The role of salt mobility in the development of supra-salt sedimentary depocentres and structural styles

Nicholas John Banbury,

B.Sc. (Hons), MRes

Thesis submitted for the degree of Doctor of Philosophy

University of Edinburgh,

Submitted for examination 1st September 2005

Dedicated to my grandmother, Betty Banbury

For her continuous support and encouragement throughout the education of myself and her other grandchildren.

The role of salt mobility in the development of supra-salt sedimentary depocentres and structural styles

Abstract

Whilst the basin morphologies that develop in a salt-free setting are generally well understood and relatively predictable, the morphology and internal architecture of sedimentary depocentres developed in salt basins are much more complex and influenced by a greater number of controls. With the aim of understanding the relative role of salt mobility and other controls on depocentre development in salt basins, results obtained from strategic, targeted observations of three different sedimentary basins are presented. These include the Paradox Basin of Utah/Colorado, USA, where sequences which are the stratigraphic response to Pennsylvanian-Triassic mobility of a Pennsylvanian salt sequence are exposed and investigated at the outcrop scale. The other basins are the Sole Pit/Silver Pit Basin (Southern North Sea) and Shearwater area (Central North Sea), both of which are exclusively subsurface examples that have experienced Mesozoic and Tertiary mobility of Upper Permian salt sequences. These later study areas are investigated using high-resolution 3D seismic data which allow the large-scale structural and stratigraphic geometries to be investigated well beyond the outcrop scale. Observations reveal a wide variety of complex depocentre styles with varying controls on their development. Controls include tectonics, differential sedimentation, availability of salt to move and potential of the overburden to flex or be penetrated. Despite this complexity, depocentre morphologies are considered to be predictable based on the concept that salt moves as a response to the pressure state in the salt layer exerted upon it by its overburden. As salt flows down pressure gradients, subsidence resulting from salt mobility is predictably greatest where the pressure from the overburden is greatest. Subsidence creates accommodation space and consequent sediment accumulation increases the load providing an intricate feedback between salt mobility and sedimentation.

Where depocentres are associated with extensional-style faulting, their morphology is influenced both by the interactions between salt mobility and sedimentation and by the relative uplift and subsidence associated with faulting. Faults in salt basins show significant variability from established concepts of fault development derived from salt-free settings and salt mobility can be seen to have a fundamental influence on how fault displacement is manifested. Observations show that footwall uplift can be of equal or greater importance in accommodating fault movement than hanging wall subsidence and salt mobility can locally both increase or decrease displacement along a fault. Fault and salt influenced depocentres do not necessarily thicken towards a fault plane and as salt must withdraw from adjacent areas into an uplifting footwall area, they may be significantly offset from the fault plane. Models of fault and depocentre development derived from salt free settings are therefore, *not* considered applicable to salt basins.

The incompactable nature of salt means that upon burial, the contents of a salt-influenced depocentre reduce in volume through compaction significantly more than the associated salt structures do resulting in the development of anticlines in overlying sequences situated directly above the salt structures. Differential compaction around salt structures is considered to provide an alternative to structural inversion or late stage salt mobility which are the favoured interpretations of many workers for the development of folds overlying salt structures.

Acknowledgements

The work presented in this thesis is the result of a CASE studentship funded jointly by NERC and Shell and Shell are gratefully acknowledged for their financial contribution and donating data to this study. Particular thanks go to Tom McKie, Mark Hempton, Simon Davey and John Horsburgh at Shell for their involvement. Shell also provided the seismic dataset used in the Southern North Sea chapter. The seismic data used in the Central North Sea chapter was provided by ExxonMobil. Seismic workstation facilities at the University of Edinburgh were financially supported by Shell/Esso and Schlumberger Geco-Prakla are acknowledged for allowing use of their Geoframe seismic interpretation software. Midland Valley Exploration Ltd are also gratefully acknowledged for providing their 2DMove and 3DMove structural restoration software to the study. Earthmoves Ltd are gratefully acknowledged for allowing me to attend one of their salt tectonics training courses in October 2003. Chris Place and James Jarvis provided invaluable computing support to the project. This work has benefited significantly from discussions with numerous people including Nick Richardson, Chris Jackson, Wendy Matthews, Gregg Farrer, Gary Hampson, Patience Cowie, Caroline Gill and Paul Post. The staff and management of the Lazy Lizard International Hostel in Moab, Utah are also thanked for assistance during the fieldwork period. Final thanks go to my supervisors, John Underhill and Bruce Trudgill. John Underhill is particularly thanked and his enthusiastic supervision which has contributed significantly to my time in Edinburgh. Steven Sawyer is thanked for allowing his photograph (Figure 3.27) to be used in the thesis and Emily Munn is also thanked for allowing inclusion of her photograph in Figure 3.58(c).

The role of salt mobility in the development of supra-salt sedimentary depocentres and structural styles

Table of Contents

Note - Figures are found in a supplement at the end of the thesis with its own numbering

List of figures

(Note - Page numbers refer to separate figures section at the end of the thesis)

Chapter 2 - Background

Chapter 3 - Paradox Basin

Chapter 4 - Southern North Sea

Chapter 5 - Central North Sea

Chapter 6 - Discussion

1.0 Introduction

In a conventional, salt-free setting, the main control on the development of a sedimentary basin is the causative tectonic regime. The direct link between tectonics and subsidence in such a setting means that the development of a sedimentary depocentre is a relatively predictable process. Extensive research has consequently led to the establishment of numerous models to explain the development of foreland (e.g. Sinclair, 1997, DeCelles and Giles, 1996), strike-slip (e.g. Aydin and Nur, 1982, Pitman and Andrews, 1985) and extensional basins (e.g. Saleveson, 1978, Leeder and Gawthorpe, 2000). The presence of a significant body of mobile salt within a sequence, however, typically complicates subsidence patterns significantly resulting in a wide variety of different depocentre morphologies, controlled by complex interactions of numerous processes. This study aims to further understand the controls on depocentre development in salt basins and the inter-relationships that exist between tectonics, salt mobility and sedimentation. Depocentres in salt basins are of two principal types, those where accommodation space is created without faulting (typically due to salt withdrawal) and those where subsidence is fault controlled. It could be argued that fault-controlled and salt withdrawal controlled depocentres develop due to separate processes and should therefore be tackled independently. Most basins which have experienced salt mobility, however, include depocentres which have developed due to both of these processes, either simultaneously or at different stages in a basins history. It is therefore hypothesised that these processes are inherently inter-related and this study investigates both styles of depocentre development simultaneously, considering their development as different aspects of a linked process.

Extensional-style faults are an extremely common feature of most salt basins and a causative link between salt mobility and extension is now well established (Jackson and Venderville, 1994). Particular emphasis is given in this study to the development of depocentres controlled by normal faults and as a fault-controlled depocentre develops as a response to the relative uplift and subsidence associated with fault displacement, a significant part of this study is involved in understanding how salt mobility influences the mechanics of fault development. There has been an extensive amount of research in recent years into the

development of normal fault systems and as a result, predictive models of fault growth, displacement-length relationships and the relative uplift and subsidence associated with faulting have become well established. These models, however, have been almost entirely based on fault systems developed in classic salt-free rift settings. It is hypothesised herein that in a salt basin, salt mobility influences the development of the fault system to the extent that models of fault development derived from salt free areas do not accurately predict their geometries, displacement-length relationships and depocentre morphologies.

The complexity of salt basins throughout the world and the great diversity in the structural styles, controls on salt mobility and morphology of depocentres in different basins makes a universal understanding of this process an unrealistic goal for a study such as this. Basins experiencing extensive salt mobility are here considered to be broadly divided into two categories. The first category are basins where salt mobility is unconstrained by an outer basin margin and experience a unidirectional sediment supply. These basins are typically found at passive continental margins and are dominated by gravity and progradation driven tectonics and include the Gulf of Mexico (USA), Kwanza (Angola) and Santos (Brazil) basins. The other group are basins constrained on all sides by a basin margin limiting the lateral movement of salt. These include the Zechstein basins of NW Europe, Paradox Basin (Colorado Plateau, western USA) and Nordkapp basin (Barents Sea, Norway). The controls and styles of salt mobility differ significantly between these types of basin and this study concentrates exclusively on the latter category. Achieving the aims of this study could be tackled in two ways, either through modelling the processes involved or through an observational study of actual faults, depocentres and salt structures in real salt basins and using targeted observations to interpret the processes involved in their development. The latter approach has been taken in this study as it is considered essential that any modelling study is preceded by observations of real world examples in order that modelled situations are realistic. This study draws its conclusions form observations and analysis of the salt structure styles, depocentres morphologies and supra-salt fault systems of three different salt basins from different parts of the world. Each of these basins developed in a different tectonic setting with varying controls on salt mobility. What they have in common, however, is that they each contain significant salt-controlled sedimentary depocentres and extensional style faults in the supra-salt sequence on the scale of tens of kilometres in length.

Study areas include two subsurface datasets based on well constrained 3D seismic data and one extremely well exposed field based study area which is also constrained in the subsurface by an extensive database of well penetrations. The field based study area is part of the Paradox Basin, an onshore salt basin of Pennsylvanian age situated in the Colorado Plateau area (western USA). The subsurface study areas are both situated on the UK continental shelf (UKCS). These include the Silverpit/Sole Pit Basin area of the Southern North Sea which is part of the Permian aged Southern Permian Basin and the Central Graben area of the Central North Sea, part of the Northern Permian Basin. The use of both surface and subsurface examples allows the processes involved to be investigated at a range of scales. 3D seismic data constrains the large-scale fault, salt structure and depocentre morphologies extremely well, which are not easily determined from field data. Field exposures do, however, allow various elements of a basins structural and stratigraphic evolution which lie below seismic resolution to be investigated. These include detailed analysis of fault systems, fracture patterns and facies distribution in the depocentres.

1.1 Rationale

The main rationale behind this research is that salt basins are extremely important hydrocarbon-bearing systems throughout the world and sequences deposited in depocentres controlled by salt mobility contain significant hydrocarbon accumulations. Understanding the nature of subsidence relating to the evolution of such a depocentre is therefore likely to significantly aid the development of depositional models for reservoir deposition and the understanding of facies distribution in the system. This is particularly significant for normal fault controlled depocentres as models for their stratigraphic development already exist based on knowledge from salt-free basins (e.g. Gawthorpe et al., 1994, Gawthorpe and Leeder, 2000). Understanding the uplift and subsidence associated with salt influenced faults is therefore critical to determining whether these models are applicable to salt basins. Similarly supra-salt fault systems frequently form structural traps for hydrocarbon accumulations and also charge reservoirs by juxtaposing them with source rocks. Consequently, understanding fully the controls that salt mobility has on the development of such faults is extremely important in understanding trap development and hydrocarbon migration in a supra-salt fault system. Aside from the clear application of this research to commercial hydrocarbon exploitation, the findings of this study are considered to be of significant academic interest. There is currently a large amount of academic interest in understanding the mechanics of how fault arrays develop which has until recently been largely restricted to salt free settings. In the classical salt free setting, tectonics is the primary control on the development of a fault system. Taking the understanding of fault development into a setting such as a salt basin where its controls are more wide-ranging can therefore, only further the understanding of how faults develop.

1.2 Organisation of the thesis

Following a literature review of the generic aspects of salt mobility, depocentre development and fault development in a salt basin (Chapter 2), this thesis consists of three stand-alone chapters, each describing one of the study areas detailed above (Chapters 3,4 and 5). Within each of these chapters are sub-sections describing the justification for inclusion of that

particular study area, the geological setting and previous work which has been carried out in that particular basin. Following this, within each chapter are presented the data and targeted observations upon which this study is based. The role of salt mobility in the development of salt structures, depocentre styles and faulting relevant to that specific area is then discussed at the end of each of these chapters. The more generic concepts which have been considered as part of this study are discussed in Chapter 6 with reference to specific examples from the preceding chapters.

1.3 Methodology

Investigations into the development of salt-controlled sedimentary depocentres are primarily based on observations of the internal morphology of particular sediment packages. It is assumed that the geometry of a supra-salt sediment package developed as a response to syn-depositional salt mobility and that by restoring these packages to their state at deposition, the morphology of the salt layer at that time can be determined. Variations in the thickness of the sediment packages associated with salt structures have therefore been investigated for each of the study areas. The varying nature of the data available in the different study areas, however, means that very different techniques are employed in different areas. In the central and southern North Sea study areas, interpretation of 3D seismic data constrained by available well penetrations is used to produce isochron maps of the time-thickness of different packages. In the Paradox Basin study area, thickness variations are observed by measuring the thickness of specific units where exposed and integrating these measurements with subsurface measurements from well penetrations to construct isopach maps. Observations of growth geometries, unconformities and fracture patterns from both seismic data and field exposures have also been used extensively to further understand the development of the study areas.

The primary techniques employed for investigating the role of salt in the structural development of fault systems are structure contour maps in the vicinity of the particular fault system and displacement-length profiles along its length. Also used are cut-off elevation profiles which plot the elevation of the footwall and hanging wall fault cut-offs alongside the maximum elevation of the top of the salt between them. Maps and profiles are constructed upon the same pre-kinematic sediment surface and derived from seismic interpretation in the North Sea study areas and from cross section construction constrained by field data in the Paradox Basin area. The specific techniques employed in each specific case study are detailed in a methodology sub-section within each chapter.

2.0 Background

2.1 Physical Properties of salt

Salt tectonics is principally concerned with the mobility of a single mineral, halite (NaCl). Halite has a melting temperature of 800°C (Talbot and Jackson, 1997) and does not undergo phase changes within a sedimentary basin. Salt mobility occurs as a response to the highly anomalous physical properties of halite relative to the other typical lithologies which make up a sedimentary basin. Relative to other lithologies, halite is typified by low strength, high thermal conductivity, extremely high solubility, low density and very low porosity (Jackson and Talbot, 1986) This section briefly reviews the properties of salt which are relevant to the process of halokinesis and compares them to the properties of carbonate and clastic sediments.

Strength of salt

According to Byerlee's law, the brittle zone of the crust displays a linear increase in the strength with depth. As Figure 2.1 illustrates, this rule applies for most rocks typically found in a sedimentary basin. Halite, however, behaves very differently with dry salt having a small amount of strength at the surface which decreases gradually with depth. Wet salt (i.e. halite aggregates that include traces of water) can be seen to be even weaker than dry salt and as Figure 2.1 shows, essentially has no strength (Jackson and Vendeville, 1994). The strength of salt has been found to vary with both temperature and grain size (Van Keken et al., 1993) with finer grained salt being weaker than coarser salt. Whilst salt can deform in a brittle manner at high strain rates (Davison et al., 1996), at typical geological strain rates it deforms as a near Newtonian viscous fluid where deviatoric stresses are linearly proportional to strain rate and viscosity (Childs et al., 1993). The much stronger overburden rocks, in contrast, deform in a time-independent, brittle manner. The low strength of salt on typical geological timescales means that salt layers are extremely inefficient at transferring shear stresses through salt layers, typically leading to a decoupling of sub-salt and supra-salt deformation (Jackson and Vendeville, 1994). Most salt sequences, however, contain significant amounts of other lithologies, particularly anhydrite, which are generally stronger and introduce a degree of strength variability to a sequence.

Density of salt

The density of salt is typically *greater* than most clastic sediments at the time of deposition but less than that of many carbonates (Talbot, 1993, Touloukian, 1981). Upon burial, most sediments progressively compact, dehydrate and cement to significantly greater densities than they have at deposition (Talbot, 1993). Salt deposits, however, have very limited potential for compaction except for at the very shallowest levels. Casas and Lowenstein (1989) observed modern salt pans as having porosities of ~50% at the surface. With 10m of burial, however, this was only 10% and by 45m the porosity was nil. Consequently, below these initial few metres, there is no potential for volume change due to compaction, dehydration or cementation in salt and it remains at a relatively similar density from a very shallow depth to deep burial. Figure 2.2 illustrates curves of density change with burial for several different lithologies and shows that despite salt having a higher density at deposition than most rocks, with burial, other lithologies rapidly overtake salt and their densities continue to rise with increasing depth. Salt in contrast shows a slight decrease in density with burial relating to a volume increase caused by the higher temperature at depth (Jackson and Talbot, 1986). As Figure 2.2 shows, salt which includes a few percent of anhydrite has a density of approximately 2200 kg m^{-3} and decreases slightly with burial.

Deformation mechanisms in salt

There is extensive evidence that salt mobility frequently occurs at shallow depths (typically <250 metres for allochthonous Gulf of Mexico salt sheets, Jackson and Vendeville, 1994) and Van Keken et al., (1993) states that salt mobility typically occurs where temperatures are <200°C. Experimental data has shown that salt can deform in two ways at these levels, either by dislocation creep or by fluid enhanced diffusional (i.e. pressure-solution) creep (Van Keken et. al., 1993). Most lithologies in overburden sequences, however, can typically only deform by brittle mechanisms at crustal levels below 8km and consequently salt deforms in a way which is very different to its overburden (Vendeville and Jackson, 1992, Jackson and Vendeville, 1994). Experiments show that dry salt will deform by dislocation creep (Urai et al., 1986), however, most natural rock salts contain trace amounts (≥0.05%) of water which significantly influences the deformation mechanism. These trace amounts of water facilitate pressure solution of material at grain boundaries allowing diffusional creep to occur at shallow depths (Urai et al, 1986, Spiers et al, 1990, Van Keken et al. 1993). As water is

present only at grain boundaries, this process is strongly controlled by grain size. Van Keken et al. (1993) describe natural salt sequences as having grain sizes between 5 and 30mm and smaller grain sizes will facilitate the most diffusional creep.

Viscosity of salt

The effective viscosity of salt depends on the deformation mechanisms involved and the relative dominance of dislocation and diffusional creep (Van Keken, et al., 1993). It is therefore strongly influenced by grain size, temperature and strain rate with smaller grain sizes facilitating a greater proportion of diffusion creep and therefore being less viscous than coarser grained salt where dislocation creep is more dominant. Figure 2.3 illustrates plots of effective viscosity of the salt as a function of strain rate for three different grain sizes of salt. Where the effective viscosity is strain rate independent, diffusion creep is considered to be dominant whereas at higher strain rates, diffusion creep is dominant. As Figure 2.3 illustrates, with larger grain sizes, the transition between the two mechanisms of deformation shifts to lower strain rates (Van Keken et al., 1993). Salt tectonics was classically modelled with both the salt layer and overburden represented by two viscous fluids (Jackson, 1995). Whilst evidence exists for the overburden behaving in a semi-viscous manner over geological timescales (Davison et al., 1996) recent modelling (e.g Vendeville and Jackson, 1992, Jackson and Vendeville, 1994, Schultz-Ela and Jackson, 1996) tends to concentrate on entirely brittle deformation in supra-salt sequences.

Thermal conductivity of salt

Salt is a very efficient conductor of heat relative to other typical constituents of a sedimentary basin (Jackson and Talbot, 1986) and salt structures tend to act as "heat chimneys" for a sedimentary basin making the lower parts of a salt structure anomalously cool and the upper areas anomalously warm (Jackson, 1995).

2.2 *Mobility of salt*

Originally horizontally bedded salt has frequently become mobilised into salt structures in salt basins around the world. A wide range of salt-structure styles have been identified which are reviewed in Jackson and Talbot (1986) and illustrated in Figure 2.4. Salt structures are broadly divided into two different types. Those in which salt mobility is accommodated in the overburden by flexure and/or sedimentary growth (e.g. salt pillows, salt-cored anticlines) and those which penetrate their overburden or appear to have penetrated it (i.e. diapirs). Three different models for the development of diapiric structures have become established, there is, however, no assumption implied of universal applicability of any single model. The oldest of these models is termed 'active diapirsim' and suggests forceful intrusion of a salt body into its overburden (Schultz-Ela, et al., 1993). Another model termed 'passive diapirism' was introduced by Barton (1933) and is based around the concept of 'downbuliding' driven by sedimentation. Rather than salt forcing its way to the surface, a down-built diapir maintains its salt crest near the surface throughout its development and grows as adjacent sediment packages sink and accumulate further sediment causing the salt structure to grow from its base downwards. The most recent concept introduced is termed 'reactive diapirism' and involves salt rising upwards to infill space created as the overburden in extended (Vendeville and Jackson, 1992).

As in any other fluid, salt becomes mobile as a response to pressure gradients within the salt body with salt flowing from areas of high pressure to areas of lower pressure (Talbot, 1993). The overburden exerts the principal pressures on a salt body and if the pressure is equal across the entire salt body (e.g. as a result of uniform deposition), no gradient will exist and the salt will not move. A specific mechanism is therefore required in which these differential pressures will develop. Numerous mechanisms have been proposed to drive and initiate salt mobility/diapirism These have been reviewed by Jackson and Talbot (1986) who discus the relative potential of salt buoyancy, sedimentary differential loading, gravity spreading and thermal convection as well as tectonic compression and extension as driving forces behind salt mobility. Jackson and Vendeville (1994) also list erosional differential loading, local heat sources (i.e. heating of salt by intrusions) and movement upon sub-salt faults as potential mechanisms. Each of these mechanism are briefly detailed below.

Mechanisms driving salt mobility

Buoyancy halokinesis

The relative buoyancy of salt with respect to overburden sequences has long been considered to be extremely important in salt tectonics (Jackson, 1995). As Figure 2.2 illustrates, upon burial, an overburden sequence will reach a critical point were it becomes denser than the underlying salt sequence resulting in a density inversion. Salt tectonics has classically been considered to be down-scalable to the point where both the salt sequence and overburden can be modelled by two viscous fluids of different densities (Jackson, 1995). In a fluid system, such a density inversion is seen to be inherently unstable (Jackson and Talbot, 1986) resulting in the overlying denser layer sinking into the less dense layer as a result of gravity and the amplification of minute pressure anomalies within the salt. The displaced layer then typically rises up in a bulbous form until a gravitationally stable morphology is attained. The morphology of diapirs modelled in this way are typically analogous to many salt structures around the world and consequently buoyancy driven diapirism with density inversion as the trigger has been widely accepted (Jackson, 1995).

As a lone mechanism for initiating salt mobility, however, buoyancy is falling out of favour. This has been due to several key observations. Firstly, seismic profiles show significant evidence that many salt structures developed at depths too shallow for a density inversion to occur at. Similarly, settings where modern-day salt tectonics is occurring (e.g. Red Sea) reveal overburden sequences which are less dense than the salt thus, ruling out density inversions as their main controlling factor (Jackson and Vendeville, 1994). Perhaps most importantly, experimental data has shown that virtually all sediments typical of an overburden sequence, deform in a brittle manner at the depths where salt tectonics occurs regardless of strain rate (Jackson and Vendeville, 1994, Weijimars et al., 1993). Consequently, ductile deformation of the overburden is considered to be unrealistic. Fluid overburdens have also been ineffective in modelling the complex structural geometries typically associated with salt structures (Vendeville and Jackson, 1992). Indeed, models which use a scaled brittle overburden (e.g. Vendeville and Cobbold, 1987, Vendeville and Jackson, 1992, Naplas and Brun, 1993) have typically reproduced much more realistic structural styles. Jackson and Talbot (1986) showed that even with a Newtonian viscous

overburden, in order for buoyancy to have the potential to cause significant uplift into a salt dome, a minimum of 150 metres of pre-existing structural relief is required. Consequently, as a triggering mechanism, buoyancy must be ruled out. Davison et al. (1996, 2000[b]), however, suggests that once diapirs are established by other means, buoyancy forces are sufficient to create topographic relief above a diapir and pierce thin, weak overburdens.

Differential loading

One mechanism which is well established as initiating salt mobility is differential loading. A salt layer with an overburden of uneven thickness or density will be experiencing different pressures in different areas and the resultant pressure gradient will therefore result in salt being displaced away from the loaded area. Any process which can create topographic or bathymetric relief in the overburden is particularly effective in creating a differential load as either air or water are significantly less dense than sedimentary rocks, regardless of their density and degree of burial (Jackson and Talbot, 1986). Whilst the most likely of these processes is sedimentary loading, salt mobility driven by erosional differential loading has also been identified (Huntoon, 1982) and Sørensen (1998) details the importance of 'unroofing' unconformities centred on pre-existing salt swells in the development of diapiric structures in the Norwegian-Danish Basin. The most likely differential loading system is that of a prograding delta or alluvial fan and Jackson and Talbot (1986) calculate that a clastic wedge with a bathymetric relief of as little as 16 metres is capable of driving salt mobility. Jackson and Vendeville (1994) suggest that in order for salt mobility driven by differential loading to be continuous, the load must be continuously dumped in the same area as otherwise deposition will migrate to more distal areas above the salt bulge and cancel out the differential nature of the load. Jackson and Vendeville (1994) also suggest that although simple salt flow is easy to initiate with differential loading, the strength of the overburden is likely to be much greater than stresses associated with the pressure differences exerted by the differential load and therefore diapiric piercement which is entirely driven by loading is difficult to initiate. Ge et al. (1997) use scaled physical models of progradation onto a salt analogue to investigate the potential of progradation driven differential loading on the development of diapiric structures (Figure 2.5). Where progradation onto salt overlying a flat sub-salt layer was modelled (Figure 2.5(a)), a salt-cored monocline was created at the progradation front but no diapiric structures developed. Where progradation was onto a stepped basement, however, steep sided salt structures (Figure 2.5(b)) and piercing diapiric

structures (Figure 2.5(c)) did develop suggesting that a buttressing of salt onto these flow obstacles was important in their development.

Gravity spreading

Salt at the surface has been observed to flow laterally under its own weight down slopes of as little as 3° in so called salt glaciers in Iran (Jackson and Talbot, 1986, Talbot and Jarvis, 1984, Wenkert, 1979). Salt flow in such a setting was seen to be extremely rapid with lateral movement of up to 2m per year being observed, (Talbot and Jarvis, 1984). This surface flow without overburden involves salt which contains large amounts of water from atmospheric precipitation which is interpreted as significantly enhancing its ability to flow (Jackson, 1995). This is, however, considered to be a highly localised mechanism of salt flowage restricted to specific, arid settings rather than being significant in the subsurface at the basin scale.

Thermal effects

As salt is a very efficient conductor of heat relative to the more usual carbonate and clastic constituents of a sedimentary basin (Jackson and Talbot, 1986), the upper parts of a salt body are likely to be warmer and the lower parts cooler than surrounding areas. Also the overburden would be expected to be cooler than the salt layer and Talbot (1978) suggested that this temperature variation has the potential to initiate convection within a salt body and drive salt flow. Jackson and Talbot (1984), however, describe this as "merely a possibility based on order of magnitude calculations" and Jackson (1995) states that salt transmits heat far more efficiently by conduction than by convection.

Compression

The role of salt layers is extremely important in developing the structural styles observed in many compressional settings throughout the world, particularly in thin-skinned foreland fold and thrust belts. There is no doubt from these settings that compression has the ability to mobilise salt. Physical modelling using brittle overburdens however, is largely unable to recreate the morphologies of most structures we would recognise as salt diapirs (e.g. Letouzey et al., 1995, Jackson and Vendeville, 1994). Compression has the result of

thickening a sequence above a salt-cored buckle fold which is therefore likely to make this the area where the pressure on the salt layer is greatest and therefore drive salt away from this area (Davison and Waltham, 2003).

Extension

Recent research, primarily driven by physical modelling has suggested that regional extension is among the most important controls on the initiation and development of salt diapirism (Vendeville and Jackson, 1992, Jackson and Vendeville, 1994, Naplas and Brun, 1993). Jackson and Vendeville (1994) highlight a distinct temporal relationship between the onset of salt diapirism and regional extension in salt basins around the world. They also point to the existence of numerous enigmatic basins which contain significant salt accumulations but are without major salt structures and conclude that extending basins typically develop salt structures whereas non-extending basins typically do not. The principals which are fundamental to this hypothesis have largely been detailed above and consider the overburden to be too strong to be intruded by extremely weak salt which is unable to effectively transfer shear stress onto it. Salt mobility driven by extension is considered to occur as it thins and weakens the strong overburden through extensional faulting and also this localised thinning exerts strong differential loads on the salt layer driving salt towards the thinned area (Jackson and Vendeville, 1994). Consequently, this form of salt mobility is termed 'reactive diapirism' (Vendeville and Jackson, 1992) as it is largely a passive, space filling response of the weak, mobile salt to extension in the overburden which is entirely within the brittle domain. Figure 2.6 illustrates the development of a salt diapir below a developing graben system in the supra-salt sequence through reactive diapirism in a physical model. Experimental results from Naplas and Brun (1993) showed that during extension, salt diapirs were frequently spatially associated with extensional faults in the sub-salt sequence. Their experiments also showed that major salt structures could also develop, significant distances away from sup-salt faults with displacement being transferred along the salt layer.

Summary

Following the work of Vendeville and Jackson (1992), Nalplas and Brun (1993), Jackson and Vendeville, (1994), extension is now widely considered to be the among most important controls driving salt mobility. Differential loading is, however, still considered to be an extremely important driving mechanism in many salt basins. Each of the other mechanisms are considered to have the potential to influence salt mobility although they are considered more likely to modify the system rather than initiate or drive it.

2.3 *The development of normal fault arrays in salt-free settings*

An extensive amount of research in recent decades has led to a detailed understanding of the way that normal fault arrays develop. Although a limited amount of research has investigated fault development in salt basins (see section 2.4), by far the most detailed understanding of the kinematics of fault array development is restricted to salt free settings. This section deals exclusively with established concepts of fault development based on salt free areas. Recent studies (e.g. Walsh and Watterson, 1989,1991, Peacock and Sanderson, 1991, Anders and Schilsche, 1994, Cartwright et al. 1995, Walsh et al. 2003) are dominated by the idea that faults grow through the processes of tip propagation and segment linkage. This process occurs with the initial nucleation of a population of small, kinematically isolated faults which grow through the radial propagation of the fault tips. Individual faults grow in an isolated manner until they overlap with incidental faults along strike and the stress fields of the two faults interact (Walsh et al., 2003). The mechanical linkage of the segments then occurs through the breaching of the overlap area resulting in the linked fault segments behaving as a single fault (Peacock and Sanderson, 1991, 1994, Trudgill and Cartwright, 1994). This concept is illustrated in Figure 2.7. Data from both observations of real fault systems in various extensional settings (e.g. Dawers et al. 1993, Cartwright et al. 1995, McLeod *et al.* 2000, Young et al. 2001) as well as numerical modelling studies (e.g. Cowie et al., 2000, Gupta et al. 1998) strongly support this model of fault array development. The implication of this model is that fault arrays develop as a large population of small faults and develop into a smaller population of large faults. Cowie et al. (2000, 2005) have shown that strain localises onto major structures as an extensional phase progresses resulting in some smaller faults being effectively switched off. A large amount of research has focused on the displacement-length relationships of normal fault systems and as Figure 2.7 shows the relationship between fault displacement and fault length between a small isolated fault and a larger linked fault is considered to be consistent. As Figure 2.8 shows, comparisons of displacement against length for a large number of fault populations around the world (e.g. Schlische et al. 1996, Morewood and Roberts, 2002) shows this relationship to be consistent at a wide range of scales. As a result, faults at a millimetre scale are considered to display similar displacement-length characteristics to those at the kilometre scale or larger.

Uplift and subsidence associated with faulting and the development of fault controlled sedimentary depocentres

Normal fault motion is manifested in components of both uplift in the footwall and subsidence in the hanging wall areas of the fault, both of which experience decay with distance away from the fault plane (Stein and Barrientos, 1985). These components also decay with distance along the length of the fault away from its point of maximum displacement resulting in a complex but predictable three-dimensional structural morphology which is illustrated in Figure 2.9. As Figure 2.9 shows, both the uplifted footwalls and downthrown hanging walls in this idealised fault system have typical 'D' shaped contour patterns. As this structural morphology governs sediment accumulation, isopach patterns in syn-rift sequences typically display this same morphology and this is consistent with the contour patterns observed in many published examples of real world faults (e.g. McLeod et al. 2000, Dawers and Underhill et al., 2000). Published accounts of relative uplift and subsidence associated with faulting, including studies of neotectonic faults exclusively imply that the magnitude of hanging wall subsidence is significantly greater than that of footwall uplift (e.g. Stein and Barrientos, 1985, Barr et al. 1985). Jackson and McKenzie (1983) consider the reduction in stress associated with a earthquake slip event to be equally distributed between the footwall and hanging wall areas of a fault and suggest the dominance of motion in the hanging wall to be due to geometric aspects of the fault plane relating to crustal scale listricity, forcing the hanging wall to subside more than the footwall is uplifted. They also suggest that as the hanging wall area is displaced, it partially unloads the footwall allowing uplift due to isostasy and estimate footwall uplift to be around $1/10^{th}$ of the magnitude of hanging wall subsidence. Other studies have suggested slightly larger ratios of between 1:6 and 1:8 (e.g. Stein and Barientos, 1985).

The accommodation space associated with a specific fault is a complex interaction of the hanging wall subsidence associated with that particular fault and the footwall uplift associated with adjacent structures, as well as longer-term isostatic movements affecting both the footwall and hanging wall areas (Gawthorpe et al., 1994). As Figure 2.9 shows, the fault morphology expected in a classic salt-free setting predicts the maximum subsidence to be directly adjacent to the fault plane, experiencing decay both with distance from the fault and along the fault as displacement decreases towards the tip. As the amount of

accommodation space reflects the amount of displacement on the controlling fault system, depocentres grow and link as the fault system grows. Consequently, as with their controlling faults, depocentres are expected to evolve from a larger number of isolated depocentres into a smaller number of large linked depocentres. This has been demonstrated from numerical modelling by Cowie et al. (2000) and also observed in seismic examples by Dawers and Underhill, (2000), McLeod et al. (2000) and Young et al. (2001).

2.4 *The development of normal faults in salt basins*

Normal faults are an extremely common feature in salt basins, both in the sequences above and below mobile salt successions and an empirical link between extensional faulting and salt mobility is becoming established (Jackson and Vendeville, 1994). A wide variety of supra-salt faulting styles are observed in salt basins around the world ranging from extremely large-scale gravity related listric growth faults (e.g. Rouby et al., 2003, Demercian et al., 1993) to small-scale radial fault patterns in the overburden to salt diapirs (e.g. Davison et al. 2000[b]). There is a widespread consensus that supra-salt faults develop with significantly different controls to the classically understood faults in salt free settings. The way that salt mobility influences factors such as displacement-length relationships, fault linkage, fault controlled uplift/subsidence and depocentre development has however, largely been neglected to date. The notable exception to this is Richardson et al. (2005), which is discussed in more detail below.

The extremely weak nature of salt means that it is unable to transmit sufficient shear stress to link supra-salt deformation to sub-salt deformation (Jackson and Vendeville, 1994) resulting in sub-salt and supra-salt deformation typically being decoupled. Stress orientations in supra-salt sequences which are 'detached' from the basement by a salt layer typically display extensive azimuthal variability whereas in a basement 'attached' salt free succession (Figure 2.10) these are typically more uniform and predictable (Bell, 1996). Similarly sub-salt and supra-salt fault systems often have entirely different orientations, dips and displacements (e.g. Helgeson, 1999, Dooley et al., 2005) and the cumulative separation may be significantly greater on one or other of the decoupled fault systems (Stewart et al., 1996).

Several studies have investigated the development of extensional faults above a salt layer through physical modelling of a brittle layer over a viscous salt analogue (e.g. Vendeville and Cobbold, 1987, Vendeville and Jackson, 1992, Childs et al., 1993, Jackson and Vendeville, 1994). Vendeville and Jackson (1992) and Jackson and Vendeville (1994) largely concentrate on the role of extensional faulting in the development of salt diapirs and do not dwell on the mechanics of fault development in their model. The keystone style graben system they show in their models (e.g. Figure 2.6) is also notably not compared with

similar geometries in real world examples making the validity of this faulting style questionable for real-world situations. Childs et al. (1993) model the development of syn-sedimentary growth faults associated with 'salt-roller' style salt structures.

Salt rollers are a characteristic structural style of many salt basins and involve low amplitude salt swells, one side of which is in conformable stratigraphic contact with the overlying sequence and the other having a faulted contact associated with a crestal listric growth fault (Jackson, 1995). As Figure 2.11 shows, the system modelled by Childs et al. (1993) did not produce diapiric salt structures and did not clarify any relationships between the salt and associated faults. They did, however, observe fault linkage through a relay zone and that displacement on the faults in their model varied in a "regular and predictable manner".

The above-described studies, only consider extension restricted to the salt layer and its overburden, whereas numerous studies have investigated the development of faults where both the overburden and sub-salt sequence are experiencing extension and particularly the relationships between sub-salt and supra-salt structures. Through observations of structures in the Central North Sea, Errat (1993) identified a variety of structural styles in supra-salt sequences as a result of movement on sub-salt faults including salt diapirs, forced folds and normal faults. He also suggested that the pre-existing pod-interpod morphology (see section 2.5) had a significant influence on structural styles with areas where the overburden was grounded on the sub-salt sequence prior to the rift episode having different structural styles to where faults developed below salt swells. Stewart et al. (1996) suggested that although frequently spatially offset, faults in the overburden sequence could still be kinematically linked to sub-salt faults along ramp-flat trajectories, similar to those observed in salt influenced thrust systems.

Numerous modelling studies, including Koyi et al. (1993), Koyi and Peterson, (1993), Schultz-Ela and Jackson (1996) and Withjack and Calloway (2000) have investigated the link between sub-salt and supra-salt faulting and have come to some generic conclusions as to the controls on the degree of linkage between fault populations separated by a salt layer. As reviewed by Stewart et al. (1996) and Richardson et al. (2005), the most important variable affecting linkage between sub-salt and supra-salt fault populations is considered to

be the displacement ratio. This is the ratio between the displacement of the controlling fault and the thickness of the salt layer with a thicker salt layer leading to greater detachment of the two. A value of 1 represents where the displacement on the sub-salt fault exceeds the thickness of the salt layer directly coupling (i.e. 'hard linking') the two fault systems (Stewart et al. 1996). Another significant control is the ratio between the thickness of the salt layer and the overburden layer (Koyi et al. 1993). Withjack and Calloway (2000) showed that overburden deformation is more widely distributed with thin overburdens. Factors such as the viscosity of the salt layer, strength of the overburden and rate of displacement of the controlling basement fault have also been shown to have an influence (Koyi et al., 1993, Withjack and Calloway, 2000).

Richardson et al. (2005) investigated a series of partially decoupled normal faults on the Norwegian continental shelf and concluded from displacement-length profile analysis of sub-salt and supra-salt faults that both groups developed through radial propagation and segment linkage. They also showed that salt mobility in the area was a response to the evolution of the fault array with salt moving towards the areas of maximum displacement on both sub-salt and supra-salt faults. The response of salt to fault array evolution is described in terms of two distinct end members (Figure 2.12). The first end-member (Figure 2.12(a)) is where faulting is entirely restricted to the sub-salt sequence and shows salt passively migrating to the area adjacent to the fault plane promoting flexure in the overburden. The second end-member is where faulting is entirely restricted to the supra-salt sequence and as Figure 2.12(b) shows, salt is considered to migrate to the areas of maximum displacement below the footwall areas.

Richardson et al. (2005) also investigate the development of fault-controlled depocentres and as Figure 2.12 shows, the pure basement fault scenario (a) predicts fault-controlled depocentres to thicken away from the controlling fault which is the exact opposite of what is expected in salt free settings. Richardson et al. (2005) suggest natural examples are likely to be a combination of these two end members with both sub-salt and supra-salt faulting controlling salt distribution and depocentre evolution.

Several studies have suggested that salt mobility associated with supra-salt normal faulting can develop precursor structures for subsequent diapirs and other salt structures. Davison et al. (2000[a]) details how numerous Central North Sea salt diapirs are associated with major normal faults near their bases and Stewart et al. (1996) suggests that salt movement associated with faulting emplaces salt at structurally high levels, facilitating subsequent passive growth through downbuilding. Richardson et al. (2005) also suggests that passive salt migration towards areas of maximum fault displacement as shown in Figure 2.12 can explain the location of subsequent diapiric structures.

2.5 The development of sedimentary depocentres in salt basins which do not involve faulting

Although faulting is a significant factor in the development of sedimentary depocentres in many salt basins, extensive sediment packages are also recognised which are not associated with faulting. The process of salt withdrawal alone has the capacity to create significant accommodation space and this section details depocentre development without faulting. One of the earliest discussions of the role of salt mobility in sedimentary depocentre development came from Trusheim (1960), who recognised that thickness variations in sediment packages could be used to infer the evolution of a salt structure.

Based on observations of salt structures in northern Germany, Trusheim (1960) proposed a model by which two types of depocentre developed, related to two stages of salt mobility (Figure 2.13). The first was termed the 'primary peripheral sink' (Figure 2.13) which develops when the salt structure is in a non-piercing pillow stage and involves expansion of sequences away from the salt swell. The second stage (secondary peripheral sink) occurs when the diapir has pierced the overburden. This change in salt structure style results in the diapiric structure draining and deflating the pre-existing salt pillow resulting in subsequent sediment packages expanding towards the diapir (Figure 2.13). Trusheim (1960) suggests that the volume of sediment in the peripheral sinks, corresponds to the amount of salt that has moved and Sørensen (1986) quantifies this, taking into account compaction of the sediments. This model is, however, clearly not universally applicable as pillow-to-diapir transitions are not recognised in the majority of salt structures and depocentre patterns are rarely this simple.

Trusheim's model involves a pre-kinematic layer in the overburden sequence although observations of many salt basins suggests that salt mobility and associated depocentres frequently develop without such an layer (e.g. Smith et al. 1993, Figure 10, Hodgson et al. 1992, Diegel et al. 1995, Figure 6, Wiemer et al. 1998, Figure 8, Stewart and Clark, 1999, Figure 7). In such situations, the nature of salt flow is likely to be very different to that described above and Trusheim's model is considered unable to predict the development of

depocentres in these settings. The development of salt structures and depocentres in such a setting has, however, been described in terms of the minibasin concept.

Minibasins are typically polygonal sedimentary depocentres bounded at their margins by salt walls and are common in various salt basins around the world. They are thoroughly documented in the Gulf of Mexico where they dominate much of the continental slope (Diegel et al. 1995) and also identified in the Precaspian Basin (e.g. Barde et al. 2002) and the Central North Sea (e.g. Stewart and Clarke, 1999). Both salt wall and depocentre morphologies in such settings typically show varying geometries and varying degrees of interconnectivity and some examples of their large-scale morphology are shown in Figure 2.14. Alexander and Flemings (1995) describe minibasins as developing due to sedimentary loading of the salt sheet which causes the migration of the salt into salt swells at marginal areas. Evacuating salt then leaves a topographic (or bathymetric) low which traps further sediment, further driving salt mobility.

Sedimentation and salt mobility associated with minibasin development are therefore considered to be intrinsically linked with salt mobility providing the accommodation space and sedimentation providing the driving force (Rowan and Weimer, 1998). Minibasin development tends to continue until the entire salt sequence has been withdrawn from below the depocentre and the package grounds out on the sub-salt package starving the system (Smith et al. 1993, Barde et al. 2002). Figure 2.15 shows a model of minibasin development specific to the Triassic in the Central North Sea although the first three stages are considered to be universally applicable. Minibasins are typified by growth geometries with very variable geometries (e.g. Stewart and Clark, figures 4,6 and 7) and include both parallel-bedded sequences such as in Figure 2.15 and strongly asymmetric sequences as shown in Figure 2.16.

3.0 The Paradox Basin

3.1 Introduction

The outstanding field exposures found in the Paradox Basin, not only reveal the presence of numerous salt structures, but also expose a significant part of the stratigraphy which can be constrained as having developed contemporaneously with them. This coupled with the extensive number of wells drilled in the area as a result of over 60 years of hydrocarbon and uranium exploration has meant that the geology can also be understood well into the subsurface. This chapter aims to document the development of salt mobility and associated depocentre development in the Paradox Basin and also to discuss the controls on its development. A significant part of this chapter is also involved in understanding the development of a system of Tertiary/Quaternary normal faults which are associated with the salt structures but appear to post-date the main (Pennsylvanian-Triassic) phase of salt mobility in the area.

The inclusion of the Paradox Basin study area into this investigation is justified largely on the outstanding nature of field exposures in the area which allow the controls of salt mobility on fault and depocentre development to be investigated at the outcrop scale. This is far more detail than is allowed from the entirely subsurface study areas and its inclusion is considered essential in order to understand the processes involved at the full range of scales.

3.2 Methodology

This investigation is based primarily on field observations, coupled with data from a large number of well penetrations in the study area, the locations of which are shown in Figure 3.1. Targeted field observations were made of key structural and stratigraphic relationships relevant to the salt-tectonic development of the study area, with particular emphasis on faults, fractures unconformity surfaces and thickness variations associated with the salt structures. Large-scale geological mapping of the entire 5525km^2 study area was not carried out, although several smaller scale areas were mapped in order to investigate certain features. Extensive amounts of dip data were also collected throughout the study area as well as map data sufficient for cross section construction. Sedimentary logging of specific units was carried out along a transect across the basin in order to assess the role of salt mobility in influencing facies distribution.

The control of salt mobility on depocentre development was investigated through integration of an extensive well database with measurements of stratigraphic thicknesses from field exposures. Well data largely consisted of information giving the elevation of the tops of various stratigraphic units accessed from the Utah Geological Survey (UGS) website (http://ogm.utah.gov). This data was then converted to give the elevation and thickness of the specific units and collected together as a spatially referenced database within the 2DMove structural restoration software. The original data from the UGS website is given as tables of well depths without justification of how the interpretations were derived. The information from this database, was however, compared with original well logs in the UGS library in Salt Lake City for all wells which provide data considered to be key to the interpretations detailed in this chapter.

Well logs were interpreted based on the guidelines detailed in McClearly et al. (1983) and a high level of confidence is expressed in this dataset. Measurements of the thickness of stratigraphic units derived from field data were measured using a barometric altimeter and the top and bottom of the units were mapped with a GPS. In order to integrate them fully with the well database, thickness measurements based on field data were then converted

through a process of cross-section construction into vertical profiles (illustrated in Figure 3.2) and added to the well database. It should be noted that vertical thicknesses rather than stratigraphic thicknesses are used throughout this chapter in order to make them consistent with the subsurface datasets in following chapters. Isopach maps were created by gridding and contouring the data using GMT and these maps include a degree of interpretation in areas where data is sparse. Thicknesses of sediment packages are consistent between isopach maps and cross sections.

The structural development of the Moab Fault System was investigated both through targeted field observations and through use of a displacement-length profile, cutoff elevation profile and structure contour map of the fault system. Each of these was derived from a series of profiles along the fault system at approximately 1km intervals where field data was collected in order to constrain the structural morphology. The structural elevation of the top of the Base Middle Jurassic horizon was then determined through basic cross section construction and the data then used to produce the maps and sections. The Base Middle Jurassic horizon was chosen as it predates the development of the fault system and is well exposed throughout the study area.

3.3 Location of study area

The Paradox Basin is situated in the Colorado Plateau geological and geomorphic province straddling the border between SE Utah and SW Colorado in the western USA (Figure 3.3). The area investigated in this thesis covers the best exposed, northern part of the Basin located in the vicinity of the town of Moab. The study area covers 5525km^2 being loosely bounded by the Book Cliffs escarpment to the north and ending several km south of Spanish Valley. It is bordered to the east by the Utah-Colorado state line and Canyonlands National Park to the west.

3.4 Geological Setting

The Colorado Plateau is a distinct structural province bounded to the south and west by the Basin and Range extensional province, and to the east and north by elements of the compressional Rocky Mountain system. The western USA has experienced an extremely complex Phanerozoic history being influenced by numerous phases of compressional, extensional and transtensional tectonism. The tectonic setting has been dominated by extensive subduction and the accretion of various terranes along its western margin. In contrast, the Colorado Plateau remained a relatively stable cratonic area (Wernicke, 1992) and has remained largely undeformed throughout this period (Barbeau, 2003). The main structural features of the Colorado Plateau are a series of large monoclines which developed in the Laramide Orogeny and can frequently be traced for several hundred kilometres (Figure 3.3). Away from these structures however, the area is dominated by a relatively undisturbed, shallow-dipping layercake stratigraphy.

Geological development of the Colorado Plateau

Pre Ancestral Rocky Mountain development

Between the Late Palaeozoic and Late Devonian, the Colorado Plateau was a cratonic area which lay to the east of a passive continental margin and was dominated by deposition in a

stable shelf environment (Poole et al. 1992). This period of relative tectonic quiescence was interrupted in the latest Devonian and Lower Carboniferous (Early Mississippian) by the Antler Orogeny, related to the collision of an island arc system with the western edge of the continent (Miller et al. 1992). Associated with this event was the development of an eastward verging orogenic thrust system situated in central Nevada and its associated foreland basin which provided a terrigenous clastic influx into adjacent basins (Poole and Sandberg, 1991). The Paradox Basin area remained a significant distance from this orogen and remained a shallow marine shelf setting throughout the Late Devonian and Mississippian (Nuccio and Condon, 1996).

Pennsylvanian – Early Permian tectonism – The Ancestral Rocky Mountains

During the Pennsylvanian and Early Permian, the Colorado Plateau and its surrounding areas was dominated by the development of the Ancestral Rocky Mountains (ARM). These are a series of around 20 structural highs of Pennsylvanian to Early Permian age which extend from Idaho to Central Texas and are most numerous in Colorado (Barbeau, 2003). Although primarily recognised from unconformities and coarse facies in adjacent basins, in some areas there is evidence of adjacent fault zones and they are widely considered to be a series of basement involved compressional structures. Five of these recognised ARM uplifts are situated in the Colorado Plateau including the Piute, Emery, Zuni, Defiance and Uncompahgre uplifts. The latter is the basin bounding structure on the NE flank of the Paradox Basin which is the largest and best exposed of the ARM basins (Barbeau, 2003). The origin of these basins is far from clear as they are situated as much as 1500 km from any contemporaneous plate boundaries (Kluth and Coney (1981)).

Two different models dominate the thinking for their development. Kluth and Coney (1981) suggest that they developed as an intra-plate response to stresses associated with the contemporaneous Ouachita-Marathon Orogeny, the suture zone of which is situated in the Gulf Coast region of western Texas. The orientation of the ARM uplifts (including the Uncompahgre) are typically oriented perpendicular to this suture zone making this interpretation problematic. Ye et al. (1996) suggest a model where deformation was related to a previously unrecognised NE dipping, Andean style subduction zone situated at the SW margin of N. America. Whatever the cause of this extensive intra-plate tectonism, it clearly

was a significant influence on the development of the Colorado Plateau with the Uncomphagre uplift creating up to 5km of accommodation space in the adjacent Paradox Basin. Kluth and Coney (1981) date ARM tectonism to have initiated in the Early Pennsylvanian, reaching its climax in the Desmoinesian (Middle Pennsylvanian) and continuing at a slower pace into the Late Pennsylvanian and Early Permian in many areas.

Middle Permian to Late Jurassic – relative tectonic quiescence

Following the ARM phase, the western margin of the USA continued to experience complex deformation. This was mainly associated with the accretion of an island arc terrane to the western margin of the continent during the Early-Middle Triassic Sonoma Orogeny (Saleeby and Busby-Spera, 1992). Widespread arc volcanism and back arc extension accompanied this event and continued through the Triassic and Jurassic. Despite all this tectonic activity to the west, the Colorado Plateau remained a stable area throughout this period without any notable deformation taking place. The only significant tectonic influences on sedimentation of this age involves extensive volcanic ash layers within Jurassic and Triassic sequences (Nuccio and Condon, 1996, Saleeby and Busby-Spera, 1992) and a gentle thickening of packages of this age towards the west indicating a gradual westward increase in accommodation space (Molenaar, 1981).

.

Late Jurassic to the Late Eocene – The Sevier-Laramide Orogenic phase

Between the Late Jurassic and Late Eocene, western North America was influenced by continued arc style compressional tectonics associated with subduction occurring at the western margin of the continent (Dickinson and Snyder, 1978). This led to the development of the major eastward migrating Cordilleran fold and thrust belt which was dominated by thin-skinned compressional tectonics and stretched from Alaska to Guatemala (Coney 1976).

In the Colorado Plateau area, this consisted of the Sevier Orogenic belt which did not migrate much further than the western margin of the plateau (Dickinson and Sydner, 1978) although marine deposition in its foreland basin stretched across most of the Colorado Plateau including the Paradox Basin. In contrast to other areas of the Cordilleran fold and thrust belt, where thin skinned tectonism continued until the late Eocene (Chapin and Cather,

1983), in the Colorado Plateau area, the Late Cretaceous saw a transition from this thin-skinned style of deformation to a style dominated by thick-skinned, basement-involved deformation.

Although essentially a continuation of the same orogenic phase, these two temporally distinct styles are generally referred to separately as the Sevier (thin-skinned) and Laramide (thick-skinned) orogenies. Although the reason of this change in structural styles is unclear, Dickinson and Sydner (1978) hypothesise that it is due to change in the dip of the associated subducting slab and an increase in the interactions of the descending slab with the base of the lithosphere. The Laramide phase saw the cessation of activity at the Sevier front and deformation instead manifested itself in basement involved uplifts with the orogenic uplift now centred at the eastern margin of the Colorado Plateau leading to the development of the Rocky Mountain uplifts and their associated basins (Chapin and Cather, 1983). Laramide deformation did, however, have a relatively subdued but significant influence to the west of the Rocky Mountains leading to the development of the inversion monoclines of the Colorado Plateau (Dickinson and Sydner, 1978) such as the Monument, San Rafael and Circle Cliffs structures (Figure 3.3).

Laramide reactivation of the Uncompahgre Uplift which bounds the Paradox Basin has also been documented (e.g. Heyman et al 1986, Jamison and Stearns, 1982). McQuarrie and Chase (2000) estimate the overall bulk shortening of the Colorado Plateau represented by Laramide monocline structures to be less than 1%. Whilst the reason for the greatly subdued deformation in the Colorado Plateau relative to the Rockies is unclear, Dickinson and Sydner (1978) suggest that pre-existing Ancestral Rocky Mountain structures played a role in localising deformation to the east of the plateau.

Early Tertiary uplift of the Colorado Plateau

The Colorado Plateau is a topographically high area and presently has an average topographic elevation of approximately 2000 metres (Pederson et al. 2002). After sediment backstripping, the Colorado Plateau is calculated to be 1200 metres higher than adjacent areas of the North American craton despite having a similar inferred pre-Laramide crustal

make-up and lithospheric buoyancy (Spencer, 1996). Marine sediments deposited in the Upper Cretaceous (Mesaverde Group), clearly pre-date this uplift and paleobotanical data from Mid to Late Eocene sequences in the northern part of the province suggest elevations of 1.5-3km (Gregory and Chase, 1992, Wolfe et al., 1998). Uplift can therefore be broadly constrained as occurring between these two dates.

Extensive magmatic activity is also identified in the Colorado Plateau which is broadly contemporaneous with the Tertiary uplift of the area. Magmatism is expressed as a series of intrusive and volcanic centres present across the area, several of which are shown in Figure 3.3. Ross (1998) describes two stages of igneous activity in the area. A NE-SW trending belt of intrusive centres is identified which developed in the Late Cretaceous to Early Tertiary and includes the La Sal Mountain and Abajo Mountain centres (Figure 3.3). A second, E-W trending belt of Late Oligocene to Early Miocene volcanic and intrusive centres is also present which includes the San Juan Dome volcanic field (Figure 3.3).

Numerous models to explain how uplift of the Colorado Plateau occurred have been proposed and most relate the uplift to mantle processes associated with the contemporaneous Sevier-Laramide orogenic phase. Bird (1984) suggests that low-angle subduction associated with the Laramide Orogeny resulted in the complete removal and eastward displacement of the lower crust below the Colorado Plateau. This model considers uplift to be the result of asthenosphere upwelling to the base of the crust and subsequently modifying its buoyancy.

Isotopic and geochemical studies have, however, suggested that native lithosphere is present beneath the Colorado Plateau (Bowring and Karlstrom, 1990) and Spencer (1996) attempts to address this by suggesting ablation/attenuation of the mantle lithosphere during low-angle subduction rather than complete removal. McQuarrie and Chase (2000) highlight the difficulties of isostatically maintaining the thick crust of the Colorado Plateau (currently 45 km) at sea level during the Cretaceous. They suggest that the Cretaceous palaeo-crustal thickness was an isostatically balanced 30 km thickness and infer crustal thickening and its subsequent isostatic response as having driven uplift. They invoke intra-crustal flow to be driven by pressure from the over-thickened lithosphere in the Sevier orogenic hinterland situated to the west. Pederson et al. (2002) consider the role of Post-Laramide erosion and

uplift on the development of the Colorado Plateau and suggest that ~650 metres of uplift is related to post-orogenic isostatic processes.

Although the details of the mechanism by which the Colorado Plateau has uplifted are not considered to be directly relevant to this study, the wider implications of this uplift and the resultant erosional down-cutting are considered to be very important. Jackson and Vendeville (1994) list erosional down-cutting as a process with the potential to initiate salt mobility and also the unroofing of a basin and resultant interactions with meteoric water have the potential to drive dissolution tectonics in a salt basin. This occurrence of this uplift is clearly a significant factor which differentiates the Paradox Basin with the other case studies in this study.

3.5 The Paradox Basin

Introduction

The Paradox Basin is classically defined by the pinchout of salt sequences in the Pennsylvanian Paradox Formation (Nuccio and Condon 1996) and forms a roughly oval shaped feature with a NW-SE trending long axis (Figure 3.3). This area stretches for 295 km along its long axis between the towns of Green River (Utah) and Durango (Colorado) and for 145 km along its short axis between Naturita (Colorado) and Bluff (Utah) with salt sequences covering an area of approximately 27,000 km^2 (Stevenson and Baars, 1986). This definition is, however, rather simplistic and Barbeau (2003) considers the shelf carbonates and algal mound sequences which are the time equivalent of evaporite sequences to have been deposited as part of the Paradox Basin. Consequently the basin width of 190 km quoted by Barbeau (2003) is likely to be more appropriate.

As a tectonically induced feature, the basin is primarily Pennsylvanian to Permian in age having accumulated up to 5 km of syn-tectonic sedimentation (Barbeau, 2003). Continued creation of accommodation space due to salt mobility is, however, widely considered to have continued through much of the Mesozoic (Doeling , 1988). The basin is flanked along its NE side by the NW-SE trending Uncompahgre Uplift, a basement-cored structure overlain by Late Triassic and younger sequences. Structurally, the basin is divided into two main zones (Figure 3.3). These include a NW-SE trending zone of approximately 50 km in width which occupies the area adjacent to the Uncompahgre front. This is known as the Paradox Fold and Fault Belt and consists of a series of salt-cored anticlines, synclines and associated normal faults. The remaining portion of the basin is here referred to as the External Paradox Basin and is characterised by shallowly dipping, undeformed sequences.

The Uncompahgre Uplift

The Uncompahgre uplift is a NW-SE trending basement high which is 40-50km wide and can be traced for over 200km (Figure 3.3). It consists primarily of Precambrian granite, gneiss and micaceous schist (Elston and Shoemaker, 1960) and continues along the entire NE margin of the Paradox Basin, forming a topographic high along much of its length. The

uplift is bounded on its SW side by a fault system known as either the Uncompahgre Front (Elston and Shoemaker, 1960) or Uncompahgre Fault (Heyman et al. 1986) and on its NE side by the a fault cored monoclinal structure here termed the Grand Mesa Fault. The morphology of the basin-bounding fault system has been subject to some debate (discussed below) but as Figure 3.4 shows, borehole data suggests this is system of reverse faults.

Stratigraphic evidence from the adjacent Paradox Basin illustrates that uplift on the Uncompahgre structure developed during the Middle Pennsylvanian (Elston and Shoemaker, 1960) and is considered to have developed as part of the Ancestral Rocky Mountains orogenic phase (Kluth and Coney, 1981, Kluth, 1986, Ye et al. 1996), continuing into the Early Permian (Barbeau, 2003). The extremely proximal facies observed in Pennsylvanian and Permian sediments adjacent to the Uncompahgre Uplift provide compelling evidence that the structure was a major highland area throughout this period (Campbell, 1979, Mack and Rasmussen, 1984) and Barbeau (2003) estimates it to have had 3-5 km of topographic relief. A sequence of Late Triassic and younger sequences is observed to blanket the structure along a flat-lying unconformity surface indicating that the Uncompahgre Uplift had become peneplaned by this time. Throughout the Early Permian to Triassic the Uncompahgre Uplift is therefore considered to have been in a state of post-orogenic denudation.

Reactivation of the Uncompahgre Uplift structure is widely believed to have occurred during the Cenozoic Laramide Orogeny (Heyman et al. 1986, Jamison and Stearns, 1982). Deformation associated with Laramide events is, however, limited and large-scale fault offsets of the Triassic and younger sequences which cover the uplift are not observed. Laramide deformation is dominantly manifested in monoclonal folding and micro-faulting on the NE flank of the uplift and varies along the SW flank of the uplift between reverse faulting, folding and systems of graben forming normal faults (Heyman et al. 1986). Heyman et al. (1986) considers the Uncompahgre Uplift to consist of a keystone style crustal block as illustrated in Figure 3.5 and suggest Laramide shortening on the order of 1-3%. It is unclear whether the Grand Mesa Fault system was active in the ARM stage of deformation and Jamison and Stearns (1982) suggest that the Uncompahgre Uplift continued for a significant distance beyond its current NE boundary in the Pennsylvanian.

The Paradox Fold and Fault Belt

The Paradox Fold and Fault belt is characterised by a series of elongate NW-SE trending salt structures oriented parallel the axis of the Uncompahgre Uplift. Salt structures occur with a wavelength of ~8-20 km and are of several different styles (section 3.8) ranging from steep sided salt walls of several km in height to gentler, salt-cored anticlines. Supra-salt sequences in the Paradox Fold and Fault belt are typically folded into gentle anticlines and synclines oriented parallel to the salt structures. Anticlines are typically situated in the crest of salt structures and synclines are situated between them. Faulting is common in this zone and with a small number of exceptions, faults are almost entirely normal faults associated with the crestal regions of salt structures. As with fold structures, the dominant orientation of faults within the basin is parallel to the axis of the Uncompahgre Uplift.

The External Zone

Despite being underlain by the evaporite sequences of the Paradox Formation, this area is characterised by an absence of salt structures. The exceptions to this are four very small, localised diapirs situated in the Cataract Canyon area. Unlike salt structures in the fold and fault belt, these are clearly Plio-pleistocene in age and related to erosional downcutting of the Colorado River (Huntoon, 1988) and are not considered relevant to this study. Sequences in the external zone are typically unfolded and have a shallow basinward dip of a few degrees.

Faulting is absent throughout most of this area with the major exception being an extensive horst and graben system situated in the area immediately SW of the confluence of the Green and Colorado rivers (Figure 3.6). This fault system covers an approximately semicircular area of 30 km x 20 km situated on the SE side of the Colorado river. As Figure 3.6 shows, this fault system has an arcuate but overall NE-SW trend which, unlike faults in the fold and fault belt, is approximately perpendicular to the Uncompahgre Uplift. This fault system is widely considered to have developed due to the downslope gravitational gliding of post Pennsylvanian sequences towards the Colorado River (Trudgill and Cartwright, 1994, Cartwright et al. 1995, Moore and Schultz, 1999, Baars, 2003, Huntoon, 1988). Decolement occurs upon the top of the Paradox evaporites and the space for gravity gliding to occur into

is created by the continued downcutting of the Colorado River. This process is illustrated in Figure 3.7. As this is clearly a fault system driven by erosional downcutting and distinct from the faulting in the Paradox Fold and Fault belt, it is not considered further in this study.

Development of the Paradox Basin

Any model for the development of the Paradox Basin must take into account both its relationship with the basin bounding Uncompahgre Uplift and also the regional tectonic setting at the time. The main Pennsylvanian-Permian phase of basin fill in the Paradox Basin is clearly contemporaneous with the development of the well-documented Ancestral Rocky Mountains system and it is widely documented as being an ARM structure (e.g. Kluth and Coney 1981, Kluth, 1986, Ye et al., 1996). Stratigraphic evidence also clearly illustrates that the Uncompahgre Uplift remained as a structural high throughout the basins Pennsylvanian-Permian history and provided a sediment source for much of the deposition in the basin (Campbell, 1980, Condon, 1997, Mack and Rasmussen, 1984). Two different models have been proposed to explain the structural development of the basin. These are that the basin is either a pull-apart basin or a flexural foreland basin. Both models are briefly detailed and discussed below.

Pull-apart basin model

The pull-apart basin model was first published by Baars and Stevenson (1981) and reinforced by Stevenson and Baars (1986). These workers consider the Paradox Basin to be a pull-apart basin situated at the intersection of two major continental-scale basement fracture zones (lineaments) which are illustrated in Figure 3.8. The main lineaments considered to influence the Paradox Basin are the NW-SE trending Olympic-Wichita Lineament and the NE-SW trending Colorado Lineament. They suggest that these lineaments were established in the early Proterozoic and repeatedly reactivated throughout the Phanerozoic as the preferred structures for deformation in the basement to be localised upon. The onset of the ARM tectonic regime is considered to have caused extensive dextral strike-slip movement of the Olympic-Wichita Lineament with the pull-apart basin developing at a tension-releasing bend in the fault system and deepening throughout the Middle Pennsylvanian. They describe this tectonic system as continuing until the end of the Desmoinesian when the strike-slip system waned. A basement high on the SW side of the Paradox Basin is notably absent and

the model explains the asymmetry of the basin by suggesting that the NW (Uncompahgre) margin of the basin was a master fault, with the present day Uncompahgre Uplift area remaining emergent throughout the episode. Extensional faulting within the subsiding zone is then invoked to explain thickness and facies changes within the syn-tectonic sequence.

Isolated foreland basin model

Several publications have suggested that the Uncompahgre Uplift developed in a compressional setting due to movement upon a controlling thrust fault with the Paradox Basin developing due to loading and flexure of the adjacent crust. (e.g. Ohlen and McIntyre, 1965, Hudec, 1995, Jackson et al. 1998). Barbeau (2003) provides a detailed analysis of this hypothesis through integrating observed stratigraphic data from wells and field exposures with flexural modelling of the basin. This model suggests that the Uncompahgre uplift was a thick-skinned (basement involved) thrust structure which experienced bulk shortening of around 10 km. Rather than being mobile like the thin-skinned thrust belts typical of the Alpine, Pyrenean and Sevier orogens, this is considered to be non-migratory and more analogous to Laramide structures in the western USA. Accommodation space in the basin is created adjacent to the basement uplift through flexural subsidence associated with this load and decreases exponentially away from the Uncompahgre front.

This model links facies distribution in the basin to different parts of the foreland basin. As Figure 3.9 shows, thick proximal alluvial fan sequences and the highly saline restricted basin facies of the Paradox Formation are located in the foredeep area. In the forebulge and backbulge areas are deposited the hydrocarbon bearing algal mound sequences (Paradox bioherms) and shelf carbonates typical of peripheral areas of the basin. Permian Cutler Group sequences which are spread across the basin are considered to be post-orogenic clastics analogous with those in many other foreland basins (Barbeau, 2003).

Discussion of models

Barbeau (2003) argues that the kinematics, geometry and subsidence history of the Paradox Basin are difficult to explain using a pull-apart model and indeed in preparing this discussion it has been impossible to determine any evidence which favours this interpretation over the

foreland basin model. Firstly, the subsidence history in the Paradox Basin is extremely asymmetric and although a pull-apart basin would not necessarily be expected to be symmetrical, some evidence of the opposing side of the pull-apart structure to the Uncompahgre Fault would be expected. Figure 3.10(a) illustrates a schematic cross section across the basin restored to late Middle Pennsylvanian time published alongside the pull-apart basin model and only shows the NE side of the basin as a significant strike-slip structure.

Comparison of Figure 3.10(a) with Figure 3.10(b) shows that the basin profile derived from Barbeau's data closely matches the late Middle Pennsylvanian basin profile of Stevenson and Baars (1986) with both showing an exponential decrease in subsidence away from the Uncompahgre front. The differences between these are that the pull-apart basin model requires stepping down upon extensional faults to account for this whereas the foreland basin model can account for this entirely through flexure.

Barbeau (2003) further casts doubt on the pull-apart basin hypothesis with respect to the geometry of the Paradox Basin. Aydin and Nur (1982) carried out an extensive review of modern and ancient pull apart basins, and concluded that pull-apart basins typically have a length range of between 0.01 and 80 km and have a scale independent aspect ratio of around 3:1. Barbeau (2003) points out that with a width of 190km and an aspect ratio of ~1.4, the Paradox Basin is far outside the geometric parameters of a pull-apart basin. As Figure 3.11 shows, the Paradox Basin plots well within the field of an isolated foreland basin. Barbeau's most decisive point with respect to the development of the basin is that borehole and 2D seismic data shows the Uncompahgre front to be a thrust fault which overhangs the most proximal basin fill and has around 10 km of heave. These observations and the inability of the pull-apart basin model to explain facies distribution within the syn-tectonic basin fill has meant it is here rejected as a plausible mechanism for the development of the basin and the Paradox Basin is confidently described in this study as a flexural foreland basin.

Development of the salt basin

Salt deposits in the Paradox Basin are exclusively found within the Pennsylvanian Hermosa Group with evaporite bearing units being mainly Desmoinesian (Middle Pennsylvanian) in age. Salt-dominated sequences are grouped into the Paradox Formation and original depositional thicknesses of salt-dominated sequences are estimated at ~1.5-1.8 km in the deeper parts of the basin (Doeling, 1988). Despite extensive salt mobility making any such estimation subject to large errors, undisturbed areas of the basin show the Paradox Formation was clearly well in excess of 1 km. The accumulation of such thick sequences requires a process of continued basin subsidence coupled with cyclic refilling, restriction and desiccation of the basin. Barbeau (2003) suggests that flexural subsidence led to the development of subsidence in the basin with the forebulge area having a role in the restriction of the basin. Base level changes due to eustatic variations and possibly with a tectonic influence are likely to have controlled the restriction and periodic flooding of the basin.

The Paradox Formation is a very diverse unit consisting mainly of dolomite, black shales, anhydrite and halite, with halite being by far the most abundant (Nuccio and Condon, 1996). Up to 40 different cycles have been identified within the basin based on black shale marker beds (Reid and Berghorn, 1981) which represent the transition between the transgressive (decreasing salinity) and regressive (increasing salinity) phases (Hite and Lohman, 1973). Reid and Berghorn (1981) describe 5 major hypersaline cycles which are correlated latterly with time equivalent shelf carbonate units at the basin margins. These are called the Alkali Gulch, Barker Creek, Akah, Desert Creek and Ismay zones (listed oldest to youngest). Reid and Berghorn (1981) divide each of these zones into marine shelf, penesaline (intermediate) and hypersaline facies and the distribution of these facies through the basin is illustrated in Figure 3.12. As Figure 3.12 shows, the hypersaline facies predominantly consisted of halite with lesser gypsum, anhydrite, black shale and shaley dolomite (Reid and Berghorn, 1981) and were situated in the deepest part of the basin adjacent to the Uncompahgre Uplift.

In contrast to the hypersaline facies, the marine shelf facies consist mainly of limestones and dolomites are situated further south towards the basin margins. Figure 3.13 illustrates an isopach map for the salt interval in the Paradox Formation and illustrates how the salt

sequences are thickest in the Paradox Fold and Fault belt where almost all of the salt mobility has taken place. Salt sequences thin dramatically towards the SW approximately where the transition between the fold and fault belt and the External Zone occurs.

Burial of the Paradox Basin

Widespread Tertiary uplift has driven extensive erosion in the Paradox Basin area and a thick Mesozoic and Tertiary succession has been removed from much of the study area. Consequently the Paradox Basin is considered to have been subjected to extensive burial which Nuccio and Condon (1996) have attempted to quantify. Figure 3.14 illustrates a burial curve for the Moab area from this publication and shows the top of the Permian sequence to have experienced approximately 3.5km of burial.

3.6 *Previous work in the Paradox Basin*

Salt tectonics in the Paradox Basin

Despite the mass of literature on the stratigraphy and structural geology of the Paradox Basin, a detailed review of salt tectonics in the basin is notably absent. The individual salt structures in the basin have been extensively described (e.g. Doeling et al. 2002, Doeling 1988, 2002, Doeling and Morgan, 2000, Doeling and Ross, 1998, Hudec, 1995, Boyers, 2000), as have the structures associated with them. The processes involved in their development however has been the subject of limited debate. Numerous processes have been suggested as being responsible for the initiation of salt mobility in the basin. Neff (1960), suggest that salt mobility was initiated by regional compression based on comparisons with the salt structures of southern Iran.

Doeling, (2002 and 2003) and Doeling et al. (2002) describe salt structures as developing due to salt flowing from the deepest part of the basin towards fault controlled "discontinuities" at the top of the sub-salt sequence. Salt is considered to rise into diapirs by exploiting weaknesses in the overburden related to these structures and Doeling (2003) relates pulses of salt movement to activity on subsurface faults. Baars (1966), speculated that that salt mobility was driven by differential loading of the salt driven by prograding wedges of Permian alluvial fan sequences derived from the adjacent Uncompahgre Uplift. This model suggests that salt structures develop due to buttressing of this loaded salt upon sub salt faults, impeding its flow and forcing it upwards. Ge (1996[a]) carried out physical modelling which led him to the same conclusion although the presence of these sub-salt faults below the salt structures has not been proven. Hudec (1995) temporally links salt structure development to the deposition of these locally sourced alluvial fan sequences at the NE margin of the basin but suggests extension had a role in the early (reactive) rise of the Onion Creek salt structure.

Timing of salt mobility

Doeling (1988) states that salt mobility began very early in the development of the Paradox Basin, a short time after the deposition of the first salt bed in the basin. Hudec (1995), in contrast, suggests salt mobility initiated in the Early Permian. Hudec (1995) also states that

most diapir development occurred during the Permian with only minor subsequent salt mobility. Doeling (1988) suggests that significant salt mobility was still occurring well into the Late Triassic and states that diapirism was "very active" during the deposition of the Late Triassic Chinle Formation. Bromley (1991) suggests that salt mobility was still occurring in the Lower Jurassic influencing deposition of the Kayenta Formation and Doeling and Morgan (2000) describe thickness variations in the Navajo Formation that they attribute to salt mobility. Doeling (1988) divides salt mobility and related deformation into 4 distinct phases based on observed stratigraphic relationships. These phases are detailed below.

Stage 1 – Pennsylvanian to Late Triassic - Period of most active salt mobility

Major salt structures developed during this period. Growth of salt structures was contemporaneous with major deposition in adjacent synclinal depocentres.

Stage 2 – Early to Late Jurassic – Period of localised salt movement

Salt mobility locally active in areas with thick salt sequences

Stage 3 - Cretaceous and Tertiary – Salt buried during this period and largely inactive

Stage 4 – Tertiary (Oligocene onwards) – Dissolution tectonics

Erosion driven by uplift of the Colorado plateau brought salt sequences near to the surface dissolving salt below the overburden causing collapse.

Structural development of the Paradox Basin

Faulting

An extensive amount of work has been done on the fault systems in the Paradox Basin, largely related to investigations into nuclear waste storage in the area (e.g. Kitcho, 1981, Olig et al. 1996, Wong et al. 1996). It is clear from geological mapping that a distinct spatial association exists between the location of faults and the zone of extensive salt mobility. Despite this, the exact relationship between salt mobility and faulting remains unclear. Faults associated with salt structures fit into 2 distinct categories, graben systems situated in the crest of salt structures and large, NE dipping normal faults. Crestal graben systems have been extensively described for many of the salt structures in the paradox basin including the

Salt Valley-Cache Valley structure, (Doeling, 1988, Chauvin, 2001), Onion Creek structure (Hudec, 1995, Boyers, 2000, Doeling 2002), and Moab-Spanish Valley structure (Doeling et al. 2002). Large basinward dipping normal faults have also been extensively described and consist of the Moab Fault (Doeling et al., 2002, Foxford et al. 1996, Olig et al. (1996), and Lisbon Faults (Ge et al. 1996, Olig, et al. 1996).

Although most authors agree that faulting in the basin was mainly occurring during the Tertiary, estimates for the age of faulting are variable. Kitcho (1981) suggests that most faults formed during Laramide time with a subsequent stage developing crestal grabens in the later Tertiary or early Quaternary. Crestal graben systems in the Salt Valley-Cache Valley (Doeling, 1988) and Onion Creek area (Doeling, 2002) are described as being related to unroofing of the Colorado Plateau and Figure 3.14 implies a post Eocene age. Ge et al. (1996) implies a post-Laramide age for both basinward dipping normal faults and crestal graben systems and Doeling et al. 2002 gives a post-Laramide age for the Moab Fault stating that it overprints folding in the area. Hecker (1993) assigns a probable Quaternary age to the Moab Fault. Olig et al. (1996) gives a post-Campanian Turonian (Upper Cretaceous) age for the Moab Fault stating that it predates dissolution. Foxford et al. (1996) however suggest the Moab Fault was active prior to the Upper Jurassic with subsequent reactivation after the mid Cretaceous. They do not, however, provide any evidence to support this interpretation and it is strongly questioned in this study.

The development of faulting in the Paradox Basin has been attributed to various processes. These include relaxation after Laramide compression (McKnight 1940), dissolution tectonics (Doeling, 1988, Doeling et al. 2002, Huntoon 1988, Oviatt 1988, Hecker, 1993) and regional (Basin and Range) extension during the Tertiary (Ge at al. 1996, Hudec 1995, Boyers 2000, Chauvin, 2001). Ge et al. (1996) tested these three hypotheses through physical modelling, subjecting pre-existing diapirs to subsequent compression, dissolution and extension, specifically in an attempt to reproduce Paradox Basin style crestal graben systems (Figure 3.15).

Experiments with compression produced re-activation of the diapirs and the development of outward-verging reverse faults (Figure 3.15(a)). Dissolution was modelled through salt

withdrawal and produced a complex system of normal faults at the margins, with external extension balanced by a reverse faulting in more central regions (Figure 3.15(b). Figure 3.15(c) shows the results from modelling regional extension and Ge et al. (1996) argued that this was the only process capable of re-creating the graben systems in the Paradox Basin. Consequently, Ge et al. (1996) concluded that faulting in the basin was the result of Tertiary regional extension.

Hudec (1995) also argues that extension is required to develop the observed faulting. He argues that the Salt Valley-Cache Valley, Onion Creek and Sinbad Valley salt structures are all one continuous trend with a collapse zone separating them even in areas where salt is deeply buried. Consequently he suggests that dissolution is less likely in these deeper areas and that extension is therefore required to develop this collapse zone. Hudec (1995) also suggests that without extension, the observed graben systems associated with the Onion Creek salt structure could not have developed as all faults are inwardly dipping and a space problem would exist.

Folding

NW-SE trending anticlines have been documented in the crests of all of the Paradox Basin salt structures, with parallel synclines situated in the intra-salt areas. Subsidence between salt structures is considered to have developed sediment-accommodating synclines between the Pennsylvanian and Late Triassic (Doeling, 1988). The fold structures situated around the salt structures, however, currently involve the entire exposed supra-salt succession. Heyman et al. (1986) document significant reactivation of the Uncompahgre Uplift during the Laramide Orogeny.

Doeling et al. (2002) and Doeling (1988, 2002), state that pre-existing salt cored structures had Laramide folding superimposed upon them and the Laramide influence on the folds in the Paradox Basin is widely stated as a matter of fact throughout much of the literature. A few exceptions to this school of thought do exist. Baars and Stevenson (1981) suggest folds were generated due to salt mobility and "little affected by Laramide compression". Ge et al. (1996) also suggest that Laramide shortening had "little effect" on the development of folds

above Paradox Basin salt diapirs. Ge et al (1996) and suggest (with specific reference to folds in the Moab and Lisbon Valley areas) that folding is due to reactive diapiric rise in the footwall and fault bend folding in the hanging wall as a consequence of the listric nature of faulting. This does not, however, explain folding in areas where significant crestal faults are absent and somewhat paradoxically the physical models presented in this work only illustrate anticlines being developed when diapirs are subjected to compression (Figure 3.15(a)). The cases of extension and salt withdrawal in contrast create synclinal structures.

Fractures

Zhao and Johnson (1992) and Kattenhorn et al. (2000) have investigated fracture development in the Paradox Basin. Both of these studies are concerned primarily with the process of joint development, are not linked to the structural development of the basin and are not considered relevant to this study.

Controls of salt mobility on deposition

Several authors have suggested that salt mobility in the Paradox Basin has had a significant impact on the development of sedimentary facies and depositional architecture in supra-salt sequences. Both Hazel (1994) and Matthews et al. (2004) have investigated the role of salt mobility in modifying facies development and sedimentary architecture in the fluvio-lacustrine Upper Triassic Chinle Formation. Hazel (1994) states that the alluvial architecture in the salt anticlines region is very different from time-equivalent units of the same age elsewhere in the Colorado Plateau and Matthews et al. (2004) suggest that the regional lithostratigraphy if the Chinle Formation breaks down in this area as a direct result of salt mobility.

Hazel (1994) describes increased fluvial channel density and interconnectivity in the salt anticlines region and suggests that salt-related uplift influenced stream gradients and subsidence rates and ultimately sinuosity, energy levels and sediment distribution.

Matthews et al. (2004) link localised salt-controlled variations in subsidence with a significant influence on facies distribution. They suggest expanded sequences of lacustrine and meandering fluvial facies are present in areas of high accommodation space between salt structures and expanded braided fluvial sandstone sequences in areas of lower accommodation space associated with salt driven uplift. Matthews et al. (2004) also document significant thickness variations in individual lithostratigraphic units within the Chinle Formation which they relate to growth of the Cane Creek salt-cored anticline. They also document variable palaeocurrent relationships within different lithostratigraphic units with some units displaying flow deflected around the salt structures and other units they display flowing across the salt structures.

Bromley (1991) also propose a significant control of salt mobility on the depositional architecture of the Lower Jurassic Kayenta Formation. He describes subsidence due to synchronous salt mobility as periodically deflecting drainage systems as recorded by palaeocurrents in Kayenta Formation fluvial sequences and also resulting in the localisation of small playa lakes.

3.7 *The Study Area*

Stratigraphy

This section briefly describes the stratigraphy of the study area with particular attention to the Cutler and Chinle formations as they are the subject to a specific discussion on the role of salt mobility in facies distribution in section 3.11. Sedimentary rocks exposed in the study area range from Pennsylvanian to Upper Cretaceous in age and Oligocene igneous intrusives are also present in the La Sal Mountains (Ross, 1998). In addition, Cambrian to Mississippian sequences are also identified from well data. As these older units lie below the salt sequence they are not considered relevant to this study and have not been described. The reader is referred to Nuccio and Condon, (1996) and Cole and Moore, (1996) for more information on these units. A Summary of the stratigraphy of the study area and adjacent areas is illustrated in Figure 3.16.

Pennsylvanian

Pennsylvanian deposition began with the Molas Formation which is a thin (0- 35 metre thick, Nuccio and Condon, 1996) palaeosol deposited upon an unconformity surface at the base of the Pennsylvanian sequence (Doeling, 1988). The Pennsylvanian stratigraphy is dominated by the overlying Hermosa Group (or Formation) which ranges in thickness from 4km to being absent in the crests of salt (Nuccio and Condon, 1996). The basal unit of this Group is the Pinkerson Trail Formation which consists of thinly bedded limestones, siltstones, dolomites, black shales and anhydrites and is interpreted as representing the transition from open marine conditions to the restricted marine conditions which dominated the rest of the Pennsylvanian (Doeling, 1988). Doeling (1988) describes this sequence as being 30-45 metres thick in the study area (salt valley area). This is overlain by the halite- dominated Paradox Formation which represents repeated transgressive/regressive cycles in a restricted marine setting.

The Paradox Formation is mainly Desmoinesian in age and its structural setting, facies and facies distribution are described in section 3.5. The Paradox Formation is the oldest lithology observed at the surface within the study area and is exposed in the crests of several of the salt

structures. Rather than representing the halite dominated facies preserved in many well penetrations, surface exposures entirely consist of caprock. This typically consists of highly contorted beds of shale and gypsum representing the insoluble residue of the sequence. Photographs of caprock exposures are shown in figures 3.17 and 3.18.

Overlying the Paradox Formation is the latest Desmoinesian to Virgillian (mainly Upper Pennsylvanian) Hoanker Trail Formation, a sequence of cyclically deposited limestones, sandstones and shales representing a return to normal, unrestricted marine conditions in the basin (Nuccio and Condon, 1996). Exposures within the study area are dominated by grey limestones containing abundant crinoid and brachiopod fossils. The Honaker Trail Formation is interpreted as a having been deposited in shallow marine shelf and near-shore environments (Doeling et al. 2002) and consists of significant aeolian and fluvial facies as well as the dominant marine carbonates (Nuccio and Condon, 1996). Barbeau (2003) describes the Honaker Trail Formation as being correlative with alluvial fan facies in the most proximal areas of the basin and representing a transition between the restricted marine system which dominated the Pennsylvanian sequence to the terrestrial system which dominated the Permian.

Permian

Pemian deposition in the basin consists of the Cutler Group. This sedimentary unit comprises the undifferentiated Cutler Formation in the main depocentre adjacent to the Uncompahgre Uplift and is divided into 5 units in peripheral areas (Condon, 1997). Although generally regarded as Permian in age, Barbeau (2003) highlights that in the most proximal parts of basin, sequences of the Cutler lithological assemblage inter-finger with time equivalent evaporite units of the Paradox Formation. Consequently a Pennsylvanian-Permian age is commonly given to this sequence (Barbeau, 2003, Condon, 1997, Mack and Rasmussen, 1984). Figure 3.19 illustrates a cross section through the Cutler Group showing the distribution if the individual units within the sequence.

The contact between the Cutler Formation and the underlying Hermosa Group (Honaker Trail Formation) is conformable and gradational and in most of the basin represents a change

from the carbonate dominance of the Honaker Trail Formation to the dominance of clastic rocks. The proximal Cutler Formation consists of a very coarse sequence of locally sourced clastic rocks derived from the adjacent Uncompahgre Uplift. Facies typically consist of deep red to purple coloured boulder to pebble sized conglomerates in the most proximal areas in the NE of the basin displaying a progressive fining into coarse sandstones and finer sequences with distance away from the source area (Condon, 1997, Barbeau, 2003). Matrix supported, bouldery debris flows have also been identified in the most proximal parts of the basin (Mack and Rasmussen, 1984).

Cutler Formation units are typically interpreted as stream-dominated alluvial fan sequences analogous to many modern fans (Campbell 1981, 1979, Mack and Rasmussen, 1984, Barbeau, 2003) and Campbell (1981) describes the system as consisting of 3 large proximal fans shedding material onto the Paradox Basin. It is generally not possible to recognise regional units in the main depocentre although as Figure 3.19 shows, away from this area the Cutler Group becomes more ordered and distinct, mapable units can be identified.

The five units of the Cutler Group outwith this main depocentre as defined by Condon (1997) are (oldest to youngest), (1.) Lower Cutler Beds, (2.) Cedar Mesa Sandstone, (3.) Organ Rock Formation, (4.) White Rim Sandstone and (5.) De Chelly Sandstone. These units consist primarily of sandstones and subordinate limestones, conglomerates and mudstones deposited in alluvial, aeolian and shallow marine environments (Condon, 1997). Limestone beds are common throughout the sequence and the toe of the Cutler fans are interpreted as having been at or near sea level throughout the period (Campbell, 1981). The Cutler Group are interpreted as having been deposited in a semi arid-arid environment (Mack and Rasmussen, 1984). The study area is primarily situated in the area where the Cutler Group is undivided and for the purposes of this study the Cutler Group will be treated as a single unit.

Triassic

Triassic deposition began with the Early (and possibly Middle) Triassic Moenkopi Formation which represents a significant marine transgression at the end of the Permian (Molenaar, 1981). The Moenkopi Formation is separated from the underlying Cutler

Formation by a significant unconformity/disconformity (Tr-1 Unconformity, Molenaar, 1981). This surface has variable angularity, with truncations typically being at their steepest around the some of the salt structures but with no discernable angular expression in other areas. This unit is interpreted as having been deposited primarily in a shallow marine and marginal marine environment influenced by a shallow, epicontinental sea situated mainly in western Utah and Nevada (Stewart et al. 1972[a]). This primarily slope forming unit is dominated by red-brown siltstones and mudstones and lesser very-fine grained and often ripple laminated sandstones in the study area.

Facies within the Moenkopi Formation are interpreted as representing various environments including (possibly tidal) mudflat and sabkha environments with a variable fluvial influence (Stewart et al. 1972[a], Doeling et al. 2002). Fluvial facies are most abundant in the eastern part of the study area representing a local influence of material shed from the Uncompahgre Uplift where Moenkopi sequences are not preserved (Molenaar, 1981, Doeling, 2002).

Another regionally recognised unconformity separates the Moenkopi Formation from the overlying, Upper Triassic, Chinle Formation (Molenaar, 1981) although with the exception of localised truncations on the NE limb of the Cane Creek Anticline, bedding either side of this contact is observed to be parallel and locally conformable throughout the study area. The Chinle Formation consists of a sequence dominated by mudstones and sandstones with lesser limestones, siltstones and conglomerates of continental origin (Stewart et al., 1972[b]).

The Chinle Formation is divided into numerous different members across the Colorado Plateau representing variable depositional environments. Figure 3.20 illustrates a section across the basin illustrating where the different members are present. As Figure 3.20 shows, the Chinle Formation consists primarily of the Church Rock, Black Ledge and Petrified Forest Members in the SW of the study area and is dominated almost entirely by the Church Rock Member in the NE of the study area.

The Church Rock Member is dominated by red-brown mudstones with lesser fine-grained and often ripple laminated sandstones (Stewart et al., 1972[b]). The Petrified Forest Member

consists of various brightly coloured mudstones (Stewart et al., 1972[b]) which are often green in the study area. The Black Ledge Unit (formally part of the Church Rock Member (Stewart et al., 1972[b])) is a sand-dominated unit consisting of densely stacked and amalgamated channel fill sandstones (Hazel, 1994, Matthews et al., 2004). These units are interpreted as having been deposited in various fluvial and lacustrine environments including floodplanes, high aspect ratio streams and fluctuating lakes (Stewart et al., 1972[b], Dubiel, 1987, Hazel, 1994, Matthews, 2004). Dubiel et al. (1991) describes the Chinle Formation as being deposited in a monsoonal climate situated at palaeolatitudes of between 5° and 15°.

A further member of the Chinle Formation is locally present at the base of the sequence in the study area and described as the Basal Sandstone Unit by Stewart et al. (1972[b]) and the Lower Chinle by Doeling and Ross, (1998) and Matthews et al. (2004). This unit consists of a complex sequence of coarse to pebbly sandstones, siltstones and lesser mudstones. These sediments typically display a bizarre multi-coloured colouration or 'mottling' effect (Figure 3.21) which has also been described in other members of the Chinle Formation outwith the Paradox Basin (Stewart et al., 1972[b]). Regionally as in the study area, this mottling effect is almost always associated with the basal member of the Chinle Formation or the upper metre or so of the formation directly beneath it (Stewart et al., 1972[b]). Doeling and Ross (1998) and Matthews et al. (2004) relate this mottling to pedogenic alteration and Dubiel (1987) suggests it is indicative of fluctuating watertables.

The Chinle Formation is considered to represent a significant base-level fall which regionally led to the incision of channels into the Moenkopi Formation (Dubiel, 1987). Subsequent base level rise then led to aggradation and infilling of these palaeo-valleys with coarse localised basal units such as the conglomeratic sands of the Shinarump Member followed by more widespread deposition of younger members. As Figure 3.21 and regional isopach data presented in Stewart et al. (1972[b]) show, the Chinle Formation shows a gradual overall thickening towards the SW across the entire Colorado Plateau with the study area being among the areas where it is thinnest.

Jurassic

A further regionally recognisable disconformity separates the Chinle Formation from the overlying Jurassic sequences. Jurassic deposition in the Paradox Basin consists of the dominantly fluvio-aeolian sequences of the Glen Canyon and San Rafael groups and dominantly fluvial Morrison Formation. At the base of the Glen Canyon Group is the Wingate Formation which is a prominent red-coloured, cliff-forming sandstone displaying abundant large scale trough cross beds and separated from the Chinle Formation by a regionally recognised disconformity (Pipiringos and O'Sullivan, 1978) which has little expression in the study area. This unit is present throughout much of the Colorado Plateau and is interpreted as a dominantly aeolian unit (Molenaar, 1981).

Overlying this is the Kayenta Formation which consists of fluvial conglomerate, aeolian sandstones and lacustrine calcareous mudstones interpreted as having been deposited by braided fluvial systems sourced from the ARM uplifts of Central Colorado (Doeling et al., 2002). Overlying the Kayenta Formation is the Navajo Formation (or Navajo Sandstone) which is a fine-grained sandstone typically containing cross beds up to several metres in height (Doeling et al., 2002). This unit represents a transition back to aeolian deposition in the area (Molenaar, 1981).

Separated from the Glen Canyon Group by another regional unconformity/disconformity with no angular representation in the study area is the San Rafael Group. Regionally, this group sees extensive facies changes and the literature varies in its consideration of where the localised members fit into regional units. For the purposes of this review the members are assigned based on the stratigraphic reclassification detailed in Doeling et al. (2002). The lowermost Carmel Formation represents a significant marine transgression at the start of the Middle Jurassic and regionally consists of marine limestones, sandstones and shales (Nuccio and Condon, 1996). In the study area the Carmel Formation consists of the Dewey Bridge Member which is a fine-medium grained muddy sandstone with a distinctive red-brown colour (Doeling et al., 2002). This unit was previously grouped into the Entrada Sandstone and is interpreted as having been deposited in a shallow marine setting marginal to the Curtis seaway situated to the east (Molenaar, 1981).

Within the study area, the Dewey Bridge Member frequently displays irregular and at times chaotic folds and contortions which are not observed outside the Paradox fold-and-fault belt. This deformation involves the lower part of overlying sequences in some areas but are completely separate from them in other areas. Several interpretations for this deformation have been proposed including soft sediment load effects of overlying sequences (Molenaar, 1981) and meteorite impact related de-watering (Alvarez *et. al.* 1998). Overlying the Carmel Formation is the Entrada Sandstone which is a silty, shallow marine sandstone in the San Rafael area (Molenaar, 1981).

In the study area, the Carmel Formation consists of the Slickrock Member which is a red coloured, typically fine to very-fine grained sandstone of aeolian origin (Doeling et al., 2002). The overlying Curtis Formation represents a marine transgression which led to an eastward migration of marine facies (Molenaar, 1981). In the study area, the Curtis Formation consists of the Moab Member (or Moab Tongue) which has frequently been extensively classified as a member of the Entrada Sandstone (Doeling et al. 2002). The Moab Member is a pale coloured, fine to very fine sandstone interpreted as a coastal dune complex deposited at the margins of the Curtis seaway (Molenaar, 1981).

Regionally, the Curtis Formation is overlain by the Summerville Formation which is a marginal marine, tidal flat sequence (Molenaar, 1981). In the study area, however, the Summerville Formation is very thin and is grouped with the Tidwell Member of the Morrison Formation by Doeling and Morgan (2000). The Late Jurassic Morrison Formation is dominated by fluvial and lacustrine sequences and is interpreted by Moelnaar (1981) as marking the start of an influence of the Sevier-Laramide orogenic phase. Various members are present in the Paradox Basin although the three main members observed in the study area are the siltstone dominated Tidwell Member, mudstone and coarse channel sandstone dominated Salt Wash Member and the siltstone/mudstone dominated Brushy Basin Member (Doeling and Morgan, 2000).

Cretaceous

Lower Cretaceous sequences in the study area consist of the Cedar Mountain and Burro Canyon Formations which conformably overlie the Morrison Formation. These units consist of conglomeratic sandstones and mudstones of fluvial origin (Nuccio and Condon, 1996). Both of these formations are time equivalent with the different designations representing deposition by two different fluvial systems (Molenaar, 1981). Upper Cretaceous sequences unconformably overlie these deposits (although significant angular relationships have not been identified in the study area) with the lowermost unit consisting of the Dakota sandstone. During the Upper Cretaceous, a major intracratonic seaway (Western Interior Seaway) developed across much of central North America (Figure 3.22) representing the foreland basin to the advancing Sevier Orogenic front. The Dakota sandstone is interpreted as a coastal plain unit deposited in front of the advancing seaway (Molenaar, 1981).

The Dakota sandstone is conformably overlain by the Mancos Shale which is a thick marine mudstone sequence representing the deepening of the basin. This is the youngest unit exposed in the area where salt structures are present being exposed in the Courthouse Syncline area. Also exposed in the Book Cliffs escarpment at the northern margin of the study area are the overlying Upper Cretaceous Mesaverde Group. This unit gradationally overlies the Mancos Shale and consists of a series of marginal marine sandstone tongues and associated delta-plain facies which interfinger with the Mancos Shale to the east (Nuccio and Condon, 1996).

The youngest rocks in the study area are intrusives of the La Sal Mountain laccolithic centres exposed in the SE corner of the study area. These consist of a series of trachytes of Oligocene age which are typically porphyritic and have a fine to very fine groundmass (Ross, 1998).

3.8 Structural Geology

Sub-salt structure

Many published cross sections illustrate faults in the sub-salt sequence to the Paradox Basin. With a small number of exceptions (e.g. Woodward-Clyde Consultants, 1984, Doeling et al., 1994, Hudec, 1995) they typically do not cite their evidence for these and in most examples their presence and location must largely be considered to be interpretive. Figure 3.23 illustrates a sketch interpretation of a seismic line across the Salt Valley salt structure from Woodward-Clyde Consultants (1984) which clearly illustrate the presence of several sub-salt normal faults. Similarly Hudec (1995) illustrates a series of down-stepping normal faults near the Onion Creek salt structure (Figure 3.24).

Sub-salt faulting has also been inferred from well data (e.g. Doeling and Ross, 1998) and the presence of a sub-salt surface at greatly different elevations in nearby wells can suggest the presence of a sub-salt faults. In order to investigate the potential of this method to identify sub-salt faults, a map of the structural elevation of the sub-salt Top Mississippian surface was produced by gridding and contouring elevation data from wells (Figure 3.25). The idea of this was that areas with closely spaced contours could indicate high gradient in the sub-salt structural topography and potentially highlight the presence of sub-salt structures.

A small number of high gradient anomalies were identified (Figure 3.25) although the absence of closely spaced well data throughout the majority of the area has meant that nothing meaningful has been identified. What Figure 3.25 does show is that the large scale sub-salt structural configuration can be represented by a surface without any major steps or anomalies that are significant at the basin scale. It also supports the flexural model for basin development of Barbeau (2003) rather than that of Stevenson and Baars (1986) which requires significant sub-salt downstepping. One thing that all of the published cross sections of the basin illustrate, whether based on seismic data or not is a significant decoupling of faulting in the sub-salt sequence from that in the supra-salt sequence. This is also clearly demonstrable from the well data in the area and full decoupling is assumed throughout this study.

Salt structures

Within the study area, six proven and two candidate salt structures are identified, the locations of which are shown in Figure 3.26. Several of these are easily identified as they are characterised by elliptical, flat-floored valleys bounded by cliff exposures of supra-salt sequences (e.g. Figure 3.27). Flat-floored valleys are typical of where salt is at the surface and form significant topographic depressions due to the highly soluble nature of the salt sequences and resultant exploitation by Holocene drainage systems. Although typically blanketed by drift deposits, the presence of salt is proveable by the presence of caprock exposures and by well penetrations which record salt sequences at shallow levels. This characteristic topographic expression is not applicable to all of the salt structures in the study area and the two candidate structures as well as the Cane Creek and Onion Creek salt structures do not display this style. It is here considered that a more thorough indication of the location and extent of underlying salt structures is determined from gravity data. Salt structures typically form major gravity anomalies due to the very low density of salt relative to the other constituents of the basin.

Gravity data

Figure 3.28(a) Illustrates a gravity map of much of the Northern Paradox Basin and adjoining areas which has been made using data from Case and Joesting (1972). This map clearly shows several major gravity lows (blues) which correspond with the orientation and location of many of the salt structures identified in the basin and several major gravity highs (reds) are also shown. One high situated in the NE of the map (Figure 3.28(a)) corresponds with the location of the Uncompahgre Uplift and is therefore interpreted as being the result of a transition from the sedimentary rocks of the Paradox Basin to the shallow igneous and metamoprhic complexes of this basement uplift. A further high area centred at approximately UTM 645250 E, 425250 N (SE corner of the study area) corresponds with the La Sal Mountain intrusive igneous complex. Although the laccolithic character of these mountains means Paradox Basin sediments are likely to underlie this area, as these denser rocks lie closer to the measuring station they are likely to mask gravity expression of the underlying sediments.

A further area with high gravity values lies in the SW corner of the gravity map. Although this area is still technically part of the Paradox Basin as defined by the presence of Pennsylvanian evaporites (Figure 3.3), Figure 3.13 shows a significant drop in the thickness of the salt interval in this area. Figure 3.12 also shows this to be near the transition zone between the hypersaline and less saline facies in the basin. Consequently this anomaly is considered to represent both a significant thinning of the salt interval and a facies change to sequences with a less anomalous density. Figure 3.28(b) illustrates a map of the gravity gradient in the same area and clearly highlights the salt structures as areas of low gravity gradient surrounded by elliptical areas of high gradient. This data is considered to illustrate very well the location and extent of the major salt structures in the subsurface and this is the main data source to delineate their location beyond their surface exposures.

Proven salt structures of the study area

The five proven salt structures in the study area (listed in order of distance from Uncompahgre Uplift) are the Onion Creek, Salt Valley-Cache Valley, Castle Valley, Moab-Spanish Valley and Cane Creek Anticline salt structures. The existence of a specific salt structure is considered to be proven if salt is constrained as being significantly above the regional level either through a field observation or a well penetration. With the exception of the Cane Creek structure, each of these salt structures is associated with a significant gravity anomaly and as Figure 3.28 shows, all have a NW-SE orientation, parallel to the Uncompahgre Uplift. The lateral extent of salt structures in the basin has frequently been illustrated based entirely on the extent of their surface expressions (e.g. Doeling, 2002). Analysis of the gravity data, however, shows that gravity anomalies typically extend laterally in the subsurface, well beyond their surface expressions (frequently by tens of km). Table 3.1 details certain aspects of the geometry of each of the proven salt structures in the basin and allows comparison of the length of the associated gravity anomaly compared to the length of the surface expression. Each of the proven salt structures in the study area are briefly described below.

Onion Creek salt structure

This structure has been previously mapped by Doeling (2002) and also described by Hudec, (1995), Boyers (2000) who largely concentrate on its associated crestal fault system. The

structure is spectacularly exposed in a 3.75 km long WNW-ESE oriented caprock exposure (Figures 3.29). The associated gravity anomaly is, however, NW-SE in orientation and appears to connect at depth with the Salt Valley-Cache Valley structure (Figure 3.28). In contrast to many other salt structures in the study area, the surface expression of this structure is not a flat-floored valley, but rather a system of steep sided mounds of caprock up to 200m in elevation (Figure 3.17). Caprock exposures in the Onion Creek area are the best exposed in the Paradox Basin and in many locations display complex deformation typically consisting of a seemingly chaotic series of largely recumbent folds, some of which are illustrated in Figure 3.18. Inliers of the Moenkopi Formation are observed sitting on top of the caprock in several locations (e.g. Figure 3.30), however, no older sequences display the same relationship implying that the Moenkopi Formation was the first sequence to blanket the structure. Figure 3.24 illustrates a published cross section through the structure and this structure is also shown in Figure 3.31.

Salt Structure	**Onion Creek**	**Salt Valley**	**Castle Valley**	**Moab Valley**	**Cane Creek a/c**
Evidence for the existence of the salt structure	Gravity anomaly, Extensive Caprock exposures (Figure 3.17), (no flat floored valley)	Gravity anomaly, flat floored valley, extensive caprock exposures	Gravity anomaly, flat floored valley, caprock exposures	Gravity anomaly, Flat floored valley Extensive caprock exposures	Wells drilled in crest (e.g. 4301910767 and 4301910987 show salt at shallow levels (no gravity anomaly or caprock exposures)
Distance of crest from Uncompahgre Uplift	16 km	28 km	29 km	43 km	55 km
Length of diagnostic flat floored valley or caprock exposure	3.75 km	39 km	9.5 km	23 km	No flat floored valley associated with salt structure
Width of diagnostic flat floored valley or caprock exposure	1.75 km	Maximum 3.5 km	3 km	1.8 km	No flat floored valley associated with salt structure
Length gravity anomaly	11.5 km	55 km	11 km	37 km	No gravity anomaly
Width gravity anomaly	3.75 km	7 km	3 km	4 km	No gravity anomaly
Approximate structural elevation of salt wall	Minimum 3250m (caprock exposed at ~1500m above sea level whereas adjacent well 4301930937 records top of salt at 1785m below s.l.)	Minimum 2811m (caprock exposed at 1525m above sea level whereas adjacent well 4301931112 records top of salt at 1287m below sea level)	Minimum 2800 m (Caprock exposed at 1341m above sea level whereas adjacent well 4301930076 records top of salt at 1460m below sea level)	Minimum 2682 m (Caprock exposed at 1222m above sea level whereas adjacent well 4301930076 records top of salt at 1460m below sea level)	Minimum 315 metres, (identified from cross section construction) very shallow relative to other salt structures
Interpreted age (see section 3.12)	Pennsylvanian to Permian (Mainly Permian)	Pennsylvanian to Triassic (Mainly Permian)	Pennsylvanian to Triassic (Mainly Permian)	Pennsylvanian to Triassic (Mainly Permian)	Tertiary (post-dates exposed sequence)
Associated fault systems	Crestal graben system – offsets upto 610m recorded (Doeling, 2002)	Extensive crestal Graben system (see Figure 3.35)	None identified although could have been removed by erosion.	Moab Fault system situated in its crest in northern area, crestal graben system in southern end	Several normal faults in in crest with a few metres of displacement (3-15m, (Doeling et al. 1994).

Table 3.1 Summary of the style and extent of the different salt structures in the study area

Salt Valley-Cache Valley salt structure

This salt structure is the longest in the study area with a gravity anomaly of around 55km in length, forming a major flat-floored valley for 39 km of this (Figure 3.32). Although it has an overall NW-SE orientation, the structure displays a significant kink at its SE end where it has an E-W trend for 7km. A major system of crestal normal faults have been identified associated with the structure which have been extensively described by Gard (1976), Doeling (1988, 2003) and Chauvin (2001) and will be discussed in more detail in section 3.12. An interpretation of the morphology of this salt structure is illustrated in figures 3.33 and 3.34 and Figure 3.23 shows a published interpretation of a seismic section through the structure.

Castle Valley salt structure

The Castle Valley salt structure is exposed as an extensive flat-floored valley which is bounded to the SW by the Tertiary La Sal Mountain igneous intrusives (Figure 3.35). Several caprock exposures are identified within this valley, confirming the existence of salt at shallow levels. Unlike many of the other salt structures in the study area, the gravity anomaly associated with the Castle Valley salt structure does not continue for a significant distance beyond the surface exposure. The salt structure does, however, clearly pre-date the intrusion of the Tertiary La Sal intrusives and the Laccolithic nature of these intrusives means that it is likely that the salt structure extends for a significant distance below these mountains.

It is possible that the Castle Valley structure connects below the La Sal Mountains with the Paradox Valley salt structure which lies directly along strike from it approximately 40 km to the SE. Doeling and Ross (1998) also suggest that a sub-salt fault they infer from wells in the Castle Valley area connects with a major sub-salt fault below the Paradox valley described by Case et al. (1963), Baars, (1966) and Carter, (1970). Aside from the large, La Sal Mountain complex, a smaller, isolated intrusive body is present in the centre of the flat-floored Castle Valley. This is called Round Mountain, covers an area of approximately 750m^2 and is shown in Figure 3.35. The presence of this intrusion, surrounded entirely by

salt suggests that the intrusive material exploited the salt body as an easy way to the surface in a similar way to that described by Fiduk et al. (2004) in the Espirito Santo Basin (Brazil). Other than a series of small normal faults of limited offset (<10m) and extent, identified in the NE end of the exposure (shown in Figure 3.35), crestal faults associated with the structure have not been identified. A cross section through the salt structure is shown in Figure 3.31.

Moab-Spanish Valley salt structure

This salt structure forms a flat-floored valley for much of its length which ends approximately in the area that the Colorado River crosses the Moab Valley (Figure 3.36). Gravity data (Figure 3.28(a)), however, suggests that the salt structure continues at a shallow depth for a significant distance (approximately 10 km) to the north of this point. In this area, a transition occurs in the exposure style from being a typical flat-floored, salt-valley, SE of the river to being an broad anticline (Moab Anticline) where salt is only present below the surface (Figure 3.27). The crest of the Moab Anticline follows exactly the crest of the underlying salt structure and wells 4301911471 and 4301911472 confirm the presence of salt at shallow levels in this area. The Moab Anticline (Figure 3.26) is therefore considered to be a salt-cored anticline. Well penetrations also show that the morphology of the salt structure changes significantly along strike. Cross sections constructed to the south of the river (e.g. Figure 3.33) are constrained by well data to show the salt structure to have a grounded supra-salt sequence and a thick Cutler Formation depocentre on its SW side. Comparison of this with the geometry shown in Figure 3.37, several km north of the river shows that well 4301930810 constrains the absence of a thick Cutler sequence and in this area the salt structure is shown to have much shallower dipping sides.

Associated with the Moab-Spanish Valley salt structure are two major crestal fault systems. A system of axis parallel normal faults are observed forming a graben system on the flanks of where the salt structure is expressed as a flat-floored valley and also extend into the crest of the Moab anticline (Figure 3.36). Another, major normal fault system, typically consisting of a single, large offset normal fault is present in the crest of the Moab Anticline (Moab Fault system).

Cane Creek Anticline

This salt structure is not associated with a flat-floored valley or a gravity anomaly and is identified entirely based on the numerous wells which record salt being above the level on its flanks. It is, however, expressed at the surface as a gentle, slightly asymmetric anticline in the supra-salt sequence with a slightly steeper NE limb. This surface expression is shown in Figure 3.38 and a cross section illustrating its morphology is shown in Figure 3.37.

Geometry of salt structures

As detailed in Table 3.1, proven salt structures in the study area range in size from 11-55km along their long axes to 3-7km along their short axes. The height of most of the structures is in excess of 2500m and minimum structural elevations have been calculated by comparing the elevation of salt in the crests of the structures to that in adjacent wells (see Table 3.1). The exception to this is the Cane Creek structure which is constrained to have an elevation of around 315m in height and is the structure furthest from the Uncompahgre Uplift. Constraining the exact 3D geometry of the salt structures is problematic without seismic data although well and field data can give a good indication of the geometry of the structures. The height of the Onion Creek, Castle Valley, Moab-Spanish Valley and Salt Valley-Cache Valley salt structures, implies that they are relatively steep-sided salt walls.

Constraining the dip of their margins is problematic without seismic data although several key observations give a good indication of this for several of the salt structures. For example in the Castle Valley area, well 4201910397 is drilled on the flanks of the flat-floored valley, 200 metres away from where salt is inferred as being at the surface. This well records the top of the Paradox Formation as being 566 metres below the surface requiring a gradient of around 3:1 to explain this morphology. Similarly on the SW flank of the Moab-Spanish Valley structure, well 4303710655 records the top of the salt sequence at a depth of 2209m, around 1km away from where salt is inferred as being at the surface requiring a gradient of at least 2:1.

Further insights into the dips of the salt structures come from the field observation that the Honaker Trail sequence is found at shallow elevations adjacent to many of the salt structures.

This is seen in field exposures on the SW margin of the Moab-Spanish Valley structure (figures 3.39 and 3.40) and is also recorded in well 4301910397 on the flanks of the Castle Valley structure. As the Honaker Trail Formation is at the base of the supra-salt sequence and is present several km below these levels in areas adjacent to the salt structures, significant flexure of the sequence is required to allow it to reach these near surface elevations and this requirement for flexure would constrain the dip of the salt structure flanks. Consequently, salt structures in the study area are inferred as having steep but not sheer sides. The geometry of the Cane Creek structure can be seen to be very different to that of the other salt structures in the study area. As Table 3.1 shows, its height is an order of magnitude smaller that the other proven salt structures in the area and it has no associated gravity anomaly. A complete overburden sequence is also present covering the entire Cane Creek salt structure which is not penetrated by salt at any point. Rather than a steep sided salt wall, this structure has the geometry of a gentle salt-cored anticline and therefore the angle of its margins is limited by the angle of dip of the supra-salt fold. Measured dips do not exceed 11° on the NE limb of the anticline and 7° on the SW limb and therefore the salt structure is inferred as being a very low amplitude structure.

Candidate salt structures

Upheaval Dome

This candidate structure is situated in the SW corner of the study area (Figure 3.26(b)) and if it were a salt structure, would be unique in the basin, having an almost perfectly circular shape and would be the furthest salt structure from the original Pennsylvanian depocentre. This complex structure is approximately 5 km in diameter and consists of a cone shaped central area where the Chinle and Moenkopi formations are situated up to several hundred metres above their elevation away from the structure. As Figure 3.41 shows this area is surrounded by a syncline with its circular axial trace situated at a radius of approximately 2 km from the centre of the structure. A further inward dipping monocline, again with a circular axis is present located approximately 2.75 km from the central area. A complex system of localised radial faults in this central area also complicate the structure, as do a series of sandstone dikes and sediment 'tongues' (Huntoon, 2000, Jackson et al. 1998).

Through the history of geological investigations in the area this structure has been variously described as a cryptovolcanic explosion, subsurface salt diapir, meteorite impact and pinched off salt diapir (citing review by Jackson, et al. 1998). A full review of these different hypotheses is beyond the scope of this study although the two processes generally considered most likely to be responsible for observed structural relationships are the meteorite impact hypothesis (Shoemaker and Herkenhoff, 1984, Kanbur et al., 2000, Huntoon, 2000) and the pinched-off salt diapir hypothesis (Jackson et al. 1998). The meteorite impact model suggests that the exposed structures represent the deeply eroded root of an impact structure and result from the complex system of strain accommodation and subsequent collapse associated with it. The pinched-off salt diapir hypothesis suggests that the structure represents an earlier salt diapir, within which all of the salt has subsequently been extruded leaving a salt weld.

Understanding the origin of this structure (and therefore its relevance to this study) is extremely problematic, especially as both the meteorite and salt diapir schools are able to provide a convincing argument. The meteorite hypothesis lacks the existence of any characteristic shocked quartz or shatter-cones whereas the salt hypothesis lacks the presence of any salt or salt residue in the area inferred to have previously been a salt diapir. Although a minor gravity high is identified above the structure (Figure 3.28(a)) Case and Joesting (1972) report that the terrain correction applied to this data is four times the magnitude of the anomaly itself casting doubt on its geological significance.

The opinion held here is that the pinched-off salt diapir hypothesis best accounts for the development of several aspects of the structure, particularly associated syn-sedimentary structures described by Jackson et al.(1998). The absence of compelling evidence of a salt tectonic origin such as well penetrations recording salt at elevations above the regional level, surface exposures of salt residue (caprock) or significant gravity anomalies has meant that this structure is not considered further in this study.

One observation has come from this study, however, which may prove significant in understanding of the origin of this structure. As Figure 3.28 shows, although Upheaval Dome is not associated with a significant gravity anomaly, it is associated with a major

gravity gradient anomaly (Figure 3.28(b)). This is where the gravity change from the high values of the External Zone to the lower values which characterise the Paradox Fold and Fault belt occurs. This gravity change is here interpreted alongside isopach data (Figure 3.13) and facies data (Figure 3.12) to indicate a significant change in the character of the salt basin and Upheaval Dome straddles the area where this change is most abrupt.

Tenmile Canyon Structure

Case and Joesting (1972) identify a small and/or deeply buried salt anticline in the Ten Mile Canyon area situated around 20 km NW of the Moab-Spanish Valley salt structure based on a minor gravity low in this area. This anomaly trends approximately parallel to other salt structures in the area and can easily be identified in Figure 3.28(a). Well data in the immediate vicinity of this area, however, does not record the presence of salt with anomalously high structural elevations in this area and consequently this proposed candidate salt structure is here not considered likely to be present.

Supra-salt faulting

Supra-salt faulting in the study area consists of populations of normal faults with variable styles which are almost exclusively restricted to the crestal regions of salt structures. These fault systems are typically oriented parallel to or sub-parallel to the underlying salt structures and fall into two distinct categories. These are isolated large offset basinward-dipping (NE) normal faults and smaller offset crestal graben systems.

Large Basinward dipping normal faults – The Moab Fault System

The only large, basinward dipping normal fault within the study area is the Moab Fault System. This is the largest fault system in the northern Paradox Basin, extending for 31 km and having a maximum vertical displacement of 862 metres. This fault system consists of two main segments, the northern Blue Hills segment and the southern Moab segment as well as several smaller splays including the Emkay Fault at its southern end (Figure 3.42). Both segments have a NW-SE orientation, dip towards the NE and are hard-linked by the complex Mill Canyon linkage zone. To the NW of the Blue Hills segment lies the WNW-ESE

oriented Ten Mile Graben which continues into the far NW corner of the Paradox Basin. Foxford et al. (1996) suggests linkage between these structures however field evidence for this has not been identified and Ten Mile Graben is not considered further in this study.

Moab segment

The Moab segment has its southern-most exposure situated at UTM 620500 E, 42747500 N, just north of where the Colorado River crosses the Moab Valley and continues to the NW for 19 Km with the surface exposure of its northern tip situated at UTM 607800 E, 4286500 N. This segment has an overall NW-SE trend, although in the 2 Km to the NW of the branch point with the Mill Canyon Linkage Zone, the fault curves to the N having an approximately N-S orientation (Figure 3.42). The fault is observed offseting the entire exposed supra-salt sequence along its length. The segment juxtaposes the Pennsylvanian Honaker Trail formation and Jurassic Salt Wash Member (Morrison Formation) in the area of maximum displacement (Figure 3.43) and the Upper Jurassic Brushy Basin Member (Morrison Formation) with the Lower Cretaceous Cedar Mountain Formation near its northern tip.

With the exception of the Emkay segment which is described below, deformation on the Moab Segment is restricted to a single fault plane and no abandoned splays or palaeo-tips have been identified. The Moab segment offsets the crestal region of the Moab Anticline along much of its length and as Figure 3.44 illustrates, bedding in the footwall area dips to the SE, away from the fault plane. Several wells drilled in the vicinity of the fault plane (e.g. 4301911471 and 4301930415) constrain salt to be present at shallow depths directly below the footwall area of the fault plane indicating salt has upwelled in this area.

The Moab segment is typically observed having a relatively shallow dip ranging from 40°-45° and having the crest of the Moab Anticline located in its hanging wall a short distance from the fault plane (Figure 3.44). The damage zone associated with the fault is complex and varies significantly along the fault. The most extensive exposure of the Moab segment is situated at UTM 617640 E, 4276770 N, in the area of maximum displacement on the entire fault system (Figure 3.43) where the fault juxtaposes the Honaker Trail Formation against the Morrison Formation (Salt Wash Member). The fault zone itself is highly complex and

consists of a 3.5-4.5 metre wide, 45° dipping zone of intensely deformed mudstones. These are primarily red mudstones derived from the footwall Honaker Trail Formation and within these, approximately 20-35% of the rock is composed of highly deformed, lens shaped sandstone blocks of various sizes. The top 10-25 cm of this unit is a distinctive yellow mudstone layer derived from mud layers in the footwall sequence which separates this intensely sheared zone from a zone of thick, highly fractured sandstone beds in the hangingwall along a flat planar fault surface. Peripheral to this central area, the damage zone consists of a 30 metre wide zone of intensely fractured sandstones which mainly influences the hanging wall.

In contrast to this highly complex damage zone style, a further exposure of the Moab segment fault plane located 1.75 km to the SW at UTM 619322 E, 4274960 N displays a much simpler damage zone. This exposure juxtaposes the Cutler Formation in the footwall against the Slickrock Member of the Entrada sandstone in the hanging wall. The damage zone consists of a 1.8 metre wide layer of intensely deformed mudstone and small (5-15mm thick) lenses of fine sandstone in the footwall to the fault plane. The fault plane itself is exposed as a flat surface which dips to the north at 45° with an azimuth of 006°. The damage zone continues into the hanging wall sequence as a 2 metre wide zone of relatively intense granulation seams, the orientations of which are approximately parallel to the fault plane. On all exposures of the Moab segment, slickenside lineations on the fault plane are parallel to the dip-direction of the fault indicating entirely dip-slip movement.

Blue Hills Segment

The Blue Hills segment is situated to the north of the Mill Canyon Linkage Zone (Figure 3.42) and continues to the NW for approximately 13km towards an unexposed northern tip. Unlike the Moab Segment, this segment displays numerous splays and significant evidence of linkage with numerous abandoned palaeo-tips are identified (Figure 3.42). The Majority of splays are identified in the footwall area and have a dominant WNW-ESE orientation which is slightly oblique to the main trend although parallel with the Tenmile Graben to the north (Figure 3.42). The Blue Hills segment is observed juxtaposing the Upper Jurassic Entrada sandstone against the Cretaceous Cedar Mountain Formation at its point of maximum displacement. A cross section through this segment (Figure 3.45) illustrates that in contrast to the Moab segment which cuts the crest of an anticline (Figure 3.44), the Blue Hills segment is located in the limb of the broad Courthouse Syncline. Bedding in the footwall, dips towards the fault plane with the same orientation as bedding in the immediate hanging wall and as Figure 3.44 shows, well penetrations and the observed structural geometry confirm the absence of salt upwelling below the fault plane.

The Blue Hills segment typically has a steeper fault-plane orientation than the Moab segment with measured dips ranging from 67° to 72°. Exposures typically juxtapose resistant sandstone units of the San Rafael Group in the footwall against mudstone-dominated parts of the Morrison and Cedar Mountain formations in the hanging wall. This results in a relatively similar outcrop style along the length of the fault (Figure 3.46). Footwall sequences typically dip at a shallow angle towards the fault plane without any fault associated folding being present. Hanging wall sequences in contrast, typically display a style of folding where sequences in the 250 metres adjacent to the fault, show a progressive increase in dip towards it. This dip variation is measurable due to the frequent presence of a laterally extensive 2-3 metre thick sandstone bed at the contact between the Morrison and Cedar Mountain formations (Figure 3.46) and dips of up to 45° have been observed adjacent to the fault plane. This appears to represent drag associated with fault movement.

The damage zone associated with the Blue Hills Faults typically exclusively influences only the footwall sequence. The best-exposed damage zone along the fault is in the Bartlett Wash area (UTM 605400 E, 4285826 N) and consists of a 5 metre wide zone adjacent to the fault

plane displaying a complex system of anatomising, sub-vertical granulation seams. These are exclusive to the Entrada Sandstone (Slickrock Member) and are typically between 1 and 5mm in width. These become increasingly frequent and intense in the area adjacent to the fault plane and frequently display minor dip-slip offsets with the side nearest to the fault plane generally being the downthrown side. These displacements are generally on the order of a few millimetres but increase to up to 50mm in the area adjacent to the fault plane (Figure 3.47).

Mill Canyon Linkage Zone

The Mill Canyon Linkage Zone represents a transition between these two styles of faulting and has the geometry of a complex breached relay ramp with bedding having an overall northward dip. Linkage occurs upon two main structures, here termed the Courthouse Rock and Tusher Canyon segments (Figure 3.48) and also a series minor structures, all of which have an E-W orientation. Hard linkage initially occurs around 1 km south of northern tip of the Moab segment where it meets the Courthouse Rock segment at a high angle branch point (labelled in 3.48). At this branch point the Courthouse Rock segment has an approximately E-W orientation but along its 2 km length it progressively curves into parallelism with the Moab and Blue Hills segments at its northern tip. This fault is then hard linked approximately half way along its length with the Tusher Canyon Fault which also shows an initial E-W trend and curves into parallelism with the Blue Hills Fault as it meets it. Abandoned palaotips have been identified of both the Blue Hills segment and an E-W trending part of the Tusher Canyon segment (labelled in Figure 3.48). This observation and the dominance of E-W trending faults in the linkage zone is interpreted as recording the linkage of the fault systems as originally consisting of soft-linked E-W trending faults. As the Moab and Blue Hills Faults propagated, however, the increasing influence of their stress regime overprinted this trend and forced the major hard-linking faults into parallelism.

Exposures of faults in the Mill Canyon Linkage Zone typically display juxtaposition of the same lithologies observed in the Blue Hills segment and similar faulting styles are observed. Fault angles are measured ranging from 68° to 75° and similar drape style folding is also observed where Entrada sequences are juxtaposed against the Morrison and Cedar Mountain formations. Within the linkage zone are areas where the Slickrock Member (Entrada

Formation) is juxtaposed against the sandstones of the Moab Member (Curtis Formation) and no folding is present. This is considered to give sufficient evidence for folding being a lithology controlled drape effect rather than being the faulted remnants of a blind-fault controlled monoclinal structure developed in the early stages of faulting (as described by Sharp et al., 2000 and Withjack et al., 1990). Slickenside lineations observed in the fault planes of the linkage zone show that fault movement had an entirely dip-slip sense.

Emkay Segment

The Emkay segment (or West Branch of the Moab Fault, Doeling et al., 2002) is exposed in the Moab Canyon area directly adjacent to Highway 191 near the entrance to Arches National Park (Figure 3.49). Periodic exposure continues along the base of the Moab Rim ending 3.6 km to the SW at UTM 622278 E, 4272145 N and further south of this point only footwall sequences are exposed (Figure 3.36). Exposures show the fault to juxtapose the Moenkopi and Chinle Formations in its hanging wall against the Hoanker Trail Formation in the footwall. Hanging wall sequences progressively become structurally lower towards the SE suggesting that fault displacement increases in this direction.

Displacement on the Emkay Segment is entirely upon a single surface which consists of a 2-3 metre thick bedding plane of Honaker Trail Formation which dips to the NE at an angle between 50° and 60° truncating the underlying Pennsylvanian sequence at a high angle (described in section 3.10). Both the Moab and Emkay segments are observed in a single exposure at approximately UTM, 6200015 E, 4274750 N (Figure 3.49) and the Emkay segment can be seen to be located in the immediate footwall to the Moab segment in this area. As illustrated in figures 3.36 and 3.27, these segments are interpreted as diverging significantly towards the SW of this location.

The faulting style of the Emkay segment appears to be controlled entirely by the fault parallel bedding plane situated in its immediate footwall, the upper bedding surface of which forms the fault plane (Figure 3.50). The Moenkopi Formation is the hanging wall lithology in all exposures of the fault plane and at the best exposure (shown in Figure 3.50), deformation within it consists of a 2 metre wide zone of extremely intensely deformed rock

dominated by typical red-brown Moenkopi Formation mudstones with a well-defined shear fabric. Also within this zone are intensely broken up lenses of the fine-very fine sandstones which are characteristic subordinate units of the Moenkopi Formation. As Figure 3.50 also shows, a large block of Honaker Trail Formation limestone is also present within this deformed unit. If this rollover structure is not considered to be part of the fault plane (see section 3.12), then deformation in the Honaker Trail sequence in the footwall to this structure is restricted to well defined slickensides on the fault surface. At UTM 630084 E, 4274722 N, this surface has a dip/dip azimuth of 63°/349° and slickensides observed upon this surface are deflected to the SE by approximately 20° from the direction of dip on this surface indicating a significant component of oblique slip was involved in fault movement.

Relationship of faulting to salt structures

Throughout the entire study area the fault system is primarily oriented parallel to the trend of the salt structures in the basin, although the exact relationship to the salt structures is variable along its length. As Figure 3.42 shows, the Moab Fault follows the crest of the buried part of the Moab-Spanish Valley salt structure as inferred from gravity data and well data. This trend is reinforced by wells 4301911471 and 4301911472 which are drilled near the fault and confirm that salt is present at shallow depths beneath the surface (569 and 884 metres above sea level respectively). Well 4301931112, however, is located near the northern tip of the fault and penetrates the top of the Paradox Formation at 1287 metres below sea level. Consequently the Moab segment is considered to be spatially related to this buried northern part of the structure along its entire length.

Gravity and well data illustrate that no upwelling salt is present beneath the Blue Hills segment and its location in the limb of the Courthouse Syncline (Figure 3.45) shows it to be in an area of salt withdrawal rather than rising salt. Stratigraphic relationships in the Permian and Lower Triassic sequence clearly illustrate that the Moab-Spanish Valley salt structure had developed prior to the development of the Moab Fault System (section 3.10).

Uplift and subsidence associated with faulting

The relative uplift and subsidence along the Moab Fault System has been investigated through analysis of structure contour data and displacement-length relationships. Figure 3.42(b) illustrates a structure contour map of the Base Middle Jurassic horizon (Top Navajo

Formation). This surface post-dates the main phase of salt mobility in the basin but pre-dates the development of the fault system and therefore is considered to accurately illustrate the fault controlled structural geometry. As this map shows, the Blue Hills Fault has a limited topographic relief and is limited to the area where subsidence in the Courthouse Syncline is at its greatest. The fault also appears to represent a hinge line where dips steepen into the syncline. In contrast to this, the Moab segment displays a very distinct structural high in the footwall area along much of its length.

Further information about the uplift and subsidence associated with faulting is determined from profiles along the fault illustrating the elevations of the footwall and hanging wall cut-offs (Figure 3.51(a) and the vertical displacement (Figure 3.51(b)). As Figure 3.51 shows, displacement is very variable across the fault system with the Blue Hills segment showing a relatively limited variation in displacement with fault length. In contrast, where it links with the Moab segment the displacement-length relationship changes significantly and the profile displays a much steeper gradient. This also corresponds with an increase in the gravity gradient, indicating that salt is beginning to rise in the same area (Figure 3.51(c)). As Figure 3.51(a) shows, along the length of the Blue Hills and Moab segments, the hanging wall cut-off varies little and remains at a relatively continuous elevation of around 1100m. The footwall cut-off, in contrast displays a dramatic increase along its length, particularly along the Moab segment. Consequently this fault segment is considered to have fault displacement primarily manifested as footwall uplift rather than hanging wall subsidence which is also illustrated by the structure contour map in Figure 3.42(b).

Ideally, a full consideration of the way strain was accommodated by the Moab Fault system would involve analysis of a heave-profile alongside the vertical displacement profile shown in Figure 3.51. Unfortunately given the nature of the field exposures of the Moab Fault system, it was judged that a heave profile could not be determined accurately enough to be meaningfully interpreted so this has been excluded. This inaccuracy is due to the fact that the fault cutoffs have to be projected onto the fault planes for a distance often over a kilometre. Due to the low dip of the projected surfaces, vertical cutoff separations are judged to be determinable from these projections with reasonable accuracy. Where the horizontal

separation is concerned however, this is not the case. In absence of a detailed heave profile, the structure map in Figure 3.42(b) gives a reasonable indication of fault heave.

Continuation of fault system to the south of the Moab Segment exposures

One problematic issue with understanding the Moab Fault system is determining how it continues to the SW of the Colorado River where no fault plane is exposed and the Moab-Spanish Valley salt structure is expressed as a flat-floored salt-valley. When beds are projected across the flat-floored valley, significant vertical offset is observed to continue from that seen in the Moab segment despite the lack of an exposed fault plane. The displacement associated with the Moab Fault System is therefore inferred to extend into this area. This offset can be clearly seen in cross sections across the flat floored valley (e.g. figures 3.52 and 3.31) and the amount of offset along the valley is shown in figures 3.51 and 3.42.

The key to understanding the continuation of the fault system is considered to be in understanding the salt structure geometry in this area and two alternative interpretations are proposed. The first (Figure 3.53(a)) implies that the change from the exposed Moab Segment to the flat-floored salt-valley is entirely related to the erosion level and that the fault continued above the current erosion level in a similar way to the way it is illustrated in Figure 3.44. The second interpretation (Figure 3.53(b)) suggests that the change in exposure style corresponds to a significant change in the morphology of the salt structure and represents a transition from extension being accommodated by a fault structure to displacement being accommodated by a piercing salt-diapir as is observed for the Schooner NE fault system (section 4.7).

It is clear from comparing figures 3.44 and 3.52 that a significant change in the salt structure style does occur in this area. Wells constrain a thick Cutler Formation depocentre on the SW side of the salt structure where it is exposed as a flat-floored valley which is not present in Figure 3.44 (section 3.10). Despite this significant change in the salt structure style, the development of this depocentre, and the resultant salt structure morphology clearly predates the development of the fault system. It is therefore difficult to relate the change from a fault

in the crest of the salt structure to a piercing salt structure accommodating extension as easily as in the Schooner NE example (Section 4.7). Both of these interpretations require the NE side of the salt structure to act as a slip surface on the fault system at depth. Consequently as illustrated in figures 3.36 and 3.27, the favoured map trace of the continuation of the fault plane in this area is to wrap around the NE side of the salt body. This is in contrast to the interpretation of Doeling et al. (2002) who places his inferred fault trace along the middle of the valley.

Crestal graben systems

Extensive normal fault systems are present in the eroded crestal regions of many of the salt structures in the study area. Fault systems typically cause down-stepping of the overburden sequence towards the centre of the structure overprinting the crestal anticline morphology. The largest offset faults are associated with the Onion Creek salt structure where the entire Pennsylvanian to Jurassic sequence is observed having been down-faulted by up to 610metres (Doeling, 2002). This fault system has a dominant E-W to WNW-ESE trend which is parallel to the outcrop trend of Paradox Formation caprock exposures. Notably, however, this is slightly oblique to the trend of the salt structure at depth which has a NW-SE trend (Figure 3.28).

The most extensive crestal graben system in the study area is associated with the Salt Valley-Cache Valley salt structure and is observed along its entire exposed length (Figure 3.32). As Figure 3.32 shows, fault orientations display a distinct change at the structures SE end from the NW-SE orientation in the Salt Valley area to the E-W trend dominant in Cache Valley. This parallels a change in the orientation of the underlying gravity anomaly and the fracture system is considered to follow the trend of the salt structure. Figure 3.54 illustrates the crestal graben system in the Cache Valley area. As Figure 3.32 shows, the fault system displays a distinct curvature, particularly on the NE side of the salt structure which corresponds with the widening of the area where Paradox Formation caprock is exposed or inferred to be at shallow depths. Fractures associated with the Moab-Spanish Valley salt structure show two different styles depending on where they are exposed.

In the area to the NW of the Colorado River where the salt structure is entirely buried beneath overburden sequences folded into the Moab Anticline, faults consist of a series of keystone-style normal faults (Figure 3.36) dipping towards the centre of the anticline but without modifying the fold geometry significantly. Faults are shallowly dipping (45-50°) and have displacements typically on the order of 5-10 metres (Figure 3.55). Detailed examination of these fault planes reveals that where sand on sand contacts are present, fault planes are open, uncemented fractures.

To the SE of the Colorado River, where the Moab salt structure forms a flat-floored salt-cored valley, the style changes significantly. In this area a series of high angle (70-90°) faults and associated folds are present along the entire valley. Downfaulted units are easily identified as they are extremely intensely fractured and sandstones are intensely bleached/stained to the extent that it is often difficult to determine their place in the stratigraphy (Figure 3.56). In contrast to NW of the river where faults are typically well-defined single planes, in this area faults are chaotic fracture zones of up to several metres in width (Figure 3.57). Faults range in displacement from several metres to several tens of metres. Significant crestal fault systems are not identified in either the Cane Creek of Castle Valley salt structures.

Crestal fault systems typically have several features in common.

1. Hangingwall areas are characterised by very intensely fractured and bleached sandstones whereas footwall areas are largely undisturbed and unbleached (e.g. Figure 3.57).
2. Faults and associated fractures are open and uncemented
3. The strike of faults typically follows the erosional extent of the salt structure and not necessarily the geometry of the buried structure (i.e. Onion Creek).
4. The amount of fault displacement is typically not greater than the topographic variation of the erosion level associated with the salt structure (Onion Creek has the highest structural elevation and consequently the deepest erosion level and also has the largest offset in its crestal graben system)

Fractures

An extensive system of fractures is present throughout much of the study area and they are particularly common around the salt structures. Fractures are typically only found in sandstone units and are particularly pervasive in Lower and Middle Jurassic sandstones, in particular the Navajo Sandstone, Moab Member (Curtis Formation) and Slickrock Member (Entrada Sandstone). The deposition of these units post-dates the main phase of salt mobility in the basin and pre-dates the development of the Moab Fault System which gives some temporal constraint on fracture development. An extensive fracture system is also present in the Cutler Formation in the region to the SW of the Moab Valley/Moab fault system area extending through much of the external zone. This unit is very infrequently exposed in the area where salt structures are present and has not been investigated in detail.

Fracture systems tend to form complex networks which are pervasive over the entire exposure of a fractured formation and can often be traced for many kilometres. Within these networks, individual fractures tend to reoccur with a frequency of several metres to several tens of metres and are easy to identify as the nature of the desert weathering style means they typically erode linear depressions separated by prominent arch or fin structures. Several examples of fracture networks in the study area are shown in Figure 3.58. Figure 3.59 shows the main strike trends of the fractures in Jurassic sandstones in the study area and illustrates that the dominant fracture trend is either parallel or sub-parallel to the trend of the salt structures. Significant variations on this trend do however exist and in many areas and fracture systems with two or more trends frequently overprint each other leading to a cross-hatched pattern in map view (Figure 3.59).

Fracture systems are also observed which display significant along strike curvature. Fractures on the SW side of the Moab-Spanish Valley salt structure have a distinctive arc shaped pattern in map view (figures 3.59 and 3.58(c)) with the strike orientation being deflected towards the salt structure in the central area. This pattern is not, however, observed on the NE flank of the Moab Valley, where fractures are oriented sub-parallel to the axis of the salt structure. A distinct relationship is also identified between fractures and the fault system morphology in the Mill Canyon linkage zone. As Figure 3.48 shows, a cross-hatched

fracture pattern is present in this area with fractures present which are oriented both parallel to the trend of the Moab and Blue Hills segments and also parallel to the linking Tusher Canyon and Courthouse Rock segments. In the eastern part of the linkage zone, fractures can be seen to curve to the NW paralleling the breaching Tusher Canyon fault segment. This fracture pattern highlights a distinct relationship between the development of fractures in this area and the development of the fault system. At the exposure scale, fractures are typically a zone of 0.3 to 1 metre in width where a series of vertical to sub-vertical granulation seams are localised. Individual granulation seams are typical on the order of 1-4 mm in width and often display up to 2 mm of extensional displacement across them (e.g. Figure 3.60).

Folds

The entire Pennsylvanian to Upper Cretaceous sequence is observed being folded into a series of broad anticlines and synclines throughout the study area. Although several small folds are present in the area which are typically associated with crestal fault systems, the area is dominated by a small number of large folds with a wavelength of 10-20 km. These folds display a distinct relationship to the salt structures with their axes being oriented parallel to them and are exclusively situated above their crests. Broad synclines are present between the salt structures and also between the most basinward Onion Creek salt structure and the Uncompahgre Front (Sagers Wash Syncline).

Figure 3.26 shows a structure contour map of the post-Permian supra-salt sequence and illustrates the fold structures in the area and their association with underlying salt structures. As Figure 3.26(a) shows, bedding is locally folded up significantly around the La Sal laccolithic igneous intrusions. Fold dips are typically relatively shallow throughout the area ranging from 5° to 28°, and dips are generally shallower, higher in the stratigraphy and showing no notable variations between the salt structures. The exception to this is the SW limb of the Moab Anticline in the area where its surface expression is in transition between a buried salt structure and a flat-floored valley near where the Colorado River cuts through the Moab Valley. In this area, the limb reaches up to 64° increasing over a 2 km towards the SE. This is in the immediate hanging wall to the Moab fault segment and a degree of fault-bend folding is considered likely.

Another notable fold structure is the Bar M Syncline which is situated in the immediate hanging wall to the Moab fault segment in the area where it has its maximum displacement. This chevron style fold has its axis 145m from the fault plane, has maximum dips of 50° on both of its SW and NE limbs respectively and can be traced for 2 km.

3.9 Unconformities associated with salt structures

Although the stratigraphic sequence exposed in the study area contains numerous regionally recognisable unconformities (Molenaar, 1981), within the study area itself, angular relationships at geological contacts are rare. The main angular relationships identified in the study area are at the base of the Triassic sequence and at the base of and within the Upper Triassic sequence. Other than these surfaces, bedding planes are generally parallel across geological boundaries, no major erosional phases or hiatuses can be identified from field data and for the purposes of this study the sequence is largely treated as conformable.

Base Triassic Unconformity

A locally angular unconformity is observed separating the Moenkopi Formation from the underlying Cutler Formation in some areas of the study area. This surface is best defined in exposures on both the NE and SW flanks of the Castle Valley salt structure where progressively older sequences become truncated by this surface with distance along the salt structure (Figure 3.61). This angular discordance reaches up to 10° in central areas directly adjacent to the salt structure although it is very localised with no truncation being present where this contact is exposed approximately 1.5 km NE of the salt structure. Exposures flanking the Onion Creek salt structure, in contrast show only very minor angular truncations which can only be observed in the Hittle Bottom area adjacent to the Colorado River. Exposures on the SW flank of the Moab-Spanish Valley salt structure show beds either side of the Cutler-Moenkopi boundary to be entirely parallel without any evidence of an erosion surface. Similarly, extensive exposures to the SW of this structure including those in the crest of the Cane Creek Anticline show no evidence of any angular relationship at this boundary and this surface erosion surface is considered to be very localised.

A 45-60 cm thick gypsum bed is present at the base of the Moenkopi Formation in exposures flanking the Castle Valley salt structure which is continuous along the entire exposed length of the salt structure (Figure 3.62, top of Log 2). This bed can be seen in exposures which are up to 2 km away from the salt structure but is not observed outside the immediate vicinity of this structure. Gypsum layers are common in the Moenkopi Formation in western parts of the Colorado Plateau where the sequence is largely of marine origin but primary gypsum has not been identified in the Paradox Basin area (Stewart et al., 1972[a]). This layer is interpreted as being secondary gypsum deposited in a localised lacustrine setting centred above the Castle Valley salt structure. The sulphate rich waters required to develop such a layer are interpreted as being derived from the Paradox Formation. Consequently this interpretation requires the erosion level associated with this unconformity to have exposed the salt structure at the surface and implies that the Moenkopi Formation would have been the first formation to blanket the salt structure, locally giving this unconformity a Pennsylvanian subcrop. Similarly, exposures of Moenkopi Formation on top of caprock in the Onion Creek area (Figure 3.30) also suggest the Moenkopi Formation has a similar localised Paradox Formation subcrop in this area.

Upper Triassic intra-formational truncations

Doeling, (1988) and Doeling et al. (2002) describe a localised truncation surface within the Chinle Formation on the SW flank of the Moab-Spanish Valley salt where progressively younger beds are truncated below the informal Black Ledge member with distance towards the salt structure (Figure 3.63). Doeling (1998) interprets this as an intraformational unconformity related to the localised uplift and erosion of the flanks of the adjacent salt structure and cite it as evidence for extensive salt mobility during Chinle time. Several other truncation surfaces have been described within the Chinle Formation in the study area (Hazel, 1994, Matthews, 2004) and as part of this study the locations of truncation surfaces within this formation have been mapped and are shown in Figure 3.64. A small number of localities have also been identified which show similar but typically much lower angle truncations at the base of the Wingate Formation Figure 3.65(c).

Figures 3.65 and 3.66 illustrate several examples of these truncations and shows the varying style of these relationships. The angles of truncated surfaces range from <5° to >90°, the highest angle of which is shown at 'Gregg's Unconformity' (Figure 3.66) where beds are rotated to the extent that they are slightly overturned. All of these surfaces display several common characteristics. Firstly truncated units are all heterolithic lithologies which are truncated below a thick, prominent sandstone unit, usually the Black Ledge Member. Secondly where beds below the truncated units are observed, they are always entirely parallel to the bedding above them indicating that this deformation is restricted to a single unit.

As Figure 3.63 illustrates, although several of these truncations are observed on the flanks of the Moab-Spanish Valley salt structure, there is no spatial correlation between them and the salt structures in the area. There is, however, a distinct correlation between their presence and the distribution of thick sandstone units (>5 m) such as the Black Ledge Member. Laterally continuous sandstone units are largely restricted to the area between the Cane Creek Anticline and the Salt Valley-Cache Valley and Castle Valley salt structures. The distribution of these truncations and their layer restricted nature is considered overwhelming evidence that they are not related to localised salt related uplift but to another process (see section 3.12). The truncation surface on the edge of the Moab-Spanish Valley salt structure described by Doeling (1988) and Doeling et al. (2002) is also situated below the black ledge unit. Although parallel sequences below these truncated beds are not exposed, sandstone beds below the truncated heterolithic unit (labelled 'x' in Figure 3.63), while still showing a discordance are at a significantly lower angle than the truncated heterolithic unit. Consequently this truncation is considered to have been formed by the same process as the others and the interpretation of Doeling (1988) is strongly questioned.

The truncation exposed in Seven Mile Canyon (Figure 3.66) shows significant thickness variations in the layers which are folded near the truncation surface with the bed labelled 'x' in Figure 3.66 changing from 48cm thick in the limb of the fold to 12cm in the axis. This is considered to be significant evidence for the folding and subsequent truncation to be related to soft sediment deformation. A further significant truncation surface is also present within

the Chinle Formation associated with the localised lower unit. This is described in detail in section 3.10.

3.10 Sediment packages associated with salt structures

Significant thickness variations indicative of syn-depositional salt mobility are observed from field exposures and well data throughout much of the study area. Although thickness variations throughout the supra-salt sequence are expected and have been hinted at in the literature, this study concentrates primarily on thickness variations in the Honaker Trail, Cutler, Moenkopi and Chinle formations. This is partly because preliminary investigations show that their deposition was synchronous with the most active phase of salt mobility in the basin. But also the present erosion level has meant that the overlying stratigraphy has been removed throughout large portions of the area meaning it is not widely represented in field or well data and making basin scale interpretations highly problematic.

Thickness variations observed from field exposures

The erosion system in the study area reveals two main types of exposure. The most extensive exposures are NW-SE trending cliff exposures on the flanks of the flat-floored valleys associated with salt structures and also in the eroded footwall scarp of the Moab Fault. Although these exposures are extensive, they are of relatively limited use for determining the salt controlled thickness variations in the basin. This is because they are oriented parallel to the strike of the salt structures whereas the main thickness variations are perpendicular to them as packages thicken into the intra-salt depocentres as determined from well data. Consequently, thickness variations shown in these exposures represent the relatively minor changes in thickness along the crest of the salt structures. Strike perpendicular exposures are present in the canyons carved by the Colorado River which follows a slightly meandering NE-SW course through the study area. Although these exposures often provide a degree of three-dimensionality, the erosion level is generally only deep enough to show part of salt influenced stratigraphy.

Thickness variations in exposures flanking salt structures

Moab Salt structure

Although obscured along much of its length by intense crestal faulting and fracturing, an 8km cliff section on the SW side of the valley to the north of the Colorado River shows extensive evidence of significant thickness variations in several formations (Figure 3.39).

Honaker Trail Formation

The Honaker Trail sequence is too deeply buried to be exposed throughout much of the study area however small exposures of the upper part of the sequence are present in the footwall of the Moab fault segment. Although the distinction between a thickness variation and a structural feature is rather blurred in this area, a very curious relationship is observed whereby the Honaker Trail sequence dramatically changes in style at the edge of the salt structure. As Figure 3.40 shows, directly adjacent to the salt structure a single, 2-3m thick bed of Honaker Trail sequence sandstone (limestone at some other locations) dips towards the salt structure (NE) at approximately 60°. Behind this bed, the sequence dips away from the salt structure (SW) at 28° with the older beds being truncated against this other upper bed. When followed up-dip, this bed continues to the top of the sequence and folds over into parallelism with bedding below. A sketch section of this curious relationship is illustrated in Figure 3.67. The upper surface of this rolled over bed forms the slip surface to the Emkay fault segment and this relationship is observed all along the entire length of this fault segment.

Figure 3.50 illustrates the nature of this rollover at a location 2 km to the NW and shows how beds underneath the rolled-over bed dramatically thin to pinchout towards it. Localised minor brecciation is present in the rolled-over layer at this location and carbonate mud is observed, moulded around the moderately broken up areas within the layer. This is interpreted as suggesting brecciation associated with this rollover occurred when the rock was semi-lithified and therefore illustrates that this deformation predates the Emkay fault segment which is observed offsetting Upper Triassic rocks.

Cutler Formation

The Cutler Formation is well exposed along the footwall scarp of the Moab fault segment and at the furthest north area where the entire section is exposed (at UTM 617517 E, 4276819 N) it is measured at approximately 200 metres in thickness. This section is observed to thin progressively with distance along the section towards the SE from the marginal shoulders of the structure towards the central area. The section thins to a pinch-out which is unexposed due to overlying sand dunes located approximately 4.75 km away at UTM 621420 E, 4273010 N). Figure 3.39(b) illustrates the gradual south-westward thinning of the Cutler sequence along this section although the sequence is almost entirely absent in the area shown in Figure 3.39(a).

Moenkopi Formation

The Moenkopi Formation shows a similar south-westward thinning along the section shown in Figure 3.39 to the Cutler Formation. Over a distance of ~2km, the sequence thins dramatically from 120 m at UTM 621256 E, 4273242 N to 25 m at UTM 622558 E, 4271536 N where the exposure ends. Although the Chinle Formation is not observed resting upon the Honaker Trail Formation, this thinning trend is expected to continue to the SW to the point where the Moenkopi Formation pinches out. Consequently the Moenkopi Formation is considered to pinch-out onto the flanks of the Moab-Spanish Valley salt structure.

The Moenkopi Formation is also observed to thin progressively along this footwall exposure north of UTM 614511 E, 4278582 N and pinch-out at UTM 612906 E, 4281380 N. The significance of this is not immediately apparent in the field due to the absence of a well-exposed salt structure adjacent to this area of pinchout. When observed in map view, however, it can be seen that the footwall scarp of the Moab fault segment becomes progressively eroded back between these two points (Figure 3.68) resulting in the exposed Moenkopi section being further from the salt structure in the areas between where pinchout is observed. At the two points where pinch-out is observed, Moenkopi exposures are at their closest to the crest of the salt structure and consequently this pinchout is interpreted as being due to a lack of accommodation space on the crest of the salt structure. The entire Moenkopi sequence is therefore interpreted as thinning to pinchout over the crest of the Moab-Spanish Valley salt structure regardless of whether or not it is buried..

Chinle Formation

In contrast to the Cutler and Moenkopi sequences the Chinle Formation displays a marked thickening to the SW in the exposure shown in Figure 3.39(a). The Chinle Formation varies from 88 m near the entrance to Arches National Park (UTM 619904 E, 4274176 N) to at least 150 m adjacent to the Colorado River (UTM 622558 E, 4271536 N). Stratigraphic expansion is largely restricted to a single unit which is the mudstone-dominated sequence between the Black Ledge Member and base of the Wingate Formation (Upper Slope Unit of Matthews et al. 2004).

Castle Valley salt structure

Cutler Formation

As Figure 3.61 shows, the observed members of the Cutler Formation show a significant thinning to the SE along the valley. This is, however, due to progressive truncation below the Base Triassic Unconformity and no primary stratigraphic expansion has been recognised (see section 3.9).

Moenkopi Formation

The most pronounced thickness variations observed in Castle Valley exposures are within this formation which displays significant thinning of the exposed sequence towards the SE in the same direction as the Cutler sequence thins due to erosion. As Figure 3.61 shows, the sequence changes from 230 metres in thickness at its northern end (UTM 635463 E, 4279778 N) to 175 metres, 4 km to the SW (at UTM 637818 E, 4276546 N). Similarly, significant thickness variations are observed in the NE-SW trending exposure at the N end of the valley where the sequence is 153 m thick (UTM 636273 E, 4280891 N) in the centre of the valley, above the crest of the salt structure. This sequence expands to 230 m, 1.4 km to the SW and to a minimum (base not exposed) of 186 m, 1.7 km to the NE. The nearest point the full sequence is exposed is 5.5 km to the east where a 248 m sequence is measured.

Chinle Formation

Exposures of the Chinle Formation in Castle Valley appear to show a similar thickness variation trend to the Moenkopi Formation (Figure 3.61). Measurements, however, show this to be largely a perspective effect as the sequence only expands from 75 to 80 metres (106%) over the same 4 km that the Moenkopi Formation expands by 55 metres (130%).

Axis parallel thickness variations in canyon exposures carved by the Colorado River

The exposures along the Colorado River which show significant thickness variations are limited to the 10 km long cliff exposure in Professor Valley (Figure 3.69) and a 4.5 km long section of the canyon in the Big Bend/Sandy Beach area. The former is situated between the northern tip of the Onion Creek salt structure and the southern (Cache Valley) end of the Salt Valley-Cache Valley salt structure. The latter is situated slightly SW of the northern end of the Castle Valley salt structure.

Professor Valley section

The Professor Valley exposure shows a progressive increase in the thickness of both the Moenkopi and Chinle Formations towards the SW (Figure 3.69). The Moenkopi Formation expands significantly more than doubling in thickness from 112m at UTM 645126 E, 4293728 N to 233m 9 km to the SW at UTM 639303 E, 4286838 N. The Chinle Formations also shows a significant thickness variation from 85 to 105 metres over the same distance.

Sandy Beach section

Only the Chinle Formation is well exposed at this location and it shows a very significant thickness variation through the exposure. Unlike the previously described exposures the thickness variation does not take place through expansion of the entire sequence but rather takes place entirely within a localised lower member of the Chinle Formation which is only exposed in this area. The mudstone dominated Chinle sequence observed in the Castle Valley and Professor Valley areas continues into this area showing no thickness or facies variations associated with the thickening underlying unit. The regionally extensive upper unit is here referred to as the 'Upper Unit' and the localised lower part as the 'Lower Unit'.

Figure 3.70 illustrates several photo-sections along this exposure and illustrates how the 'Lower Unit' pinches out at the NE and SW ends of this exposure where the Upper Unit is observed sitting conformably on top of the Moenkopi Formation. The Lower Unit then thickens progressively towards the centre of the exposure towards the Sandy Beach area.

Two different thickening styles are observed in this 'Lower Unit' which include an upper sequence (X) within which, stratigraphic expansion occurs through growth geometries. The main lower part of the sequence (I – V) is separated from the X unit by angular truncations of up to 20° with units on either side of the package dipping towards the central area and progressively younger units being truncated below this surface with distance towards the centre. A sketch section illustrating the structural and stratigraphic relationships in this area are shown in Figure 3.71 and Figure 3.72 shows the outcrop pattern of this lower member in map view. The exact thickness of this unit is not known as its base is only seen at its margins. The maximum exposed thickness is 60m and a projection of beds below the surface predicts this unit to be in the region of 150m thick. The Upper Unit is ~110m thick in this area highlighting the significance of this localised thickening.

Large-scale thickness variations determined from integration of field and well data

Field exposures within the study area typically show relatively limited thickness variations, largely due to their association with the crestal regions of salt structures. Well penetrations situated between the salt structures, in contrast, frequently reveal significantly expanded sequences illustrating the presence of significant depocentres between the salt structures. Thickness variations determined from comparisons of field and well data are here described for the four investigated formations.

Honaker Trail Formation

The Honaker Trail Formation is the most difficult formation to assess as the very limited nature of surface exposures makes its exact relationships with the salt structures very difficult to determine. Spatially limited Honaker Trail Formation exposures are present in the crest of the Cane Creek anticline and also in the crest of the Moab-Spanish Valley salt

structure in the uplifted footwall area of the Moab Fault segment. The sequence is, however, absent in the crests of the Onion Creek, Salt Valley-Cache Valley and Castle Valley salt structures and the lack of exposure means it is not clear whether this is due to non-deposition or pre-Triassic erosion. Well penetrations record a relatively consistent thickness of 380 – 480 metres in the area to the SW of the Salt Valley-Cache Valley and Moab salt structures with a gradual thinning to the SW in the external zone. Well penetrations in the deepest part of the basin in contrast, reveal a Honaker Trail sequence reaching 1459m in well 4301930206 situated 5.7 km to the NW of the Onion Creek salt structure (See Figure 3.31). Figure 3.24 also shows a significantly thicker Honaker Trail sequence on the N side of the Onion Creek structure to that on the S side suggesting that the salt structure had a role in this thickness change. Well 4301930076, situated midway between the Castle Valley and Moab-Spanish Valley salt structure (Figure 3.31) penetrates a 725m thick sequence whereas wells 4301931180 and 4301910397 on the NE flank of the Castle Valley structure penetrate a 288m and 246m sequence respectively. Well data therefore clearly demonstrates that the Honaker Trail varies significantly in thickness around the salt structures. An isopach map of the Honaker Trail sequence in the study area derived from well and field data is shown in Figure 3.73.

Cutler Formation

The presence of Moenkopi Formation deposits resting directly on top of the Paradox Formation in Onion Creek exposures (Figure 3.30) suggests the absence of the Cutler Formation from the crest of the salt structure. Similarly the presence of the gypsum layer at the base of the Moenkopi Formation in Castle Valley is interpreted as evidence for the absence of the Cutler Formation from the crest of this structure. Although exposures flanking the Salt Valley-Cache Valley salt structure do not penetrate this far down in the stratigraphy, wells 4301910232 and 4301911566 on the SW and NE sides of the salt structure show the Moenkopi Formation sitting directly upon the Paradox Formation (Figure 3.34). This clearly illustrates that the Cutler Formation is absent from the crest of this structure. The presence of the locally angular, Base Triassic Unconformity makes it difficult to determine whether or not this is due to non-deposition or erosion. Exposures on the flanks of the Moab-Spanish Valley salt structure, however, show the progressive thinning to pinch-out of the Formation onto its flanks and clearly implicates non-deposition over the crestal area of this salt structure (Figure 3.39(b)). As Figure 3.37 shows, no notable thickness variations have been

observed across the Cane Creek salt structure and a full Cutler Formation/Group sequence is exposed in its crest.

Well penetrations illustrate that the Cutler Formation shows some very dramatic thickness variations between the salt structures. From being absent in the crest of the Onion Creek and Castle Valley salt structures, the sequence thickens significantly into the foredeep of the basin reaching 1216m in well 4301930206 (5.7 km NE of the Onion Creek structure) and 1125m at 4301930455 (4.7 km SW of the Salt Valley-Cache Valley structure). Also from being absent in the crest of the Castle Valley and Moab-Spanish Valley salt structure the sequence thickens to 1400m in well 4301930076, approximately midway between the structures. To the SW of the main salt structures in the basin the Cutler Formation maintains a relatively uniform thickness of 390-420m through into the External Zone. At the SW margins of the Moab-Spanish Valley and Salt Valley-Cache Valley salt structures, the sequence also locally thickens significantly. The best constrained thickening is shown by wells 4301931112 and 4301930455 which show the package increasing from 684m to 1125m over a distance of 3km towards the Salt Valley-Cache Valley salt structure to the NE (Figure 3.74). As figures 3.37 and 3.39 show, a package with a similar style is present on the SW side of the Moab-Spanish Valley salt structure which is constrained by wells 4301930113, 4303730031, 4301910655 and 43019563. Figure 3.75 illustrates an isopach map of the Cutler Formation in the study area derived from well and field data.

Moenkopi

Field evidence, largely described in the previous section suggests that the Moenkopi Formation blanketed the Onion Creek and Castle Valley salt structures. The Moenkopi Formation is also observed to cover the crest of the Salt Valley-Cache Valley salt structure at its SW end in Cache Valley area (Figure 3.54). The absence of blocks of Moenkopi Formation in the collapsed crest of the Salt Valley area (Figure 3.32), however, suggests it may not have done so in the structurally larger central area of the salt structure. Exposures flanking the Moab-Spanish Valley salt structure in contrast display stratigraphic pinch-out of the formation which clearly did not blanket this structure.

As Figure 3.37 shows, a complete sequence of un-varying thickness covers the Cane Creek Anticline. The Formation typically has a relatively consistent thickness of 100-175 metres throughout most of the study area which is observed both in field exposures and the majority of well penetrations. The maximum observed thickness in the field is 248m, although several wells locally record much thicker sequences. As Figure 3.74 shows, wells on the SW side of the Salt Valley-Cache Valley salt structure show a progressive thickening of the sequence towards the structure, reaching 740m in thickness at well 4301930122 around 1.75 km from the edge of the flat-floored, salt-cored valley. The sequence also reaches 352m in well 4301930076 situated midway between the Castle Valley and Moab-Spanish Valley structures. Although wells on the NE side of the Salt Valley-Cache Valley salt structure typically record relatively thin Moenkopi sequences (172m and 253m at wells 4301920146 and 4301930055 respectively) one well (4301930110) records an anomalously thick sequence of 599m on the structures NE side at its northern end. An isopach map of the Moenkopi Formation in the study area is shown in Figure 3.76.

Chinle

The Chinle Formation is generally thinner and much less variable in thickness than the underlying sequences and is typically 70-135m thick throughout most of the study area. The Chinle Formation is also notable as it is the youngest sequence observed to blanket the Uncompahgre Uplift (Figure 3.77) making it the youngest sequence to not be constrained by the Pennsylvanian foreland Basin morphology. The Chinle Formation has a similar thickness where it covers the Uncompahgre Uplift, to that throughout much of the Paradox Basin and therefore the influence of salt mobility on its deposition is clearly limited. Exposures of Chinle Formation and older sequences in the crests of the Salt Valley-Cache Valley and Onion Creek salt structures illustrate how the sequence blanketed these structures. The same relationships which suggest that the Moenkopi sequence blanketed the Castle Valley salt structure, similarly suggests that the Chinle Formation also covered its crest. Also the re-interpretation of the intra-formational truncations flanking the Moab-Spanish Valley structure (section 3.9) suggests that the Chinle Formation also blanketed this structure (in contrast to the interpretations of Doeling, (1988) and Mathews et al. (2004)).

Well penetrations which record a Chinle sequence which is significantly thicker than that observed elsewhere in the basin are situated on the SW side of the Salt Valley-Cache Valley salt structure and include wells 4301911035 (221m), 4301930122 (247m), 4301930455 (259m), 4301931112 (282m) and 4301910361 (216m). Another well (4301930076) which lies along strike from this but between the Castle Valley and Moab-Spanish Valley salt structures also records an anomalous thickness of 259m. The only field exposure where significant thickening of the Chinle sequence is observed is in the Sandy Beach area (described above) where the sequence thickens due to the localised presence of a sand-dominated lower member with angular relationships with the regionally extensive Chinle sequence.

Analysis of gamma ray logs from all of the wells in this area with an anomalously thick Chinle sequence, shows that they have several features in common. Wells show the sequence to be roughly divided into two portions, the upper portion showing the variable but relatively high gamma values typical of the Chinle Formation throughout the study area and the region (Figure 3.78). The lower part of the sequence in contrast, shows significantly lower values and where present (e.g. 4301931112), mud logs describe a sand dominated lower unit. This gamma ray response is consistent with that recorded from exposures in the Sandy Beach exposures where the upper and lower Chinle members are present (W. Matthews, Pers. Comm, 2005) and consequently the lower units in the wells are correlated with the Lower Unit in the exposure. Table 3.2 shows the thicknesses of the regionally extensive, mudstone dominated upper unit and localised sandstone dominated lower unit interpreted from well logs. The thicknesses of the interpreted upper units are on the order of those found for the Chinle Formation throughout the study area.

If the relationships observed in the Sandy Beach exposures are assumed to continue into these subsurface areas as shown in Figure 3.79(c), then stratigraphic expansion of the Chinle Formation recorded in these wells can also be considered to be restricted to this localised lower member with the sequence as a whole showing very limited thickness variations and therefore illustrating that salt mobility was very limited at this time. Figure 3.79 illustrates an isopach map of the Chinle Formation as well as isopach maps of the upper and lower units.

Well Number	Lower unit thickness (m)	Upper unit thickness (m)
4301931112	112	170
4301911035	75	146
4301930455	111	147
4301930076	125	134

Table 3.2. Thicknesses of the sand dominated 'lower unit' and mudstone dominated 'upper unit' of the Chinle Formation in several wells which show a sequence significantly thicker than the regional.

Sedimentary depocentres

From the thickness variations identified in the study area, several major salt-mobility controlled sedimentary depocentres have been identified. The locations of these depocentres are shown in Figure 3.80(a) and are briefly described Table 3.3.

Depocentre morphology

The absence of seismic data in the study area makes interpreting the depocentre morphology extremely difficult. Several locations are present where well data is sufficient to interpret the morphology of the depocentre. As Figure 3.74 shows, a line of five wells is present on the SW side of the Salt Valley-Cache Valley salt structure which show the Moenkopi and Cutler sequences to thicken progressively towards an inferred salt weld at the edge of the salt structure. Well data constrains a similar morphology on the SW margin of the Moab-Spanish Valley salt structure which is shown in Figures 3.37 and 3.52. Further information on the depocentre morphology comes from a cross section published by Hudec (1995) which is interpreted from seismic data at depth (Figure 3.24). Figure 3.24 shows the illustrated part of the Sagers Wash depocentre to be strongly asymmetric, thickening towards the Onion Creek salt structure which Hudec (1995) interprets as a salt-roller morphology. Similarly Figure 3.24 illustrates an asymmetric morphology for the Mary Jane Canyon depocentre, thickening away from the Onion Creek structure towards the Castle Valley structure.

Further insights into the depocentre morphology can be determined from field exposures. The Professor Valley exposure (Figure 3.69) shows an asymmetric thickening of the Moenkopi sequence towards the Castle Valley/Salt Valley-Cache Valley salt structures. As exposures in the Sandy Beach area, however, (figures 3.70 and 3.71) show a much more symmetrical morphology it is inferred that the main Chinle depocentre has a more symmetrical geometry.

Depocentre Name	Location relative to salt structures	Formations displaying significant thickness variations
Sagers Wash Depocentre	Between the SW margin of the Uncompahgre uplift and the Salt Valley-Cache Valley and Onion Creek structures	Honaker Trail Fmn. Cutler Fmn.
Mary Jane Canyon Depocentre	Between Onion Creek and Castle Valley salt structures	Cutler likely but no well penetrations Moenkopi thickens slightly onto NE margin of Castle Valley structure
Courthouse Depocentre	On SW side of Salt Valley-Cache Valley	Cutler Fmn Moenkopi Fmn. Chinle Fmn. (Lower Mbr.)
Sand Flats Depocentre	Between Castle Valley and Moab-Spanish Valley salt structures	Cutler Fmn. Moenkopi Fmn. Chinle Fmn. (Lower Mbr.)
Kings Bottom Depocentre	SW side of Moab-Spanish Valley salt structure	Cutler Fmn.

Table 3.3. Key characteristics of the main depocentres identified in the study area

Salt Welds

Figure 3.81 illustrates an isopach map of the Paradox Formation in the study area (a) and a map of the inferred salt welds in the area (b). The absence of seismic data makes many of the salt welds highly interpretive although several are constrained by well data. The Paradox Formation was likely to have been well over 1km thick throughout most of the study area

and therefore a well penetrating <200m of Paradox Formation is a good candidate for a salt weld as this would be a good upper estimate of the residual/immobile constituents of the sequence. Well 4301930076 records a Paradox Formation sequence of 150m underlying a 1400m thick Cutler sequence indicating a salt weld developed at the base of the Sand Flats Depocentre. Well 4304710655 records a 115m thick Paradox sequence implying a salt weld of the Kings Bottom Depocentre on the SW edge of the Moab-Spanish Valley salt structure. A further salt weld is implied on the SW side of the Salt Valley-Cache Valley salt structure through projection of the base of the salt and top of the salt NE from wells 4301931112 and 43030455 (Figure 3.74).

3.11 Facies variations

Although originally intended as a bigger part of this study, an investigation into the role of salt mobility on facies distribution in supra-salt sequences was largely sidelined. This was primarily due to the discovery that another student was simultaneously working on the role of salt mobility on facies distribution in the Paradox Basin, concentrating on the Chinle Formation. What is presented here should therefore be considered as a preliminary investigation and basis for further work rather than an authoritative review of the role of salt mobility in facies distribution in the basin.

Of the supra-salt formations investigated in this study, the poor exposure of the Honaker Trail Formation and relative consistency of facies through the basin in the Moenkopi Formation means that only the Chinle Formation and Cutler Formation are considered suitable for such a study. Due to the crossover with the other student, and conclusion that the Chinle Formation was deposited at a time of very limited salt mobility (section 3.12), the emphasis is here placed upon the Cutler Formation. Both the Cutler and Chinle Formations were investigated through analysis of sedimentary logs carried out along a NE-SW trending transect, approximately following the course of the Colorado River across the zone of salt mobility.

Cutler Formation

Thickness variations in the Cutler Formation clearly illustrate a fundamental control of salt mobility on the deposition of the sequence. Investigations into facies distribution were primarily concerned with testing the hypothesis that the associated uplift and subsidence had a significant role in modifying sedimentary environments. The Cutler Formation has a strongly unidirectional source in the proximal part of the basin with sediments being shed to the SW from the Uncompahgre Uplift into the basin. Therefore if logs show a relatively uniform proximal to distal transition across the basin, this suggests the role of salt mobility in influencing sedimentation was minor. In contrast, if sediments record significant compartmentalisation of facies in specific depocentres and a highly irregular proximal to distal transition, this would suggest that salt structures did have a significant control on

facies distribution. Figure 3.62 illustrates these sedimentary logs and shows their position in the basin. The facies found in each log are briefly described below.

1. Fisher Towers section. This log was carried out in an exposure on the northern (proximal) flank of the Onion Creek salt structure and the base is not seen in the exposure making it an incomplete sequence. At this location the Cutler sequence consists almost entirely of extremely coarse grained red-purple to red-orange coloured micaceous sandstones and conglomerates. The sequence typically displays beds with deeply scoured bases, well developed cross bedding and clasts up to 10's of cm in width. The sequence is interpreted as an alluvial fan deposit deposited by a very high energy, braided depositional system.

2. Castle Valley section. This log was carried out in an exposure on the NE flank of the Castle Valley salt structure and its base is not seen. Throughout the lower part of the exposure, the sequence consists of similar facies to those at Fisher Towers although with an increasing proportion of fine to medium grained sandstones. The upper 80 metres of the exposure are dominated by purple mudstones interbedded with beds of coarse sandstone.

3. Moab Canyon Section (a). A complete Cutler sequence is logged in the Moab Canyon area as part of the growth package observed on the SW flank of the Moab-Spanish Valley salt structure. The sequence is dominated by fine to medium grained red-orange sandstones frequently displaying large scale cross beds and interpreted as aeolian deposits. A significant portion of the sequence, consists of beds of coarse-very coarse grained and frequently pebbly red-purple sandstones. Although finer grained, these are very similar to those observed at Fisher Towers and interpreted as alluvial fan sandstones. In contrast to the Castle Valley exposures, mudstones constitute only a small part of the sequence in this area (<5%).

4. Potash section. A complete Cutler sequence is also exposed in the Potash area in the crest of the Cane Creek Anticline. Facies at this location are similar to those in Moab Canyon consisting of inter-bedded orange-red, aeolian sandstones and coarser grained fluvial sandstones, frequently with scoured bases. Exposures at this location contain numerous thin (<2m) beds of limestone which frequently display extensive marine fauna. Mudstones are

much more abundant at this location than in Moab Canyon and are typically of fluvial origin but carbonate mudstone layers are also frequently associated with limestone beds.

Although not logged due to accessibility problems, on the opposite (SW) side of Castle Valley to log 2, is exposed a significant thickness (~75m) of fine grained orange or white aeolian sandstone at the top of the Cutler sequence which is not present to the NE of the salt structure (Figure 3.61). Unlike the Cutler sequence logged elsewhere, this unit is not inter-bedded with other facies and clearly represents aeolian sedimentation uninterrupted by fluvial deposition for a long period. Well 4301930076 records a 137m thick unit of extremely clean sandstone with a very low gamma ray response (Figure 3.82) situated 4km to the SW which is here correlated with the Castle Valley exposure. Based on these observations, the preliminary interpretation is that in this area, sedimentation was locally shielded from the fluvial influence from the NE by the Castle Valley salt structure. The interpretation of these logs in terms of interactions between sedimentation and salt mobility is discussed in section 3.12.

In addition to log 3. (Figure 3.62), another log was carried out in the Moab Canyon area 2 km to the SE along the cliff section shown in Figure 3.39 where the Cutler sequence thins to pinchout. These logs are shown in Figure 3.83 and were carried out in order to determine how sedimentary growth affects facies distribution. As Figure 3.83 shows, both logs display very similar facies distribution through the sequence although beds of finer grained aeolian units are typically significantly thicker in the expanded sequence than in the condensed sequence. Coarser, fluvial units, in contrast have a similar thickness and abundance in both logs and the preliminary interpretation of this is that sedimentary growth was primarily accommodated by aeolian units with fluvial deposition being periodic and short lived.

Chinle Formation

The very limited isopach variations in the Chinle Formation and the observation that the most significant thickness changes are associated with a single, isolated unit which is unconformable with the regionally extensive sequence (Section 3.10) makes invoking salt mobility as a control on facies distribution somewhat problematic. Observation of the Chinle

sequence shows however that significant facies variability is present within the sequence and this is briefly described below.

Upper (regionally extensive) Unit

In this unit, the Moab-Spanish Valley salt structure appears to represent some kind of transition zone in the basin. Exposures to the NE of this structure are dominated by red mudstones with typically fine-grained, isolated sandstone units of varying frequency forming a lesser part of the sequence. This sequence does not change significantly in thickness or character where the transition from the Paradox Basin to the Uncompahgre Uplift occurs suggesting that salt mobility has little control on its character. SW of the Moab-Spanish Valley salt structure, however, the sequence varies significantly, consisting of a typically green basal mudstone unit (Petrified Forest Unit of Stewart et al., 1972[b]) and thick amalgamated channel sequence (Black Ledge Unit) which are laterally extensive and not exposed to the NE. It is, however, unclear how abrupt this change is and the role that the salt structure has in this as exposures with the different characters are separated by 3km.

Lower Unit (Localised in Sandy Beach area)

Compared to the facies represented in the 'Upper Unit', the Lower unit varies significantly. The six informal units (I-X) consist of a sequence of intensely mottled siltstones and coarse-very coarse sandstones divided into specific units by variations in coloration or abundance of their varying constituents. One significant variation between the two sequences is that larger clasts in the Lower Unit frequently consist of vein quartz whereas any clasts bigger than sand size in the upper unit are typically intra-clasts. This is significant as it suggests the units have a different provenance, with the Lower Chinle potentially being derived from the Uncompahgre Uplift whereas the Upper Unit (which blankets the uplift) is derived from a more regional depositional system.

3.12 Discussion

Development of salt mobility in the basin

Timing of salt mobility in the basin

Certain key relationships between the stratigraphic units and the salt structures are used to determine the timing of salt mobility in the basin. The most useful relationship is sedimentary growth, as salt migrating into a salt structure must be withdrawn from adjacent areas which will consequently have a response in terms of creating accommodation space. Evidence for a stratigraphic unit pinching-out onto the margins of a salt structure indicates that the salt structure was active during deposition. Deposition of a sequence over the crest of a salt structure, in contrast, indicates a period of less dynamic activity, particularly if the sequence is not greatly condensed. Table 3.4 summarises the observed stratigraphic relationships for each of the salt structures in the study area.

As detailed in Table 3.4, the most dramatic thickness variations are present in the Honaker Trail and Cutler sequences and the main phase of salt mobility is therefore inferred as being during the Upper Pennsylvanian and Permian. The presence of smaller, but significant growth sequences in Triassic depocentres, indicates that salt mobility continued beyond this time. Major salt-controlled depocentres have not been identified, which post-date the deposition of the Lower Unit of the Chinle Formation and basin- wide salt mobility is inferred as having largely ceased by this time.

As shown in Table 3.4 an attempt has been made to estimate the timing of the development of salt welds associated with the major salt structures in the study area. This has been done through analysis of the stratal geometries associated with the associated depocentres. The interpretation of when welds develop relies on the assumption that a supra-salt sequence, locally looses its ability to move at the point when it becomes welded to the sub-salt sequence. At this point, salt movement therefore also locally looses the ability to control sedimentary growth in the supra-salt sequence. The time at which a weld develops is therefore interpreted as the last time when the stratal growth sequences associated with the

weld change from showing a control of salt mobility to showing no control on salt mobility. It should be stressed however, that in this dataset, the absence of seismic data means that growth geometries are constrained with a very low resolution and this is a highly subjective interpretation.

Deposition controlled by salt-mobility is un-evenly distributed in the basin through time. Isopach maps show some of the thickest sequences of the Cutler and Honaker Trail formations (figure 3.73 and 3.75) to be situated in areas adjacent to the Uncompahgre Uplift in the NW of the study area. Isopach maps of the Moenkopi and Chinle Formations, in contrast (figures 3.76 and 3.79), show relatively thin sequences in these areas and the main Triassic depocentres are located to the SW of the Salt Valley-Cache Valley and Castle Valley structures. This suggests a significant migration of the locus of salt mobility over time, similar to that observed in the Southern North Sea study area (section 4.9). This is interpreted as the result of early salt welds developing in the NE of the basin during Cutler time which result in the salt-starvation of the system and do not allow subsequent salt mobility to occur in the area. Salt in areas further from the Uncompahgre Uplift (and the sediment load driving salt mobility) in contrast, is interpreted as not having withdrawn so completely by this time allowing further subsequent salt mobility and depocentre development to occur.

In contrast to Baars, (2003) who suggests (or perhaps speculates) that the Cane Creek Anticline was active from the Permian to Jurassic time, non of the isopach maps in this study show any evidence of any activity of this structure during this time and its development is inferred as post-dating the main phase of salt mobility in the basin. Matthews et al. (2004) and Hazel, (1994) also interpret this structure as having had significant activity during the deposition of the Chinle Formation based largely on sedimentogical evidence. The finding of this study is that no stratigraphic thickness variations can be constrained in the entire exposed supra-salt sequence (Honaker Trail to Wingate formations). As it is difficult to envisage a situation where a salt structure could develop without either major stratigraphic expansion or a major unconformity surface developing, the Cane Creek Anticline is interpreted as having developed after the deposition of this sequence.

	Onion Creek salt structure	Salt Valley-Cache Valley salt structure	Castle Valley salt structure	Moab-Spanish Valley salt structure	Cane Creek Anticline
Distance of crest from Uncompahgre Front (km)	6km	28km	29km	43km	55km
Estimated height of the salt column	3250m (min)	2811m (min)	2800m (min)	2682m (min)	315m
Sequences showing sedimentary growth associated with the structure	Mainly Cutler. Although significant differences in thickness of Honaker Trail observed across the structure	Mainly Cutler but significant thickness variations present in Moenkopi and possibly in Honaker Trail. Moderate thickness variations observed in Chinle (SW side only)	Mainly Cutler. Also moderate thickness variations in Moenkopi on both sides and in Chinle on SW side. Honaker Trail thick on SW side	Mainly Cutler. Moenkopi thins to pinchout onto its flanks and thickens on the NE side. Minor variations in the Chinle.	None of the exposed Honaker Trail to Wingate sequence is observed showing any significant thickness variations across the structure
Sequences pinching out onto or beign removed from its crest (prior to Tertiay erosion)	Honaker Trail and Cutler	Honaker Trail Cutler and possibly Moenkopi	Honaker Trail and Cutler	Honaker Trail, Cutler, Moenkopi	None – complete Honaker Trail to Wingate sequence preserved over crest
Earliest sequences deposited over its crest	Moenkopi	Moenkopi or Chinle	Moenkopi	Chinle	Honaker Trail
Salt Welds associated with structure?	Yes – Probably Cutler age welds	Yes – Probably Cutler age welds	Yes – Probably Cutler age welds	Yes - Probably Cutler age welds	No
Interpreted periods of movement	During Honaker Trail and Cutler time	Mainly during Honaker Trail and Cutler time. Also movement in Moenkopi and Chinle time on SW side	Mainly during Honaker Trail and Cutler time. Also movement in Moenkopi and Chinle time on	Honaker Trail, Cutler and Moenkopi	Post Lower Jurassic

Table 3.4. Summary of the constrained timing of salt mobility for each of the salt structures in the study area.

A thickness change in the Chinle Formation across the structure of ~9% was reported by Matthews et al. (2004) (from 103-113 metres). This is not here considered significant as the margin of error on measuring field exposures, particularly while simultaneously logging a sedimentary section is likely to be in this area. Consequently a late-stage phase of salt mobility, possibly contemporaneous with the development of the Moab Fault System is inferred in this part of the basin which is not well constrained by stratigraphic evidence due to erosion of the sequence.

Constraints on salt mobility in the basin

In the Paradox Basin the amount of salt with the potential to become mobile is largely constrained by the original basin morphology. As described in section 3.5 the Pennsylvanian basin showed an exponential decay in subsidence away from the Uncompahgre Front which corresponds to an exponential decrease in the original thickness of the salt sequence. The basin is also constrained by facies changes from the highly mobile saline facies in the foredeep to the immobile basin-margin facies where the equivalents of the supra-salt sequence in the salt basin become effectively coupled. The exact location of this facies change and consequently the outer limits of mobile part of the salt basin are difficult to determine. Figure 3.12 illustrates the margins of the hypersaline facies in the basin to be approximately in the vicinity of the confluence of the Green and Colorado rivers throughout the sequence. This transition is likely to occur in a complex manner with basin margin facies increasingly inter-fingering with salt beds away from the basin. From a salt mobility point of view, however, the point where the proportion of salt in the sequence is low enough to retard salt mobility is likely to be a significant distance basinward of the pinchout of the hypersaline facies.

Gravity data is interpreted as giving a good indication of the location of this point as it is sensitive to the density change associated with salt sequences. As Figure 3.28(a) shows, a significant increase in the gravity field is present 15-20 km SW of the outermost salt structures in the basin illustrated by a change from the green colours typical of the mobile part of the basin to the red colours of the external zone. In the absence of any significant geological changes in this area, this is interpreted as being related to a facies change in the buried Pennsylvanian sequence and consequently represents the outer limits of salt mobility

in the basin. The proximity of this gravity change to the salt structures in the basin suggests there is little or no potential for further salt mobility in the basin.

Initiation of salt mobility in the basin

Although numerous different hypotheses have been proposed to account for the initiation of salt mobility in the basin summarised in section 3.6, the process by which this occurred is far from clearly defined. The interpretation of Doeling, (2002 and 2003) and Doeling et al. (2002) that salt moved as a response to activity on sub-surface faults and exploitation of weaknesses in the overburden, is here considered to be rather ambiguous. This interpretation is difficult to justify according to modern concepts of the initiation of salt mobility (detailed in section 2.2) and the tectonic episode responsible for this proposed sub-salt fault movement is not supported by any other evidence. Hudec (1995) also suggests the influence of a tectonic phase in the initiation of salt mobility in the basin suggesting the Onion Creek salt structure was reactive to extension, again evidence for such an episode is not apparent.

The hypothesis here considered to be best supported by the observations in this study is that salt mobility was initiated by differential sedimentary loading from material shed onto the basin from the Uncompahgre Uplift during the Pennsylvanian and Permian. This is primarily because the main Upper Pennsylvanian-Permian phase of salt mobility recorded by the thickest salt-controlled packages are contemporaneous with this strongly unidirectional depositional system. All regional and local evidence suggests that the Permian was a time of post-orogenic tectonic quiescence in the Colorado Plateau and the development of such significant salt mobility controlled depocentres at this time suggests it was largely independent of tectonism. Further evidence comes from the demonstrated migration of salt mobility away from the Uncompahgre Uplift with time. This indicates that salt mobility ceased first in the areas which were most proximal to the Cutler depositional system despite them being where the salt sequence was thickest. This is interpreted as evidence that the most dramatic salt mobility was proximal to the Cutler system where the sedimentary loads would have been largest.

The system of early proximal salt weld development is also predicted by analogue modelling of progradation over a salt basin published by Ge et al. (1997) as are the growth geometries observed on the SW flank of the Moab-Spanish Valley salt structure, the most distal Permian age salt structure in the basin (Figure 3.84(a)).

Salt structure development – Passive growth or active piercement?

One critical aspect of understanding salt mobility in the basin is concerned with whether it developed through active (or reactive) piercement of its overburden or through passive growth/downbuilding. The presence of Honaker Trail sequences at elevated levels at the margins of the salt structures (section 3.10) is considered to provide substantial evidence that growth occurred in a passive manner. If the salt had actively pierced the supra-salt sequence, then this sequence would be expected to have been truncated at depth. Its presence on the flanks of the salt structures, up to several km above its elevation in intra-salt areas therefore indicates that these areas were passively rotated to these elevations as the salt structure developed through salt being withdrawn from intra-salt areas. Depocentre morphologies and observed growth geometries in the Cutler Formation also strongly support passive growth rather than dynamic piercement.

Role of salt mobility in depocentre development

The reliance of this study upon well data to constrain the large scale depocentre morphology in the basin means that, at best depocentre morphologies can be broadly constrained by conveniently spaced well data (e.g. Courthouse Depocentre (Figure 3.74) and Kings Bottom Depocentre (Figure 3.44)) and at worst, not constrained at all or by single published seismic lines. Consequently the potential to understand the role of salt mobility in depocentre development from this data is limited. Where constrained, depocentres can typically be seen to be strongly asymmetric and in the case of the best constrained Courthouse and Kings Bottom depocentres which are the most distal Cutler age depocentres to the Cutler depositional system, they are observed to have their maximum thickness and therefore greatest subsidence directly adjacent to the salt structures (figures 3.74 and 3.44). This geometry implies that salt was free to move into the salt structure from the area directly adjacent to it and consequently that salt was at or near the surface throughout the depocentres development. The implication of this is that salt mobility was unconstrained by a significant

overburden sequence throughout this period as otherwise the depocentre would record evidence of folding and piercement of the sequence.

Although not constrained by sufficient well data to determine their morphology, depocentres in the NE part of the basin are traversed in published cross sections derived from seismic data shown in figures 3.24and 3.23. Both of these sections display the most proximal Cutler depocentres thickening towards the most proximal salt structure reaching their maximum thickness directly adjacent to the structure. This style of proximal depocentre morphology is notably not predicted by analogue models of progradation onto a salt basin by Ge et al. (1997) which predict maximum withdrawal and complete grounding in the most proximal part of the basin (Figure 3.84). An interpretation proposed here is that this geometry is based on the most proximal part of the Desmoinesian (Paradox equivalent) sequence in the basin consisting of immobile basin margin facies and proximal clastics (as described by Barbeau, 2003). It is here suggested that this has, from a salt tectonics point of view effectively pinned the sequence in the most proximal part of the basin and that this thickening sequence is partially accommodating the flexural bend in the Late Pennsylvanian sequence over this pinned area.

Structural development of the Basin

The Moab Fault system

One of the most puzzling aspects of the development of the study area is the presence of the Moab Fault system as despite its large displacement and extensive length, a driving mechanism for its development is far from apparent. Although estimates for the timing of its development vary (section 3.8), it clearly post-dates the Pennsylvanian to Lower Cretaceous sequence which it juxtaposes giving it a Laramide or post-Laramide age. Outside the Paradox Basin, there has been no documented evidence of a significant extensional phase elsewhere in the central Colorado Plateau at this time which was dominated by compressional tectonics and regional uplift. It seems improbable that many of the mechanisms suggested for the development of faulting in the basin are capable of developing a fault system of the size and structural style of the Moab Fault system. For example, dissolution related collapse and relaxation after compressional shortening would be expected

to develop a complex system of small offset faults with variable dip. The Moab system in contrast, is well organised with strain almost entirely localised on a single, basinward dipping normal fault.

Analysis of the uplift and subsidence associated with the fault system also shows its footwall area to be significantly elevated above the regional level (Figure 3.42(b)). If the fault system were driven by some kind of collapse mechanism, the system would be expected to be dominated by an overall bulk downward movement of sequences rather than dominated by uplift. Perhaps the most compelling evidence against any kind of collapse hypothesis is that the Moab Fault system continues well beyond the Moab-Spanish Valley salt structure with significant displacement continuing across the Blue Hills segment. In order for dissolution collapse to be viable, salt dissolution would be required along its entire length which clearly is not the case in the Blue Hills area where no underlying salt structure is present (Figure 3.45). Similarly a post-Laramide relaxation mechanism requires the structure to be associated with an area structurally elevated by this tectonic phase (i.e. an anticline) whereas no such structure is present in the Blue Hills area. This leaves either bulk tectonic extension of the entire crust (thick-skinned) or extension restricted to the supra-salt sequence and driven by processes restricted to the salt basin (thin-skinned) as the most plausible driving force.

Although the absence of evidence for a Tertiary extensional phase in the central Colorado Plateau outside the basin would seem to rule out regional extensional tectonics, it is here considered that this is a plausible hypothesis. Although largely considered not to have affected the Colorado Plateau, a very significant extensional phase did influence the Basin and Range province to the west and south which was contemporaneous with the broadly constrained Moab Fault system. Much less dramatic, but still significant extension also affected the SE margin of the Colorado Plateau at this time leading to the development of the Rio Grande Rift which suggests that extensional stresses affected a wider area of the western USA area than just the area where extensive Basin and Range faulting is present.

When considered in isolation, the Moab fault system appears to be a very large structure. A maximum of 850 metres of heave is measured across the Moab segment which represents a

fraction of 1% of bulk extension across the entire Colorado Plateau province. A salt basin, by its very nature is an area where strain is likely to localise due to the mechanical weakness of a significant part of the sequence in these areas. Movement of salt into diapiric structures will magnify this weakness and make their overburdens, the areas where the 'minimum work' is required to fracture the supra-salt part of the sequence. Consequently the Paradox Basin salt structures could feasibly allow the localisation of this minor amount of extension onto a small number of large structures. Elsewhere in the Colorado Plateau, this same strain could feasibly be accommodated by a much larger population of small faults or micro-fractures. One possible criticism of this hypothesis could be that the NW-SE oriented Moab fault system is oriented oblique to the dominant N-S trending faults of the Basin and Range. It is notable, however, that experiments by Ge et al. (1996) showed that when extension was applied to modelled salt structures oriented oblique to the direction of extension, fault structures followed the trend of their associated salt structures rather than the extensional system (Figure 6.2).

The final hypothesis considered here is that the fault system developed in the supra-salt layer to accommodate folding of this sequence elsewhere in the basin. Folding of the supra-salt sequence driven by salt mobility is unbalanced by equivalent shortening of the sub-salt layer and as this is effectively pinned at the basin margins, shortening of the layer through folding requires equivalent extension to balance it elsewhere in the layer (see sections 4.9 and 6.1). As described in section 3.8, the supra-salt sequence is folded into a series of salt-cored anticlines and intra-salt synclines. Both these folds and the Moab Fault system influence the entire supra-salt sequence and can be dated as Tertiary in age. It is therefore possible that the two phases of basin development are contemporaneous. This argument hinges on the interpretation of how folds developed. The most widely accepted interpretation (e.g. Doeling et al. (2002) and Doeling (1988, 2002), is that folds were superimposed upon the pre-existing salt structures by Laramide compression. As this would have been thick-skinned, bulk crustal shortening affecting the entire crust, there would be no requirement for it to be balanced by equivalent extension in the supra-salt sequence.

Interpretations where folding is restricted to the supra-salt sequence (e.g. Baars and Stevenson, 1981), developing as a response to salt mobility in contrast do require a

mechanism such as faulting or diapirsim to accommodate this layer restricted shortening. The key to deciding between this and the extensional hypothesis lies in the sub-salt sequence. If crustal shortening in the sub-salt sequence equivalent to that represented by folding in the supra-salt sequence could be demonstrated, this would rule out the fold-driven hypothesis. Alternatively, if equivalent sub-salt extension to that represented in the Moab Fault system could be demonstrated, this would strongly support the extension hypothesis. Unfortunately the data available to this study is insufficient to accurately decide between these.

Crestal graben systems

The crestal graben systems associated with salt structures in the Paradox Basin are clearly a very different structural style to that represented by the Moab Fault system. Most notably they are typically complex zones, consisting of large numbers of small faults, strictly limited to the crestal regions of salt structures. The Moab system in contrast is limited to a small number of well organised, uniformly dipping segments which extend well beyond the limits of the underlying salt structure (Figure 3.45). The leading hypotheses are that these faults are either collapse structures related to dissolution collapse (Doeling, 1988, Doeling et al., 2002, Huntoon, 1988, Oviatt, 1988) or that they are due to the process of diapir fall as a response to regional extension (Ge at al. 1996, Hudec 1995, Boyers 2000, Chauvin, 2001).

Ge et al. (1996) suggest that their analogue modelling (see figure 3.15) strongly supports the extensional hypothesis as this is the only mechanism which re-created similar structures to those found in the basin. This interpretation is, however, strongly questioned due to the nature of the experiments carried out to test the hypothesis. Ge et al. (1996) rule out the dissolution collapse hypothesis as models predict the development of a series of peripheral extensional faults but also a system of inward dipping reverse faults which are not observed associated with any of the salt structures. It is here felt, that they did not accurately model the process of salt dissolution which is likely to have taken place in the Paradox Basin. As Figure 3.15(c) shows, they model dissolution through complete withdrawal of salt sequence. Evidence abounds, however, that upwards of 3km of salt is still present in salt structures in the study area and therefore the actual dissolution would be likely to be a small percentage of the complete removal that they model. It is also felt that bulk salt withdrawal does not

accurately model dissolution. This is because dissolution is here understood as a very localised process with salt depletion and any consequent structural response restricted entirely to the crest of the structure. Bulk salt withdrawal in contrast, assumes the salt to behave in a plastic manner at these timescales and therefore the volume loss in the salt sequence would be spread over the entire salt body influencing a much wider area of overburden.

The observations of this study are considered to strongly support a the hypothesis that faulting was a response to the erosional unroofing of the basin rather than a tectonically driven mechanism. This is based on several lines of evidence. Firstly, the orientations of the crestal fault systems appear to strongly mirror the erosional extent of the supra-salt sequence. For example, the cliffs bounding the surface expression of the Moab-Spanish Valley salt structure are extremely straight and the flanking fault system parallels these NW-SE oriented cliffs rigidly (figures 3.36 and 3.56). Similarly the cliffs bounding the Salt Valley-Cache Valley structure have a more arcuate trend and again the fault system parallels this, particularly on its NE side (Figure 3.32). Also, surface exposures of the Onion Creek salt structure trend approximately E-W and the majority of crestal faults are oriented parallel to this (Figure 3.29). Gravity data (Figure 3.28) in contrast, shows this structure to have a NW-SE trend at depth and consequently it is concluded that the fault systems parallel the exposure rather than the actual salt structure.

Further observations that suggest unroofing/collapse is responsible for the development of crestal faults is concerned with their style. Where individual crestal faults juxtapose sandstones with other sandstones, they can typically be observed to consist of open, uncemented fractures. This is interpreted as evidence that they developed near the surface rather than at depth. Similarly their typically steep fault planes and intensely fractured and bleached hanging wall areas relative to their typically undisturbed footwall areas (see Figure 3.57) are interpreted as evidence for downward collapse of the unsupported hanging walls relative to the supported footwall areas. Hudec (1995) argues against the collapse hypothesis by suggesting there is a space problem associated with crestal faults downfaulting the overburden towards the centre of the salt structure without extension. These observations in contrast, suggest that relative fault motion was dominantly downwards rather than inwards

and as dissolution would primarily create accommodation space below the downthrown area, no space problem is here considered to exist. Consequently, crestal graben systems are here interpreted as being a result of late stage dissolution collapse and erosion driven gravity collapse into the developing salt valleys. Their origin is therefore considered to be completely separate from the development of the Moab Fault system.

The role of salt mobility in the development of the Moab Fault system

The observations detailed in this investigation show that the Moab Fault system is extremely complex displaying significant variability along its length. Stratigraphic relationships illustrate that the fault developed after the main Permian to Lower Triassic phase of salt mobility in the basin and therefore the main sedimentary depocentres and probably the main salt welds had developed prior to its development. Consequently, the Moab-Fault system deformed a salt and supra-salt sequence with substantial inherited heterogeneity including significant variability in the along strike morphology of the associated salt structure. In the southern part of the fault system, the salt structure consists of a steep sided structure with a significant Permian depocentre and probably a salt weld on its SW side (Figure 3.52). In contrast, further north where the Moab Segment offsets the sequence, this has developed into a gentler salt-cored anticline without a major Permian package at its SW flank but with sequences thickening away from the structure to the NE into a depocentre on the SW side of the Salt Valley-Cache Valley structure (Figure 3.44). Further north still, the fault system offsets a supra-salt sequence unrelated to an underlying salt structure (Figure 3.45).

Other inherited factors are also likely to have influenced the development of the fault system. Most notably, salt welds of probable Permian age were developed throughout the majority of the NW half of the study area, retarding salt flow throughout much of the basin. The part of the fault system to the north of the Colorado River is considered to represent the most basinward part of the study area where pre-existing salt welds were not inhibiting salt flow at the time the Moab Fault developed.

Evidence for a significant influence of salt mobility on the development of the fault system comes from the nature of the displacement-length plot of the fault system. As Figure 3.51

shows, at the point where the fault system transfers from the Blue Hills segment to the Moab Segment, the gravity profile shows a significant change corresponding with an increase in the elevation of the underlying salt sequence. This also corresponds with a significant increase in the gradient of the throw profile which continues along the entire length of the Moab segment as the elevation of the underlying salt increases. The much steeper displacement gradient observed in the Moab segment which cuts the crest of the salt structure, relative to the Blue Hills segment where underlying salt is subdued, is considered evidence that the presence of salt has enhanced displacement on the fault. As the cut-off elevation profile in Figure 3.51(a) shows, the increase in the displacement gradient in the Moab segment approximately 15km along its length is coupled with a dramatic increase in the elevation of the footwall cut-off only. The hanging wall cut-off in contrast, maintains a relatively consistent elevation along the entire profile and appears to have remained relatively static throughout the development of the fault system.

Similarly the structure contour map in Figure 3.42 shows the footwall area to the Moab segment to be dramatically elevated from the surrounding area with little evidence of any subsidence in the hanging wall. Consequently the Moab segment is considered to have its displacement almost entirely manifested in footwall uplift. As Figure 3.44 shows, wells constrain upwelled salt as being present beneath the footwall area of the Moab segment and consequently it is interpreted that the movement of salt during faulting is facilitating this footwall uplift. Figure 3.85 illustrates a model for this process which interprets the lack of mobility in the hanging wall to it being effectively pinned by the distal salt weld inferred as being present on the SW side of the Salt Valley-Cache Valley salt structure (Figure 3.74). Movement of the area to the SW of the Moab Fault system, in contrast, is not restricted by a salt weld (Figure 3.44). The footwall is therefore the only side of the fault that can easily move and fault displacement is consequently concentrated on uplift of the footwall relative to the hanging wall and accommodated by the rise of salt beneath it.

The lack of subsidence in the hanging wall indicates that this was not the source of this rising salt and consequently it must have been derived from further beneath the footwall. As Figure 3.85 shows, this requirement for salt withdrawal from the SW to balance uplift of the

footwall therefore provides a mechanism for the development of the Kings Bottom syncline synchronously with the fault system.

Relationship of the Emkay segment to the Moab Fault System

Although exposed within a few tens of metres of each other at the entrance to Arches National Park, the Moab and Emkay segments are interpreted as diverging significantly with distance to the SE (figures 3.27 and 3.36). The Emkay segment can clearly be observed to follow the SW flank of the Moab-Spanish Valley salt structure where it is exposed (Figure 3.36). Slip on the major Moab segment, in contrast, is interpreted as following the NE side of the valley and using the NE margin of the salt structure as a slip surface. Several observations are considered key to understanding the relationship of these structures. Firstly, the footwall slip surface along the entire length of the Emkay segment is observed to be the rolled over bed at the top of the Honaker Trail sequence as described in section 3.10 which is interpreted as having developed prior to the development of the Moab Fault system. Also the amount of displacement on the Emkay segment is around 150m. This is significantly greater than any of the collapse faults flanking the Moab and Spanish Valleys or in the crest of the Moab Anticline and the Moab and Emkay segments are also observed to have the same dip orientation. Two distinct hypotheses have been considered for the development of the Emkay segment which are detailed below.

Hypothesis 1 – The segment significantly post-dates the Moab Segment and developed as a late-stage collapse fault which related to the unroofing of the basin. The pre-existing rolled over bed in the Honaker Trail Formation was locally exploited as a slip surface

Hypothesis 2 – The segment is contemporaneous with the development of the Moab Fault system and is where extensional stresses were originally focused in this area as the system developed. The fault was likely to have originally nucleated on this pre-existing, rolled over Honaker Trail bed as it presented a minimum work slip surface. With the continued development of the fault system, the NE side of the Moab-Spanish Valley salt structure become increasingly important in accommodating strain and the Moab segment developed as

a shortcut fault joining the early Emkay fault with the NE side of the salt structure, upon which all subsequent displacement occurred. This interpretation is illustrated in Figure 3.86.

Invoking collapse for the development of the Emkay segment would be relatively straightforward in areas where exposures flank the salt-cored Moab Valley as sufficient space is present for hanging-wall sequences to collapse into. A significant space problem is, however, considered to exist in the northernmost exposures where the overburden sequences to the salt structure have not yet been removed by erosion and therefore there would be nowhere for sequences to move into. Similarly it is difficult to envisage, in these areas, why collapse would be centred on a newly developed fault, a short distance into the footwall of the Moab segment, which would presumably have provided an efficient slip surface. Hypothesis 2 is therefore, considered to best explain the observed relationships and also explains the relatively low dip of the Moab segment in this area.

Development of folds in the basin

As the major folds in the study area are observed to affect the entire exposed, supra-salt sequence, it is clear that they developed after the main Pennsylvanian-Lower Triassic phase of salt mobility in the basin. Consequently this phase of salt mobility alone cannot be exclusively responsible for their development. It is widely accepted that the major folds in the Paradox Basin were superimposed upon the pre-existing salt structures by Laramide compressional stresses (e.g. Doeling et al. (2002) and Doeling (1988, 2002)). The absence of major folds in areas of the Paradox Basin away from the salt structures, however, either implies that compressional deformation was focused upon the salt structures or that they developed as a response to another process.

Observations of the basin bounding SW flank of the Uncompahgre Uplift suggest that large scale Laramide inversion of the basin did not take place. Although an extensive system of relatively small, Laramide age faults are present on this margin (Heyman, et al. 1986), the Uncompahgre Fault is not observed to penetrate the Upper Triassic and younger sequence at any point and its buried crest is overlain by a very broad fold rather than a prominent monocline typical of Laramide structures in the Colorado Plateau. The NE margin of the

Uncompahgre Uplift, in contrast, is a very distinctive monocline structure which displays the same eastward vergence, typical of Laramide structures in the region. Consequently, the idea that Laramide compressional stresses were efficiently focused on structures on the NE side of the Uncompahgre Uplift, requiring no compressional folding in the Paradox Basin is explored. Baars and Stevenson (1981) have suggested that folds developed due to late stage diapiric uplift on the Paradox Basin salt structures. With the exception of the Cane Creek Anticline, however, all of the salt structures in the basin are inferred to have become at least partially bounded by salt welds prior to the Jurassic, significantly inhibiting salt mobility by the time the folds developed. It is therefore unlikely that there would be the potential for such a phase of halokinesis driven folding throughout much of the basin during this time.

A hypothesis proposed here which has not previously been suggested for the development of folds in the basin is that they developed as a passive response to compaction in the basin. It is notable that the majority of anticlines in the basin are situated above the salt structures and that the synclines are situated above the major salt controlled depocentres. Nuccio and Condon (1996) estimate burial of the top of the Permian sequence (which is generally roughly the same elevation as the top of the salt in diapiric structures) to be in excess of 3km in the Moab area. As the salt structures are made almost entirely of halite which has practically no porosity, the large salt bodies which are typically on the order of ~3km in structural elevation would be expected to experience minimal compaction during burial. The carbonate and clastic sequences present in intra-salt areas in contrast, would be expected to experience extensive compaction and subsequently intra-salt areas would subside significantly relative to the salt structures during burial. This process is considered to be capable of producing many of the folds in the area and is discussed further in sections 5.9 and 6.3. As the basement sequences of the Uncompahgre Uplift would be similarly difficult to compact, this could explain the development of the Sagers Wash Syncline which lies between this and the most proximal salt structures in the basin. The fold which can-not be interpreted as developing in this way is the Cane Creek Anticline as the salt structure is not considered to have developed prior to at least the Middle Jurassic and it is not bounded on both sides by major sedimentary depocentres. The above described interpretation for the development of footwall uplift in the Moab Fault system, requires salt withdrawal from the Kings Bottom Syncline area and this late-stage salt withdrawal at the margins of the zone of salt mobility could feasibly be responsible for the development of folds in this area.

The differential compaction hypothesis is here presented as an alternative to inversion for the development of many folds in the Paradox Basin. It should be stressed, however, that the main conclusion of this section is to show that the major folds in the basin are not the result of late-stage salt mobility. Despite the above discussion, it is considered that sufficient evidence to conclusively prove that either the differential compaction or inversion hypothesis is correct is not present. A very detailed analysis of the compaction history of the basin would be required to do this which is very problematic due to the widespread removal of the overburden. One observation which suggests that inversion was responsible for the development of these folds is that basin scale cross sections show beds in these salt-cored folds to be significantly elevated above the regional level (e.g. Figure 3.33 and Figure 3.34). It is notable however that this is less apparent on the 1:1 scale sections shown in these figures and the reader is reminded that the regional elevation of a surface is also partly a function of compaction.

Development of fractures in the basin

The extensive fracture system observed in Jurassic sandstones in the study area clearly post-dates the main Pennsylvanian-Triassic phase of salt mobility in the basin and its development is therefore related to some later process. Fracture systems are typically oriented parallel to the axis of the salt structures in the study area (Figure 3.59) and frequently show similar orientations to faults present in the sequence. Although typically displaying identical orientations to crestal faults, fractures are generally pervasive throughout the area where salt structures are present and are as abundant in the synclines as they are in the crests of salt structures. Consequently they are not considered to be related to dissolution related crestal collapse or any other fold crest specific process. Fracture orientations do, however, also show a distinctive relationship to the Moab Fault system, particularly in the Mill Canyon linkage zone where fractures locally display a crosshatched pattern with orientations paralleling both the main Blue Hills and Moab segments and the oblique linking segments of the fault system (Figure 3.48). More difficult to explain are the fracture patterns observed on the SW side of the Moab-Spanish Valley salt structure which show a very distinct curvature, which neither parallels the fault trace or the crest of the salt structure.

Any relationships between this fracture pattern and the fault/salt structure system are not immediately apparent from Figure 3.59. Figure 3.87, however, illustrates the fracture system overlain on the Base Middle Jurassic structure contour map shown in Figure 3.42(b). As this maps shows, two major structural highs are shown on the SW side of the Moab-Spanish Valley salt structure where red colours are present. Approximately mid-way between these points, fractures are oriented parallel to the salt structure but with distance towards the structural highs, fracture orientations become increasingly deflected towards the high areas. The north-western structural high is the footwall area of the Moab segment where salt influenced footwall uplift accompanied faulting and the other structural high is also likely to be related to the development of the fault system. Consequently, fracture development is interpreted as having been strongly influenced by the development of the Moab Fault system and as fractures typically display minor extensional offsets, they are considered to be linked to either layer restricted or bulk crustal extension.

Development of Unconformities in the basin

Base Triassic Unconformity

Field observations give strong evidence that the development of this unconformity is strongly linked to salt mobility in the basin. Observations flanking the Castle Valley salt structure show progressively older sequences being truncated below it with distance towards the salt structure on both its NE and SW flanks. With distance away from the salt structure, the angular relationships become increasingly poorly defined and 2km to the NE of the salt structure, no unconformity can be defined in terms of angular or erosional relationships and this contact is interpreted as a correlative conformity in intra-salt areas. In contrast to the Castle Valley area, no unconformity is observed in exposures flanking the Moab-Spanish Valley salt structure despite evidence that salt mobility was very active during Cutler/Moenkopi time with both sequences pinching out onto the flanks of the salt structure. Similarly, only very minor angular relationships are observed associated with the Onion Creek salt structure which clearly illustrates that this was a very localised process, ruling out large-scale erosion of the basin. Consequently, this unconformity is interpreted as being due

to localised salt-mobility, largely restricted to the Castle Valley salt structure elevating Cutler sequences above the regional level.

Intra-Chinle Unconformities

Truncation surfaces within the Chinle Formation have two different associations which are here considered to be related to fundamentally different processes. Firstly there are the small scale truncations typically observed below thick sandstone layers where bedding both above and below the truncated units is parallel described in section 3.9. The second association is the surface which separates the 'X' member of the Lower Chinle sequence from the underlying Lower Chinle members in the Sandy Beach area described in section 3.10. Other than the fact that this surface covers a much greater area (can be traced for ~2.5km in the Sandy Beach exposures), the most significant observation which differentiates these is that in the latter association, bedding in sequences below the truncated units is parallel to that of the truncated units rather than parallel to the beds above the truncation surface.

Truncations separating parts of the Lower Chinle sequence

As Figure 3.71(a) shows, stratigraphic growth within the localised Lower Unit of the Chinle Formation occurs in two different ways. The uppermost, 'X' unit expands into the centre of the package through sedimentary growth being conformable with the Upper Unit above. The lower (I – V) sequences in contrast, are separated from 'X' by a significant erosion surface and become progressively truncated by it until they pinch-out. The erosion surface and the extent of the 'X' unit occupy approximately the same area which suggests that the process which controlled the development of this growth package was also responsible for the development of the erosion surface. A model is proposed, herein whereby the observed relationships develop as a response to continued salt withdrawal throughout the I – X period of deposition which did not continue into the time represented by the Upper Unit. This model is illustrated in Figure 3.88.

This model is considered to successfully account for the observed relationships in this sequence. One implication of this interpretation, however, is that this localised Lower Unit

has more in common with the underlying Moenkopi Formation which it is observed to be entirely conformable with the regionally extensive Chinle Formation.

Small-scale, layer-restricted truncations

Previous interpretations of the development of smaller scale truncation surfaces within the Chinle Formation are largely restricted to the most accessible exposure at the Portal which is shown in Figure 3.63. Doeling (1988) attributes the development of this structure to contemporaneous uplift on the adjacent salt structure. As detailed in section 3.9, several key observations suggest that this is not a satisfactory interpretation. Numerous other truncation surfaces have been identified in the study area which do not show any spatial relationship to the salt structures. They do, however, show a distinct spatial relationship with the presence of thick amalgamated sandstone units such as the Black Ledge Member, the base of which always form the truncating surface. Other key observations are that where the sequence below the truncated unit is exposed, (e.g. figures 3.65(a) and 3.66), bedding within it is seen to be entirely parallel with beds above the truncated unit. This observation illustrates that the process developing these truncations is restricted to a single layer. Salt related uplift can therefore not be responsible for the development of these truncations as this would cause uplift of the entire sequence with all beds below the truncation surface displaying angular relationships. Consequently, a process is required which would account for the observed relationships. Four hypotheses are introduced and briefly discussed below.

Hypothesis 1 – Truncations developed through slumping due to regional tilt, possibly as a result of salt mobility.

Hypothesis 2 – Truncations are primary sedimentary structures caused by lateral accretion of the fluvial depositional system. This has also been proposed by Hazel (1994) and G. Hampson (Pers. Comm., 2005).

Hypothesis 3 – Truncations developed due to large scale de-watering of part of the sequence, possibly due to contemporaneous seismicity

Hypothesis 4 – Truncations developed as soft sediment deformation as a response to loading by the thick overlying sand layers.

Each of these mechanisms satisfy the basic criteria that the causative process must not be directly, spatially associated with salt structures and must be capable of being restricted to a single layer within the sequence. Detailed observations do, however, cast substantial doubt on several of these. The lateral accretion hypothesis is considered the least likely as it is not considered capable of creating the observed bedding discordances which reach up to 90° (Figure 3.66). Similarly it is considered that the heterolithic nature of beds below the truncations with mud/sand interbeds typically being regularly spaced and on the order of 10's of cm in thickness would be unlikely to develop due to lateral accretion in a fluvial system.

The dewatering hypothesis is also cast into doubt as the observed structures do not resemble typical dewatering structures and nowhere is evidence of water escape identified. The slumping hypothesis is considered more feasible but requires movement to have occurred on an extremely small slope (<1°) in order to give the observed parallelism of bedding above and below these units. The only one of these hypotheses which is considered to successfully account for the observed, exclusive relationship of truncation surfaces with thick overlying sand-bodies is Hypothesis 4. This model suggests that large channelised sand-bodies began to develop above a sequence of weak, wet and poorly consolidated sandstones and mudstones developed above a better-consolidated and largely immobile sequence. Under the weight of these overlying sand bodies, the weaker underlying units were then effectively squeezed outwards and their tops truncated and overlain by subsequent deposition. This hypothesis is not without its problems and would require significant extra work to convince even myself. It is, however, considered the model which best accounts for the observed relationships and is therefore the preferred hypothesis in this study. For the purposes of this investigation, these structures are considered to be well enough understood to rule of a direct control of salt mobility on their development.

The role of salt mobility in facies distribution in the basin

Chinle Formation

Although Hazel, (1994) and Matthews et al. (2004) suggest that salt mobility has had a fundamental control upon facies distribution within the Chinle Formation in the study area,

the observations carried out in this study suggest that salt mobility during this time was minimal. The majority of stratigraphic expansion identified within the Chinle Formation is entirely restricted to the localised 'Lower Unit'. Stratigraphic relationships illustrate that this unit predates the regionally extensive Upper Unit and is largely unconformable with it. It is, however, conformable with the underlying Moenkopi Formation which displays significant stratigraphic expansion in the same areas and consequently from a salt-tectonics point of view, the 'Lower Unit' is considered to be more related to the Moenkopi sequence than the 'Upper Unit'. Observations in this study do acknowledge significant facies changes in the Chinle Formation in the study area, particularly with respect to the distribution of the Black Ledge and Petrified Forest members.

When the 'Lower Unit' is excluded, the very limited isopach variations (Figure 3.79(b)) strongly question the occurrence of significant salt mobility at this time. Consequently in this study, caution has been exercised in attributing facies variations in the Chinle Formation to salt mobility.

Cutler Formation

Unlike the Chinle Formation, the salt tectonic controls in the Cutler Formation are unambiguous and this preliminary investigation suggests that salt mobility has had a significant control on facies distribution within this sequence. As introduced in section 3.11, it has been suggested that salt mobility could be inferred to control facies distribution if significant interruptions in the proximal to distal facies transition could be identified in this sequence associated with the salt structures. The observations in this study are interpreted as suggesting such a control, although it should be stressed that this is a preliminary investigation and a significant amount of further work is required to confirm these relationships.

The most proximal logged section in the sequence is Log 1 (Figure 3.62) which consists of extremely coarse-grained alluvial fan sandstones and conglomerates. Although displaying similar coarse facies in the lower part of the log, Log 2 shows the upper 85 metres of the sequence to be dominated by mudstones. Despite its relatively proximal location, this

represents the finest grained Cutler sequence observed anywhere in the study area with much coarser facies observed in far more distal parts of the basin. The Cutler sequence at this location was situated in the depositional lee of the Onion Creek salt structure and it is proposed that a topographic barrier associated with this structure prevented proximal facies from reaching this area. A similar interpretation is also suggested to explain the presence of the thick localised, aeolian sandstone unit on the SW side of the Castle Valley salt structure which is not present on the NE side of the structure. Logs 3 and 4 show sequences to the SW of the Castle Valley salt structure to consist of fine-medium grained aeolian facies which are periodically interbedded with coarser, alluvial fan facies similar to those seen in Log 1. The extremely clean, localised sandstone unit seen on the SW side of Castle Valley and in well 4301930076 (where it reaches 137m in thickness) represents an long period of aeolian deposition without interruption by fluvial deposition. The localisation of this unit on the SW side of the salt structure is interpreted as suggesting that towards the end of Cutler time, this area was in the depositional lee of the Castle Valley salt structure which shielded it from this the coarse grained sediment input from the Uncompahgre Uplift.

3.13 Summary

The development of the Paradox Basin is illustrated in Figure 3.89 and summarised below. As detailed by Barbeau (2003), the Paradox Basin is considered to have developed as a flexural foreland basin in the Pennsylvanian (Desmoinesian). Contemporaneous with basin development was the deposition of the halite dominated Paradox Formation, the main depocentre of which was in the foredeep area of the basin adjacent to the Uncompahgre Uplift (Stage 1). Into the Missourian and Virgillian, deposition changed to the carbonate dominated Honaker Trail Formation. Carbonate deposition in the basin was contemporaneous with alluvial fan deposition at the basin margin with sediments derived from the Uncompahgre highlands (Barbeau, 2003). These sediments provided a differential load onto the salt layer and initiated the mobility of the salt sequence and the early development of salt structures, which in-tern led to the initiation of salt controlled depocentres (Stage 2). Into the Permian, coarse clastic deposition sourced from the Uncompahgre highlands became more widespread throughout the basin. The differential loading associated with this, drove the most dramatic phase of salt mobility in the basin, leading to the development of tall (2-3km high) salt structures, thick Cutler depocentres and locally, the complete removal of the salt sequence (Stage 3). An unconformity which was locally angular around some of the salt-structures then separated the Cutler Formation from the overlying Triassic sequence. Subsequent deposition, largely limited to the Moenkopi Formation and Lower Unit of the Chinle Formation was then centred in depocentres 30-40km from the Uncompahgre Uplift where all of the salt had previously not been withdrawn during the Permian (Stage 4). Subsequent deposition largely blanketed the salt structures and was largely unaffected by the movement of salt which had largely been entirely withdrawn into the salt structures (Stage 5). Extensional stresses then led to the development of the Moab Fault system in the outermost part of the basin where salt had not been completely withdrawn (Stage 6). Faulting was accompanied by salt withdrawing from behind the footwall into the immediate footwall area and uplift of the footwall was the dominant mechanism by which fault displacement was accommodated. Burial led to the compaction of the overburden around the uncompactable salt structures and subsequent regional uplift led to the unroofing of the basin. Erosion of the crests of the salt structures led to the dissolution of the salt at the surface and the subsequent development of crestal collapse grabens in overburden sequences.

4.0 The Southern North Sea

4.1 Introduction

As a consequence of hydrocarbon exploration in the area, an extensive history of salt mobility has been recognised in the Southern North Sea spanning much of the Mesozoic and Tertiary. Extensive faulting is also recognised which can also be constrained as being contemporaneous with salt mobility and spans a similarly long period. This chapter documents and discusses the role of salt mobility in faulting and depocentre development in a large portion of the UK sector of the Southern North Sea. This is done both with the aim of understanding the controls on the long-term development of salt structures in the basin and also to aid the development of generic concepts of fault and depocentre development which are the ultimate aims of this research.

The inclusion of the Southern North Sea study area into this thesis is partly justified based on the long-lived nature of salt mobility in the basin. Various different depocentre styles are identified and their extent varies both spatially and temporally. This allows the way that salt mobility evolves and migrates with time to be investigated in detail and allows the long-term controls on their development to be investigated. The nature of faulting in the basin also makes it a key area in achieving the more generic aims of this study. This is because extensive extensional-style faulting is identified which is not contemporaneous with a regionally recognised extensional phase or balanced by equivalent extension in the sub-salt sequence. Analysis of this apparently thin-skinned faulting is therefore considered to give an extremely important insight into the way that salt mobility can influence faulting.

Further justification for the use of this area is based on the extent and quality of the data available to the study. The concentration of exploration targets in sub-salt reservoirs in the Southern North Sea has meant that well control of the entire sequence including both the sub-salt, and supra-salt sequence is much better than that in other areas of the North Sea. This coupled with the extremely well imaged nature of these relatively shallow salt

structures and basins gives a very high-resolution dataset where concepts can be established with confidence.

4.2 Methodology

Investigations in this chapter are based primarily on interpretation of a large seismic survey, the location of which is shown in figures 4.1 and 4.2. This is full stack, time migrated 3D data with a line spacing of 25 metres. Seismic interpretation was constrained by surface picks from the numerous released wells in the area, the locations of which are shown in Figure 4.2. The main technique employed was analysis of thickness variations and sedimentary growth geometries in supra-salt sedimentary sequences which were used to assess the role of salt mobility in their deposition. Thickness variations were investigated using both isochron maps derived from seismic interpretation as well as measurements from well data in the area. 2D structural restorations of seismic sections also proved extremely useful in understanding the developing morphology of the salt structures. Restorations were carried out using the 2DMove structural restoration software provided by Midland Valley Exploration Ltd. Fault profiles were investigated using displacement-length plots which were depth converted using the method detailed in Appendix 1.

4.3 Location of the study area

The area investigated in this study is located in the UK sector of the Southern North Sea, centred approximately 150km east of the East Yorkshire coast. The study area consists of a 2850km^2 area of 3D seismic coverage spanning areas of UK licensing quads 43, 44, 48 and 49 (Figure 4.1). This is mainly situated in the area informally referred to as the Silverpit Basin, with the SW of the dataset being part of the NW margin of the Sole Pit Trough

4.4 Geological setting – the Southern North Sea

This study is concerned primarily with the UK sector of the Southern North Sea, situated between the Mid-North Sea High and London – Brabant Massif which have been structural highs throughout much of the basins history (Cameron et al., 1992). The basin is bounded to the west by the East Midlands Shelf and continues across the Anglo-Dutch median line towards the Dutch Central Graben to the east. The basin is structurally dominated by the Sole Pit Basin, a NW-SE oriented basin which has been the major depocentre in the UK sector throughout much of the Mesozoic (Stewart and Coward, 1995). To the northwest of the Sole Pit Basin are the Silverpit Basin and Clever Bank High areas where salt-cored anticlines are the dominant structural style. Halokinesis in the basin is concerned primarily with the mobility of Upper Permian Zechstein Group salt facies although thinner Triassic evaporite horizons have locally had a role in accommodating deformation in the basin (Stewart et al., 1996).

Faulting

Although not as pervasive as in the Central Graben, extensive faulting has been documented in the Southern North Sea in both the sub salt and supra-salt sequence. Supra-salt faults typically, sole out into the Zechstein sequence and therefore are effectively decoupled from faulting in the basement (Arthur 1993, Cameron *et al.* 1992, Stewart and Coward, 1995). Fault orientations in the sub-salt sequence show an overwhelming dominance of a NW-SE trend (Figure 4.3) which is considered to have developed prior to the Base Permian (Saalian) Unconformity (Oudmayer and De Jager, 1993) and with the exceptions of the Outer Silverpit Fault, Vale of Pickering/Flamborough Fault Zone and Central Fracture Zones (Figure 4.1) most of the major structures have this same NW-SE orientation (Cameron *et al.* 1992, Jenyon 1988). Despite their decoupled nature, sub-salt and supra-salt faults in many areas are frequently described as being associated with each other. The present day fault pattern observed at sub-salt (pre-Zechstein) levels has had a complex history of fracturing and reactivation spanning various Palaeozoic to Tertiary stress regimes. The still dominant NW-SE trend is thought to have developed in the Late Carboniferous to earliest Permian due to dextral strike-slip deformation in an overall extensional setting (Oudmayer and De Jager, 1993). Faults were subsequently affected by selective reactivation due to Variscan compression, Late Cimmerian rifting, and Late Cretaceous and Tertiary inversion.

Sub-salt faulting is much more pervasive throughout the basin than in the supra-salt package and typically, seismic sections show smaller apparent bed offsets on sub-salt faults than those in the supra-salt sequence. Seismic sections show that sub-salt faults frequently have either normal or reverse throw and fault patterns interpreted as flower structures have been documented (Gibbs, 1986). Fault orientations rarely coincide with regional stress orientations (Oudmayer and De Jager, 1993) and strike-slip/oblique-slip is considered to be the main deformation mechanism in the sub salt sequence (Cameron et al.1992, Oudmayer and De Jager, 1993). Glennie and Boegner (1981) suggest that faults in the Mesozoic section are also strike-slip, although they do not detail any evidence of lateral movement. A study by Arthur (1993), demonstrates that supra-salt faults in blocks 49/28, 48/23 and 48-11 are clearly extensional in style, concluding that although Mesozoic faults are frequently associated with sub-salt structures in terms of location and trend, they are controlled by Mesozoic forces not the inherited structural grain.

Among the main Mesozoic fault systems in the basin (Figure 4.1) are the NW-SE oriented Dowsing Graben System (using the nomenclature from Stewart and Coward, 1995) and Swarte Bank Hinge Zone at the margins of the Sole Pit Basin (Cameron *et al.* 1992). Other major structures are the Outer Silverpit Fault, Flamborough Head Fault and Central Fracture Zones which are oblique to the regional structural trend (Figure 4.1). Another major structure is the North Dogger Fault Zone which, along with the Dowsing Graben System are considered to be major basin bounding structures (Allen *et al.* 1994, Griffiths *et al.* 1995, Stewart and Coward 1995). Stewart and Coward (1995) also document a system of extensional faulting called the Sole Pit High Collapse Zone in the thickest part of the Sole Pit sedimentary wedge.

Basin development

Pre Permian development

Basement rocks in the Southern North Sea are considered to be a continuation of the crystaline Lower Palaeozoic rocks of the London – Brabant Massif (Stewart and Coward, 1995), mildly deformed by Caledonian events and overlain by Devonian and Carboniferous sediments (Cameron *et al.* 1992). These are separated from overlying rocks by the Base Permian (Saalian) Unconformity related to Variscan and Saalian tectonics (Oudmayer and De Jager, 1993). A detailed discussion of the pre-Permian development of the Southern North Sea is beyond the scope of this study. However, both Cameron et al. (1992) and Oudmayer and De Jager, (1993) agree that the dominant NW-SE structural fabric of the basin which is still present in Tertiary structures was established prior to the base of the Permian and Cameron et al., (1992) suggest it may have been inherited from Early Palaeozoic basement trends.

Permian development

The Permian saw the development of two distinct, but interconnected E-W oriented basins across much of NW Europe (Gatliff et al. 1994, Glennie et al., 2003, Jenyon et al., 1984). These are termed the Southern and Northern Permian basins and extend across the present

day Southern North Sea and Central North Sea respectively (Figure 5.4). Although Lower Permian deposition was dominated by sub-aerially deposited clastics which may have been deposited below sea level (Jenyon and Cresswell, 1987), a major marine transgression in the Upper Permian led to the widespread deposition of halite dominated evaporite facies of the Zechstein Group across the basin (Cameron et al., 1992). Five cycles are recognised representing five separate transgressive events when the Permian basins were temporarily connected with the Boreal Ocean to the north (Ziegler, 1982). In contrast to the Northern Permian Basin which has been directly linked to contemporaneous extension (Hodgson et al., 1992), the tectonic controls on subsidence in the Southern Permian Basin are less well understood. Cameron et al., (1992) describe the area as part of the post-orogenic Variscan foreland basin and in their review, Stewart and Clark (1995) suggest thermal subsidence associated with Carboniferous extension to have had a control. Hughes and Davison (1993) suggest that the Zechstein sequence was deposited contemporaneously with a weak extensional phase.

Mesozoic Basin development- Triassic to Lower Cretaceous

Sedimentation continued in the Triassic with a similar depositional style to that observed in Permian (Stewart and Coward, 1995). The Sole Pit Trough became the major depocentre in the basin at this time although with little influence of faulting along the Dowsing or Swarte bank trends (Arthur 1993). The Triassic saw initial onset of mobility of Zechstein Group salt sequences (Hughes and Davison, 1993) and is also the time when the North Dogger Fault Zone began to become active (Allen et al, 1994, Griffiths et al. 1995). Subsidence of the Sole Pit Trough was accentuated in the Jurassic by the development of the Dowsing fault zone to the SW (Cameron et al. 1992, Stewart and Coward, 1995) with the earlier sag induced depocentre developing into a fault bounded basin (Oudemayer and De Jager, 1993). Jurassic tectonics were dominated by thermal doming and extension. The Middle Jurassic saw widespread thermally driven uplift associated with the development of the Central North Sea Dome (Underhill and Partington, 1993, 1994) which developed into the Late Jurassic rift system in which the Central and Viking grabens developed along the axis of the North Sea. Deep seismic studies suggest, however, that the Southern North Sea was not influenced by significant crustal extension in the same way as the rift basins to the NW (Cameron et al., 1992) and Glennie and Boegner (1981) relate enhanced Jurassic subsidence in the Sole Pit area to strike-slip movement on basement faults.

Several other Jurassic extensional basins are also present in the Southern North Sea at similar latitudes to the Sole Pit Basin. These all lie within the Dutch sector and include the Dutch Central Graben, Broad 14's and West Netherlands basins. Consequently a Jurassic rift control is here considered likely to have had a major influence on its development. Middle Jurassic thermal doming led to widespread uplift of the eastern part of the basin resulting in the development of a regional tilt to the west and the development of the major Base Cretaceous (Cimmerian) Unconformity with Triassic and Jurassic stratigraphy becoming progressively less complete beneath it towards the NW (Stewart and Coward, 1995).

Upper Cretaceous and Tertiary

The Upper Cretaceous and Tertiary history of the Southern North Sea is considered to have been dominated by tectonic inversion due to Sub-Hercynian (Oudemayer and De Jager, 1993) and Alpine events. The initial phase of inversion was Late Albian to Late Campanian in age (Walker and Cooper, 1987) and was followed by further pulses in the Early Palaeocene (affecting mainly the Dutch Jurassic Basins) and another in the Mid Tertiary (affecting mainly the Sole Pit Basin, Oudemayer and De Jager, 1993). Inversion of the Sole Pit Basin caused it to develop into a structural high (Stewart and Coward, 1995) and widespread erosion took place developing a major unconformity in many areas (Oudemayer and De Jager, 1993). Although some halokinesis had occurred in the preceding period which was limited in spatial extent, the Tertiary was also the main phase of salt mobility in the basin. This period saw the extensive development of salt structures in the central part of basin (Stewart and Coward, 1995), particularly the un-inverted Silverpit Basin area. Salt structures in this area typically consist of shallow-sided salt pillows underlying the crests of buckle folds in the Triassic to Cretaceous sequence. These have an overall NW-SE structural trend (Figure 4.4), parallel to the sub-salt fault trend and Figure 4.5 shows a seismic section illustrating their style.

Regional Stratigraphy

Sedimentary deposition in the Southern North Sea spans the Devonian to Pleistocene. Sub-salt stratigraphy is, however, largely irrelevant to this study and consequently only the post

Carboniferous sequence is described. The post Carboniferous stratigraphy of the Southern North Sea is summarised in Figure 4.6 and the lithostratigraphic units are briefly described below.

Permian

Uppermost sub-salt deposits in the Southern North Sea are part of the Rotliegend Group. In the SW of the basin these consist of the fluvio-aeolian Leman Sandstone Formation which pinches out towards the NW, approximately along the NW margin of the Sole Pit Trough. In the northwest of the basin (including the study area) the Lower Permian is composed almost entirely of the Sabkha and Lacustrine silty claystones and minor evaporites of the Silverpit Formation (Cameron et al., 2005).

Upper Permian deposition consisted of the evaporite dominated facies of the Zechstein Group which are estimated prior to halokinesis to have been in excess of 1 km thick in the centre of the basin (Cameron et al., 1992). Hughes and Davison (1993) give estimated original depositional Zechstein thicknesses of around 1300m at around 54°N decreasing to 470m around 55°N. The overall trend is for thicker Halite dominated sequences in the basin centre and thinner carbonates and anhydrites at the basin margins. Basin margin facies grade laterally into terrestrial sandstone and siltstone facies into the onshore area. Although locally variable, Zechstein Group deposits are divided into 5 groups related to basin-wide transgressive events (Cameron et al., 1992). Each cycle shows an upward facies variation representing increasing restriction of the basin.

Triassic

Following the final Upper Permian marine transgression, continental deposition which was previously restricted to the basins western and southern margins became established across the entire basin in the early Triassic (Cameron et al., 1992). The Lower Triassic Bacton Group consists of fluvial mudstones and sandstones deposited in an arid environment (Cameron et al., 1992). The overlying Middle and Upper Triassic Haisborough Group consists of various mudstones punctuated by frequent dolomite, anhydrite and halite intervals. From a structural point of view, the most significant Triassic halite interval is the

Main Röt member of the Dowsing Dolomitic Formation which is typically on the order of 60-100m in thickness (Cameron et al., 1992) and lies near the base of the Haisborough Group.

Jurassic

Jurassic deposits in the Southern North Sea are dominantly marine facies and consist of the Lower Jurassic Lias Group, Middle Jurassic West Sole Group and Upper Jurassic Humber Group. Considerable facies variation occurs in these deposits but the Lias Group is largely mudstone dominated and the West Sole Group largely sandstone dominated. Both the West Sole and Humber groups contain significant carbonate formations, including the Corralian Limestone Formation (Cameron et al., 1992) which is a major seismic marker in the basin (Arthur, 1993). Jurassic deposition ends with the organic-rich Kimmeridge Clay Formation which extends over much of the North Sea.

Cretaceous

Fully marine conditions continued into the Cretaceous with deposition of the mudstones, shales and sandstones of the Cromer Knoll Group (Lower Cretaceous). These were deposited in a basin which extended from the Southern North Sea to the Viking Graben and into the developing Atlantic (Cameron et al., 1992). A substantial Albian transgression (Haq et al. 1987) flooded the previous terrigenous source areas and the pelagic carbonates of the Chalk Group dominated deposition on the continental shelves through the rest of the Cretaceous (Cameron et al., 1992).

Tertiary

Cretaceous carbonate deposition continued into the Early Palaeocene (Danian) and ceased as Palaeocene uplift of the British Isles developed (Cameron et al., 1992). The North Sea had a basin morphology similar to its current configuration throughout most of the Tertiary and the Tertiary section consists of the various marine clays, sands and siltstones of the North Sea Group. A major regional unconformity related to a eustatic sea level fall at the end of the Oligocene led to the development of a major unconformity. Consequently, Late Oligocene and Early Miocene deposits are largely absent in the basin (Cameron et al., 1992).

4.5 Previous work

Halokinesis in the Southern North Sea

Halokinesis in the Southern North Sea is thought to have initiated in the Mid Triassic (Brunstrum and Walmsley, 1969), initially developing only on the margins of the Sole Pit Trough and then becoming more widespread in the Jurassic as erosion associated with the major Late Cimmerian unconformity thinned the overburden (Glennie and Underhill, 1998). Various salt structure styles have been described in the UK sector of the Southern North Sea although only a very small number of large salt diapirs which pierce the overburden are identified (Jenyon and Cresswell, 1987). Jenyon and Cresswell describe these as being typically restricted to the to basin margins and associated with sub-salt faults. By far the most numerous salt structures in the basin are the shallow-sided, non-piercing salt-cored buckle folds which are illustrated in figures 4.4 and 4.5. Hughes and Davison (1993) describe these as having typical wavelengths of 3-17km, with wavelengths increasing to the SW as the original salt thickness increases. Hughes and Davison (1993) detail their development as being mainly during the Tertiary (primarily Eocene-Oligocene) although they recognise a very minor stage of growth in the Lower Triassic, restricted to the northern part of the basin.

Several workers, including Griffiths et al. (1995) and Jenyon and Cresswell (1987) suggest a significant influence of sub-salt fault reactivation on salt mobility. Hughes and Davison (1993) however, note the absence of any correlation between the location of salt structures and suggest that inversion may have had a role in the development of the salt structures. Stewart and Coward (1995) in contrast, suggest that salt mobility is a passive response to gravity driven buckle-fold formation associated with tectonic tilt of the basin and link diapir development with intrusion into the crests of these folds. Stewart and Cowards model is described in more detail below.

Supra-salt fault development in the Southern North Sea

Cameron et al. (1992) describe numerous supra-salt fault systems in the Southern North Sea, largely attributing them to basement controlled strike-slip faulting. Many of these structures developed synchronously with basin-wide halokinesis although with the notable exceptions of Griffiths et al. (1995) and Stewart and Coward, (1995) little attempt has been made to understand the relationship between salt mobility and faulting. Most of this previous work has concentrated on the development of the major basin margin fault systems such as the Dowsing Graben System and North Dogger Fault Zones. Although described by Cameron et al. (1992) as a Jurassic extensional graben systems, Griffiths et al. (1995) propose a hypothesis whereby their development is related to halokinesis. Their model suggests extensional structures developed at the edge of the mobile Zechstein sequence to accommodate overall horizontal shortening of the supra-salt sequence as salt cored anticlines developed in the centre of the basin. Stewart and Coward (1995) propose a similar origin for the fault system detailed below. Stewart et al. (1996) detail the role of salt layers within the Triassic sequence in the development of the Jurassic faulting in the Flamborough Head area in the west of the basin. They describe detachments occurring on several Triassic evaporite layers with fault displacements occurring along complex ramp-flat style fault geometries.

Integrated structural and halokinetic development of the Southern North Sea Basin

Stewart and Coward (1995) provide the most thorough investigation of salt tectonics in the Southern North Sea and propose a regional model to explain both the structural and salt-tectonic development of the basin. This model is described in two parts reflecting two distinct periods of tectonics and halokinesis.

Permian to Early Cretaceous basin model

Like Griffiths et al. (1995) and Allen et al. (1994), Stewart and Coward (1995) consider the supra-salt Dowsing Graben System and North Dogger Fault Zones to be situated at the edge of the mobile part of the Zechstein evaporite basin. They propose a gravity driven model whereby the areas basinward of the fault systems have slid under a tectonically induced slope towards the centre of the basin (Figure 4.7). They suggest a combination of tectonic

subsidence across the sub-salt Dowsing fault zone and rift flank uplift due to Jurassic rifting and thermal doming as being responsible for the generation of this slope. This model is schematically summarised in Figure 4.8(a). Supra-salt extensional-style faulting in the peripheral graben systems is considered to lie in the vicinity of the facies change in the Zechstein Group from the highly mobile halite sequences dominant in the basin to the much less mobile carbonates which effectively pin the margins of the salt basin. These faults are likened to bergschrunds at the upslope limit of ice glaciers being due to the tensions between the mobile down-slope part of the overburden and the pinned up-slope area.

The above described model is analogous to models proposed for the development of extensional systems at passive margins (e.g. Wu et al., 1990, Demercian et al., 1993 and Duval et al., 1992) except that unlike in these areas, overburden in the Southern North Sea is ultimately constrained and unable to slip indefinitely (Stewart and Coward, 1995). Consequently, in this model, up-slope extension is balanced by down-slope contraction which is manifested in a series of asymmetric salt cored buckle folds in central parts of the basin, the tops of which are largely removed by erosion associated with the Late Cimmerian Unconformity. This model considers salt mobility to play a passive part in this process with salt structures effectively moulding around deformation in the overburden.

Late Cretaceous to Tertiary basin model

In the second part of their model (illustrated schematically in Figure 4.8(b)), Stewart and Coward (1995) invoke tectonic inversion as the main tectonic control in the Late Cretaceous and Tertiary. As well as inversion of individual fault structures (such as the Dowsing fault zone and Flamborough head fault) and the development of extensive salt-cored buckle folding, this manifested itself in a reversal of the previous regional tilt which was towards the SW in the Jurassic. The model suggests that inversion of the basement meant widespread uplift of the Sole Pit Trough. This then led to gravity spreading of the post salt section causing extensional-style faulting in the thickest part of the wedge (i.e. the Sole Pit High collapse zone) and amplification of the buckle folds down-slope (Figure 4.8(b)).

4.6 The study area

Stratigraphy

The stratigraphy of the study area is largely as described for the whole basin in section 4.4. More specific aspects of the local stratigraphy relevant to this study are described below. The stratigraphic development of the study area is also summarised in Figure 4.9. Maximum depths of burial for Carboniferous sequences in the basin are estimated by Bulat and Stoker (1987) to be 3-4 km in un-inverted areas such as the Clever Bank High and 4-5 km in the Sole Pit area. Depths to the Top Carboniferous in the largely un-inverted study area are typically on the order of 3.6km and therefore with the exception of erosion at Base Cretaceous level, the succession is largely considered to be complete.

Tertiary

Tertiary sequences are largely undifferentiated within wells in the study area. 49/1-3 is the only well in the study area to thoroughly differentiate the North Sea Group and records a thick (1712m) and almost complete Tertiary section. This includes a 183m thickness of Late Oligocene – Early Miocene sequence which is significant as a sediments of this age are largely absent in the Southern North Sea where a regional unconformity due to a major eustatic sea level fall during this time marks this time period (Cameron et al. 1992). Wells in the study area record the North Sea group to be composed almost entirely of marine mudstones and siltstones with infrequent sandstone layers. The thick (262m) Pliocene sequence recorded in 49/1-3 is, however, almost entirely composed of sandstone which is frequently glauconitic and contains abundant marine fauna. A 75m thick Pliocene sequence of similar lithology is also recorded in 49/1-4.

Mesozoic

Chalk deposits in the area are entirely Upper Cretaceous in age. Compared to the thick Chalk Group which reaches 906m thickness in 48/10b-5, wells show Lower Cretaceous deposits of the Cromer Knoll Group to be typically very thin (12-25m). Well penetrations of Jurassic sequences in the study area record only the Lower Jurassic Lias Group. A major angular

unconformity (Cimmerian Unconformity) is, however, clearly resolvable on seismic data and in some areas, erosion of the Jurassic is frequently less than where well penetrations exist so the presence of younger Jurassic sequences in the are is not ruled out. As well as numerous anhydrite and dolomite units, the Mid-Upper Triassic Haisborough Group in the area contains 3 halite layers of significant thickness. These are the Keuper, Muschelkalk and Röt halite members and each is around 70m thick in the study area. The Röt Halite is effectively the base of the Haisborough Group and the underlying Bacton Group consists of relatively uniform thicknesses of the Bunter sand and shale formations.

Palaeozoic

In the study area, the Zechstein Group deposits are dominated by anhydrite, dolomite and limestone facies in the areas between the major salt structures. In the diapiric structures, wells record an overwhelming dominance of halite. The Zechstein Group sequence is around 90% halite in well 49/1-1 and around 98% in upper two thirds of the penetrated salt diapir. In the study area, the Zechstein sequence is sub-cropped by the Permian Silverpit Formation. Hughes and Davison (1993) estimate the original salt thickness in the area to be around 1300 metres. This estimate is based on parallel NE-SW oriented 2D seismic lines and no account has been made for salt flowing in or out of these sections. As part of this study a three-dimensional restoration of the original salt thickness has been carried out using 3DMove structural restoration software. This restoration takes into account lateral movements and estimates an original salt thickness of 986m. A full description of this restoration and the assumptions and limitations associated with it are described in Appendix 2.

4.7 Structural geology

Sub-salt structure

The base salt, Top Rotliegend reflector is shown from well and seismic data to have a relatively uniform depth (approximately 3.6km below mean sea level) and time depth (approximately 2.4 seconds two-way travel time) throughout the study area and its surface is generally largely parallel to the seabed. Major fluctuations in the travel time to this horizon occur below the major salt structures which are interpreted as velocity pull-up effects associated with the rapid seismic velocity of the salt relative to surrounding successions. These effects have largely obscured the sub-salt imaging in much of the SW half of the study area where no sub-salt faults can be interpreted with confidence at Top Rotliegend level (Figure 4.10(a)). A suitable interpretation has, however, been carried out in the NE half of the survey area which is shown in Figure 4.10(a). As Figure 4.10(a) shows, the sub salt structural trend is entirely NW-SE in orientation showing none of the minor oblique trends reported in other areas of the Southern North Sea (e.g. Cameron et al. 2005, Oudmayer and De Jager, 1993).

Sub-salt faults typically have relatively small vertical displacements generally not in excess of 75 milliseconds. Figure 4.11 illustrates a seismic section through the NE of the study area showing the typical sub-salt structural styles imaged in the study area. As Figure 4.11 shows, sub-salt fault styles show both normal and reverse apparent fault displacements. Faults are frequently clustered in groups which dip towards a central area and could reasonably be interpreted as flower structures. In agreement with Oudmayer and De Jager (1993), the small amount of displacement on these faults coupled with their varying slip style is interpreted as evidence that strike-slip/oblique-slip deformation is dominant in the sub-salt sequence. As Figure 4.11 shows, all sub salt faults are observed being truncated at the base of the Zechstein Group sequence and no relationships have been identified between sub-salt structures and those in the supra-salt sequence within the study area.

Salt structures

Several salt structure styles are present in the study area ranging from sheer sided salt diapirs which penetrate their overburden to gentle, non–penetrating salt-cored anticlines. Figure 4.12 shows an isochron map of the Zechstein Group succession upon which the individual salt structures described below are labelled. Salt structures are also shown as a 3D view in Figure 4.13 which illustrates more clearly their varying morphology. As figure 4.12 shows, most salt structures have a dominant NW-SE trend with their axes typically parallel to the sub-salt fault trend. Each of the nine individual salt structures are described in the following section and an attempt has been made to classify them according to their morphology, relationship to surrounding rocks and timing. Each diapir is given a maximum structural elevation in two way travel time (TWTT) and also and an estimate of its actual height in metres. This estimate is derived from the measured one way time thickness multiplied by the mean velocity of the Zechstein Group in diapir penetrating wells (4543m/sec).

S_1 - S_1 is a tall, sheer sided diapiric structure with a maximum 1370msec (~3110m) of structural relief. It is an elongate structure which is up to 6km wide at least 22km long with both lateral tips lying outside the survey area. The structure has an overall NNW-SSE trend with a substantial kink at its southern end corresponding with a dip in the elevation of the top of the salt. As figure 4.14(a) shows, the margins of the structure truncate bedding in Triassic, Jurassic and Cretaceous sequences at high angles. Tertiary sequences in contrast, show less truncation, thinning significantly over the diapirs crest. From structural and stratigraphic relationships, the structure is interpreted as having developed as a salt cored anticline in the mid to late Jurassic with a pillow to diapir transition occurring in the Cretaceous. A seismic sections through this structure is shown in 4.14(a).

S_2 – S_2 is another sheer sided diapiric structure with up to 1700msec (~3860m) of structural relief. It is an elongate structure which is 10km in length and 1.5-2km in width. Like S_1, it truncates the Triassic to Cretaceous sequence at a high angle and the Tertiary sequence thins over its crest. A seismic section through this structure is illustrated in figures 4.15 and 4.16(a).

S_3 – S_3 is a salt-cored dome structure with 730msec (~1660m) of structural relief (approximately 1660 metres) and does not penetrate its overburden. Although much of the structure clearly lies outside the survey area, from the part that is imaged, it is assumed to have an elliptical shape with a NW-SE trend to its long axis. Jurassic sediments get thinner towards the structure and are progressively truncated by the Base Cretaceous Unconformity. Consequently the structure is interpreted as having developed between the Mid Jurassic and Lower Cretaceous. This salt structure is illustrated in Figure 4.17.

S_4 – S_4 is a tall, elongate diapiric structure with 1440msec (~3270m) of structural relief and a NW-SE oriented long axis. It is approximately 1.5km wide and continues for 9km within survey area, continuing to the SW outside its boundaries. The structure truncates Triassic and Jurassic growth sequences on its SW margin. On this SW margin, a Cretaceous growth sequence thins towards the structure without any truncation (Figure 4.17). On its NE side, however, the Cretaceous sequence is truncated at a high angle by the salt structure. The structure is interpreted as having initially developed in the footwall to a fault controlled growth sequence in the Triassic and Jurassic with subsequent modification occurring in the Cretaceous and Tertiary.

S_5 – S_5 is the most complex of the salt structures in the study area and its morphology is shown in a seismic section in Figure 4.14(b). It is situated approximately 6km along strike from the NW margin of S_2 and has a structural elevation of 470msec (~1070m). It is approximately 10km long and has a NE-SW trending long axis. Unlike the other salt structures in the area which have the top of the Rotliegend Group at their base, this structure has the top of the Lower Triassic Bacton Group at its base implying a complex process of detachment has occurred on the Röt halite horizon. The salt body is overlain by highly disturbed deposits interpreted as being of the Haisborough Group. No Jurassic sediments are present on the structures crest or NE side although the structure truncates a thick Jurassic growth sequence on its SW side (Figure 4.14(b)). The structure is interpreted as having developed in the footwall to a Jurassic growth fault and been further modified by subsequent Cretaceous and Tertiary salt mobility. The structure is also associated with a NW-SE oriented, NE dipping normal fault located in its crest. This fault cuts through the entire

preserved Tertiary section and meets the NE margin of the salt structure at its base. This structure is also illustrated in figures 4.18(a) and 4.16(a).

S_6 – S_6 is a dome-shaped, salt-cored anticline which is almost circular but slightly elliptical in shape with a NW-SE oriented axial trace and 1050msec (~2385m) of structural relief. Jurassic and Triassic sequences become progressively eroded/truncated onto its SW flank and are not present on NE side. It is interpreted as having developed during the mid-late Jurassic with its development continuing through the Cretaceous and Tertiary. This salt structure is illustrated in Figure 4.19.

S_7 – S_7 is another dome-shaped, salt-cored anticline with elliptical but nearly circular contour patterns. In contrast with S_6 its axial trace has a NE-SW orientation parallel to the axis of the adjacent salt withdrawal syncline which separates it form S_8. The structure does not penetrate its overburden and has a structural relief of 1230msec (~2790m). This structure is shown in Figure 4.19.

S_8 – S_8 is a dome-shaped, salt-cored anticline which does not penetrate its overburden and displays circular structure contour patterns. It has 740 milliseconds (approximately 1680m) of structural relief and along with S_7 forms part of a pair of similar structures which are separated by the main Tertiary salt withdrawal depocentre (section 4.8) Based on growth geometries in this depocentre, structures are interpreted as having initiated in the Mid Eocene with development continuing into the Pliocene.

S_9 – S_9 is another tall, elongate diapiric structure having up to 1660msec (~3770m) of structural relief. It has a NW-SE orientation and continues for around 20km as a diapiric structure of approximately 2km in width. Beyond this, the elevation of the top of the salt drops significantly and its margins develop into a faulted salt-cored anticline with the same orientation. This changing morphology along strike can be seen from Figure 4.13 and also by comparing parts (a) and (b) of Figure 4.20. This structure continues as a non-penetrating salt-cored anticline for a further 8km to the NW of the steep sided part and for at least 2km to the SE where it meets the edge of the seismic survey. Despite being a diapiric structure which penetrates its overburden for much of its length, the style of this salt structure is very

different to that of the S_1 and S_2 structures. Unlike the S_1 and S_2 structures, this structure does not truncate the Triassic sequence at a high angles as is seen in Figure 4.14(a), instead these sequences are folded up in towards the structure with beds lying parallel to the base of the salt (Figure 4.20(b)).

The angle of the diapir sides in this lower area are therefore limited to the flexural potential of folding of these beds and consequently this isn't a sheer sided structure for its entire length. As Figure 4.20(b) shows the salt has a steady increase in height from its flanking salt welds to around 1.1 seconds TWTT. It then becomes a steep sided diapir above this level. Growth sequences in the Chalk Group suggest the structure initiated in the Cretaceous as a salt-cored anticline and continued to grow though fold amplification and then subsequently developed into a diapir penetrating its overburden in the Tertiary.

The salt structures described above have been grouped into 4 different types according to various characteristics. These groups are detailed below.

Type 1

- Steep sided diapirs truncating the Triassic and Jurassic section at high angles (S_1 and S_2) and with growth geometries in the Cretaceous and Tertiary sequences.

Type 2

- Diapirs flanked by Triassic/Jurassic growth packages on one side and with no evidence for sedimentary growth or Jurassic sequences preserved on the opposite side (S_4 and S_5).

Type 3

- Diapirs which are steep sided in their upper areas with gentler dipping margins in the lower area with Triassic beds folded up towards the salt structure rather than truncated by it (S_9).

Type 4

- Dome shaped salt-cored antclines which fold and do not penetrate their overburden. Structures typically have elliptical but near circular structure contour patterns (S_3 S_6, S_7 and S_8).

Supra salt faulting

Numerous faults have been identified in the supra-salt sequence within the study area, displaying several different styles. The location of the main supra-salt faults are shown in Figure 4.10(b) and four distinct styles have been identified. Figure 4.17 shows a seismic section which illustrates each of these styles which are described below.

Reverse faults

Faults with a reverse sense of displacement are interpreted as being present in the highly disturbed area between the S_9 salt structure and the along strike trend which consists of the S_5, S_4 and S_2 structures (Figure 4.17). Faults are typically relatively small in throw with vertical offsets of <50 msec. Although displacements are entirely within Triassic sequences, the faulted topography is not planed flat by the Base Cretaceous Unconformity and movement is therefore considered to post-date this surface. Minor growth geometries have also been identified in the lower parts of the Chalk Group (Figure 4.17) and a Cretaceous age of movement is therefore implied. Reverse faults are oriented parallel to the NW-SE trend of the salt structures and all are observed verging towards the NE. These structures are situated in a zone of high structural complexity and poor data quality has made mapping them in 3D difficult. The trends of some of these faults are shown in Figure 4.10(b)

Large normal faults in the crests of salt structures

Two large normal faults are found within the study area, both of which are associated with salt structures and penetrate most of the supra-salt sequence. These structures are shown in Figure 4.16(a) and are here named the Schooner NE and Schooner SW faults. Faulting described here should not be confused with faulting associated with the nearby Schooner hydrocarbon field which is associated with sub-salt structures (Moscariello, 2003)

Schooner NE Fault system

This fault structure is associated with the S_9 salt structure exhibiting the same NW-SE orientation and with displacements occurring along the structures crest. Displacement develops initially as a SE dipping normal fault at the NW end of the S_9 salt structure. At this

point the morphology of the salt structure is of a gentle salt-cored anticline with the fault located in the structures crest. Figure 4.21 shows a plot of the elevation of the faults footwall and hanging wall cut-off elevations as well as the maximum elevation of the top of the salt between the two cut-offs along the fault/salt-diapir system. As Figure 4.21(a) shows, displacement along this fault structure increases progressively towards the SE for approximately 8km. This increase in displacement is coupled with a progressive increase in the elevation of the underlying salt and also a progressive increase in the dip of the limbs of the salt-cored anticline.

8km along the structure, a significant change occurs and as Figure 4.21(a) illustrates, a dramatic increase in the elevation of the top of the salt occurs. This change in the elevation of the top of the salt can also be seen in Figure 4.13 and illustrates a significant change in the style of the S_9 salt structure from being a gentle faulted salt-cored anticline (Figure 4.20 (a)) to being a steep sided diapiric structure (Figure 20(b)). Where this transition occurs, bed displacement ceases to occur across a dip-slip normal fault plane (Figure 20(a)) and transfers to become displacement across the diapiric salt wall (Figure 20(b)). The fault has its maximum displacement (625msec at Top Chalk level) 2km to the NW of where this transition occurs. Away from the fault, significant bed displacement continues to occur across the diapiric salt wall for its entire 20 km length. 20km to the SE, the elevation of the top of the salt rapidly drops again and the style of deformation changes back to being a faulted salt-cored anticline in a similar way to that seen at the NW margin of the diapir. Again, deformation occurs on a NW-SE oriented, SW dipping normal fault which decreases in displacement with distance from the diapir. This decrease in displacement is also coupled with a decrease in the elevation of the salt and the dip of the limbs of the salt-cored anticline mirroring the style seen at the NW end of the salt structure.

The SE tip of the fault system lies beyond the margins of the survey area although this trend is expected to continue to the SE in a similar manner to that seen in the NW of the structure. Figure 4.21(b) illustrates a displacement-length profile along the Schooner NE fault/salt diapir system. In the area where displacements are occurring across the diapiric salt wall, the footwall equivalent NE side is interpreted as having been influenced by a degree of erosion resulting in a flat top to the profile in its central area (Figure 4.21 (a)). Therefore in this

central area, Figure 4.21(a) is inferred as recording an underestimate in the elevation of the footwall equivalent. Consequently an underestimate in the overall vertical separation of beds illustrated in Figure 4.21(b) is also implied. Despite this, structural restorations show that this erosion is minimal and the overall trend shown by the profile is considered to be representative of the true displacement on the structure. As Figure 4.21(b) shows, the trend is for displacement to decrease significantly where a transition in the styles of bed separation from displacement across a normal fault to displacement across the diapiric salt wall occurs.

The fault offsets the entire post-salt section to the level where the data becomes complicated by sea bed multiples (around 200 milliseconds) and was clearly active in the Tertiary. Growth structures in Cretaceous sequences flanking the salt structures suggest that it was an unfaulted salt-cored anticline at this time. Consequently the fault is considered to be entirely Tertiary in age and therefore not contemporaneous with the Jurassic and Triassic episodes of crustal extension in the basin.

Schooner SW Fault System

This fault system is located in the crest of the S_5 salt structure (Figure 4.16(a) and shares the WNW-ESE orientation of the underlying salt body. The fault has a NE dip which is of the opposite orientation to the Schooner NE Fault System which faces it. The fault is 9.5 km in length and offsets the Top Chalk horizon by a maximum of 128msec, significantly less than that of the Schooner NE Fault System. The hanging wall of this fault overlies a growth sequence associated with an earlier Jurassic growth fault (described below) which had ceased to by active at the time the Schooner SW fault developed. It is notable that despite their similar location, the orientation of the Schooner SW fault has the opposite polarity to that inferred for the underlying growth fault and no reactivation is implied. The fault offsets the entire sequence from the top of the Bacton Group (Lower Triassic) to the top of the preserved Tertiary succession. The fault does not, however, penetrate the Lower Triassic sequence and is interpreted as being detached on a decolement horizon in the lower Haisborough Group (likely to be the Röt halite).

The fault is interpreted as having been active in the Tertiary based on observed stratigraphic relationships and although a major Cretaceous depocentre exists in the hanging wall area, growth geometries within this sequence suggest this was not fault controlled. Despite having a similar age and orientation to the Schooner NE Fault System, the style of faulting is very different. This structure does not see displacement transferring from a fault to a salt structure, nor is it associated with a pre-existing salt-cored anticline.

Growth faulting

Significant growth sequences are seen on the SW sides of both the S_4 and S_5 salt structures with the former displaying growth geometries in the Jurassic sequence (Figure 4.14(b)) and the latter displaying sedimentary growth in both Jurassic and Triassic sequences (Figure 4.17). In both examples, packages thicken towards the NE where they are truncated against the S_4 and S_5 salt structures. Growth sequences are entirely restricted to the Triassic and Jurassic sequences. On the SW flank of the S_5 salt structure, the growth sequence is underlain by a Triassic sequence which has undergone complex ramp-flat style deformation (Figure 4.18). On the opposite side of the related salt structures, no Jurassic sediments are present and no evidence of any sedimentary growth is observed in the Triassic sequences. This morphology matches the definition of a 'salt-roller' given by Jackson (1995) as described in section 2.4. Consequently, these structures are interpreted as having developed as salt-roller style growth faults with substantial salt withdrawal from the hanging wall area resulting in the development of a thick growth package, while significant thicknesses of salt still existed in the footwall area.

The amount of offset on these faults is difficult to assess due to a combination of the erosion of the upper part of the growth sequence and the extensive subsequent subsidence of the footwall area during the development of the Schooner SW fault in the Tertiary. These factors have combined to remove any reliable datum surface by which to constrain the amount of Jurassic fault displacement .

Small-scale normal faults

A population of small normal faults are present at the SE extreme of the study area. Their locations are shown in Figure 4.10(b) and a seismic section illustrating their style is shown in Figure 4.17. Faults have a NW-SE trend and generally have an offset of <50 milliseconds. Faults dip to both the NE and SW although the NW dipping trend is dominant. These faults dissect the entire Middle Triassic to Jurassic sequence but are truncated by the Base Cretaceous Unconformity at their top and sole out near the base of the Haisborough Group. Well penetrations are absent in the area where these faults are present but this lower termination is interpreted as being on the Röt halite horizon near the base of the Haisborough Group. These structures are particularly common on the NE flank of the S_3 salt structure (Figure 4.17) and are interpreted as having developed in the Jurassic due to gravity induced faulting on a Jurassic slope.

4.8 Salt controlled depocentres

Since the end of Zechstein Group deposition, up to 3.5 km (post compaction) of sedimentation has occurred in basins bounded by the previously described salt structures. Reflector geometries within much of the post salt sequence display extensive evidence of sedimentary growth related to these structures and salt mobility can be seen to have locally in one area or another controlled deposition in almost the entire post salt sequence. The morphology of depocentres and their relationships with salt structures varies significantly through time and space in the study area and the individual depocentres are described in the following sections according to their age.

Triassic

Although the isochron map (Figure 4.22) clearly shows significant thickness variations do occur in the Triassic sequence, throughout the majority of the area, reflectors within this sequence are entirely parallel and thickness variations are clearly the result of variable amounts of erosion at the Base Cretaceous Unconformity. The exception to this is a Triassic package (Tr_1) which displays sedimentary growth towards the north onto the SW side of the S_4 salt structure (Figure 4.17) covering an area of approximately 25 km^2. This package appears from reflector geometries to be conformable with the overlying Lower Jurassic package which also shows a similar growth sequence. This sequence is interpreted as having been deposited in a fault controlled growth depocentre as described in the preceding section. The thickness change in this growth sequence is, however, minimal compared to the large thickness variations in the Triassic sequence associated with erosion and this depocentre does not show a significant thickness anomaly on the isochron map (Figure 4.22)

Jurassic

Jurassic sequences are only preserved in the W and SW parts of the study area (Figure 4.23) having experienced extensive erosion at the Base Cretaceous Unconformity. A sequence of 1100m thickness is preserved in well 48/9-1 in the SW of the area although the sequence is completely absent in the NE part of the study area. Like the Triassic package, most of the Jurassic sequence shows parallel reflectors and significant thickness variations within the

sequence are attributed to differential erosion at this unconformity rather than salt withdrawal controlled sedimentary growth. Two areas have, however, been identified where reflector geometries in the Jurassic sequence show of extensive sedimentary growth. These are named Ju_1 and Ju_2 and their locations are shown in Figure 4.23. These Jurassic depocentres are interpreted as being the result of growth faulting described in the previous section. It should be noted, however, that no Jurassic sequences are preserved to the N or NE of where these two growth packages are truncated against their associated salt structures.

A small isolated pod of sediment, interpreted as being Jurassic in age is present on the NE flank of the S_2 salt structure (Figure 4.23). Geometries within this package are however parallel and therefore the package is not inferred as being influenced by salt mobility.

Ju_1 – This depocentre is located on the S side of the WNW-ESE oriented S_5 salt structure with reflectors diverging towards the north and truncating against the salt structure where the package is at its thickest (Figure 4.14(b)). This WNW-ESE oriented depocentre is 10km long, covers an area of approximately 30km^2 and has 'D' shaped isochron contours (Figure 4.23). Beds in the upper part of the growth sequence are truncated at the overlying Base Cretaceous Unconformity and this erosion means the exact thickness of the package is unknown (Figure 4.14). The maximum preserved time thickness of the package is 1350msec (TWTT).

Ju_2 – This package is located on the SW margin of the S_4 salt structure and displays the same style of sedimentary growth towards the salt structure as the Tr_1 package which occupies the same area (Figure 4.17). As in Ju_1 and Tr_1 the package truncates against the adjacent salt structure at its thickest point. This package is considered to have been deposited in a fault-controlled depocentre which is the continuation of the Triassic depocentre in the same area described above (described in detail in Section 4.7).

Cretaceous

Cretaceous depocentres all have the major Base Cretaceous erosion surface as their base and their morphology and development appear to be completely distinct from earlier packages.

Five major depocentres have been identified in the study area which are shown in Figure 4.24 and are described below.

Cr_1 – The Cr_1 depocentre is located on the SW side of the S_1 salt structure and is at its thickest directly adjacent to the salt structure which the package is truncated against (Figure 4.14(a)). Towards the SW, the sediment package thins significantly, pinching out 3–7.5km away from the salt structure. The converging reflectors in this package illustrate the syn-depositional sedimentary growth of this sequence and the package is at its thickest where Base Cretaceous level erosion has removed the greatest amount of the Jurassic sequence. As Figure 4.14(a) shows, Jurassic reflectors are truncated against the package at a high angle.

Cr_2 – This depocentre is bounded to the SW by the S_1 salt structure and by the elongate trend consisting of the S_2, S_4 and S_5 structures to the NE. The package is also bounded to the SE by the S_3 salt structure (Figure 4.14(a)). As in Cr_1, the reflectors within the package diverge towards the S_1,S_2,S_4 and S_5 salt structures and the thickest parts of the package are adjacent to these structures where reflectors become truncated by the salt structure (Figure 4.14(a)). Each of these salt structures are steep sided and diapiric in morphology (Figure 4.13). In contrast to this overall trend of thickening towards the salt structures, the package thins significantly onto the S_3 salt structure which is a shallow salt-cored dome structure (Figure 4.17). The thinnest part of the package is situated between the salt structures where erosion at the Base Cretaceous Unconformity leaves the thickest Jurassic sequence (compare Figures 4.24 and 4.23). Like in Cr_1, Jurassic reflectors are truncated against this package at a significant angle (Figure 4.14(a)).

Cr_3 – The Cr_3 depocentre is a NW-SE trending, trough shaped package bounded to the SW by the S_2,S_4 and S_5 trend of salt structures and the S_9 salt structure to the NE (Figure 4.24). It continues for approximately 25km although its morphology changes significantly across this distance and is subsequently described in 3 parts (a, b and c).

(a) This southernmost section of the package is a maximum of 4.5 km wide and located between the S_4 and S_9 salt structures (Figure 4.17). Towards the SW of the package, reflectors diverge significantly towards the S_4 structure and are truncated against it at their thickest point which is around 650msec (TWTT). To the NE, the reflectors converge and the

package thins to a pinchout on the SW flank of the S_9 salt structure (Figure 4.17). The underlying package is entirely Triassic in age and no Jurassic sediments are preserved in this area.

(b) Towards the NW, into part B of the depocentre, the Cretaceous sequence thins significantly to having a time thickness that is generally less than 350msec (TWTT) across much of the area (Figure 4.24). The Cretaceous package is a maximum of 5.3 km wide in this area and locally thickens slightly towards the S_2 salt structure. Its greatest thickness is in the NE part of the Cretaceous package where a 2km wide trough is present which displays an anomalously thick package with synclinal growth geometries (Figure 4.15). This package is penetrated by well 49/1-4 which records a 1350m Cretaceous sequence. As Figure 4.15 shows, other than this anomalously thick package in the NE of the unit, the sequence is underlain by a thick, isolated Jurassic package which is limited to the area directly to the NE of the S_2 salt structure and does not continue into (a) and (c) parts of the depocentre.

(c) Further NW into part (c) the package thickens again and has a morphology very similar to that seen in part (a). Like in (a) the Cretaceous package thickens towards the SW and becomes truncated against the margin of the S_2 salt structure and thins to a pinchout on the SW margin of the S_9 structure (Figure 4.14(b)). The package is 4.75km wide at this point and contains a maximum of 730msec (TWTT) of Cretaceous sediments.

Cr_4 – The Cr_4 package is situated to the NE of all of the major salt structures in the area except for the S_7 and S_8 structures which stratigraphic relationships constrain as not having developed until the Tertiary (Figure 4.24). Cretaceous sediments in this package thin almost to pinchout towards the NE flanks of the S_9 and S_6 salt structures (Figure 4.19). Other than this, thickness variations within the package are generally less dramatic than other parts of the study area. A gentle decrease in the time thickness of the Cretaceous package occurs in the area that would later become the Te_4 depocentre. Curiously this package appears to show the reverse trend to the Te_4 package getting, thinner as the Tertiary package gets thicker (Figure 4.19). This decrease in time thickness towards the centre of the syncline is likely to be partly due to its deeper burial and therefore increased seismic velocity and compaction although some thickening is observed in this package which is not associated with an increase in burial. Consequently this time thickness variation which shows the inverse thickening style to that seen in the Tertiary sequence is considered to be related to true sedimentary thinning.

Cr_5 – Cr_5 is a small depocentre situated between the S_5 and S_6 depocentres. The package progressively thins to pinchout onto the margins of the S_6 structure and thins significantly but does not pinchout over the crest of the S_5 salt structure connecting it to the Cr_1 package.

Tertiary

Tertiary depocentres are present throughout the survey area and are generally more interconnected than earlier depocentres. Four major packages have been identified which are illustrated in Figure 4.25 and are described below. Tertiary sequences are all conformable with the underlying Chalk Group and the depocentres in the SW of the area generally follow the growth and morphology trends of the underlying Cretaceous successions. Depocentres to the NW of the S_9 and S_6 salt structures where significant subsidence had not occurred prior to the Tertiary (Te_3 and Te_4) in contrast, show very different trends.

Te_1 – This depocentre is located to the SW of the S_1 salt structure displaying a similar morphology to the underlying Cr_1 depocentre with the thickest sequence located next to the salt structure (Figure 4.14(a)). As in the Cr_1 package, sequences show significant growth towards the salt body and are largely truncated against it. Sequences do, however, begin to thin significantly in the 1 – 2 km directly adjacent to the diapir giving it more of a bowl shaped morphology than is seen in the underlying depocentre. A maximum time thickness of 900msec (TWTT) is seen in this depocentre, although angular truncation of reflectors by sea bed multiples suggest the uppermost part of the sequence has been removed by erosion.

Te_2 – This depocentre is located between the S_1, S_2, S_3, S_4 and S_5 salt structures in the approximate area of the underlying Cr_2 depocentre. Unlike the Cretaceous sequences, this package is not bound by the S_5 or S_4 salt structures and also covers the area of the Cr_3 and Cr_5 depocentres (figures 4.24 and 4.25). Tertiary sediments blanket the crests of these structures, which earlier sequences thinned significantly above or were truncated against (Figure 4.17). The package does, however, thin significantly over the S_2 salt structure which Cretaceous sequences are truncated against. Like the Cr_2 depocentre, the sequence is truncated at its SW margin by the S_1 salt structure and thins significantly in the area where

the Base Cretaceous level erosion has left the thickest Jurassic sequence. The thickest Tertiary sequence in this package is located in a broad WNW-ESE oriented trough the area above the $Cr_3(c)$ depocentre (marked 'a' in Figure 4.25). A maximum time thickness of 1025msec (TWTT) is seen in this area, although as in Te_1, significant erosion of the top of the sequence is inferred.

Te_3 – This depocentre consists of a pair of broad, NW-SE oriented synclinal sags bounded to the SE by the S_8 structure and to the SW by the S_6 structure. Angular reflector terminations against seabed multiples at the top of the package suggest erosion of the upper part of the sequence and the package is absent over the crests of the S_6 and S_8 salt structures. Reflector geometries show this is due to erosion not pinchout of the sequence and within the package, sedimentary growth was minimal. A maximum time thickness of 640msec (TWTT) is preserved in this area although erosion means this is clearly an underestimate of the true Tertiary thickness

Te_4 – This depocentre is by far the most significant of the Tertiary depocentres in the study area and contains an almost complete Tertiary sequence displaying sedimentary growth strata aged from Eocene to Pliocene (shown to the NE of the S_9 salt structure in Figure 4.28). This package has a maximum time thickness of 1470msec (TWTT) which is recorded as 1712m in well 49/1-3. This package is an elongate NE-SW oriented synclinal trough which extends for 40km from the NE margin of the S_9 salt structure to beyond the margins of the study area (Figure 4.28). Almost the entire Tertiary sequence in this package thins to pinchout against the S_7, S_8 and S_9 salt structures (Figure 4.19). This package displays the opposite trend to the underlying Cr_4 package which thins slightly over roughly the same area that this package thickens over. Unlike over the rest of the area, no evidence for major erosion of the top of the package is found in this area.

Timing of salt weld development

The timing of salt weld development is very important in the development of salt structures and supra-salt depocentres as it marks salt starvation and therefore the cessation of the

halokinetic system at a given location. The three-dimensional nature of salt mobility means that two-dimensional restorations alone, such as those shown in figures 4.16 and 4.28 are unable to constrain salt-weld timing exactly and the observations from such restorations have been used alongside more subjective methods to determine the timing of salt welds in the study area. The timing of when a specific salt weld developed is here considered to be constrained as broadly simultaneous with the deposition of the earliest stratigraphic package that *does not* show evidence of major stratigraphic expansion in a depocentre. Consider the situation shown in Figure 4.28 for example. In the area to the NE of the S_9 salt structure, the Base Cretaceous to Base Pleistocene package shows significant stratigraphic expansion to the NE and is therefore considered to have been deposited prior to welding. The Base Pleistocene to seabed package in contrast does not show such expansion. In order differentiate between a post-weld package and a pre-weld package deposited during a period of minimal salt mobility however it is necessary that the timing must be *broadly* contemporaneous with that determined from a structural restoration.

An interpretation of the timing of weld development is shown in Figure 4.26. Most of the welds are interpreted as developing in the Tertiary which is where salt mobility is interpreted as being at its greatest and most widespread. Through most of the area, well data does not allow these welds to be constrained more accurately than to give a Tertiary age and Figure 4.26 dates these welds as 'Tertiary undifferentiated'. Well 49/1-3 allows the stratigraphy in the Te_4 depocentre to be constrained more accurately and an Oligocene age is given for the development of most of the major weld in this area with the exception of the SW end of the weld which is given a Plio-Pleistocene age.

Several other welds developed prior to the Tertiary including the weld in the SW end of the study area where no significant deposition has occurred since the development of the Base Cretaceous Unconformity and a Jurassic age is given. A Cretaceous age is given to a weld (or near weld) in the area between the S_1 and S_3 salt structures in the area adjacent to the S_1 structure where growth geometries observed in the Cretaceous sequence are almost absent in Tertiary sequences. The weld which is present between the S_1 and S_2 structures is given a Tertiary age, although there is evidence that along a NW-SE trending line along the centre of

this area where the Jurassic sequence is at its thickest, the weld developed earlier, possibly in the latest Cretaceous.

Unconformities associated with salt structures

The extensive erosion associated with the regional Base Cretaceous Unconformity is well documented throughout the North Sea and although extensive erosion is clearly present at this level throughout the study area, the amount of erosion clearly varies significantly. Figure 4.27 shows a subcrop map on the Base Cretaceous unconformity and shows the subcrop to be dominantly Jurassic to the SW of the S_5-S_2-S_4 salt structure trend and dominantly Upper Triassic to the NW of this trend. Estimating the amount of erosion locally, however, is difficult as this trend represents the transition from the Sole Pit Basin to the SW which was the major Jurassic depocentre in the Southern North Sea (Cameron et al. 1992) to the peripheral areas to the NE where Jurassic sequences were likely to be significantly condensed or even absent. Therefore the level to which erosion occurred to does not necessarily equate to the amount of erosion that has occurred. What is clear is that the style of this unconformity varies significantly across the area from being a bedding parallel unconformity in the NE where it has an Upper Triassic sub-crop to being highly angular in the SW where it has a Jurassic sub-crop. As Figure 4.28(a) shows, where this unconformity has a Jurassic sub-crop, erosion associated with it increases progressively towards the S_1 salt structure and the S_5-S_2-S_4 trend of structures suggesting that salt mobility has locally influenced the amount of erosion at the Base Cretaceous level.

4.9 Discussion

Salt tectonic controls on fault development

Development of Triassic and Jurassic growth faulting

The growth packages observed in the predominantly Jurassic sequences to the SW of the S_4 and S_5 salt structures typically converge towards their associated salt structures, leading to the interpretation that they are growth faults as described in section 4.7. These packages are, however, not simple growth packages and are typically associated with very complex structural geometries, particularly within the underlying Triassic sequence. Understanding these geometries is therefore considered to be key to the understanding of the structural controls on these depocentres. In order to develop a geologically feasible interpretation of these structures, sections must be balanceable and structural restoration of the geometries was carried using 2DMove. The complex and poorly imaged nature of these structures in the areas where Jurassic growth packages are at their thickest (e.g. Figure 4.14(b)) has made attempts at restoring packages in these areas unsuccessful. A successful restoration has been carried out in a section from a peripheral area (Figure 4.18(a)) where sedimentary growth is less dramatic but structural geometries are better imaged.

As Figure 4.18(a) shows the Triassic sequence is detached throughout much of the section at the Base of the Haisborough Group, probably on the basal Röt Halite Member and displaying complex 'ramp-flat' geometries. The Upper Triassic sequence is split into several sections, two of which are completely independent of the Lower Triassic sequence. One forms a keystone block, below which Lower Triassic sequences are absent and another forms an anticline cored by the S_5 salt body between the two Triassic sequences. This geometry has been restored and successfully balanced and is shown in Figure 4.18(b). From balancing this section the Triassic sequence can bee seen to have been extended by 2140m during the development of the structure, which strongly implies that tectonic extension has occurred in the area. Extension of the Triassic sequence, associated with the development of Jurassic growth faults is therefore interpreted as having been accommodated, not by a single fault structure but rather by a complex system of layer restricted faults and flat areas similar to

those described by Stewart et al. (1996) (Flamborough Head area, Southern North Sea) and Hudec, (2004) (NE German Basin).

Development of the Schooner NE fault system

Timing of faulting relative to salt mobility and tectonic episodes

The Schooner NE fault system is assigned a Tertiary age as it cross cuts the entire supra-salt sequence with no evidence for any fault development prior to the base of the Tertiary. The Tertiary age of this structure is curious as despite being a major extensional style normal fault with up to 650m of vertical displacement, it developed in a time where the Southern North Sea was widely considered to be dominated by inversion tectonics (section 4.4). Also the other major structures which developed contemporaneously with the fault are large scale buckle style salt cored folds which are also structures normally associated with compressional tectonics.

With the absence of any evidence of contemporaneous crustal extension, in either the sub-salt or supra-salt sequences, a simple extensional model is therefore considered insufficient to explain the development of the fault system. Structural restorations (figures 4.28 and 4.16) and interpretations of salt weld timing (Figure 4.26) illustrate that by the initiation of Tertiary deposition, widespread salt mobility in the SW of the Schooner NE Fault had led to the grounding of salt structures in several locations. Cretaceous sequences in this area are frequently observed thickening towards and truncating against salt structures indicating that they were steep sided diapiric structures at this time. In contrast, in the vicinity of the S_9 salt structure, sedimentary growth geometries flanking the structure suggest it was a gentle salt-cored anticline during the Cretaceous and the area to the NW shows no evidence of any sedimentary growth or salt mobility until the development of the Te_4 depocentre in the Tertiary.

The partial grounding of salt structures to the SW would have substantially limited salt mobility in this area whereas there was potential for extensive salt mobility in the vicinity of the Schooner NE fault and the area to the NE. Consequently at the time when the fault

system developed, the area to the SW of the study area was considered to have been a grounded and therefore semi-pinned area at the margins of the Sole Pit Basin where there was limited potential for salt mobility. The area to the NW, in contrast, was part of the Silverpit Basin where there was only limited previous salt mobility, no grounding restricting salt flow and therefore extensive potential for salt mobility. The Schooner NE fault system is therefore considered to be situated at the boundary of these zones.

Mechanisms driving the development of the fault system

Two possible models for the driving mechanism behind fault development have been considered which take into account the lack of an obvious extensional tectonic control. These models are outlined and discussed below.

Mechanism 1 – This model suggests that the fault system developed due do to crestal collapse in the overburden of the S_9 salt structure related to dissolution. Normal faulting is a common feature in the crest of salt structures which have undergone significant dissolution and is identified extensively in the Paradox Basin study area (section 3.8). There are, however, several significant arguments against this hypothesis. Firstly the maximum offset due to faulting is located entirely in the marginal areas at the NW and SE of the salt structure where its morphology is of a salt-cored anticline rather than a diapiric structure. Away from this area where the top salt elevation increases dramatically developing the morphology of a diapiric salt wall, the vertical displacement decreases dramatically (Figure 4.21). As the structurally much higher diapiric area is likely to have been much closer to groundwater sources and therefore display the greatest amount of dissolution, this is the area where most dissolution driven displacement would be expected to occur which is the opposite to the actual observations. Further arguments against this hypothesis are concerned with the style of faulting. The Schooner NE fault system consists of a single large normal fault situated at either end of the salt structure. Crestal collapse structures are typically complex graben systems consisting of numerous small structures situated along the crest of the salt structures.

Mechanism 2 – This model suggests that the fault developed due to extensional stresses related to folding restricted to the supra-salt layer and is the favoured hypothesis in this

study. The extensive buckle folding style found in the Silverpit Basin described in both this study and others (e.g. Hughes and Davison, 1993, Stewart and Coward, 1995) represents significant amounts of bed length shortening in the supra-salt sequence across the basin.

Observations of the sub-salt sequence do not reveal evidence of any major folding that cannot be attributed to velocity effects below salt structures. Similarly no fault structures in the sub-salt sequence have been observed that represent sufficient shortening to balance the amount of shortening in the supra-salt sequence. Consequently shortening in the supra-salt sequence is considered to be a thin-skinned process limited entirely to the folded layers and not due to an overall bulk shortening of the crust. As such, if neither bulk crustal shortening or stretching is assumed, amounts of bed length shortening due to folding in the supra-salt sequence need to be balanced by equivalent gaps in the bed length across faults or salt diapirs (section 6.1). As such, faulting is attributed to thin-skinned stretching associated with the process causing these buckle folds. This concept is not new and has been invoked by Griffiths, et al. (1995) and Stewart and Coward, (1995) to explain the development of the basin bounding Jurassic and Triassic aged Dowsing and North Dogger fault systems in the Southern North Sea. Up-dip extensional style structures related to down-dip compressional structures are also a well-documented feature of many salt basins at continental margins (e.g. Demercian et al., 1993, Duval et al., 1992 and Wu et al., 1990). What is clear is that in order for a fault to occur by this mechanism, the process causing buckle fold deformation must be strong enough to overcome the mechanical strength of the faulted sequence.

Proposed mechanisms driving faulting include gravity gliding related to regional tilt (Stewart and Coward, 1995) tectonic inversion (Hughes and Davison, 1993) and halokinesis related to basement tectonics (Jenyon and Cresswell, 1987). Of these processes, inversion and basement related tectonics would be unable to account for the lack of equivalent deformation in the sub-salt sequence and it is difficult to envisage how gravity alone could cause folds in excess of 1.5km in height unless the differential uplift was on this scale. It is here proposed that the folds developed due to feedbacks between differential deposition and salt mobility in a similar way to the minibasin concept detailed in section 2.5. The principal difference between this setting and the classic minibasin concept is that the presence of the thick Triassic sequence which cannot be easily penetrated must be folded in order to allow salt

mobility to accommodate salt mobility. Folding and therefore the development of the Schooner NE fault system are considered to be by-products of this differential load driven salt mobility. This process is discussed in more detail in section 6.2.

Location of the fault system and localisation of deformation

The location of the Schooner NE fault system is considered to be very relevant to the discussion of its origin. Based on the observations detailed in section 4.8 the fault system is considered to be located at the transition between the area where salt mobility was limited due to grounding in the Tertiary and the area to the NE where there was extensive potential for salt mobility at this time. As described by Stewart and Coward, (1995), faults at the basin margin accommodating folding in the basin are considered to be localised where facies changes occur within the Zechstein Group. This change from the mobile halite dominated facies in the basin to the less mobile facies at the margins forms an effective pin, localising the strain associated with folding and leading to the development of the faults. Although the situation is different in this setting where faulting is located in the centre of the basin, the observed grounding to the SW of the Schooner NE fault system is considered to provide an equally effective pin. This therefore explains the location of the fault system in this area a short distance to the NW of this pinned zone rather than at some other point in the mobile part of the basin.

The association of the Schooner NE fault system with the S_9 salt structure raises the question as to whether the salt structure developed as a result of the faulting or whether the faulting exploited a pre-existing salt structure. The location of the fault in the crest of the salt-cored anticline is significant as growth geometries in the Cretaceous sequence flanking the salt structure suggest that a salt-cored anticline with gently dipping limbs was present in this location prior to the development of the fault. Salt-cored anticlines further NE than S_9 do not tend to show evidence of pre-Tertiary activity in this way and this crestal area would therefore have the thickest sequence of weak salt beneath the overburden and make it the point at which the minimum work was required to fracture the supra-salt sequence. The above discussion therefore explains satisfactorily the development of the fault in this location within the confines of the favoured mechanism for the faults development.

The development of the fault/salt diapir system

The discussion of the manner in which the fault system developed is strongly related to the discussion of the mechanism behind faulting described above. If Mechanism 1 was the main controlling factor, then the development of the diapiric salt wall would pre-date the development of the fault. Mechanism 2, in contrast implies that the process of late stage (mainly Tertiary) salt mobility leading to the development of the S_9 diapir was the same process responsible for the development of the faulting and therefore their development would have been synchronous. As discussed above, little evidence exists for Mechanism 1 being the main control on faulting and Mechanism 2 is considered dominant. Subsequently Mechanism 2 is used as the basis for this interpretation of the development of the fault/salt diapir system.

The displacement-length profile shown in Figure 4.21(b) illustrates that significant vertical displacement of beds continues to occur across the diapiric part of the S_9 salt structure away from the area where normal faulting is observed. The salt diapir system is here considered as having had a significant role in accommodating Tertiary bed displacement. As this displacement-length profile shows, at both ends of the fault system, a significant drop in vertical displacement occurs at the point of transition where displacement transfers from fault to diapir. As Figure 4.10(b) shows, however, despite the major drop in vertical displacement at this point, the horizontal component of bed separation continues to increase at the S_9 salt structure. The interpretation is that this point represents the point where the bed separation became sufficient for salt to flow into the fault plane between the two cut-offs. This therefore represents the transition between a style of deformation where tension in the layer was accommodated by dip-slip faulting to where salt could flow into the space between beds and provide the necessary gaps to accommodate overall bed length shortening in the sequence (see section 6.1). The drop in vertical displacement recorded in Figure 4.21(b) at this transition is therefore interpreted as being due to this change in the style of deformation.

In the faulted section, the gaps in bed length required to accommodate overall shortening of the layer would be manifest in the heave component of fault displacement with the vertical component being a mechanical requirement allowing this horizontal bed separation to occur. Where bed separation was accommodated by salt flowing between the separated areas,

however, no vertical component of displacement would be required to obtain the same bed separation. Therefore where the transition from fault displacement to displacement across a diapir occurs, the horizontal requirement is no longer needed to accommodate bed length shortening explaining the significant displacement drop at this point in Figure 4.21(b). A model is therefore proposed to explain the development of the Schooner NE fault system which is illustrated in Figure 4.29.

Stage 1 – The area that would later become the Schooner NE fault developed initially as a relatively gently and un-faulted salt cored anticline displaying minor sedimentary growth of flanking Cretaceous sequences.

Stage 2 – Stage 2 begins as thin-skinned bed length shortening due to the development of buckle folds to the NE leads to the development of a minor fault in the overburden centred at the crest of the pre-existing anticline.

Stage 3 - Thin-skinned bed length shortening continues to enhance displacement on this fault to a critical point where bed separation is sufficient for the salt upweling below the fault plane to penetrate it.

Stage 4 – Salt penetrates the fault plane and is able to lubricate the horizontal bed movements. Subsequent bed separation is accommodated by salt flowing into the area between the two fault cut-offs rather than by offsetting them. Consequently, the horizontal component of fault movement is no longer required and subsequent vertical bed displacement will therefore not contribute further to the total vertical displacement recorded in the displacement-length profile.

Stage 5 – Horizontal bed separation continues without any vertical movement and a diapiric salt structure develops as salt flows in to fill the gaps left by the separating beds. Salt continues to upwell into the salt structure until all salt is withdrawn from adjacent areas. The dips of flanking sequences are progressively steepened due to salt withdrawal into the adjacent structure.

This model only describes the situation in the centre of the structure where bed displacement was at its greatest and while bed separation would be sufficient in the centre of the fault system for salt to penetrate the fault plane. Simultaneous deformation at the margins of the structure would therefore still be occurring through fault displacement. The lateral propagation of the system is therefore considered to have continued through dip-slip faulting with the transition point from fault to diapir progressively moving outwards as displacement increased explaining the presence of fault structures at the margins of the salt structure and a diapiric structure in the centre. The observed vertical displacement across the diapiric part of the S_9 salt structure is therefore considered to be remnant vertical displacement from when tension was previously accommodated by faulting.

Development of the Schooner SW fault system

Despite being located above the area where an inferred Jurassic growth fault was present and having the same strike orientation as this inferred structure, the Schooner SW fault has the opposite polarity. The Tertiary age of this structure also means that its development is unable to be explained by the Jurassic extensional mechanism responsible for the underlying growth fault. It is here proposed that its development is related to the same mechanism described for the Schooner NE fault system. As in the Schooner NE fault system, the location of this structure in the crest of a pre-existing salt structure is interpreted as being due to it being where the minimum work was required to fracture the supra-salt sequence as the weaker salt was thicker here. One notable aspect of this fault is that its opposite polarity to the underlying structure is inferred as being controlled by salt mobility. The amount of potential fault displacement in a supra-salt sequence is restricted to the amount of salt that can move away from a faults hanging wall allowing subsidence relative to the footwall or the amount of salt that can move into the footwall area allowing movement relative to the hanging wall. It is therefore proposed that as the early stage (Jurassic) faulting created a thick sequence restricted to the SW side of the salt structure, the area where subsequent relative subsidence could occur most efficiently would be on the opposite side of the salt structure hence developing the polarity reversal between these structures.

Development of small-scale faults in vicinity of the S_3 salt structure

The timing of fault movement in the small-scale faults associated with the S_3 salt structure can be constrained with confidence as they crosscut the entire Upper Triassic sequence as well as the preserved Jurassic sequence but are truncated by the Base Cretaceous Unconformity. As faults all sole out onto the Röt Halite horizon and no evidence of equivalent extension is preserved in the Lower Triassic section, these faults are interpreted as being due to a passive localised stress regime rather than regional tectonic stresses. Clusters of these faults typically have a similar dip and although this dip is not always in a downslope direction in the present day structural configuration, it is highly likely that this dip has been modified by subsequent salt mobility. These faults are therefore interpreted as thin-skinned, gravity induced faults associated with a Jurassic slope and facilitated by the Röt Halite decolement horizon. Similar faults have been described in the Upper Triassic sequence above the same halite horizon in the Flamborough Head Fault Zone by Stewart et al. (1996) by who describe them as 'a train of domino fault blocks'.

Development of reverse faults

The presence of reverse faulting in the area between the S_5-S_2-S_4 salt structure trend and the S_9 salt structure is difficult to explain, especially as this is the area where imaging of the structures is at its poorest. Reverse faulting offsets the Base Cretaceous horizon (which is frequently also the Top Triassic horizon in this area) and is also interpreted as controlling minor growth geometries observed in the Cretaceous sequence (Figure 4.17) suggesting a Cretaceous age. Two plausible mechanisms exist which could explain their development. As reverse faults are typically associated with compressional tectonics, the most obvious explanation is that they are related to tectonic inversion. Stewart and Clark (1999) describe similar thrust structures in the Horn Graben and Feda Graben areas of the Central North Sea attributing them to basement involved shortening (see Figure 23 in their paper). The reverse faults in the study area, however, do not penetrate the entire Triassic succession and are entirely restricted to the area between the S_9 salt structure and the S_5-S_2-S_4 trend of salt structures. An alternative interpretation is that these structures are simply accommodating space problems in the supra-salt sequence as this package subsides in the Cretaceous.

Interactions between salt mobility and erosion

The extensive erosion associated with the regional Base Cretaceous Unconformity is well documented throughout the North Sea and although extensive erosion is clearly present at this level throughout the study area, the amount of erosion varies significantly around the different salt structures in the study area. Salt structures in the SW of the study area typically show major angular discordances at this surface whereas in the NE of the area, pre-Cretaceous sequences are typically parallel to the Cretaceous sequence.

The above described variation is clearly related to the variation in the development of salt mobility relative to the timing of the unconformity. Figure 4.28(b) shows a cross section restored to this time and illustrates how stratigraphic relationships in the SE of the area show evidence of extensive salt mobility prior to the Base Cretaceous. In the NE, in contrast, there is no evidence for salt mobility prior to this time. Salt structure styles also vary significantly between these two areas. Steep-sided types 1 and 2 salt structures which truncate the supra-salt sequences at their margins are present where salt mobility was early and major angular truncations exist at this surface. In the NE of the area in contrast, where angular truncations are not present and salt mobility post-dated erosion, only types 3 and 4 salt structures are present where the base of the supra-salt sequence is typically parallel to the top of the salt. The implication of this is that erosion had a significant control on the development of salt structure styles. The implication of the restoration shown in Figure 4.28(b) is that prior to the Base Cretaceous Unconformity, a salt-cored anticline was present in the site of the S_1salt structure. It is considered that salt mobility in this early structure was restricted by this overburden and it could only develop into a diapiric structure when erosion removed the crest and allowed salt to move more freely. This situation is illustrated in Figure 4.30 and corresponds with the pillow to diapir transition concept described by Sørensen, (1998) and the transition between the primary and secondary peripheral sinks of Trusheim (1960). The relative timing of erosion and salt mobility is therefore considered to have had a significant control on salt structure development.

Salt tectonic controls on depocentre development

As described in section 4.8 a wide range of depocentre styles are observed within the study area which have varying relationships to their associated salt structures. Interpretations of salt structure and depocentre evolution have been determined from Isopach data and through using restorations of seismic sections to restore the earlier morphologies. Figures 4.28 and 4.16 illustrate structural restorations of two NE-SW oriented 2D seismic lines across the study area. These restorations have two way travel time as their vertical scale and have not been decompacted during the restoration. No attempt has been made to balance structures in the sub-salt section as structures are typically small and deformation is likely to be largely out of section. An attempt has, however, been made to manually remove velocity pull-up effects in the sub salt sequence as salt structures are removed.

Depocentre morphology

The depocentre styles observed in the study area vary significantly from the typical honeycomb minibasin morphology described in many basins (e.g. Figure 2.14) in that salt structures have a distinct preferred orientation. This preferred NW-SE trend is also observed in sub-salt faults 4.10(b) and is also largely reflected in the orientation of salt controlled depocentres with the exception of the Te_4 depocentre which has a NE-SW orientation. Supra-salt sedimentary depocentres have developed as either fault controlled depocentres or salt withdrawal controlled depocentres, although these two styles are considered to be fundamentally linked.

Fault controlled depocentres

Despite the actual detachments being structurally complex, the depocentres associated with Jurassic growth faults (Ju_1 and Ju_2) have a relatively straightforward morphology. Growth packages typically thicken towards the associated faults and display the characteristic 'D' shaped contour patterns that are typical of salt free settings (Figure 4.23). The Tertiary Schooner NE and Schooner SW fault systems in contrast, do not display a classic hanging wall growth sequence thickening towards the faults. In contrast, the Tertiary package is observed to thin slightly towards the Schooner NE fault rather than thicken towards it

(Figure 4.20(a)) and consequently the uplift and subsidence associated with faulting is considered not to conform to the established concepts of fault-controlled subsidence derived from salt free areas. The development of the Schooner NE fault system above a pre-exiting salt cored anticline (Figure 4.29) and associated with salt withdrawal into the contemporaneously developing S_9 salt structure means that subsidence is far more complex than in a classic salt free setting. Fault controlled subsidence is therefore considered to be intricately integrated with associated salt withdrawal related subsidence to produce the observed geometry.

Salt withdrawal controlled depocentres

Figures 4.14, 4.15, 4.19, 4.28(a) and 4.16(a) illustrate numerous different depocentre styles and morphologies, many of which are relatively complex. Despite this complexity, with respect to the relationship of depocentres to their associated salt structures, only two different relationships exist. Sequences are observed to either thin towards the associated salt structures or thicken towards them. This is consistent with the relationships detailed by Trusheim (1960) and refined assuming a brittle rather than fluid overburden by Venderville, (2002) for the primary and secondary peripheral sink concepts respectively (see section 2.5). As with Trusheim's concept, packages which thin towards their associated salt structures are associated with salt structures which do not pierce the overburden at their time of deposition. Packages which thicken towards salt structures in contrast are associated with salt which is at the surface during deposition allowing downbuilding to take place. As a thick Triassic, and possibly Jurassic succession blanketed the entire area prior to the development of major salt mobility in the basin, for this latter style to develop requires either active piercement or erosion of the salt structures crest.

As Figure 4.28(b) suggests, erosion is considered to be the main factor allowing salt structures to penetrate to the surface in this study area. Several individual depocentres show asymmetric relationships where one side of the package thickens towards, and is truncated by a salt structure and the other side the package thins towards another salt structure (e.g. Cr_2 and Cr_3). These packages represent the transition between the parts of the basin where the different styles are dominant.

Depocentre migration

Structural restorations (e.g. figures 4.28 and 4.16) and Isochron maps of the supra-salt packages illustrate that both salt structure development and associated salt withdrawal was not uniform across the basin throughout the history of the study area. The earliest preserved supra-salt depocentres in the SW of the study area, developed in the Jurassic and Cretaceous whereas subsidence in the NE of the study area (Te_4) was very minor until the main Te_4 depocentre developed in the Tertiary. Restorations and isochron maps record an overall NE migration of the major depocentres through time with Jurassic growth packages being thickest to the SW of the S_5-S_2-S_4 salt trend (Figure 4.23), Cretaceous packages being thickest between the S_5-S_2-S_4 trend (Figure 4.24) and the S_9 structure and Tertiary packages thickest to the north of this (Figure 4.25). Similarly Figure 4.26 illustrates a NW migration of salt weld development with the earliest welds developing in the SW in the Jurassic and Cretaceous welds developing slightly further to the NE. Although salt welds developed in the Tertiary throughout the SW of the study area, these welds represent later stage salt mobility. The result of enhanced localised salt withdrawal related to a pillow to diapir transition and each of the sediment packages to the SW of the S_5-S_2-S_4 salt trend can be seen to have originally touched down on the sub-salt sequence prior to the Tertiary.

Depocentre migration is interpreted as being the result of changes in the area where the most potential for salt mobility is present. The amount of growth that a salt structure can achieve is directly controlled by the amount of salt locally available to be withdrawn into it and when a salt structure has exhausted its salt supply it will become largely inactive. This is unless a factor such as erosion causes a change in the salt structure style allowing withdrawal of small isolated salt pockets. In a system such as this where salt was plentiful on the basin scale, upon the grounding and starvation of a particular structure, providing there is a still a mechanism driving salt mobility, halokinesis is likely to migrate to the nearest point where salt is plentiful. Depocentres are therefore likely to progressively step away from their original locations until all salt in the system is mobilised.

Effects of pre-existing sediment packages on depocentre development

The simple relationship between salt structure style and depocentre style detailed above is not considered to fully explain the varying geometries of the depocentre styles observed in

this study and the influence of pre-existing sediment packages is considered to have a significant control. As the potential for salt withdrawal-controlled depocentre development is limited by the amount of salt available to withdraw, the presence of a thick sediment package related to earlier salt mobility in the same area will significantly limit the potential for the development of later packages. Perhaps the most dramatic illustration of this involves the Tertiary depocentres in the study area. As Figure 4.25 shows, by far the greatest thickness of Tertiary sequences is in the Te_4 depocentre which has a time thickness of up to 1470 milliseconds (TWTT), which is almost double that of any other Tertiary depocentre. This package shows very well defined growth geometries throughout the Tertiary sequence (Figure 4.19). In contrast, other Tertiary packages elsewhere in the study area show much less significant growth and less dramatic geometries.

The thinner packages are all situated in areas where major earlier depocentres are present and therefore are effectively infilling the remaining space in the basin. The Te_4 package in contrast is unaffected by any such constraints. Another example is the Cr_3 depocentre which although being a single interconnected package, shows significant variability in its thickness along its length. As Figure 4.24 shows, parts (a) and (c) of this package show relatively thick packages which span the whole area between the bounding salt structures. In contrast part (b) is generally thinner but locally thickens significantly in the NW part of this package in a tight growth syncline illustrated in Figure 4.15 and penetrated by well 49/1-4. As Figure 4.27 shows, in this area the Cretaceous sequence is underlain by an isolated pod of Jurassic sediment which is not present below parts (a) and (c) of the depocentre. The tight growth syncline in part (b) is located just beyond the NE margin of this Jurassic sediment pod illustrating that subsidence in this area was locally controlled by the presence of this pod and a thicker sequence could only develop away from its influence.

Controls of salt mobility on sedimentation

Except for the major depositional hiatus represented by the Base Cretaceous Unconformity, both salt mobility and sedimentation are considered to have continued in the area throughout the entire Mesozoic and Tertiary history of the basin. Consequently a dynamic link is suggested between sedimentation and salt mobility with feedbacks occurring between the two processes. Although the infrequency of well data makes finding direct evidence for a salt tectonic control on sedimentation from facies distribution problematic, one specific area does

show a significant control of salt mobility on sedimentation which can be determined from seismic data. As Figure 4.31 shows, the Pliocene succession in the Te_4 depocentre displays distinct clinoform geometries typical of a classic deltaic sequence. Figure 4.32 shows an isochron map of this package which shows it being locally derived from the flanks of the adjacent S_9 salt structure and having a fan shaped geometry reinforcing the interpretation of it being a deltaic sequence. This sequence is interpreted as being derived from the uplifted footwall area of the Schooner NE fault system and deposited directly into the adjacent salt withdrawal basin.

Summary

An approximately 1km thick sequence of halite dominated Zechstein Group evaporites are considered to have been deposited across the study area in the Upper Permian. These were blanketed by a thick Triassic and Jurassic sequence across the area which was largely parallel bedded and relatively undisturbed by salt mobility other than where two growth faults locally developed in the SW of the area. Between the Early Jurassic (end Lias) and the end of the Jurassic, a NW-SE oriented salt-cored anticline developed in the SW of the area which was later decapitated by erosion associated with the Base Cretaceous Unconformity. This led to salt being exposed at the surface and the structure subsequently developed into a steep sided diapir which grew through downbuilding. Salt mobility at this time was restricted to the SW of the study area and in the NE, the unconformity was parallel to bedding in the Triassic sequence.

The Cretaceous saw extensive salt mobility in the SW of the study area and also the development of the S_9 salt structure in the centre of the area as a gentle salt-cored anticline. Salt welds in the SW of the study area are also thought to have first developed during this time. The Tertiary saw the most widespread salt mobility in the area and for the first time, it extended into the NE part of basin where a system of salt-cored buckle folds developed driven by a feedback relationship between salt mobility and differential sedimentation in the intra-salt depocentres. Folding driven by this mechanism was balanced by normal faulting in the Schooner NE fault system which developed in the crest of the S_9 salt structure. At this time the S_9 structure represented the furthest SW salt structure in the basin which was not bounded by salt welds. Fault displacement was accompanied by salt moving into the footwall area which eventually penetrated the fault plane in the central area of the fault system. This caused the associated salt structure to develop from a faulted salt-cored anticline into a diapiric structure and subsequent extensional stresses were accommodated by bed separation filled by upwelling salt rather than fault displacement.

5.0 The Central North Sea

5.1 Introduction

Hydrocarbon exploration in the Central North Sea has identified extensive evidence for the mobility of Upper Permian (Zechstein Group) evaporites throughout the Mesozoic and Tertiary history of the basin. Much of the most dramatic salt mobility is associated with Triassic and Late Jurassic extensional structures, particularly in the Central Graben area. The aim of this chapter is to investigate the interactions between salt mobility and faulting in the Central Graben with a view to understanding the role that salt mobility has had on the development of the fault system, basin subsidence and the evolution of sedimentary depocentres in time and spaces. This is done with the ultimate aim of aiding the development of more generic concepts of the interactions between salt mobility and faulting. Due to constraints relating to data availability, this study is limited to observations of the Shearwater hydrocarbon field and its immediate vicinity. This chapter is an extension of the work published in Banbury and Underhill (2004). The concepts detailed in this paper have, however, developed significantly since this paper was accepted (December 2003) and the concepts detailed in this chapter should be considered to be the findings of this study.

Rationale

Although a link between salt mobility and extension is well established from a theoretical and modelling point of view (e.g. Jackson and Vendeville, 1994, Vendeville and Jackson, 1992), little attempt has been made to provide detailed observations of this link in actual examples. The Shearwater Fault System is considered to be an ideal example for identifying such relationships. This is partly due to the good quality seismic data and well coverage of the supra-salt sequence but mainly due to its spatial and temporal position. In many of the salt-influenced faults detailed in this study, the tectonic controls on fault development are somewhat ambiguous and have required extensive discussion. The Shearwater Fault System in contrast is situated in an extremely well documented, Late Jurassic extensional basin where extensional structures continue well beyond the extent of the salt basin (Figure 5.1).

The development of the Shearwater Fault System can be entirely constrained as contemporaneous with this rift phase and therefore the tectonic controls on its development can be differentiated from the controls of salt mobility with confidence. One advantage of this fault system over many others in the Central Graben is that the associated salt structure has not experienced extensive post-rift diapirsm. Although typically associated with large normal faults at Triassic or Jurassic levels (Davison et al., 2000[a]), many of the salt structures in the Central Graben penetrate well into the Tertiary sequence and obscure much of the underlying fault geometry. The salt diapir associated with the Shearwater Fault System in contrast, does not penetrate the Base Cretaceous Unconformity into the post-rift sequence, effectively preserving the fault geometry with its morphology at or near the end of the rift phase.

Aside from aiding the establishment of generic concepts of the interactions between salt mobility and faulting, which is one of the ultimate aim of this study, understanding the development of the Shearwater Fault System has direct implications for exploiting hydrocarbon resources in the Central Graben area. The fault system provides the trap to the extensive Shearwater gas condensate field (Blehaut *et. al.,* 1999) and understanding the role of salt mobility on the development of this structure is likely to aid in the exploitation of this resource. Numerous other analogous structures are also present in the Central Graben and this knowledge is likely to be transferable to other fault systems.

Methodology

The primary mode of investigation in this study involves interpretation of a high resolution 3D seismic dataset covering an area of approximately 15km^2 in UK blocks 22/30, 23/26, 29/5 and 30/1. This is full stack time migrated data with a line spacing of 25 metres. Interpretation was constrained by horizon picks from released wells in the survey area, the locations of which are illustrated in Figure 5.2. As well as observations of seismic sections, the concepts detailed in this study make use of structure contour maps, isochron maps and subcrop maps derived from this data. Fault development has been analysed through use of displacement-length plots which have been depth converted using the technique described in

Appendix 1. The fault-controlled depocentre morphology was investigated using 3D visualisation techniques within the 3DMove software of Midland Valley Exploration Ltd.

Location of the study area

The study area is situated primarily in UK licence block 22/30 but also covers areas of blocks 23/26, 29/5 and 30/1 approximately 200 km east of Aberdeen and around 30 km west of the UK/Norway median line. This is one of the deepest parts of the Central Graben and the Shearwater field is part of the so-called high pressure-high temperature (HPHT) province The study area is located approximately equidistantly between the Forties-Montrose and Josephine Ridge intra-basinal highs and its situation relative to the main Jurassic structures in the area is illustrated in figures 5.1 and 5.3.

5.2 *Geological setting – The Central North Sea*

The Upper Permian saw the development of the extensive Zechstein evaporite basin over much of NW Europe. In the North Sea area this consisted of two distinct but interconnected, approximately E-W oriented basins, partially separated by the Mid North Sea High (Gatliff et al., 1994, Glennie *et al.*, 2003, Jenyon et al., 1984). These are termed the Southern and Northern Permian basins and extend across the present day Southern North Sea and Central North Sea respectively (Figure 5.4) with evaporite sequences in this study area being contemporaneous with those detailed in Chapter 4. Although post-depositional salt mobility has made understanding the development of the North Permian basin problematic, Gatliff et al. (1994) suggests that contemporaneous extension had a role in its development and Hodgson et al. (1992) describes the basin as a sediment-starved, intra-continental rift basin.

Deposited in the Northern Permian Basin were halite-dominated evaporite sequences estimated at between 1km (Buchanan et al. 1995) and 3km (Hodgson et al. 1992) in thickness as well as equivalent basin margin facies. The Triassic saw the development of a significant, approximately N-S oriented rift system in the central and northern North Sea which is becoming increasingly well understood (e.g. Tomasso et al., 2002, Færeseth, 1996). Widespread salt mobility has largely hindered the understanding of the Triassic rift geometry in the Central North Sea although, Erratt et al. (1999) states that Triassic depocentres are thickest to the east of the Jurassic graben system which is consistent with the trend observed in the better imaged Northern North Sea by Tomasso.et al, (2002). Extensive mobility of Zechstein salt has also been documented during the Triassic throughout the Central North Sea (Hodgson *et al.,* 1992, Smith *et al.,* 1993, Gatliff et al., 1994, Johnson et al., 1986) with extension likely to have had a significant role in its development. The Triassic rift and salt-controlled structural geometry was overprinted in the Late Jurassic by another subsequent extensional phase which resulted in the development of a three-armed rift system intersecting around a collapsing thermal dome which had developed in the Early to Middle Jurassic (Underhill and Partington, 1993, 1994). These include the Viking Graben, Central Graben and Moray Firth rift arms (Figure 5.1), although, only the southern (Central Graben) arm influenced the salt basin. Figure 5.5 illustrates, the rift morphology in the Central

Graben which consists of a series of N-S oriented Jurassic sub-basins occurring along an approximately NW-SE oriented en-echelon trend (Erratt et al.1999).

Sears et al. (1993) and Bartholomew et al. (1993) highlight how the observed structural geometry shows a distinct relationship with a pre-existing Early Palaeozoic structural trend and propose a model whereby the rift system developed with widespread reactivation of pre-existing structures and requiring a significant component of oblique slip. Erratt et al. (1999) propose a similar polyphase model with a significant influence of pre-existing trends leading to the basins being offset in an en-echelon fashion. In contrast to the models of Sears et al. (1993) and Bartholomew et al. (1993), however, they highlight the absence of convincing evidence for strike-slip deformation and suggest that the observed fault system developed with extensional faulting and salt mobility as the primary controls with a significant rotation of the extensional kinematic vectors occurring through the rift phase.

By the Early Cretaceous, the rift axis had migrated westward from the North Sea to the North Atlantic (Knott et al., 1993) and the basin entered a prolonged phase of thermal subsidence. Numerous authors recognise a Late Cretaceous inversion phase in the Central North Sea (e.g. Farmer and Barkved, 1999, Erratt et al., 1999, Gatliff et al., 1994, Stewart and Clark, 1999) related to early Alpine compression and considered to be contemporaneous with inversion of the Sole Pit Basin in the Southern North Sea (Ziegler, 1987, Gatliff et al., 1994). This inversion phase is considered to be most apparent in the Norwegian sector of the Central North Sea and is attributed to the development of the (NNW-SSE oriented anticlinal structures along the Lindesnes Ridge (Gatliff et al. 1994, Farmer and Barkved, 1999). Continued thermal sag continued through the Tertiary in conditions of relative tectonic quiescence although salt diapirism continued into this time, with structures locally penetrating much of the Tertiary section (Davison et al. 2000[a], 2000[b], Bishop, 1996).

5.3 *Previous work*

Salt tectonics in the Central North Sea

Salt tectonics in the Central North Sea influences the entire supra-salt sequence with Upper Permian salt penetrating well into the Tertiary sequence in many areas. Bishop (1996) described three salt tectonic zones in the basin consisting of the platform areas bounding the Central Graben, the Central Graben itself and an intermediate zone located between the two. Salt-related deformation in platform areas is characterised by an assemblage of salt structures with a relatively low width to height ratio overlying a moderately faulted, basinward-dipping basement (Bishop (1996). These structures are frequently associated with listric normal faults and the typical structural style is illustrated in Figure 5.6. The Central Graben in contrast, has a much different structural/salt tectonic style consisting of a sub-salt structural topography with numerous very large offset normal faults, variable salt thicknesses and characterised by a series of very tall (up to 6200 metres described by Buchanan et al. 1995) but typically narrow salt diapirs (Figure 5.7).

Most of the literature agrees that the Triassic was the most important phase of salt mobility in the basin. Much of the Triassic sequence is divided into minibasins separated by salt walls with a dominant N-S trend although sediment bodies encircled by salt ridges are identified (Hodgson et al., 1992). Hodgson et al. (1992) and Smith et al. (1993) propose a model they term 'podology' (Figure 2.15) whereby minibasins and salt walls initiate due to a extension and continue to develop through a passive system of salt withdrawal and sedimentation which continues until salt-starvation. Penge et al. (1993, 1999) in contrast, propose a model (specific to the East Central Graben) of 'raft tectonics' whereby the observed geometries are due to extension driven rafting with salt upwelling between the rafted blocks of Triassic sediment. Stewart and Clark (1999) discuss these mechanisms and highlight that many areas, particularly on the platforms show significant evidence of growth geometries within the Triassic sediment pods indicative of salt-withdrawal style growth. In contrast, the Triassic sequences separated by salt walls in the graben areas show little evidence of salt-withdrawal related growth suggesting the 'rafting' was post-depositional and related to Jurassic extension.

In contrast to the typically elongate salt walls associated with the Triassic minibasin/raft assemblage which typically do not extend beyond the Jurassic sequence, the tall diapirs, exclusive to the deepest parts of the Central Graben typically have a sub-circular shape in timeslice view and penetrate well into the Cretaceous and Tertiary section. Figure 5.3 shows the location of many of the major diapiric structures in the Central Graben and one of these is also shown in Figure 5.7. Davison et al. (2000[a]) notes that these structures are typically associated with major faults in the Mesozoic sequence and observations of published seismic sections (e.g. Figure 5.7 (this study), Figure 8 of Erratt et al. 1999, Figure 4 of Bishop, 1996) show many are also associated with large faults in the sub-salt sequence. Despite their apparent intrusive nature, Davison et al. (2000[a]) suggests they penetrated the Cretaceous and younger (post-rift) sequences through a process of down-building and slump structures and debris flows in cored Palaeocene-Eocene units indicate they were at or near the surface at this time (Davison et al. 2000[b]).

Numerous authors have suggested that post-rift basin inversion has influenced these diapirs with compressional structures superimposed on the salt structures (e.g. Buchanan et al. 1995, Davison et al. 2000[a], Stewart and Clark, 1999). Stewart and Clark (1999) link the variable ellipticity of these sub-circular structures in plan view to compression suggesting they behaved as strain ellipsoids during Tertiary compression.

Faulting in the Central North Sea

Although numerous publications describe faulting associated with the Triassic and Jurassic rift phases in the Central North Sea (e.g. Penge et al., 1993, Smith et al., 1993, Buchanan, 1996, Hodgson et al. 1992), compared with the salt-free Northern North Sea, the mechanics of fault development in the basin and the evolution of the rift system is relatively poorly understood. This is primarily due to the great complexity of the fault systems in the basin and as both the northern and central North Sea experienced a very similar tectonic history, this complexity highlights the dramatic influence of salt on fault geometry. As Figure5.7 shows, fault-controlled subsidence is greatest in the Late Jurassic Central Graben area where sub-salt faults show offsets of up to 3km and can be traced for up to 30km (Stewart and

Clark, 1999). Supra-salt faults, however, show very little relationship to the underlying rift geometry, typically soling out into the salt and displaying more of a relationship to the salt geometry than the basement fault geometry (Hodgson et al., 1992).

The most significant factor in the development of Late Jurassic faulting in the supra-salt sequence appears to be that the rift system overprinted a system of pre-existing salt structures and inter-salt minibasins developed during the main Triassic phase of salt mobility (Erratt, 1993, Stewart and Clark, 1999, Hodgson, 1992). Supra-salt faulting has clearly exploited heterogeneities in the pre-rift sequence due to this salt mobility with faults developing at points of structural weakness, typically at the minibasin-salt wall interfaces (Hodgson et al. 1992). Hodgson et al. (1992) details differences in the structural wavelength of sub-salt and supra-salt faulting (Figure 5.8) and points out that the sub-salt faults develop with a similar frequency to those in the salt free Northern North Sea whereas the salt control requires supra-salt faults with smaller offset and greater frequency to accommodate the same extension.

Erratt (1993) investigated the role of basement structures in influencing supra-salt structures and highlighted that a wide range of supra-salt structural styles developed as a response to Late Jurassic extension. These styles include faulting, diapirism, forced folding and gravity sliding with the specific style being controlled by the location of underlying basement faults relative to the pre-rift salt structure/minibasin morphology. Stewart and Clark (1999) detail a degree of detachment of sub-salt and supra-salt deformation based on the ratio of salt thickness to basement fault displacement and illustrate a model of the changing supra-salt deformation styles with changing salt thickness and pre-existing supra-salt structure (Figure 5.9). Helgeson (1999) also proposes a model of supra-salt fault development in the Central Graben concerned with the interaction with sub-salt structures. As this study directly refers to the study area, however, it is reviewed in the following section.

Structural geology and development of the Shearwater Fault System

Several previous publications have discussed the structural configuration of the fault system associated with the Shearwater hydrocarbon field which is here termed the Shearwater Fault

System. Although primarily a review of the development history of the Shearwater field, Blehaut et al. (1999) illustrate a structural interpretation of the fault system (Figure 5.10). Hydrocarbon accumulations are shown to be trapped by what is illustrated as two distinct faults labelled A and B in Figure 5.10 and which are linked by two smaller faults labelled C and D. In this interpretation, the faults are separated by an area labelled as "area of poor seismic definition" which is where the 'Northern Block' of the Shearwater Field is present which they describe as "a salt induced structure located on the downthrown side of the same (i.e. NE side of fault labelled B) fault". In Figure 5.10 this interpretation shows both faults (A and B) to display a large amount of strike curvature from tip to tip. This is approximately 75° in segment A and 65° in segment B. Blehaut et al. (1999) do not discus this structural configuration and their publication concentrates largely on the technical aspects of hydrocarbon recovery. Helgeson (1999), however, provides a structural model for the development of the Jurassic HPHT play of the Central Graben and the maps and sections in this publication as well as the proposed model include the Shearwater Fault System.

Helegeson (1999) highlight several key structural features of faults in the area most notably the highly irregular fault pattern in the supra-salt sequence. The paper also describes a significant mismatch in fault locations and orientations between sub-salt and supra-salt levels which is particularly apparent in the Shearwater area. This is shown in Figure 5.11 which illustrates structure maps at Base Upper Jurassic (Top Pentland Formation) and Top Rotliegend (Base Salt) levels. In this figure the Shearwater Fault System as described in this study is marked with an 'S'. Figure 5.12 shows an interpreted seismic section through the area and Helgeson notes several observations which are illustrated in this section. These observations are that each fault block appears to be grounded on the edge of a basement horst and that the crests of supra-salt faults always overlie a basement fault with the opposing dip. Helgeson (1999) also notes that salt, upwelling to varying degrees is typically associated with these faults and that salt structures are generally circular in map view, located in the hanging wall to faults and almost always situated at the apex of the rotated fault block. Figure 5.12 illustrates the salt bodies associated with the fault planes, including one associated with the Shearwater Fault System. As shown in Figure 5.12, these salt bodies are typically illustrated as being located in the hanging wall area of the faults.

Helgeson, (1999) proposes a model whereby the complex supra-salt structural framework in the area is due to interactions between the sub-salt structural topography and the supra-salt sequence during Late Jurassic rifting. The complex structural geometry and mismatch between sub-salt and supra-salt structural styles is explained by a model where the supra-salt fault blocks are considered to rotate about a fulcrum at the first point of contact with the underlying sub-salt fault block. Subsequent faulting then occurs due to continued rotation of fault blocks associated with salt withdrawal as extension of the basement continues. This model is illustrated in Figure 5.13. Diapiric salt structures are considered in this model to have developed after Late Jurassic block rotation (Figure 5.13) and as overlying Lower Cretaceous sequences are folded around the salt structure, Helgeson (1999) suggests that salt diapirism is Lower Cretaceous in age. Despite this, however, the model suggests that salt diapirism was initiated due to Late Jurassic extension.

Dooley et al. (2005) briefly discuss the Shearwater Fault System with reference to an analogue modelling study of basement controls on salt tectonics. This paper illustrates the Shearwater Fault System as a 3 armed "tri-spoke" fault pattern intersecting around a central, sub-circular salt diapir (Figure 5.14). In contrast to the interpretation in Helgeson (1999), Dooley et al. (2005) illustrate the fault plane as having been breached by the salt diapir with the slip surface located on the hanging wall side of the salt diapir (Figure 5.14(b) rather than on the footwall side as illustrated in Figure 5.13. In this paper, these aspects of the Shearwater Fault System are likened to structures developed in analogue models described in the same paper and the fault system is considered to have developed above a basement corner or intersection point in the sub-salt fault system.

5.4 The study area

Stratigraphy

Well penetrations do not penetrate beyond Middle Jurassic level in the study area. Well penetrations elsewhere in the Central Graben, however, confirm the presence of thick sequences of halite-dominated Zechstein Group evaporites (Upper Permian) overlying the fluvial, aeolian and sabkha deposits (Gatliff et al. 1994) of the Rotliegend group (Lower Permian) which represents the salt-tectonic basement. Whilst Triassic sequences are dominated by the largely lacustrine Smith Bank Formation, the Triassic saw a progressive increase in coarse clastic input with time and the fine fluvial sandstones and siltstones ascribed to the Skagerrak Formation often dominate the Upper Triassic in the Central Graben (Hodgson et al., 1992). Lower Jurassic sediments are largely absent from the Central Graben, probably due to widespread erosion associated with thermal doming (Underhill and Partington, 1993, 1994) and the Middle Jurassic Pentland Formation is the first Jurassic sequence to be encountered in well penetrations in the study area and is expected to be the oldest Jurassic sequence preserved. This sequence consists of stacked fluvial sand channels, crevasse splay and overbank fines (Gilham et al., 2005) in the study area which are contemporaneous with volcanic and volcanoclastic rocks elsewhere in the basin (Gatliff et al., 1994).

Upper Jurassic deposition began with the reservoir shoreface sands of the Fulmar Formation which grade into the offshore marine shales of the Heather Formation representing deepening marine conditions later in the period (Gatliff et al., 1994, Gilham et al., 2005). Organic-rich, black shales of the Kimmeridge Clay Formation were the latest Jurassic unit to be deposited and were largely contemporaneous with the Late Jurassic rift episode. A very thin Lower Cretaceous sequence (mudstones/marls) is present overlain by the Upper Cretaceous Chalk Group which has a thin limestone/chalk unit (Hidra Formation) and organic rich mudstone unit (Plenus Marl Formation) at its base. The top of the Plenus Marl Formation forms a very strong seismic marker in the study area which marks the base of the limestone/chalk-dominated Hod and Tor formations. Tertiary deposition in the area is

dominated by a thick sequence of mudstones and lesser sandstones of the Rogaland and Hordaland Groups. The stratigraphy of the study area is summarised in Figure 5.15 .

Seismic interpretation issues

Observations of the Shearwater Fault System are based entirely on seismic data coupled with geological data from released wells. The seismic data available to this study covers a limited area encompassing the Shearwater Fault System but not the surrounding area and consequently, published material is entirely relied upon to place the fault system into a wider structural framework. This dataset has several significant limitations. Firstly the seismic data has been clipped off at a depth of 5 seconds two way travel time (TWTT) removing much of the sub-salt sequence from the dataset and making links between sub-salt and supra-salt deformation highly problematic. Secondly none of the wells in the area penetrate the entire supra-salt sequence and therefore salt has to be delineated entirely by its seismic facies characteristics. Well control is also entirely absent from the hanging wall sequence although the distinct seismic characteristics of the pre-rift sequence and particularly the strong Base Upper Jurassic reflector mean a high level of confidence is given to correlations across the fault and certain horizons can also be correlated around the fault tips.

5.5 Structural Geology

Sub salt structure

The absence of seismic data below 5 seconds (TWTT) in the dataset means that determining the sub-salt structural geometry is highly problematic as the base of the salt is typically near or below this level. Helgeson (1999) and Dooley et al. (2005) both publish sub-salt structure maps which include the study area at the top Rotliegend (base salt) horizon, one of which is shown in Figure 5.11(b). As Figure 5.11(b) shows, this interpretation illustrates the area to be dominated by a series of WNW-ESE or NW-SE trending normal faults with a less extensive group of approximately N-S trending faults also present.

An opportunity was taken as part of this investigation to view a regional seismic dataset which did include the sub-salt sequence which was not released to this study. The sub-salt data was found to be of extremely poor quality with the top salt reflector mapable with a very low level of confidence. The tenuous and often forced interpretation of this data set suggested the presence of a WNW-ESE oriented, southward dipping normal fault directly below the Shearwater fault system which is similar to the interpretation shown in Figure 5.11. This candidate sub-salt fault has a maximum offset of ~300 milliseconds (msec), significantly less than the maximum of 752msec in the supra-salt fault system. The orientation of this candidate sub-salt structure is oblique to both the Late Jurassic and Triassic structural trends but is consistent with the inferred Permian trend. Consequently this is inferred as a remnant of the fault system controlling the Permian basin and its low offset and oblique orientation means it is not considered to be a major structure accommodating Late Jurassic extension.

Salt structures

Although data coverage and resolution issues mean that a full survey-wide interpretation of the top and base of the salt sequence is not possible, where salt has upwelled into diapiric structures it can be delineated with confidence. Timeslices reveal sub-circular areas of extremely poor seismic coherence in areas which are generally characterised by very

coherent reflection patterns. These areas are interpreted as being bodies of upwelling salt and have been mapped as diapiric salt structures using these characteristics. Figure 5.16 illustrates a timeslice through this area (a) and a 3D view (b) illustrating the morphology of the interpreted diapiric structure in the vicinity of well 22/30-15.

Within the survey area, two distinct diapiric structures have been identified, both displaying a distinctive sub-circular shape. The larger of the two is here referred to as the Martha salt structure (after Helgeson, 1999) and is located in the NW margin of the survey area, around 1 km NNE of well 22/30-15 (Figure 5.17). Due to its peripheral location with respect to the Shearwater Fault System, this structure will not be discussed in much detail. The other salt structure in the survey area is here termed the Shearwater salt structure and is located in the vicinity of the Shearwater field, centred around 250m NE of 22/30-15 (Figure 5.17). The base of the salt has not been identified for either structure so no idea of their structural elevation can be determined however this is a minimum of 1100msec (TWTT) for the Martha structure and 950msec (TWTT) for the Shearwater salt structure.

This study is primarily concerned with the Shearwater salt structure due to its relationship with the Shearwater Fault system. Although an entire supra-salt sequence is not imaged due to clipping of the data, where observed, reflectors in the Triassic and Middle Jurassic (pre-rift) packages are typically parallel. Therefore no evidence for salt mobility prior to the Late Jurassic can be constrained although given the regional trend and the limited amount of data from this sequence, Triassic salt mobility in the area is not ruled out. Salt structures penetrate through the entire Triassic and Jurassic succession although neither penetrate the Base Cretaceous Unconformity. Both structures are directly overlain by circular anticlinal domes at Cretaceous and Early Tertiary level.

Structures in the Pre-rift sequence

The structural geometry in the sequence below the Base Cretaceous Unconformity is dominated by a complex array of extensional faults. As well as a series of smaller faults, the study area is dominated by the large Shearwater Fault System which spans most of the survey area.

The Shearwater Fault system

The Shearwater hydrocarbon accumulations are trapped by a complex system of extensional faults here termed the Shearwater Fault System. This fault system offsets the Jurassic and Triassic sequence but does not penetrate the Base Cretaceous Unconformity and is therefore considered to have become inactive before the beginning of Cretaceous deposition. The fault morphology at Base Upper Jurassic level is illustrated in Figure 5.18. As Figure 5.18 shows, the fault system is interpreted as a complex network of four fault segments which increase in displacement towards a central area in the vicinity of the Shearwater salt structure. In contrast to the interpretation illustrated in Blehaut et al. (1999) where the fault system is interpreted as consisting of two distinct faults, each with a high degree of strike curvature (Figure 5.10), the fault system is here interpreted as an interconnected fault system consisting of four separate arms which intersect at the salt diapir. The intersecting nature of the fault segments is difficult to visualise from the structure map in Figure 5.18 although the timeslice shown in Figure 5.16(a) illustrates very clearly how the faults intersect around the salt diapir.

The individual segments of the fault system have two distinct orientations, the northern and southern segments have a NNW-SSE orientation and dip to the WNW whereas the oblique western and eastern segments have an E-W orientation and both dip towards the north. The fault system continues for 11 km along this NNW-SSE trend and for 7.5 km along the E-W trend. The fault system has a maximum throw of 752msec which has been depth converted to approximately 1200 metres (Appendix 1). In the central area, the margin of the Shearwater salt diapir is interpreted as forming part of the slip surface of the fault system and in Figure 5.16, the fault surface is inferred as running around the NE margin of the salt structure. This interpretation is also shown as a seismic section in Figure 5.19 which illustrates how the fault surface continues above the salt diapir towards the Base Cretaceous Unconformity having a distinct curved profile around the crest of the salt body. Consequently, this interpretation implies that the salt is situated in the *footwall* area of the fault system rather than the hanging wall as suggested in Helgeson (1999).

The NNW-SSE trend of the fault system is here considered to be the dominant orientation due to it having a greater combined length than the E-W trend and also due to its parallelism with the regional fault trend. This orientation is also parallel with the majority of minor faults at Base Upper Jurassic in the survey area (Figure 5.18) which strongly suggests that this was the principal stress orientation at the time. Further evidence for this being the dominant trend comes from the observation that a latest Jurassic seismic surface is offset slightly by the NNW-SSE trending segments but not by the eastern segment indicating that this NNW-SSE trend was active as a single structure after the E-W trend had ceased moving. This surface is tenuously matched with the SJU600 sequence boundary described by Jeremiah and Nicholson (1999) and dated by them as being earliest Middle Volgian in age. Figure 5.20(a) illustrates a profile along the Shearwater Fault System calculated along this NNW-SSE trend which plots the elevation of the footwall and hanging wall cut-offs along the fault. This elevation profile illustrates that cut-off elevations vary significantly along the fault and they are significantly dissected by the E-W trending segments which are oblique to this profile. These oblique segments divide the fault system into a structurally high southern area and a structurally lower northern area.

The footwall structural highpoint on the fault system is offset by around 2 km from the structural lowpoint and the gradient of the hangingwall profile displays a significant change approximately 2km along the profile. Also shown on this profile is the maximum elevation of the top of the salt between the two fault cut-offs. The salt diapir is shown to be located directly below the footwall high point and directly adjacent to the hanging wall lowpoint. Figure 5.20(b) illustrates a displacement-length plot along the same profile which has been depth converted using the technique described in Appendix 1. This profile shows a very different trend in the northern part of the fault system to that in the south. The southern part displays a relatively gentle increase in fault throw with length whereas the northern part has a much steeper overall gradient and also displays significant further increases in gradient at 2.25 km and 5.5 km along the fault giving the profile a distinctive bell shaped top. Comparison of figures 5.20(a) and 5.20(b) show that the point of maximum displacement is situated in the vicinity of the structural lowpoint on the fault system rather than the structural highpoint indicating that hanging wall subsidence rather than footwall uplift was the dominant factor controlling fault displacement.

Small scale faulting

Numerous minor normal faults have been mapped in the survey area and with a very small number of exceptions, they typically have either a NW-SE or NNW-SSE orientation (Figure 5.21). Faults are observed being both synthetic and antithetic to the Shearwater fault trend and the majority are clustered in either the area between the northern and western segments or the area between the eastern and southern segments. Two faults have been mapped which have an E-W trend, both of which are antithetic to the E-W trending segments of the Shearwater Fault System.

5.6 *Sedimentary depocentres*

Sedimentary packages in the pre-Base Cretaceous sequence displaying sedimentary growth are only identified in the uppermost Kimmeridgian and Volgian parts of the sequence with older sequences displaying parallel reflectors. Growth sequences within the survey area are all associated with the Late Jurassic fault blocks and are restricted to two main areas. Figure 5.22 shows an isochron map of these growth sequences which are isolated from each other by the uplifted and eroded fault block crests between them. The northernmost of these depocentres in situated in the hanging wall to the Shearwater Fault System, however, it is restricted entirely to the hanging wall area of the northern and eastern segments. This package contains a maximum thickness of 790msec (TWTT) of Upper Jurassic sediments (including the pre-rift Heather and Fulmar Formations) with reflectors diverging dramatically towards the fault plane (Figure 5.19). This package has an irregular trough shape which has a distinct curvature to it on the isochron map (Figure 5.22) and contour patterns in the pre-rift Base Upper Jurassic structure map (Figure 5.18) have a distinctive pear shaped morphology.

The second syn-rift growth package identified is located behind the Shearwater Fault System in the rotated footwall area to the western and southern fault segments. This package has an approximately NW-SE trending trough shaped morphology (Figure 5.22) and also links to the north with the area in the immediate footwall of the western segment of the Shearwater Fault System where it continues for 3 km with an E-W trend. This package is offset from the fault plane by approximately 1.5-2 km where the Base Cretaceous sup-crops truncated pre-rift units rather than syn-rift growth sequences (Figure 5.23). The package increases in thickness progressively with distance to the SW (away from) the Shearwater Fault System with its depocentre axis located ~3.5 km to the SW of well 22/30-2. The package has a maximum time thickness of 548msec (TWTT) of Upper Jurassic sequences within the study area and reaches its maximum thickness outside the study area. This package is interpreted as a combination between a footwall salt withdrawal basin and a hanging wall growth sequence associated with another fault system on the margins of the survey area (in the vicinity of the Elgin and Franklin hydrocarbon fields). It is also possible that very minor growth sequences are also present in the hanging wall areas of the southern and western fault

segments. Seismic resolution is, however, not good enough in these areas to either confirm or disprove the presence of the diverging reflectors indicative of sedimentary growth in this area. The level of the Base Cretaceous unconformity relative to the base Upper Jurassic surface in these areas suggests that these areas are likely to be either truncated pre-rift packages or very thin growth sequences overlying partially truncated pre-rift sequences.

5.7 *Structures in the Cretaceous and Tertiary section*

Faulting associated with the Shearwater Fault System is entirely truncated by the Base Cretaceous Unconformity and does not continue into the Cretaceous and Tertiary sequence. Other than very minor layer-restricted polygonal faults in the Eocene to recent package, faulting is largely absent from the post Base Cretaceous sequence. Despite this, structural features have been identified in this sequence which are considered highly relevant to the development of the survey area. The most significant of these are two dome-shaped, doubly-plunging anticlines (periclines) present at the base of the Cretaceous sequence and continuing throughout much of the Cretaceous and Tertiary sequence. Figure 5.24 illustrates a structural elevation map on the top of the Campanian age Top Plenus Marl seismic surface illustrating the location of these two folds.

The axis of the fold structure in the NW of the survey area is located approximately 1 km NNE of well 22/30-1 and the structure located centrally in the survey area is approximately 250m NE of well 22/30-15. These circular folds are not associated with bounding synclines and have their steepest limb angles located at Base Cretaceous level with dips progressively decreasing with decreasing depth through the section.

Several significant relationships have been identified between the structural configuration of the pre-Cretaceous (syn-rift) sequence and that of the overlying post-rift sequence which is nowhere penetrated by diapiric salt in the survey area. Firstly the axes of both of these fold structures are located directly above the crests of the underlying Martha and Shearwater salt structures and decrease in fold height rapidly with distance away from the diapirs. This relationships is clearly illustrated by comparing figures 5.17 and 5.24 and also by the seismic section in Figure 5.19. Also as Figure 5.24 shows, the structurally low areas on structural elevation maps of post Base Cretaceous surfaces are located in the areas directly above where Figure 5.23 shows the Base Cretaceous Unconformity to have a syn-rift subcrop rather than a pre-rift subcrop and hence where there is the greatest thickness of Kimmeridge Clay formation below the unconformity surface. Similarly, isochron maps in the post-rift sequence (e.g. Figure 5.25) show an anomalously thin sequence directly above the crests of

the salt structures and the areas above the thickest syn-rift packages show anomalously thick sequences.

Helgeson (1999) describes onlap of lowermost Cretaceous seismic surfaces onto the margins of these anticlinal structures suggesting this onlap can be used to date the timing of salt mobility. Observations in this study, however, have not revealed any evidence of convincing onlap onto these structures. A close-up seismic section of the anticlinal structure above the Shearwater salt structure is shown in Figure 5.26 and clearly illustrates a decrease in the number of seismic loops onto this structure, particularly from the northern (footwall) area around the Plenus Marl reflector. These geometries are here, not considered to be sufficient to demonstrate sedimentary onlap and are interpreted as being due to tuning of the seismic data. More convincing suggestions of onlap are observed onto the Base Cretaceous surface in Figure 5.26 but this onlap does not show evidence of being related to the anticlinal structure and the footwall high of the fault block is onlapped much more convincingly suggesting the anticline was not a major feature of the Base Cretaceous topography. Consequently, the interpretation favoured in this study differs significantly from that of Helegeson (1999) and his use of it to date diapir movement is strongly questioned.

5.8 Unconformities

The main unconformity surface in the survey area which is clearly observable from seismic data is the Base Cretaceous Unconformity and is recognised in the footwall areas of the fault system by significant angular reflector truncations. This surface is present throughout much of the North Sea and in the areas affected by the Late Jurassic rift episode, typically separates rotated fault blocks and syn-rift sequences from the flatter lying and un-faulted post-rift sequence. Truncations are not, however, identified in hanging wall areas within the study area. As Figure 5.22 shows, syn-rift sequences are not found blanketing the survey area but instead are restricted to two distinct depocentres in the hanging wall to the Shearwater Fault System and to the SW of the faults footwall. These packages are bounded at their top by the Base Cretaceous surface and Figure 5.23 illustrates a subcrop map on this horizon. As Figure 5.23 shows, the footwall crests of the Shearwater Fault System have been eroded significantly with the Base Cretaceous subcrop getting progressively older with distance towards the fault. The areas where the unconformity has its oldest subcrop (Middle Jurassic) are directly above both the Martha and Shearwater salt structures suggesting that they coincided with the structural culminations on their respective controlling fault systems.

5.9 Discussion

Relationship between salt mobility and faulting

The Shearwater salt structure is located directly at the intersection of the four arms of the Shearwater Fault System and a similar relationship between faults and salt structures are also seen for many other salt structures in the Central Graben (Helgeson,1999). This spatial relationship is the therefore considered highly unlikely to be coincidental indicating that a causative relationship is likely to exist between salt mobility and fault development. Such an interpretation, however, raises a significant chicken and egg problem with respect to the timings and relative importance of the two processes. Three distinct hypotheses are proposed.

(a) Salt mobility post-dates faulting and has exploited the fault plane. This model is proposed by Helgeson (1999) and illustrated in Figure 5.13.
(b) Salt mobility pre-dates faulting and the fault plane has exploited the pre-existing salt diapir as a minimum work slip surface.
(c) The salt diapir and fault system developed simultaneously as an inter-related system with both being reactive to extension.

Testing these hypotheses is relatively straightforward in a situation such as this where 3D seismic data is available and significant sedimentary growth geometries associated with the fault system are resolvable. If (a) were true, and salt diapirism post-dated faulting, growth geometries associated with the fault system would not be expected to show evidence of any relationship or control of the developing salt structure on their development. The salt diapir would therefore be expected to simply penetrate the pre-existing growth package with all deformation being limited to intrusion or diapir margin drag and showing no evidence for sedimentary growth. If (b) were true then evidence for sedimentary growth associated with salt mobility would be expected in the pre-rift sequence underlying the fault controlled growth package. Structures could include rim synclines or pillow to diapir transition geometries or any sedimentary growth that suggests salt mobility pre-dates faulting. If (c) were true then the syn-sedimentary growth sequence would be expected to show evidence of a control of both tectonic fault-controlled subsidence and subsidence related to salt withdrawal.

Observations of the Triassic to Oxfordian (pre-rift) sequence in the survey area show seismic reflectors prior to the Kimmeridgian growth sequence to be parallel suggesting that no sedimentary growth occurred prior to this time. No evidence is therefore considered to exist for any pre-rift salt mobility and consequently hypothesis (b) is considered unlikely. Evidence that salt mobility post-dated the faulting is, however, considered rather more ambiguous. Helgeson (1999) suggests that the pericline structures in the post-rift sequence overlying the salt structures are the result of post-rift diapirism. If this mechanism was clearly defined as the controlling process on the development of these folds then this would clearly indicate that at least part of the salt mobility was post-rift. It is here considered that the Lower Cretaceous onlap (Figure 5.13) invoked by Helgeson (1999) to justify this interpretation is an equivocal interpretation at best for the Shearwater example and seismic tuning is considered much more likely (Figure 5.26). Two other processes are considered to

have the potential to create these structures, tectonic inversion and differential compaction and this issue forms part of a discussion later in this chapter.

Observations of the syn-rift growth geometries associated with the hanging-wall depocentre to the Shearwater Fault System are considered to give the strongest evidence as to the relationship between salt mobility and faulting. The isochron map of the syn-rift sequence illustrated in Figure 5.22 shows its thickest point directly adjacent to the northern segment of the fault system. This point is, however, also directly adjacent to the Shearwater salt diapir. Similarly the structural elevation map of the pre-rift Base Upper Jurassic horizon shown in Figure 5.18 shows the maximum subsidence to be directly adjacent to the fault and also directly adjacent to the salt diapir. The morphology of this subsidence pattern does not conform to the typical fault-controlled depocentre morphology described in Section 2.3 where subsidence gradually decreases with distance from the fault plane creating a 'D' shaped contour pattern. Instead, Figure 5.18 shows this package to have its maximum subsidence located in a N-S oriented trough with 'pear' shaped contour patterns with subsidence gradually decreasing towards the north, away from the salt structure, rather than simply away from the fault plane.

Growth geometries in this package are perhaps easiest to understand when viewed on a 3D visualisation. Figure 5.27 shows a 3D view looking through the Shearwater Fault System to the NE towards the hanging wall growth sequence and the salt diapir. As this visualisation illustrates, the hanging wall growth packages thicken very dramatically in the vicinity of the Shearwater salt structure and the point of maximum subsidence can be seen to be directly adjacent to the salt diapir. Consequently a very distinct relationship is considered to exist between the morphology of the hanging wall growth sequence and that of the salt diapir. The interpretation of these observations is that the tectonic fault controlled subsidence associated with the Late Jurassic rift phase has been locally and very dramatically overprinted by subsidence associated with salt withdrawal into the Shearwater salt diapir. As this subsidence has clearly affected growth geometries in the syn-rift growth sequence it can be constrained to be contemporaneous with faulting. Consequently salt mobility is considered to have developed contemporaneously with faulting as suggested in (c). As discussed in a following paragraph, the fold structure in the post-rift sequence above the Shearwater salt structure is

considered to be unrelated to post-rift salt movement and the entire phase of salt diapirism is therefore constrained to be contemporaneous with the Late Jurassic rift episode.

Morphology of the fault system and its relationship with salt mobility

A description of the morphology of a fault system consists of two parts, the orientation of the slip surfaces and the degree of uplift and subsidence either side of these slip surfaces. As detailed in section 5.5, the Shearwater Fault System is considered to be dominated by the NNW-SSE trending Northern and Southern segments. Although Mesozoic fault orientations in this part of the Central Graben are very irregular (Helgeson, 1999, Dooley et al., 2005), this trend is consistent with the main basin bounding faults (Figure 5.3) and is considered to be parallel with the Late Jurassic stress orientation in the area. The E-W trending Eastern and Western segments are, however, oblique to this trend indicating that the controlling stress regime was much more complex than in salt free areas of the rift province.

The discussion described in the previous section both temporally links the development of the Shearwater Fault System with that of the Shearwater salt diapir and highlights the role that salt mobility had in locally influencing fault-controlled subsidence. Analysis of the relative amounts of uplift and subsidence associated with the development of the Shearwater Fault System is aided by the cut-off elevation profile shown in Figure 5.20(a). This profile is calculated along the main NNW-SSE trending segments and also plotted is the maximum elevation of the top of the salt between the footwall and hanging wall fault cut-offs in order to illustrate the spatial relationships between salt mobility, uplift and subsidence. As described in section 5.5, the most significant observations of this profile are that the fault system is very clearly dissected by the oblique Eastern and Western fault segments into a structurally high southern part and a structurally much lower northern part. Also, the footwall structural culmination on the fault system is located in the higher southern area situated directly above the salt diapir and to the immediate south of the two oblique fault segments. The structural low-point of the fault system in contrast, is located in the structurally much deeper northern part of the fault system in the immediate hanging wall to the oblique segments. This observation is significant as for the situation of a classic salt-free fault, the hanging wall high would be expected to be situated at the same length along the

profile as the footwall low as they would be adjacent in a section perpendicular to the profile. In this example, these two points are not adjacent and are offset by approximately 2 km. This relationship is interpreted as being a result of the influence of salt withdrawal on subsidence in the fault system (also identified in Richardson et al., 2005).

The elevation trend for the hanging wall cut-off can be seen to change significantly approximately 2 km along the fault and at this point the proportion of subsidence relative to distance along the fault increases dramatically and continues to be anomalously high for the next 5 km until the elevation of the salt increases dramatically. As described in the previous section, it is proposed that in this area, fault-controlled subsidence is locally overprinted by extensive salt withdrawal related subsidence as the Shearwater salt diapir develops. This area of anomalously high subsidence on the fault profile represents this same area identified on syn-rift isochron maps and pre-rift structure maps. As this profile illustrates, enhanced subsidence is only seen in the structurally lower northern part of the fault system suggesting that the salt mobility feeding the Shearwater diapir was strongly unidirectional being largely restricted to north to south flow from this area. This highly unidirectional salt flow is suggested as a primary control on the development of the E-W oriented oblique fault segments.

It is proposed that the southern part of the fault system was being actively propped up by the developing salt diapir whereas the northern part of the fault was being subjected to extensive salt withdrawal. Oblique faults are therefore considered to have developed as release structures accommodating this differential subsidence and to have increased in displacement as differential subsidence continued. The implication of this is that salt mobility was the major control on their development rather than extension.

While the northern half of the cut-off elevation profile (Figure 5.20(a)) is dominated by relative subsidence in both the hanging wall and footwall areas, the southern part of the profile shows a very different trend. Prior to fault development, the lines that would later become the footwall and hanging wall fault cut-offs are assumed to have both been along the same flat lying isochronal datum line. Cut-off elevations that are currently above or below this inferred line therefore are considered to represent either fault-controlled uplift or

subsidence respectively. In the northern part of the fault, the hanging wall cut-off can be seen to decrease very significantly in elevation along the profile. In the southern part of the fault, in contrast, the cut-off elevation sticks rigidly to an isochronal line at approximately 4275 milliseconds. The implication of this is that hanging wall subsidence did not occur in this southern area and that all fault displacement was locally manifested in footwall uplift. Although it could be argued that hanging wall subsidence did occur and that the profile was subsequently rotated to this isochronal level, the above interpretation is considered more plausible.

Observations of growth sequences associated with faulting, illustrate that no convincing syn-rift package exists in the hanging wall to the southern segment (Figure 5.22). For a growth package to develop, hanging wall subsidence would be required to provide the appropriate accommodation space and therefore the absence of such a package suggests that hanging wall subsidence did not occur. In a situation such as this, finding a mechanism to explain this extensive footwall uplift is relatively straightforward. In the model proposed by Helgeson (1999), rotation of the footwall area due to pivoting on a basement fault block fulcrum is considered to be the dominant process in the latter stages of fault development (Figure 5.13). As a result of salt withdrawal from the distal footwall area this pivot would lead to footwall uplift equivalent to the amount of subsidence on the other side of the pivotal point. As Figure 5.20 illustrates, this model predicts a steeply dipping, uplifted footwall area and a much shallower hanging wall area. Applying such a mechanism to the Shearwater Fault System while still allowing for extensive subsidence in the northern part of the fault system requires pivotal back-rotation of the area in the footwall to the Western and Eastern fault segments.

Another mechanism where extensive footwall uplift could be invoked is where diapiric upwelling below the footwall area effectively pushes up the footwall of the fault block. Figure 5.20(a) clearly illustrates that the footwall highpoint on the fault system is situated directly above the salt diapir and upward movement of the diapir could lead to upward movement of the footwall area.

Displacement – length relationships

Analysis of a complex four-armed fault system such as this where the uplift and subsidence associated with faulting is a complex three-dimensional process is difficult to assess using a classical, two-dimensional displacement-length profile. The profile shown in Figure 5.20(b), however, shows several significant features. In contrast to the established model illustrated in Figure 2.7, the observed profile for the Shearwater Fault System shows several significant differences in the displacement gradient which is strongly variable along the fault system. Firstly, the southern part of the fault system, from ~5750m onwards along the profile shows a relatively consistent displacement gradient. This is in the structurally high part of the fault system to the south of the oblique segments where Figure 5.20(a) shows salt-influenced footwall uplift to be the dominant process in fault displacement. To the north of this area, however, where the oblique segments begin to influence the fault system and salt withdrawal occurred, hanging wall subsidence becomes the dominant process, the gradients become significantly steeper. This steeper gradient is most dramatic in the 3-4 km directly adjacent to the salt diapir where salt withdrawal is considered to have enhanced tectonic, fault-controlled subsidence. Salt withdrawal is consequently considered to have locally steepened the displacement gradient in this area and the distinctive bell-shaped top to the profile is considered to be the result of salt withdrawal significantly enhancing fault-controlled displacement. One consequence of this is that unlike the classic profile shown in Figure 2.7, the point of maximum displacement in the Shearwater profile is not half way along the fault, but rather at the point where salt withdrawal is at its greatest around one third of the way along the fault.

Development of anticlinal structures in the post-rift sequence

The spatial relationship between the doubly plunging anticlines in the post-rift succession and the salt structures which penetrate the pre and syn-rift sequences is direct and unequivocal. The mechanism by which these structures developed, however, is less clearly defined. Helgeson (1999) and Gilham et al. (2005) interpret these structures as the result of post rift salt diapirism, in contrast, it is here considered that compressional inversion and

differential compaction are also valid candidate mechanisms for their development. Each of these three mechanisms are discussed below.

Post Jurassic structural inversion, focused on salt diapirs in the Central North Sea has been suggested by several authors (e.g. Buchanan et al. 1995, Davison et al. 2000[a], Stewart and Clark, 1999). Although clearly having the potential to develop anticlinal structures centred above salt diapirs, several arguments against this hypothesis are considered. The most important of these is that any inversion phase would be restricted to a specific period in the development of the basin. Sequences post-dating this phase would therefore be expected to be marked by an unconformity or onlap onto the fold structure with overlying sequences being deposited parallel to each other. No such surface is identified in the study area and the interpretation detailed above suggests that the onlap illustrated by Helegeson (1999) (Figure 5.13) in the Cretaceous sequence is not present. Rather than being restricted to a specific level in the stratigraphy, the fold structure is present throughout the sequence showing a gradual decrease in amplitude and slight increase in fold length up-section from the Base Cretaceous surface. The implication of this is that either another mechanism is responsible for their development or that the last inversion phase post-dates the entire sequence, in which case it is difficult to link with Alpine tectonics.

Post-rift salt diapirism is another mechanism with potential to develop the observed fold geometry. The presence of the Machar salt structure which penetrates to Mid Miocene levels (Pooler and Amory, 1999) and is situated a few kilometres E of the eastern margin of the study area illustrates that there was significant salt available for post-rift salt diapirism in the area. Seismic data however shows that the salt diapir does not pierce the Late Jurassic fault which would be a requirement for significant post-rift diapirism to occur. Further arguments against this concern an apparent lack of a mechanism to drive salt mobility. As the fold structure involves several kilometres of overlying sediment without an associated intrusive salt structure, buoyancy forces alone are not considered to be capable of doming such a volume of overburden. No other potential driving mechanism such as differential loading, erosional downcutting or extension is apparent from the seismic data which leaves inversion (discussed above) as the only mechanism capable of driving this salt mobility.

The final mechanism discussed here is that folds developed due to passive differential compaction of the sequence with the largely porosity free Zechstein sequence forming the salt diapir acting as an uncompactable pillar around which the surrounding pre and syn-rift sequence compact and subside. This would be expected to leave the sequences directly above the salt structurally elevated relative to the peripheral sequences forming a fold structure mirroring the shape of the salt structure located directly above it. This would successfully explain the spatial relationship of the folds relative to the salt structure, the presence of the fold through the entire post-rift sequence and the progressive decrease in the amplitude of the fold up-section relating to an exponential decay in the porosity with burial. What is here considered the most convincing evidence for this hypothesis concerns the relationship between the sub-Base Cretaceous basin morphology and the structure and isopach patterns in the post rift sequence.

One consequence of the development of the Shearwater Fault System is that large thicknesses of Late Jurassic, Kimmeridge Clay Formation mudstones were localised in two specific depocentres in the footwall and hanging wall areas of the fault system (Figure 5.22). As mudstones have a much higher porosity at deposition than other lithologies (Scalater and Christie, 1980), these thick syn-rift sequences are consequently expected to compact much more than the sand prone pre-rift units.

Figure 5.24 illustrates a structural elevation map of the Upper Cretaceous, Top Plenus Marl horizon which is overlain by an outline of where the Base Cretaceous Unconformity has a syn-rift subcrop illustrating the location of the Late Jurassic depocentres. As Figure 5.24 shows there is a direct correlation between the structural elevation of this surface and the underlying basin morphology. The structural lowpoints on this surface are situated above where the syn-rift packages are present which is where the pre-Base Cretaceous package inferred as having its greatest porosity and potential for compaction at this time. The structural highpoints (and also the fold axes) in contrast are situated above the salt structures where the least potential for compaction is present. A similar relationship is also observed in isochron maps in the post-rift sequence. Figure 5.25 shows an isochron map of much of the post-rift chalk sequence in the basin and illustrates how the thickest sequences are located directly above the Late Jurassic depocentres illustrating that during this period, these were

the areas where the maximum subsidence was occurring. The thinnest sequences in contrast, are situated in the areas above the salt structures. These relationships are very difficult to explain using either the inversion or post-rift salt mobility hypothesis. They are therefore considered to clearly demonstrate that passive differential compaction of the sequence controlled subsidence throughout the post-rift period and hence the structural geometry and isopach patterns of the sequence.

Differential compaction is therefore considered to be the preferred mechanism for the generation of doubly plunging anticlines in this area and also other areas where salt structures have experienced significant burial. Similar fold/salt structure associations are identified in the western platform area of the Central North Sea which have previously been described as inversion structures (Stewart and Clark, 1999). These are discussed in more detail in section 6.3.

Timing and initiation of salt mobility

The observations made as part of this study require a significant revision of the established timings of salt mobility in the Shearwater area from those previously implied by Helgeson (1999), Dooley et al. (2005) and Gilham et al. (2005). Each of these studies either suggests or implies from their diagrams (e.g. Figure 5.13) that salt diapirism was at least partially post-rift. The presence of numerous salt diapirs in the Central North Sea, which grew throughout the post-rift period means that it is tempting to suggest that the Shearwater salt structure was also active at this time. These tall diapirs are interpreted as growing through down-building (Davison et al. 2000[a]) requiring salt to be at or near the surface throughout their development. The Shearwater salt structure in contrast, can be seen to have been overlain by overburden (including syn-rift sequences) throughout its development (Figure 5.19) meaning it is highly unlikely that it developed in the same way as the post-rift structures. Also, observations of the fault system and its associated depocentres in this study provide strong evidence that the fault system and salt structure developed simultaneously.

The above reinterpretation of the anticlinal structures above the salt structures as the result of differential compaction rather than post-rift salt mobility coupled with the absence of salt

penetrating the post rift-sequence indicates that active diapirism of the Shearwater salt diapir had ceased by the end of the Jurassic. Consequently, although taking care not to entirely rule out Triassic salt mobility in the area, the Shearwater salt diapir is considered to have developed in the Late Jurassic. The implication of this is that it is entirely coincident with the contemporaneous rift episode in the basin and therefore salt mobility is considered to be reactive to crustal extension as a response to pressure gradients in the salt sequence related to the tectonic thinning of the overburden.

Role of the Basement

The lack of a well-imaged sub-salt sequence in this study makes understanding the basement controls on salt mobility and the development of the supra-salt fault system problematic. Although several aspects of the interpretations of Helgeson (1999) have been questioned in this study, his structural model for the development of the supra-salt fault systems in the Central Graben is considered to be largely compatible with the observations and interpretations detailed here. Although not fully understood, the sub-salt structural topography is considered likely to have had a significant control on the development of the fault system and may be responsible for the largely uni-directional flow of salt during the development of the Shearwater salt structure. The interpretation of Dooley et al. (2005) however, that the fault system developed at an intersection point in the sub-salt fault pattern is considered to not be supported by sufficient evidence and is clearly model led. What can be determined from the limited observations of the sub-salt sequence in this study is that the sub-salt fault pattern underlying the Shearwater Fault System is largely oblique to it and displays significantly less displacement. At the local scale therefore, the morphology of the Shearwater Fault System is considered to be controlled more by processes in the salt and supra-salt sequences than processes linked to the basement.

Summary

The Shearwater Fault System is considered to have developed due to a complex interaction between extension and reactive salt withdrawal associated with the development of the Shearwater salt structure. Figure 5.28, illustrates a summary model for the development of the fault system where initial faulting of the overburden sequence leads firstly to the mobility of salt to accommodate the relative movement of the offset fault blocks (Stages 1 and 2). As extension continues (Stage 3), extensive salt mobility occurs which is dominated by north to south salt flow into the developing salt diapir. This strongly unidirectional salt flow is accommodated by a pair of oblique, E-W oriented fault segments which divide the fault system into a structurally low, northern part and a structurally high southern part (Stage 4). Salt withdrawal related subsidence significantly overprints tectonic subsidence in the development of the fault system and has a strong influence on the displacement-length relationships of the fault system and the fault-influenced depocentre morphology. Salt mobility is considered to have ceased by the end of the rift phase and anticlinal structures developed above the salt diapir are interpreted as being related to differential compaction rather than inversion or post-rift salt mobility (Stage 5).

6.0 Discussion

6.1 Controls of salt mobility on the development of supra-salt normal faults

Localisation of faults

Salt mobility prior to the development of faulting in both the Moab and Schooner NE areas is considered to have significantly influenced the localisation of fault systems through time. In both basins, extensive salt mobility had taken place prior to the development of these faults and had continued to the extent that major salt welds developed which limited the mobility of salt through much of the basin. Both the Moab and Schooner NE fault systems developed in the crestal region of pre-existing salt-cored anticlines (see Figure 4.16(b) stage 2 and Figure 3.85(a)). This association is considered to be predictable and represent the point where the succession contained its maximum thickness of salt and subsequently the minimum thickness of overburden. Such areas will therefore be where the sequence is weakest and the minimum work is required to fracture the overburden. Consequently, supra-salt faults which are driven by bulk-crustal or layer-restricted supra-salt extension are considered likely to preferentially develop above pre-existing salt structures. Similarly, the particular salt structure which these fault systems develop above is also considered to be predictable.

Restoring the basin morphology to its state prior to the development of both the Moab (Figure 3.89) and Schooner NE (Figure 4.16) fault systems shows that these faults developed at the outermost margin of where prior salt mobility had led to the grounding of the sequence, i.e. peripheral to the outermost salt weld in the basin. This association is intuitive since in order for an entirely supra-salt fault to accrue displacement, salt must be able to flow to accommodate relative movements of the footwall and/or hanging wall (Figure 6.1). Therefore, where a salt-weld inhibits the flow of salt, a major fault is considered unable to develop without an involvement of the sub-salt sequence.

Salt controls on the geometry of the fault systems

Each of the fault systems in this study show a significant relationship to the underlying salt structure. Where the salt structure is elongate in the Moab and Schooner NE examples, the strike of the fault system develops exactly parallel to the long axis of the salt structure. This is consistent with modelling by Ge et al. (1996) which shows that fault structures are likely to develop parallel to an elongate salt structure even if the extension direction is oblique to its axis (Figure 6.2). In such a situation, strain is considered to localise on the salt high as it represents the weakest point in the sequence and it is therefore far easier to fracture in this location than in areas where the sequence is thicker. Consequently, where pre-existing elongate salt structures exist, these are considered to be sites of strain localisation and single, large fault systems are expected to develop in their crestal regions rather than more widely distributed arrays of faults.

The sub-circular and spatially more restricted Shearwater salt structure is only associated with the central portion of the fault system (Figure 5.17) and has an altogether different control on the geometry of the fault system. This complex, four armed fault system including segments which are almost perpendicular to each other is considered to have developed as a response to an extremely complex stress regime, strongly influenced by salt withdrawal (section 5.9). Although oblique faults have frequently been documented in various salt free settings, these are generally small relative to the offset on the main fault. The oblique faults in the Shearwater Fault System in contrast, accumulate displacements on the order of several hundred milliseconds which equates to hundreds of metres of throw. As detailed by Bell (1996), in settings where deformation in cover sequences is considered to be 'attached' to that of the basement, stress orientations are expected to be relatively organised and unidirectional (see Figure 2.10). The highly variable stress regime responsible for the development of the Shearwater Fault System is therefore considered to be a direct result of salt decoupling sub-salt from supra-salt deformation with salt flow influencing subsidence and displacement on individual segments.

The role of salt structures as slip surfaces for supra-salt faults

The role of salt layers as preferred fault surfaces is well documented in thrust settings (e.g. Boyer and Elliott, 1982, Butler and Coward, 1987) and the association between salt structures and faulting in diapiric basins has also been widely established (section 2.4). In each of the examples detailed in this study, the margins of the salt structure associated with the fault system is considered to have behaved as a slip surface. This can be clearly seen on seismic sections of the Schooner NE (Figure 4.20) and Shearwater fault systems (Figure 5.19) and is also inferred from well data and the observed structural geometry for the Moab segment of the Moab Fault System (Figure 3.44).

In situations such as the Moab and Schooner NE fault systems, where the salt structure pre-dates the fault, the link can be attributed to the fault surface nucleating in the crestal region and propagating to the margin of the salt structure as displacement increased. In a situation such as the Shearwater example in contrast, where there is no evidence of a salt structure pre-dating the fault system and the diapiric structure is considered to be reactive to the faulting, a different relationship exists. In such a situation, the fault and salt structure are considered to have developed as a linked system with the salt structure initially being manifested as an area of elevated salt situated below the faults footwall and developing into a salt diapir as the fault system developed (Figure 5.28). As such, the salt structure is considered to have behaved as a slip surface throughout its development. A salt body is likely to make a preferential slip surface due to its relative weakness making it an efficient detachment horizon.

Using the margins of a salt structure as a slip surface has significant implications for the shape of the fault planes. Where a pre-existing salt structure is exploited as a slip surface, the slip surface is expected to follow the geometry of that margin. As fault movement is considered unable to occur unless it is accommodated by salt mobility allowing relative movements of the footwall and hanging walls, any fault movement is likely to significantly modify the salt structure geometry. In the Shearwater example, where the fault plane continues above the salt structure, its geometry changes significantly as it ceases to be constrained by the morphology of the salt structure and could be described as having a ramp-

flat geometry. As Figure 5.19 shows, the fault plane consists of a steep-sided fault surface on the flanks of the salt structure, shallowing significantly to a relatively flat plane over its crest. This then increases in dip again in the area between the crest of the salt structure and the Base Cretaceous Unconformity but has a much lower dip than that observed below on the flanks of the salt structure. Although this change in dip could be interpreted as being due to late stage salt movement effectively bending the fault plane, the interpretation favoured here is that this is at least partially due to compaction.

It is proposed that as the faulted sequence compacts, the dip of the fault plane shallows as a response to the overall volume reduction (as established by Xiao and Suppe, 1989). Salt structures, however, are considered to be uncompactable (Rowan, 1993) and where they form the slip-surface to a fault system, this shallowing effect will not take place. A similar ramp-flat style geometry is considered to exist at the top of the Moab-Spanish Valley salt structure in the Moab canyon area where the exposure style changes from being a fault entirely in the overburden to the salt structure, to where salt is exposed at the surface and slip is interpreted along its NE flank (see figure 3.27).

The role of salt mobility in influencing the uplift and subsidence associated with faulting

The uplift and subsidence associated with faulting is considered to be relatively predictable in salt-free settings with hangingwall subsidence largely considered to be by far the dominant manifestation of fault movement (section 2.3). The primary tools used to investigate the uplift and subsidence associated with faulting are structure contour maps and cut-off elevation profiles based on surfaces which were inferred to be flat prior to the development of the fault system. Observations of such maps and profiles for the salt-influenced faults investigated in this study, however, reveal that in salt-influenced settings, footwall uplift can be *equally or significantly more* important than hanging wall subsidence. As detailed in section 3.12, both cut-off elevation profiles (Figure 3.51(a)) and structure contour maps (Figure 3.42(b)) for the Moab Fault System reveal that the hanging wall experienced negligible subsidence. The footwall area, in contrast, which is underlain by a body of upwelled salt, has experienced extensive uplift and in this example, the majority of fault movement is considered to be manifested as footwall uplift.

In the Shearwater example, despite the maximum offset on the fault being related to extensive hanging wall subsidence restricted to the northern and eastern segments (Figure 5.18), the hanging wall to the southern segment appears to have experienced negligible subsidence (figure 5.20(a)). In contrast, the footwall to this segment which is underlain by the Shearwater salt structure at its apex has experienced extensive relative uplift. Similarly, the cut-off elevation profile for the northern segment of the Schooner NE fault system appears to show a slight dominance of footwall uplift (Figure 4.21(a)). Although it could be argued that enhanced footwall uplift observed in these examples occurs simply as a response to salt buoyancy below the fault plane, this is insufficient to explain why footwall uplift occurs at the expense of hanging wall subsidence in the Moab Fault system. As has previously been mentioned in this discussion, it is considered that an entirely supra-salt fault requires salt mobility to take place in order for the footwall and/or hanging wall to be able to move relative to each other. Consequently salt withdrawing from a subsiding hanging wall must migrate somewhere else which could be either into the adjacent footwall or into the footwall of another structure (Figure 6.1). This migration of buoyant salt from hanging wall to footwall is considered to have the potential to enhance footwall uplift although it is the ability of salt mobility to accommodate fault displacement at shallow crustal levels which is considered to be more significant.

According to Jackson and McKenzie (1983), the stress reduction which occurs across a fault during a slip event is equal in both the footwall and hanging wall and they consider the dominance of the hanging wall component of fault movement, typical in salt free settings to be a consequence of the large-scale listric geometry of the controlling fault (Figure 6.3(a)). In such a situation, a large fault would be expected to continue to the brittle-ductile transition zone gradually decreasing in dip due to rheological changes with depth with displacement being eventually accommodated by thinning of the mantle lithosphere and upwelling of the asthenosphere. As Figure 6.3(a) suggests, this geometry, therefore requires the rotation of the fault block to be largely restricted to the hanging wall.

In contrast to an fault involving the entire lithosphere, an entirely supra-salt fault is able to accommodate its displacement within the salt layer where it soles out. At these depths, the

rheology variations in the supra-salt sequence are not considered to require significant shallowing of the fault plane and therefore there is considered to be no large-scale geometric control on the relative uplift and subsidence associated with faulting. It is therefore argued that *for a supra-salt fault, footwall uplift is likely to be an equally important method of accumulating fault displacement as hanging wall subsidence.* For a situation such as the Moab segment of the Moab Fault system, where a pre-existing salt weld in the hanging wall area made hanging wall subsidence problematic, it is considered that fault displacement could be efficiently accommodated entirely by uplift of the footwall. This situation is illustrated in Figure 3.85 which shows the salt required to move below the footwall area to accommodate this fault displacement to be more efficiently withdrawn from the distal footwall area rather than the immediate hanging wall.

A similar situation is considered to also exist in the SW quadrant of the Shearwater Fault System with salt withdrawn from the distal footwall into the footwall area accommodating some of the fault movement (Figure 5.28). The Shearwater example also illustrates how syn-tectonic salt withdrawal is able to locally enhance hanging wall subsidence. As detailed in section 5.9, salt withdrawal associated with the reactive rise of the Shearwater salt structure is considered to significantly locally overprint tectonic fault-controlled hanging wall subsidence. Salt mobility is therefore considered to have a very significant influence on the relative uplift and subsidence associated with faulting and faults which detach at a salt layer behave very differently from those in salt-free areas.

Controls of salt mobility on displacement-length relationships

The salt-influenced faults investigated in this study reveal extensive evidence of a significant control of salt mobility on their displacement-length relationships. As figures 3.51(b) and (c) show, the cumulative throw across the Moab Fault system experiences a dramatic increase in both bulk displacement and the displacement gradient at the point where the Blue Hills segment hard-links with the Moab segment. As is detailed in section 3.8, the Blue Hills segment is not underlain by any salt structure. Gravity and well data, however, reveal the Moab segment to be underlain by a significant amount of upwelled salt along its entire length. It is therefore proposed that this mobile salt has locally enhanced the amount of

displacement upon the fault. The exact details of how this has occurred are unclear, although it is speculated that the salt mobility associated with faulting is of greater magnitude than the simple passive migration of salt required to allow the footwall and hanging wall to move relative to each other. It is suggested that enhanced salt movement could lead to further uplift of the footwall area and consequently enhance the amount of fault displacement.

Processes that could be invoked to drive additional salt mobility could be buoyancy or sedimentary differential loading associated with deposition in adjacent fault-controlled depocentres. The Shearwater fault system also locally displays a dramatic, localised increase in fault displacement which is related to salt mobility. Unlike the Moab Fault system, this is not related to salt upwelling below the footwall but rather to salt being locally withdrawn from the hanging wall into the adjacent Shearwater salt structure as detailed in section 5.9.

The Schooner NE fault system also displays a significant change in fault displacement in its central area associated with salt mobility. This transition occurs where the fault system experiences a transition from displacement across a fault to displacement across a salt wall. In contrast to the previously described examples, however, where displacement has become enhanced by the salt structure, this transition represents a significant drop in displacement. The reasons for this displacement are discussed in a following section. As a result of these observations, it is considered that salt mobility can have a very significant control on the displacement-length relationships of a supra-salt fault and can lead to displacement being locally enhanced or reduced along a fault system. Such displacement variations are not, however, necessarily expected in all supra-salt normal faults. Childs et al. (1993) model faults developed above a salt analogue (see Figure 2.11) and show that in these faults "displacement varies in a regular and predictable manner". As Figure 2.11 shows, the only salt mobility associated with faulting in their models is the passive migration required to allow relative motion of the rotated blocks (Figure 6.1).

In contrast to the observations of Childs et al. (1993), each of the fault systems detailed in this study involve either diapirism which is reactive to faulting or faults which develop above pre-existing salt structures. It is therefore considered to be the dynamic movement of

salt which influences displacement-length relationships locally along the fault rather than passive movement.

Relative role of extension in the development of extensional style supra-salt faults

Although each of the study areas represented in this investigation contain large-scale (in excess of 500m throw) extensional-style normal faults, the tectonic driving forces behind their development are variable and frequently ambiguous. The easiest faults to explain in terms of their tectonic controls are the Late Jurassic Shearwater Fault System and the Jurassic growth faults observed in the Southern North Sea study area (figures 4.14(b) and 4.17). These faults are synchronous with a well-documented, regional extensional phase (Roberts et al., 1999, Rattey and Hayward, 1993), which is also recognised outside of the salt basin and fault orientations are largely consistent with those of this rift episode implying that bulk crustal extension was responsible for their development.

In contrast to the Jurassic faults of the North Sea, the Moab fault system is not contemporaneous with any extensional phase recognised in the Colorado Plateau region outwith the salt basin despite having accumulated throw in excess of 850 metres. The lack of control on faulting in the sub-salt sequence means that it can not be determined whether supra-salt extension is balanced by sub salt extension and therefore whether or not extension is a bulk (tectonic) extension or is restricted to the supra-salt sequence. This raises the question about whether a small amount of regional extension was focused on the Paradox Basin due to the presence of salt making it a point of regional weakness or whether extension is an entirely thin skinned process and not balanced by equivalent large scale crustal extension (see section 3.12).

In the Schooner NE example (Chapter 4), the entirely thin-skinned nature of faulting is less ambiguous as the sub-salt sequence is resolved on seismic data and does not contain extensional structures with equivalent displacement. The fault system is not contemporaneous with any recognised extensional phase. It did, however, develop contemporaneously with an extensive system of salt-cored buckle folds which are entirely restricted to the supra-salt sequence situated immediately to the NE (figures 4.4 and 4.16(a)).

These folds are largely oriented parallel to the fault system (Figure 4.4) and are the dominant structural style of the Silverpit Basin.

It has previously been proposed that basin margin faults such as the Dowsing Graben System and North Dogger Fault systems developed to accommodate compressional-style structures elsewhere in the basin (Allen et al. 1994, Griffiths et al. 1995, Stewart and Coward, 1995). As detailed in section 4.9, it is also here proposed that the Schooner NE fault system developed to accommodate shortening of the sequence by these contemporaneous folds. As Figure 6.4 shows, when folding in the supra-salt sequence is not matched by equivalent bulk crustal shortening, there is a line-length deficit associated with this thin-skinned shortening which must be accommodated by extensional-style structures in the same sequence. This line-length deficit and therefore the potential amount of apparent extension on accommodating structures is proportional to the wavelength and amplitude of the fold structures.

This amount of extension which could be related to folding has been quantified experimentally using structural restoration software (2DMove) to restore folds of varying wavelengths and amplitudes to flat lines. The line-length deficit (*d*) (and therefore the apparent extension required to balance it of a single anticline-syncline pair) is calculated by subtracting the unfolded line length (*l*) from the fold wavelength (*w*) (Figure 6.5(a)). As Figure 6.5 shows, folds with shorter wavelengths and larger amplitudes have the greatest line length deficit and therefore the greatest potential to develop extensional structures. The maximum heave across the part of the Schooner NE fault system where heave is entirely manifested in fault displacement is 1200m. Folds to the NW of the fault system are on the order of 13-17km in wavelength and typically have amplitudes of 500-1000m. As Figure 6.5(b) shows, a fold with a wavelength of 16km and an amplitude of 500m (point 'A') accounts for 170m of line-length deficit and it would therefore take 7 anticline/syncline fold pairs to account for the heave across the Schooner NE fault system. Similarly a fold with the same wavelength and a 1000m amplitude (point 'B') would account for 682 metres of line length deficit and it would take 1.75 fold pairs to account for the observed fault heave. It is therefore considered that this is a plausible mechanism to account for the development of the

Schooner NE fault system and it also explains the contemporaneous development of extensional-style normal faults and compressional-style folding.

Several significant constraints are considered on this method of developing normal faults in the supra-salt sequence which should be considered when applying this concept elsewhere. Firstly it is considered that this can only occur if folds are entirely thin-skinned buckle folds. Folding due to bulk crustal shortening and differential compaction would not be able to account for extensional stresses in the supra-salt sequence as there would be no difference in line length between the sub-salt and supra-salt sequences. Secondly, the driving force behind thin-skinned fold development (in this case differential load-driven salt mobility) must be able to overcome the strength of the overburden in order to be able to develop faults. Finally, salt mobility must be constrained by an overburden layer in order for buckle-folds to develop. If salt was easily able to reach the surface as diapiric structures throughout the basin then buckle folds, and therefore related folds, would be unlikely to develop (see section 6.2).

It has previously been hypothesised that such a mechanism could potentially account for the development of the Moab fault system (section 3.12). Numerous supra-salt folds are present in the Paradox Basin which are associated with the numerous salt structures in the area. To the NE of the fault system, however, these folds are situated in areas where the supra-salt sequence is inferred as having become grounded on the sub-salt package prior to the development of the fault system. Consequently these folds are unlikely to be thin-skinned buckle folds as in the Silverpit Basin. One fold does, however, fit this criteria, the Cane Creek anticline and adjacent Kings Bottom Syncline (Figure 3.26(b)) are inferred as having developed at a late stage in the basins development which was potentially synchronous with the fault system. This fold pair has a wavelength of 15km and an amplitude of approximately 200m. Figure 6.5(b) shows this fold geometry to only account for a line length deficit of 25 metres and therefore this mechanism is considered unable to account for the 850m of maximum heave estimated for the Moab segment.

The role of faults and salt structures in accommodating extension in salt basins

Upwelled salt is observed separating the footwall and hanging wall cutoffs and consequently, partially accommodating the horizontal component of fault slip in central areas of both the Shearwater and Schooner NE fault systems. A similar relationship may also apply in the case of the Moab Fault system where the associated Moab-Spanish Valley salt structure is expressed as a flat-floored valley (Figure 3.31). One significant observation in the Schooner NE example is that where the transition occurs from a faulted salt-cored anticline to displacement across the S_9 salt structure, the fault throw (Figure 4.21) decreases significantly. It is here proposed that this drop in the vertical component of fault displacement is related to differences in the way that salt and overburden sequences accommodate extension.

Regardless of whether it is at the crustal scale or restricted to a specific layer, extension effectively requires a particular volume of rock to be redistributed over a wider area and as such, this requires the sequence to be thinned vertically. In rocks which typically deform by brittle means, a sequence is thinned through normal faulting with extension accommodated through both the horizontal heave component of fault movement coupled with a rotational component facilitated by dip-slip movement (Figure 6.6(a)). A medium which deforms through ductile creep, such as a salt layer or the mantle lithosphere, in contrast accommodates extension simply by redistributing its volume over the new surface area. As such, salt layers and their overburden sequences are considered to accommodate extension in very different ways and the way that extension is accommodated in a salt basin is considered to be a complex interaction between these processes.

Vendeville and Jackson (1992) showed that diapiric salt structures can develop as a response to extension and also suggested that when a diapiric structure has reached the surface, extension can be accommodated by salt flowing into the structure. Salt flowing into a salt structure is here considered to accommodate extension in two ways. Firstly, rising salt effectively drains the salt layer and therefore has a role in thinning the sequence. Secondly, salt moving between two overburden blocks also facilitates extension by allowing the overburden sequence to be distributed over a wider area and effectively lubricating the

boudinage of the overburden sequence. Two end-members are therefore considered to exist by which extension is accommodated in a supra-salt sequence which are illustrated in Figure 6.6. The first end member is where extension is accommodated entirely through brittle faulting in the overburden sequence, accompanied by passive salt movement beneath the rotated fault blocks (Figure 6.6(b)). The other is where extension is accommodated entirely through boudinage of the brittle overburden sequence lubricated by salt moving between rafted blocks (Figure 6.6 (c)).

Significant differences clearly exist between a thin-skinned setting where only the supra-salt sequence is being extended and the crustal scale where the entire sequence, including the salt layer is being extended. These principles are, however, considered to remain the same with salt able to facilitate extension of the supra-salt sequence in both settings. Each of the end members illustrated in Figure 6.6 have different implications in terms of how displacement is accommodated in the overburden sequence. Extension through normal faulting (Figure 6.6 (a and b)) requires both a horizontal (heave) component and a vertical (throw) component of relative displacement across the fault blocks. Salt-lubricated boudinage, in contrast (Figure 6.6(c)) can account for an identical amount of extension entirely with horizontal motion (i.e. heave).

As detailed in section 4.9, the displacement-length profile for the Schooner NE fault system (Figure 4.21) shows a much smaller amount of vertical displacement in the area where bed separation occurs across the salt diapir, than the peripheral areas where bed separation is across the normal fault segments. This is despite the diapir being in the central area of the fault system and where the bed separation is greatest. The interpretation of this, is that where fault displacement is sufficient for the salt upwelling beneath the fault plane to penetrate the surface, upwelling salt is locally able to accommodate the extension. This then results in a cessation of the vertical component of fault movement and extension becomes entirely accommodated by the heave component (see Figure 4.29). As salt is unlikely to be able to penetrate through a thick overburden sequence without first exploiting a fault system (Vendeville and Jackson, 1992), this transition between fault structure and salt structure would be expected before salt was able to accommodate extension. Therefore in an area

where salt was accommodating extension in the way shown in Figure 6.6(c), remnant vertical displacement would be expected from the prior fault phase.

It is difficult to assess the applicability of the above-described concept to the other fault systems in this study due to several complicating factors. The Moab fault system shows a very dramatic drop in displacement which corresponds with the point where the Moab segment ceases to be exposed and the Moab-Spanish Valley salt structure begins to be at the surface, exposed as a flat floored valley (figures 3.36 and 3.27). Although it is tempting to suggest that this represents a similar fault-to-salt-wall transition as observed in the Schooner NE example, field exposures and well penetrations are not considered to be sufficient to distinguish this exposure pattern from that expected from the erosional unroofing of the upper part of the salt structure. It is therefore not easy to say with confidence whether or not the Moab-Spanish Valley salt structure was a diapiric structure present at the surface and accommodating extension during the development of the Moab Fault System or not. This area is also complicated by the observation that a major Permian depocentre and related salt weld are present where the salt structure is expressed as a flat-floored valley which is not present where the fault is exposed (compare figures 3.44 and 3.52). This means that at the time the fault system developed, there would have been a significant difference in the amount of salt available to move in this area and consequently in the potential to accumulate fault displacement. This drop in displacement could therefore be adequately explained by the transition from where salt was available to move and accommodate displacement (NE) to where the sequence was largely grounded (SW).

The Shearwater fault system does not display any decrease in displacement in the vicinity of where the salt structure influences the structure (Figure 5.20(b)). The limited extent of the salt structures influence on the fault system, however, means any associated displacement drop would be unlikely to have a significant influence on the profile. Syn-rift geometries also suggest that the salt structure never reached the surface (Figure 5.28) and therefore that salt was unable to accommodate extension. Despite the apparent lack of universality to this concept, it is considered that in any extending salt basin, salt flow is a significant, and previously overlooked mechanism accommodating extension.

6.2 *Development of supra-salt sedimentary depocentres*

Numerous different styles of salt influenced sedimentary depocentre have been identified in this study which include depocentres influenced by a combination of faulting and salt mobility and those controlled entirely by salt mobility. The different depocentre styles have varying relationships to their associated salt structures and these relationships and controls are detailed below.

Fault controlled sedimentary depocentres

Established models of fault controlled sedimentary depocentre development (e.g. Gawthorpe et al. 1994, Gawthorpe and Leeder, 2000) are typically based on the assumption that hanging wall subsidence is the dominant process by which accommodation space is generated resulting in hanging wall growth packages which thicken dramatically towards the fault plane. What has been identified in this study is that in a salt-influenced setting, the relative motion of a faults footwall and hanging wall are not necessarily the same as would be expected in a salt-free setting. As it is this relative fault motion that creates accommodation space, the depocentre styles identified in a salt-influenced setting would therefore be expected to vary significantly from established models.

Although some depocentres are observed to be dominated by hanging wall subsidence, such as the Jurassic growth faults in the Southern North Sea study area (see figures 4.17 and 4.16(b)), in this study, this is the exception rather than the rule. Despite the Schooner NE, fault systems extensive amount of displacement, at first glance it appears not to have a fault-controlled sediment package associated with it. Sequences on the hanging wall side however, are significantly thicker than those on the footwall side despite the lack of growth geometries and hanging wall sequences can be seen to thicken slightly away from the fault rather than towards it (Figure 4.20(a)). Although the Shearwater fault system clearly shows its greatest syn-rift thickness situated in the hanging wall area and displays a distinct thickening towards the fault plane (Figure 5.19), the pre-rift footwall sequence can be seen to have been rotated to a steeper angle than in the hanging wall. Consequently, subsidence of the footwall area a

few kilometres away from the fault plane which is responsible for this rotation is also considered to have had a significant role in accommodating faulting. The synclinal syn-rift growth sequence in this area (Figure 5.22) is therefore considered to also be a significant fault controlled depocentre despite not being adjacent to the fault plane or thickening towards it.

The role of the footwall is even more dramatic in the Moab Fault System where the structure contour map shown in Figure 3.42 illustrates no identifiable subsidence in the hanging wall implying uplift of the footwall was the only process accommodating fault displacement. Although the current erosion level of the Moab Fault System means that no fault controlled growth packages are identified, the implication of this is that as uplift was the dominant process and localised uplift does not create any accommodation space. As Figure 3.85 illustrates, in a salt basin, the footwall is considered unable to rise without salt withdrawing into the risen area and salt upwelling in one area means subsidence in an adjacent area. As Figure 3.85 therefore suggests, the fault controlled subsidence associated with the development of the Moab Fault system is considered to be a synclinal footwall sequence which thins towards the fault.

The salt-influenced, fault-controlled sedimentary depocentres identified in this study are therefore considered to show very significant variability from the classically understood depocentre styles identified in salt-free settings. Salt mobility as a response to extension is considered to be equally as important as extension itself in the development of fault controlled depocentres and it should not be assumed that a depocentre will thicken towards a fault or be restricted to hanging wall areas. In a salt influenced setting the footwall is considered to have a much more significant role in accommodating fault displacement. Similarly, depocentres in the footwall due to fault controlled salt withdrawal are likely to be a feature of many salt basins.

Salt withdrawal controlled depocentres not influenced by faulting

Three major depocentre styles have been observed in this study which are not influenced by faulting. These include the growth fold style depocentre (Figure 6.7) where growth packages

are present above a developing buckle fold. This is typical of the Silverpit Basin (Figure 4.4) and is also similar to the style observed on a much smaller scale in the Sandy Beach area of the Paradox Basin (Figure 3.71(a)). As Figure 6.7(c) shows, this style is associated with non-piercing salt pillows and sediment packages are observed to thin onto the shoulders of the salt structures and reach their maximum thickness midway between them. Another style (Figure 6.7(b)), observed only in the Southern North Sea study area consists of sequences which thicken progressively towards a steep-sided, piercing salt structure as shown in Figure 4.14(a). As detailed 4.9 this style is associated with an unconformity at the base of the sequence and the restored geometry indicates the presence of a pre-existing salt-cored fold which was decapitated by this unconformity (figures 4.28(b) and 4.30).

The final major depocentre style observed in this study (Figure 6.7(a)) is present in the Cutler Formation in the Paradox Basin study area where sedimentary differential loading is interpreted as the main control on salt mobility. This is the least well-constrained depocentre style, only being identified in field exposures and well penetrations as well as published seismic lines. Well correlations (e.g Figure 3.74) frequently show the sequences to thicken towards the salt structures, although where depocentres are situated between two salt structures, the depocentre morphology is typically poorly constrained. One significant observation is that despite displaying growth towards the salt structures, sequences are observed to thin dramatically to pinchout onto the shoulders of the salt structure (Figure 3.37). It is interpreted from this morphology that the salt structure remained near the surface throughout the development of the sequence.

Each of the depocentre styles identified in this study are considered to be explainable through analysis of the pressure state in the salt layer through their development. Salt is considered to move as a response to pressure variations in the salt layer exerted upon it by its overburden with salt moving down the pressure gradients (Talbot, 1993, Davison and Waltham, 2003). Although not identified in this study, the minibasin concept detailed in section 2.5 is considered to be the simplest situation and provides the basis for this discussion. As Figure 6.8 shows, in such a situation, deposition is considered to begin with a small differential load on the top of the salt layer which locally increases the pressure below driving salt away down the pressure gradient. Salt movement then causes further subsidence

in the area above and therefore more sediment accumulates in the depocentre increasing the pressure on the salt layer. This feedback between sedimentation and salt mobility then continues until the salt layer is depleted. It is considered that the buckle-fold growth depocentres observed in the Silverpit Basin developed with a similar influence of differential loading. The lack of an equivalent amount of shortening in the sub-salt sequence and long term nature of the observed growth geometries which span the entire Tertiary is considered to be sufficient evidence to rule out a compressional tectonic origin in their development.

As detailed by Davison and Waltham (2003), buoyancy forces in the salt alone are considered unable to produce a salt-cored buckle fold. As Figure 6.9(a) shows any uplifted area below a salt swell will cause the pressure at the base of the salt layer to be highest in this area and the resultant pressure gradient will drive salt mobility away from the swell, reducing the amplitude of the structure. If sedimentation is occurring on the flanks of the swell, however (Figure 6.9(b), the pressure gradients will be reversed amplifying salt mobility and promoting further sedimentation in a the same way that sedimentation does in the minibasin setting. The development of these buckle-fold related depocentres is therefore considered to be analogous to the simple minibasin model shown in Figure 6.8. The complicating factor, however, is the presence of the pre-existing, parallel-bedded Triassic to Cretaceous sequence. In order for the folds and depocentres to develop, this sequence needs to flex whereas the simple minibasin setting where such a layer is not present the sequence is free to move anywhere that salt can withdraw. The morphology of the resultant depocentre is therefore considered to be constrained by the flexural wavelength of these folds and the buckle fold geometry requires subsidence to be spread over a wide area resulting in packages which progressively thin onto the shoulders of the salt structure.

In a situation where the salt was able to pierce the crest of a salt-cored buckle fold (as shown in Figure 6.10), then the constraint of the fold wavelength on the depocentre geometry would be removed and the nature of subsidence would change dramatically. The absence of the flexural control would then allow salt to upwell through sedimentary downbuilding and subsidence of the directly adjacent areas coupled with synchronous sedimentation in an adjacent depocentre. The geometry observed in this depocentre style (which is equivalent to the secondary peripheral sink of Trusheim, 1960) where sequences expand towards the salt

structure is considered to be controlled by the availability of salt to move into the salt structure. The pre-existing salt-cored anticline meant that more salt was available in crestal areas and therefore as salt was drained into the new diapiric structure, these adjacent areas were subsidence was greatest.

The sedimentary differential load-driven depocentre style identified in the Paradox Basin can also be explained in terms of the pressure regime in the salt layer if buttressing on a step in the sub-salt sequence is inferred as localising the initial upwelling of salt as suggested by Ge et al. (1997). As detailed in section 3.12, the growth of the sequence onto the loadward side of the most proximal salt structure in the basin (figures 3.23 and 3.33) is interpreted as being a result of a facies change restricting salt movement in this area. This therefore requires flexure of the supra-salt sequence in order for salt to move to accommodate the load (Figure 6.11) and would produce a thickening towards the salt structure in the most proximal area. The thickening observed onto the most distal salt structure in the basin (Figure 3.74), in contrast is interpreted as being related to the tapering of the clastic wedge with distance from the sediment source. This means that on the distal side of the salt swell, the area directly adjacent to it is where the load is greatest and consequently this is where subsidence is greatest. This depocentre style is considered to ultimately be a minibasin-style although the strongly unidirectional nature of the sediment source significantly influences the depocentre morphology.

Controls on depocentre morphology

Each of the depocentre styles identified in this study is considered to be explainable using the concept of pressure variations in the salt layer as discussed above. Salt mobility is characterised by salt moving from the areas of high pressure into the areas of lower pressure and therefore, where pressure is highest, subsidence is expected to be highest and where pressure is lowest subsidence is expected to be lowest. This is considered to be applicable to depocentres developed with the exclusive influence of salt withdrawal as described above but also to those where fault controlled subsidence influences their development. As Figure 6.12(a) shows, the depocentre style associated with the Shearwater Fault System can be explained by salt flowing down the pressure gradients which develop initially due to faulting

and then due to the combined influence of faulting and fault/salt controlled deposition. Similarly the pre-established pressure gradients associated with the salt-cored anticline which pre-dates the Schooner NE fault system appears to have a significant control on where subsidence associated with this fault systems develops (Figure 6.12(b)).

Further controls on depocentre morphology concern the availability of salt to move. The development of a salt-mobility controlled depocentre is limited by the thickness of the salt layer and once all of the available salt has withdrawn, there is no further potential for accommodation space development (other than due to differential compaction as described in section 6.3). The morphology of a basin including pre-existing and simultaneously developing sub-salt topography therefore can strongly control the potential for salt controlled depocentre development. Similarly, factors such as salt welds and viscosity-increasing facies changes in the evaporite sequence can also control the availability of salt to move. This is reflected in the progressive migration of depocentres through time identified in the Southern North Sea study area and to a lesser extent in the Paradox Basin. The freedom of salt to move is also a key factor in determining depocentre morphology. If salt mobility requires flexure of an overburden sequence in order to move, salt mobility will be constrained by the flexural potential of this sequence which will consequently influence the depocentre morphology. If a salt body is at the deposition surface, however, salt mobility can occur freely through sedimentary downbuilding if sufficient salt and sediment supply is available and the depocentre morphology will reflect this.

Role of compaction in salt basins

As detailed in section 2.1, salt has effectively no porosity even at shallow depths in a basin meaning that there is no potential for it to compact or dewater upon burial. Salt is therefore considered to be an uncompactible, solid mass throughout a basins development (Rowan, 1993). The consequences of this are that after a salt structure has developed a significant topographic expression, the surrounding clastic and carbonate sequences will compact around the salt structure leaving sequences deposited over the crestal area of at a higher structural elevation than sequences on its flanks. It is here hypothesised that this differential compaction has the potential to cause significant folds to develop above salt structures.

A control of differential compaction on structural geometries has been suggested in several areas (e.g. Barr, 1991, North Sea, Gómez and Vergés, 2005, Norwegian Atlantic margin) although this has previously been restricted to basement structures rather than salt structures. One exception to this is Buchanan et al. (1995) who discuses the restoration of structural sections in the Central North Sea and describes drapes over salt structures as "disappearing" during decompaction. The Shearwater example in this study is considered to be a very important test of this compaction hypothesis. A significant fold developed above the Shearwater salt structure has been attributed to late stage salt diapirism by Helgeson (1999). It has been proposed here (see section 5.9) that this fold developed after the development of the salt structure due to passive compaction of the supra-salt sequence, with the area directly above it remaining elevated. Perhaps the most striking evidence for this comes from structure maps (Figure 5.24) and isochron maps (Figure 5.25) in the post rift sequence which, not only show the structural highs and thinnest sequences to be situated above salt structures but also the structural lows and depositional thicks, match the morphology of the underlying syn-rift basins. The significance of this observation is that as these packages below the Base Cretaceous Unconformity contain thick sequences of mudstones which are more compactable than the underlying sequences which contain abundant, less compactable sandstones. One significant feature of the fold overlying the Shearwater salt structure is that sequences thin slightly onto it and it gradually reduces in amplitude up-section.

In order to determine whether compaction could be responsible for such a geometry, modelling was carried out whereby a sequence including a diapiric structure was progressively compacted as a sequence was deposited. The lack of seismic data below 5 seconds (TWTT) in the Shearwater example meant that the base of the salt and therefore the thickness of the supra-salt sequence could not be constrained making such modelling inaccurate.modelling was based on a salt structure from the Fyne area of the Western Platform, Central North Sea where similar folds are present and salt and overburden sequence were better constrained.

The methodology used to do this is detailed in Appendix 3 and Figure 6.13 illustrates both the original seismic line upon which modelling is based (a) and the resultant modelled compacted section (b). As Figure 6.13(b) shows, the modelled, compacted section develops a fold structure with the same decrease in amplitude up-section as shown in the original seismic section (Figure 6.13(a)) which is the same relationships observed above the Shearwater example. Consequently, differential compaction is considered to be responsible for the development of the fold in the Shearwater area and this requires a reinterpretation of the timing of salt mobility (section 5.9) and also introduces a new depocentre concept.

As Figure 5.25 shows, deposition in the post-rift sequence is centred around the more compactable areas of the underlying sequence and directed away from the underlying salt structure. Therefore, in areas where a significant-salt controlled depocentre morphology has developed, sequences are likely to be thickest overlying the more compactable areas.

Differential compaction as an alternative to inversion?

Many salt basins have been described as having been subjected to significant inversion including each of the areas used in this study. Compressional-style fold development and diapir reactivation are widely cited as evidence for this (e.g. Stewart and Clark, 1999). It is argued herein, however, that in some cases, differential compaction around pre-developed salt structures can be responsible for the development of these structures, previously attributed to inversion. Stewart and Clark (1999) describe differential compaction developing drape structures in the Central North Sea. Somewhat paradoxically, however, they describe

the drapes developing over Triassic minibasins rather than the salt structures implying that it was the halite dominated Zechstein Group which compacted the most (Figure 6.14).

This is curious as these areas would be expected to be largely uncompactable whereas the minibasins would be dominated by highly compactable mudstones of the Smith Bank Formation. It is therefore suggested that the drape shown in Figure 6.14 does have a differential compaction control and that the interpretation of Stewart and Clark (1999) is considered to be incorrect. The favoured interpretation here is that the largely transparent package labelled 'Triassic' in Figure 6.14 is actually a salt structure and the sequence labelled 'Zechstein' is actually a Triassic minibasin. Furthermore, the findings of this study disagree significantly with the interpretation of Stewart and Clark (1999) who consider an anticline developed above an inter-pod salt structure to be diagnostic of shortening in the cover sequence (Figure 6.15(a)). The situation shown in Figure 6.15(a) is based on the Triassic minibasin system of the Western Platform (Central North Sea), the same area shown in Figure 6.13. In Figure 6.13, a similar geometry to that shown in Figure 6.15(a) has been modelled entirely by differential compaction, even down to the up-section decrease in fold amplitude which is difficult to explain within the constraints of inversion. This geometry is therefore considered to be better explained by compaction and not diagnostic of inversion as they suggest.

In section 3.12 it is proposed that differential compaction around salt structures can provide an alternative interpretation to Laramide inversion in the development of folds in the Paradox Basin. A critical test of this is whether compaction of the observed sequence is capable of developing folds of the amplitude observed given the known constraints. This has been investigated through modelling of a situation where a salt-controlled depocentre of the same height as the adjacent salt structure has been compacted with varying loads (Figure 6.16). The amount that this package compacts is then considered to represent the maximum amplitude of fold that can be developed due to differential compaction with these parameters.

Compaction was modelled in 2DMove using the initial porosity and depth coefficients for sand, shale and shaley sand shown in Table 6.1. Figure 6.17 illustrates graphs of the potential

compaction due to burial for given salt structure heights/depocentre thickness for various thicknesses of overburden. Although the values used in this modelling are not based on actual data from the Paradox Basin, Figure 6.17 is considered to give a suitable ballpark figure for the potential compaction in the Paradox Basin. Maximum thicknesses of the sandstones in these depocentres determined from well penetrations are 1400-1700m and the Permian sequence is interpreted as being buried by 3500m by Nuccio and Condon (1996).

For a 3500m overburden and a sandstone depocentre/salt structure of 1000m in height (A), Figure 6.17(a) predicts a fold height of 290m and with a depocentre of 2000m in height (B) a 521m fold height is predicted. Folds in the Paradox Basin are typically on the order of 350-500m in height and therefore on the same scale as is predicted through differential compaction. Differential compaction is therefore considered to be a plausible alternative to inversion as the mechanism responsible for the development of these folds.

Lithology	Initial porosity	c $x10^{-5}$ cm^{-1} (depth coefficient)
Shale	0.63	0.51
Sand	0.49	0.27
Shaley sand	0.56	0.39

Table 6.1. Initial porosities and depth coefficients used in the compaction modelling detailed in Figures 6.16 and 6.17. Values are from Scalater and Christie (1980) and based on typical values in the Central North Sea .

Role of salt mobility in controlling facies distribution

As detailed in section 3.12, observations of the facies distribution in the Cutler Formation (Paradox Basin study area) suggest that salt structures may have had a significant role in controlling facies distribution in the sequence. Facies variations in this area imply that salt structures may have interrupted the proximal to distal transition of the depositional system and therefore led to partial compartmentalisation of the basin. Beyond this, this study has not identified detailed stratigraphic evidence for controls of salt mobility in sediment

distribution. What has been identified are significant controls on uplift and subsidence in a basin related directly to salt mobility.

Topographic/bathymetric variations, related to this uplift and subsidence would be expected to have a significant role in controlling facies distribution in many sedimentary environments. Environments which are particularly sensitive to this include fluvio-lacustrine, shallow marine and turbidite settings. In many of the depocentre styles identified in this study, the control of salt mobility on the topographic/bathymetric elevation of the deposition surface would be expected to be relatively minimal. This is because of the close inter-relationship between salt mobility and sedimentation with accommodation space being in-filled soon after being created leaving a relatively flat deposition surface. In settings where depocentres are influenced by faulting, however, the combined influences of salt mobility and faulting on the deposition surface are likely to be more dramatic.

Models of the stratigraphic development of active extensional basis such as Gawthorpe et al., (1994) and Gawthorpe and Leeder (2000) are based around a pre-determined assumption of the relative uplift and subsidence associated with faulting where hanging-wall subsidence is dominant. The findings of this study show that in a salt-influenced setting, this can be much more variable with footwall uplift being potentially dominant and with maximum fault-controlled subsidence not necessarily being situated directly adjacent to the fault plane. This variability has wide implications for facies distribution in an active extensional setting and models based upon salt-free settings should therefore not be applied to a salt influenced basin.

7.0 Conclusions

The conclusions contained within this thesis are of two types. Firstly there are those which are specific to each of the three study areas detailed in this study. Although not the primary aim of this thesis, this investigation has revealed an enhanced understanding of many aspects of each of these study areas which constitute a significant contribution to that particular region. Each of these study areas has been the subject of extensive academic and commercial interest and despite being a secondary aim of this thesis, the significance of this knowledge should not be overshadowed. Secondly there are the more generic aspects of this study which are considered to be the main contributions that this study offers. In this section the conclusions specific to the individual study areas are considered separately to the generic aspects.

7.1 Generic conclusions of this study

Faulting and fault related depocentres in salt basins

- Both the faulting styles and depocentre styles associated with salt-influenced faults in this study differ significantly from those in salt-free settings. It is therefore concluded that supra-salt faulting is a significantly different process in a salt basin to in a salt free area and that classic models of fault development based on salt free areas are not applicable in such settings.
- Entirely supra-salt faults are spatially restricted to areas where sufficient salt is available to move to accommodate relative movements of the footwall and hanging wall.
- Salt mobility associated with faulting can significantly influence the displacement-length scaling relationships along a faults length and can locally both increase or decrease the displacement gradient along a specific fault.
- In contrast to faults in salt-free areas where fault displacement is classically considered to be dominated by hanging wall subsidence, for supra-salt faults, footwall uplift has been shown to be equally or even more important in accommodating displacement.

- Supra-salt faults can develop both to accommodate crustal-scale stresses and stresses which are entirely restricted to the supra-salt layer. Significant extensional-style faults can therefore develop in salt basins which are not experiencing tectonic extension.
- The crests of pre-existing salt structures are considered to represent preferential locations for later faults to develop at. This is because they have the thinnest overburden and the low strength of salt makes them the sites where the minimum-work is required to fracture the salt/supra-salt sequence.
- Where fault displacement is sufficient for salt upwelling below a fault's footwall to penetrate the fault plane and reach the surface, extension can be accommodated entirely by the upwelling salt. At the point when this happens, the vertical component of fault displacement ceases to be required and extension can be entirely accommodated by the heave component of fault displacement with salt flowing in to fill the space created.
- In contrast to salt-free settings where subsidence associated with a specific normal fault typically results in hanging wall depocentres which thickens progressively towards the fault, in a salt basin this is not necessarily the case. Depocentres related to salt-influenced faults can thicken both towards or away from a faults hanging wall or can be situated entirely in the faults footwall (compare Figure 2.9 with Figure 6.7).

Supra-salt sedimentary depocentres

- Salt mobility can result in the development of numerous different depocentre styles which are summarised in Figure 6.7.
- Depocentres which thicken towards an associated salt structure are typically associated with salt structures which grew through downbuilding with salt being at or near the surface.
- Depocentres which thicken away from an associated salt structure are typically associated with salt structures where an overlying sediment layer stops salt reaching the surface.
- Regardless of the style of a specific depocentre (including fault influenced depocentres), the geometry of the growth package can be explained by considering the pressure state in the salt layer during deposition. Salt will flow from areas where the pressure from the overburden is greatest to where it is least and therefore subsidence will be greatest where the overburden sequence is thickest.

- Salt controlled depocentres are shown to migrate with time as salt welds locally inhibit further halokinesis at a given point. Salt mobility and consequently depocentre development will then move to the nearest point where salt is available to move.
- Differential compaction of the clastic and/or carbonate constituents of a sedimentary depocentre around their associated salt structures has the potential to develop both anticlinal structures above salt structures and influence the thickness of the post-halokinesis sequence. Differential compaction around salt structures is considered to provide a plausible alternative interpretation to inversion in the development of many salt related anticlines.

7.2 Conclusions specific to individual study areas

The Paradox Basin study area

- The structural and stratigraphic development of the Paradox Basin can be explained in terms of an integrated model with halokinesis as a dominant control on sedimentation and structural styles (as shown in Figure 3.89).
- In agreement with Barbeau (2003), the basin is considered to be a Pennsylvanian foreland basin with salt mobility triggered by differential loading of material shed from the adjacent basement high (Uncompahgre Uplift).
- The main phase of salt mobility has been shown to be during the deposition of the Pennsylvanian-Permian Cutler Group and by the end of this time, major salt welds had developed leaving no further potential for salt mobility in the proximal parts of the basin. Subsequent salt mobility was very limited and restricted to the more distal parts of the basin where sufficient salt was available to move.
- Significant post-Permian salt mobility was largely restricted to the Triassic during the deposition of the Moenkopi Formation and the localised 'lower member' of the Chinle Formation. In contrast to previous studies which have suggested that the Chinle was a time of significant salt mobility in the basin, it is here concluded that by this time, the major salt welds had developed and halokinesis was largely inactive. The earlier interpretation is considered to be related to a miss-interpretation of the field outcrop shown in Figure 3.63 and the absence of stratigraphic expansion in the main Chinle package is considered to be indicative of deposition without the influence of halokinesis.
- Supra-salt faulting in the Paradox Basin has been shown to have developed at a relatively late stage in the basins history. While the main phase of subsidence-controlling salt mobility is considered be restricted to the Pennsylvanian to Triassic, the main faults in the basin crosscut the entire exposed stratigraphy indicating a Tertiary age.
- Faults in the basins are considered to be of two separate groups, related to two separate processes. The extensive system of crestal normal faults associated with the exposed salt structures are considered based on several lines of evidence to be due to erosion-related dissolution collapse during the Oligocene to recent period. The more extensive Moab Fault System in contrast is considered to be related to regional extension.

- Despite significantly post-dating the main phase of salt mobility in the basin, the Moab Fault system is considered to have had both the pre-existing salt morphology and contemporaneous salt mobility as significant controls on its development. The fault system is shown to have developed in the crest of the of the only major salt structure in the basin which was not entirely constrained by salt welds on both sides and was therefore the only place in the basin where sufficient salt was able to move to allow the footwall and hanging walls to move relative to each other.
- Displacement on the Moab Fault was almost entirely restricted to footwall uplift and as the hanging wall was effectively pinned by a salt weld, the movement of salt into the uplifted footwall is considered to have been derived from the more distant footwall area.
- A preliminary investigation into the control of salt mobility on facies distribution in the basin suggests that halokinesis did significantly control facies distribution in the Cutler Group. The lack of stratigraphic expansion observed in the Chinle Formation however casts doubt on previous interpretations of a salt mobility control on facies distribution in this sequence.

The Southern North Sea Study area

- Salt structures in this area are of three principal types and it is concluded that their specific morphologies are predictable and related to the situation in which they developed. Salt structures which are gentle salt-cored buckle folds either developed after the major Base Cretaceous Unconformity or in positions where erosion did not remove all of the overburden in their central areas. Salt structures which are steep sided and truncate their associated depocentres at high angles in contrast, lie in areas where Base Cretaceous erosion removed the overburden from the central area of the structure. The timing of the salt structure development relative to the Base Cretaceous Unconformity and the level in the stratigraphy that this erosion locally reaches is therefore considered to be a fundamental control on salt structure style in the region.
- A further salt structure style is identified in the S_9 salt structure where despite being a steep-sided salt-wall the base of the supra-salt sequence lies parallel to the top of the salt. This style is considered to be associated with the development of the Schooner NE fault

system with salt upwelling to accommodate thin-skinned extension of the supra-salt sequence.

- A progressive SW-NE migration of depocentres in the study area is identified through time related to a migration in the locus of salt mobility as certain areas become starved of salt as salt welds develop.
- The mainly Jurassic growth faults in the study area have highly complex structural geometries, often consisting of layer restricted ramp-flat fault systems. Structural restorations show that they are associated with significant extension and they are considered to be the result of contemporaneous crustal extension with the complexity being the result of decollement on thin intra-Triassic evaporite layers.
- The entirely Tertiary, Schooner NE and Schooner SW faults, in contrast, are shown to have developed at a time when the basin is documented as having been more influenced by inversion. These faults are considered to have developed at the outer margin of the most basinward salt weld in the basin, at the time as a response to thin-skinned shortening associated with buckle fold development in the Silverpit Basin.
- The Schooner NE fault system and S_9 salt structure are considered to have developed contemporaneously as a dynamically interlinked system. The structure is considered to have initially developed as a fault in the crest of a salt-cored buckle fold. When fault displacement had increased to the extent that salt could penetrate the fault plane however, salt upwelling into this area took over from fault displacement in accommodating the thin-skinned extension.

The Central North Sea study area

- The Shearwater Fault System is considered to be a complex four-armed fault system intersecting around the Shearwater salt structure rather than two separate faults, as suggested in previous studies. In contrast to the interpretation of Helgeson (1999) the Shearwater salt structure is interpreted as being situated in the footwall area of the fault rather than the hanging wall area.
- Both the Shearwater Fault System and Shearwater salt structure are considered to have developed as an integrated system. Salt mobility is considered to have been reactive to Late Jurassic extension and both the salt movement and fault displacement are considered to

have been jointly responsible for the development of the subsidence associated with faulting. The displacement gradient on the Shearwater Fault System is consequently shown to steepen dramatically in areas where salt withdrawal is greatest.

- The doubly-plunging anticline which directly overlies the Shearwater salt structure is considered not to have existed at the beginning of the Cretaceous and previously reported onlap onto this structure (see Figure 5.13) is considered not to be present. This anticline is interpreted as the result of differential compaction around the salt structure during the Cretaceous and Tertiary rather than late-stage diapirism. Consequently it is concluded that actual salt mobility is entirely contemporaneous with the Late Jurassic rift episode.
- Both the structural and isopach patterns in the Cretaceous and Tertiary sequence overlying the Shearwater Fault System are shown to have been controlled by the underlying fault geometry despite the cessation of fault activity by the end of the Jurassic. Structural highs and depositional thins are shown to be situated directly above the salt structure. Areas where these sequences are both thickest and structurally lower in contrast are situated above the syn-rift depocentres. It is concluded that this is entirely the result of differential compaction with the more compactable, mud-filled syn-rift depocentres compacting the most and therefore causing greater subsidence and thicker overlying packages. The areas above the uncompactable salt structure in contrast subside much less and cause much thinner overlying sequences.

References

Alexander, L.L. and P.B. Flemings, 1995, Geologic evolution of a Pliocene-Pleistocene salt-withdrawal mini-basin: Eugene Island Block 330, Offshore Louisiana, American Association of Petroleum Geologists Bulletin, Vol.79, p.1737-1756

Allen, M.R., P.A., Griffiths, J. Craig, W.R. Fitches and R.J. Whittington, 1994, Halokinetic initiation of Mesozoic tectonics in the southern North Sea; A regional model, Geological Magazine, Vol. 131, p.559-561

Alvarez, W., E. Stanley, D. O'Connor, and M.A., Chan, 1998, Syn-sedimentary deformation in the Jurassic of southeastern Utah, a case of impact shaking?, Geology, Vol.26, p.579-582

Anders, M.H. and R.W. Sclische, 1994, Overlapping faults, intrabasin highs and the growth of normal faults, Journal of Geology, Vol.102, p.165-180

Arthur, T.J., 1993, Mesozoic structural evolution of the UK Southern North Sea: Insights from analysis of fault systems, in J.R. Parker (ed), Petroleum Geology of Northwest Europe: Proceedings of the 4th conference: The Geological Society, London, p.1269-1279

Aydin, A., and A. Nur, 1982, Evolution of pull-apart basins and their scale independence, Tectonics, Vol. 1, p.91-105

Baars, D.L. and G.M. Stevenson, 1981, Tectonic evolution of the Paradox Basin, Utah and Colorado, in D.L. Wiegand (ed.), Geology of the Paradox Basin, Rocky Mountain Association of Geologists Publication, p.23-31

Baars, D.L., 1966, Pre-Pennsylvanian palaeotectonics – key to basin evolution and petroleum occurrences in Paradox Basin, Utah and Colorado, American Association of Petroleum Geologists Bulletin, Vol. 50, p.2082-2111

Baars, D.L., 2003, Geology of Canyonlands National Park, in D.A. Sprinkel, T.C. Chidsey Jr. and P.B. Anderson (eds.), Geology of Utah's parks and monuments, Utah Geological Association Publication 28, second edition, p.61-83

Banbury, N.J. and J.R. Underhill, 2004, The role of halokinesis in supra-salt fault development: insights from the North Sea, In P.L. Post, D.L. Olson, K.T Lyons, S.L. Palmes, P.F. Harrison and N.C. Rosen (eds.) Salt-sediment interactions and hydrocarbon prospectivity: Concepts, applications and case studies for the 21st century, 24th GCSSEPM Foundation Bob F. Perkins Research Conference

Barbeau, D.L., A flexural model for the Paradox Basin: implications for the tectonics of the Ancestral Rocky Mountains, Basin Research, Vol. 15, 97-115

Barr, D., J.A. McQuillin and J.A. Donato, 1985, Footwall uplift in the inner Moray Firth Basin, offshore Scotland, Journal of structural Geology, Vol. 7, p. 267-268

Barr, D., 1991, Subsidence and sedimentation in a semi-starved half-graben: a model based on North Sea data, in A.M. Roberts, G. Yielding and B. Freeman (eds.), The geometry of normal faults, Special publication of the Geoloical Society, London, No. 56, p.17-28

Bartholemew, I. D., J.M. Peters and C.M. Powell, 1993, Regional structural evolution of the North Sea: oblique slip and the reactivation of basement lineaments. in J.R. Parker, (ed.), Petroleum Geology of Northwest Europe: Proceedings of the 4th conference: The Geological Society, London, p.1109-1122

Barton, D.C., 1933, Mechanics of formation of salt domes with special reference to Gulf Coast salt domes of Texas and Louisiana, American Association of Petroleum Geologists Bulletin, Vol. 17, p.1025-1083

Bell, J.S., 1996, In-situ stresses in sedimentary rocks (part 2): applications of stress measurements: Geoscience Canada, Vol. 23, p. 135-153

Bird, P., 1984, Laremide crustal thickening in the Rocky Mountains foreland and Great Plains, Tectonics, Vol.3, p.741-758

Bishop, D.J., 1996, Regional distribution and geometry of salt diapirs and supra-Zechstein Group faults in the western and central North Sea: Marine and Petroleum Geology, v. 13, p. 355-364.

Blehaut, J.F., F. Van Beek, C. Billeau, J.K. Gause, S. Kimminau, A. Paardekam, N. Radcliffe, R. Rademaker, L. Storms, B.J. Welsh, and A. Wittemann, 1999, Shearwater prospect development: a high Pressure/high temperature challenge, *in* A.J. Fleet, and R. Boldy, R. eds., Petroleum Geology of Northwest Europe: Proceedings of the 5th conference: The Geological Society, London, p. 1021-1027.

Bowring, S.A. and K.E. Karlstrom, 1990, Growth stabalization and reactivation of the Proterozoic lithosphere in the southwestern United States, Geology, Vol 18, p.1203-1206

Boyer, S.E. and D. Elliott, 1982, Thrust Systems, American Association of Petroleum Geologists Bulletin, V.66, No.9., p.1196-1230.

Boyers, W.C., 2000, Structural style and normal faulting adjacent to the Onion Creek salt diapir, Paradox Basin, Utah, MSc thesis, Baylor University, Waco, Texas

Bromley, M.H., 1991, Architectural features of the Kayenta Formation (Lower Jurassic), Colorado Plateau, USA: relationship to salt tectonics in the Paradox Basin, Sedimentary Geology, Vol.73, p77-99

Brunstrom, R.G.W. and P.J. Walmsley, 1969, Permian evaporites in the North Sea Basin, American Association of Petroleum Geologists Bulletin, Vol. 53, p.870-883

Buchanan, P.G., D.J. Bishop and D. N. Hood, 1996, Development of salt-related structures in the Central North Sea: results from section balancing, in G.I. Alsop, D.J. Blundell and I. Davison, (eds.) Salt Tectonics, Special Publication of the Geological Society, London, No. 100, p.111-128

Bulat, J. and S.J. Stoker, 1987, Uplift determination from interval velocity studies, UK southern North Sea, in J. Brooks and K. Glennie (eds) Petroleum Geology of Northwest Europe: Proceedings of the 3rd conference, The Geological Society, London, p.293-305

Butler, R.W.H., M.P Coward, G.M. Harwood, and R.J Knipe, R.J., 1987, Salt control on thrust geometry, structural style and gravitational collapse along the Himalayan mountain front in the salt range of northern Pakistan, in Dynamical geology of salt and related structures, Academic press, p. 339-418

Cameron, D., J. Munns and S. Stoker, 2005, Remaining hydrocarbon exploration potential of the Carboniferous fairway, UK southern North Sea, in J.D. Collinson, D.J. Evans, D.W. Holliday, N.S. Jones (eds.) Carboniferous hydrocarbon reserves: the southern North Sea and surrounding onshore areas, Volume 7, Occasional publication series of the Yorkshire Geological Society, p.209-224

Cameron, T.D.J., A. Crosby, P.S. Balson, D.H. Jeffery, G.K. Lott, J. Bulat and D.J. Harrison, 1992, The Geology of the Southern North Sea: United Kingdom offshore regional report, British Geological Survey, HMSO, London,

Campbell, J.A., 1979, Lower Permian depositional system, Northern Uncompahgre Basin, in D.L. Baars (ed.) Permianland, Four Corners Geology Society, 9th Field Conference guidebook, p.13-21

Campbell, J.A., 1980, Lower Permian depositional systems and Wolfcampian palaeogeography, Uncompahgre Basin, eastern Utah and southwestern Colorado, in T.D. Fouch and E.R. Magathan (eds.), Palaeozoic palaeogeography of west central United States, West central United States palaeogeography symposium 1, Rocky Mountain section SEPM, Denver Colorado, p.327-340

Campbell, J.A., 1981, Uranium mineralization and depositional facies in the Permian rocks of the northern Paradox Basin, Utah and Colorado, in D.L. Wiegand (ed.) Geology of the Paradox Basin, Rocky Mountain Association of Geologists Publication, p.187-194

Carter, N.L., 1976, Steady state flow of rocks, Reviews of geophysics and space physics, Vol. 14, p.301-360

Cartwright, J.A., B.D. Trudgill, and C.S. Mansfield, 1995, Fault growth by segment linkage: an explanation for scatter in maximum displacement and trace length data from the Canyonlands grabens of SE Utah, Journal of Structural Geology, Vol. 17, p.1319-1326.

Casas, E. and T.K. Lowenstein, 1989, Diagenesis of saline pan halite: comparison of peterographic features of modern; Quaternary and Permian halites, Journal of Sedimentary Petrology, Vol. 59, p.724-739

Case, J.E. and H.R Joesting, 1972, Regional geophysical investigations into the central Colorado Plateau, U.S. Geological Survey Professional Paper No. 736

Chapin,C.E. and S.M. Cather, 1983, Eocene tectonics and sedimentation in the Colorado Plateau – Rocky Mountain area, In J.D. Lowell (ed.) Rocky Mountain foreland basins and Uplifts, Rocky Mountain Association of Geologists Publication

Chauvin, P.C., 2001, Structural styles of a normal fault system above the Salt Valley salt wall, Paradox Basin, Utah, MSc thesis Baylor University, Waco, Texas

Childs, C., S.J. Easton, B.C. Vendeville, M.P.A. Jackson, S.T. Lin, J.J. Walsh and J. Watterson, 1993, Kinematic analysis of faults in a physical model of growth faulting above a viscous salt analogue, Tectonophysics, Vol. 228, p.313-329

Cole, R.D. and G.E. Moore, 1996, Stratigraphic and sedimentologic characterisation of McCracken sandstone member of Elbert Formation (Upper Devonian) at Lisbon Field, Paradox Basin, San Juan County, Utah, in Huffman, A.C. Jr., Lund, W.R. and Godwin, L.H. (eds.), Geology and resources of the Paradox Basin: Utah Geological Association Guidebook 25, p.117-128

Colorado School of Mines website, 2005 (viewed 16/08/05), Bruce Trudgill – Research page, http://www.mines.edu/academic/geology/faculty/btrudgil/research.html

Condon, S.M., 1997, Geology of the Pennsylvanian and Permian Cutler Group and Permian Kaibab Limestone in the Paradox Basin, southeastern Utah and southwestern Colorado, United States Geological Survey Bulletin 2000-P, US Department of the interior

Coney, P.J., 1976, Plate tectonics and the Laramide Orogeny, in L.A. Wood and S.A. Northrop (eds.) Tectonics and mineral resources of southwestern North America, Special Publication of the New Mexico Geological Society No. 6, p.5-10

Cowie, P.A., J.R. Underhill, M.D. Behn, J. Lin and C.E. Gill, 2005, Spatio-temporal evolution of strain accumulation derived from multi-scale observations of Late Jurassic rifting in the northern North Sea: A critical test of models for lithospheric extension, Earth and Planetary Science Letters, Vol. 234, p.401-419

Cowie, P. A., S. Gupta and N. H. Dawers, 2000, Implications of Fault Interaction for early syn-rift sedimentation: insights from a numerical fault growth model. Basin Research, 12, 241-262

Davison, I and D. Waltham, 2003, North Sea salt tectonics, practical workshop and lectures, course notes, Earthmoves Ltd

Davison, I., G.I. Alsop, P. Birch, C. Elders, N. Evans, H. Nicholson, P. Rorison, J. Wade, J. Woodward, and M. Young, 2000[a], Geometry and late-stage structural evolution of Central Graben salt diapirs, North Sea, Marine and Petroleum Geology, v. 17, p. 499-522.

Davison, I., G.I. Alsop, N.G. Evans and M. Safaricz, 2000[b], Overburden deformation patterns and mechanisms of salt diapir penetration in the Central Graben, North Sea, Marine and Petroleum Geology, v. 17, p.601-618

Davison, I., I. Alsop and D. Blundell, 1996, Salt tectonics: some aspects of deformation mechanics, In G.I. Alsop, D.J. Blundell and I. Davison (eds.), Special publication of the Geological Society, London 100, p.1-10

Dawers, N.H. and Underhill, J.R., 2000, The role of fault interaction and linkage in controlling synrift stratigraphic sequence development: Late Jurassic, Statfjord East Area, Northern North Sea, American Association of Petroleum Geologists Bulletin, Vol. 84, p.45-64

Dawers, N.H., M.H. Anders and C.H. Scholz, 1993, Growth of normal faults: displacement-length scaling, Geology, Vol. 21, p.1107-1110

DeCelles, P.G. and K.A. Giles, 1996, Foreland basin systems, Basin Research, Vol. 8. p.105-123

Demercian, S., P. Szatmari and P.R. Cobbold, 1993, Style and pattern of salt diapirs due to thin skinned gravitational gliding, Campos and Santos basins, offshore Brazil, Tectonophysics, 228, 393-433

Dickinson, W.R. and W.S. Snyder, 1978, Plate tectonics of the Laramide Orogeny, In V. Matthews (ed.) Laramide folding associated with basement block faulting in the western USA, Geological Society of America Memoir 151, p.355-366

Diegel, F.A., J.F. Karlo, D.C. Schuster, R.C. Shoup and P.R. Tauvers, 1995, Cenozoic structural evolution and tectono-stratigraphic framework of the northern gulf coast continental margin, in M.P.A. Jackson, D.G. Roberts and S. Snelson (eds.) Salt tectonics: a global perspective, American Association of Petroleum Geologists Memoir, No. 65, p.109-151

Doeling, H.H. and C.D. Morgan, 2000, Geologic map of the Merrimac Butte Quadrangle, Grand County Utah, Utah Geological Survey, Report accompanying map No.178

Doeling, H.H. and Ross, M.L., 1998, Geologic map of the Big Bend quadrangle, Grand County, Utah, Utah Geological Survey, Report accompanying map No. 171

Doeling, H.H., 1988, Geology of Salt Valley anticline and Arches National Park, Grand County, Utah, in Salt deformation in the Paradox Basin, Utah Geological and Mineral survey Bulletin, Vol. 122, p.1-60

Doeling, H.H., 2001, Geologic map of the Moab and eastern part of the San Rafael Desert 30' x 60' quadrangles, Grand and Emery counties, Utah and Mesa County, Colorado, Utah Geological Survey, Report accompanying map No. 180

Doeling, H.H., 2002, Geologic map of the Fisher Towers Quadrangle, Grand County, Utah, Utah Geological Survey, Report accompanying map No. 183

Doeling, H.H., 2003, Geology of Arches National Park, in D.A. Sprinkel, T.C. Chidsey Jr. and P.B. Anderson (eds.), Geology of Utah's parks and monuments, Utah Geological Association Publication 28, second edition, p.11-36

Doeling, H.H., M.L. Ross, and W.E. Mulvey, 2002, Geologic map of the Moab quadrangle, Grand County, Utah, Utah Geological Survey, Report accompanying map No. 180

Doeling, H.H., W.A. Yonkee and J.S. Hand, 1994, Geologic map of the Gold Bar Canyon quadrangle, Grand County, Utah, Utah Geological Survey, Report accompanying map No. 155

Dooley, T., K.R. McClay, M. Hempton and D. Smit, 2005, Salt tectonics above complex basement extensional fault systems: results from analogue modelling, In A.G. Dore and B.A. Vining (eds.) Petroleum Geology: northwest Europe and global perspectives, Proceedings of the 6th petroleum geology conference, The Geological Society, London, p.1631-1648

Dubiel, R.F., 1987, Sedimentology and new fossil occurrences of the Upper Triassic Chinle Formation, southeastern Utah, in J.A. Campbell (ed), Geology of Cataract Canyon and vicinity, Four Corners Geology Society, 10th field conference guidebook, p.99-107

Dubiel, R.F., J.T. Parrish, J.M. Parrish and S.C. Good, 1991, The Pangean megamonsoon – evidence from the Upper Triassic Chinle Formation, Colorado Plateau, Palaios, Vol. 6, p.347-370

Duval, B., C. Cramez, and M.P.A. Jackson, 1992, Raft tectonics in the Kwanza Basin, Angola, Marine and Petroleum Geology, Vol. 9, p.389-405

Elston, D.P. and E.M. Shoemaker, 1960, Late Palaeozoic and early Mesozoic structural history of the Uncompahgre Front, In K.G. Smith (ed.), Geology of the Paradox Basin Fold and Fault Belt, Four Corners Geology Society, 3rd field conference guidebook, p.47-55

Erratt, D, G.M. Thomas, and G.R.T. Wall, 1999, The evolution of the Central North Sea Rift, In A.J. Fleet, and R. Boldy, R. eds., Petroleum Geology of Northwest Europe: Proceedings of the 5th conference, The Geological Society, London, p.63-82.

Erratt, D., 1993, Relationship between basement faulting, salt withdrawal and Later Jurassic rifting, UK Central North Sea, In J.R. Parker, ed., Petroleum Geology of Northwest Europe: Proceedings of the 4th conference, The Geological Society, London, p. 1211-1219

Færeseth, R.B., 1996, Interaction of Permo-Triassic and Jurassic extensional fault blocks during the development of the Northern North Sea, Journal of the Geological Society, London, Vol. 153, p.931-944

Farmer, C.L. and O.I. Barkved, 1999, Influence of syn-depositional faulting on thickness variations in chalk reservoirs – Valhall and Hod fields, in A.J. Fleet, and R. Boldy, eds., Petroleum geology of Northwest Europe: Proceedings of the 5th conference, The Geological Society, London, p.949-957

Fiduk, J.C., E.R. Brush, L.E. Anderson, P.B. Gibbs and M.R. Rowan, Salt deformaion, magmatism and hydrocarbon prospectivity in the Espirito Santo Basin, offshore Brazil, In P.L. Post, D.L. Olson, K.T Lyons, S.L. Palmes, P.F. Harrison and N.C. Rosen (eds.) Salt-sediment interactions and hydrocarbon prospectivity: Concepts, applications and case studies for the 21st century, 24th GCSSEPM Foundation Bob F. Perkins Research Conference

Foxford, K.A., I.R. Garden, S.C. Guscott, S.D.Burley, J.J.M. Lewis, J.J. Walsh, and J. Watterson, 1996, The Field Geology of the Moab Fault, in Huffman, A.C. Jr., Lund, W.R. and Godwin, L.H. (Eds.), Geology and resources of the Paradox Basin: Utah Geological Association Guidebook 25, p.265-283

Gard, L.M. Jr., Geology of the north end of the Salt Valley Anticline, Grand County, Utah, United States Geological Survey, Open-file report 76-303,

Gatliff, R.W., P.C. Richards, K. Smith, C.C. Graham, M. McCormac, N.J.P. Smith, D. Long, T.D.J. Cameron, D. Evans, A.G. Stevenson, J. Bulat and J.D. Ritchie, 1994, The Geology of the Central North Sea, British Geological Survey, UK Offshore Regional Report, HMSO, London

Gawthorpe, R.L. and M.R. Leeder, 2000, Tectono-sedimentary evolution of active extensional basins, Basin Research, Vol. 12, p. 195-218

Gawthorpe, R.L., A.J. Fraser and R.E.L. Collier, 1994, Sequence stratigraphy in active extensional basins: implications for the interpretation of ancient basin-fills, Marine and Petroleum Geology, Vol. 11, p.642-658

Ge, H., 1996[a], Kinematics and dynamics of salt tectonics in the Paradox

Basin, Utah and Colorado: Field observations and scaled modelling, PhD Dissertation, University of Texas at Austin, Austin, Texas

Ge, H., M.P.A. Jackson, B.C. Vendeville, 1996, Extensional origin of breached diapirs, Utah and Colorado: field observations and scaled physical models, in Huffman, A.C. Jr., Lund, W.R. and Godwin, L.H. (eds.), Geology and resources of the Paradox Basin: Utah Geological Association Guidebook 25, p.285-294

Ge, H., M.P.A. Jackson, B.C. Vendeville, 1997, Kinematics and dynamics of salt tectonics driven by progradation, American Association of Petroleum Geologist Bulletin, Vol. 81, No. 3, p.398-423

Gibbs, A.D., 1986, Strike-slip basins and inversions: a possible model for the Southern North Sea gas area, In J. Brooks, J.C. Goff and B. Van Hoorn (eds.) Habitat of Palaeozoic gas in NW Europe, Special Publication of the Geological Society, London, No.23, p.251-266

Gilham, R., C. Hercus, A. Evans and W. DeHaas, 2005, Shearwater (UK Block 22/30b: managing challenging uncertainties through field life, in A.G. Dore and B.A. Vining (eds.) Petroleum Geology: northwest Europe and global perspectives, Proceedings of the 6th petroleum geology conference, The Geological Society, London, p.663-673

Gill, J.R. and W.A. Cobban, 1973, Stratigraphy and geologic history of the Montana Group and equivalent rocks, Montana, Wyoming and South Dakota: United States Geological Survey Professional paper No. 776

Glennie, K., J. Higman, and L. Stemmerik, 2003, Permian, In D. Evans, C. Graham, A. Armour, and P. Bathurst, eds., Millennium Atlas: Petroleum geology of the Central Graben and Northern North Sea, Geological Society of London, Ch. 8, p. 211-225

Glennie, K.W. and J.R. Underhill, 1998, Origin, development and evolution of structural styles, In K.W. Glennie (ed), Petroleum geology of the North Sea, basic concepts and recent advances, p.42-82, Blackwells, Oxford

Glennie, K.W. and P.L.E. Boegner, 1981, Sole pit inversion tectonics, in L.V. Illing and G.D. Hobson (eds) Geology of the continental shelf of north-west continental Europe, (Heyden and Sons, London), p.110-120

Gómez, M. and J. Vergés, 2005, Quantifying the contribution of tectonics vs. differential compaction in the development of domes along the Mid-Norwegian Atlantic margin, Basin Research, Vol. 17, p.289-310

Gregory, K.M.,.and C.G., Chase, 1992, Tectonic significance of palaeobotanically estimated climate and altitude of the late Eocene erosion surface, Colorado, Geology, V.12, p.116-119

Griffiths, P.A, M.R. Allen, J. Craig, W.R. Fitches and R.J. Whittington, 1995, Distinction between fault and salt control of Mesozoic sedimentation on the southern margin of the Mid-North Sea High, In S.A.R. Boldy (ed.) Permian and Triassic rifting in Northwest Europe, Special publication of the Geological Society, London, No. 91, p.145-159

Gupta, S., P.A. Cowie, N.H. Dawers and J.R. Underhill, 1998, A mechanism to explain rift-basin subsidence and stratigraphic patterns through fault array evolution, Geology, Vol. 26, p.595-598

Haq, B.U., J. Hardenbol, and P.R. Vail, 1987, Chronology of fluctuating sea levels since the Triassic, Science, Vol. 235, p. 1156-1167

Hazel, J.E. Jr., 1994, Sedimentary response to intrabasinal salt tectonism in the Upper Triassic Chinle Formation, Paradox Basin, Utah, U.S. Geological Survey Bulletin 2000-F, 34

Hecker, S., 1993, Quaternary tectonics of Utah with emphasis on earthquake hazard characterisation, Utah Geological Survey Bulletin, Vol. 127, p. 157

Heyman, O.G., P.W. Huntoon and M.A. White-Heyman, 1986, Laramide deformation of the Uncompahgre Plateau – Geometry and mechanisms, In D.S. Stone (ed.), New interpretations of NW Colorado geology, Rocky Mountain Association of Geologists Publication

Hite, R.J. and S.W. Lohman, 1973, Geological appraisal of Paradox Basin salt deposits for waste emplacement, United States Geological Survey, open-file report, p.73-114

Hodgson, N.A., J. Farnsworth, and A.J. Fraser, 1992, Salt related tectonics, sedimentation and hydrocarbon plays in the Central Graben, North Sea, UKCS, In R.F.P. Hardman, (ed.), Exploration

Britain, Geological insights for the next decade: Special Publication of The Geological Society, London, no. 67, p. 31-63.

Hudec, M.R., 1995, The Onion Creek salt diapir: an exposed diapir fall structure in the Paradox Basin, Utah, 16th Annual GCSSEPM Foundation Bob F. Perkins Research Conference, salt sediment and hydrocarbons, p.125-134

Hudec, M.R., 2004, Salt intrusion: time for a comeback?, In P.L. Post, D.L. Olson, K.T Lyons, S.L. Palmes, P.F. Harrison and N.C. Rosen (eds.), Salt-sediment interactions and hydrocarbon prospectivity: Concepts, applications and case studies for the 21st century, 24th GCSSEPM Foundation Bob F. Perkins Research Conference

Hughes, M. and I. Davison, 1993, Geometry and growth of kinematics of salt pilliows in the southern North Sea, Tectonophysics, Vol. 228, p.239-254

Huntoon, P.W., 1982, The Meander Anticline, Canyonlands, Utah – an unloading structure resulting from horizontal gliding on salt, Geological Society of America Bulletin, Vol. 93, p.941-950

Huntoon, P.W., 1988, Late Cenozoic gravity tectonic deformation related to the Paradox salts in the Canyonlands area of Utah, Utah Geological and Mineral survey Bulletin, Vol. 122, p.79-93

Huntoon, P.W., 2000, Upheaval Dome, Canyonlands, Utah: Strain indicators that reveal an impact origin, In Sprinkel, D.A., Chidsey, T.C. Jr., and Anderson, P.B. (eds.), Geology of Utah's parks and monuments, Utah Geological Association publication 28, first edition, p.619-628

Jackson, M.P.A. and Talbot, C.J., 1986, External shapes, strain rates, and dynamics of salt structures, GSA Bulletin, Vol. 97, p.305-323

Jackson, M.P.A., 1995, Retrospective salt tectonics, in M.P.A. Jackson, D.G. Roberts and S. Snelson (eds.) Salt tectonics: a global perspective, American Association of Petroleum Geologists, Memoir 65, p.1-28

Jackson, M.P.A., and B.C. Vendeville, 1994, Regional extension as a geologic trigger for diapirism: Geological Society of America Bulletin, v. 106, p.57-73

Jackson, M.P.A., E.D.D. Schultz, M.R. Hudec, I.A. Watson, M.L. Porter, 1998, Structure and evolution of Upheaval Dome: a pinched-off salt diapir, GSA Bulletin, Vol. 110, p.1547-1573

Jamison, W.R. and D.W. Stearns, 1982, Tectonic deformation of Wingate sandstone, Colorado National Monument, American Association of Petroleum Geologists Bulletin, Vol. 66, p.2584-2608

Jenyon, M.K, 1988, Fault-salt wall relationships, southern N. Sea, Oil and Gas Journal, September 1998, p 76-81

Jenyon, M.K. and P.M. Cresswell, 1987, The Southern Zechstein salt basin of the British North Sea, as observed in regional seismic traverses, In J. Brooks and K. Glennie (eds.) Petroleum Geology of North West Europe, p.277-292

Jenyon, M.K., P.M. Cresswell and J.C.M., Taylor, 1984, Nature of the connection between the Northern and Southern Zechstein basins across the Mid North Sea High, Marine and Petroleum Geology, Vol.1, p.355-363

Jeremiah, J.M., and P.H. Nicholson, 1999, Middle Oxfordian to Volgian sequence stratigraphy of the Greater Shearwater area, In A.J. Fleet, and R. Boldy, eds., Petroleum geology of Northwest Europe: Proceedings of the 5th conference, The Geological Society, London, p. 153-170.

Johnson, H.D., T.A. MacKay and D.J. Stewart, 1986, The Fulmar Oil Field (Central North Sea): Geological aspects of its discovery, appraisal and development, Marine and Petroleum Geology, Vol. 3., p.99-125

Kanbur, Z., J.N. Louie, S. Chavez-Perez, G. Plank, and D. Morey, 2000, Seismic reflection study of Upheaval Dome, Canyonlands National Park, Utah, Journal of Geophysical Research (Planets), Vol.105, No.E4, p.9489-9505

Kattenhorn, S.A., A. Aydin and D.D. Pollard, 2000, Joints at high angles to normal fault strike: an explanation using 3D numerical models of fault perturbed stress fields, Journal of Structural Geology, Vol.22, p.1-23

Kitcho, 1981, Characteristics of surface faults in the Paradox Basin, in D.L. Wiegand (ed.), Geology of the Paradox Basin, Rocky Mountain Association of Geologists Publication, p.1-21

Kluth C.F., 1986, Plate tectonics of the Ancestral Rocky Mountains, In J.A. Peterson (ed.), Paleotectonics and sedimentation in the Rocky Mountian region, united states, American Association of Petroleum Geologists Memoir 41, p.513-540

Kluth, C.F and P.J. Coney, 1981, Plate tectonics of the Ancestral Rocky Mountains, Geology, v.9, p.10-15

Knott, S.D., M.T. Burchell, E.J. Jolley, and A.J. Fraser, 1993, Mesozoic to Cenozoic plate reconstructions of the North Atlantic and hydrocarbon plays of the Atlantic margins, In J.R. Parker, (ed.), Petroleum geology of Northwest Europe: Proceedings of the 4th conference: The Geological Society, London, p. 953-974.

Koyi, H. , M.K. Jenyon and K. Peterson, 1993, The effect of basement faulting on diapirism, Journal of Petroleum Geology, Vol. 16, p.285-312

Koyi, H. and K. Peterson, 1993, Influence of basement faults on the development of salt structures in the Danish Basin, Marine and Petroleum Geology, Vol. 10, p. 82-94

Lasocki, J., A. Guemene, A. Hedayati, C. Legorjus, and W. M. Page, 1999, The Elgin and Franklin fields: UK Blocks 22/30c and 29/5b, In A.J. Fleet, and R. Boldy, eds., Petroleum geology of Northwest Europe: Proceedings of the 5th conference: The Geological Society, London, p. 1007-1020.

Letouzey, J., R. Colletta, R. Vially and J.C. Chermette, 1995, Evolution of salt-related structures in compressional settings, in M.P.A. Jackson, D.G. Roberts and S. Snelson (eds.), Salt tectonics: a global perspective, American Association of Petroleum Geologists Memoir 65, p. 41-60

Mack, G.H. and K.A. Rasmussen, 1984, Alluvial-fan sedimentation of the Cutler Formation (Permo-Pennsylvanian) near Gateway Colorado, Geological Society of America Bulletin, Vol.95, p.109-116,

Marsden, D., 1992, V (sub 0) –K method of depth conversion, Geophysics: The leading edge of Exploration, 11 (8), p.53-54

Matthews, W., G. Hampson, B. Trudgill and J. Underhill, 2004, Impact of salt movement on fluvio-lacustrine stratigraphy and facies architecture: Late Triassic Chinle Formation, northern Paradox Basin, SE Utah, USA, In P.L. Post, D.L. Olson, K.T Lyons, S.L. Palmes, P.F. Harrison and N.C. Rosen (eds.) Salt-sediment interactions and hydrocarbon prospectivity: Concepts, applications and case studies for the 21st century, 24th GCSSEPM Foundation Bob F. Perkins Research Conference

McClearly, J., T. Rogers and R. Ely, 1983, Stratigraphy, structure and lithofacies relationships of Devonian through Permian sedimentary rocks: Paradox Basin and adjacent areas – Southeastern Utah, Technical report prepared by Woodward-Clyde consultants for Office of nuclear waste isolation, ONWI-485, Battele Memorial Institute, Columbus, Ohio, USA

McKnight, E.T., 1940, Geology of the area between Green and Colorado river, Grand and San Juan Counties, Utah, United States Geological Survey Bulletin, Vol. 908, p.147

McLeod, A.E., N.H. Dawers, and J.R. Underhill, 2000, The propagation and linkage of normal faults: Insights from the Strathspey-Brent-Statfjord fault array, Northern North Sea, Basin Research, 12, p. 263-284.

McQuarrie, N. and C.G. Chase, 2000, Raising the Colorado Plateau, Geology, Vol. 28, No.1, p.91-94

Miller, E.L., M.M. Miller, C.H. Stevens, J.E. Wright and R. Madrid, 1992, Late Palaeozoic palaeogeographic and tectonic evolution of the western U.S. Cordillera, In B.C. Burchfield, P.W. Lipman, M.L. Zoback (eds.), The Geology of North America, Vol. G-3, The Cordilleran Orogen: Conterminous US, The Geological Society of America, p.57-106

Molenaar, C.M., 1981, Mesozoic stratigraphy of the Paradox Basin – an overview, in Wiegand (ed.), Geology of the Paradox Basin, Rocky Mountain Association of Geologists Publication

Moore, J.M. and R.A. Schultz, 1999, Processes of faulting in jointed rocks of Canyonlands National Park, Utah, Geological Society of America Bulletin, Vol. 111, p.808-822

Morewood, N.C and G.P. Roberts, 2002, Surface observations of active normal fault propagation: implications for growth, Journal of Structural Geology, Vol.159, p.263-272

Moscariello, A., 2003, The Schooner Field, Blocks 44/26a, 43/30-a, UK North Sea, in J.G. Gluyas and H.M. Hichens (eds.) United Kingdom oil and gas fields , Commemorative Millennium volume, Geological society, London, Memoir, 20, p.811-824

Naplas, T. and J-P Brun, 1993, Salt flow and diapirism related to extension at crustal scale, Tectonophysics, Vol. 228, p.349-362

Neff, A.W., 1960, Comparisons between the salt anticlines of south Persia and those of the Paradox Basin, in K.G. Smith (ed.), Geology of the Paradox Basin Fold and Fault Belt, Four Corners Geology Society, 3rd field conference guidebook, p.56-63

Nuccio, V.F. and S.M. Condon, 1996, Burial and thermal history of the Paradox Basin, Utah and Colorado, and petroleum potential of the middle Pennsylvanian Paradox Formation, US Geological Survey Bulletin 2000-O

Ohlen, H.R. and L.B. McIntyre, 1965, Stratigraphy and tectonic features of Paradox Basin, Four Corners area, American Association of Petroleum Geologists Bulletin, Vol. 49, p.2020-2040

Olig, S.S., C.H.Fenton, J. McCleary, and I.G.Wong, 1996, The earthquake potential of the Moab Fault and its relation to salt tectonics in the Paradox Basin, Utah, in Huffman, A.C. Jr., Lund, W.R. and Godwin, L.H. (eds.), Geology and resources of the Paradox Basin: Utah Geological Association Guidebook No. 25, p.251-264

Oudmayer, B.C. and J. De Jager, 1993, Fault reactivation and oblique slip in the southern North Sea, in J.R. Parker (ed.), Petroleum geology of Northwest Europe: Proceedings of the 4th conference, The Geological Society, London, p.1281-1290

Oviatt, C.G., 1988, Evidence for Quaternary deformation in the Salt Valley Anticline, southeastern Utah, Utah Geological and Mineral survey Bulletin, Vol. 122, p.61-78

Peacock, D.C.P. and D.J. Sanderson, 1991, Displacements, segment linkage and relay ramps in normal fault zones, Journal of Structural Geology, Vol. 13, p.721-733.

Peacock, D.C.P. and D.J. Sanderson, 1994, Geometry and development of Relay Ramps in normal fault systems, American Association of Petroleum Geologists Bulletin, Vol.78, p.147-165

Pederson, J.L., R.D. Mackley and J.L. Eddleman, 2002, Colorado Plateau uplift and erosion evaluated using GIS, GSA Today, August Issue, Geological Society of America, p.4-11

Penge, J., B. Taylor, J.A. Huckerby and J.W. Munns, 1993, Extension and salt tectonics in the East Central Graben, In J.R. Parker, (ed.), Petroleum Geology of Northwest Europe: Proceedings of the 4th conference, The Geological Society, London, p. 1197-1209

Penge, J., J.W. Munns, B. Taylor and T.M.F. Windle, 1999, Rift-raft tectonics: examples of gravitational tectonics from the Zechstein basins of northwest Europe, In. A.J. Fleet, and R. Boldy, (eds.), Petroleum geology of Northwest Europe: Proceedings of the 5th conference: The Geological Society, London, p.201-213

Pfiffner, O.A. and J.G. Ramsay, 1982, Constraints on geological strain rates: arguments from finite strain rates of naturally deformed rocks, Journal of Geophysical Research, Vol. 87, B1, p.311-321

Pimpiringos, G.N. and R.B. O' Sullivan, 1978, Principal unconformities in Triassic and Jurassic rocks, western interior United States – A preliminary survey: United States Geological Survey, professional paper 1035-A

Pitman, W.C.III and J.A. Andrews, 1985, Subsidence and thermal history of small pull-apart basins, in K.T. Biddle and B.N. Christie (eds.) Strike-slip deformation, basin formation and sedimentation, SEPM special publication No.37, p.45-119

Poole, F.G. and C.A. Sandberg, 1991, Mississippian palaeogeography and conodont biostratigraphy of the western United States, In J.D. Cooper and C.H. Stevens (eds.), Palaeozoic palaeogeography of the western United States-II Pacific section, Society of economic palaeontologists and mineralogists Book 67, Vol.1, p.107-136

Poole, F.G., J.H. Stewart, A.R. Palmer, C.A. Sandberg, R.J. Madrid, R.J. Ross, Jr., L.F. Hintze, M.M. Miller, C.T. Wruke, 1992, Latest Precambrian to latest Devonian time: development of a continental margin, In B.C. Burchfield, P.W. Lipman, M.L. Zoback (eds.), The Geology of North America, Vol. G-3, The Cordilleran Orogen: Conterminous US, The Geological Society of America, p.9-56

Pooler, J. and M. Amory, A subsurface perspective on ETAP – integrated development of seven Central North Sea fields, 1999, In. A.J. Fleet, and R. Boldy, R. eds., Petroleum Geology of Northwest Europe: Proceedings of the 5th conference: The Geological Society, London, p.993-1006

Rattey, P. and A.B. Hayward, 1992, Sequence stratigraphy of a failed rift system: the Middle Jurassic to Early Cretaceous basin evolution of the central and northern North Sea, In J.R. Parker, ed., Petroleum geology of Northwest Europe: Proceedings of the 4th conference: The Geological Society, London, p.215-249

Reid, F.S. and C.E. Berghorn, 1981, Facies recognition and hydrocarbon potential of the Pennsylvanian Paradox Formation, in D.L. Wiegand (ed.) Geology of the Paradox Basin, Rocky Mountain Association of Geologists Publication, p.111-117

Richardson, N.J., J.R. Underhill and G. Lewis, 2005, The role of evaporite mobility in modifying subsidence patterns during normal fault growth and linkage, Halten Terrace, Mid-Norway, Basin Research, Vol. 17, p.203-233

Roberts, D.G, M. Thopmson, B. Mitchener, J. Hossack, S. Carmichael and H.M. Bjørnseth, 1999, Palaeozoic to Tertiary rift and basin dynamics: mid-Norway to the Bay of Biscay – a new context for hydrocarbon prospectivity in the deep water frontier, In A.J. Fleet, and R. Boldy, R. (eds.), Petroleum geology of Northwest Europe: Proceedings of the 5th conference: The Geological Society, London, p.7-40

Ross, M.L., 1998, Geology of the Tertiary intrusive centres of the La Sal Mountains, Utah – influence of pre-existing structural features on emplacement and morphology, United States Geological Survey Bulletin, Vol. 2158, p.61-83

Rowan, M.G. and P. Weimer, 1998, Salt sediment interaction, northern Green Canyon and Ewing Bank (offshore Louisiana), Northern Gulf of Mexico, American Association of Petroleum Geologists Bulletin, Vol. 82 p.1055-1082

Rowan, M.G., 1993, A systematic technique for the sequential restoration of salt structures, Tectonophysics, Vol. 228, p. 331-348

Saleeby, J.B. and C. Busby-Spera, 1992, Early Mesozoic tectonic evolution of the western U.S. Cordillera, In B.C. Burchfield, P.W. Lipman, M.L. Zoback (eds.), The Geology of North America, Vol. G-3, The Cordilleran Orogen: Conterminous US, The Geological Society of America, p.107-169

Salveson, J.O., 1978, Variations in the geology of rift basins – a tectonic model, Paper presented at Rio Grande Rift Symposium, Santa Fem New Mexico

Scalater, J.G. and P.A.F. Christie, 1980, Continental stretching: an explanation of the post-Mid-Cretaceous subsidence of the Central North Sea Basin, Journal of Geophysical Research, Vol. 85, p.3711-3739

Schlische, R.W., S.S. Young, R.V. Ackermann, and A. Gupta, 1996, Geometry and scaling relations of a population of very small rift-related normal faults, Geology, 23, 683-686.

Schultz-Ela, D.D. and M.P.A. Jackson, 1996, Relation of subsalt to suprasalt structures during extension, American Association of Petroleum Geologists Bulletin, Vol. 80, p.1896-1924

Sears, R.A., A.R. Harbury, A.J.G. Protoy and D.J. Stewart, 1993, Structural styles from the Central Graben in the UK and Norway, In J.R. Parker, (ed.), Petroleum geology of Northwest Europe: Proceedings of the 4th conference: The Geological Society, London, p.1231-1243

Sharp, I.R., R.L. Gawthorpe, J.R. Underhill and S. Gupta, 2000, Fault-propagation folding in extensional settings: examples of structural style and syn-rift sedimentary response from the Suez Rift, Sinai, Egypt, Geological Society of America Bulletin, Vol. 112, p.1877-1899

Shoemaker, E.M. and K.E. Herkenhoff, 1984, Upheaval Dome impact structure, Lunar and Planetary Science, 15th Lunar and Planetary science conference, part 2, p.778-779

Sinclair, H.D., 1997, Tectonostratigraphic model for under-filled peripheral foreland basins, an Alpine perspective, Geological Society of America Bulletin, Vol. 109, p.324-346

Smith, R.I., N. Hodgson, and M. Fulton, 1993, Salt control on Triassic reservoir distribution, UKCS Central North Sea, In J.R. Parker, ed., Petroleum geology of Northwest Europe: Proceedings of the 4th conference, The Geological Society, London, p. 547-557.

Sørensen K., 1998, The salt pillow to diapir transition: evidence from unroofing unconformities in the Norwegian-Danish Basin, Petroleum Geoscience, Vol. 4, p.193-202

Sørensen, K., 1986, Rim syncline volume estimation and salt diapirism, Nature, Vol. 319, p.23-27

Spencer, 1996, Uplift of the Colorado Plateau due to lithospheric attenuation during Laramide low-angle subduction, Journal of Geophysical Research, Vol 101, NO. B6, p.13595-13609

Spiers, C.J., P.M.T.M, Schutjens, R.H. Brezesowsky, C.J. Peach, J.L. Liezenberg and H.J. Zwart, 1990, Experiential determination of constitutive parameters governing creep of rocksalt by pressure solution, in R.J. Knipe and E.H. Rutter (eds.) Deformation Mechanisms, Rheology and Tectonics, Special publication of the Geological Society, London, No.54, p.215-228

Stein, R.S. and S.E Barrientos, 1985, Planar high-angle faulting in the Basin and Range: geodetic analysis of the 1983 Borah Peak , Idaho, earthquake, Journal of Geophysical Research, Vol. 90, p.11355-11366

Stevenson, G.M. and D.L. Baars, 1986, The Paradox: a pull-apart basin of Pennsylvanian age, In J.A. Peterson (ed.), Paleotectonics and sedimentation in the Rocky Mountian region, united states, American Association of Petroleum Geologists Memoir No.41, p.353-370

Stewart, J.H., F.G. Poole and R.F. Wilson, 1972[a], Stratigraphy and origin of the Triassic Moenkopi Formation and related strata in the Colorado Plateau region, United States Geological Survey, Professional Paper No. 691

Stewart, J.H., F.G. Poole and R.F. Wilson, 1972[b], Stratigraphy and origin of the Chinle Formation and related Upper Triassic strata in the Colorado Plateau region, United States Geological Survey, Professional Paper No. 690

Stewart, S.A. and J.A. Clark, 1999, Impact of salt on the structure of the Central North Sea hydrocarbon fairways, In A.J. Fleet, and R. Boldy, (eds.), Petroleum geology of Northwest Europe: Proceedings of the 5th conference, The Geological Society, London, p.179-200

Stewart, S.A., and M.P. Coward, 1995, Synthesis of salt tectonics in the

Southern North Sea, UK, Marine and Petroleum Geology, Vol. 12, p.457-475

Stewart, S.A., M.J. Harvey, S.C. Otto and P.J. Weston, 1996, Influence of salt on fault geometry: examples from the UK salt basins, in G.I. Alsop, D.J. Blundell and I. Davison (eds.) Salt tectonics, Special Publication of the Geological Society, London, No.100, p.175-202

Talbot, C.J. and M.P.A. Jackson, 1987, Internal kinematics of salt diapirs, American Association of Petroleum Geologists Bulletin, Vol. 71, No. 9, p. 1068-1093

Talbot, C.J. and R.J. Jarvis, 1984, Age, budget and dynamics of an active salt extrusion in Iran, Journal of Structural Geology, Vol. 6, p.521-533

Talbot, C.J., 1978, Halokinesis and thermal convection, Nature, Vol. 273, p.739-741

Talbot, C.J., 1993, Spreading of salt structures in the Gulf of Mexico, Tectonophysics, Vol. 228, p.151-166

Tomasso, M., M.J. Young, J.R. Underhill, R. Cooper, L. Sides, and R.A. Hodgkinson, 2002, Unmasking Triassic structural and depositional patterns in the Northern North Sea: A new vision for

the evolution of the Triassic system. American Association of Petroleum Geologists annual meeting, Houston, Texas (Extended Abstract)

Touloukian, Y.S. Judd, W.R. and R.F. Roy (eds.) Physical properties of rocks and minerals, 1981, McGraw-Hill/CINDAS data series on material properties, Volume II-2, McGraw-Hill, New York, p.502

Trudgill, B. and J. Cartwright, 1994, Relay-ramp forms and normal-fault linkages, Canyonlands National Park, Utah, Geological Society of America Bulletin, Vol. 106, p.1143-1157

Trusheim, F., 1960, Mechanism of salt migration in northern Germany, American Association of Petroleum Geologists Bulletin, Vol. 44. p.1519-1540

Underhill, J.R. and M.A Partington, 1993, Jurassic thermal doming and deflation in the North Sea: implications of the sequence stratigraphic evidence, In Parker, J.R. (ed.) Petroleum Geology of Northwest Europe: Proceedings of the 4th conference, The Geological Society, London, p.337-345

Underhill, J.R., and M.A. Partington, 1994, Use of maximum flooding surfaces in determining a regional control on the Intra-Aaelenian (Mid–Cimmerian) sequence boundary: Implications for North Sea basin development and Exxon's sea level chart, In H.W. Posamentier, and P.J. Weimer, (eds.), Recent advances in siliciclastic sequence stratigraphy American Association of Petroleum Geologists Memoir, No. 58, p.449-484.

Urai, J.L., C.J. Spiers, H.J. Zwart and G.S. Lister, 1986, Weakening of rock salt by water during long term creep, Nature, Vol. 324, p.554-557

Van Keken, P.E., C.J. Spiers, A.P. van den Berg and E.J. Muyzert, 1993, The effective viscosity of rocksalt: implementation of steady-state creep laws in numerical models of salt diapirism, Tectonophysics, Vol. 225, p.457-476

Vendeville, B.C. and M.P.A Jackson, 1992, The rise of diapirs during thin-skinned extension, Marine and Petroleum Geology, Vol. 9, p.331-353

Vendeville, B.C. and P.R. Cobbold, 1987, Synsedimentary gravitational sliding and listric normal growth faults: insights from scaled physical models, C.R. Acad. Sci. Paris, Vol. 305, p.1313-1319

Vendeville, B.C., 2002, A new interpretation of Trusheim's classic model of salt-diapir growth, Gulf Coast Association of Geological Societies Transactions, Volume 52, p.943-952

Walker, I.M. and W.G. Cooper, 1987, The Structural and stratigraphic evolution of the northeast margin of the Sole Pit Basin, In J. Brooks and K. Glennie (eds.) Petroleum geology of Northwest Europe: Proceedings of the 3rd conference, The Geological Society, London, p.263-275

Walsh, J.J. and J. Watterson, 1989, Displacement gradients on fault surfaces, Journal of Structural Geology, Vol. 11, p.307-316

Walsh, J.J. and J. Watterson, 1991, Geometric and kinematic coherence and scale effects in normal fault systems, in A.M. Roberts, G. Yielding and B, Friedman (eds.), The geometry of normal faults, Special publication of the Geological Society, London, No. 56, p.193-203

Walsh, J.J., W.R. Bailey, C. Childs, A. Nicol and C.G. Bonson, 2003, Formation of segmented normal faults: a 3-D perspective, Journal of Structural Geology

Weijermars, R., M.P.A. Jackson and B. Vendeville, 1993, Rheological and tectonic modelling of salt provinces, Tectonophysics, Vol. 217, p.143-174

Weimer, P. M.G. Rowan, B.C. McBride and R. Kligfield, 1998, Evaluating the petroleum systems of the northern deep Gulf of Mexico through integrated basins analysis: an overview, American Association of Petroleum Geologists Bulletin, Vol. 82, p.865-877

Wenkert, D.D., 1979, The flow of salt glaciers: Geophysical Research Letters, Vol. 6, p.523-526

Wernicke, B., 1992, Cenozoic extensional tectonics of the US Cordillera, In B.C. Burchfield, P.W. Lipman, M.L. Zoback (eds.), The Geology of North America, Vol. G-3, The Cordilleran Orogen: Conterminous US, The Geological Society of America, p.553-581

Withjack, M.O. and S. Calloway, 2000, Active normal faulting beneath a salt layer: an experimental study of deformation patterns in the cover sequence, American Association of Petroleum Geologists Bulletin, Vol. 84, p.627-651

Withjack, M.O., J. Olson and E. Peterson. 1990, Experimental models of extensional forced folds, American Association of Petroleum Geologists Bulletin, Vol.74, p.1038-1045

Wolfe, J.A., C.E. Forest, P. Molnar, 1998, Palaeobotanical evidence of Eocene and Oligocene palaeolatitudes in mid latitude western North America, Geological Society of America Bulletin, Vol. 110, p.664-678

Wong., I.G, S.S. Olig, J.D.J. Bott, Earthquake potential and seismic hazards in the Paradox Basin, southeastern Utah, In Huffman, A.C. Jr., Lund, W.R. and Godwin, L.H. (eds.), Geology and resources of the Paradox Basin: Utah Geological Association Guidebook 25, p.251-264

Woodward-Clyde Consultants, 1984, Geologic characterisation report for the Paradox Basin study region – Utah study areas, Volume VI, Salt Valley, Office of nuclear waste isolation, ONWI-290, Battele Memorial Institute, Columbus, Ohio, USA

Wu, S. A.W. Bally, C. Cramez, 1990, Allochthonous salt, structure and stratigraphy of the north-eastern Gulf of Mexico. Part II, Structure, Marine and Petroleum Geology, Vol. 7, p.334-370

Xiao, H-B and J. Suppe, 1989, Role of compaction in listric shape of growth normal faults, American Association of Petroleum Geologists Bulletin, Vol. 73, p.777-786

Ye, H., L. Royden, C. Burchfiel and M. Schuepbach, 1996, Late Palaeozoic deformation of interior north America: the Greater Ancestral Rocky Mountains, American Association of Petroleum Geologists Bulletin, v.80, No.9, p.1397-1432

Young, M.J., R.L. Gawthorpe, S. Hardy, 2001, Growth and linkage of a segmented normal fault zone: the Late Jurassic Muchison-Statfjord North Fault, northern North Sea, Journal of Structural Geology, Vol. 23, p.1933-1952

Zanella, E., and M.P. Coward, 2003, Structural Framework, In D. Evans, C., Graham, A. Armour, and P. Bathurst, (eds.), Millennium Atlas: Petroleum geology of the Central Graben and Northern North Sea: Geological Society of London, p. 45-59.

Zhao, G. and A. M Johnson, 1992, Sequence of deformations recorded in joints and faults, Arches National Park, Utah, Journal of Structural Geology, Vol.14, p.225-236

Ziegler, P.A., 1982, Geological Atlas of Western and Central Europe, Shell Internationale Petroleum Maatschappij BV, Amsterdam,

Ziegler, P.A., 1987, Late Cretaceous and Cenozoic intra-plate compressional deformations in the Alpine foreland – a geodynamic model, Tectonophysics, Vol. 137, 389-420

Appendices

Appendix 1 – Description of the technique used for depth conversion of displacement-length profiles for faults based on 3D seismic data

In order to compare displacement-length profiles from faults where observations were based on seismic data with published examples and those based on field data, profiles were depth converted. This was done by measuring the two way travel time to both the footwall and hanging wall cutoffs at various points along the profile, converting the travel times to depths and subtracting the elevation of the footwall cutoff from that of the hanging wall cutoff. Depth conversions were done using the technique detailed in the 2DMove help files which is based on the work of Marsden (1992). The nature of the different faults meant slightly different approaches were taken. The Schooner NE profile was based on the Base Tertiary (Top Chalk) horizon which is constrained by stratigraphic relationships to pre-date the development of the fault system. Above the chalk sequences are a thickness of mudstones and minor sandstones which velocity logs from wells in the area show to have a relatively linear increase in velocity with depth. As such this was treated as a single layer. The time thickness (minus the travel time taken to get through the thickness of seawater) was then used to determine the thickness of the layer using the following equation.

$$Z = V_1(e^{kt}-1)/k$$

Z	Thickness of layer (i.e. depth to top chalk below seabed in SNS e.g.)
V_1	Velocity at top of layer
k	Rate of velocity change with increasing depth
t	One way travel from top to bottom of layer

The thickness of seawater is then added to this thickness to give the depth to the Top Chalk reflector from the mean sea level datum. With the absence of any seabed bathymetry observed on the seismic data an average seawater thickness of 30m was determined from local wells.

In the Shearwater example the faulted horizons are much deeper (>5 seconds two way travel time compared to <1 second in the Schooner NE example). Therefore the depth conversion needed to take into account velocity variability in the thick and complex stratigraphy above the faulted horizons. Sections were divided into several stratigraphic units and the thickness of each unit was then calculated from velocity logs using the above formula. The depth to the fault cutoffs in the faulted horizon (Base Upper Jurassic horizon in this case) was then calculated as the sum of each stratigraphic unit plus the thickness of the seawater. In the Shearwater example many of the units had very variable velocities without a linear change in velocity with depth. Above the Base Cretaceous reflector the stratigraphy has a layercake style with relatively uniform thicknesses of the units and more accurate depths were therefore determinable using interval velocities for the units instead of calculating them from velocity change with depth. Using an interval velocity for the whole unit instead of a velocity at the layer top (V_1) and a rate of change (k) changes the above equation to that below with V_i being the interval velocity.

$$Z = V_i t$$

A note on d-l profiles derived from deep basins

Care should be exercised when comparing d-l profiles derived from deep basins to those observed in neo-tectonic settings as the latter are likely to have been modified significantly by the effects of compaction. Faults in porous rocks near the surface which have subsequently been deeply buried will have significant changes in the thickness of both hanigingwall and footwall layers due to compaction typically leading to a decrease in recorded fault displacement with burial. Faulted units have been buried to ~5500m in the Shearwater example, upto 700m in Schooner NE example and >3000m in the Moab Fault example (Nuccio and Condon, 1996)

Appendix 2 – Description of the technique used to determine original depositional thickness of salt in Southern North Sea study area

An estimated original depositional thickness of the Zechstein Group in the southern North Sea was carried out from a bulk 3D restoration of the salt sequence using the 3DMove structural restoration software. This is simply the result of restoring the 'Top Salt' surface to an assumed original flat surface while maintaining the volume of salt in the model. The restoration gave a restored time thickness of 421 milliseconds two-way travel time, however, several assumptions are made in getting this value. It is assumed that no volume change has occurred in the salt sequence, i.e. no salt has moved laterally in or out of the boundaries of the study area and also that no volume has been lost through dissolution. It is also assumed that no bulk shortening or extension of the crust has occurred since the deposition of the salt sequence (i.e. the area that salt sequence covered hasn't changed) and that the base of the salt at deposition is a flat planar surface and therefore no account has been made for any kind of sub-salt structural topography locally varying the thickness of Zechstein Group deposits. Also no attempt has been made to decompact the sequence and although no compaction is thought to have occurred in the halite sequence, the other constituents of the Zechstein Group will have compacted significantly.

As the restored value is in two way travel time, this had to be converted to a true thickness using the appropriate seismic velocities for the succession. The Zechstein sequence was arbitrarily assumed to consist of 85% halite and 15% other lilthologies (generally dolomite, anhydrite and limestones). For the halite, an average seismic velocity of 4543 m/sec was determined from wells 49/1-1 and 48/10-1 which penetrate salt diapirs. For the other lithologies, a seismic velocity of 5425 m/sec was used which is an average of the velocities of non-halite constituents of wells 48/10b-5, 48/10-4 and 49/1-1. Although the velocity of these deposits would vary significantly with depth, at the present day these lithologies are generally found in the lowest part of the sequence and this velocity is representative of these depths. Using this technique, an original depositional thickness of 984m has been calculated for the Zechstein Group. This should be treated with caution due to the assumptions involved. It is, however, considered to give a much more accurate estimate than that of Hughes and Davison

(1993) which is based on 2D seismic data and therefore does not take into account salt moving laterally in or out of the 2D sections.

Appendix 3 – Description of the technique used for modelling compaction around salt structures in the Fyne area, Western Platform, Central North Sea

In order to assess the potential of differential compaction around salt structures to develop folds in overburden sequences, observations of the fold geometry in a real world example from the Central North Sea was compared with a modelled situation using the same parameters. The first stage involved depth converting the original seismic section to image the true fold geometry (Figure DIS-M(A)). This was done using the depth conversion and seismic restoration tools in 2DMove. The model was then constructed for the original salt-influenced Triassic package which was considered to be equal in thickness to the height of the salt structure and had a flat upper surface (Figure DIS-M(B)). The modelled Triassic package was then given the porosity and depth coefficient values of a typical Central North Sea mudstone from Scalter and Christie, (1980) to represent the Smith Bank Formation in this package and the salt sequence was given a porosity of zero as detailed by Rowan (1993). The overburden sequence was then progressively added to the section layer by layer and the section compacted using the compaction algorithm in 2DMove at each stage. The thicknesses of overburden sequence deposits were derived from backstripping well 21/28-1 which is situated in the crest of a fold. Subsequent layers were then added as flat-topped layers and thicknesses calculated from the top of the developing fold.

Figures section

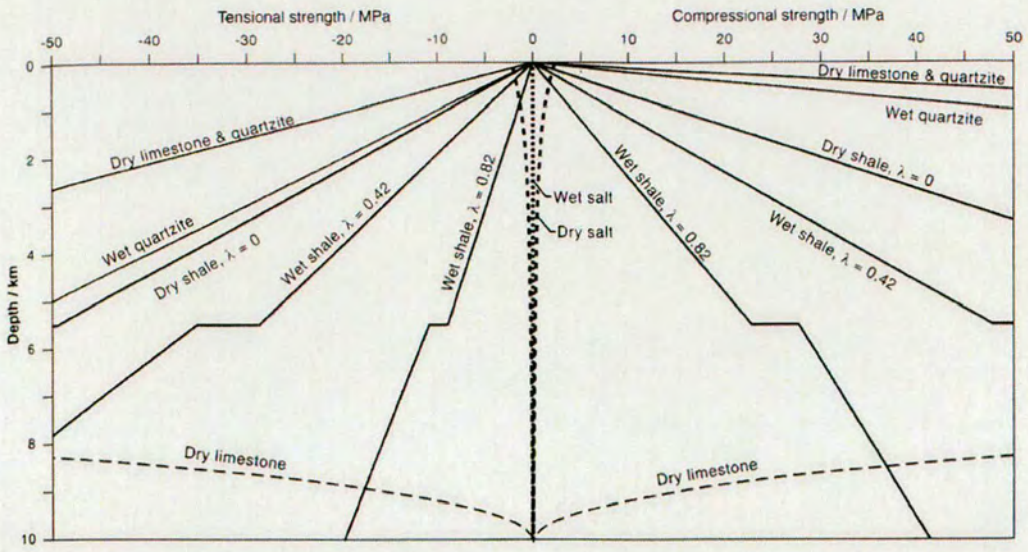

Figure 2.1 Plot illustrating how the strength of salt and certain other lithologies varies with burial. Salt strengths are for a representative strain rate of 10^{-14} s^{-1} (considered a datum strain rate for most geological processes by Carter, 1976, Pfiffner and Ramsay, 1982). λ is the pore pressure coefficient. From Jackson and Venderville, (1994).

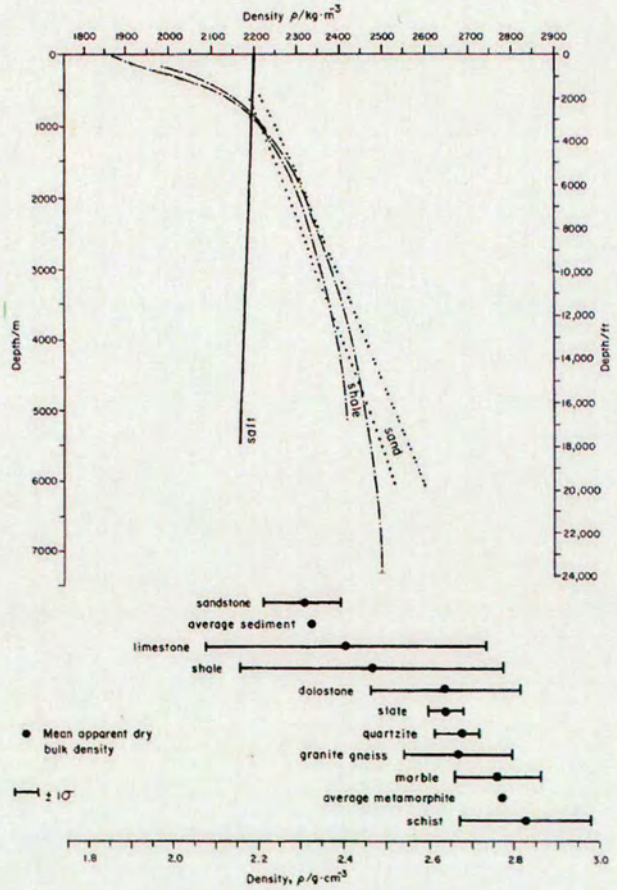

Figure 2.2. Plot illustrating the density change with depth for salt compared to that of sand and shale. Also shown are the mean bulk densities of certain common lithologies. From Jackson and Talbot, (1986).

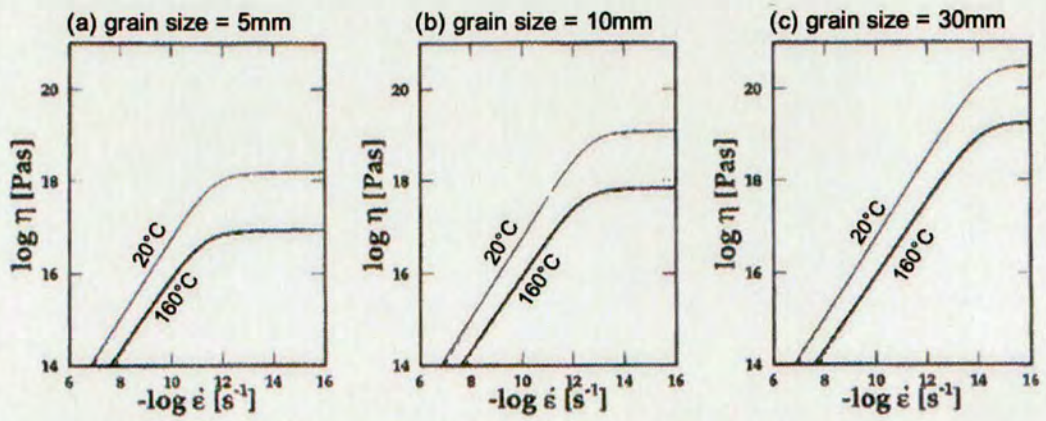

Figure 2.3. Log-log Plots of strain rate (ε) against effective viscosity (η) for three different grain sizes of salt deforming by combined dislocation and diffusion creep. Strain rate independent viscosity is considered to be dominated by diffusion creep whereas deformation at higher strain rates is dominated by dislocation creep. Note how the increase in grain size from 5mm (a) to 10mm (b) results in an effective viscosity increase of approximately one order of magnitude at low strain rates. Similarly the increase in temperature of 40°C results in a decrease in viscosity of one order of magnitude. From Van Keken et al. (1993).

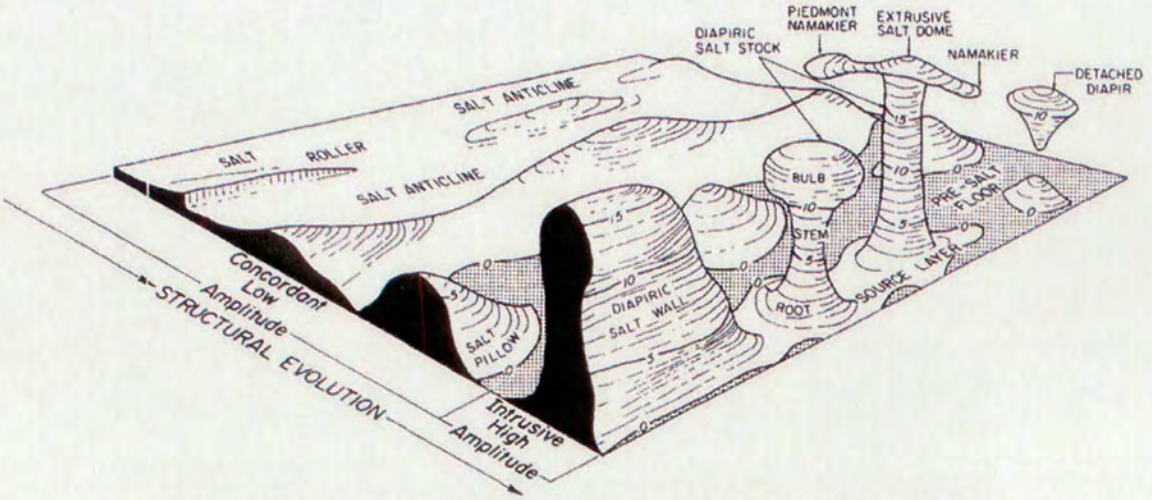

Figure 2.4. Sketch illustrating the nomenclature for different salt structure styles. From Jackson and Talbot (1986).

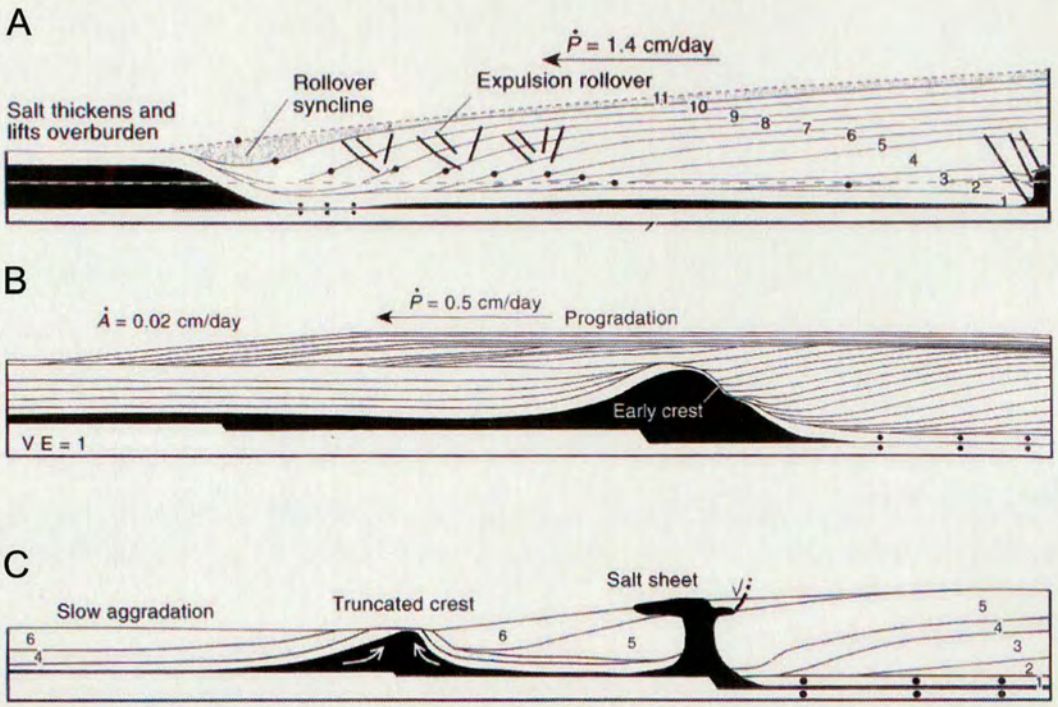

Figure 2.5. Geometries produced by analogue modelling of the progradation of a clastic wedge onto a buoyant salt analogue. (A), illustrates progradation onto a salt sequence with a flat base and shows that no diapiric structures develop. (B) and (C) in contrast have a stepped base to the salt and show significant salt structures developed above basement steps including a piercing structure with an overhanging salt canopy (C). From Ge et al. (1997).

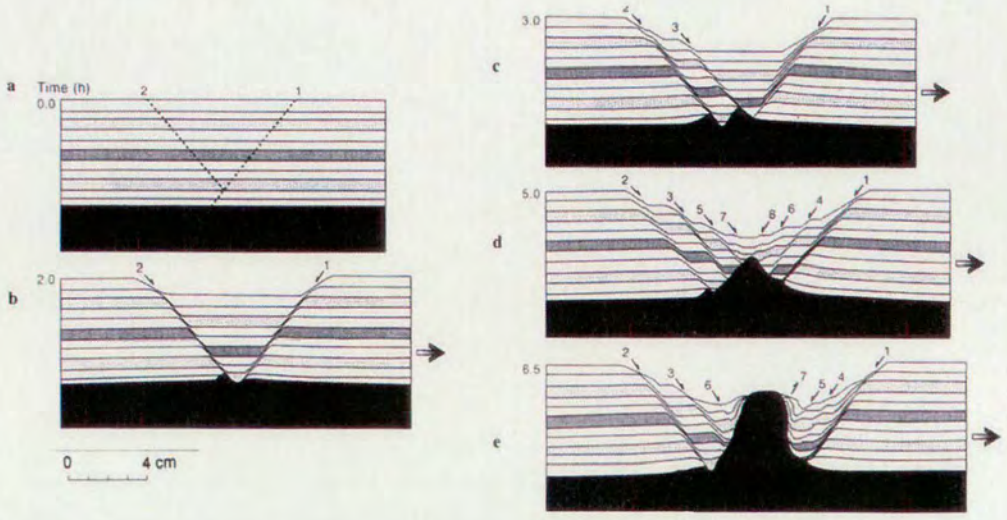

Figure 2.6. Cross sections through an analogue model of brittle overburden sequences overlying a salt analogue. The different stages represent progressive extension and a reactive diapir can be seen to develop below the developing graben system. From Jackson and Vendeville, (1994).

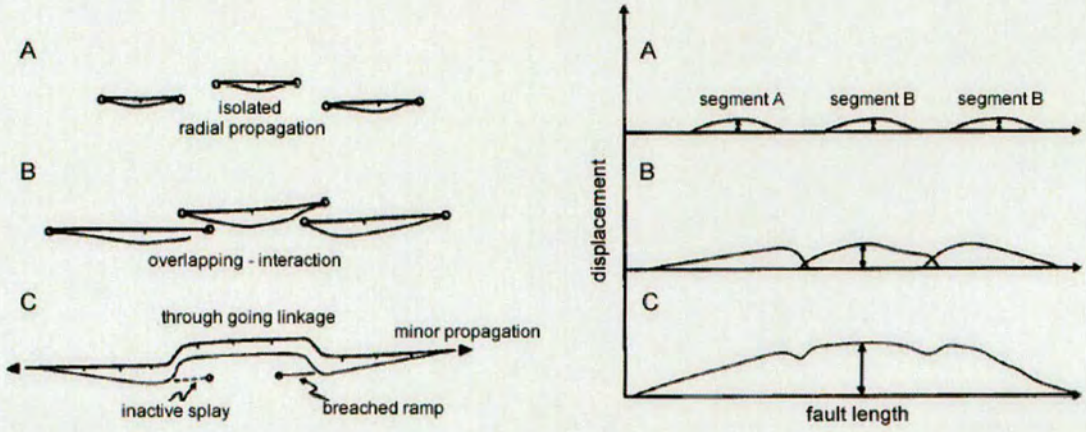

Figure 2.7. Model of fault growth through tip propagation and segment linkage. Shown as map view (left) and as displacement-length profiles (right). After Cartwright et al. (1995).

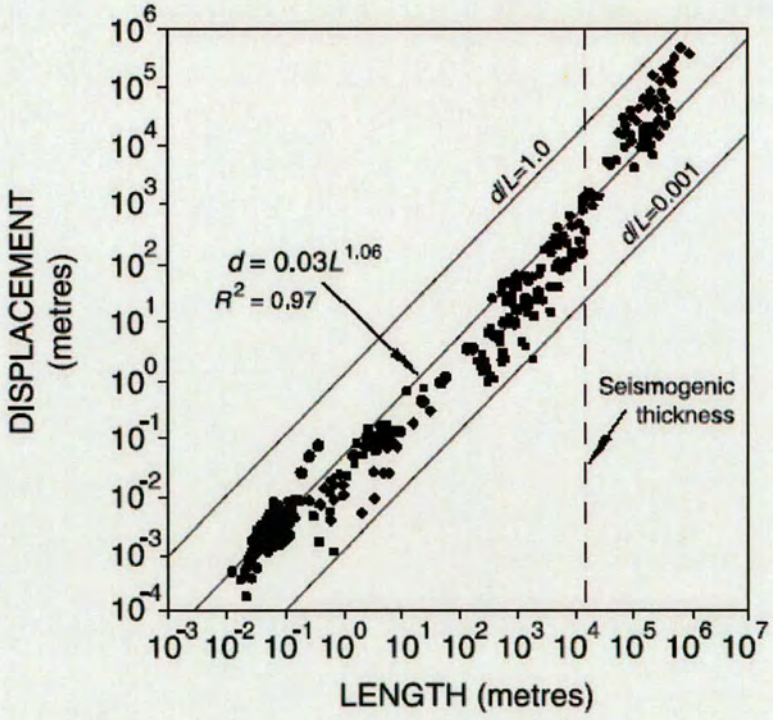

Figure 2.8. Log-log plot of displacement against length for a large number of faults from various different fault populations around the world. This illustrates the scale independence of the relationship between fault displacement and fault length at crustal scales. From Morewood and Roberts (2002).

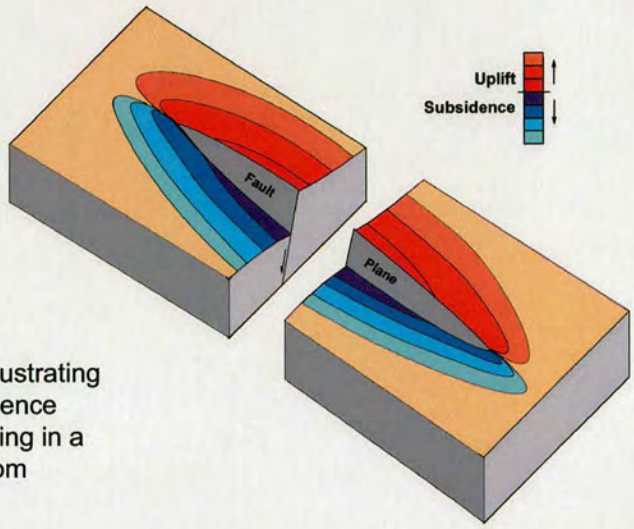

Figure 2.9. Block diagram illustrating the relative uplift and subsidence associated with normal faulting in a salt free setting. Modified from Gawthorpe et al. (1994).

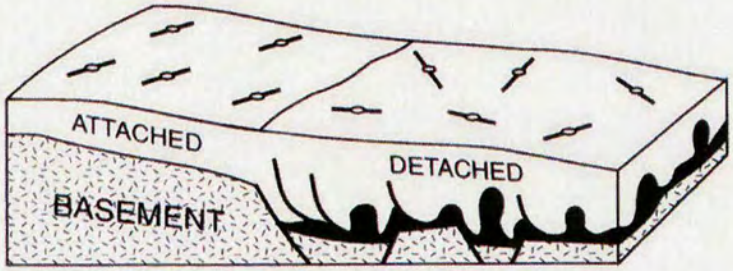

Figure 2.10. Schematic diagram illustrating the typical stress orientations in cover sequences which are either kinematically 'attached' to the basement or 'detached' by a mobile salt or overpressured shale layer. Stress orientations as determined from borehole breakouts and other stress indicators are typically coherent and predictable in attached sequences but more irregular in detached areas. From Bell (1996).

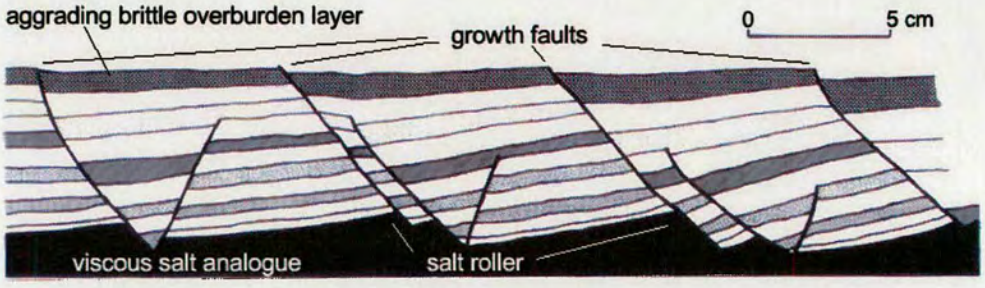

Figure 2.11. Cross section through a physical model consisting of a brittle overburden sequence overlying a viscous salt analogue. The model is experiencing both extension and aggradation and growth faults develop in the overburden sequence and 'salt roller' style structures develop in the salt analogue. After Childs et al. (1993)

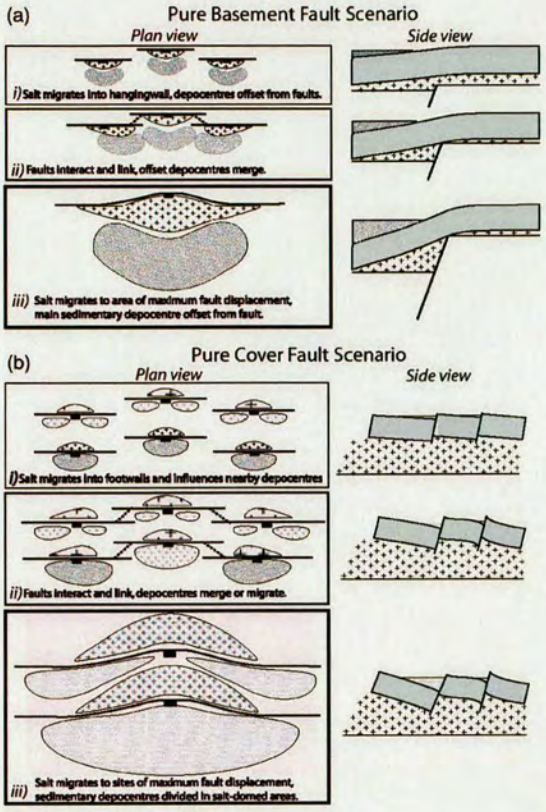

Figure 2.12. Schematic model of the evolution of salt influenced fault systems and their associated fault controlled depcoentres. The model illustrates two end members, a situation where faulting is entirely within the sub-salt succession (a) and where faulting is entirely within the supra-salt sequence (b). From Richardson et al. (2005)

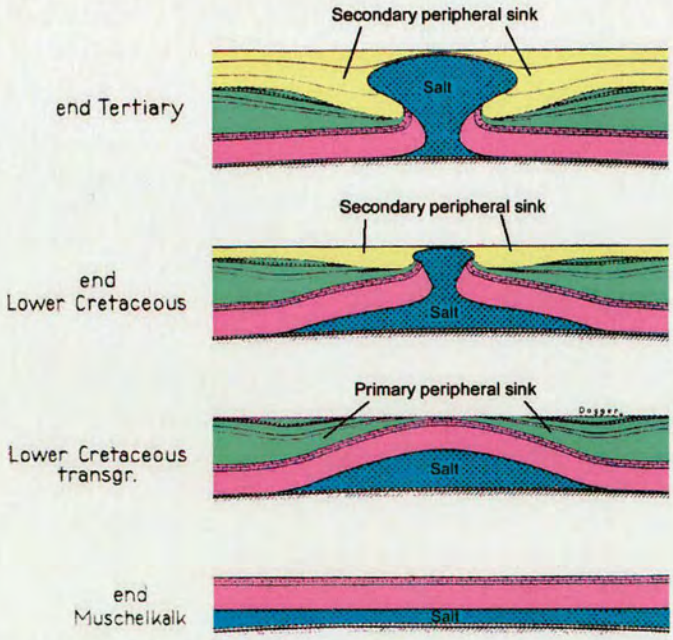

Figure 2.13. Model illustrating the development of salt structures in northern Germany and the way their associated depocentres develop as the salt structure style evolves. Shown are the 'primary peripheral sink' depocentre style (green) related to salt upwelling in a pillow style and the 'secondary peripheral sink' (yellow) style developing as the salt pierces its overburden. From Trusheim (1960).

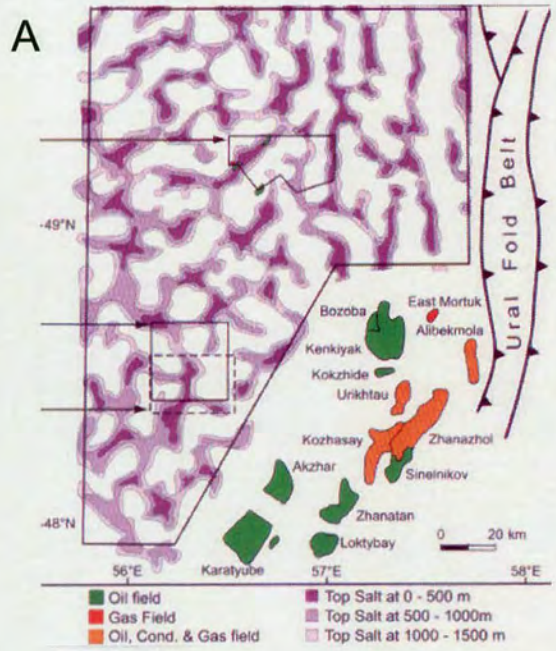

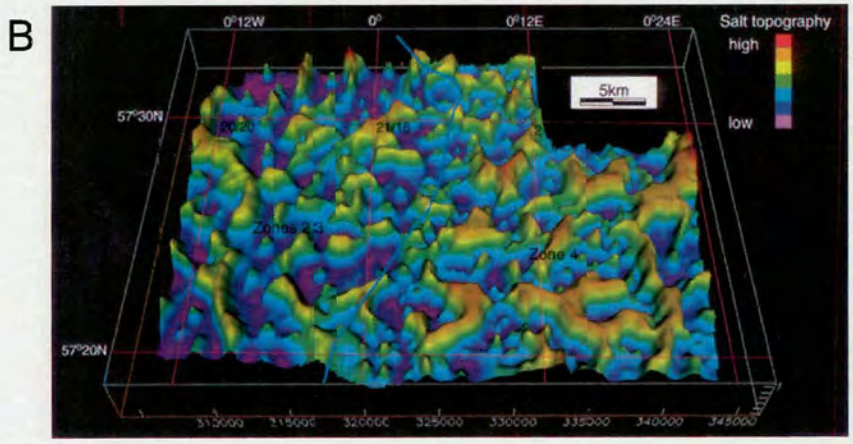

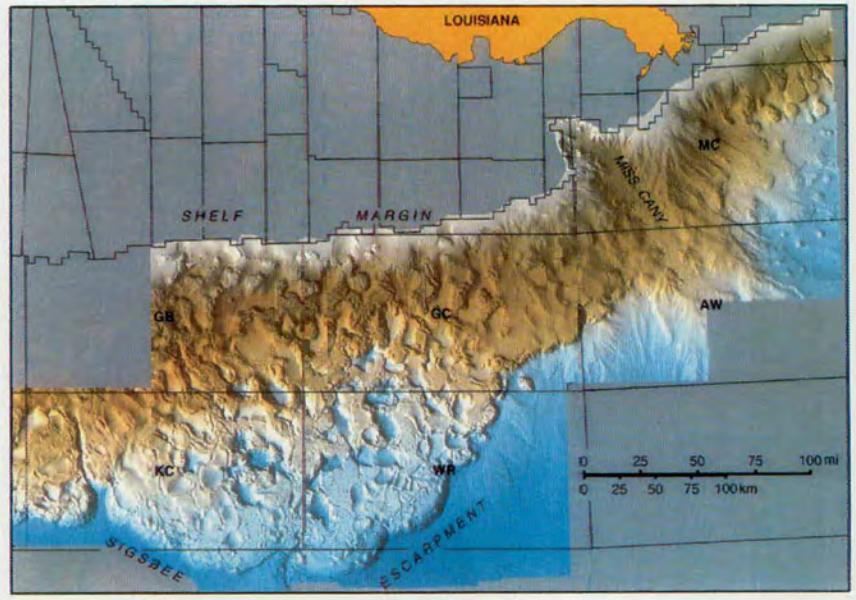

Figure 2.14. Published views of minibasin morphologies in various salt basins. Shown are top salt structure maps for the Precaspian basin (A) and Central North Sea (B). Also shown is a seabed structure map (C) for the minibasin province of the Gulf of Mexico. On this map blues are deep and browns are shallow and most minibasins show up as depressions due to sediment starvation. Figures are from Barde et al. 2002 (A), Stewart and Clark, 1999 (B) and Diegel et al ., 1995 (C).

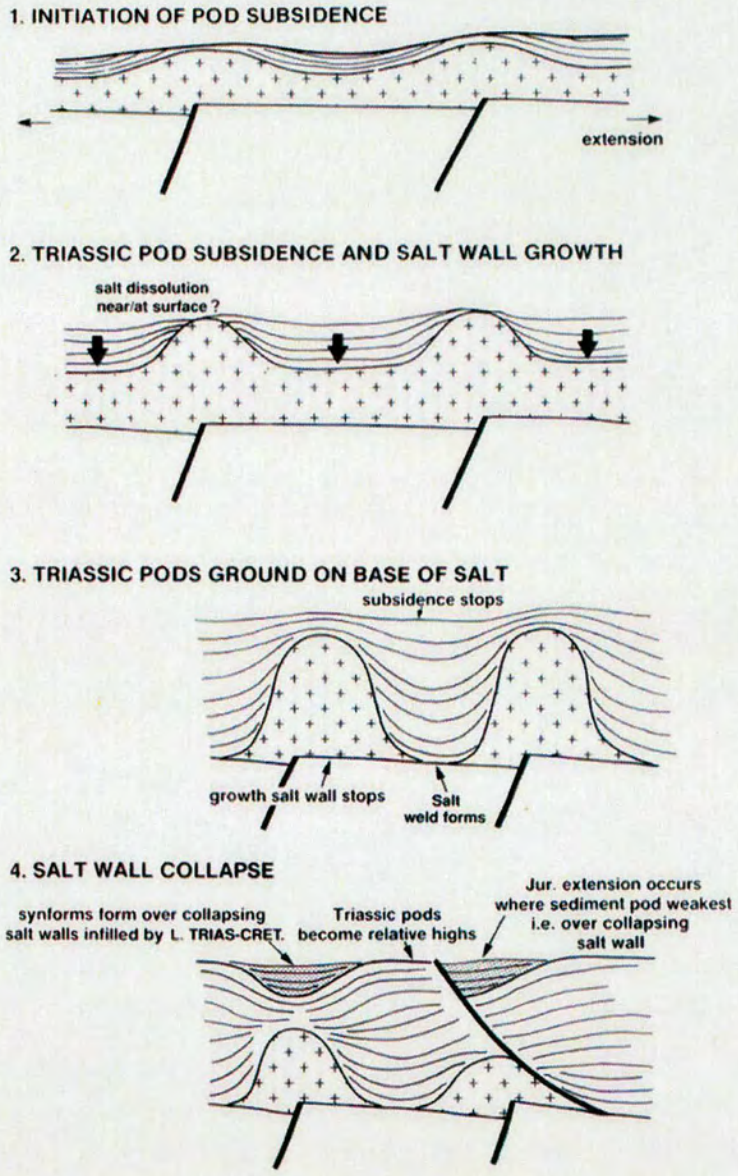

Figure 2.15. Cartoon diagram illustrating the 'podology' model of Triassic minibasin (pod) and salt wall development in the Central North Sea. From Hodgson et al. (1992).

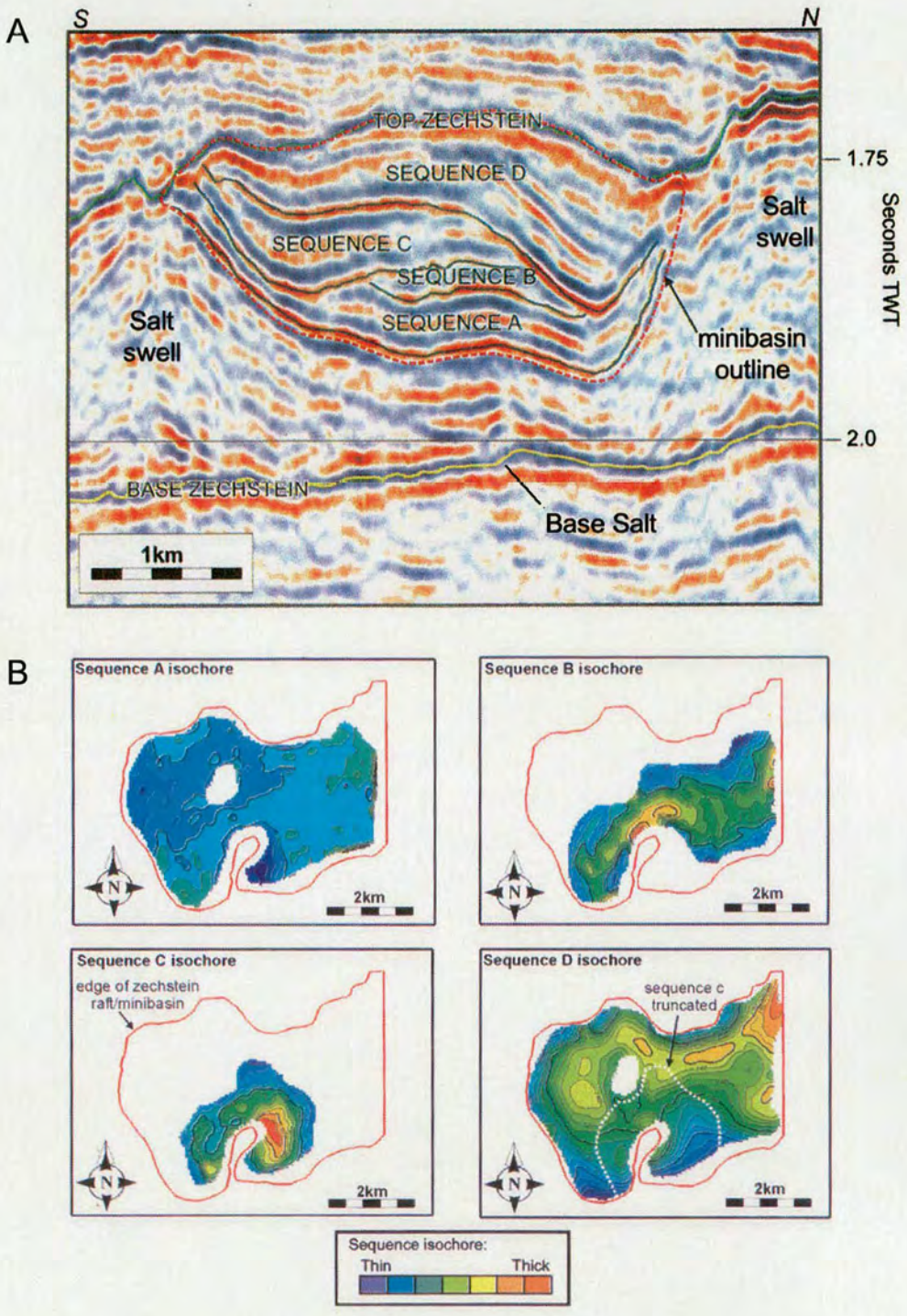

Figure 2.16. Seismic section through a Permian minibasin in the Central North Sea illustrating the variable reflector geometries in the package (A) and isochron maps of the individual labelled packages in this section (B) illustrating their three dimensional geometry. From Stewart and Clark (1999).

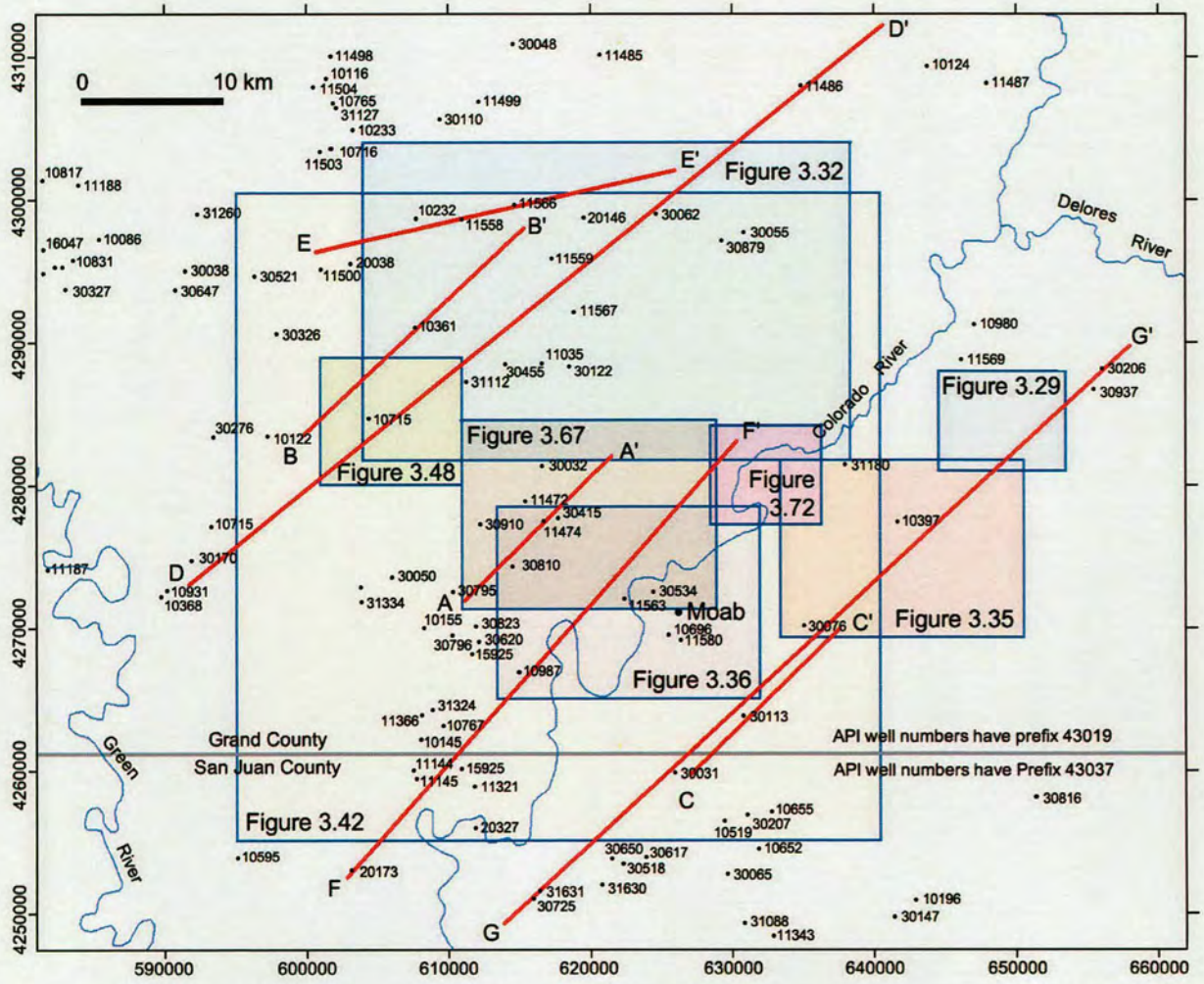

Figure 3.1. Map illustrating the extent of the study area and the locations of well penetrations within it. Also shown are the locations of maps and cross sections featured within this chapter

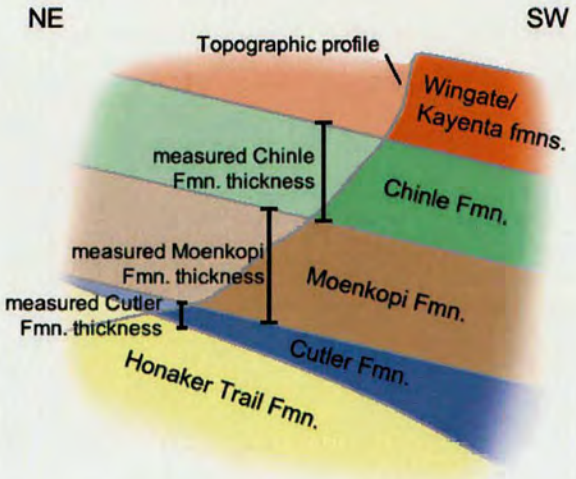

Figure 3.2. Section illustrating the technique used to integrate measured sediment package thicknesses from field exposures with data from well penetrations. The technique involves measuring the elevation between where the top and base of a specific unit is exposed and the map location of these points as well as orientation of bedding in the sequence. A cross section is then plotted for each point and the top and base of the sequences projected according to the dip of the bedding. The vertical thickness is then measured from this data.

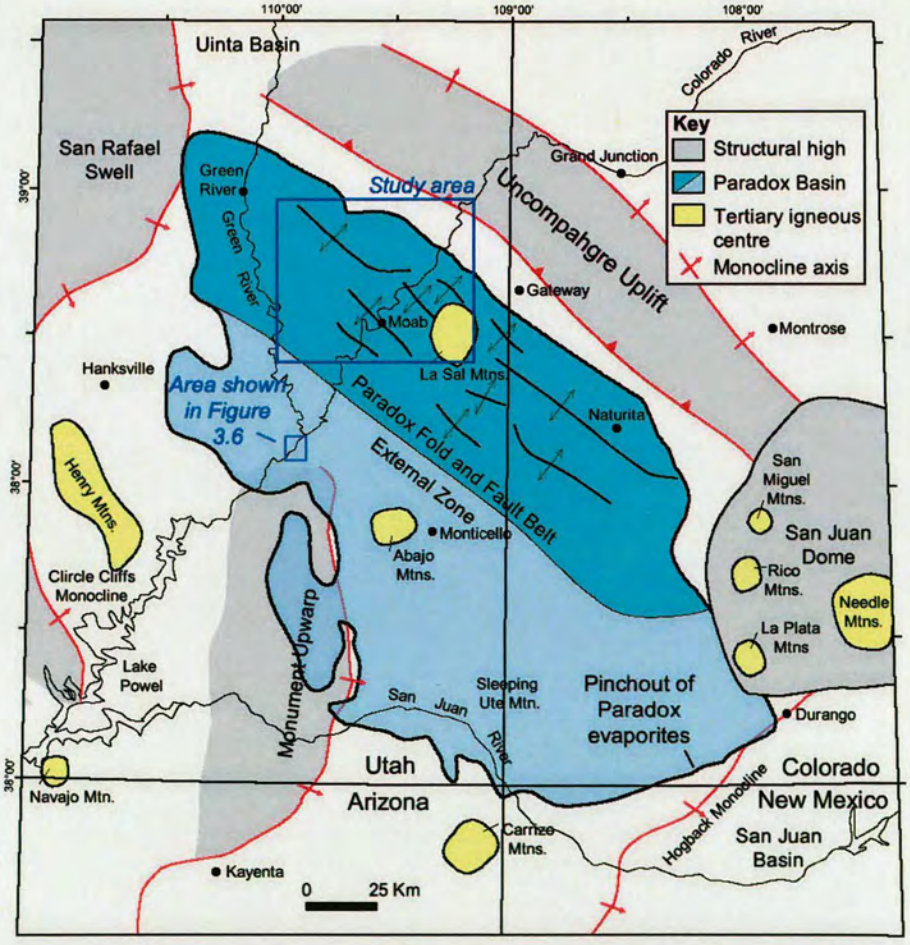

Figure 3.3. Map illustrating the extent of the Paradox Basin and the major structural elements in the area – Modified from Nuccio and Condon, 1996)

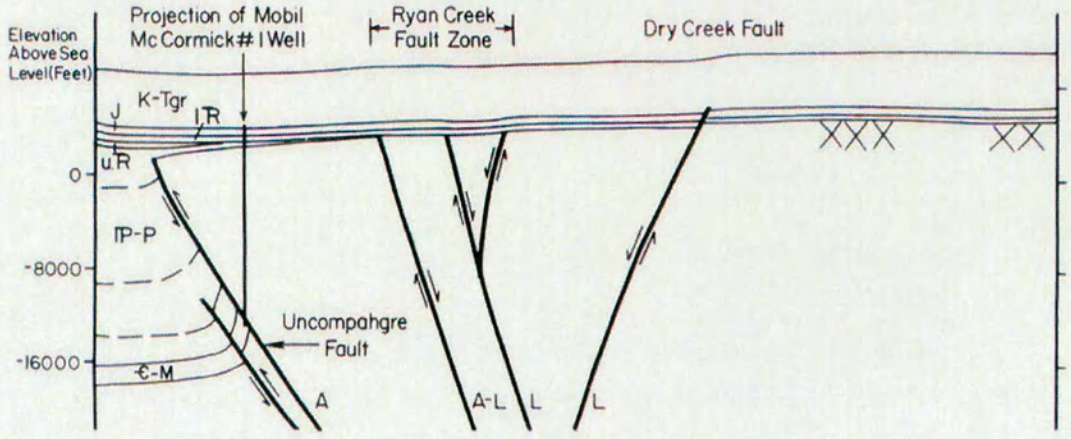

Figure 3.4. Cross section across the Uncompahgre front illustrating the nature of the fault geometry. From Heyman et al. (1986)

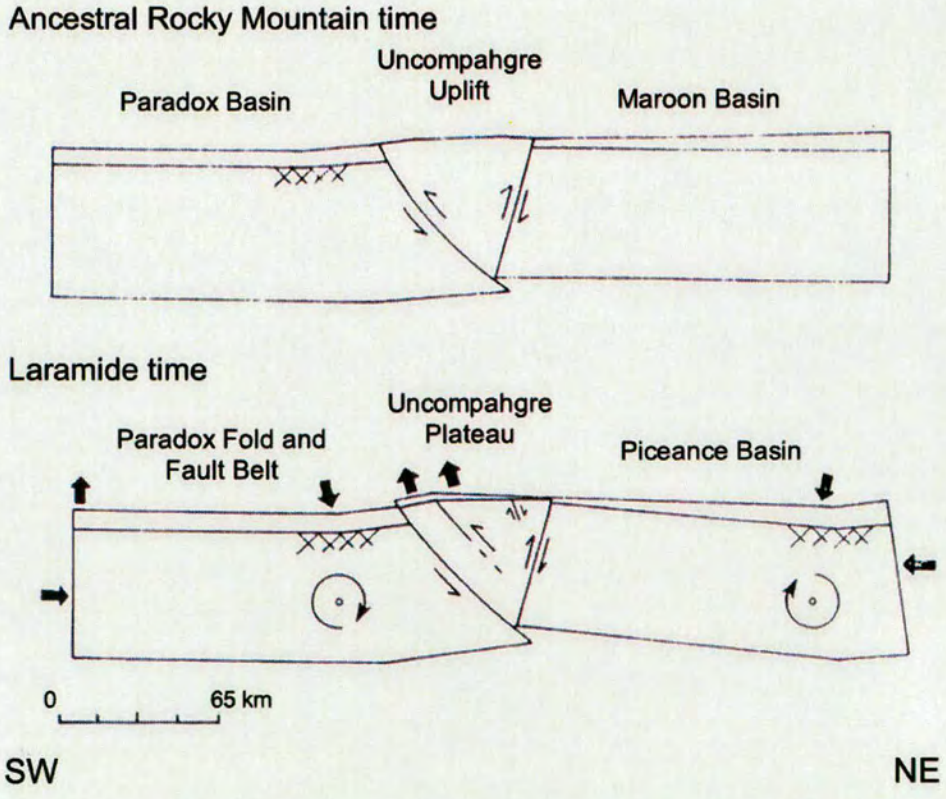

Figure 3.5. Sketch section illustrating the crustal geometry inferred by Heyman et al. (1986) for the Uncompahgre uplift in ARM and Laramide time. After Heyman et al. (1986).

Figure 3.6. Map of faults in the Grabens area of Canyonlands National Park. Faults are considered to have developed due to gravity sliding of sequences towards the Colorado River canyon upon a weak evaporite layer. The location of map shown in Figure 3.3. Map from Colorado School of Mines, 2005

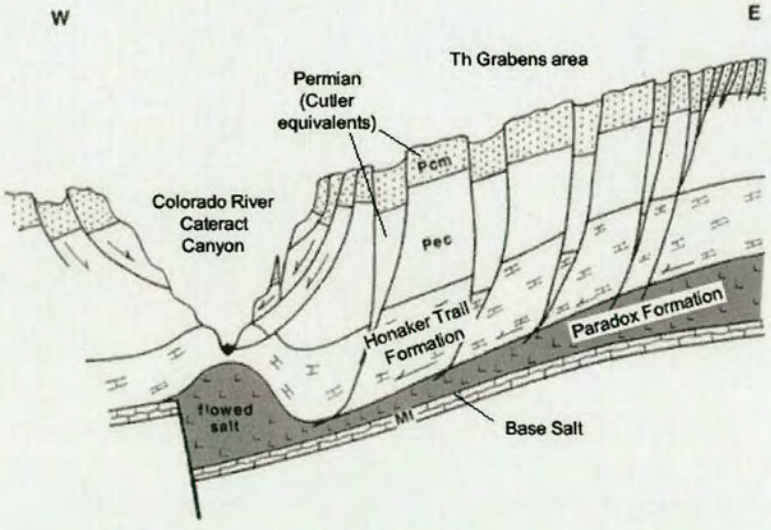

Figure 3.7. Diagrammatic cross section through the Grabens normal fault system illustrating the relationship between the fault system and the canyon carved by the Colorado River in the area. After Baars, (2003).

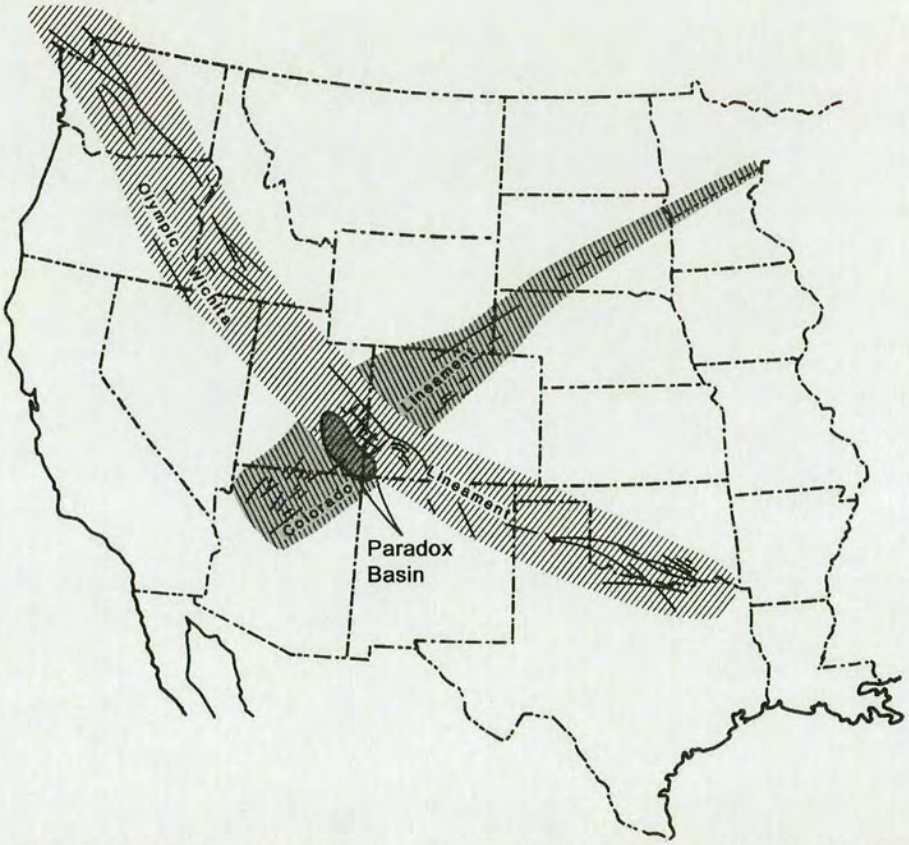

Figure 3.8. Map of the basement lineaments proposed as being responsible for the development of the Paradox Basin by Stevenson and Baars (1986). They interpret the Paradox Basin as a strike slip basin at the intersection of these lineaments

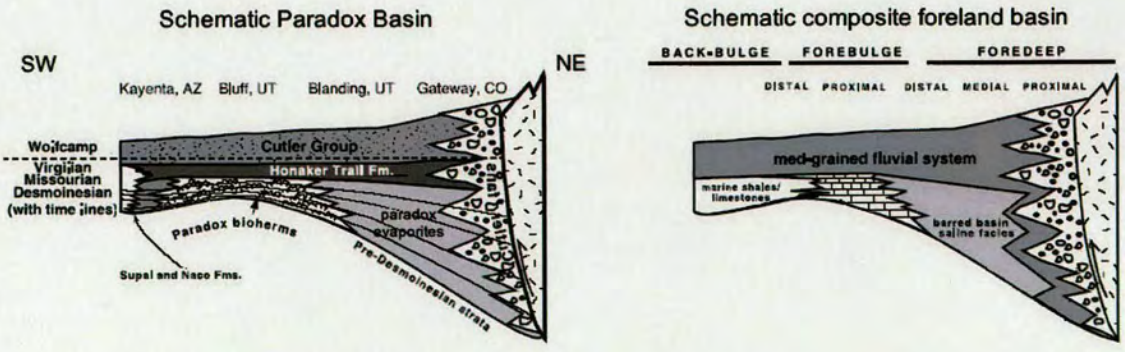

Figure 3.9.Comparison of the facies architecture of the Paradox Basin with a composite facies architecture model for a restricted flexural basin (after Barbeau, 2003)

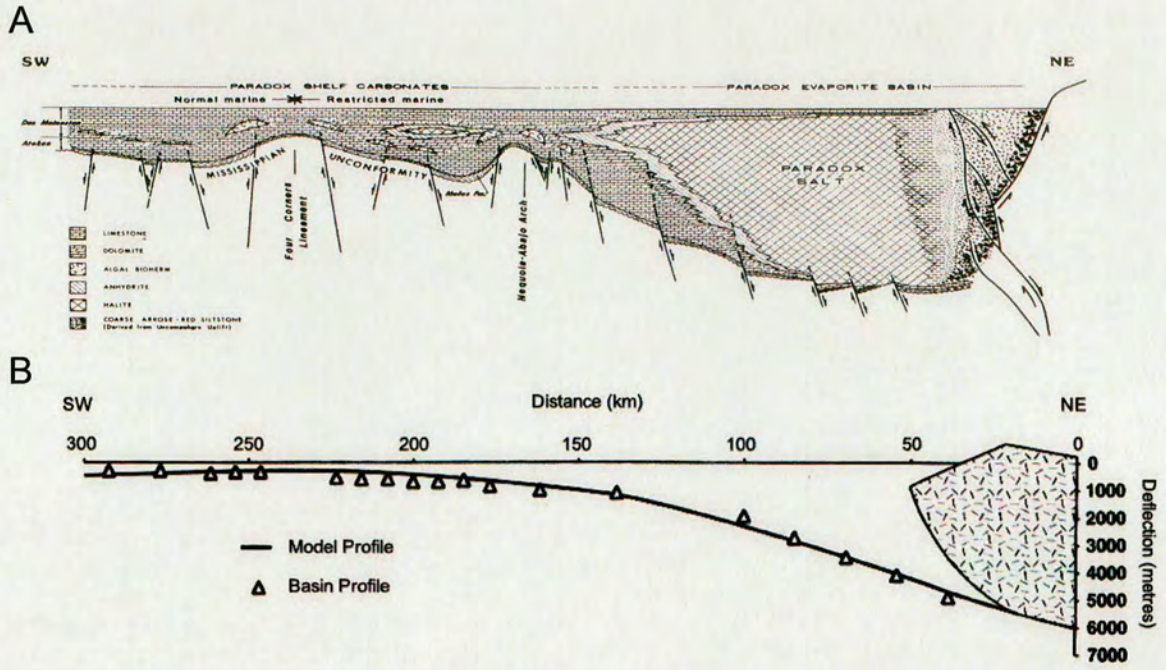

Figure 3.10. Schematic section through the Paradox Basin restored to Late Middle Pennsylvanian time illustrating salt basin morphology (a) (From Stevenson and Baars, 1986). And plot of restored basin profile along a transect through the Paradox Basin (Modified from Barbeau (2003))

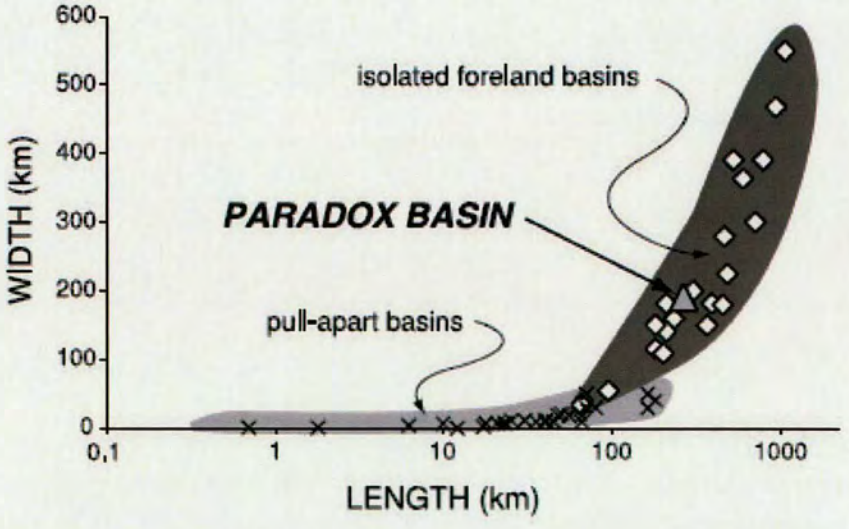

Figure 3.11. Plot of length vs width for various pull-apart basins and isolated flexural foreland basins from around the world (From Barbeau, 2003). Note how the Paradox Basin plots well within the foreland basin field

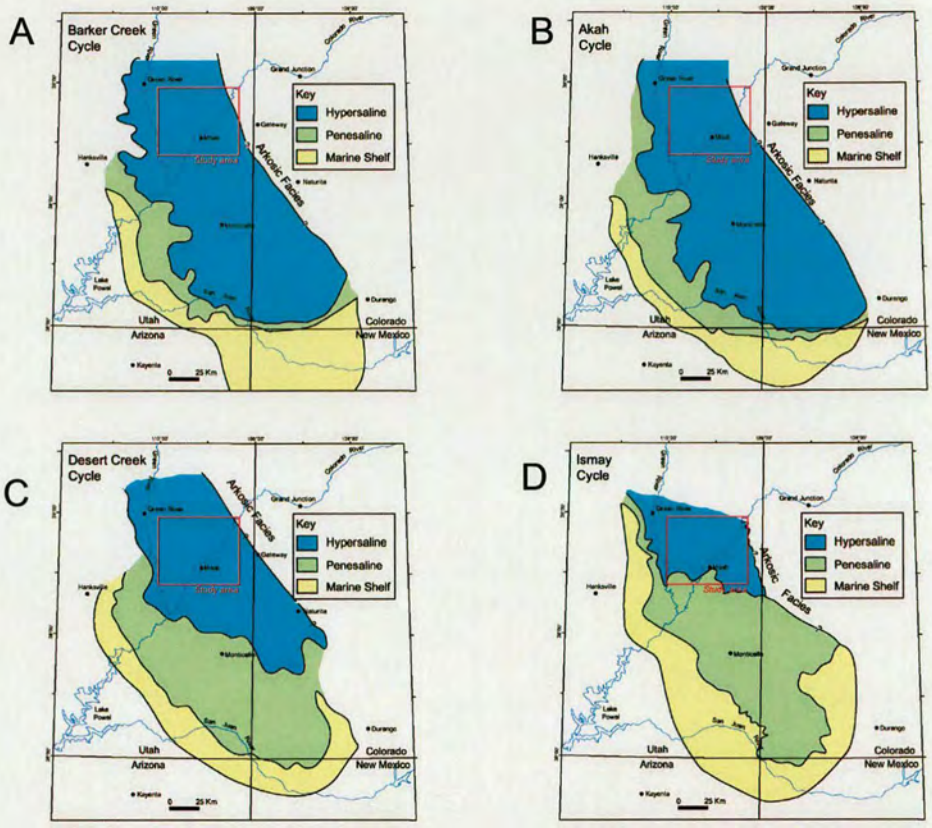

Figure 3.12. Maps illustrating facies distribution in the various cycles of the Paradox Formation – (note Alkali Gulch and Barker Creek are combined) Redrawn from Reid and Berghorn, 1981

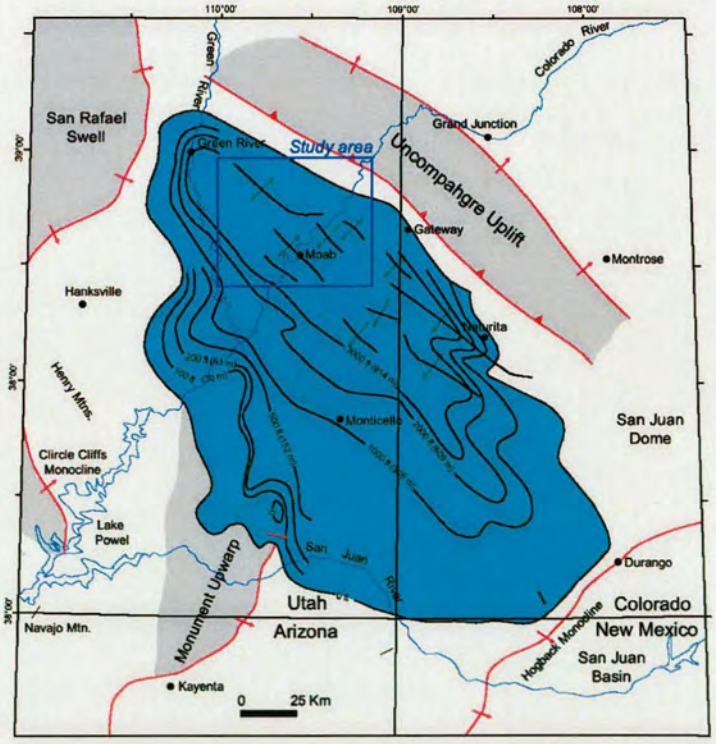

Figure 3.13. Isopach map of salt interval in Paradox Formation – After Baars and Stevenson, 1981

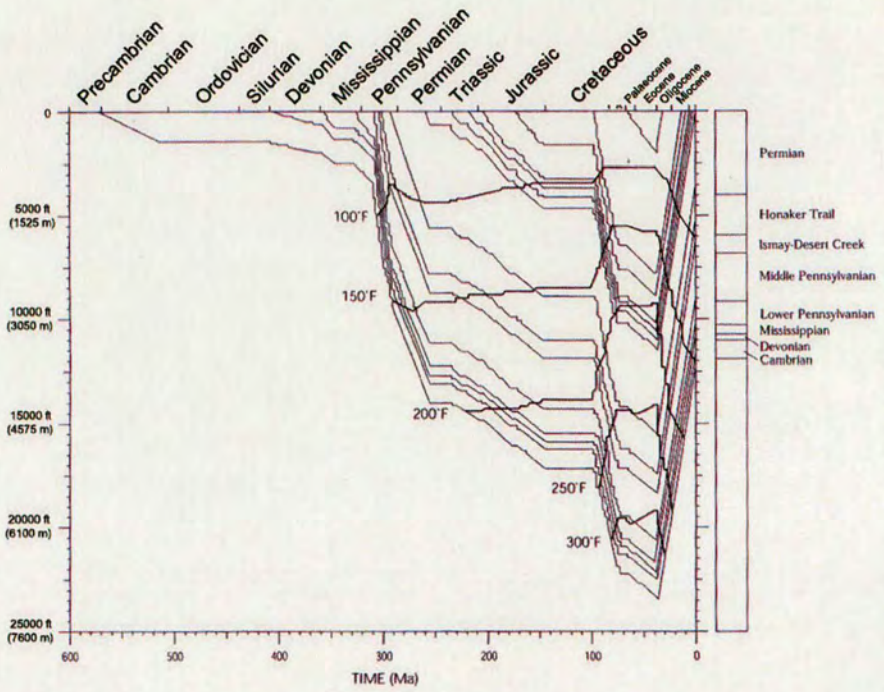

Figure 3.14. Burial and thermal history plot of the Phanerozoic sequence in the Moab area of the Paradox Basin – Using top Permian as a datum – Modified from Nuccio and Condon (1996)

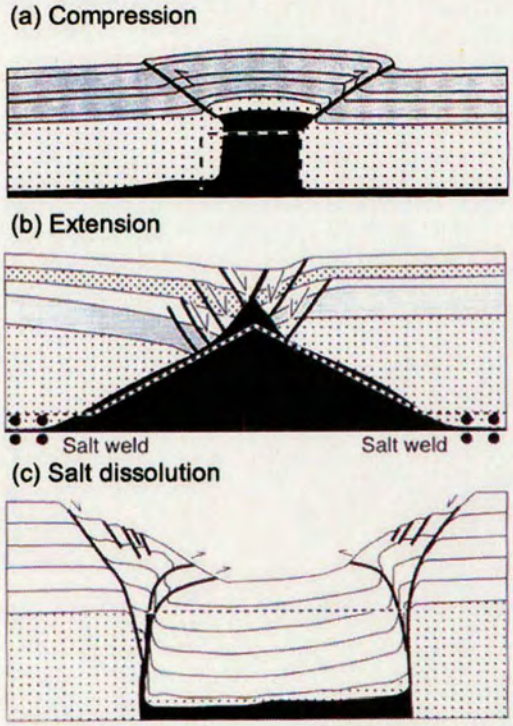

Figure 3.15. Sections from physical models of Ge et al. (1996) used to test the origin of supra-salt faulting in the Paradox Basin. Models were subjected to compression (a), extension (b) and salt dissolution (c). Black areas represent the salt analogue in the model and dotted lines illustrate the morphology of the modelled salt structure prior to deformation

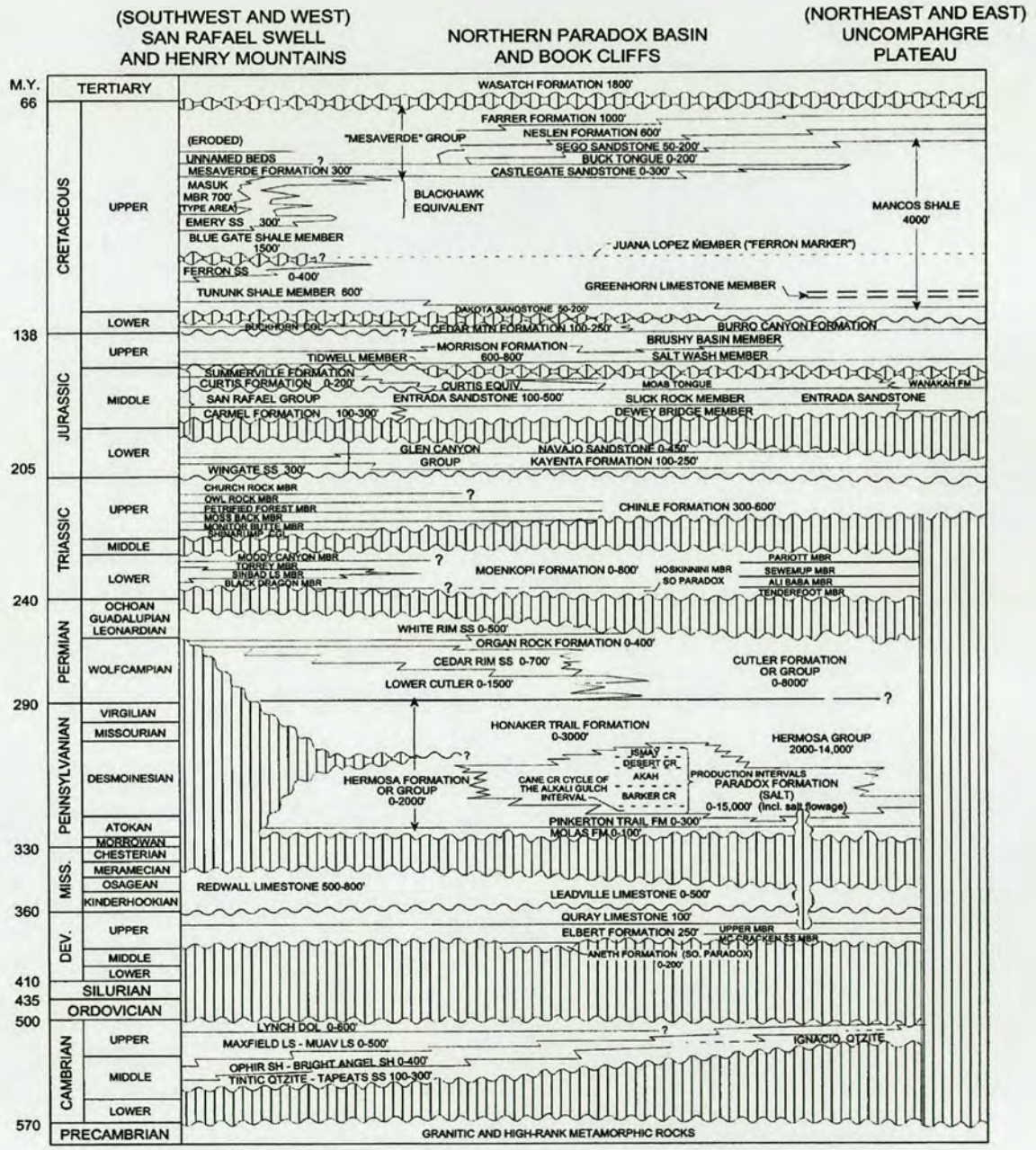

Figure 3.16. Stratigraphy of Paradox Basin and surrounding areas – From Nuccio and Condon, 1996

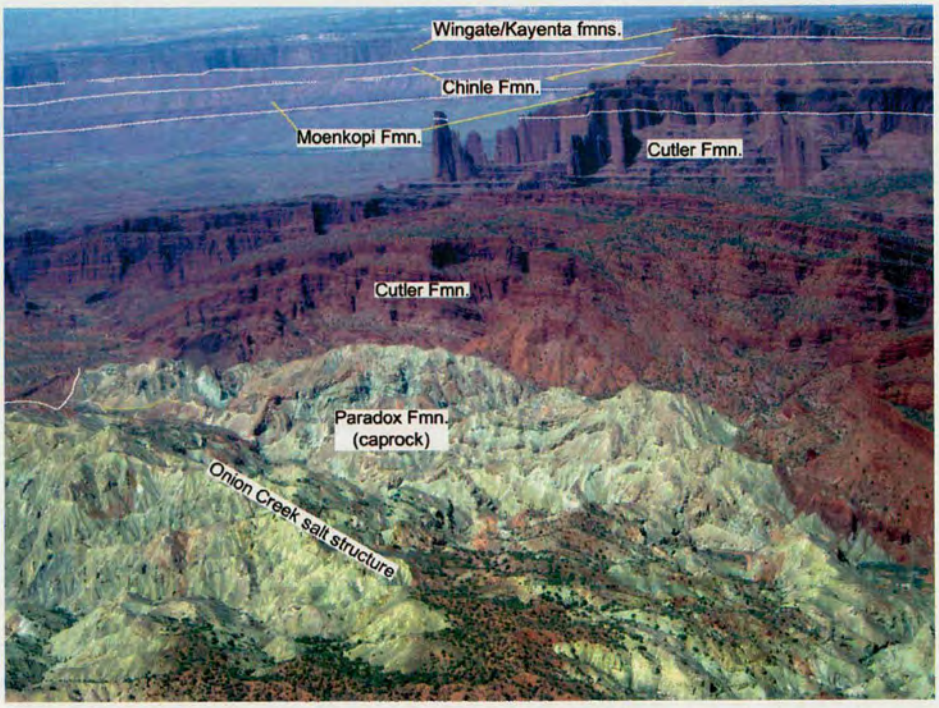

Figure. 3.17. Aerial photograph of the Onion Creek area illustrating the caprock exposures which are the surface expression of the Onion Creek salt structure. View is looking to the NE towards Fisher Towers from above Fisher Valley.

Figure 3.18. Photograph illustrating a typical caprock exposure in the the Onion Creek area and the complex folding observed within the rock. Photo taken looking north from UTM 649566 E, 4284798 N near the Stinking Spring area. Bedding in the deformed sequence is highlighted with yellow lines.

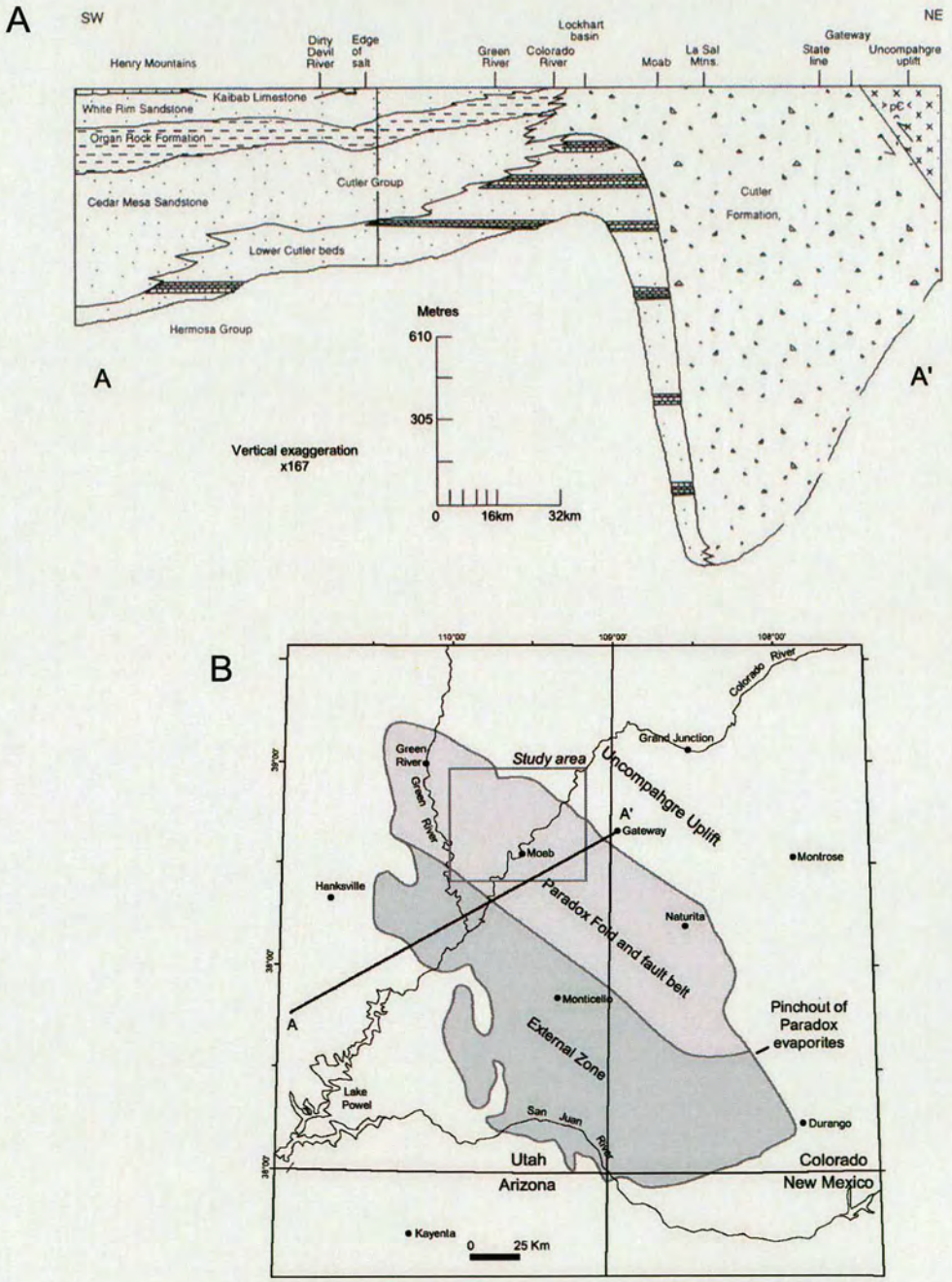

Figure 3.19. Cross section showing stratigraphic relationship and nomenclature used for the Cutler Group/Formation in the Paradox Basin and adjacent areas (a) and Location map showing location of section (b) (After Condon, 1995)

A

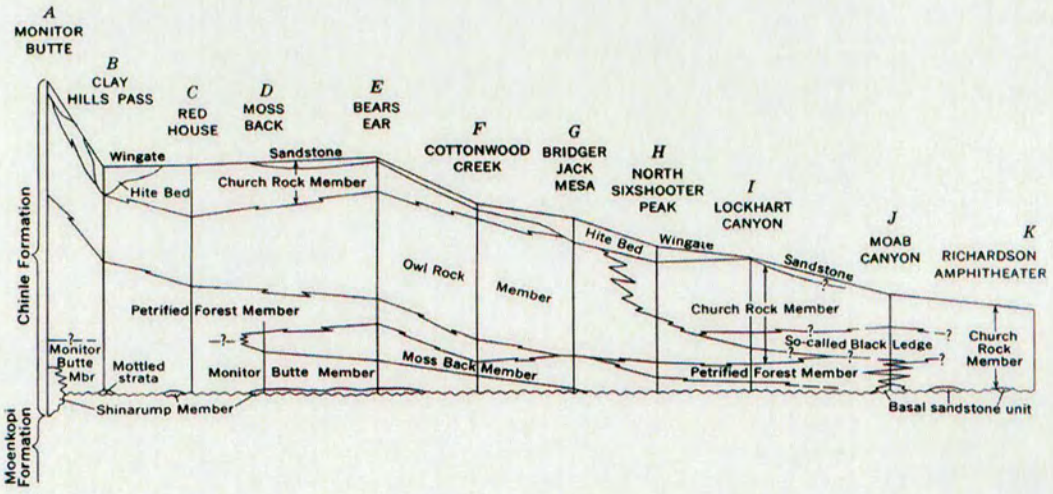

B

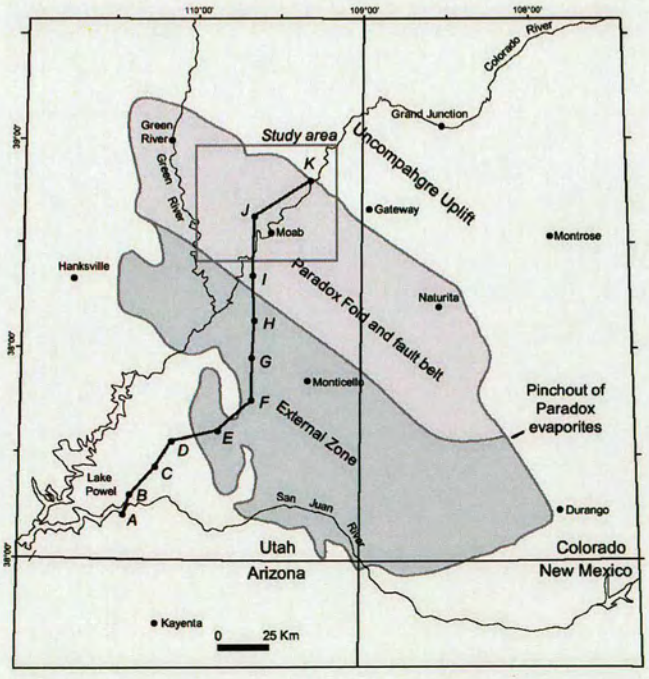

Figure 3.20. Correlation diagram illustrating the extent of various members of the Chinle Formation across the basin (a) and a location map illustrating the location of the chart in the transect (b). Both after Stewart et al. (1972[b])

Figure 3.21. Photo of mottling effect in 'Lower Unit' of the Chinle Formation (Taken in the Sandy Beach area at UTM 630682E, 4280717N). Pen for scale

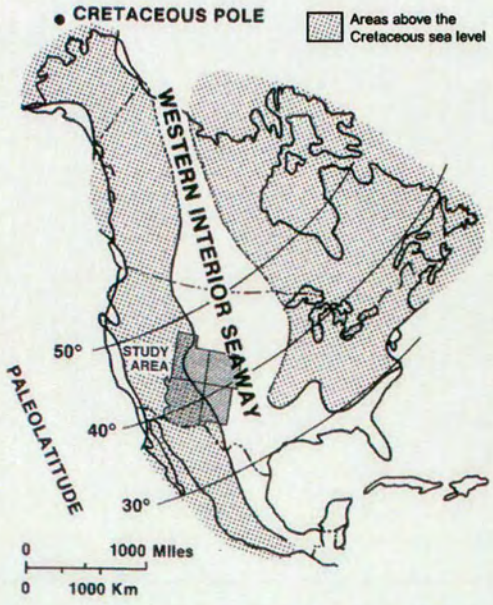

Figure 3.22. Cenomanian to Turonian (Upper Cretaceous) palaegeographic map of North America illustrating the extent of the Western Interior Seaway at maximum highstand conditions (after Gill and Cobban, 1973)

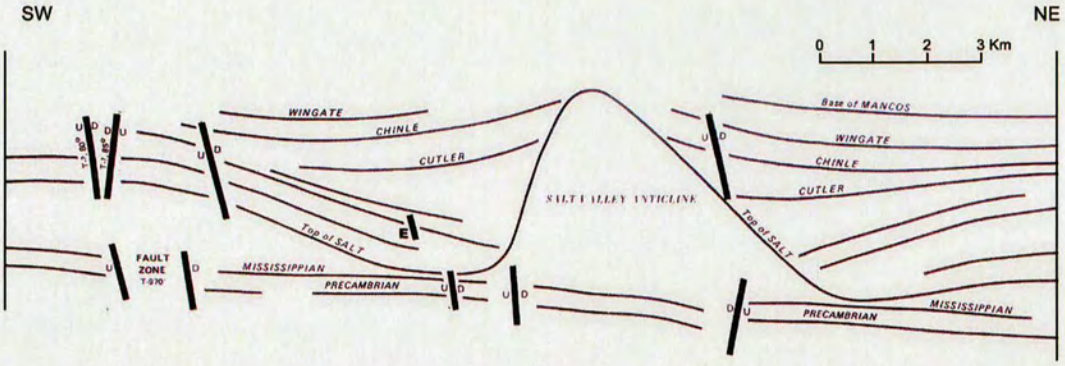

Figure 3.23. Line drawing of a seismic line through the Salt Valley salt structure. From Woodward Clyde Consultants 1984

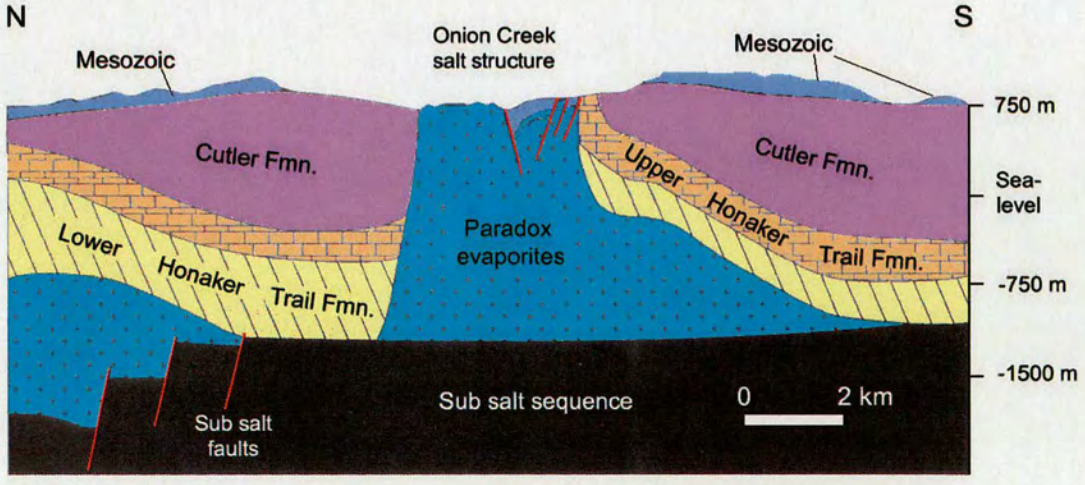

Figure 3.24. Cross section through the Onion Creek salt structure. Note that the interpretation of structure at depth is based on seismic data. After Hudec (1995)

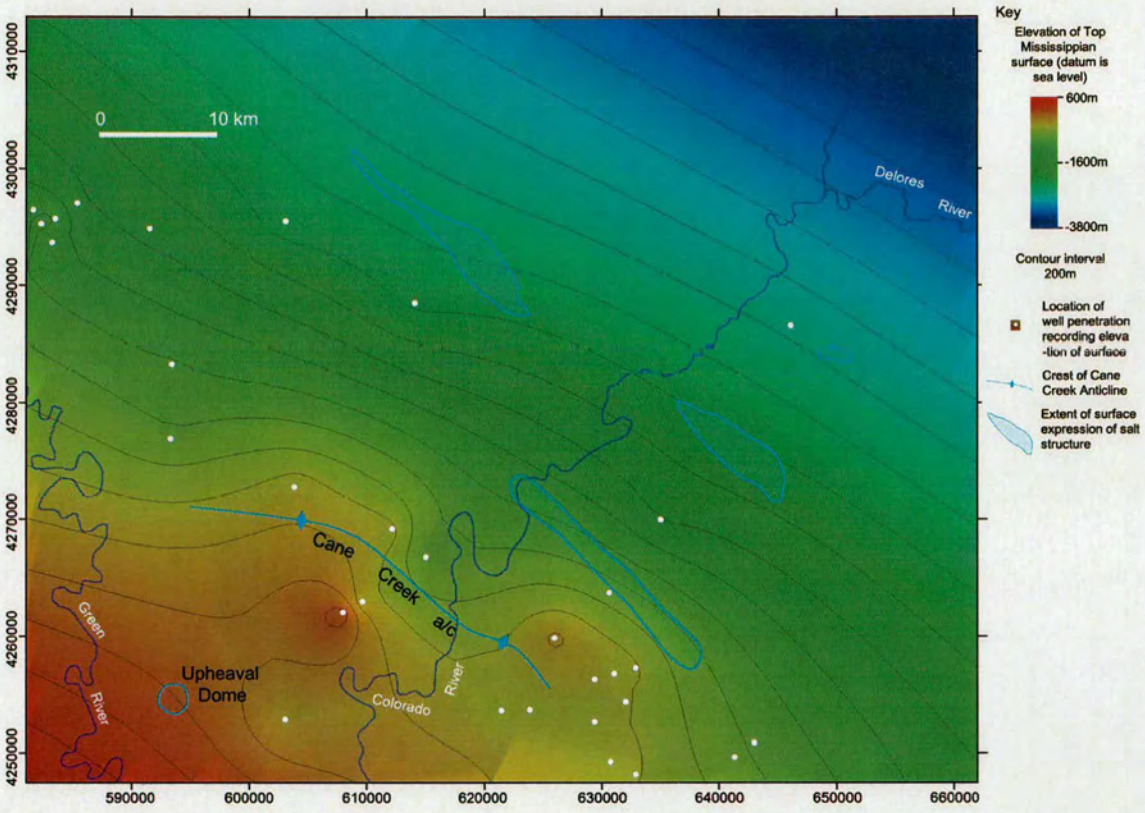

Figure 3.25. Structure contour map on the top of the Mississippian sequence in the study area. This surface is near to the top of the sub-salt sequence and illustrates the large scale foreland basin morphology.

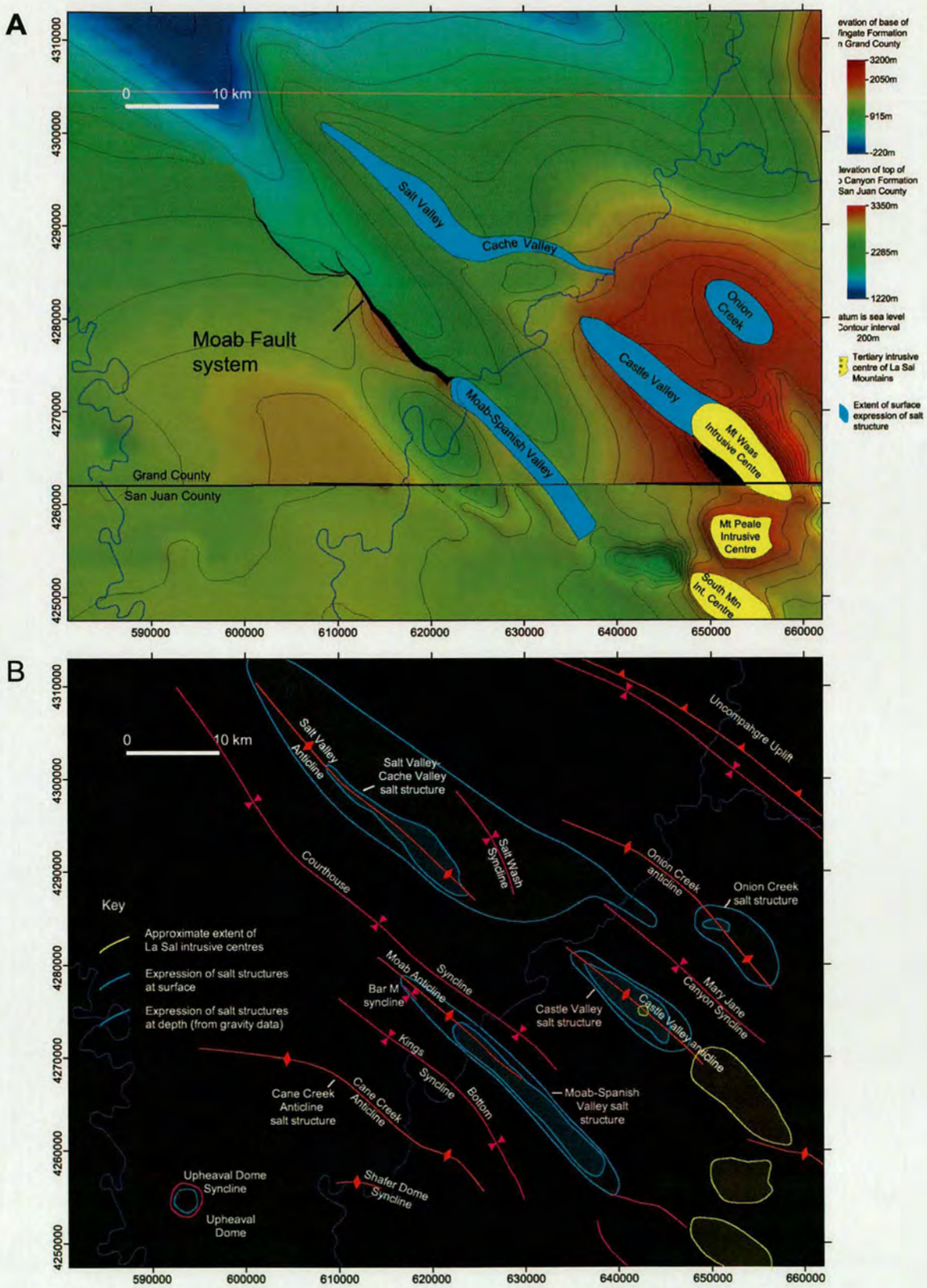

Figure 3.26. Structure contour map of the supra-salt sequence (A) and a map illustrating the location of major salt structures and major folds in the study area (B). Structure contour data in (A) is based on the Base Jurassic (Top of Chinle Formation) horizon in Grand County and Base Cretaceous (Top of Burro Canyon Formation) in San Juan County. Based on data from Doeling (2001) Grand County and Doeling, 2004 (San Juan County). Note different elevation scales are used in Grand and San Juan counties.

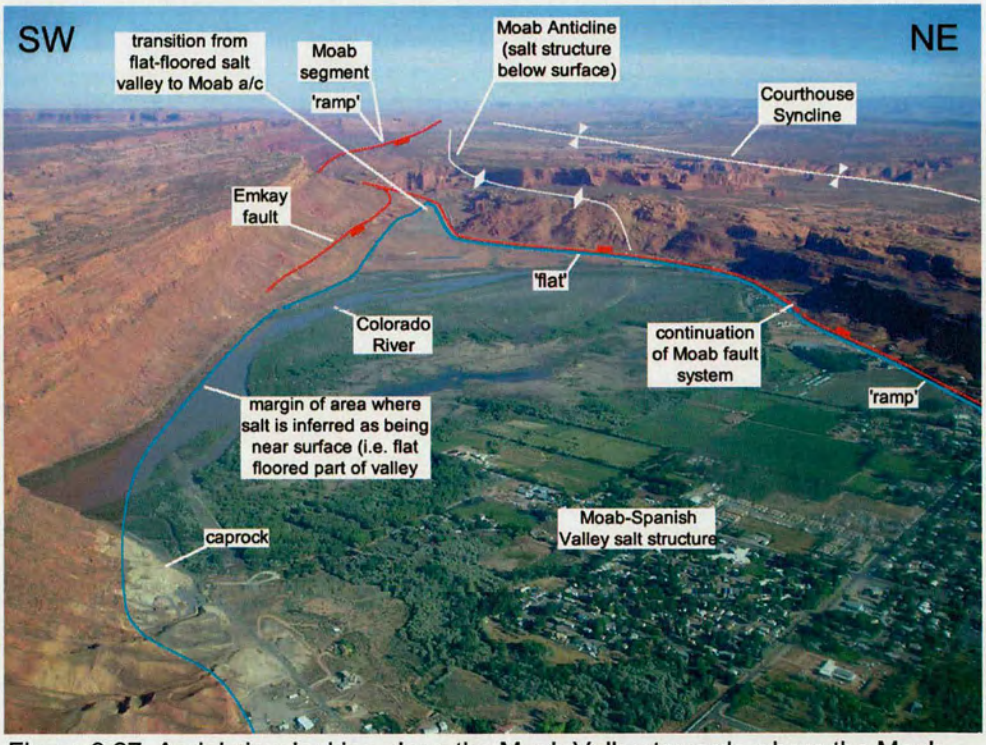

Figure 3.27. Aerial view looking along the Moab Valley towards where the Moab-Spanish Valley salt structure changes from being expressed as a flat- floored salt valley to where salt is buried below the surface and expressed as the salt-cored Moab Anticline. Also shown is the morphology of the Moab Fault system in the area. Photo taken from approximately UTM 626000 E, 4269500 N. looking towards the NW.

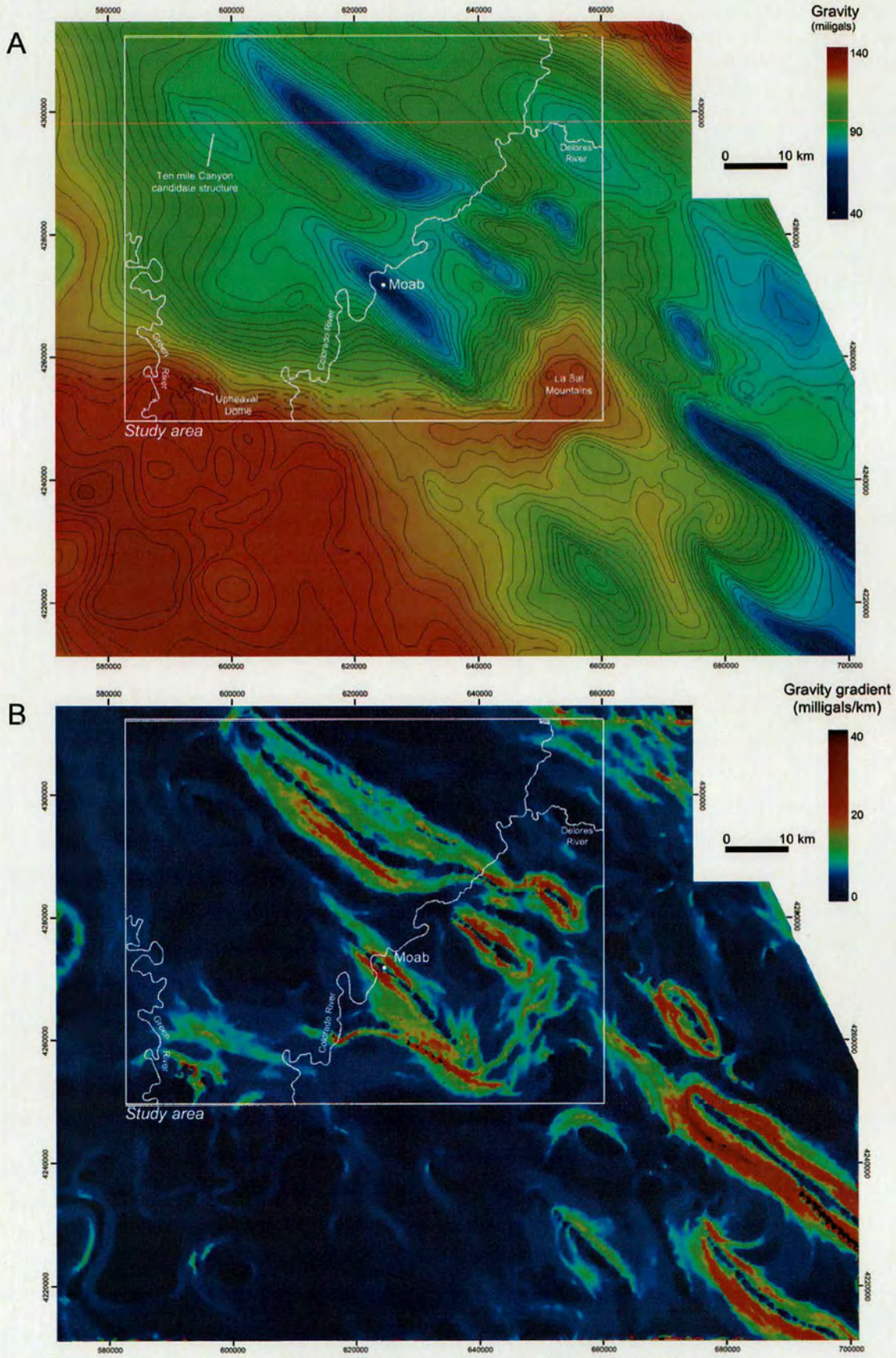

Figure 3.28. Gravity map (A) and gravity gradient map (B) of the study area and surrounding areas of the Paradox Basin. Maps made from digitising and colouring data published by Case and Joesting (1972)

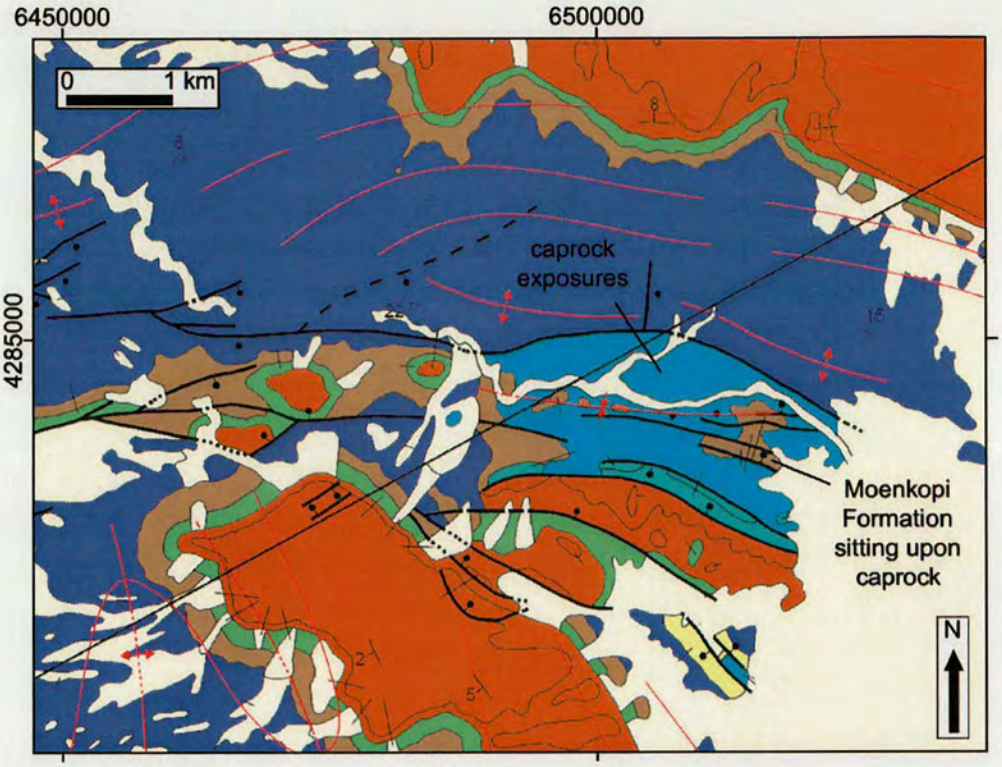

Figure 3.29. Geological map of the area around Onion Creek where extensive caprock exposures form the surface expression of the Onion Creek salt structure. The map illustrates the dominant orientations of a system of normal faults associated with exposures. Note how the faults have a dominantly E-W to ENE-WSW orientation. Modified from Doeling, 2001. The location of this map is shown in Figure 3.1.

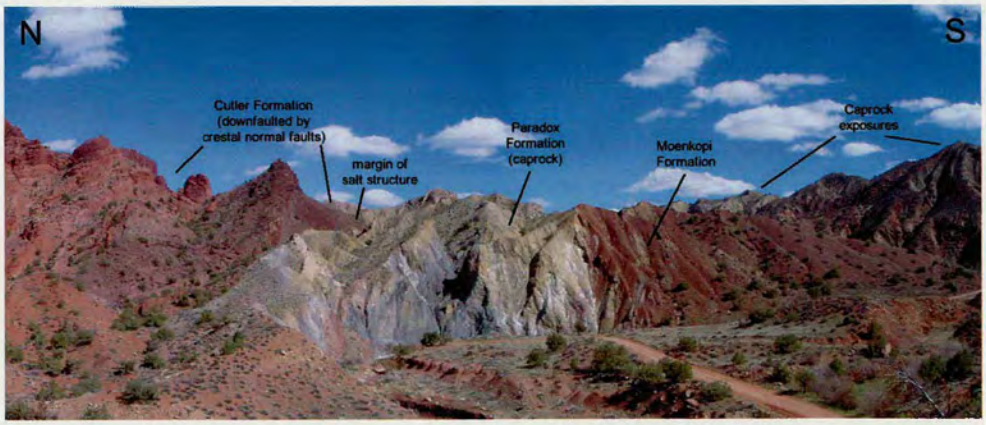

Figure 3.30. Photograph taken in the Onion Creek area illustrating how the Moenkopi Formation is locally exposed sitting directly upon caprock of the Onion Creek salt structure. This and several other exposures are the basis for the interpretation that the Moenkopi Formation was the first to blanket the salt structure. View is looking east from UTM 648561 E, 4284729 N.

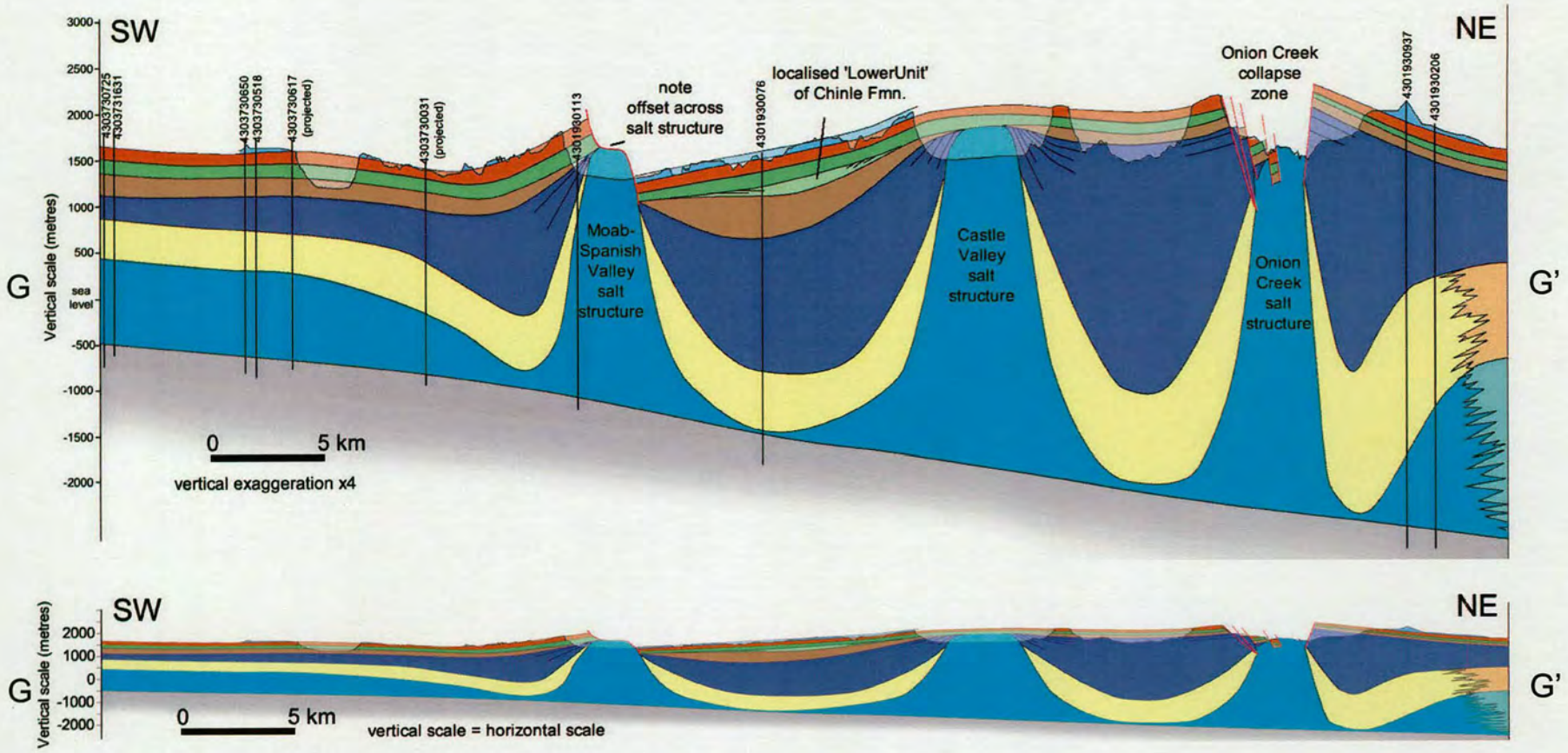

Figure 3.31. Cross section through the study area illustrating the interpreted subsurface extent of the Moab-Spanish Valley, Castle Valley an Onion Creek salt structures. Location of section is shown in Figure 3.1.

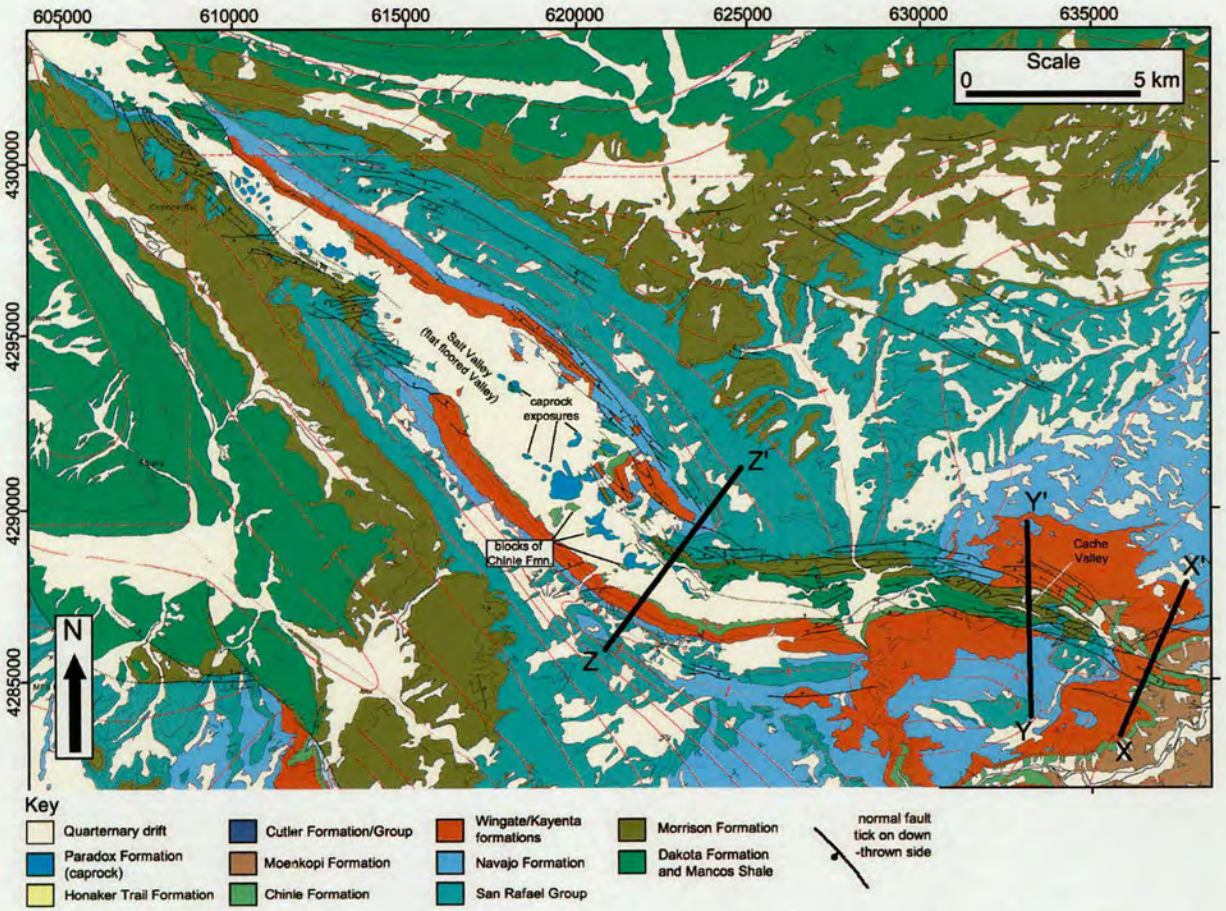

Figure 3.32. Geological map of the Salt Valley and Cache Valley areas and surrounding areas illustrating the outcrop expression of the Salt Valley-Cache Valley salt structure and the extensive crestal fault system associated with it. Map is based on published map data from Doeling (2001) (A). Also shown are several cross sections illustrating the style of faulting in the salt structures crest (B). Sections are from Doeling (1988).

B

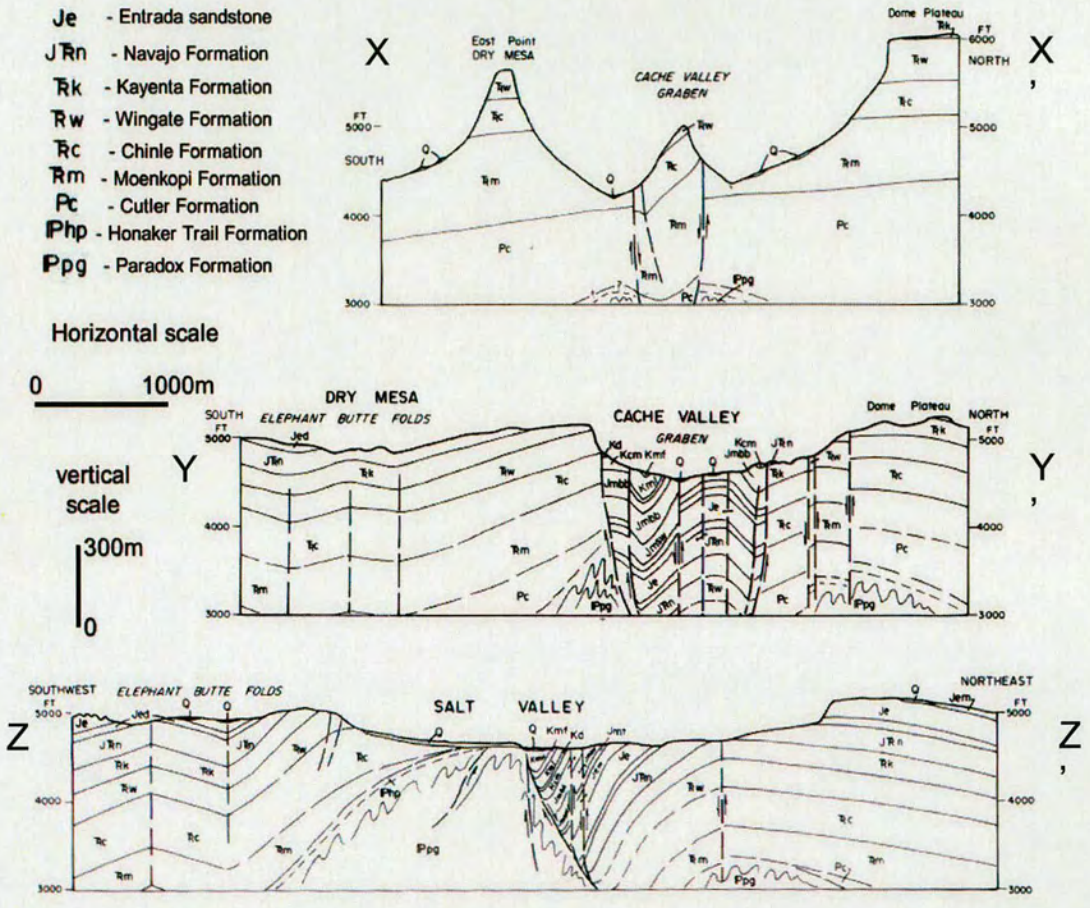

Figure 3.32 continued

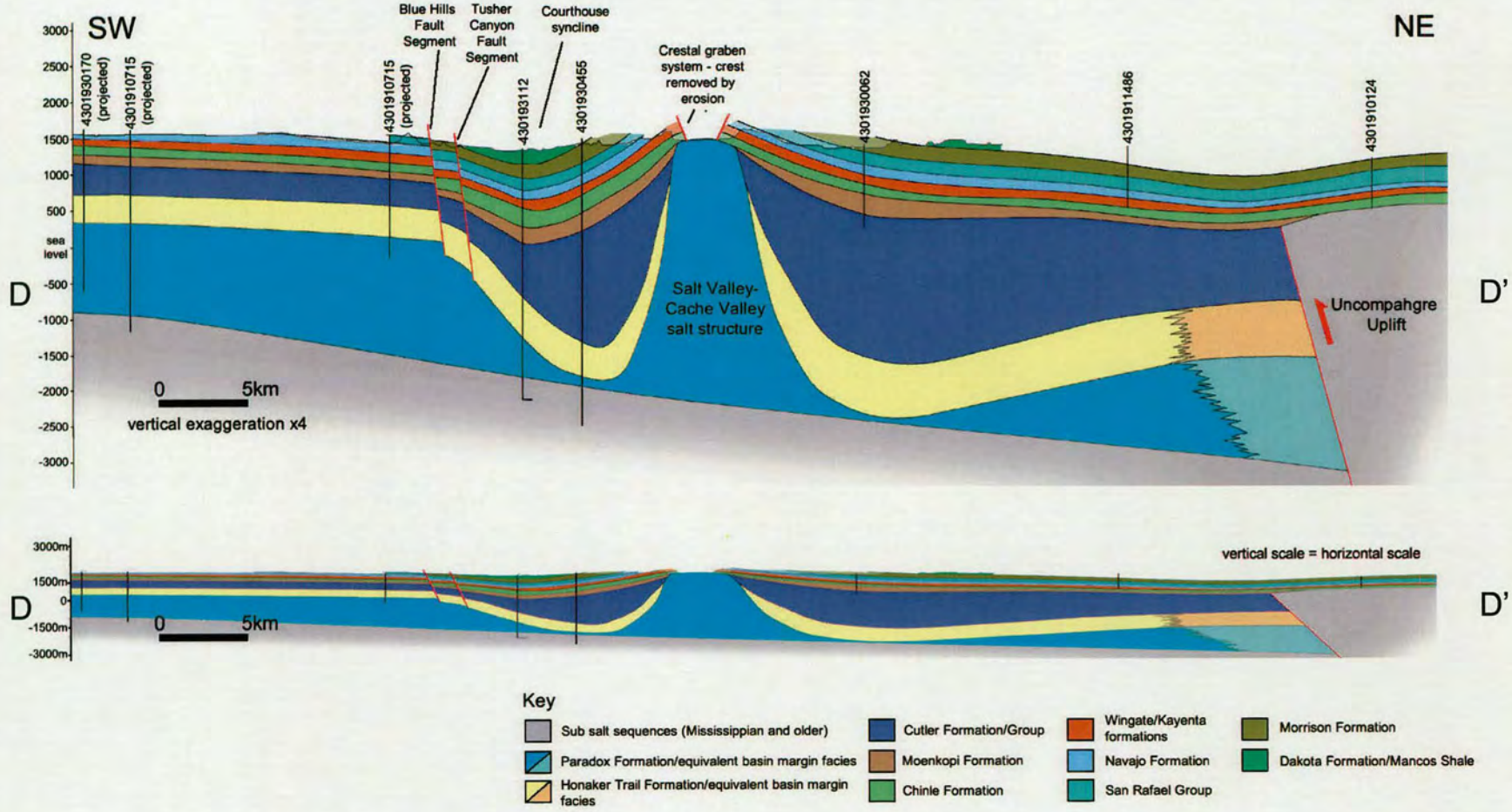

Figure 3.33. Cross section through the northern part of the study area showing the Salt Valley-Cache Valley salt structure, Uncompahgre Uplift and northern part of the Moab Fault System. The location of the section is shown in Figure PB-A.

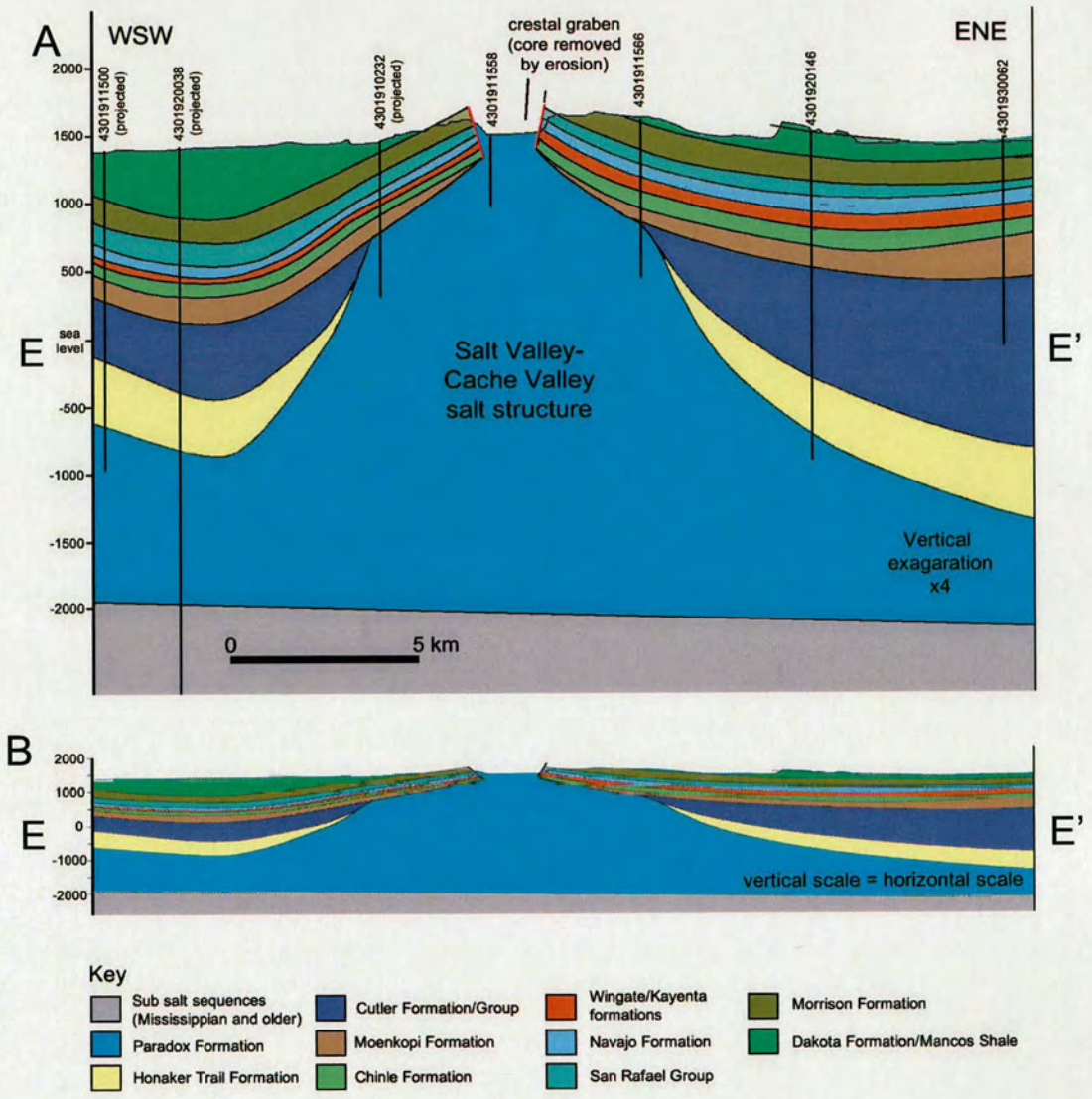

Figure 3.34. Cross section through the northern part of the Salt Valley-Cache Valley salt structure. Shown are a section in which the vertical scale has been exaggerated by 4 (A) and a section where the vertical and horizontal scales are equal (B). The location of the section is shown in Figure 3.1.

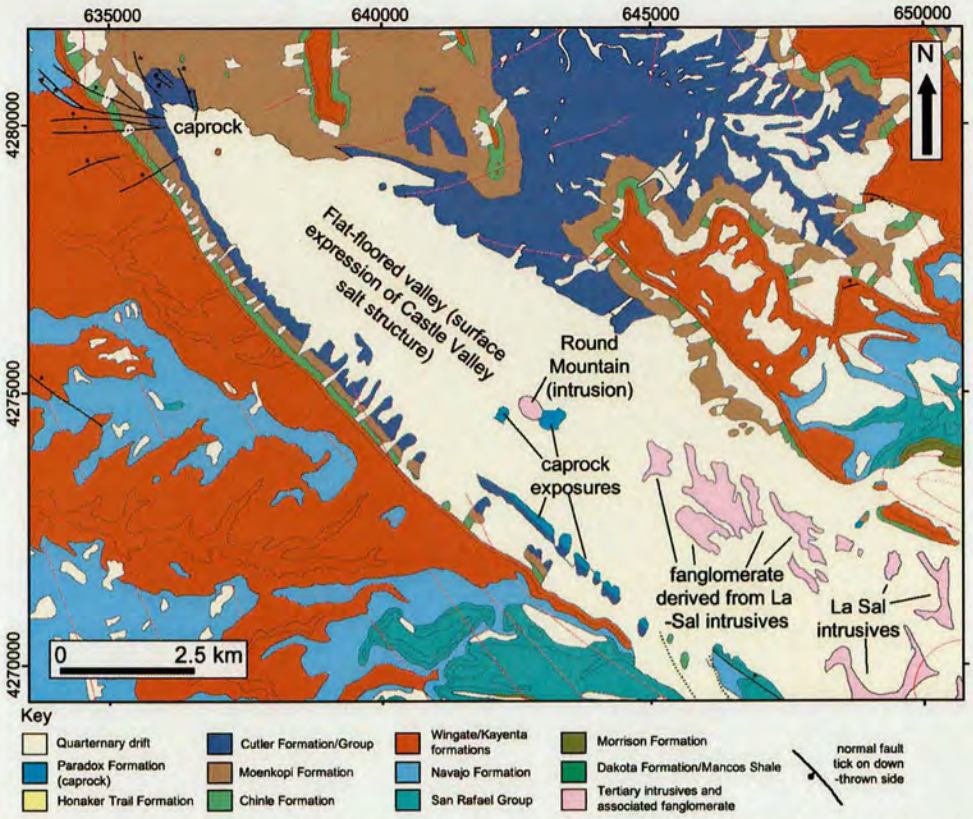

Figure 3.35. Geological map of the Castle Valley area illustrating the outcrop expression of the Castle Valley salt structure and the location of intrusives associated with the salt structure. Map based on published map data from Doeling (2001) and Doeling and Ross (1998). The location of the map is shown in Figure 3.1.

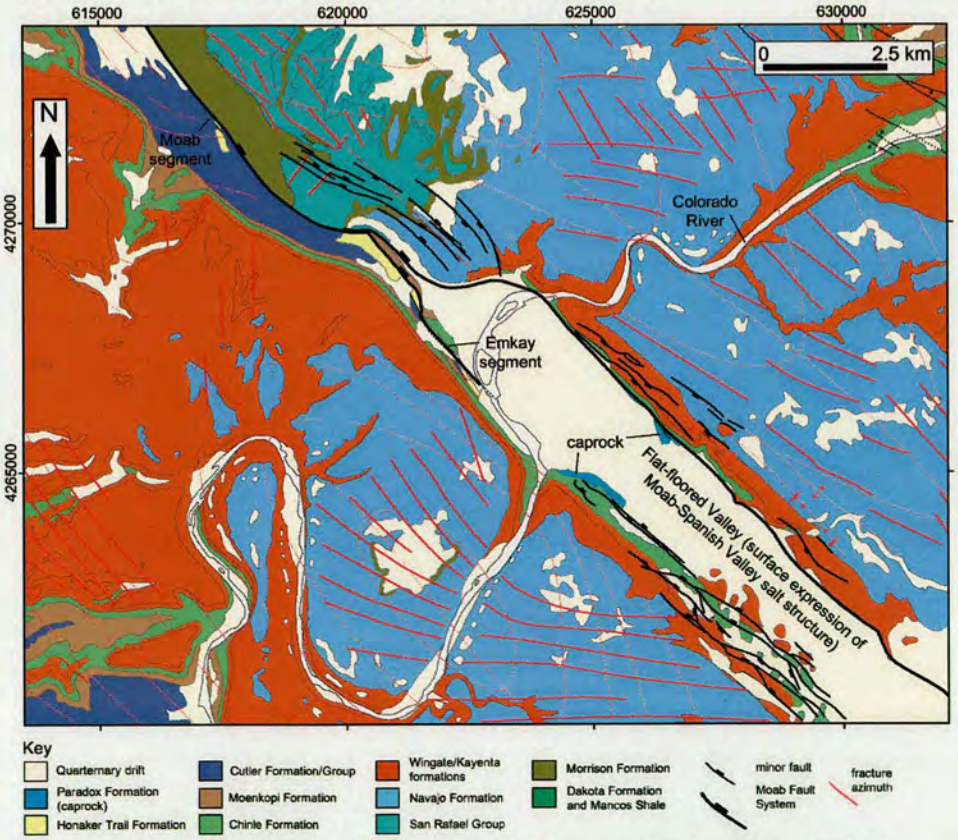

Figure 3.36. Geological map of the Moab Valley area and northern end of Spanish Valley areas. The map illustrates the surface expression of of the Moab-Spanish Valley salt structure and its associated faults. Lithology mapping is based primarily on Doeling (2001) but the illustrated extent of the Moab and Emkay segments of the Moab Fault System, fracture azimuths and faults to the NW of the Colorado River shown were mapped as part of this study. Minor faults to the SE of the Colorado River are based on Doeling et al. (2002).

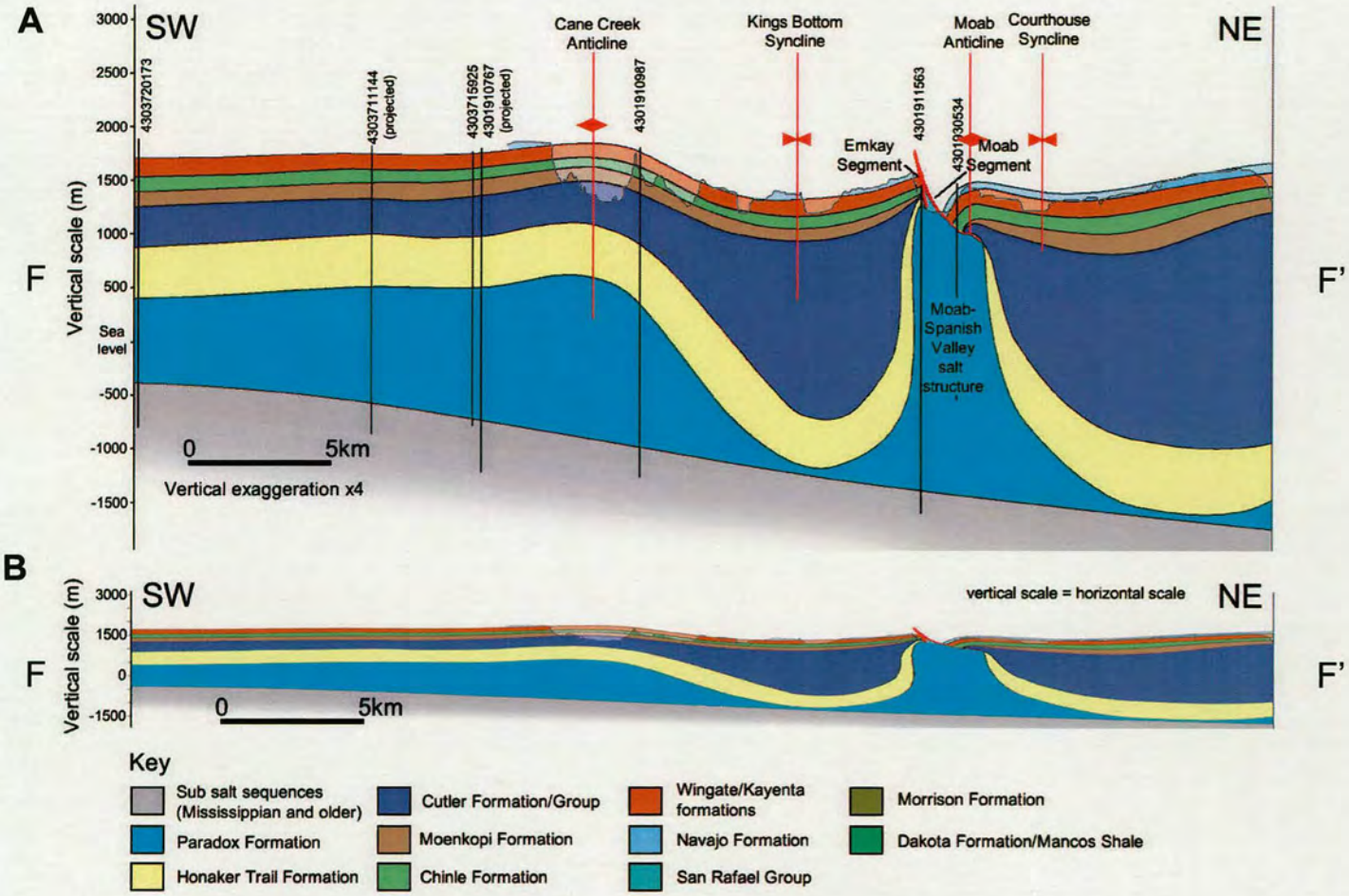

Figure 3.37. Cross section through the Cane Creek Anticline and Moab-Spanish Valley salt structures. Shown are a section in which the vertical scale has been exaggerated by 4 (A) and a section where the vertical and horizontal scales are equal (B). The location of the section is shown in Figure 3.1.

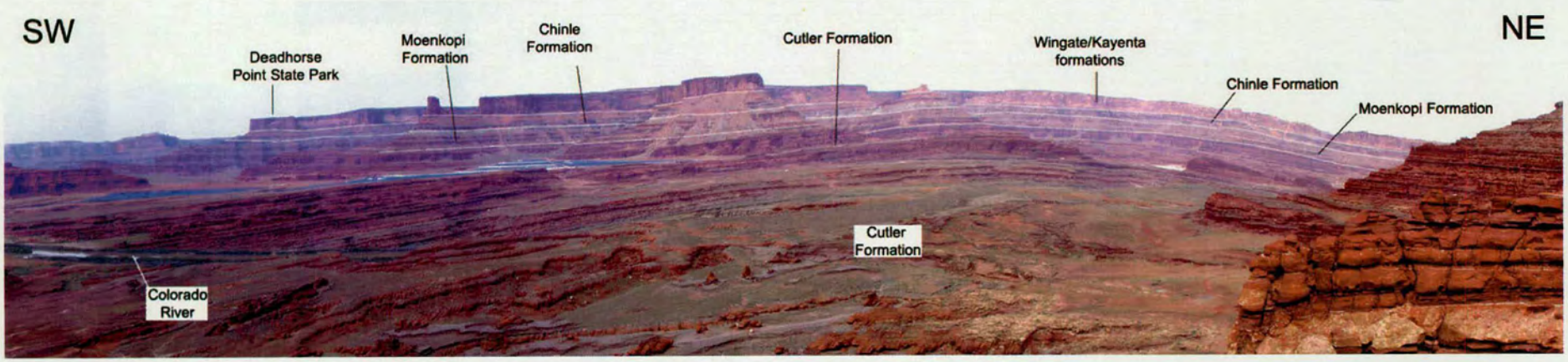

Figure 3.38. Photograph of the Cane Creek Anticline in the Potash Amphitheatre area looking to the NW from UTM 619815 E, 4260179 N (near Hurrah Pass). The cliff exposes and photograph show an approximately strike perpendicular section. Note the absence of any significant thickness variations observed in any of the exposed sequences.

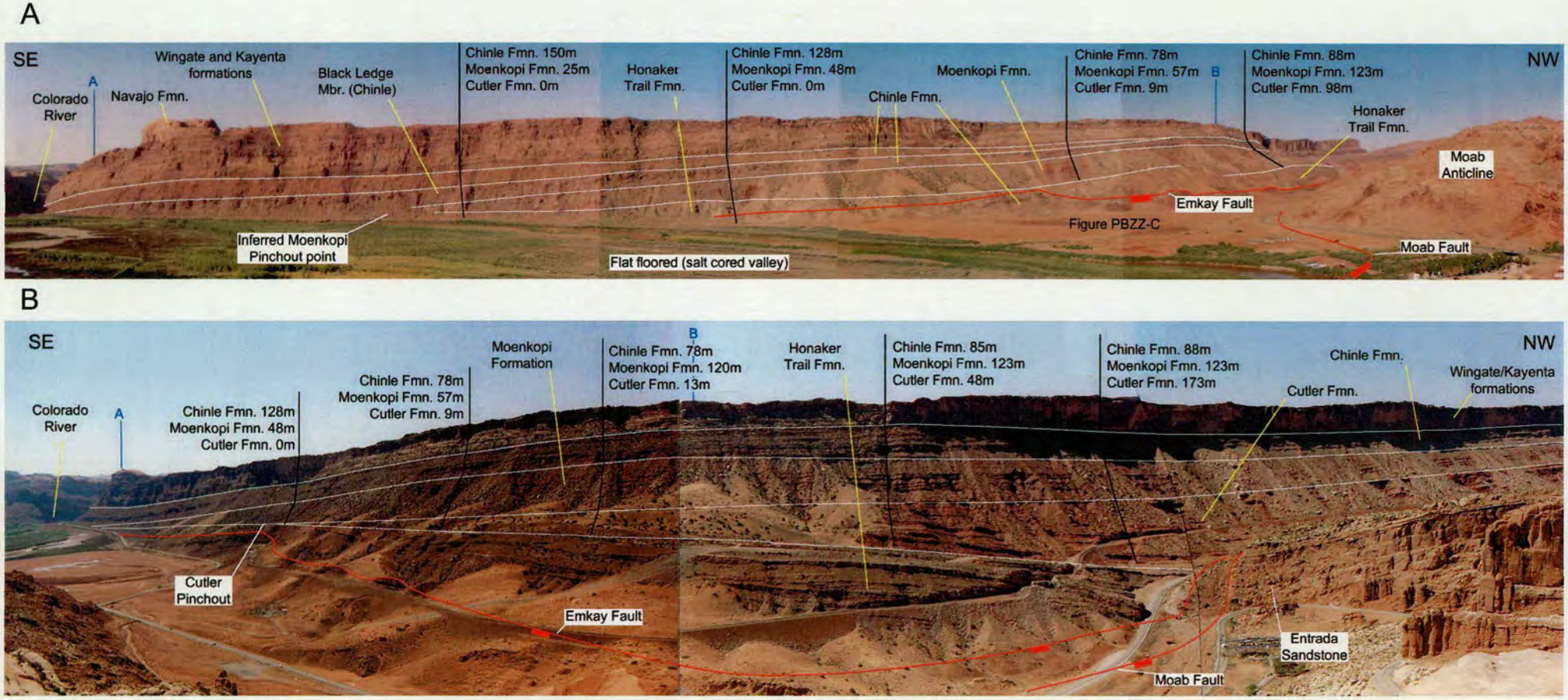

Figure 3.39. Photographs of the cliff section at the northwest end of the Moab Valley illustrating thickness variations in the Cutler to Chinle sequence. Photographs are of different parts of the same cliff section and two points common to both sections are labelled A and B. The measured thickness of the exposed formations are shown at various points along the section.

Figure 3.40. Photograph of the Emkay fault and the 'rolled over' bed of Honaker Trail Formation which locally forms its slip surface. Note how the underlying Honaker Trail sequence is truncated by this bed. Photograph is taken at UTM 621450E, 7273190N looking towards the south.

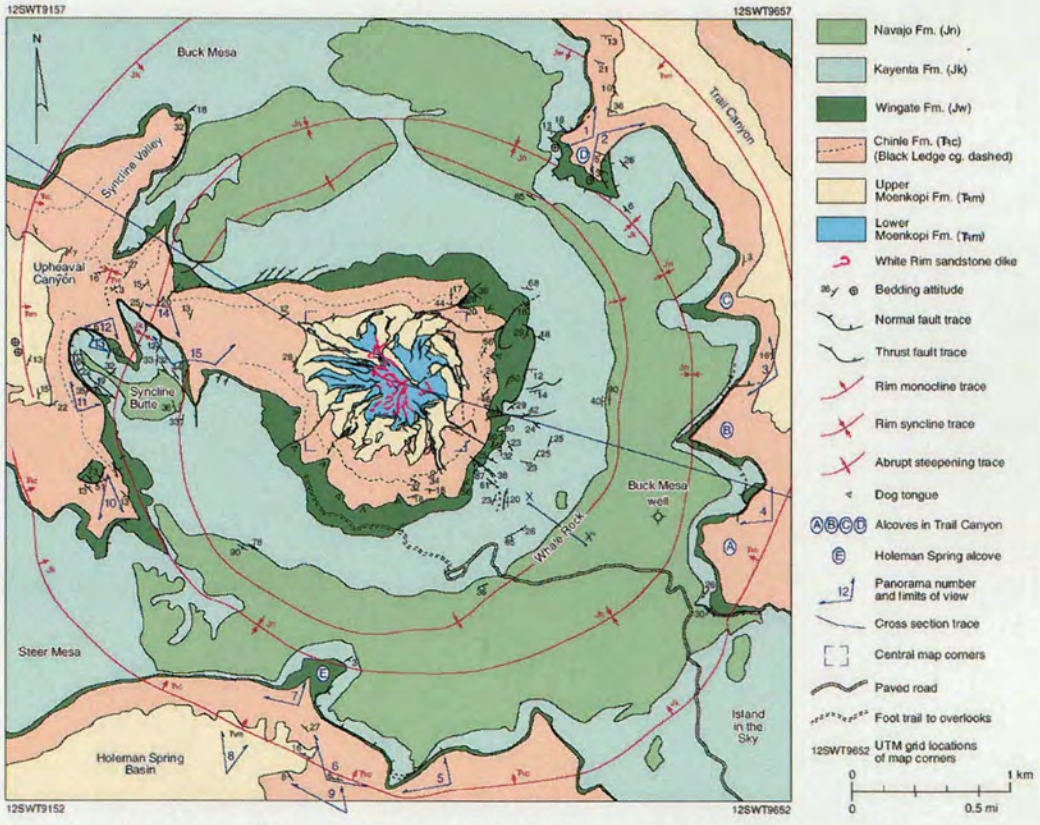

Figure 3.41. A map illustrating the structural elements of of the Upheaval Dome structure, a circular candidate salt structure within the Paradox Basin. From Jackson et al. (1998).

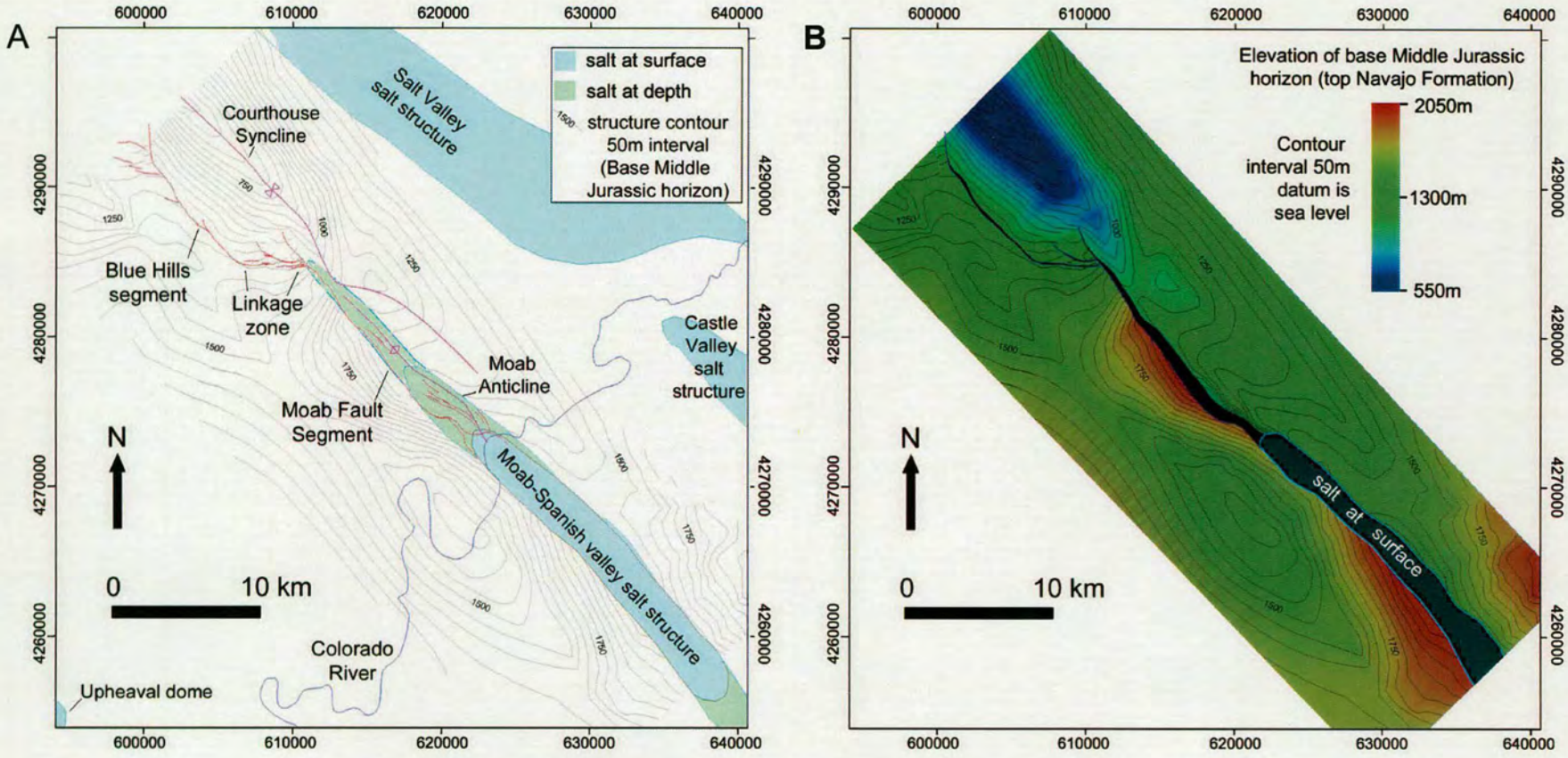

Figure 3.42. Maps illustrating the surface extent of the Moab Fault system and the location of the associated salt structures (A) and a structure contour map on the Base Middle Jurassic (Top Navajo) horizon (B) illustrating the uplift and subsidence associated with the fault system.

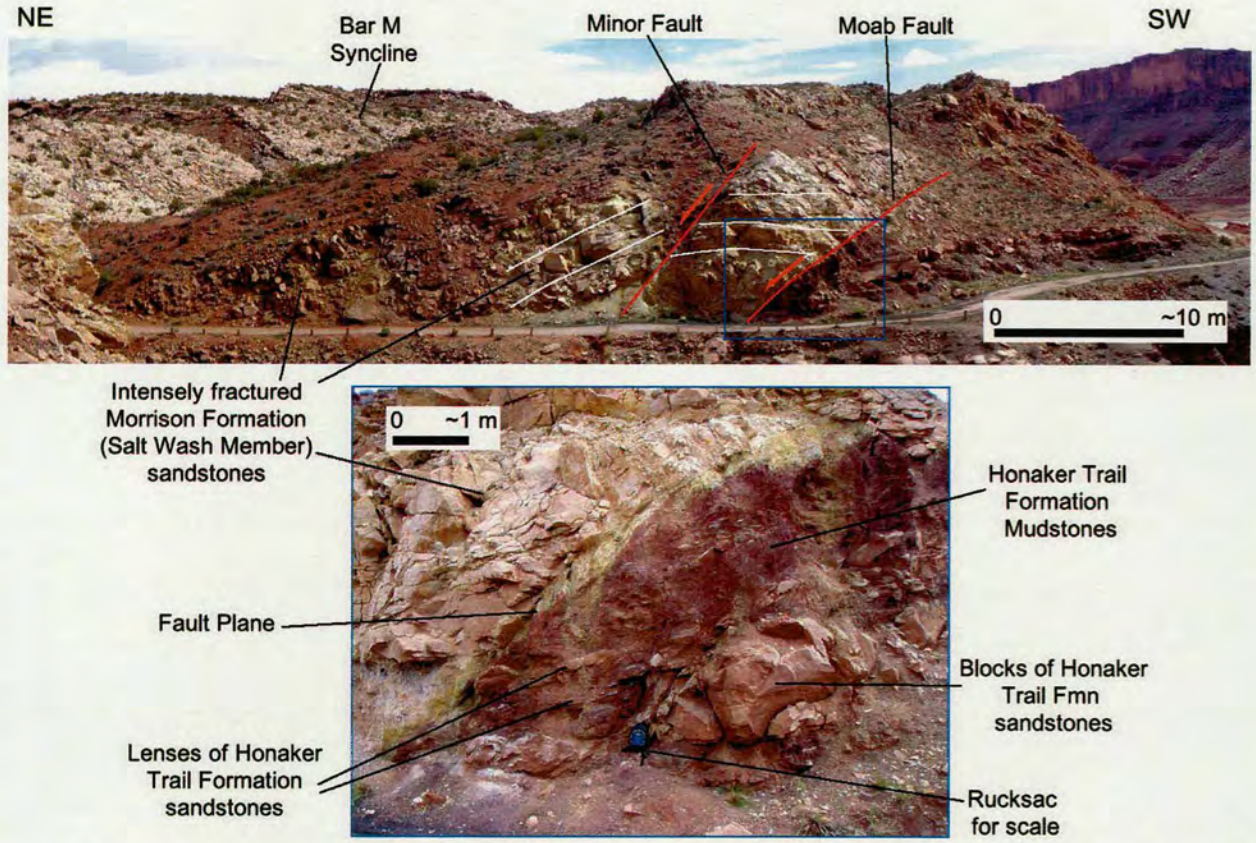

Figure 3.43. Photograph of the Moab segment of the Moab Fault System and its associated damage zone. Photograph taken at UTM 617577 E, 4276835 N along the old Crescent Junction to Moab highway. Shown are both a view of the whole damage zone and also a close-up of the fault plane itself. This is approximately the area of maximum displacement on the entire Moab Fault system and sees the Pennsylvanian Honaker Trail Formation juxtaposed against the Jurassic Morrison Formation. Note the Bar M Syncline is situated in the immediate hanging wall to the fault in this location.

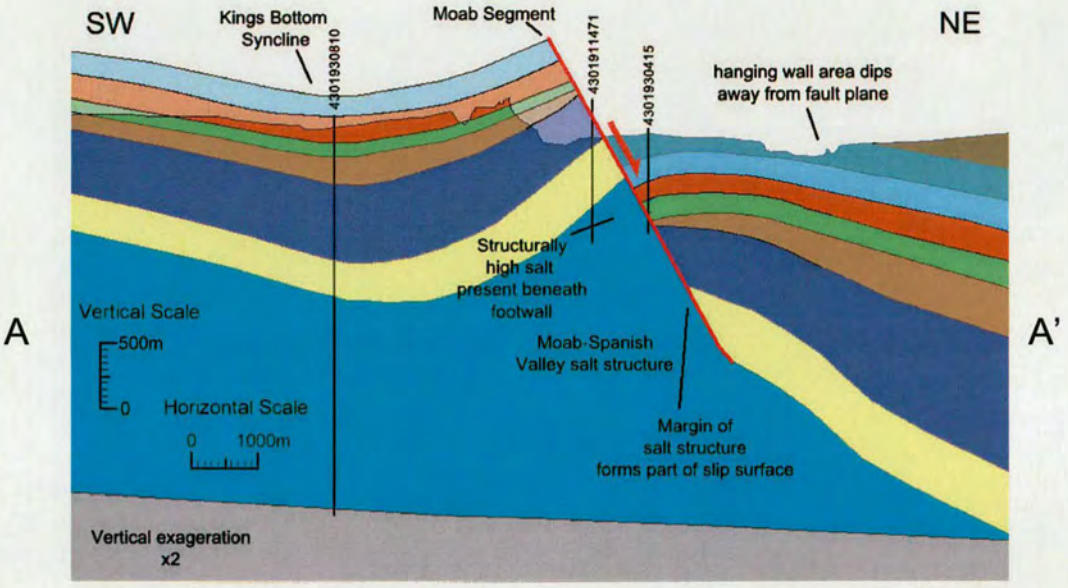

Figure 3.44. Cross section through the Moab segment of the Moab Fault system in the vicinity of where it has its maximum displacement. Note how well data constrains salt as having upwelled beneath the footwall area of the fault. The location of this section is shown in Figure 3.1.

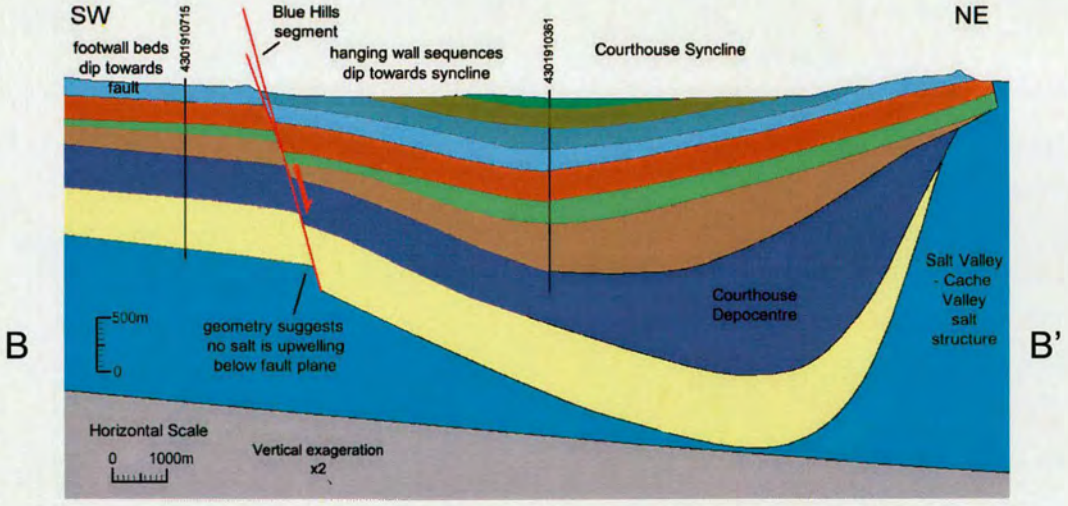

Figure 3.45. Cross section through the Blue Hills segment of the Moab Fault system illustrating the inferred structural morphology in this area. Note how no salt can be constrained as having upwelled beneath the fault plane in this area. The location of this section is shown in Figure 3.1.

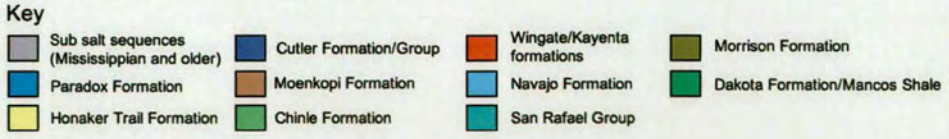

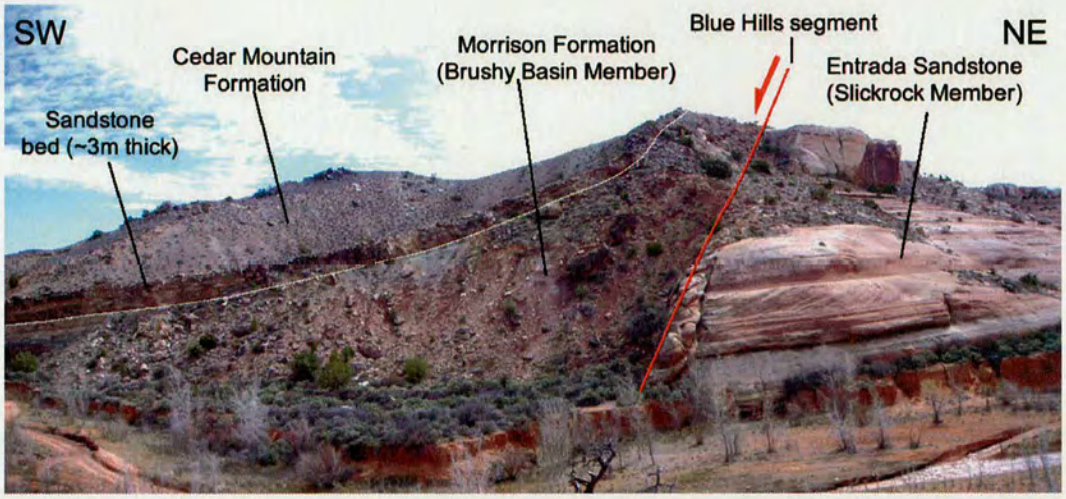

Figure 3.46. Photograph of Blue Hills Fault segment in the Bartlett Wash area taken at UTM 605403 E, 4285828 N looking SW. Note the presence of a 'drag style' fold in the hanging wall area highlighted by a prominent sand bed at the base of the Cedar Mountain Formation.

Figure 3.47. Photograph of granulation seams in the Slickrock Member of the Entrada Sandstone in the immediate footwall to the Blue Hills segment. Note how several cm of dip-slip offset is observed across granulation seams in this exposure. Photo taken in Bartlett Wash at UTM 605403 E, 4285828 N. Pen for scale.

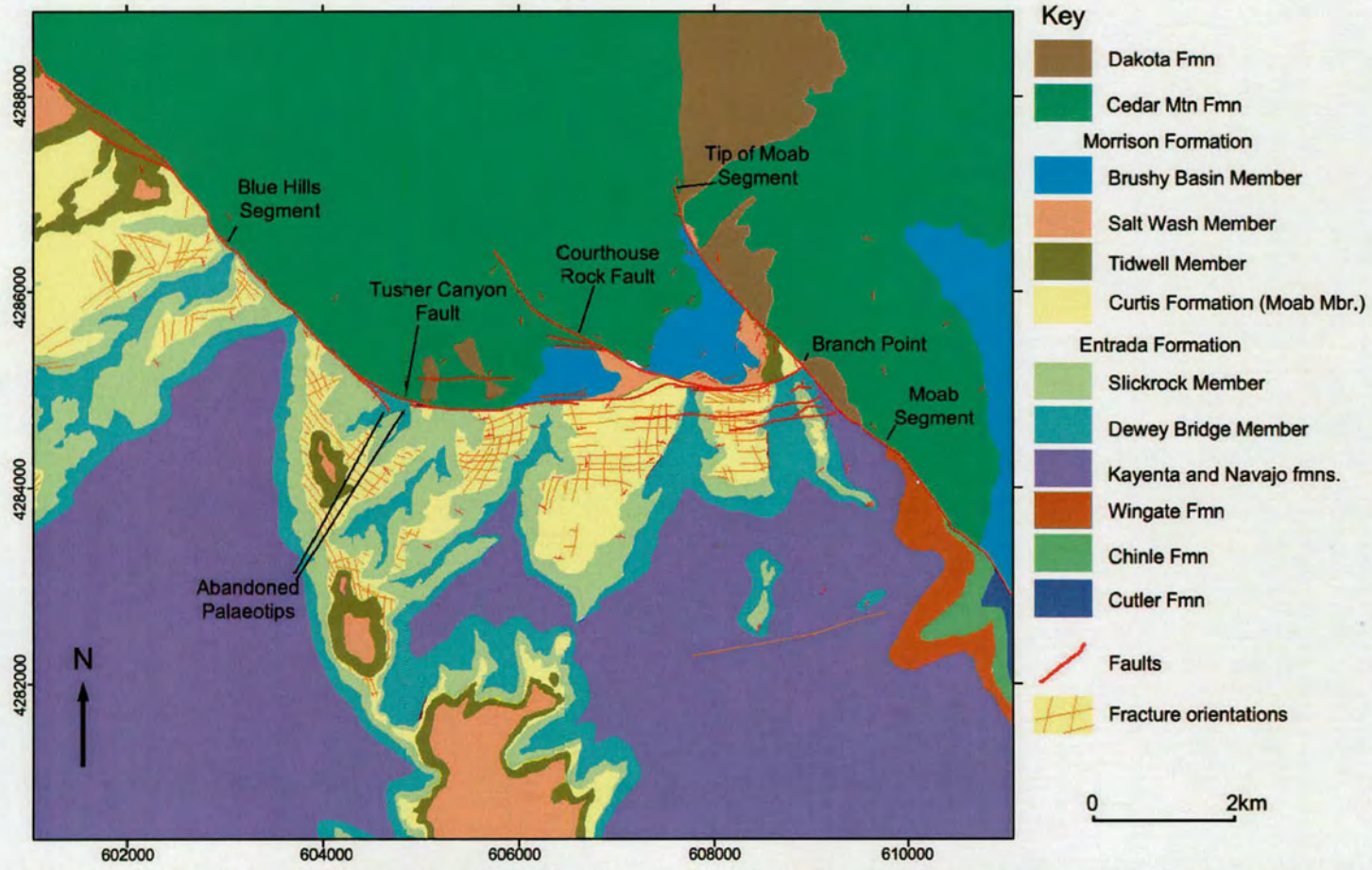

Figure 3.48. Bedrock geology map of the Mill Canyon linkage zone illustrating the fault geometry and fracture orientations in the Moab Tongue Member of the Curtis Formation

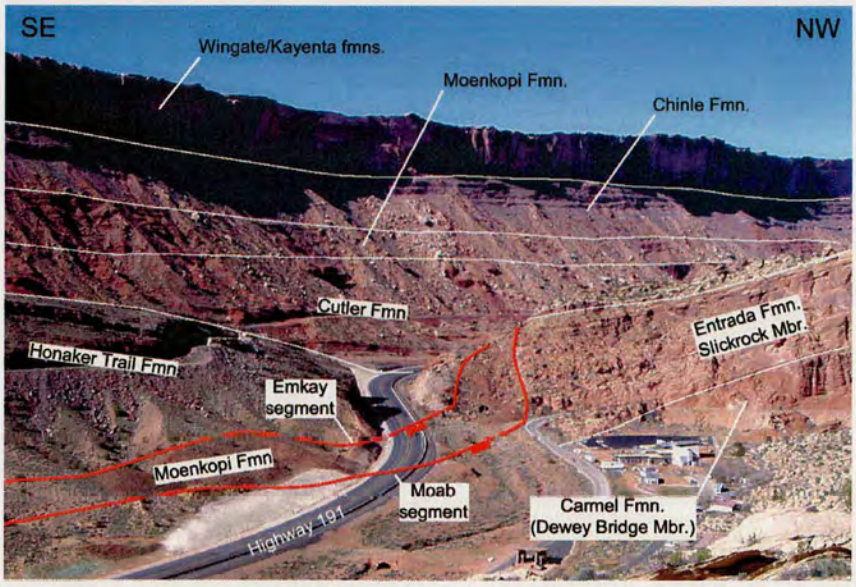

Figure 3.49. Photograph of the entrance to Arches National Park illustrating the location of the Moab and Emkay segments of the Moab Fault System. Photo is looking west from UTM 621000 E, 4275175 N.

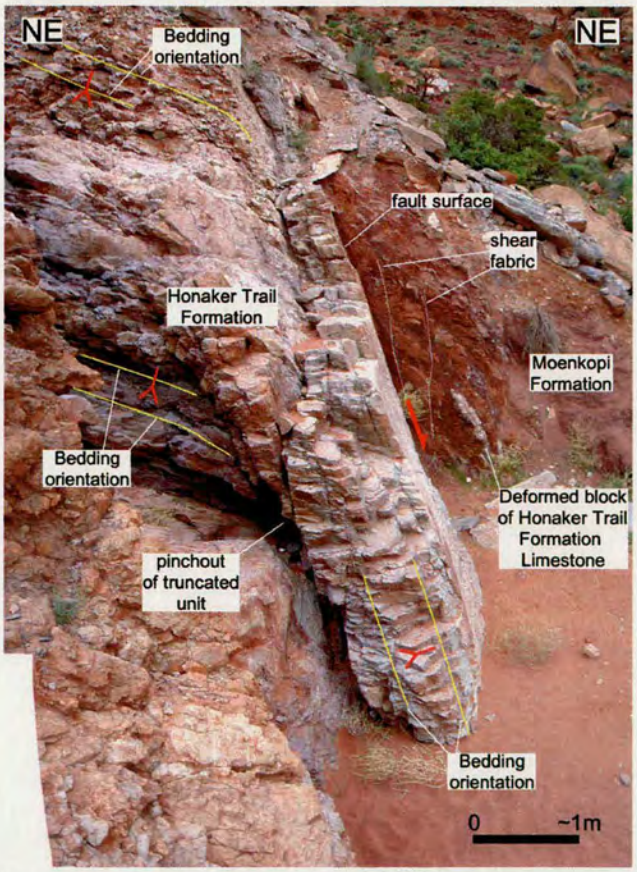

Figure 3.50. Photo of the Emkay Fault exposure at near the entrance to Arches National Park. Photograph taken at UTM, 620118 E, 4275117 N looking south

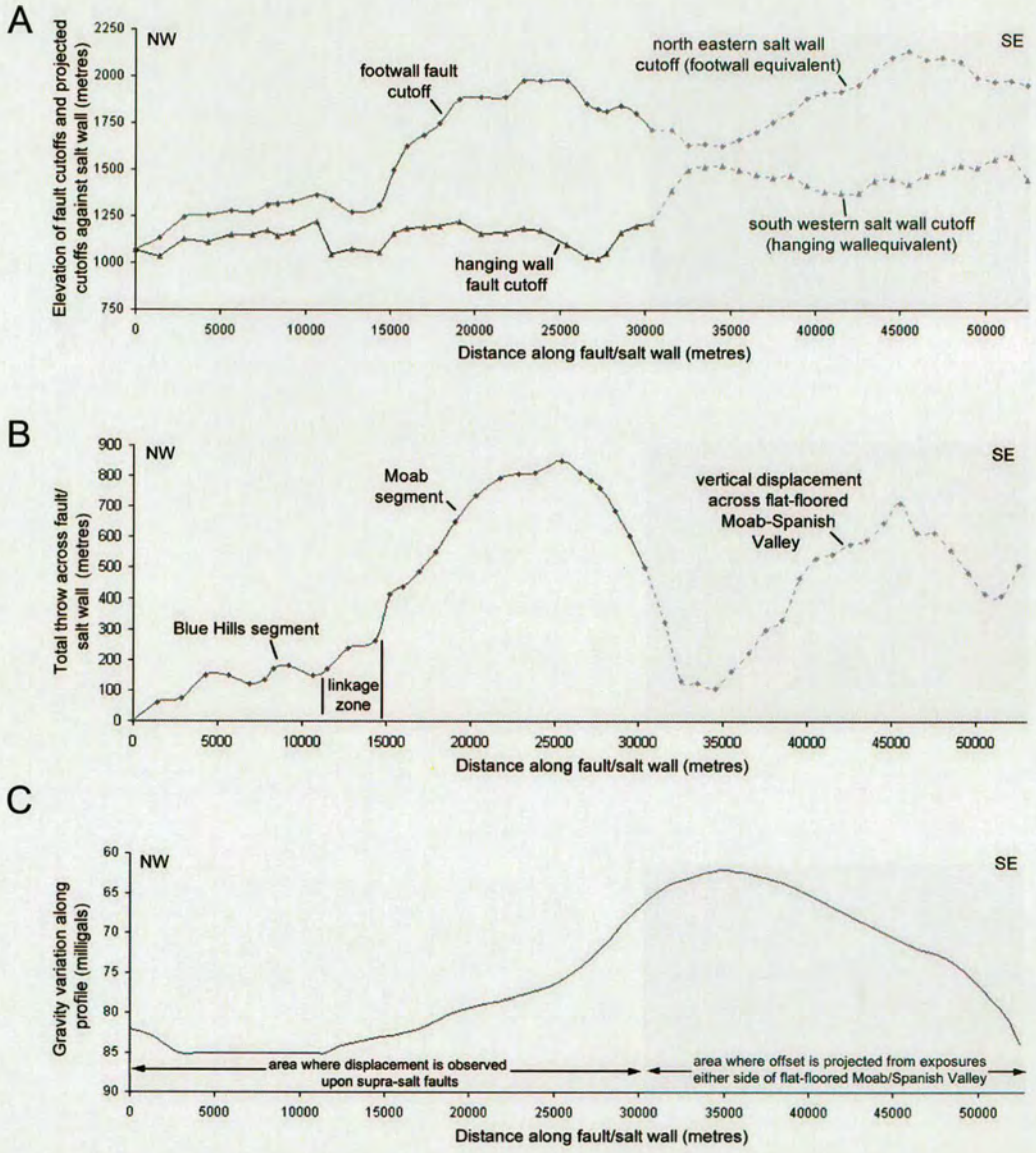

Figure 3.51. Profiles along the Moab Fault system illustrating the elevation of the fault cut-offs (A), cumulative throw across the fault system (B) and a gravity profile which gives an indication of the elevation of the salt below the surface. The shaded area on the SE side of the profiles is where no fault plane is exposed and displacement is observed either side of the flat-floored Moab-Spanish Valley. Note that faults in the linkage zone are oriented oblique to the profile and therefore gradients appear steeper than the are in reality. Also the scale on the gravity profile (C) is reversed so that low values (representing elevated salt) appear as highs. Fault cutoffs and displacement-length profile are for the Top Navajo Formation (Base Middle Jurassic) horizon.

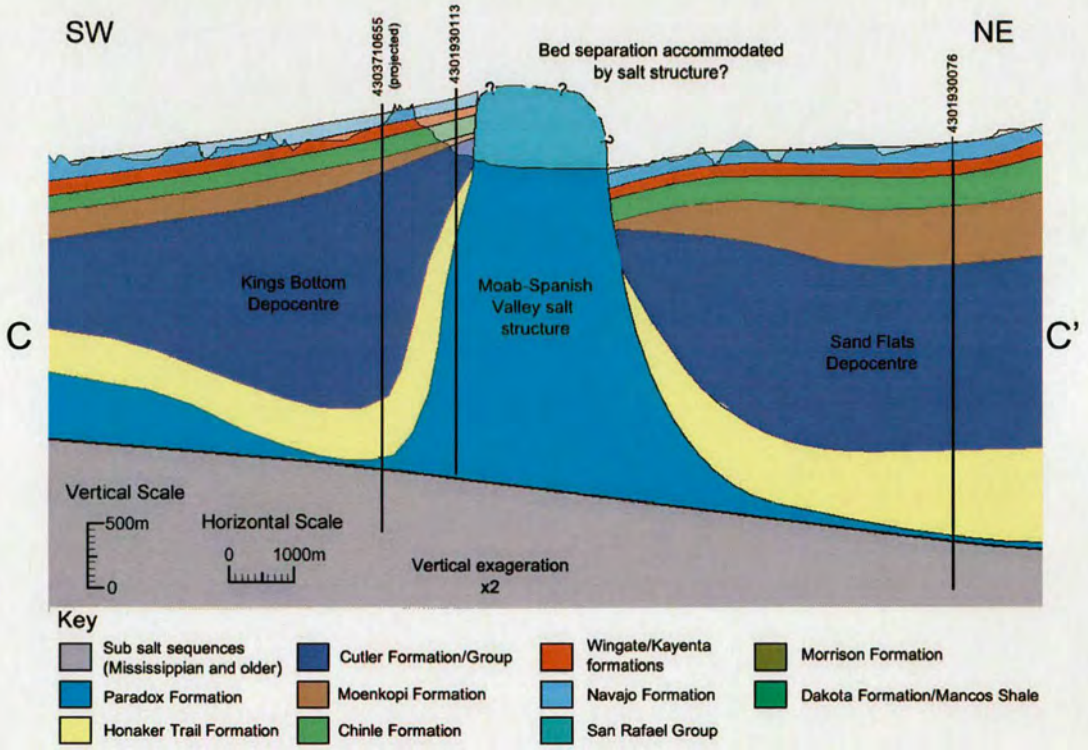

Figure 3.52. Cross section through the southern part of the Moab Fault System where significant bed separation is observed but no fault plane is observed. The section illustrates one interpretation in which displacement is accommodated by the Moab-Spanish Valley salt wall. Note how the morphology of the Cutler sequence is very different to that observed in Figure 3.45.

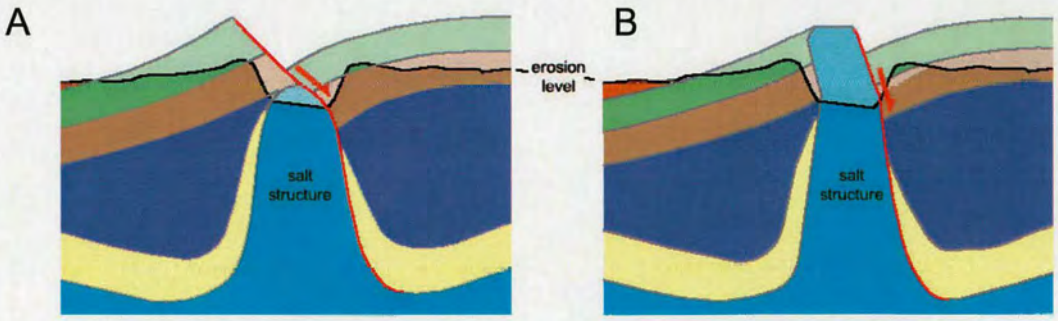

Figure 3.53. Sketch sections to illustrate two different interpretations of the relationship between the Moab-Spanish Valley salt structure and the Moab Fault System in the area where the salt structure is expressed as a flat floored salt valley. (A) illustrates a situation where the structural style remains the same as is observed to the NW with the erosion level removing the overlying fault structure. (B) illustrates a situation where the style of the salt structure changes and extension becomes accommodated by the salt wall which pierces the overburden.

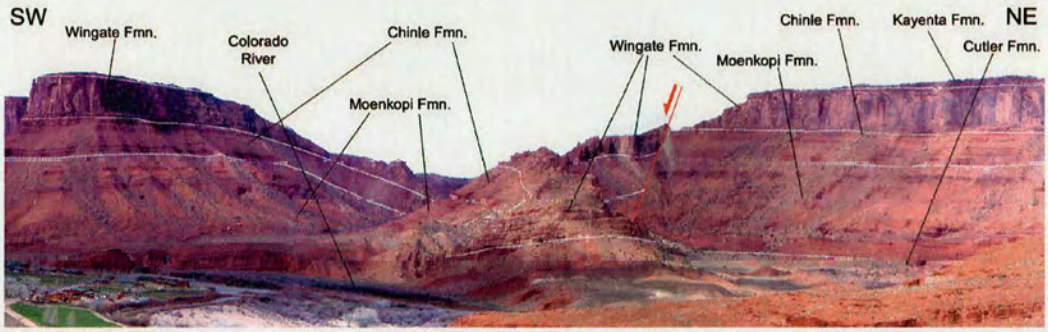

Figure 3.54. Photograph illustrating deformation in the crest of the Salt Valley-Cache Valley salt structure in Cache Valley. Photo taken looking ESE from UTM 640276 E, 4284843 N. Note the bleached sandstones and intense fracturing of the down-faulted Wingate Formation

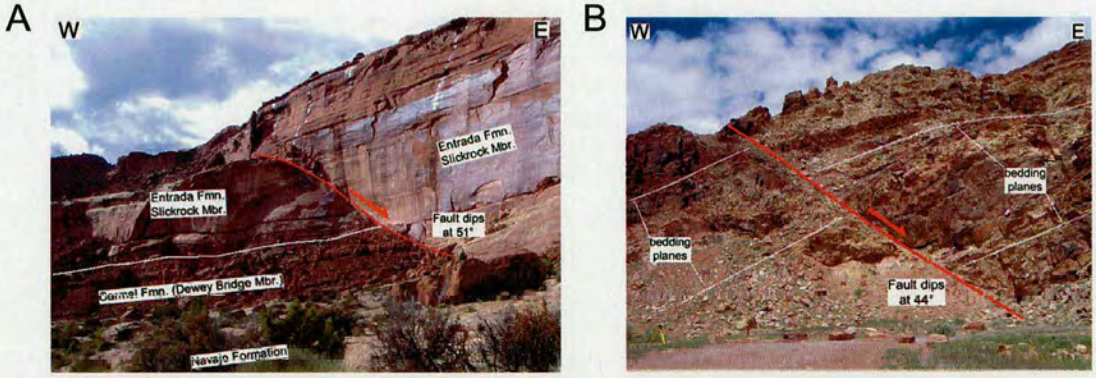

Figure 3.55. Photographs of minor faults in the SW limb of the Moab Anticline. (A) shows a fault in the San Rafael Group with 6m of displacement and (B) shows a fault in the Kayenta Formation with approximately 4m of displacement. Both faults are observed to be open, uncemented fractures where sand-on-sand contacts are observed. Note the intensely fractured nature of the Kayenta Formation in (B) and the presence of localised areas where sandstones are intensely bleached.

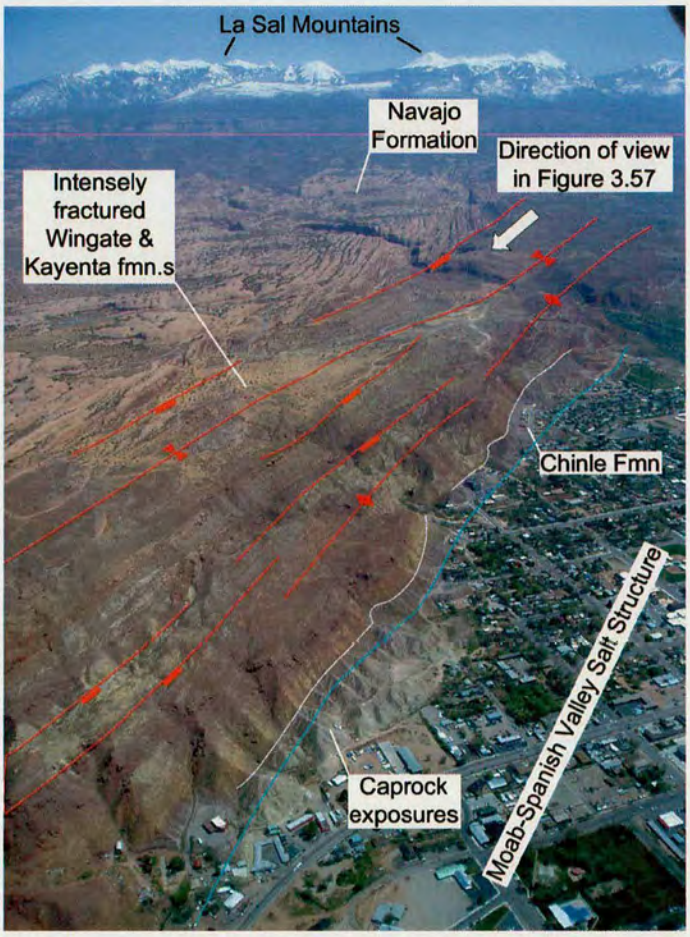

Figure 3.56. Aerial view of the NE side margin of the Moab-Spanish Valley salt structure illustrating deformation in sequences at the edge of the flat floored Moab Valley where salt sequences are very near the surface. Deformation consists of a complex system of folds and normal faults with supra-salt sequences being down-stepping towards the centre of the salt structure. View is looking approximately ESE.

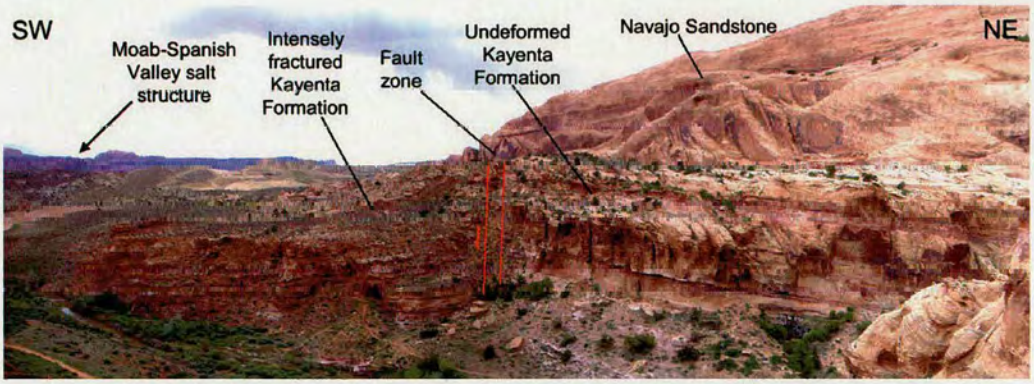

Figure 3.57. Photograph of a crestal fault associated with the Moab-Spanish Valley salt structure in Mill Canyon taken at UTM 629998 E, 4269202 N looking NW. The area to the left is down-faulted upon a high angle fault zone. Note the extremely broken-up nature of the downfaulted Kayenta Formation relative to that in the footwall

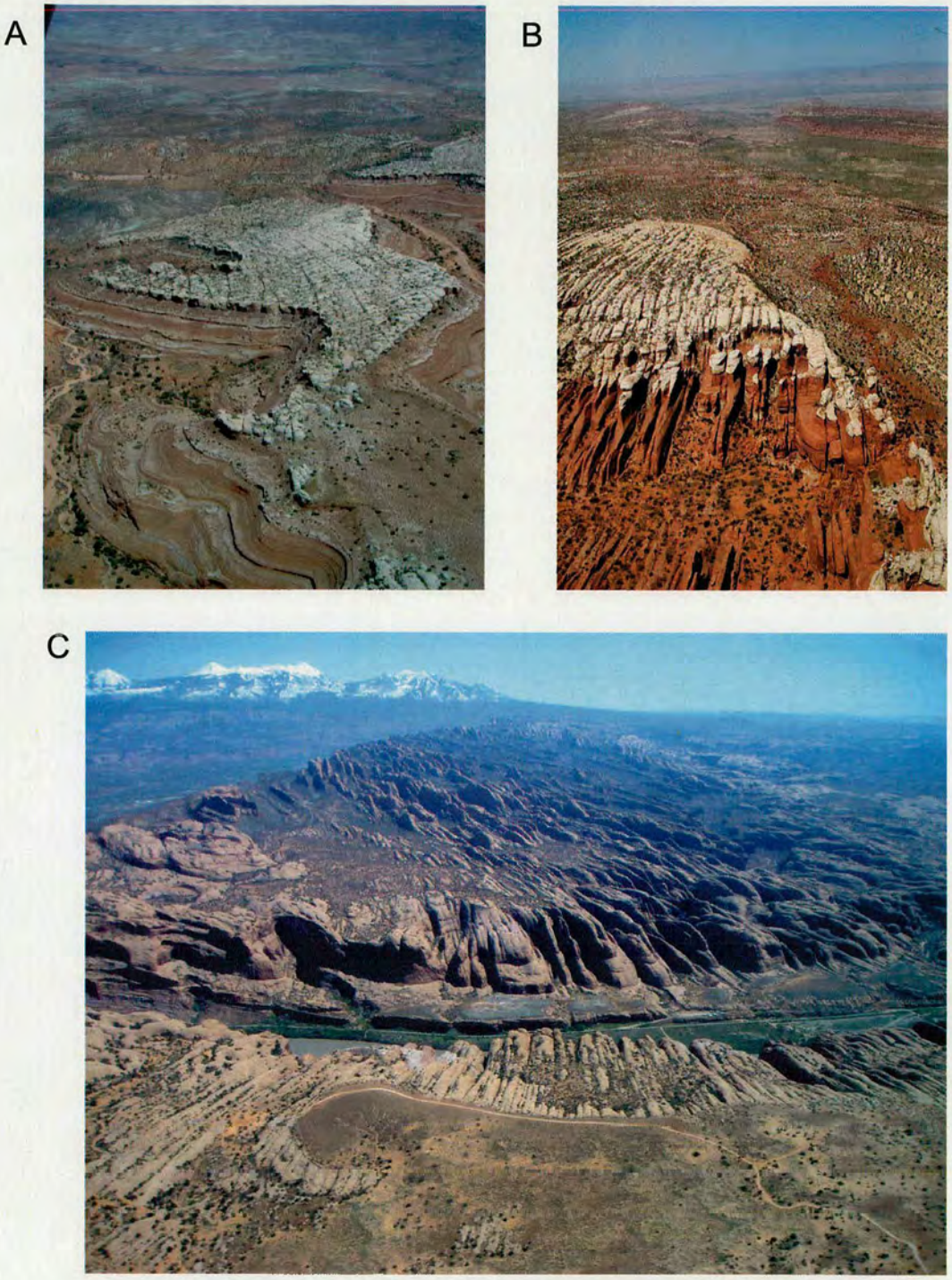

Figure 3.58. Aerial photographs of fractures within the study area. Fractures are in the Moab Tongue and Slickrock members (A and B) and the Navajo Formation (C). The location of photographs is shown in Figure 3.59.

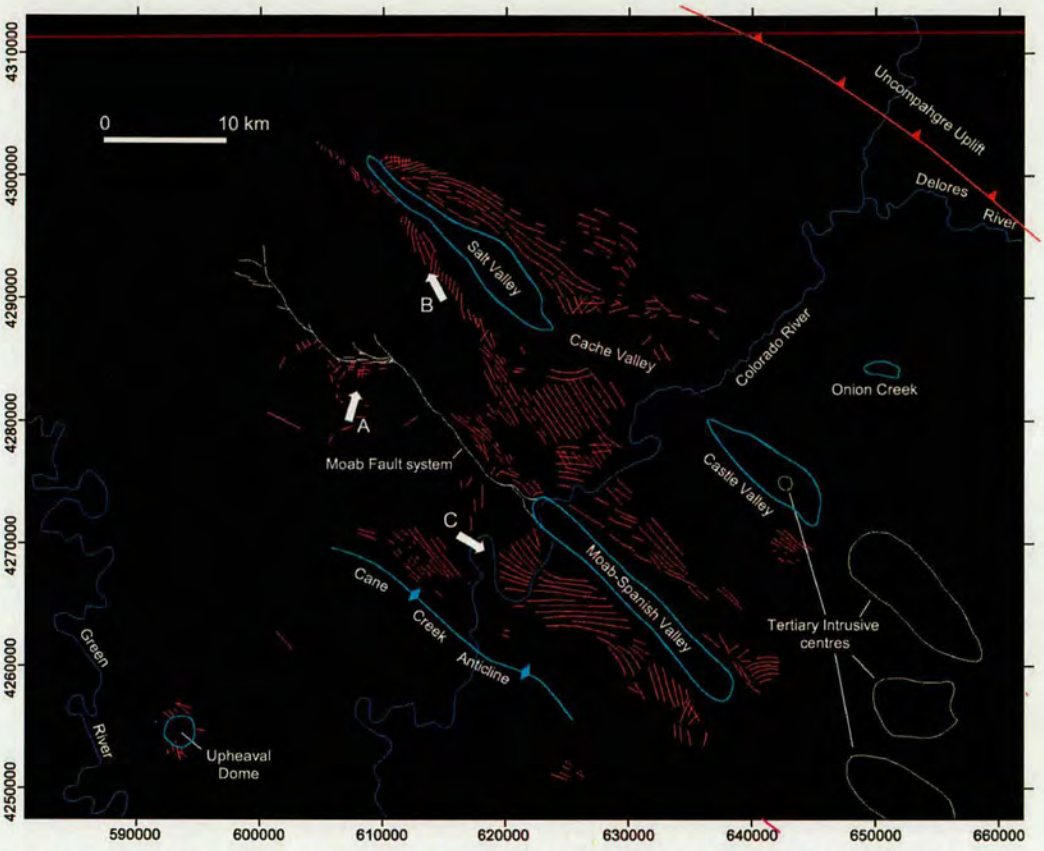

Figure 3.59. Map illustrating strike orientations of fracture systems within Jurassic sandstones in the study area. Fractures are typically vertical/sub-vertical and are pervasive wherever Jurassic sandstones are exposed around salt structures. Arrows show directions of view of aerial photographs in Figure 3.58.

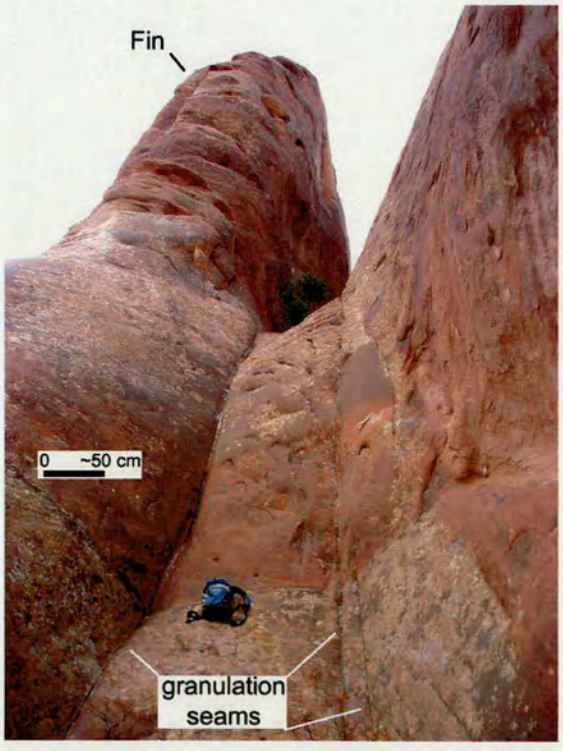

Figure 3.60. Photograph of a fin related to fractures in the Slickrock Member of the Entrada Formation. These are the typical geomorpic expression on fractures in this unit. Fins typically form in undisturbed areas whereas the more eroded, intra-fin areas are typically zones of around 1m in diameter with numerous sub-vertical, granulation seams of 1-4mm in diameter. Photograph shows a fin in the Devils Garden area of Arches National Park taken at UTM 622108 E, 4293431 N.

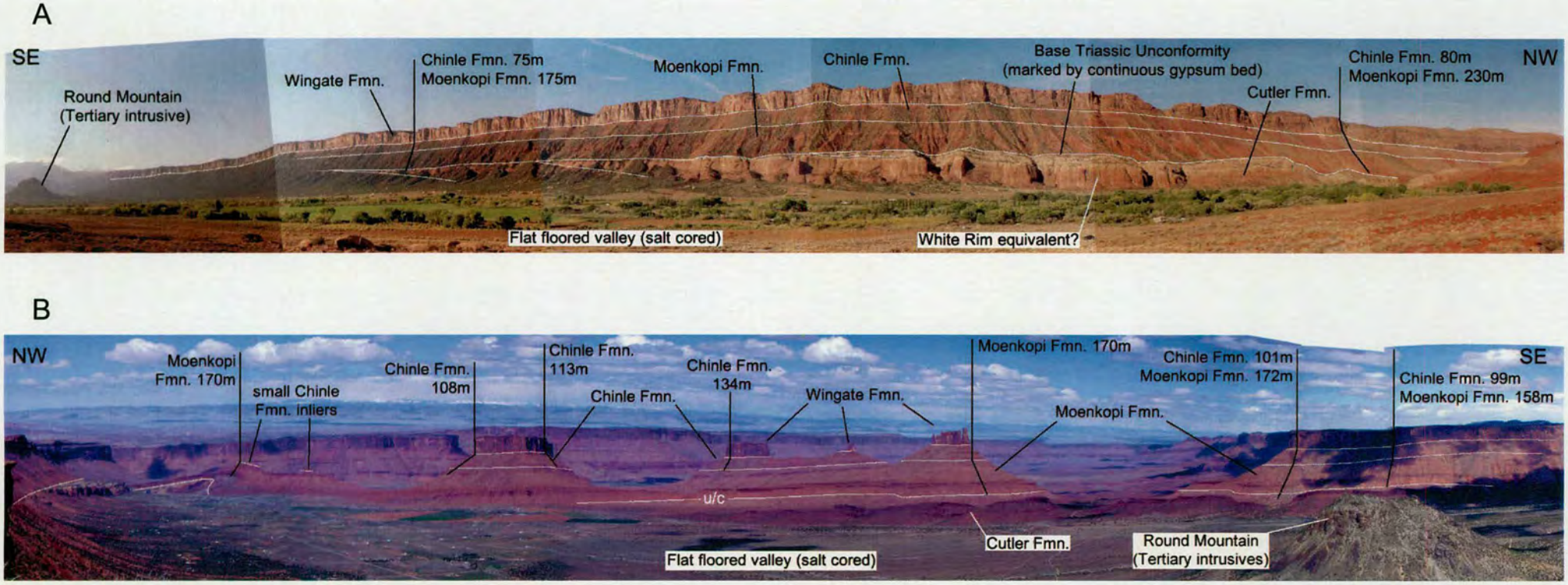

Figure 3.61. Photo panoramas along the SW (A) and NE (B) side of Castle Valley illustrating thickness variations associated with the Castle Valley salt structure which is expressed as a flat-floored salt valley in both panoramas. Note the angular unconformity at the base of the Moenkopi Formation.

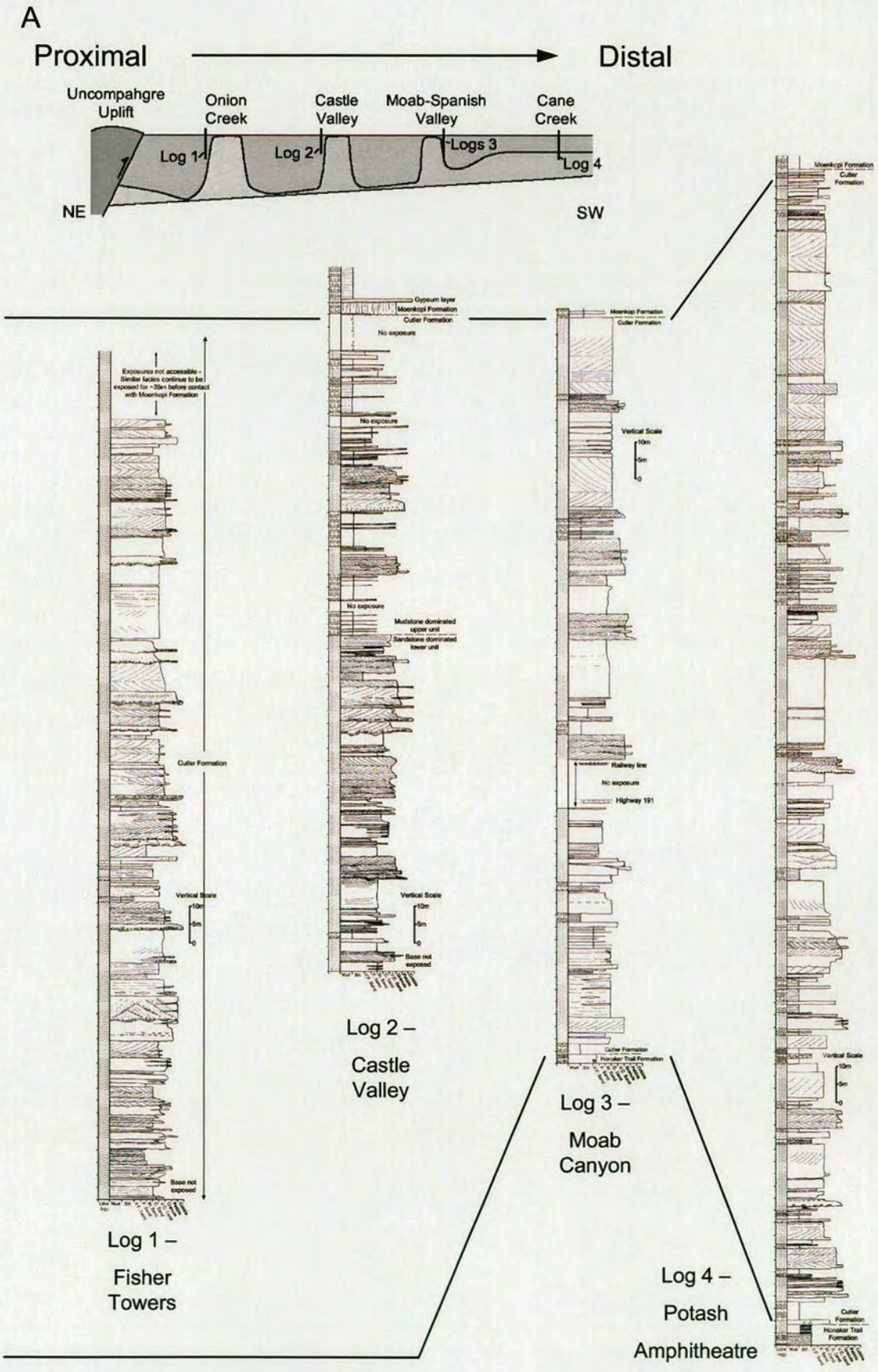

Figure 3.62. Sedimentary logs through the Cutler sequence in a NE-SW traverse of the basin representing the proximal to distal transition in the sequence. The location of logs relative to salt structures is shown in 'A'.

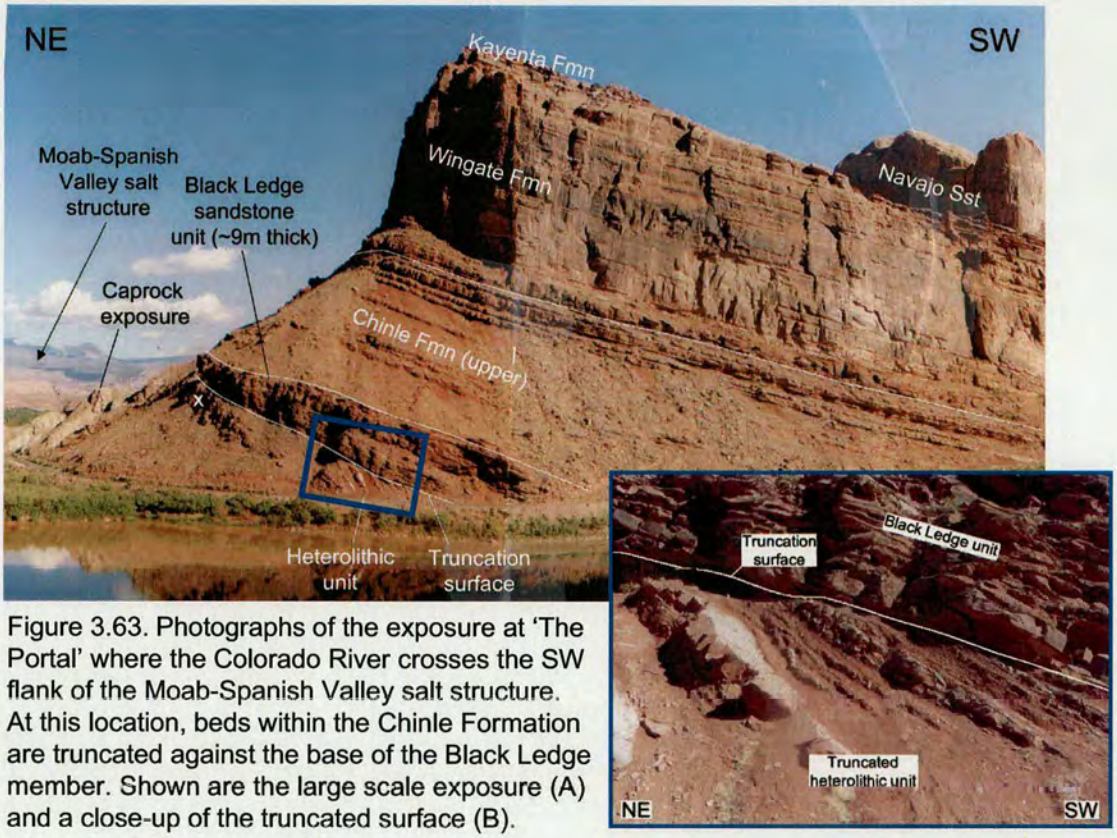

Figure 3.63. Photographs of the exposure at 'The Portal' where the Colorado River crosses the SW flank of the Moab-Spanish Valley salt structure. At this location, beds within the Chinle Formation are truncated against the base of the Black Ledge member. Shown are the large scale exposure (A) and a close-up of the truncated surface (B).

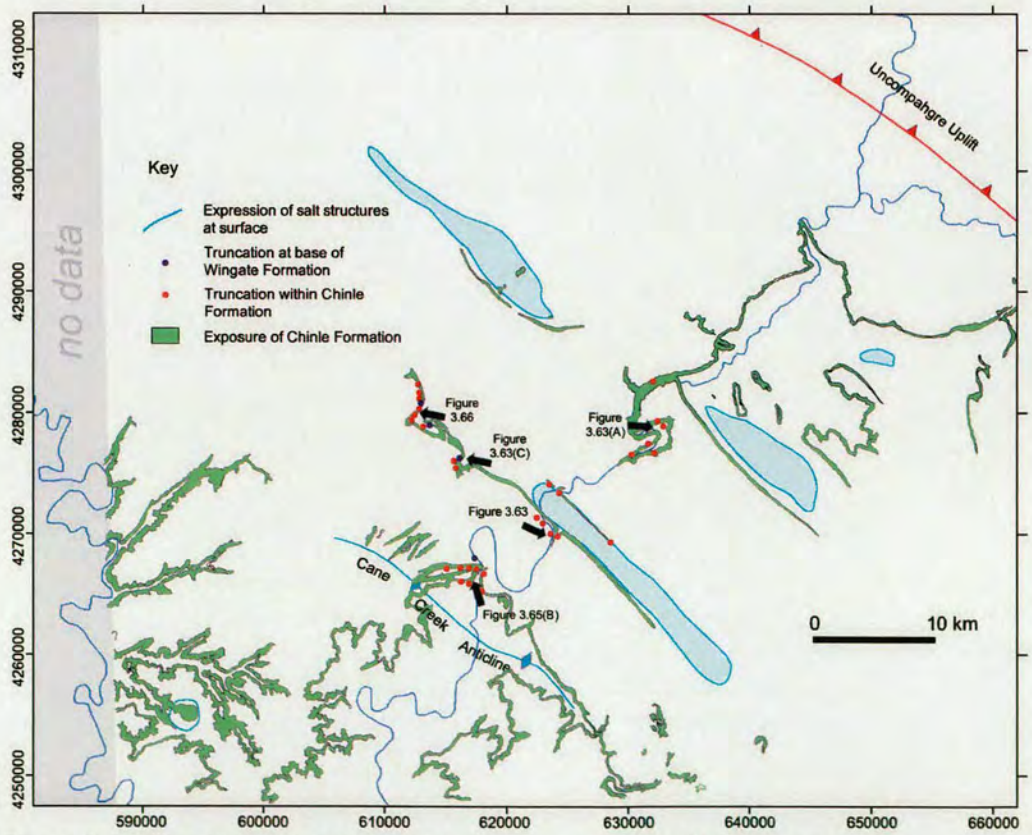

Figure 3.64. Map illustrating the extent of exposure of the Chinle Formation in the study area and the location of exposures where angular truncations are observed within the Chinle Formation. The locations and directions of view of photographs in Figures 3.63, 3.65 and 3.66 are illustrated by arrows.

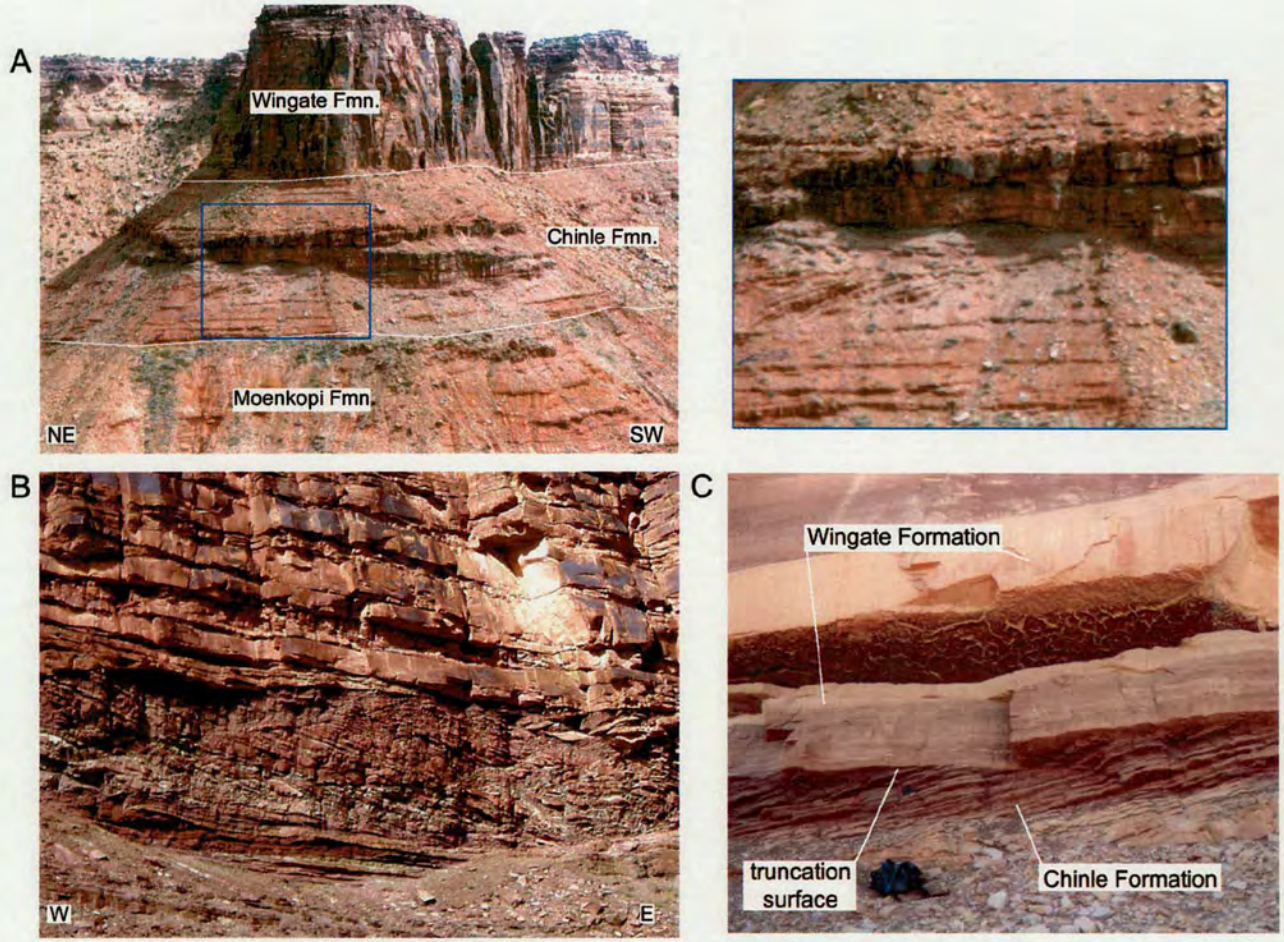

Figure 3.65. Photographs of truncations within the Chinle Formation at Big Bend (a), Long Canyon (b) and between the Chinle Formation and Wingate Formation (c). The location of these photographs is shown in 3.64.

Figure 3.66. Photograph of 'Greggs Unconformity' in Seven Mile Canyon. The exposure shows high angle truncations within the Chinle Formation. Photos taken at UTM 612432 E, 4279828 N (lower photo) and 612620E, 4279686 N (upper photo). Note how bedding below the truncated surface is parallel to bedding above it (upper picture). The location of this exposure is shown in Figure 3.64.

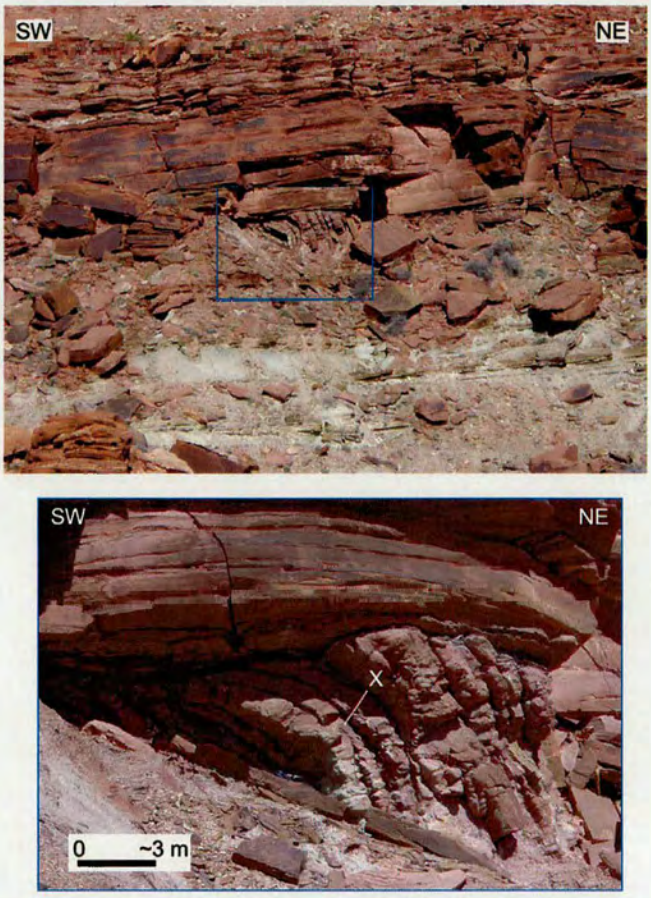

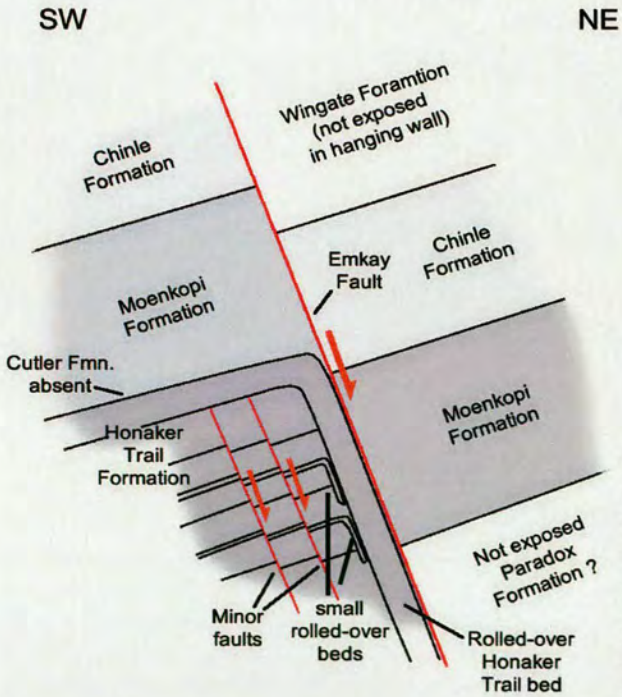

Figure 3.67. Sketch section through the Emkay fault at the location shown in Figure 3.40 illustrating the interpreted structural geometry in this area. Note that the Cutler Formation is absent in this area.

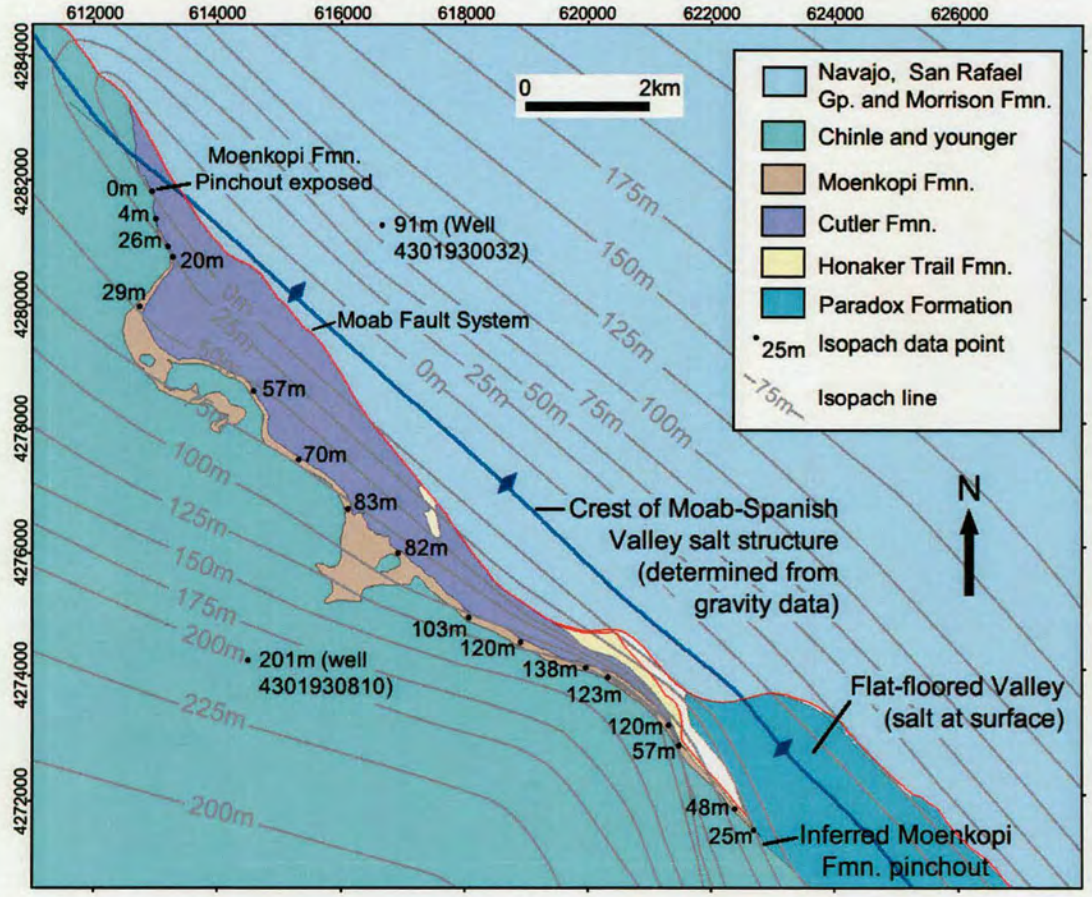

Figure 3.68. Map of the area between the two points where the Moenkopi Formation is observed to pinch out in the Moab Anticline area. Shown are the measured thickness of the Moenkopi Formation in field exposures and wells and also an interpretation of the isopach lines in the area. The Moenkopi Formation can be seen to thin to pinchout towards the crest of the salt structure, both where it is buried and where salt is at the surface.

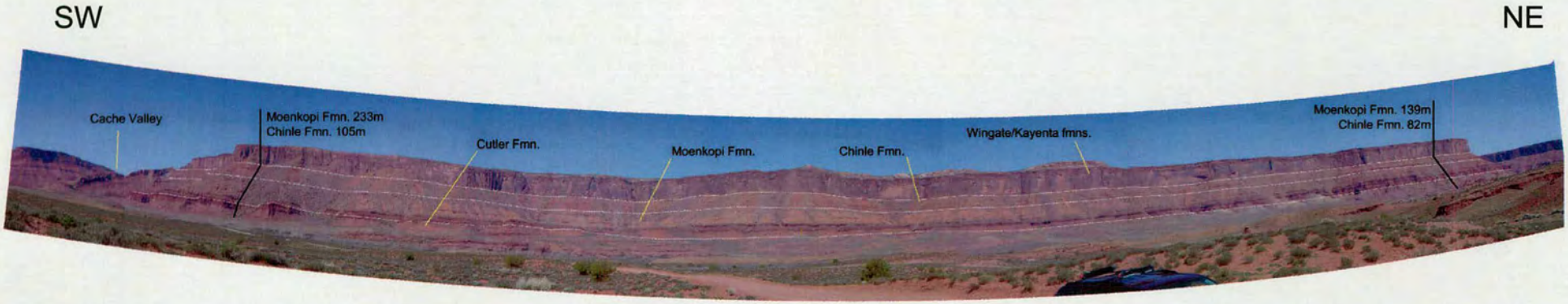

Figure 3.69. Photograph of the Professor Valley cliff exposure on the NW side of the Colorado River taken from UTM 643360 E, 4287092 N looking NW. Also shown are the measured thicknesses of the Chinle and Moenkopi formations at each end of the exposure. Note that although a very slight synclinal morphology is present in this cliff exposure, this has been significantly enhanced by the process of stitching photographs together to form this panorama.

Panorama 1

Panorama 2

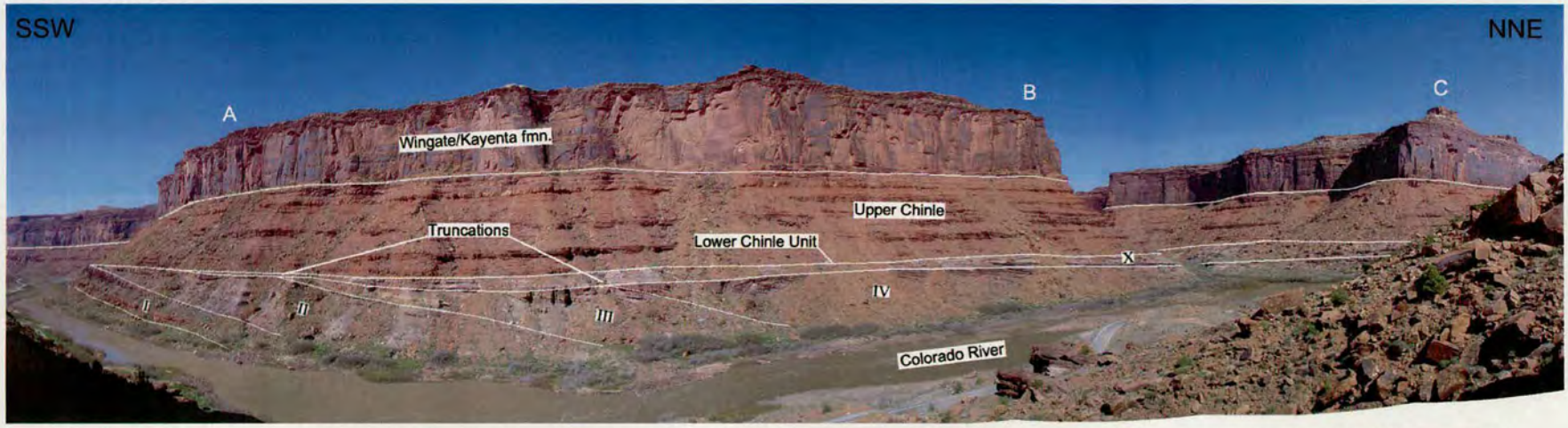

Figure 3.70. Photo panoramas along the Sandy Beach section of the Colorado River illustrating the nature of exposure in the localised 'Lower Unit' of the Chinle Formation. The location of each panorama is shown in Figure 3.72. Points common to two or more panoramas are labelled A-D.

Panorama 3

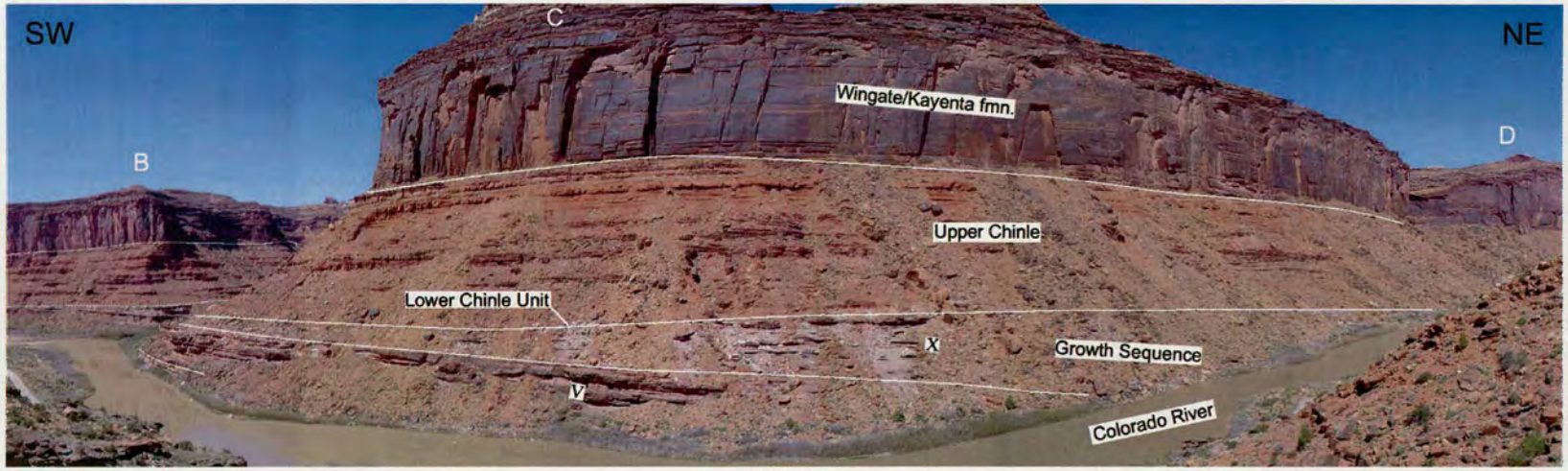

Panorama 4

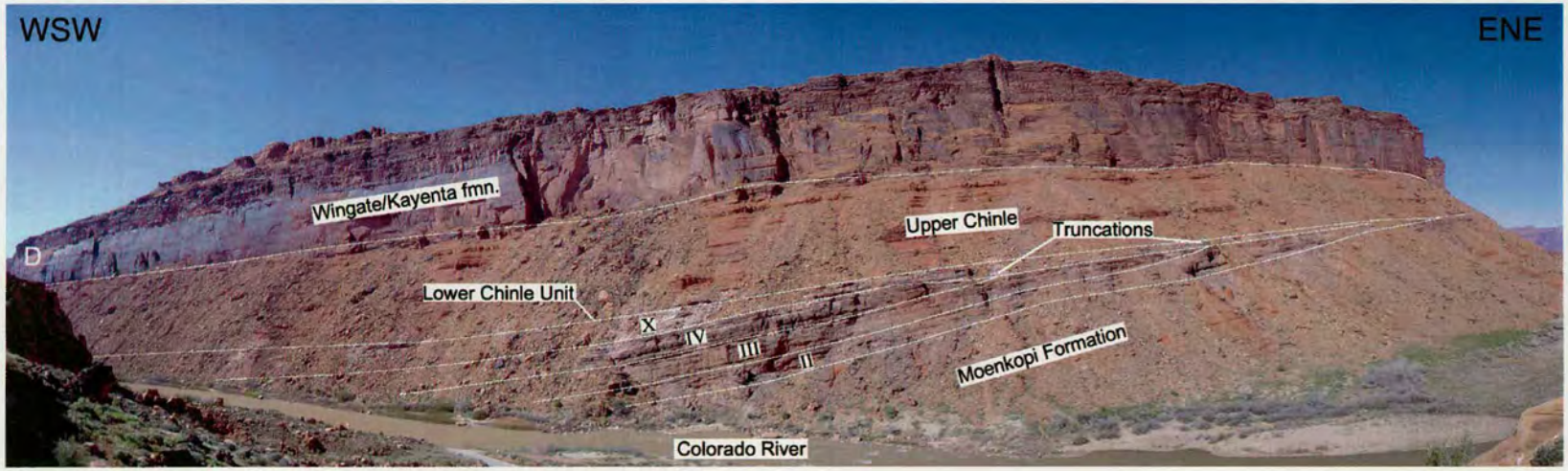

Figure 3.70. Continued

Figure 3.71. Sketch section illustrating the stratigraphic relationships in the Chinle Formation in the Sandy Beach area (A) and a series of sedimentary logs along this section illustrating the sedimentary facies in the 'Lower Unit' of the Chinle Formation in this area (B).

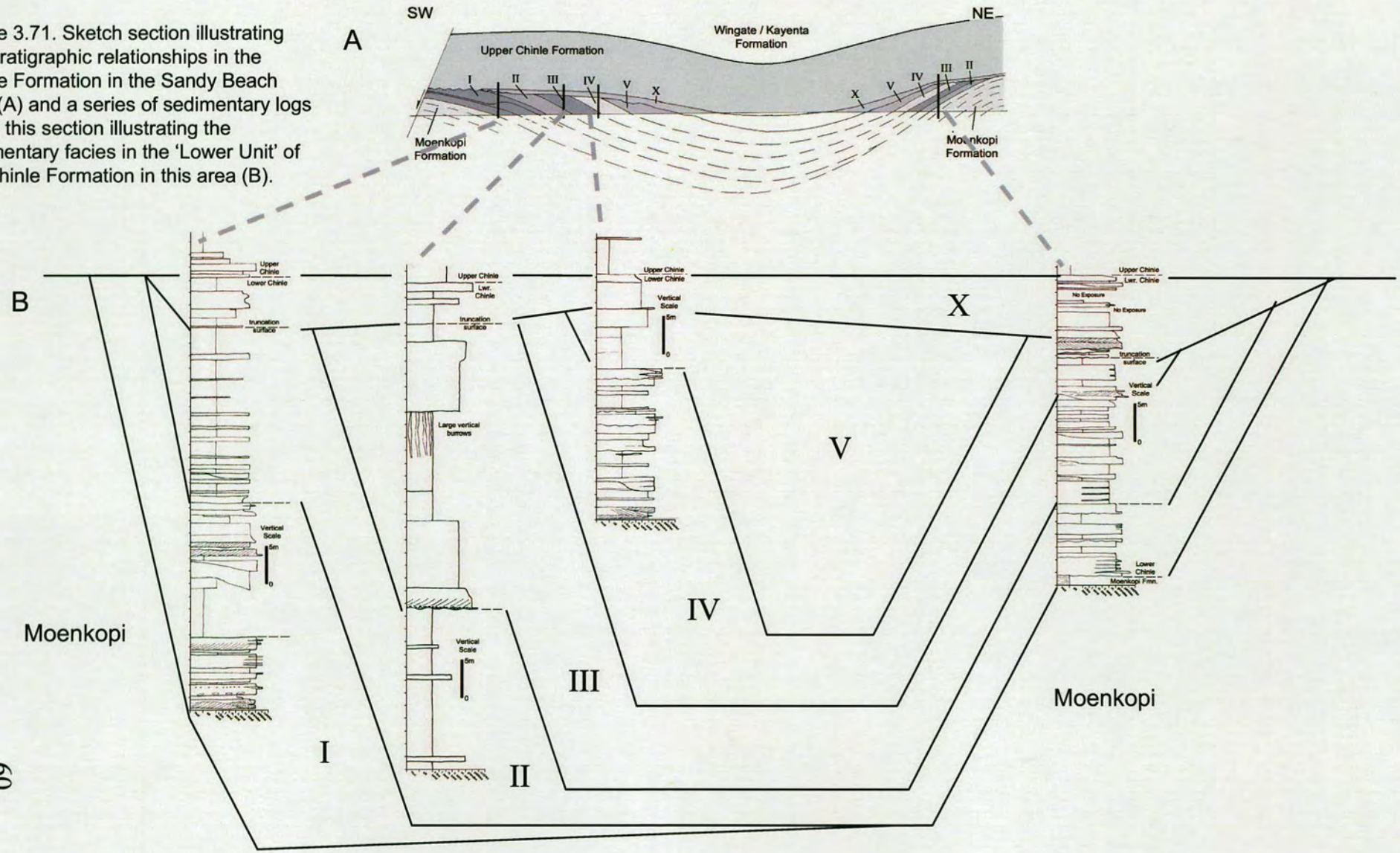

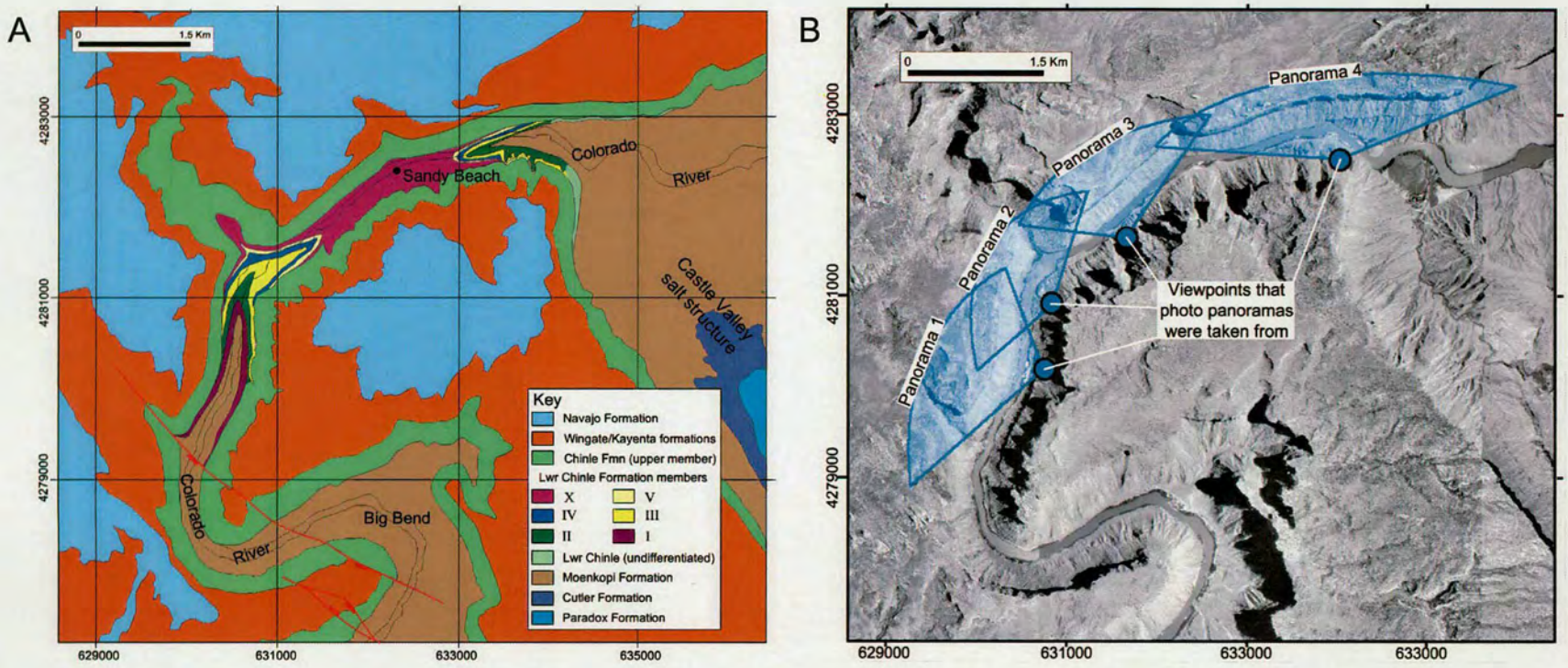

3.72. Geological map of the Sandy Beach area illustrating the distribution of members in the localised Lower Chinle Unit (A) and a composite aerial photograph of the same area showing the location of photo-panoramas shown in Figure 3.70 (B). Mapping carried out as part of this study.

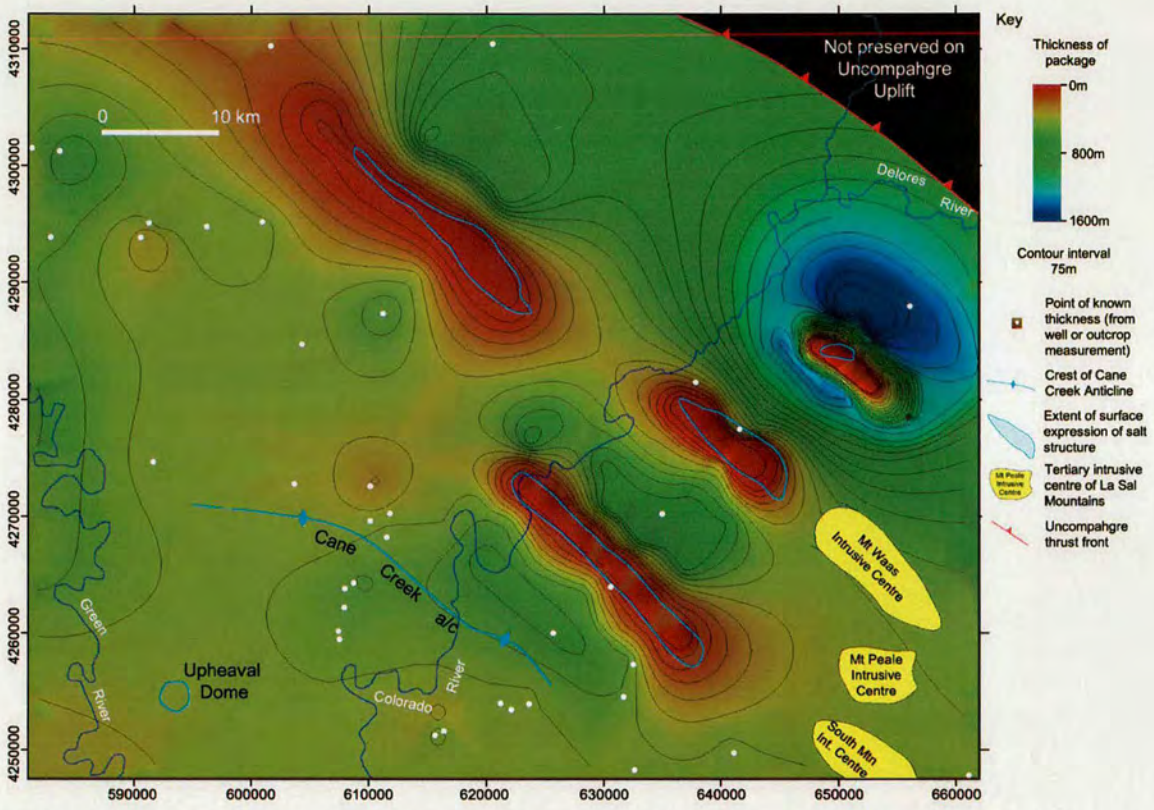

Figure 3.73. Isopach map of the Honaker Trail Formation within the study area. Note that in areas where data is sparse, the isopach pattern has been interpreted based on regional cross section construction and published seismic data.

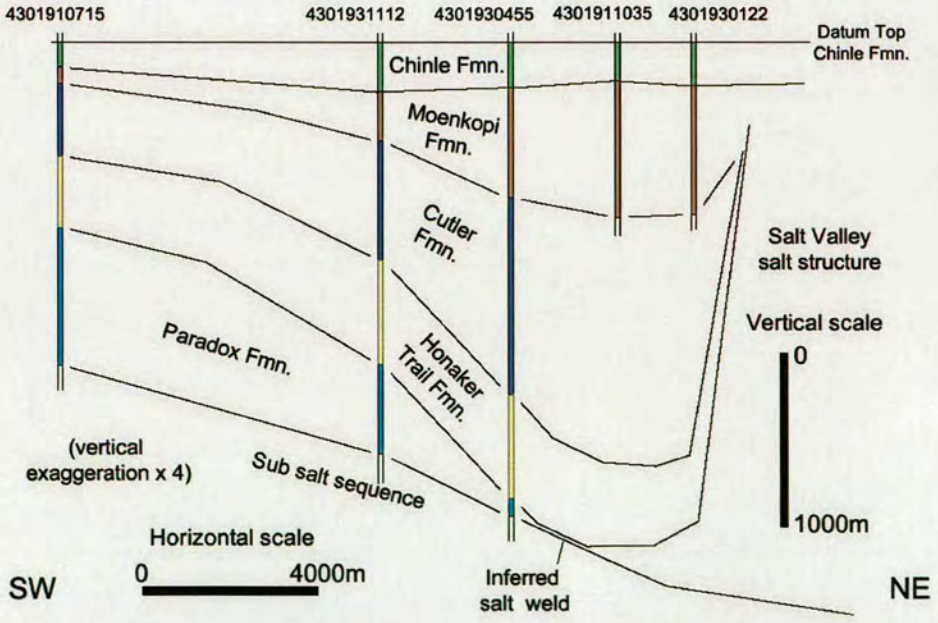

Figure 3.74. Well correlation profile illustrating growth in Cutler and Moenkopi formations in the Courthouse depocentre (SW side of Salt Valley salt structure). The location of wells is shown in Figure 3.1

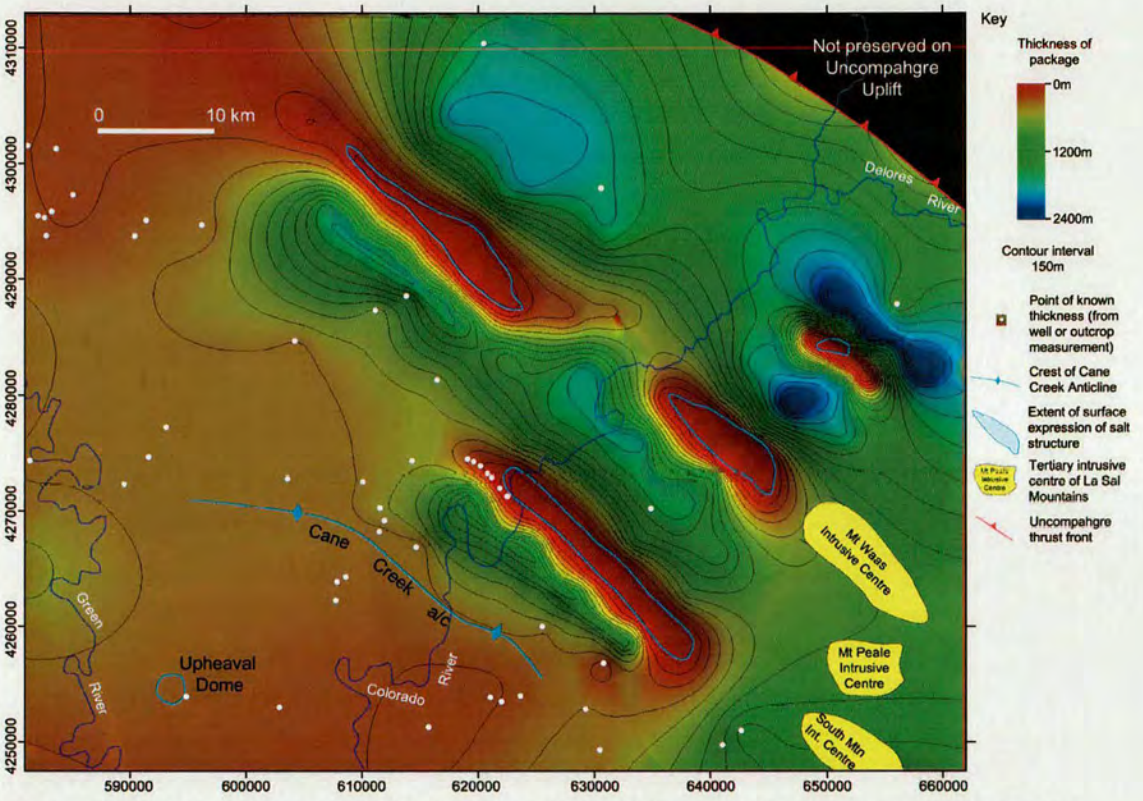

Figure 3.75. Isopach map of the Cutler Formation within the study area. Note that in areas where data is sparse, the isopach pattern has been interpreted based on regional cross section construction and published seismic data.

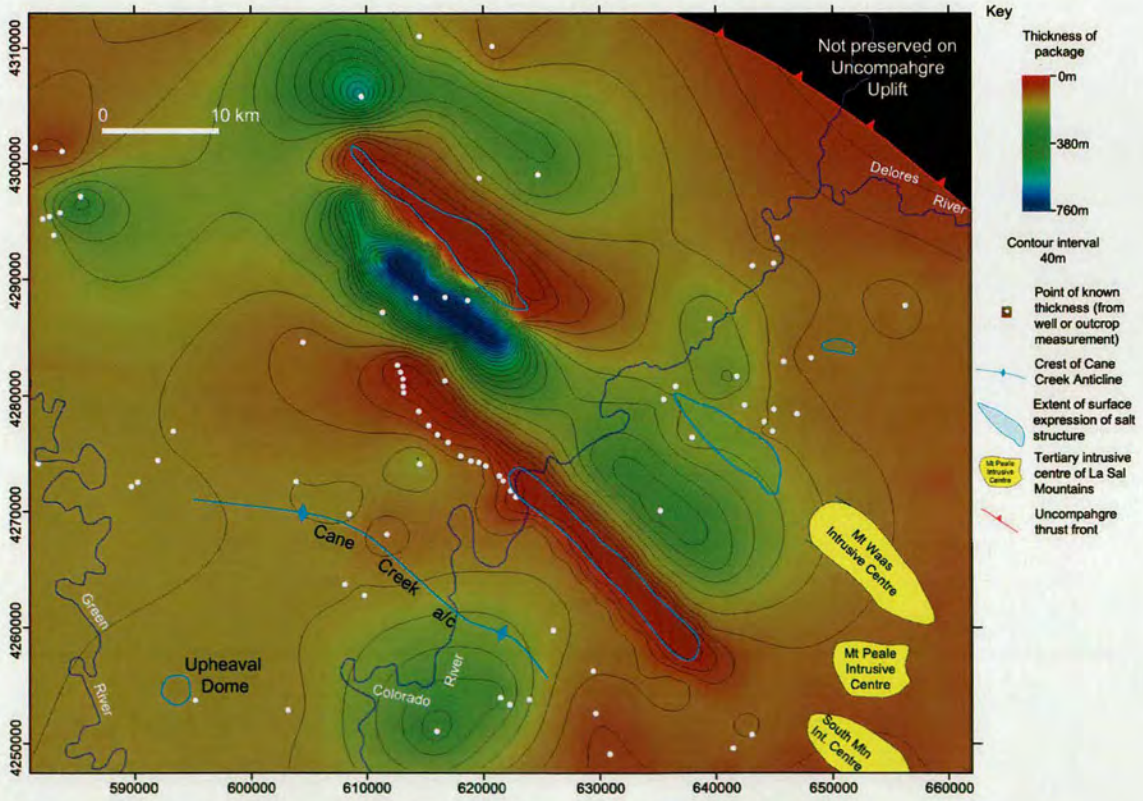

Figure 3.76. Isopach map of the Moenkopi Formation in the study area

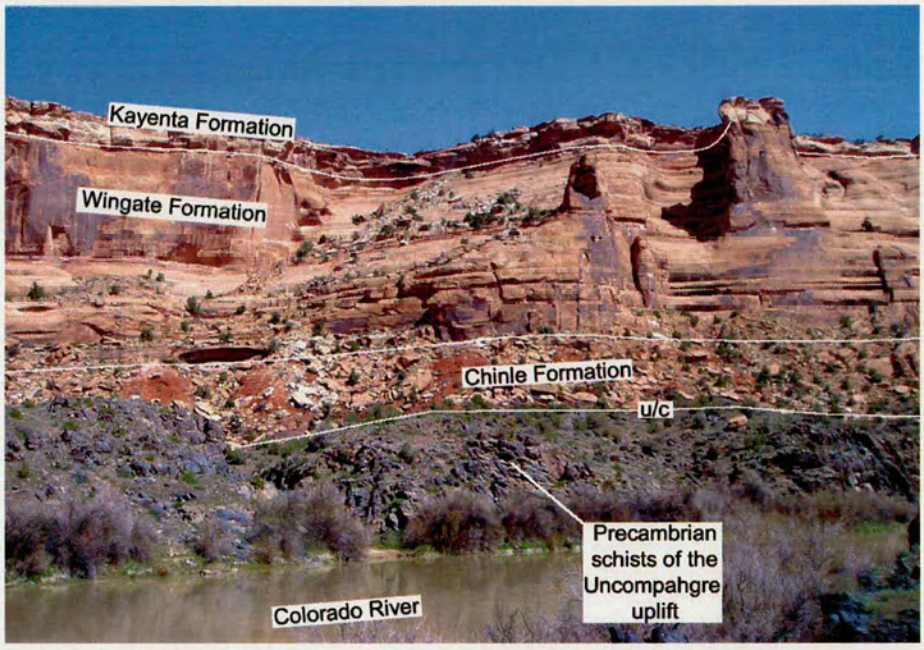

Figure 3.77. Photograph illustrating the unconformity which separates the crystalline basement rocks of the Uncompahgre Uplift with the overlying sedimentary sequence. Note how the unconformity is directly overlain by the Chinle Formation. This is the youngest sequence observed to blanket the Uncompahgre Uplift. Photo taken in the Westwater Canyon area, looking N from UTM 660705 E, 4320371 N.

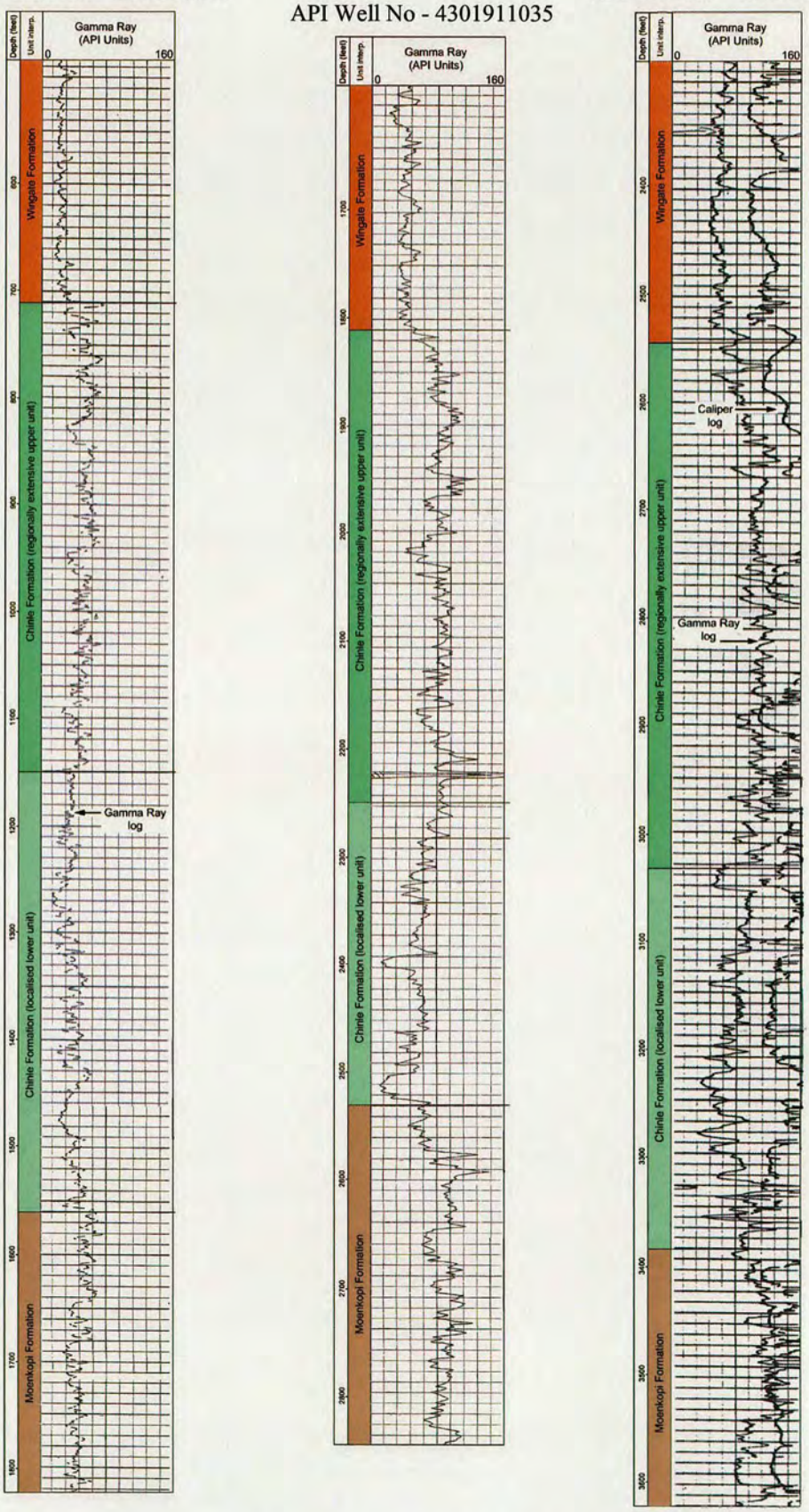

Figure 3.78. Gamma ray logs for several wells showing an anomalously thick Chinle Formation sequence. Note how in each log, the lower part of the section displays a lower gamma response than the upper part. These lower parts are interpreted as the continuation of the localised 'Lower Unit' of the Chinle Formation observed in the Sandy Beach area which contains a significantly larger proportion of sand than the regionally extensive upper unit.

A

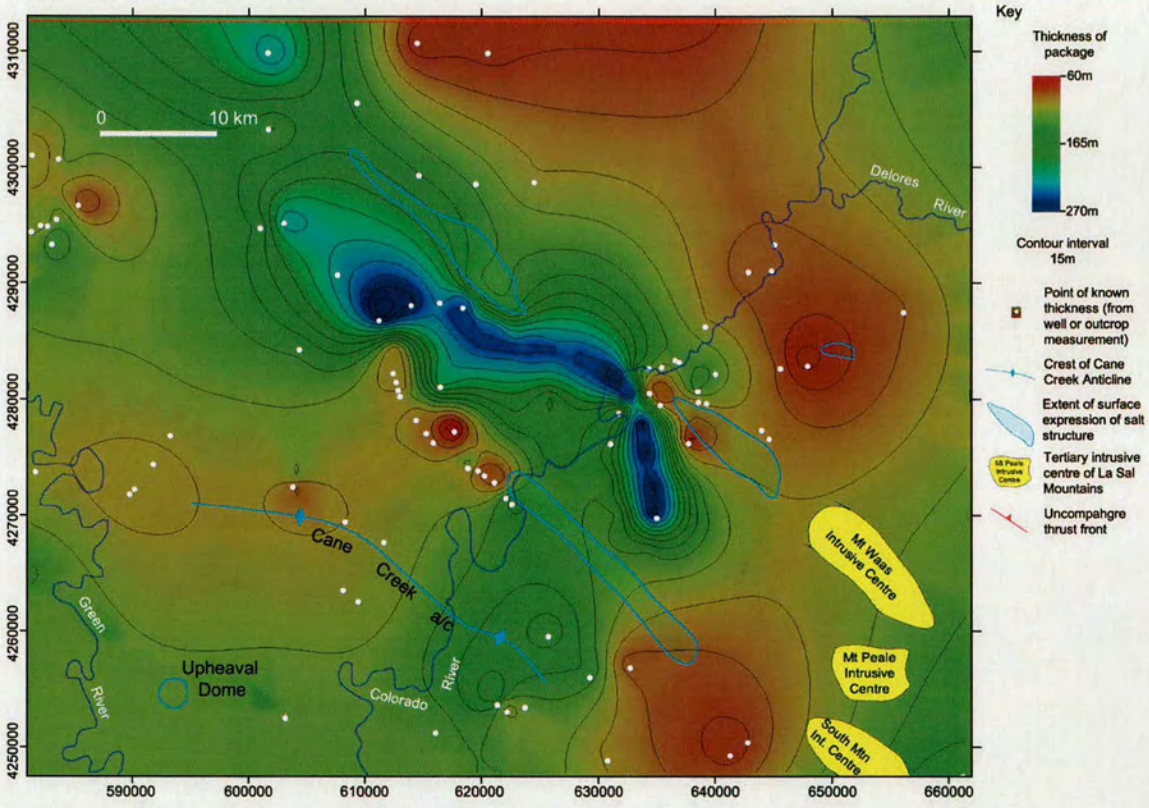

Figure 3.79. Isopach maps of the whole of the Chinle Formation (A), the regionally extensive 'Upper Unit' (B) and the localised 'Lower Unit' (C) within the study area.

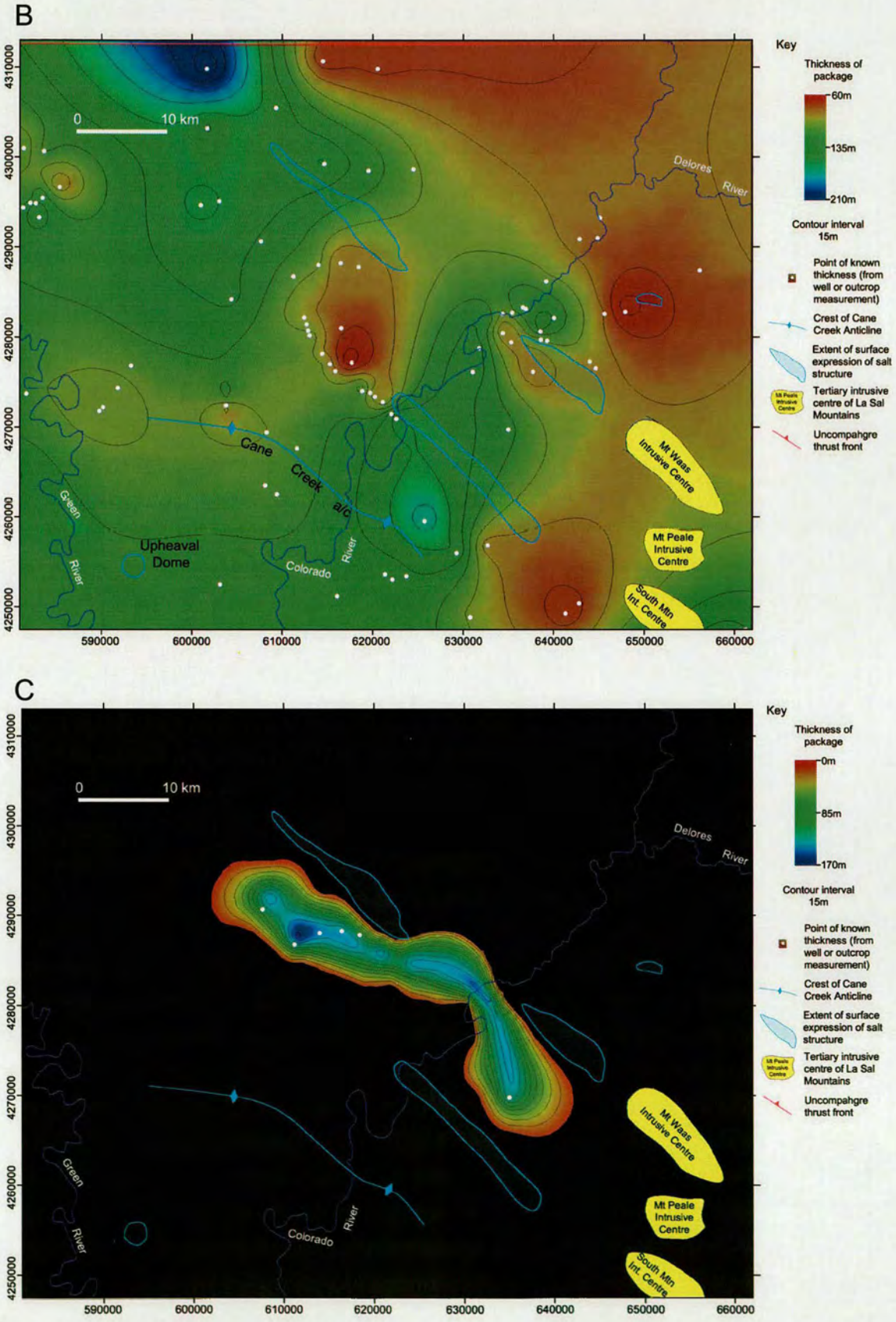

Figure 3.79 Continued

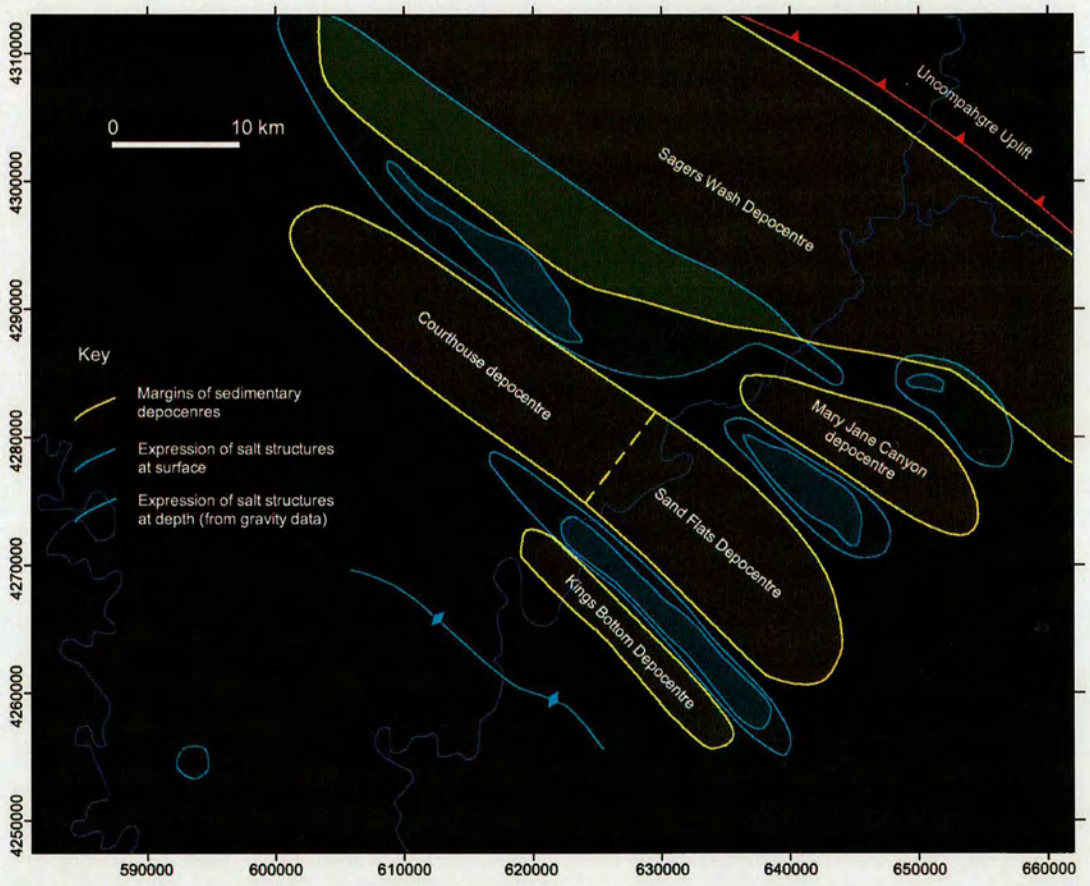

Figure 3.80. Map illustrating the extent of main sedimentary depocentres in the study area and their association with salt structures.

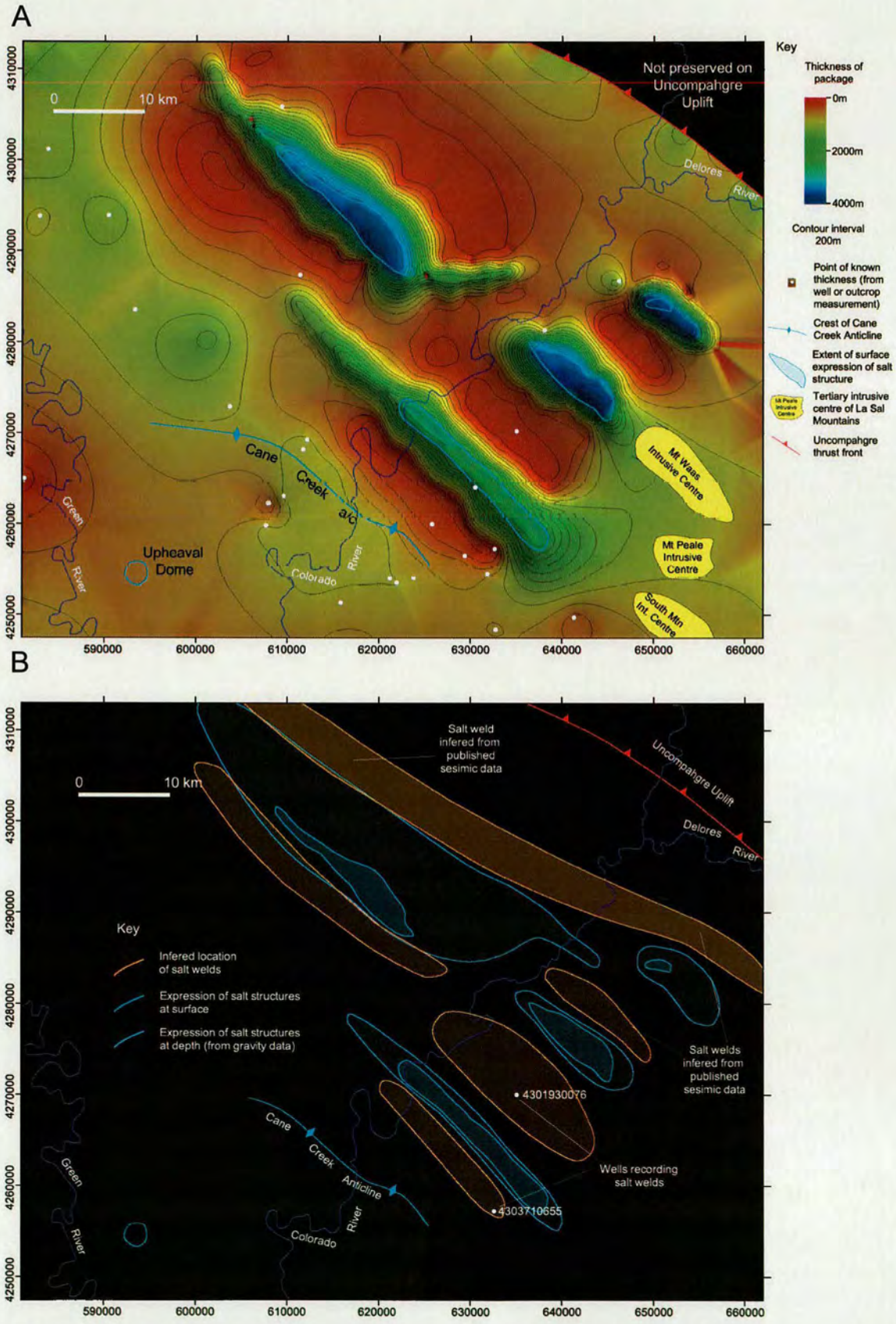

Figure 3.81. Isopach map of the Paradox Formation within the study area (A) and a map illustrating the location of salt welds identified from well data in the study area or inferred from published seismic data (B). Note that where well data is sparse, the thickness of the Paradox Formation has been interpreted based on regional cross section construction

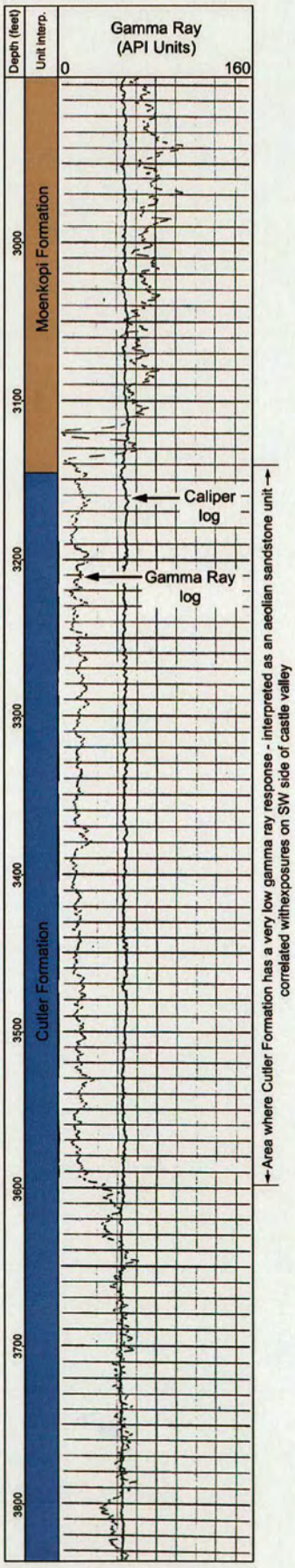

Figure 3.82. Part of a gamma ray log from well 4301930076 illustrating the gamma ray response of the top of the Cutler Formation. The gamma ray log shows a 137m thick sequence with an extremely low gamma ray response interpreted as an extremely clean aeolian sandstone correlated with exposures on the SW side of Castle Valley.

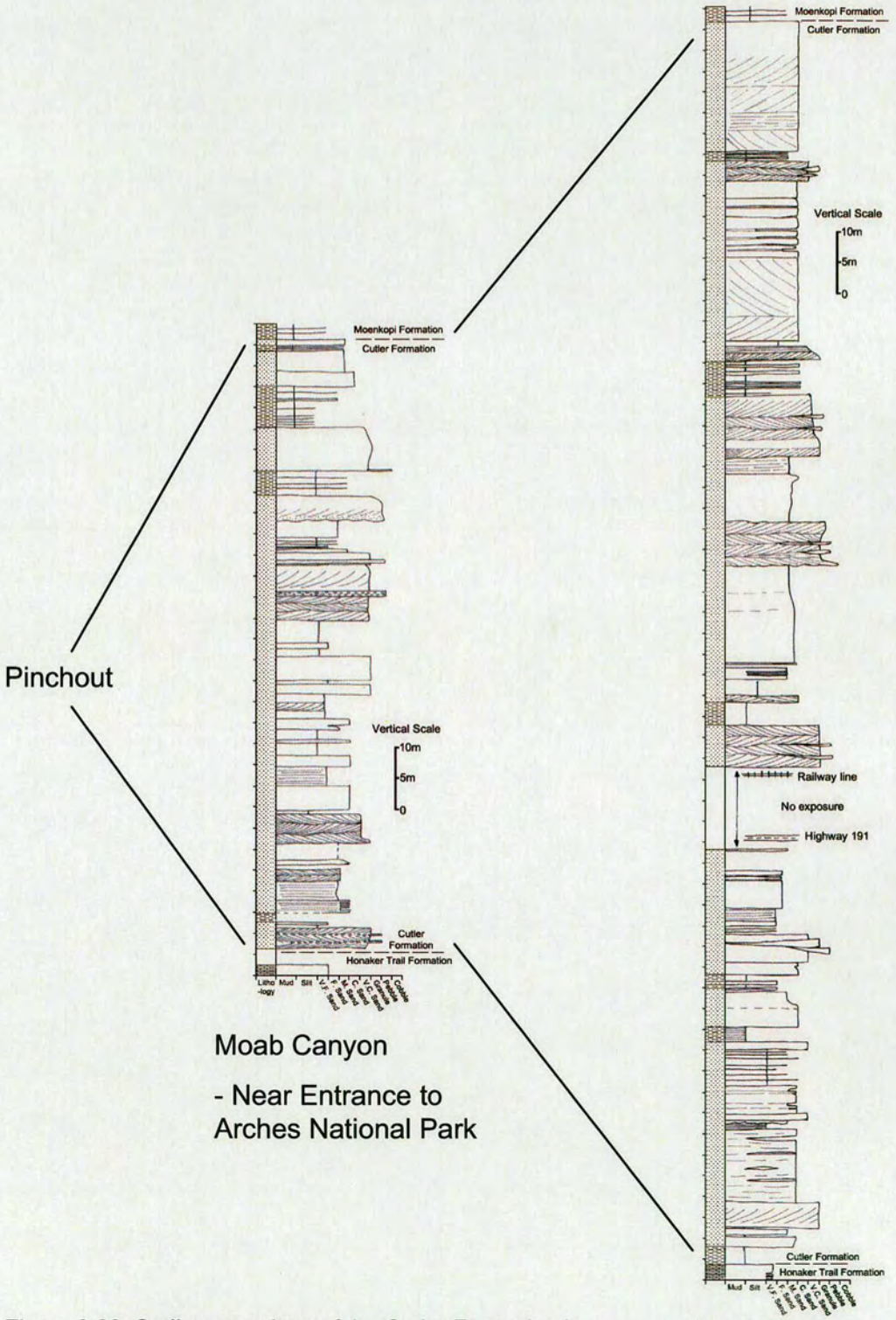

Figure 3.83. Sedimentary logs of the Cutler Formation in the Moab Canyon area illustrating along strike facies variations. Both logs show a complete sequence and there is no evidence of erosion at the upper contact

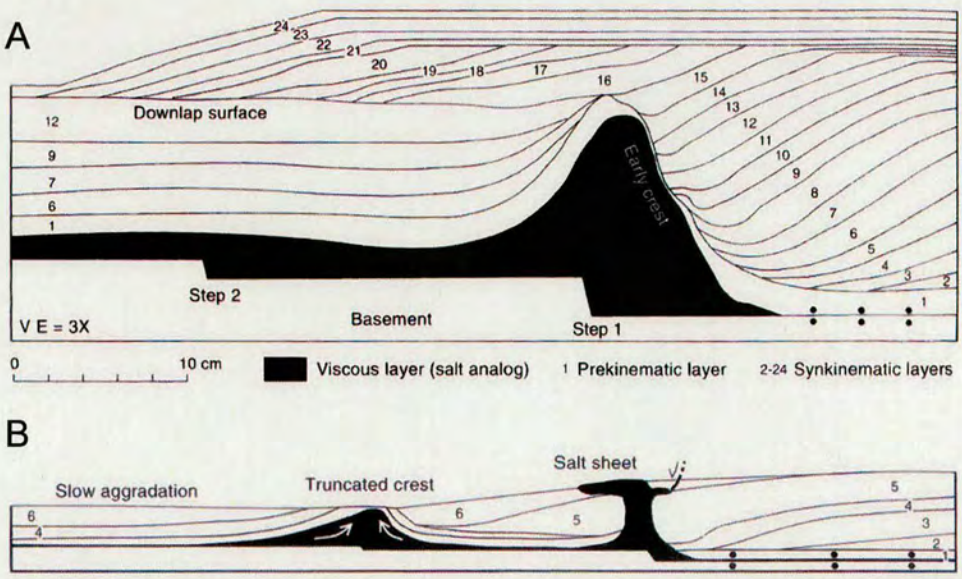

Figure 3.84. Cross sections illustrating the results of analogue models of the development of salt structures through progradation of sediment over a viscous salt analogue. Modelling results are compared with geometries observed in the Paradox Basin in the text. From Ge et al. (1997).

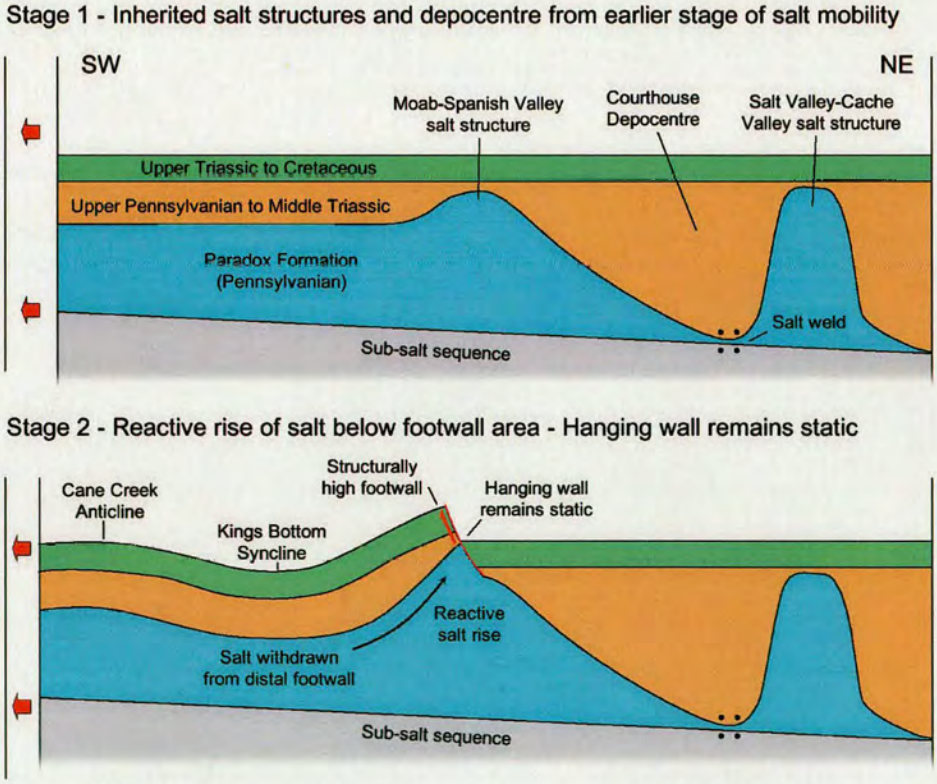

Figure 3.85. Cartoon model illustrating the development of the Moab segment of the Moab Fault system. Note how fault displacement consists entirely of footwall uplift.

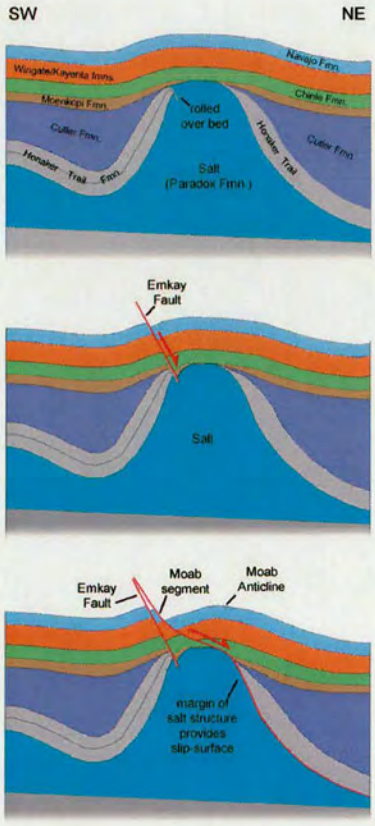

Figure 3.86. Schematic sketch illustrating one interpretation of the association of the Emkay Segment to the Moab Segment. This model suggests that the Emkay fault develops to accommodate early extensional stresses and then the Moab segment develops as a shortcut fault as displacement begins to involve the edge of the salt structure.

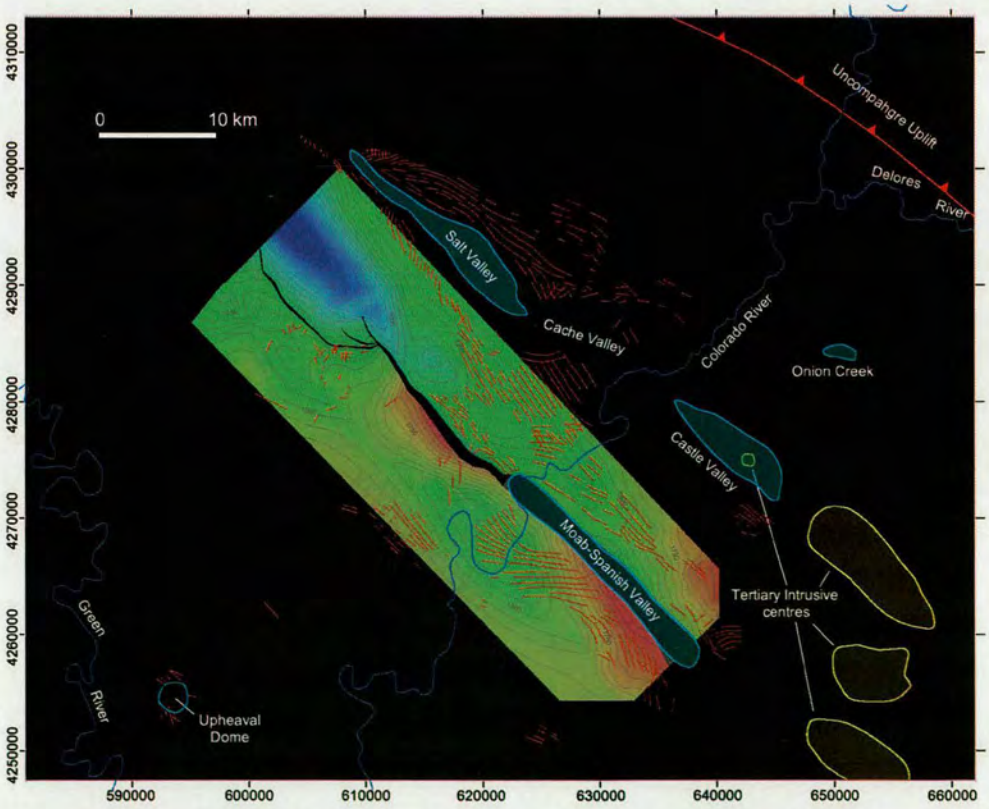

Figure 3.87. Map of the fracture pattern in the study area overlying the structure contour map of the Base Middle Jurassic horizon shown in Figure 3.42(B). Note how fractures on the SW side of the Moab-Spanish Valley salt structure are deflected towards the structural high areas.

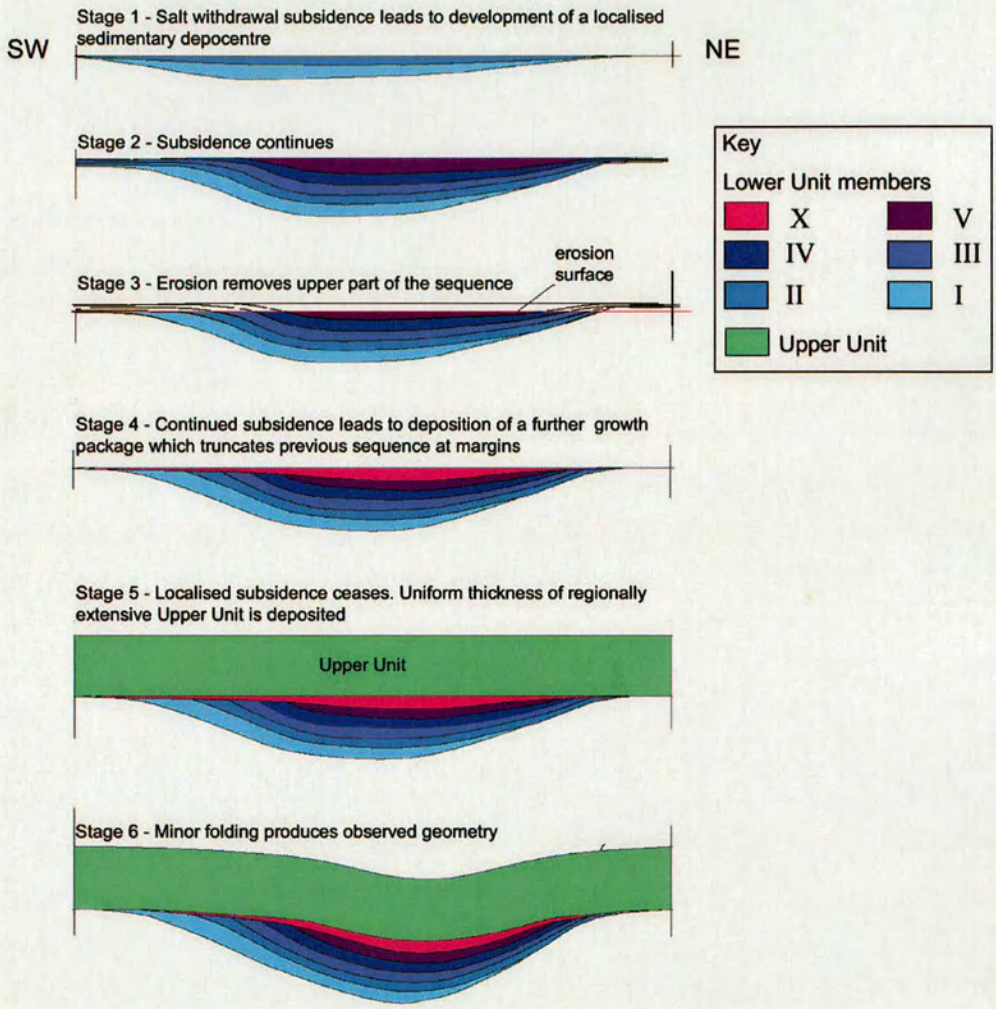

Figure 3.88. Cartoon model illustrating the evolution of the Chinle sequence in the Sandy Beach area and the development of truncations within this sequence

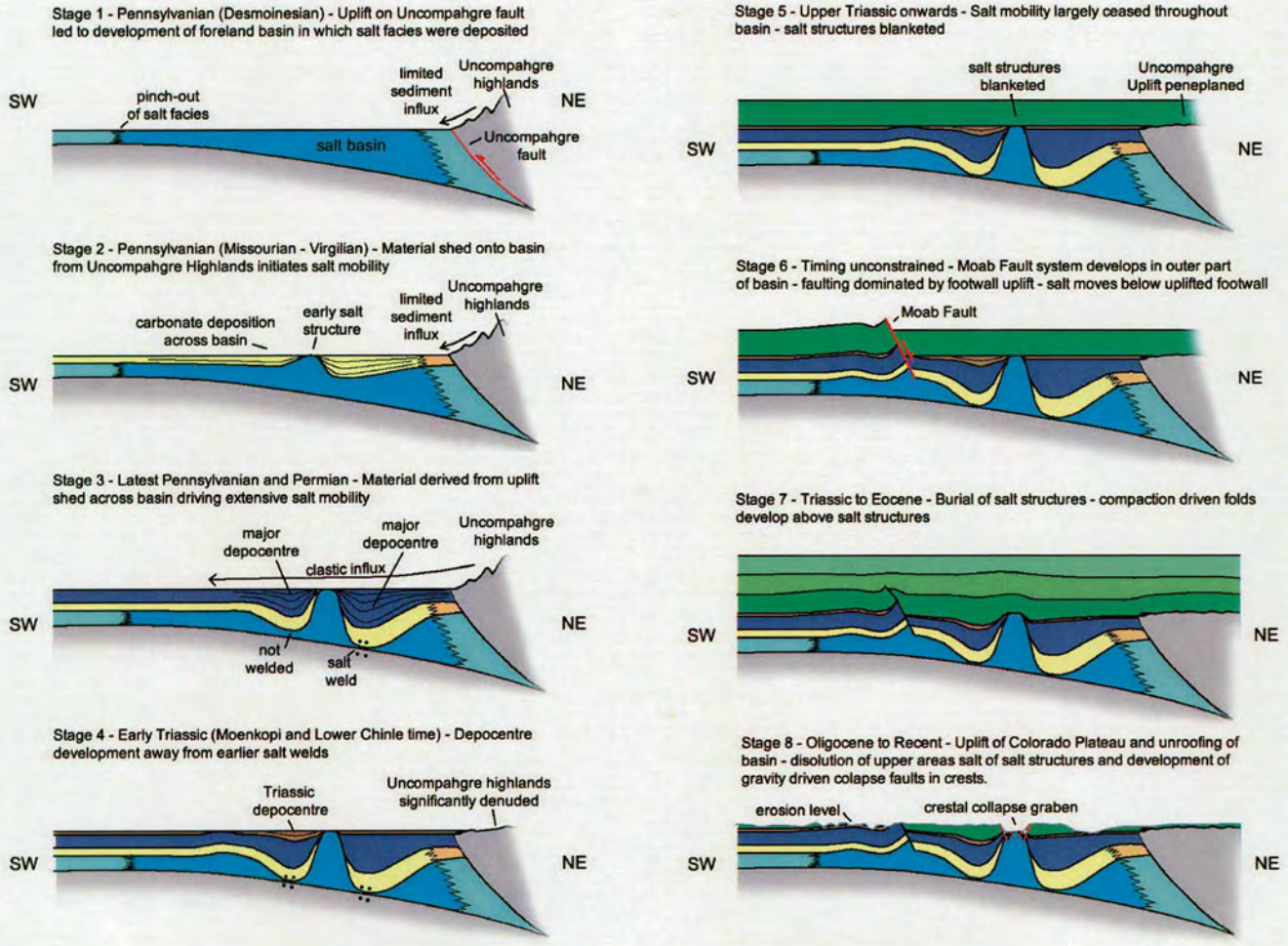

Figure 3.89 Cartoon model illustrating the structural and stratigraphic development of the Paradox Basin. The model is based on SW-NE traverse of the basin incorporating the Salt Valley salt structure and the northern end of the Moab-Spanish Valley structure.

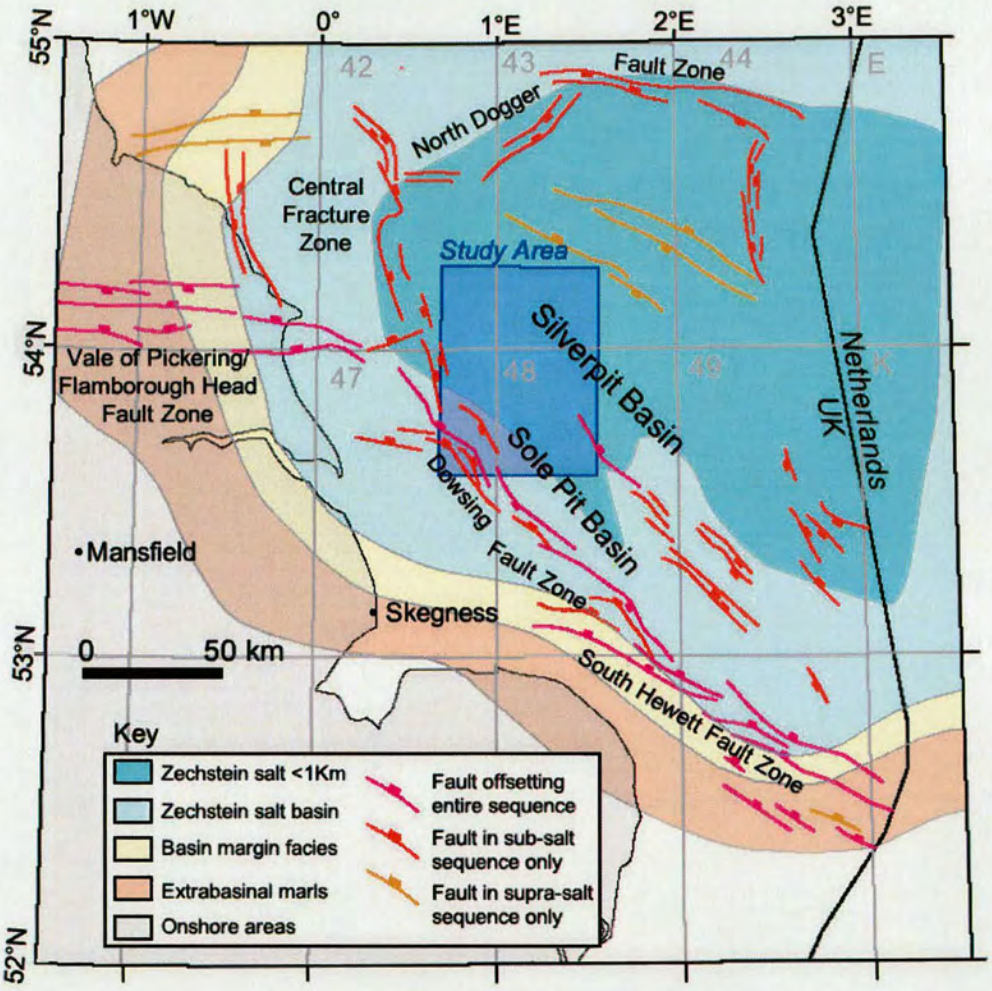

Figure 4.1. Map of the UK sector of the Southern North Sea illustrating the location of the study area, major faults in the area and the extent of the salt basin as well facies variations in the Upper Permian sequence. Compiled after Cameron et al. (1992) and Stewart and Coward (1995).

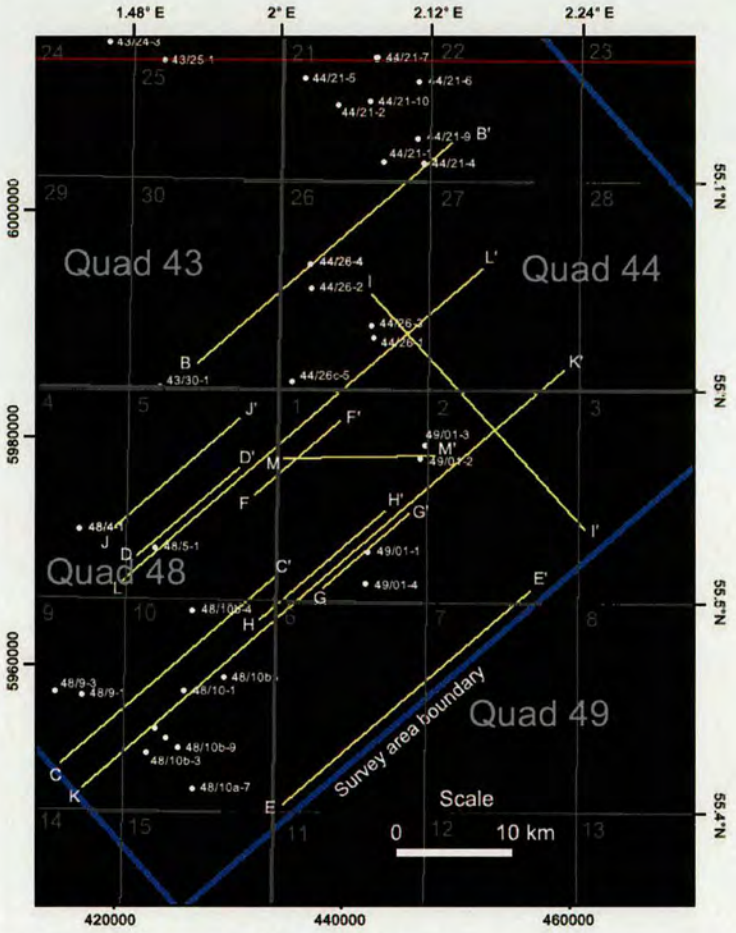

Figure 4.2. Map of study area illustrating the location of well penetrations in the area. Also shown are the locations of seismic sections shown in this chapter

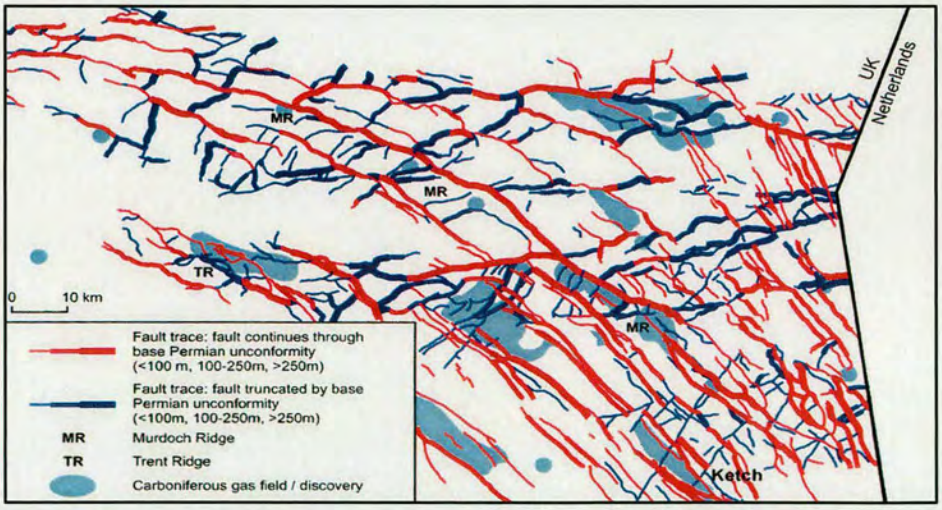

Figure 4.3. Map of the Silverpit basin area of the Southern North Sea illustrating sub-salt fault trends. From Cameron et al. (2005)

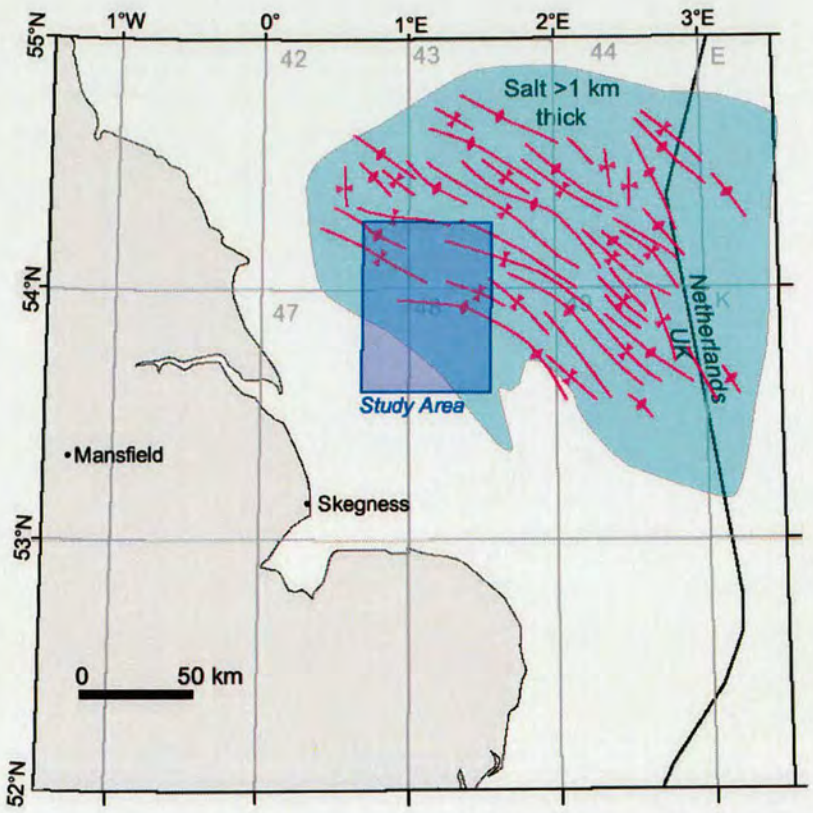

Figure 4.4. Map of the UK sector of the Southern North Sea illustrating the location of major salt-cored buckle folds in the basin. Note how these are exclusively situated in the area where the salt sequence is thickest and are the dominant structural style to the NE of the study area. After Stewart and Coward (1995).

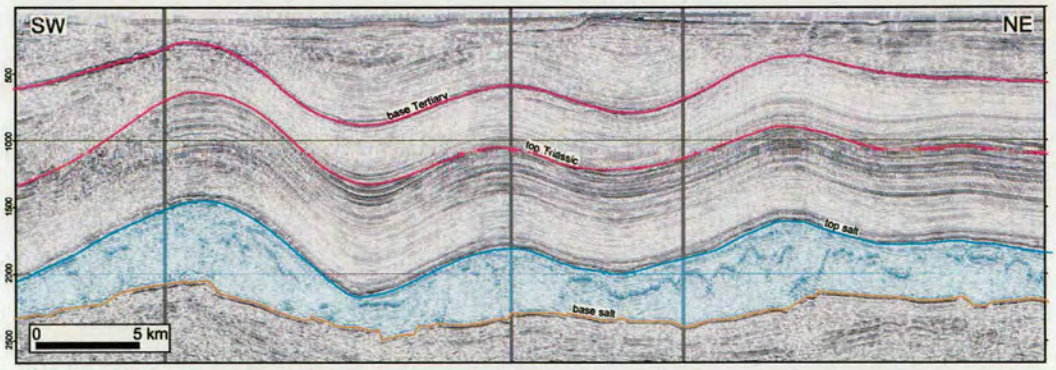

Figure 4.5. Cross section through part of the Silverpit Basin illustrating the dominant structural style in the area. The area is dominated by a series of salt-cored buckle folds in the supra-salt sequence which are not related to similar compressional structures in the sub-salt sequence.

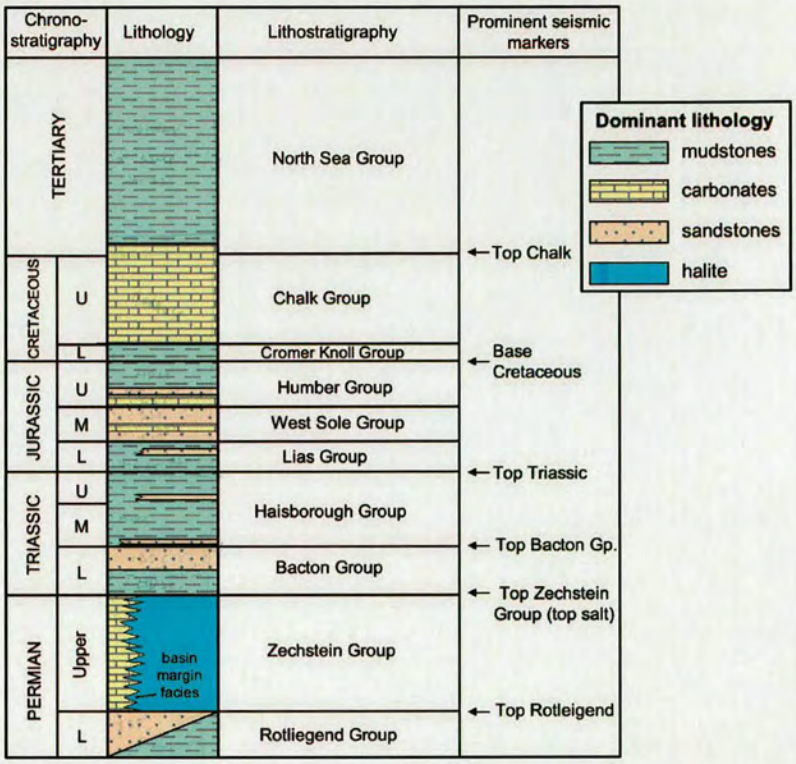

Figure 4.6. Generalised stratigraphy of the Southern North Sea and the prominent seismic markers in the study area

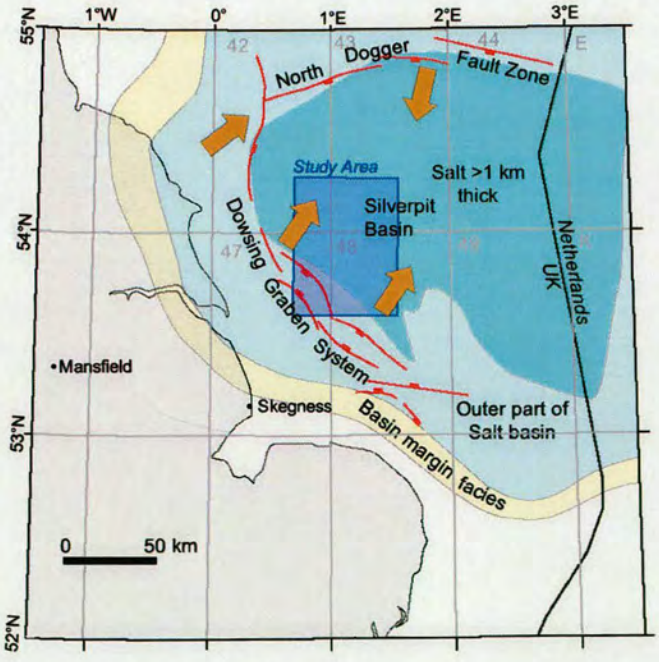

Figure 4.7. Map of the UK sector of the Southern North Sea illustrating the direction of movement of the supra-salt sequence suggested by Stewart and Coward (1995) to explain the development of the Dowsing Graben system and North Dogger Fault Zones which are supra-salt, basin margin fault systems. After Stewart and Coward (1995).

(a) Permian to Early Cretaceous

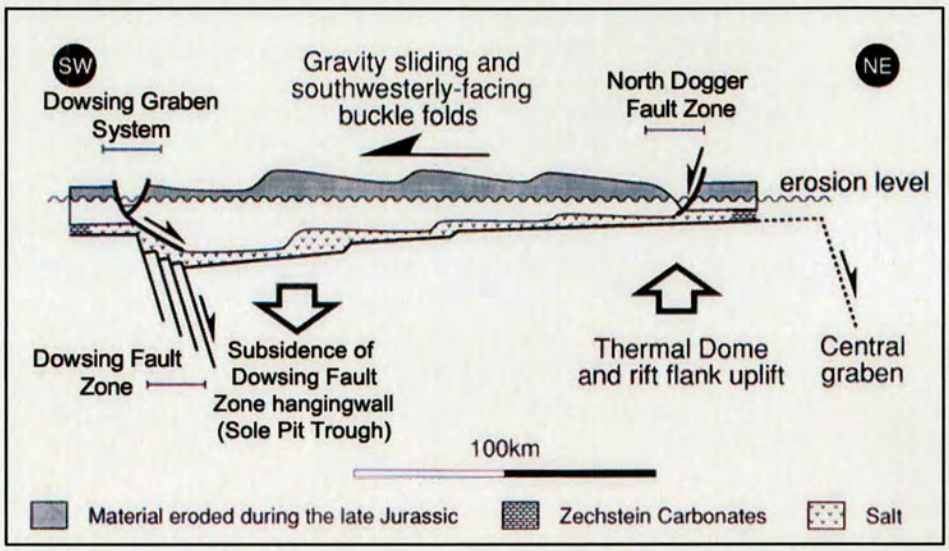

(b) Cretaceous and Tertiary

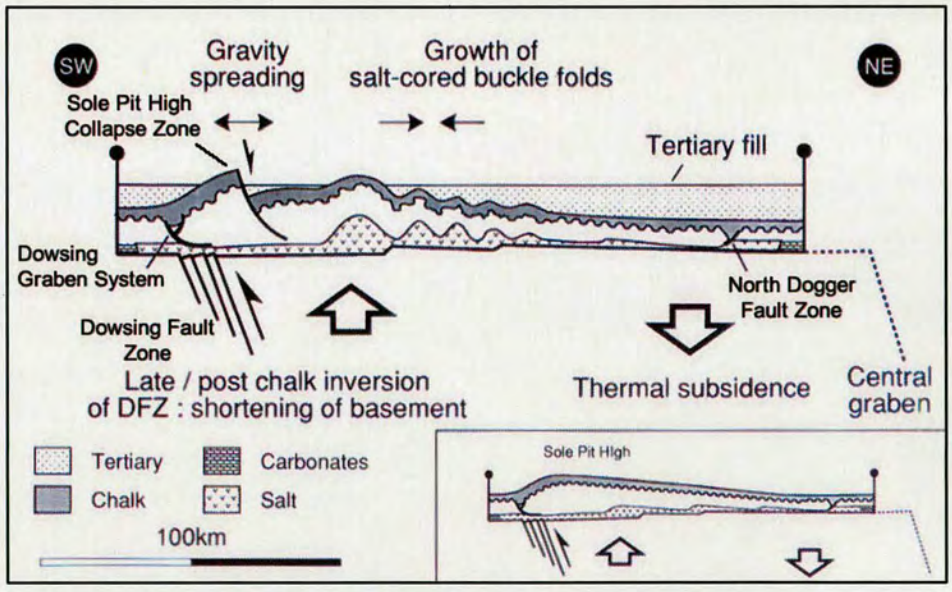

Figure 4.8. Cartoons illustrating Stewart and Coward's model for the development of the Southern North Sea. (A) illustrates the Permian to Lower Cretaceous development of the basin and (B) illustrates the Cretaceous and Tertiary basin development. From Stewart and Coward (1995)

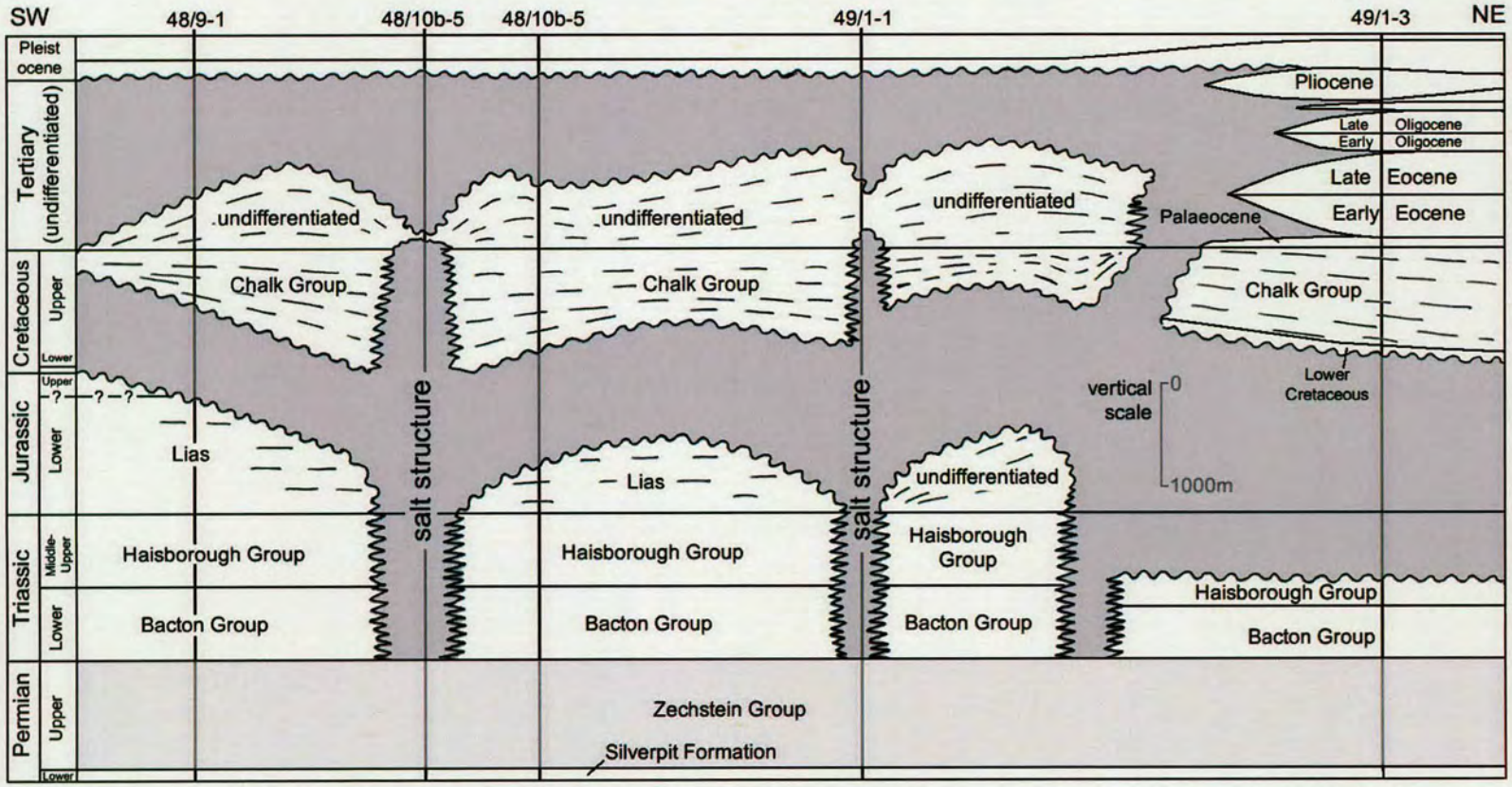

Figure 4.9. Chronostratigraphic diagram for the Southern North Sea study area. The diagram represents the stratigraphy along a SW-NE transect incorporating the illustrated wells.

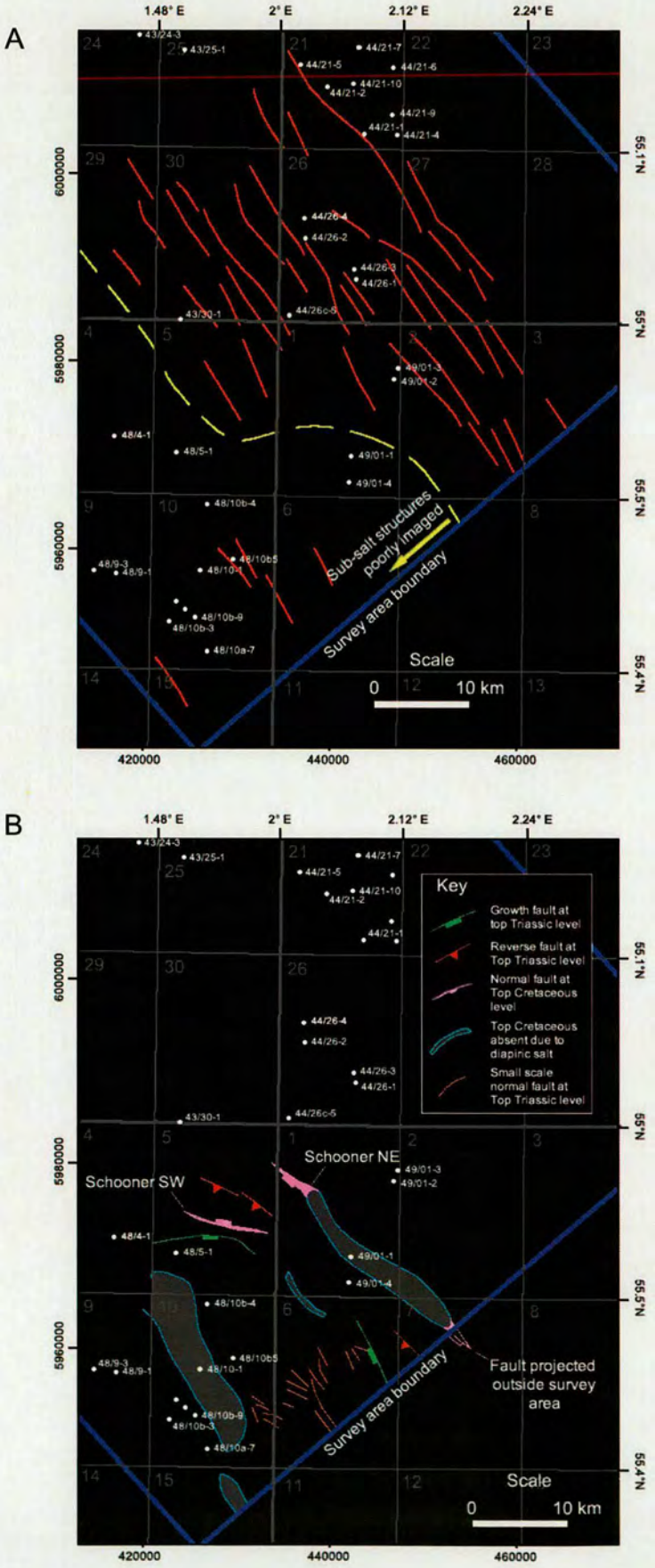

Figure 4.10. Maps illustrating the fault orientations in the sub-salt (A) and supra-salt (B) sequence within the study area. Note sub-salt faults are poorly imaged in the SW of the study area. Faults are likely to be present in this area which are not shown as they can not be imaged with confidence.

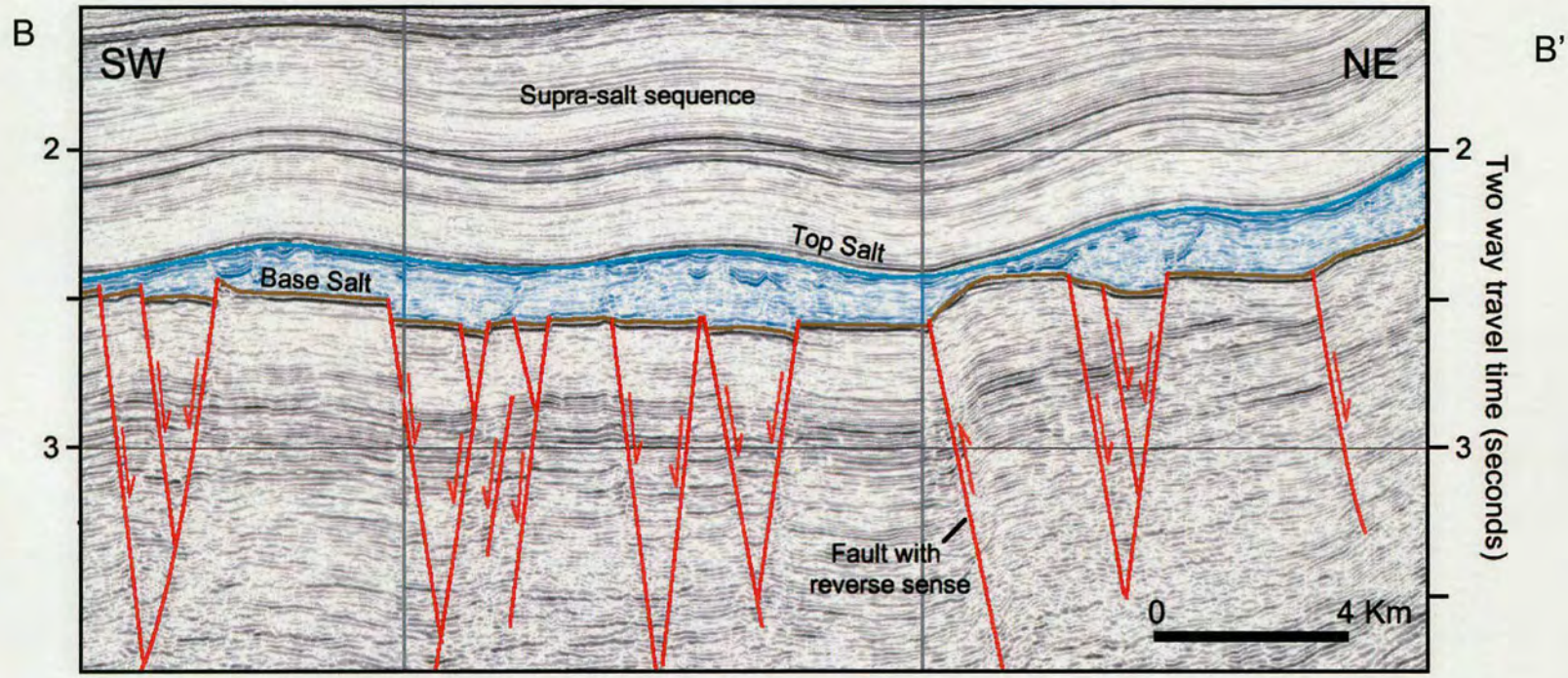

Figure 4.11. Seismic section illustrating the faulting style in the sub-salt sequence in the study area. Where imaged, faults are typically pervasive and display vertical displacements which are significantly less than those observed in supra-salt faults.

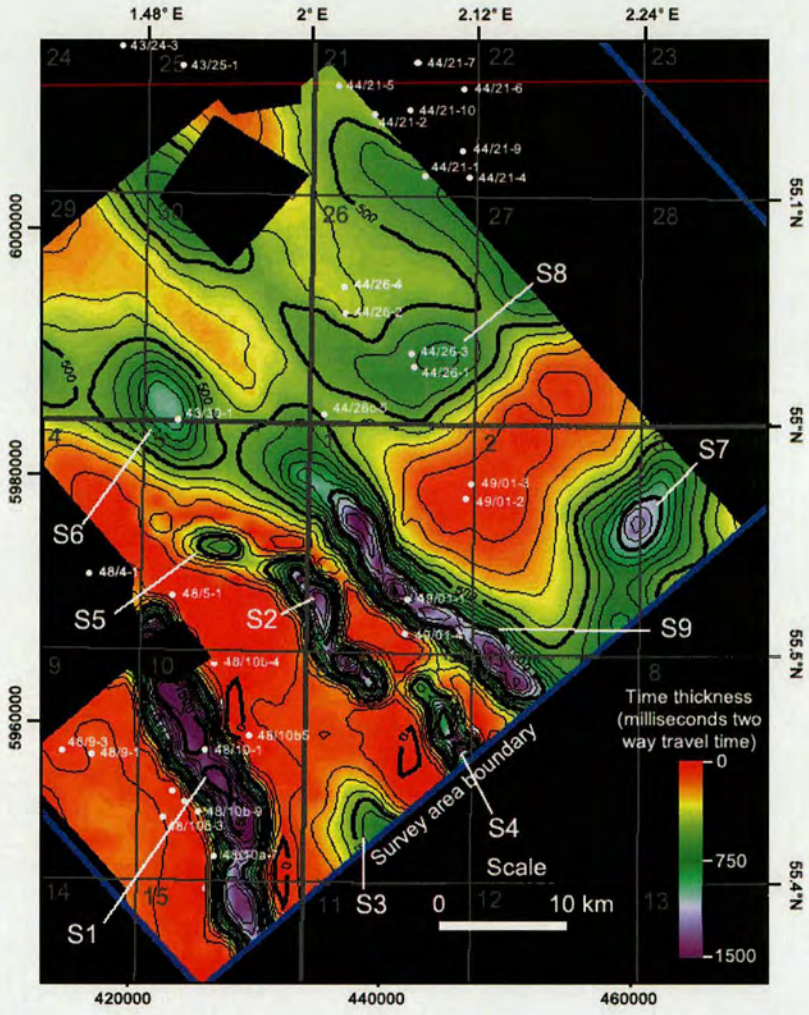

Figure 4.12. Isochron map of the halite dominated Upper Permian Zechstein group illustrating the location of salt structures in the study area.

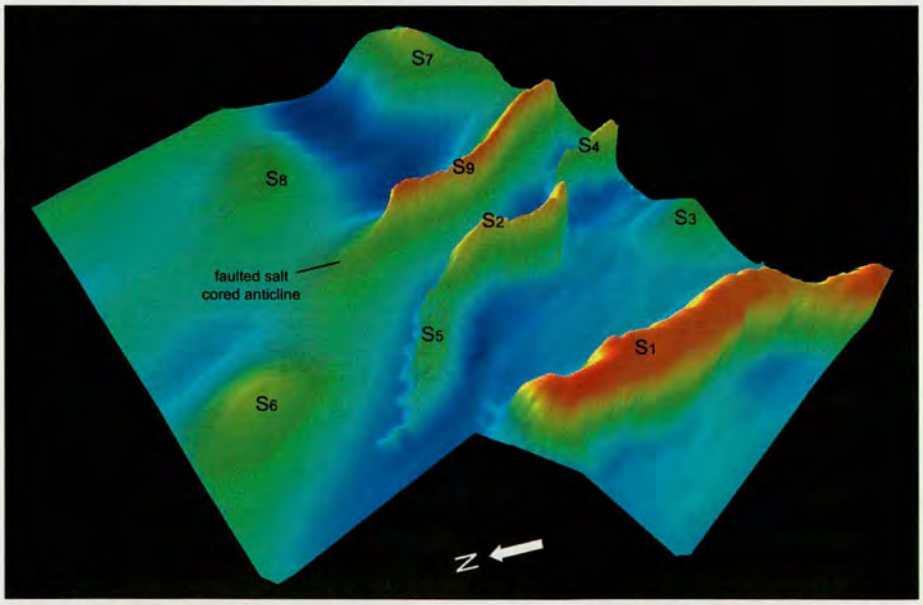

Figure 4.13. 3D view of the top Zechstein (top salt) horizon illustrating the varying morphology of salt structures in the study area

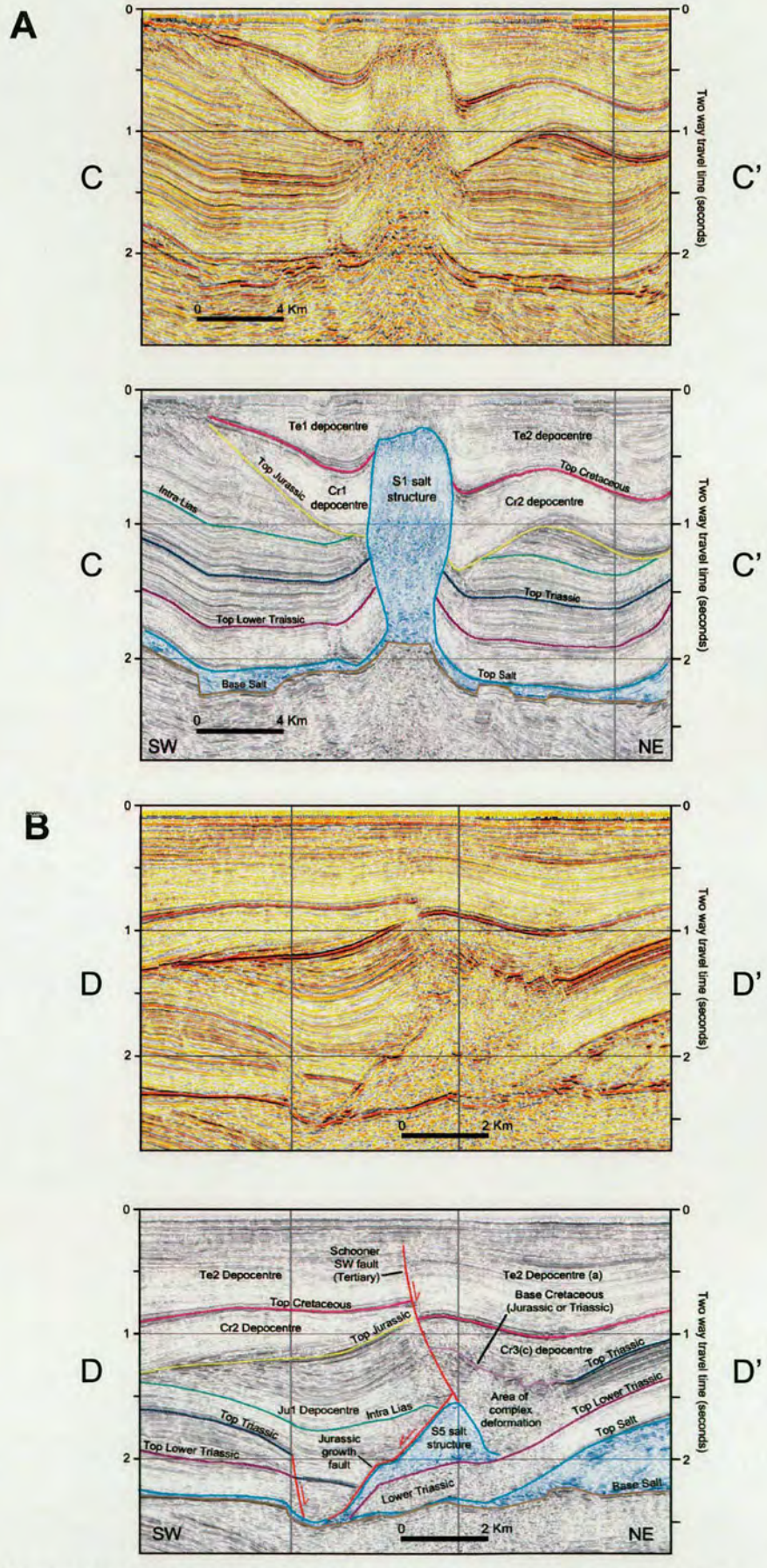

Figure 4.14. Uninterpreted and interpreted seismic sections through the S_1 and S_5 salt structures and their associated depocentres. The locations of sections are shown in Figure 4.2

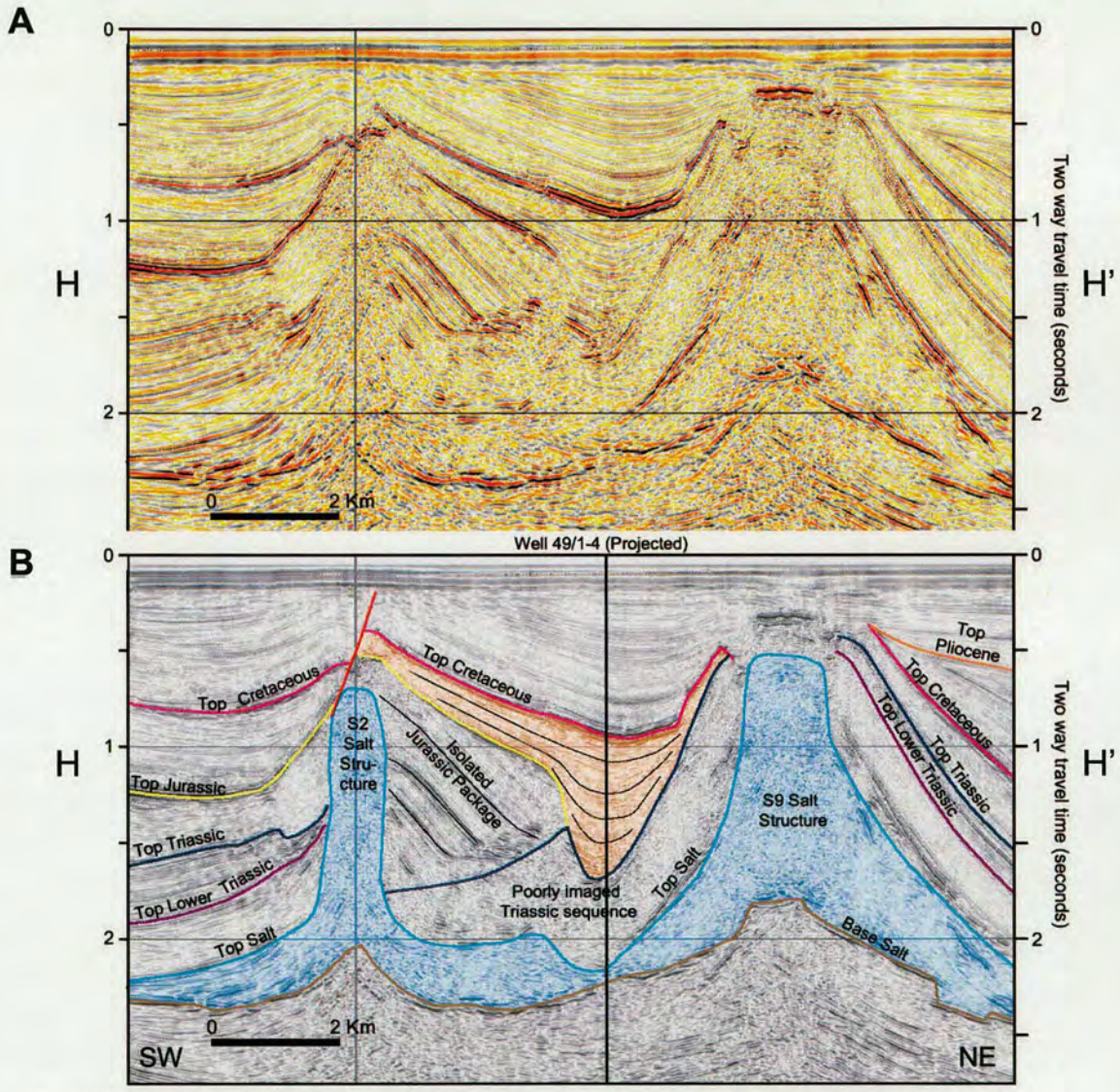

Figure 4.15. Uninterpreted (A) and interpreted (B) seismic sections illustrating the Cr_3(b) depocentre and surrounding salt structures

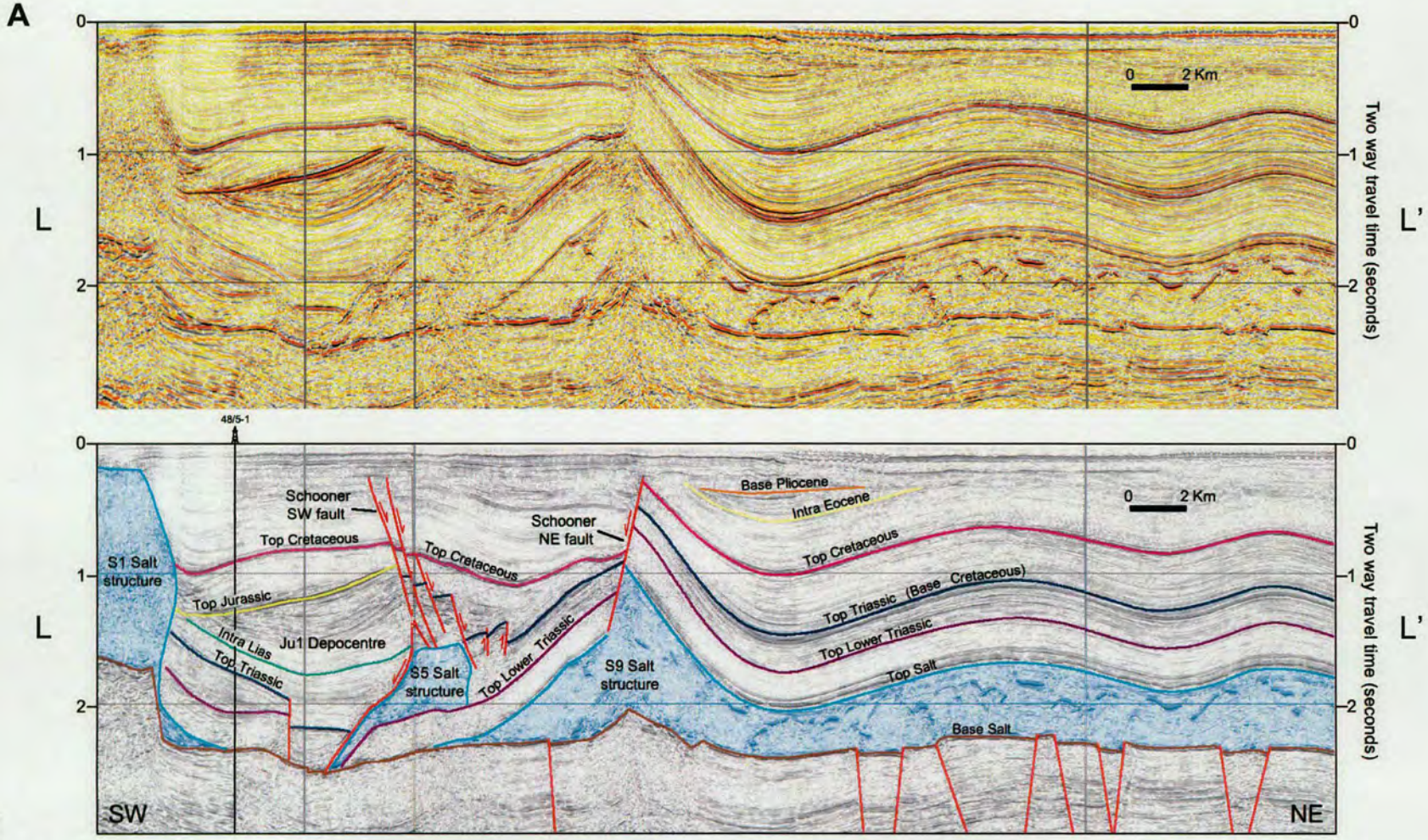

Figure 4.16. Uninterpreted (top) and interpreted (bottom) seismic sections across the study area including the Schooner NE fault system (A) and a structural restoration of this section (B).

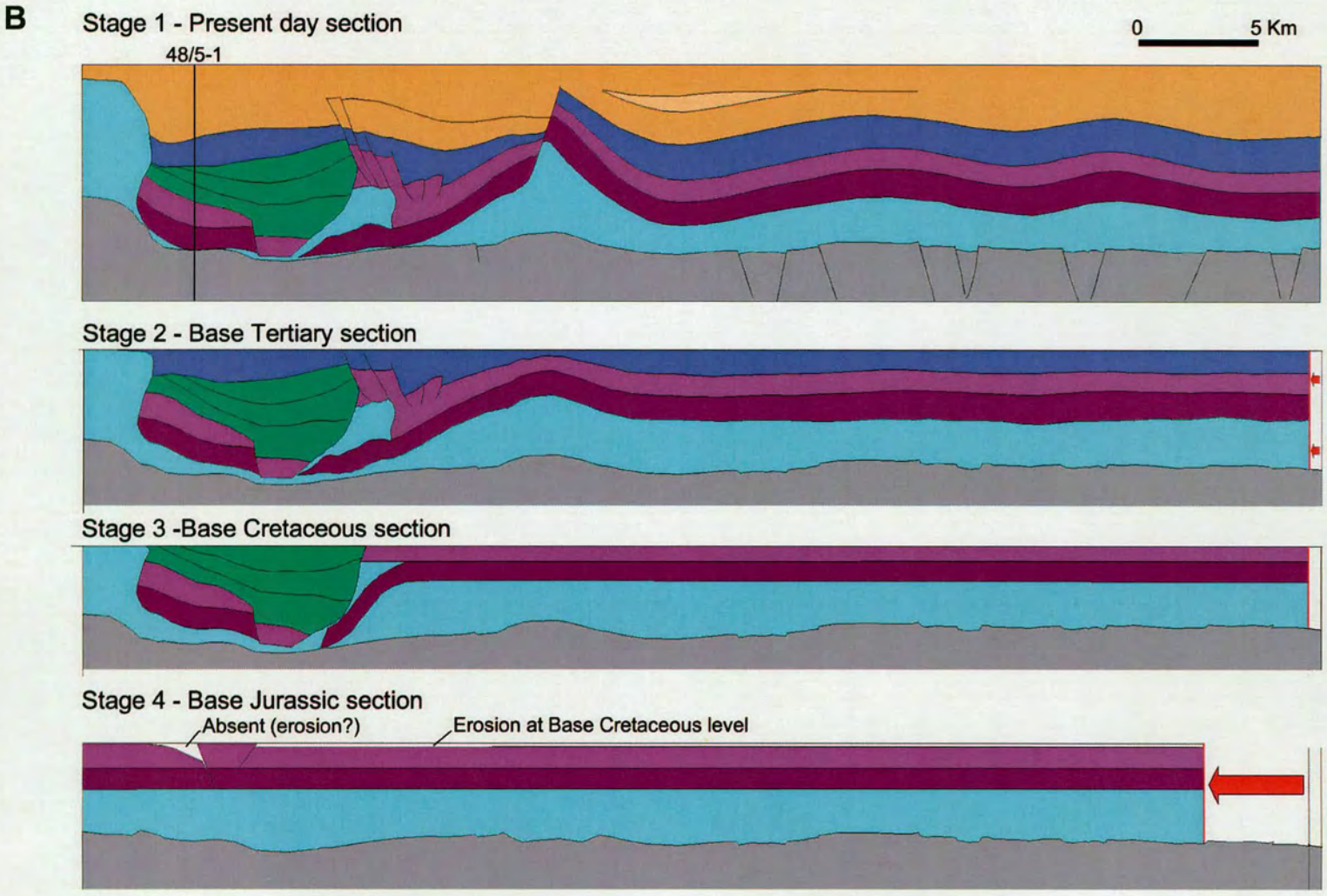

Figure 4.16. Continued

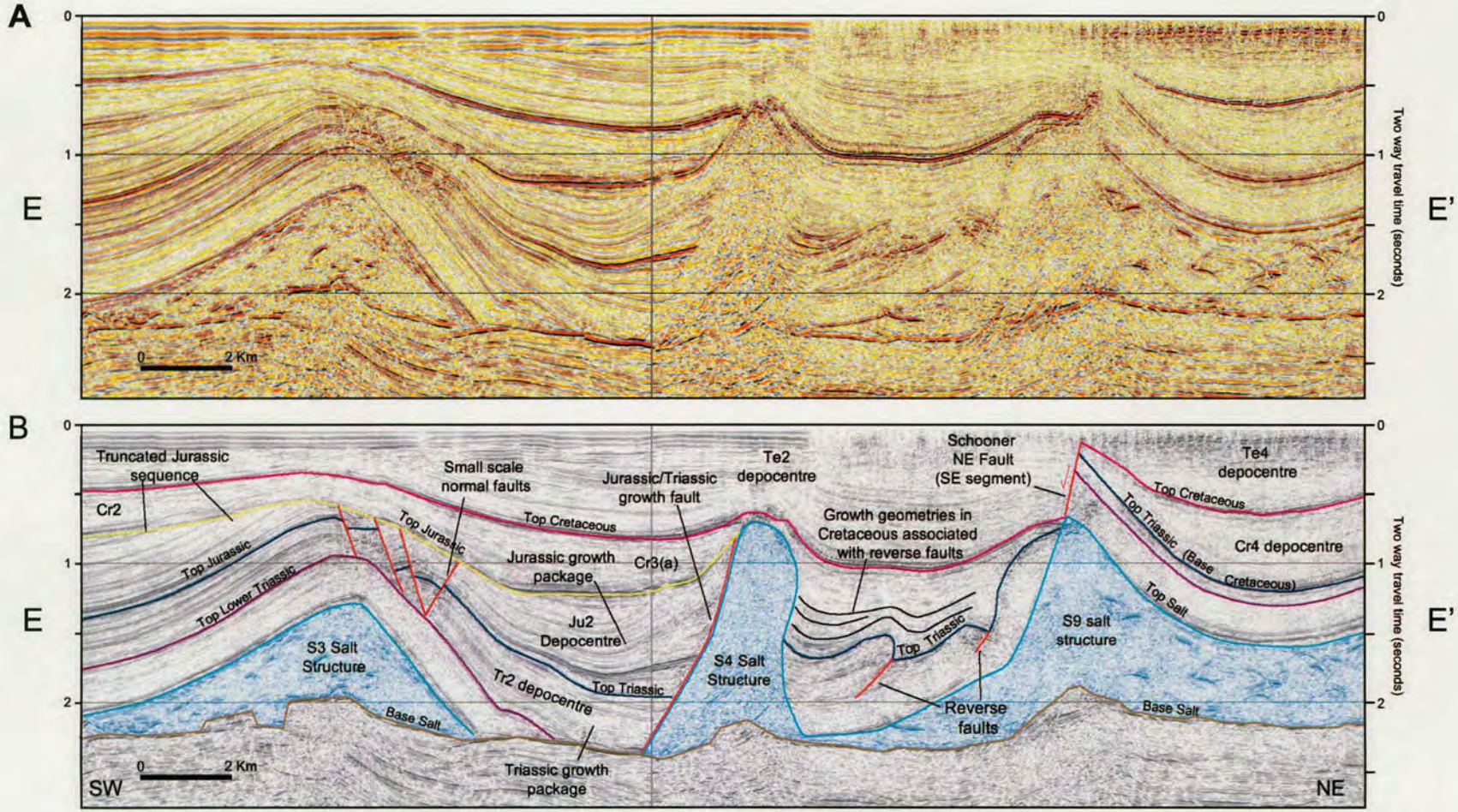

Figure 4.17. Uninterpreted (A) and interpreted (B) seismic section through SE margin of study area illustrating each of the different supra-salt faulting styles identified in the study area

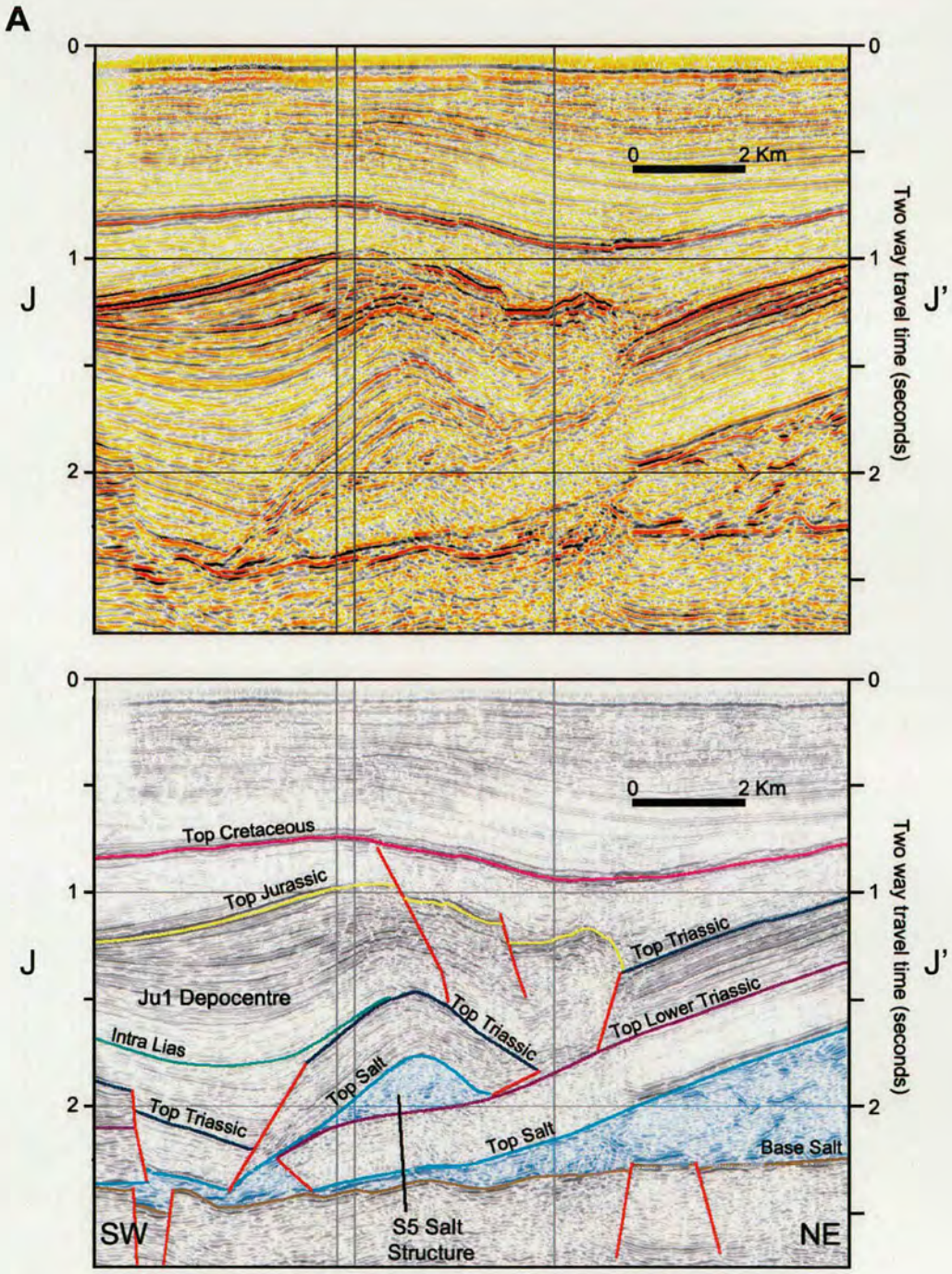

Figure 4.18. Uninterpreted and interpreted seismic section of the NE end of the S_5 salt structure illustrating the complex structural geometry in the area (A) and a structural restoration of this section (B)

B

Stage 1 - Present day section

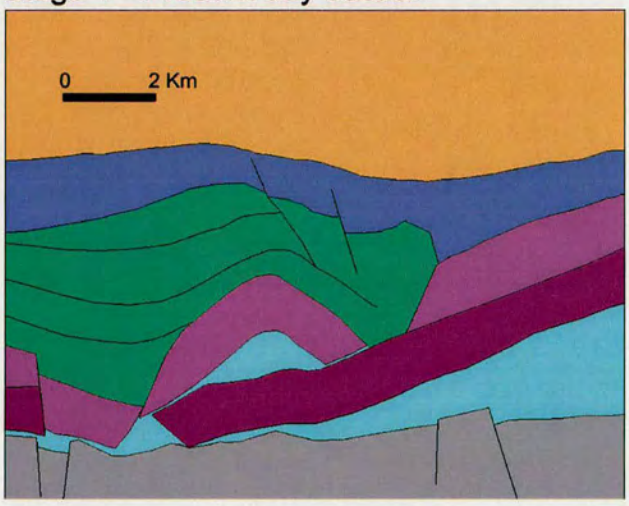

Stage 2 - Base Tertiary section

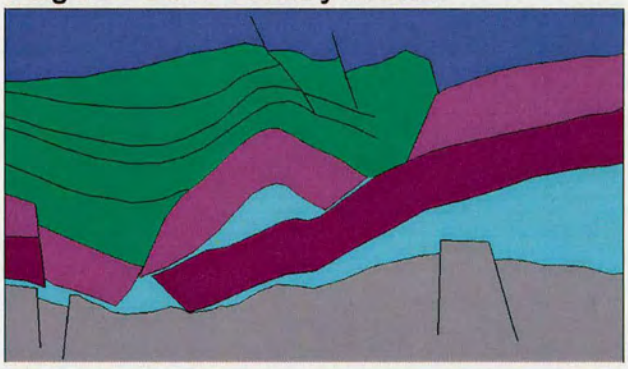

Stage 3 - Base Cretaceous section

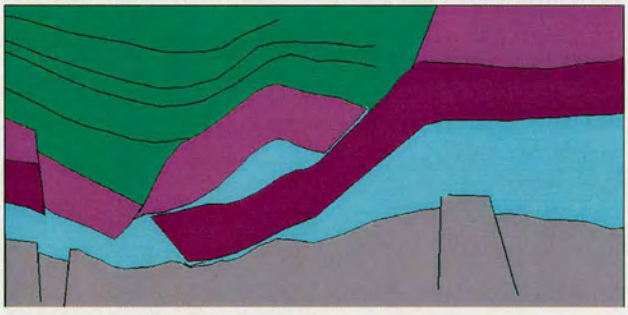

Stage 4 - Base Jurassic

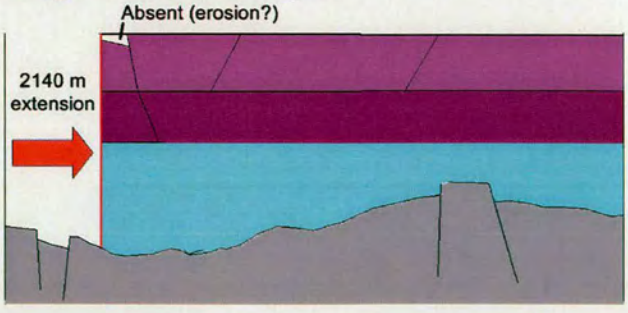

Figure 4.18. Continued

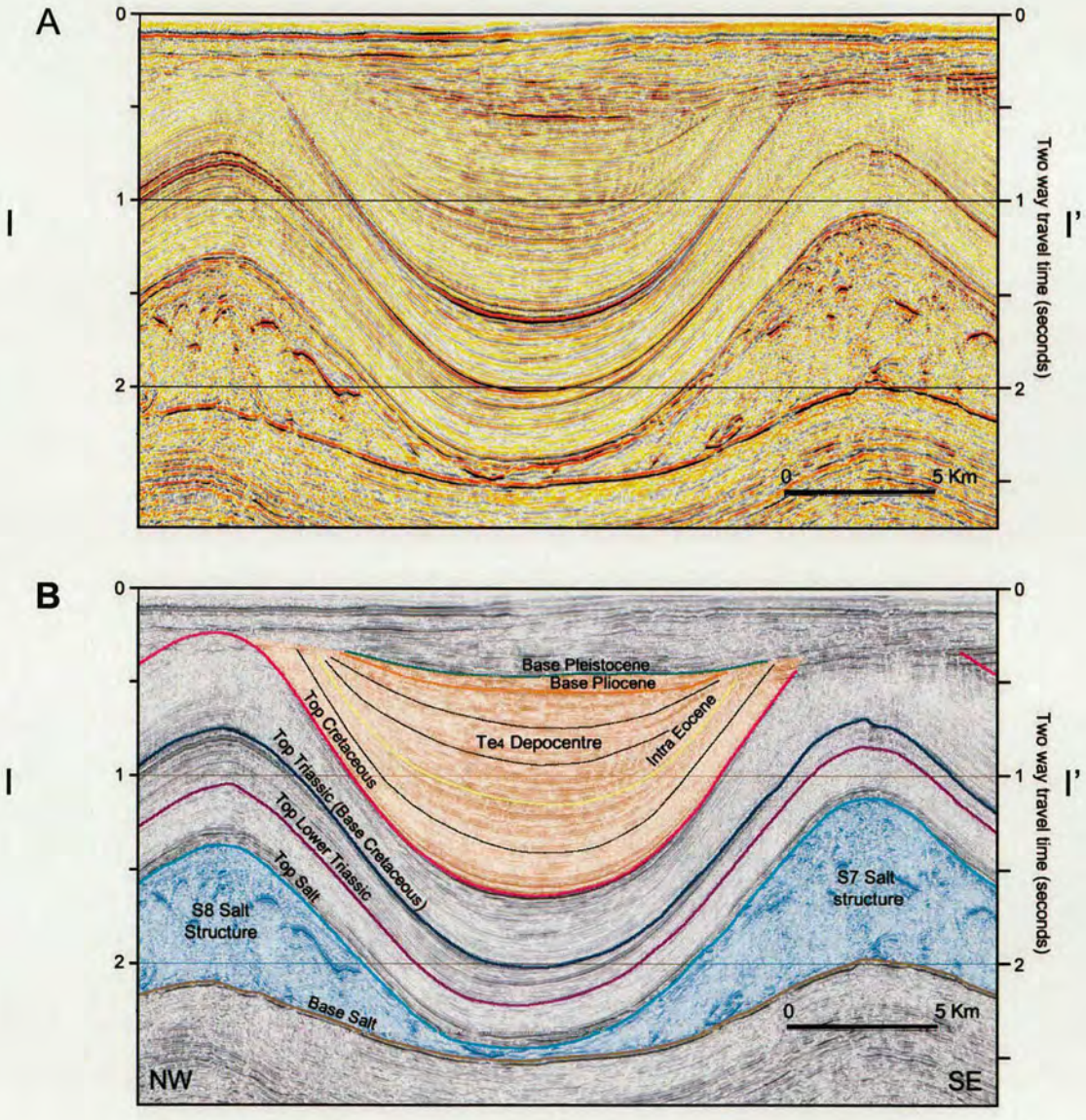

Figure 4.19. Uninterpreted (A) and interpreted (B) seismic section through the Te_4 depocentre

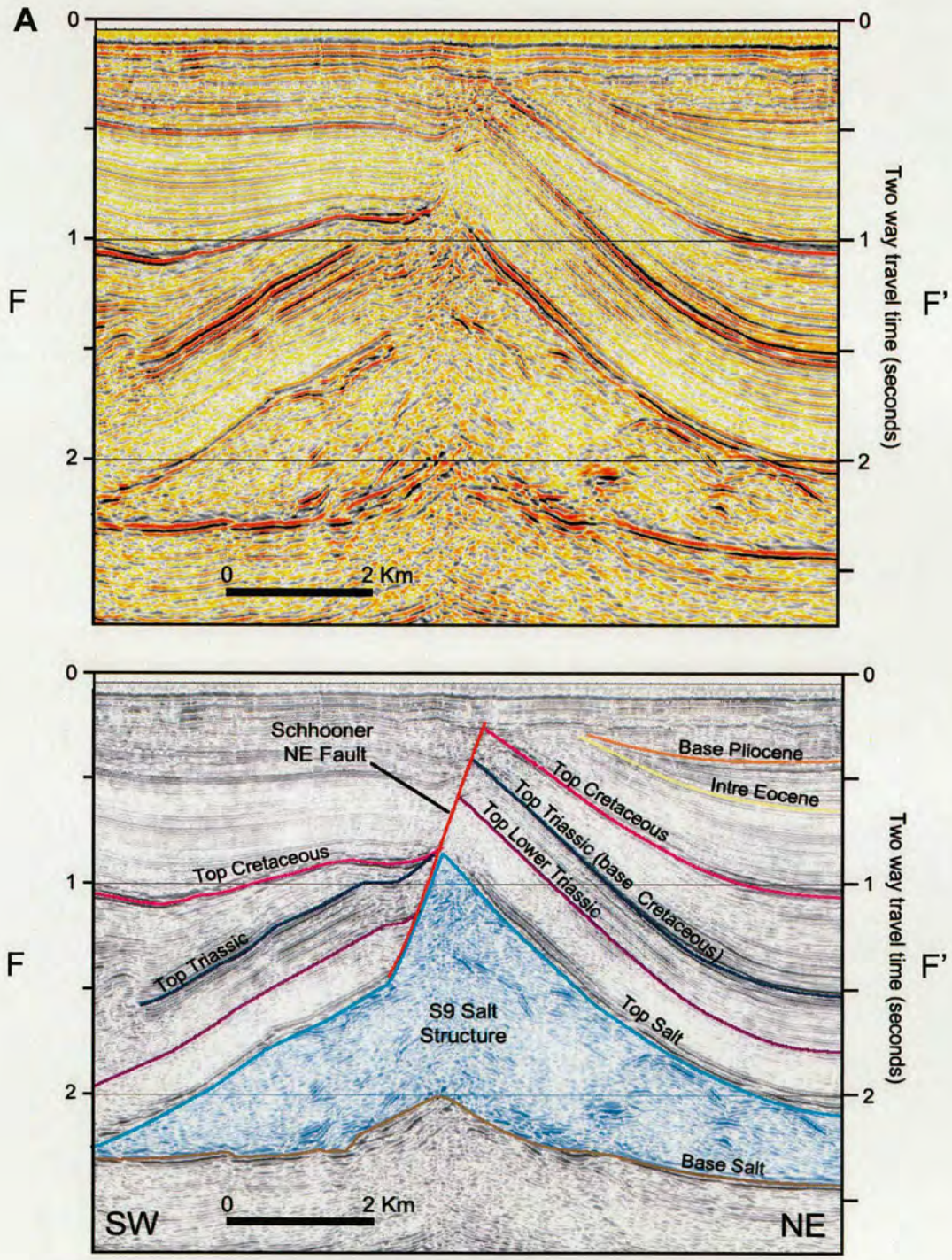

Figure 4.20. Uninterpreted and interpreted seismic sections through the Schooner NE fault system illustrating the changing nature of the S_9 salt structure along strike. In (A) the fault system is a faulted salt-cored anticline. Further to the SE, vertical bed separation occurs across a steep sided diapiric structure (B)

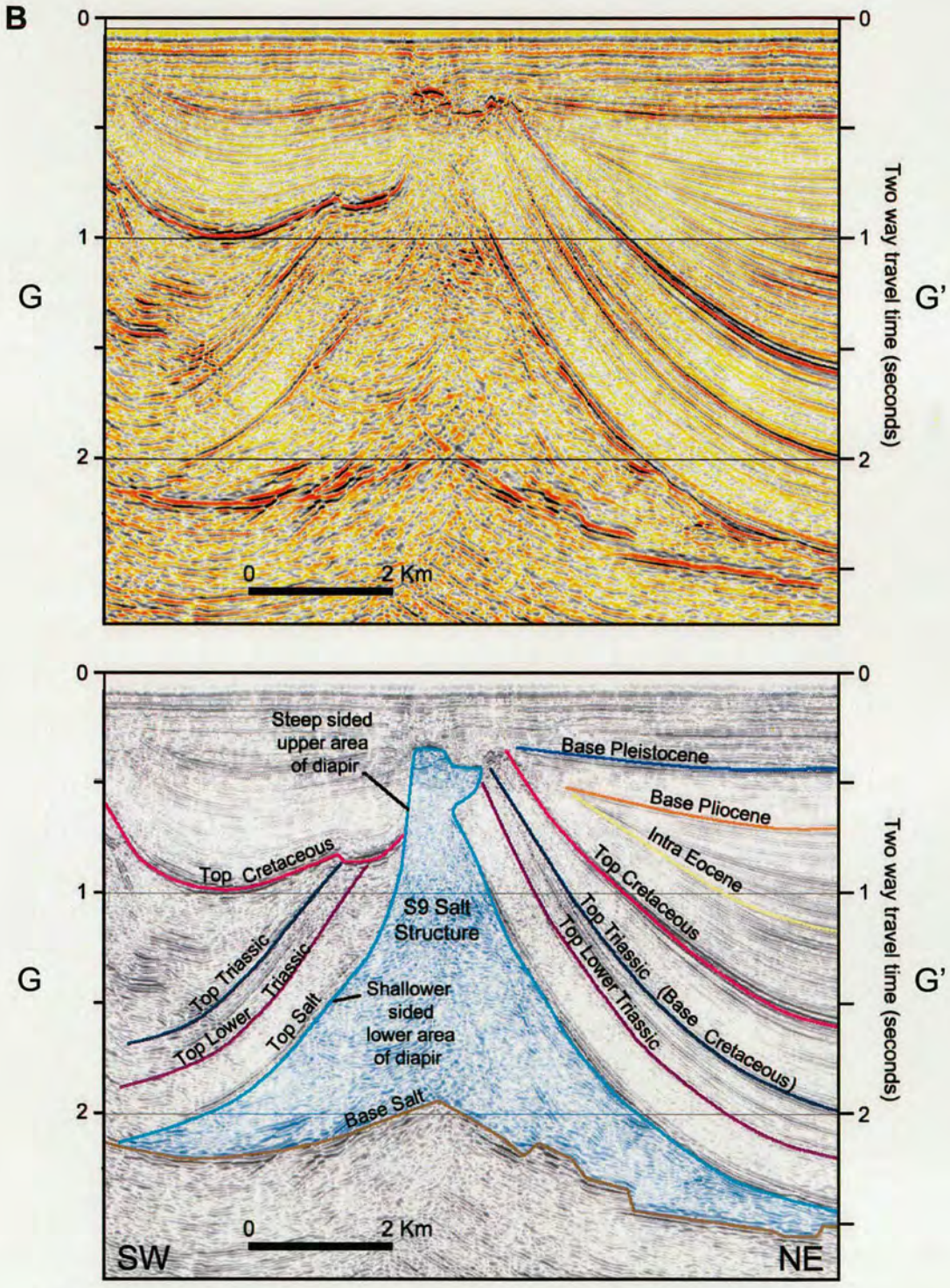

Figure 4.20. Continued

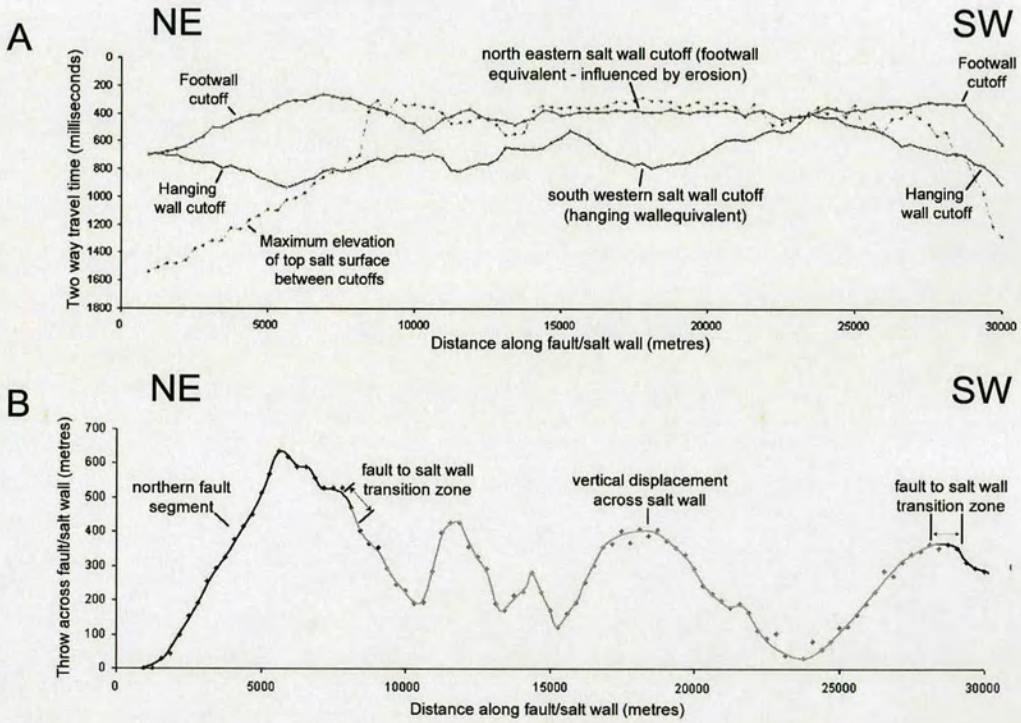

Figure 4.21. Cut-off elevation profile (A) and displacement-length profile (B) along the Schooner NE fault system. Note that separations are shown for fault segments and also where vertical separation is across the S_9 salt structure

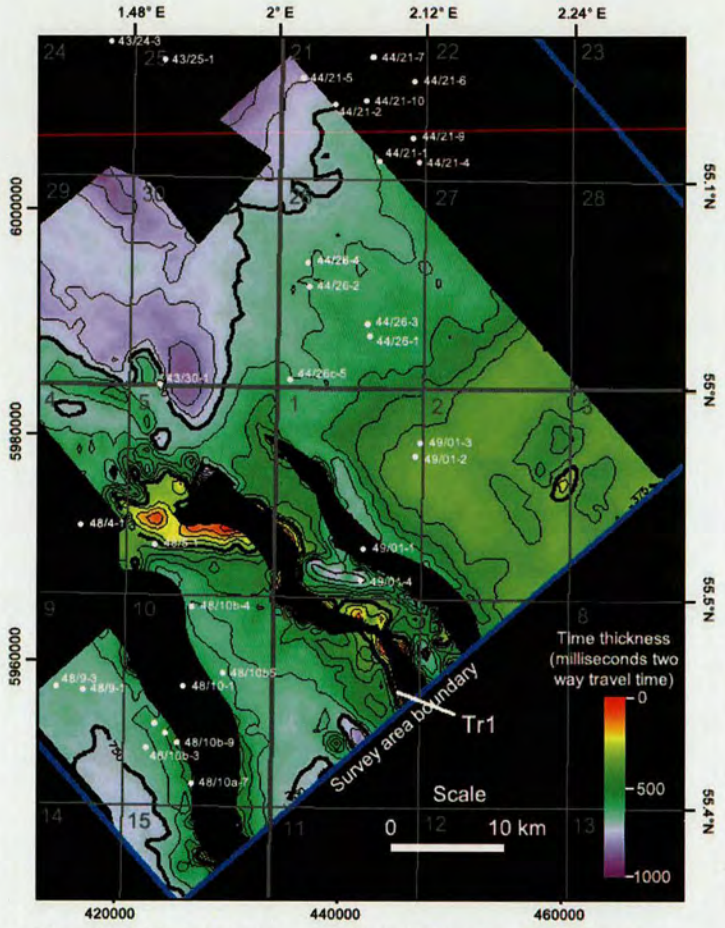

Figure 4.22. Isochron map of the Triassic sequence

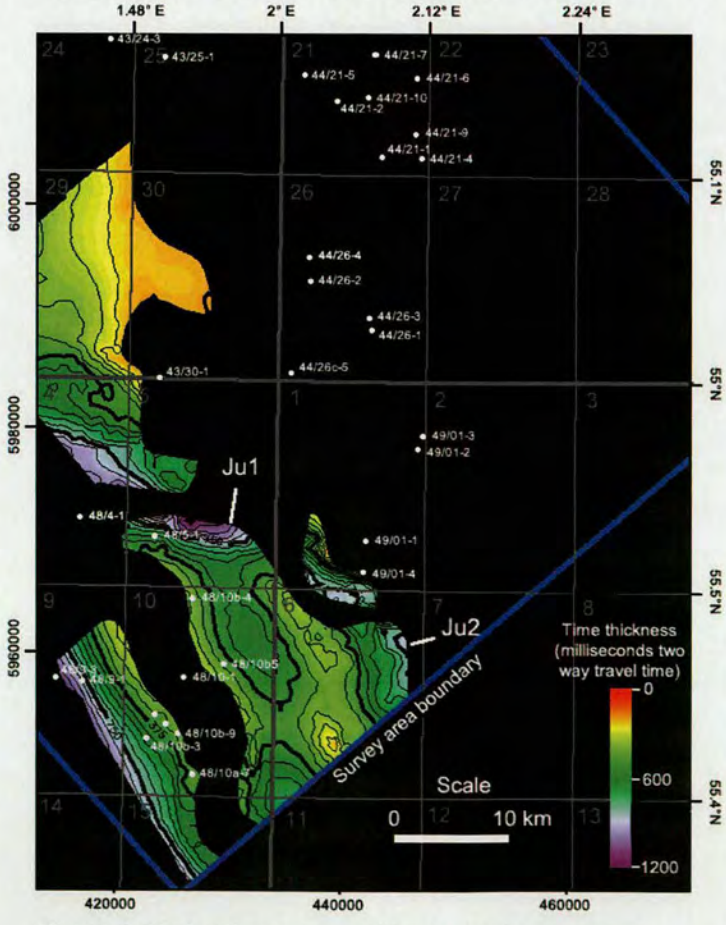

Figure 4.23. Isochron map of the Jurassic sequence

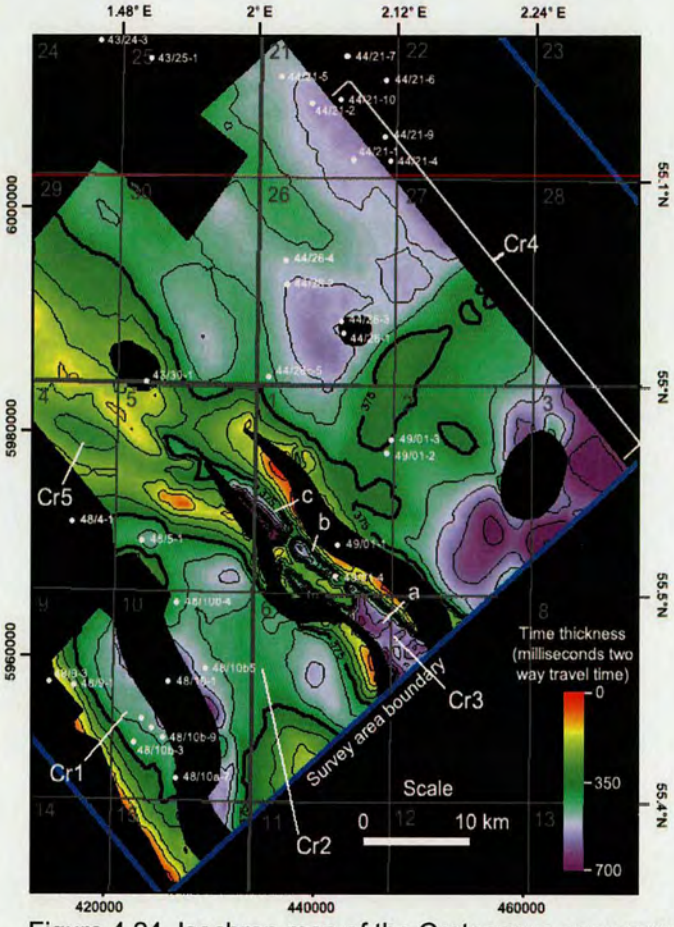

Figure 4.24. Isochron map of the Cretaceous sequence

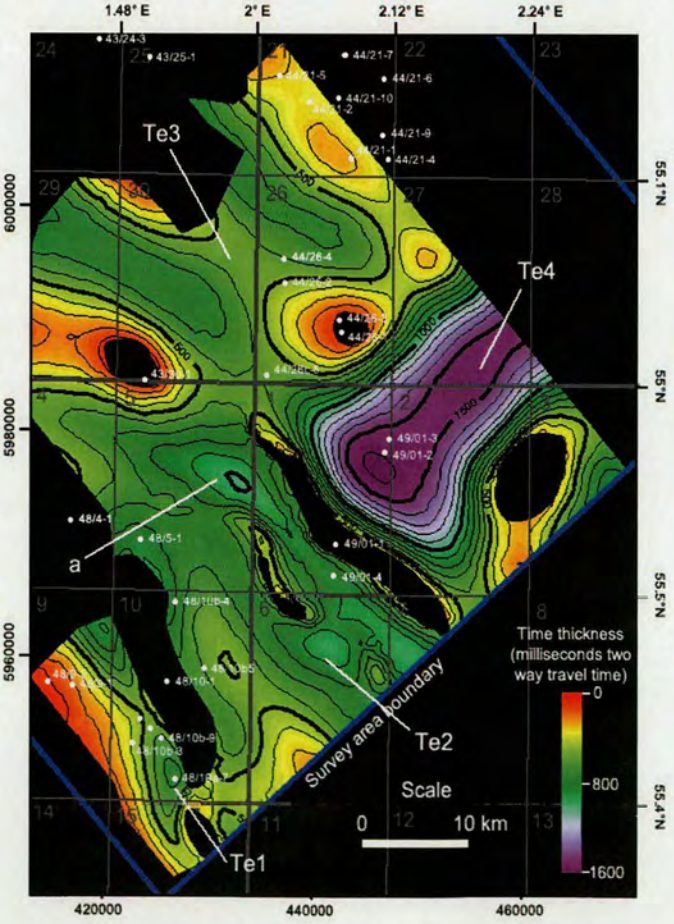

Figure 4.25. Isochron map of the Tertiary sequence

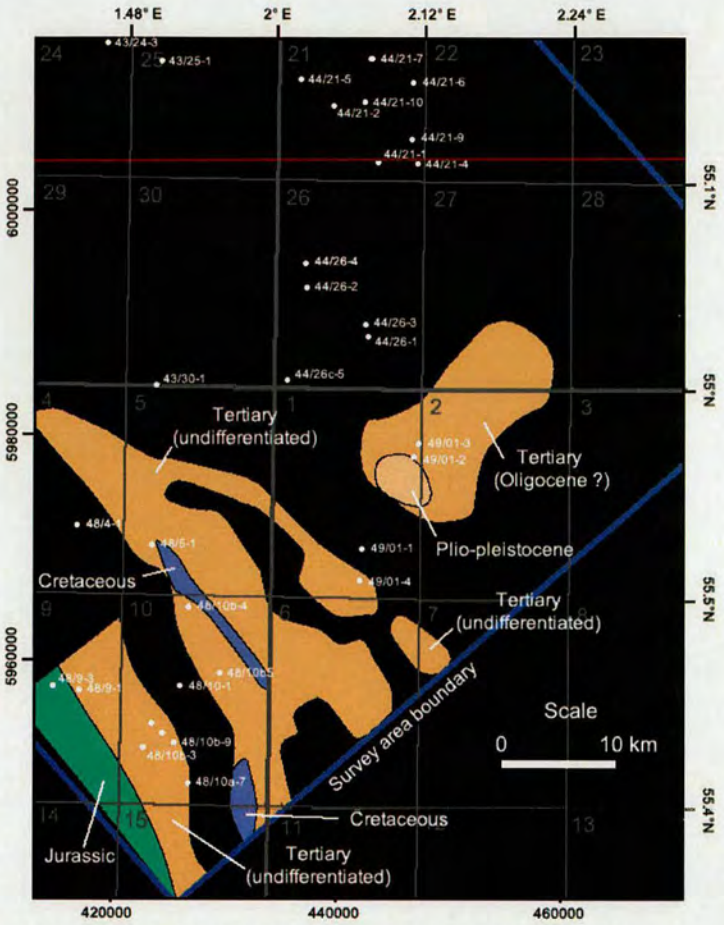

Figure 4.26. Map illustrating the timing of salt weld development in the study area

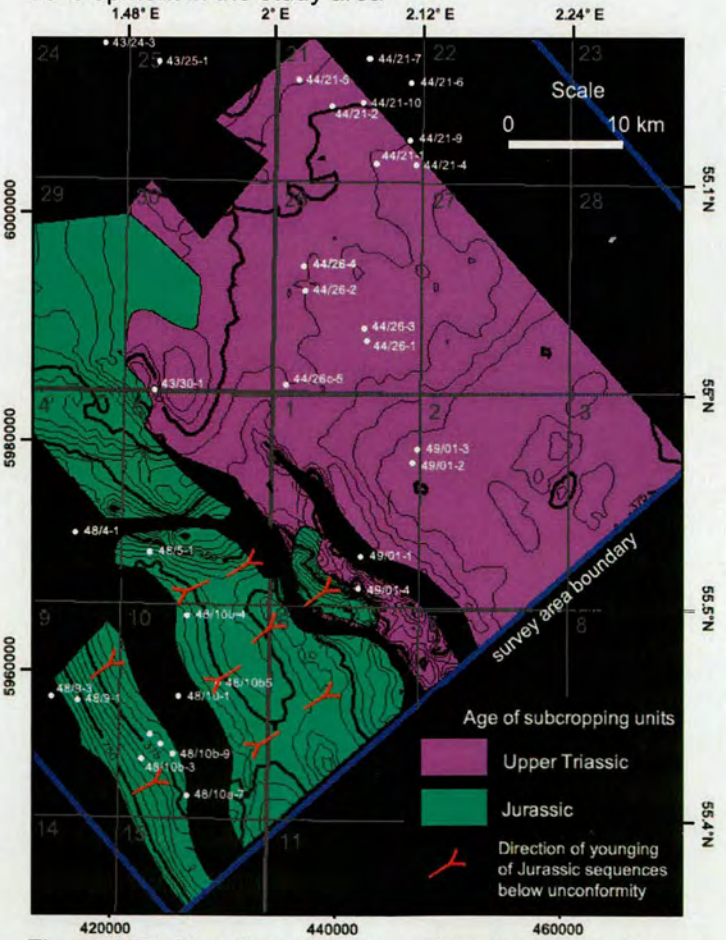

Figure 4.27. Map illustrating the units subcropping the Base Cretaceous Unconformity in the study area

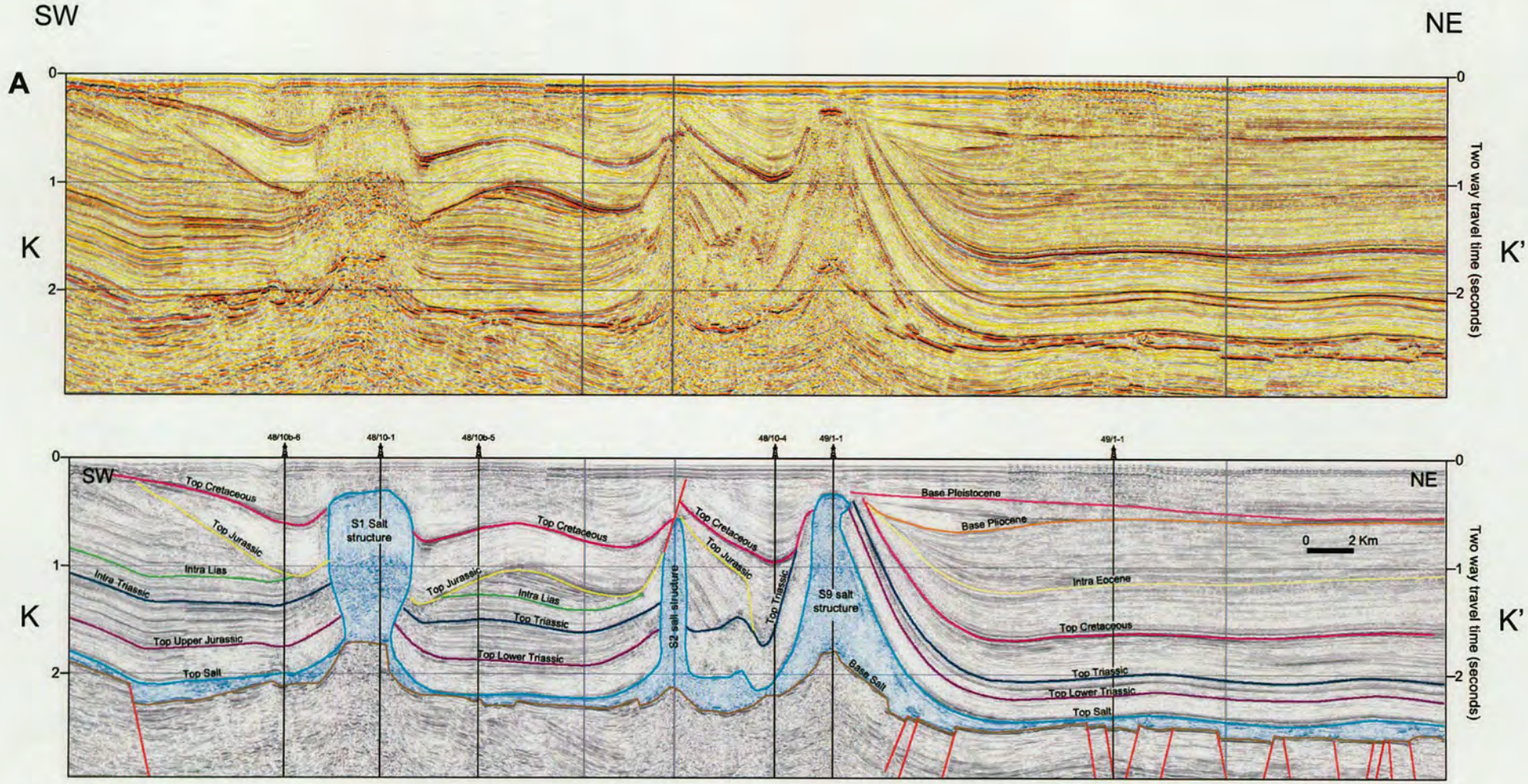

Figure 4.28. Uninterpreted (top) and interpreted (bottom) seismic sections across the study area (A) and a structural restoration of this section (B).

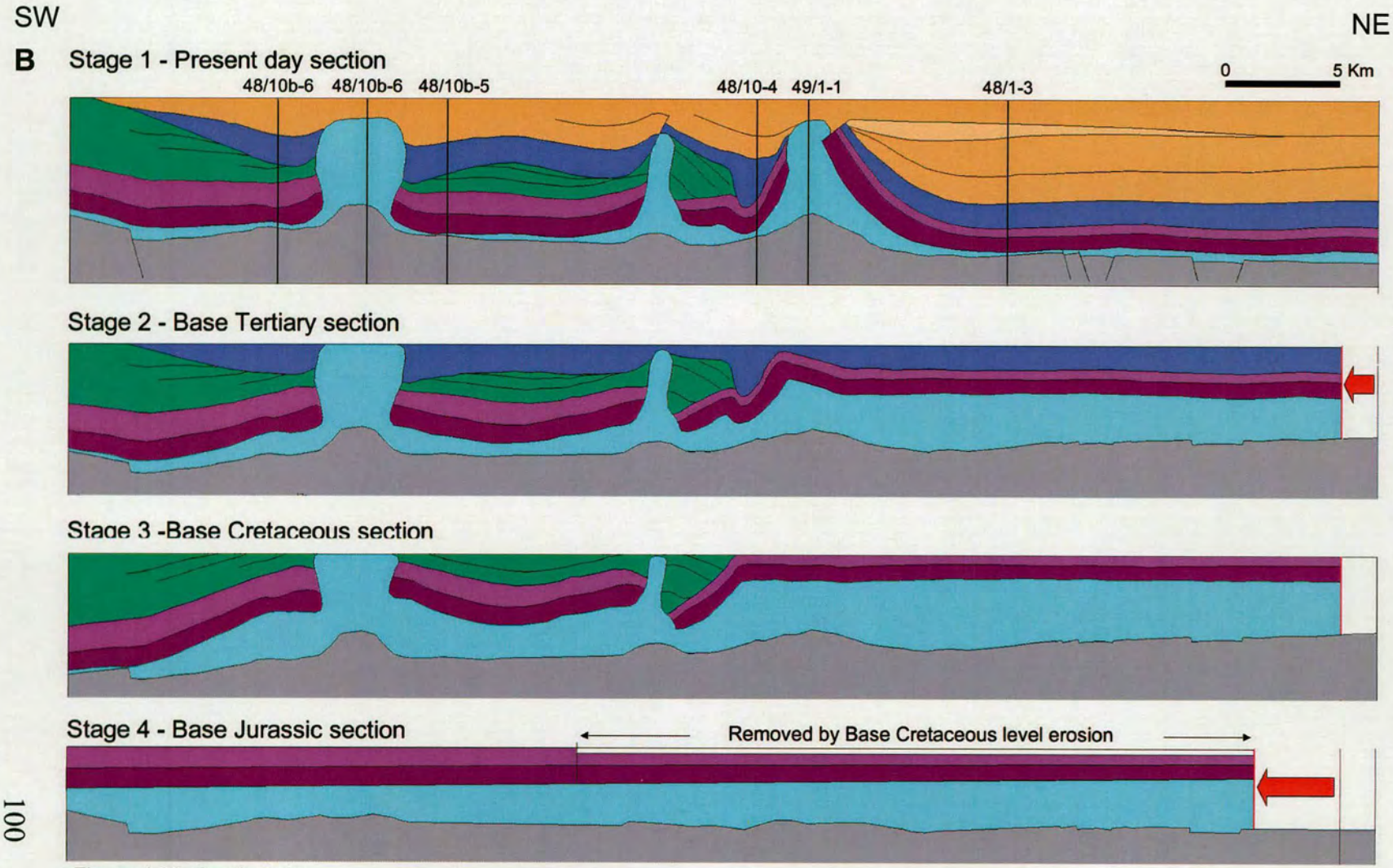

Figure 4.28. Continued

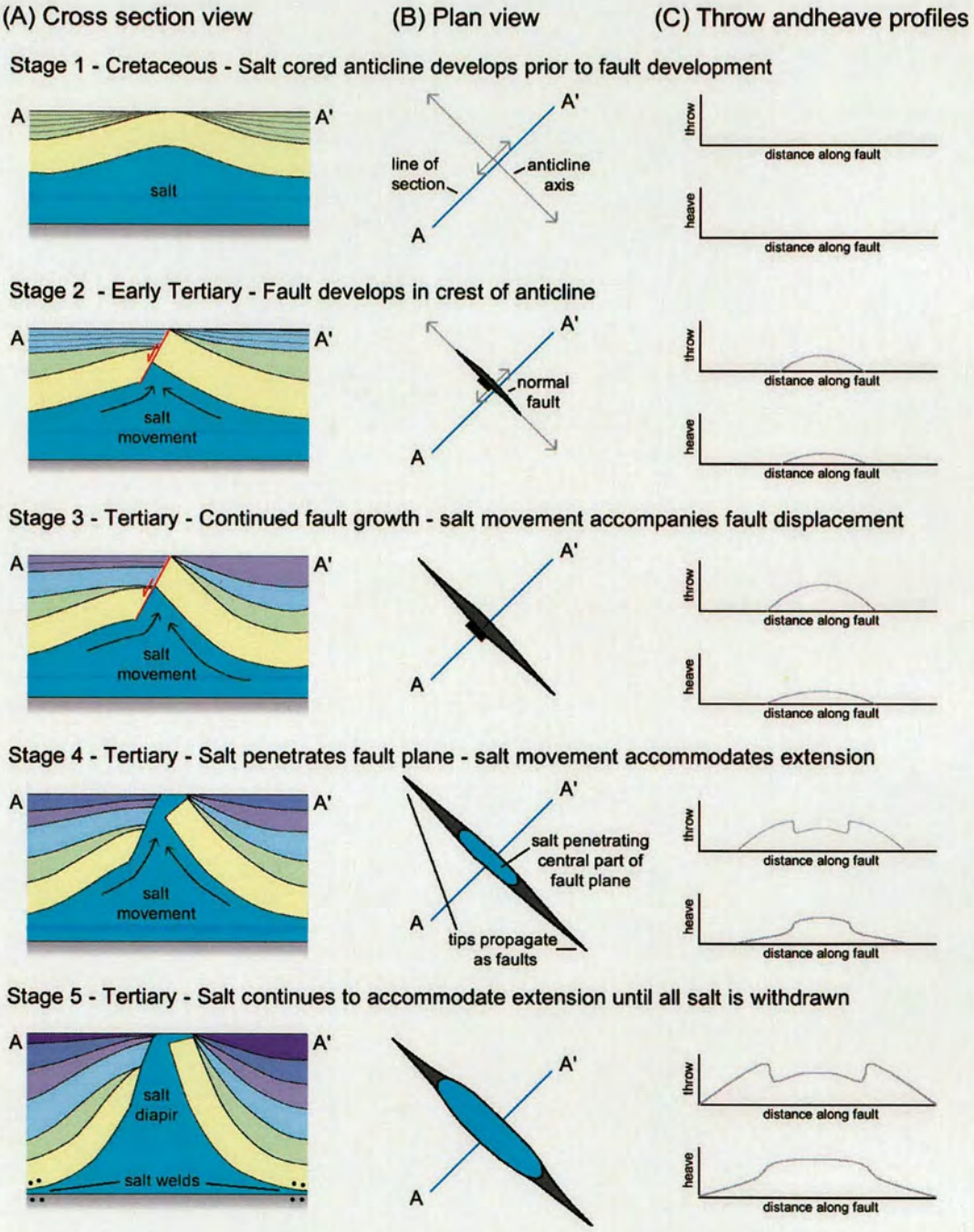

Figure 4.29. Model illustrating the development of the Schooner NE fault system. The model is shown in cross section (A) and plan (B) views and also as throw and heave profiles along the fault system. Note how throw profiles show a significant drop as salt penetrates the fault plane and begins to accommodate extension.

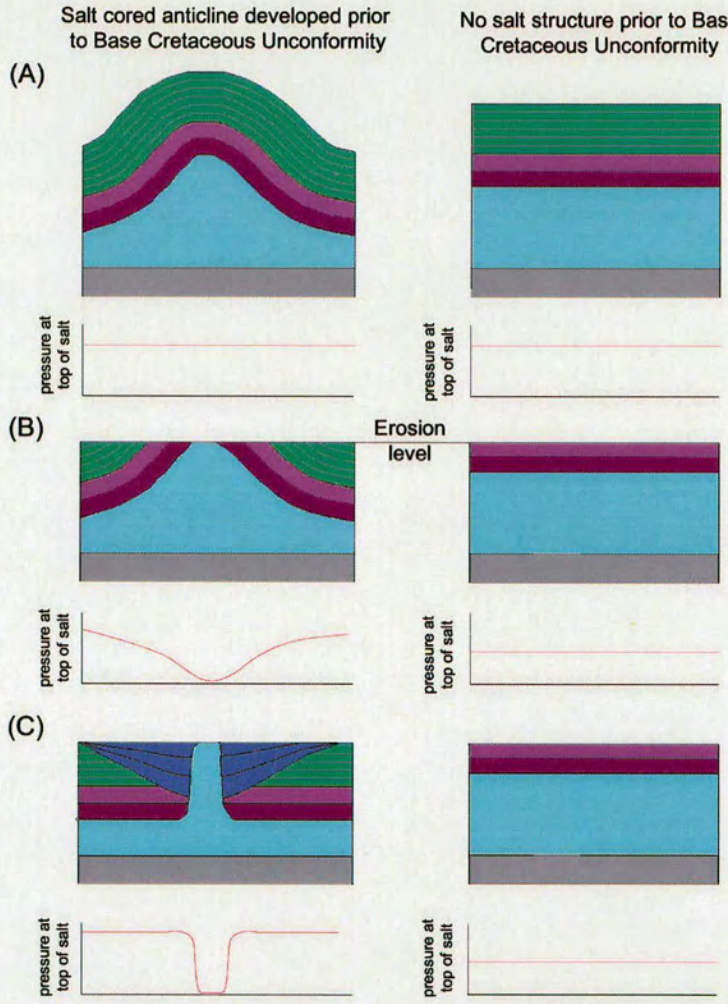

Figure 4.30. Schematic diagram illustrating the varying influence of Base Cretaceous erosion on two different structural geometries. Left shows erosion decapitating a pre-existing salt-cored anticline (I.e as in SW of study area) and right shows a a flat lying sequence as in the NE of the study area. Note how the pressure state in the salt layer is only influenced where a pre-existing salt structure is present

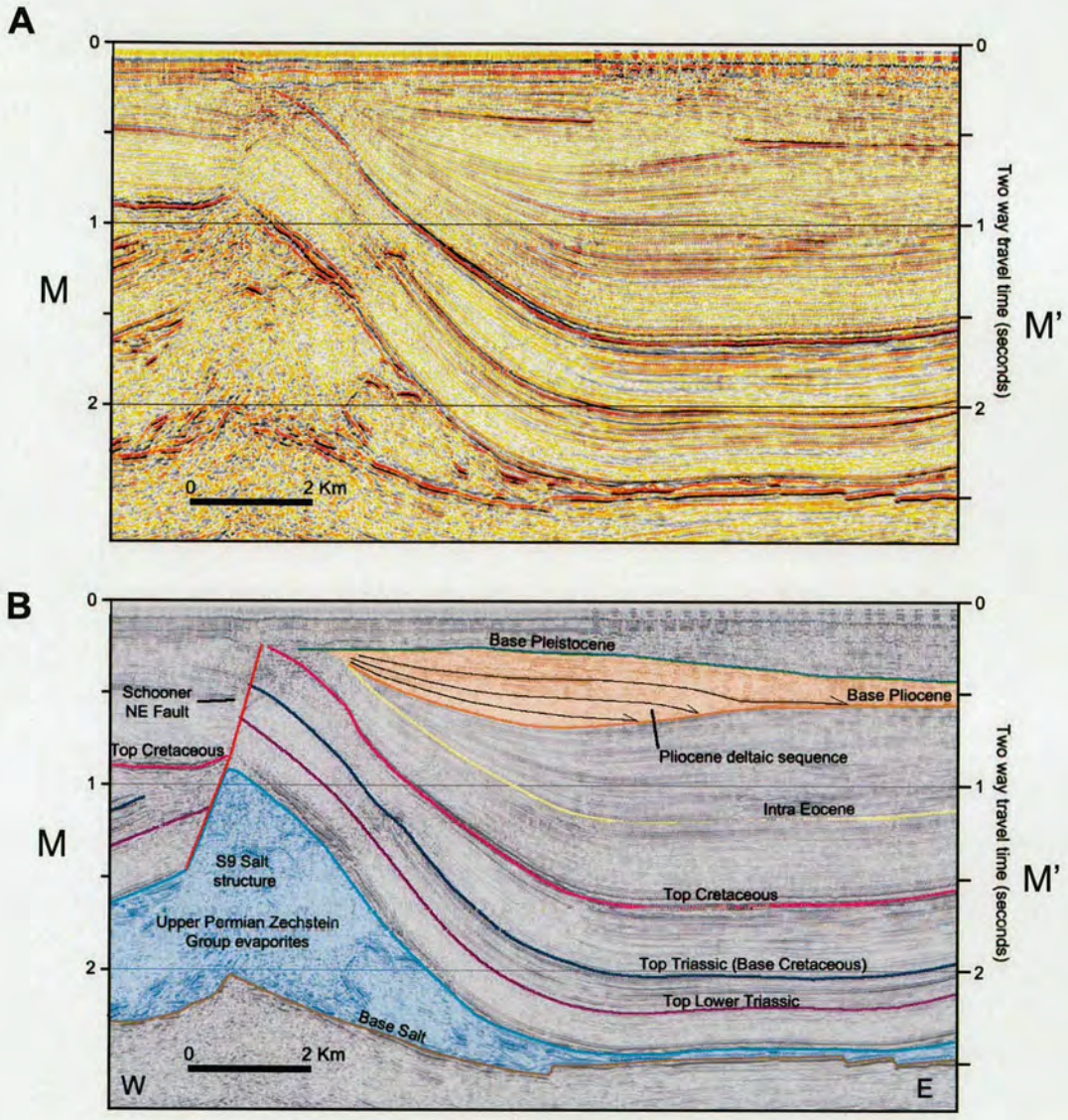

Figure 4.31. Uninterpreted (A) and interpreted (B) seismic sections through the Pliocene deltaic sequence restricted to the Te_4 depocentre.

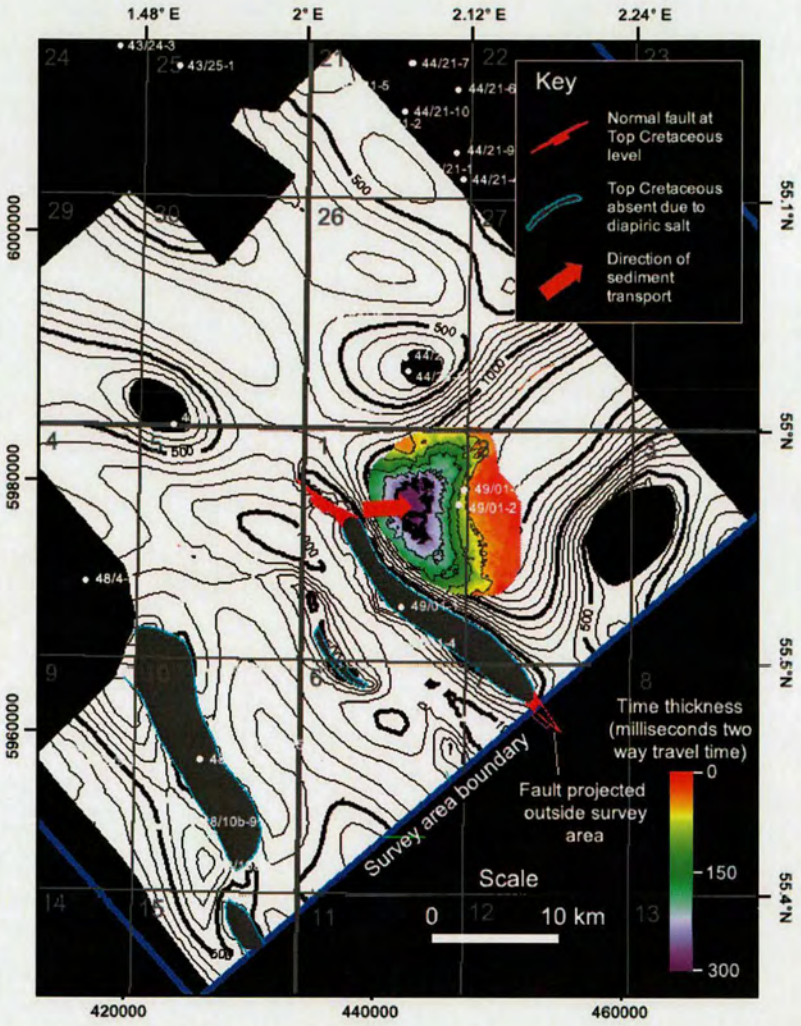

Figure 4.32. Isochron map of the Pliocene deltaic sequence in the Te_4 depocentre (coloured). Where this sequence is not present, contours of structural elevation of the Base Tertiary horizon are shown to illustrate the basin morphology. This sequence is interpreted as being restricted to the Te_4 depocentre and locally sourced from the footwall area of the Schooner NE fault system

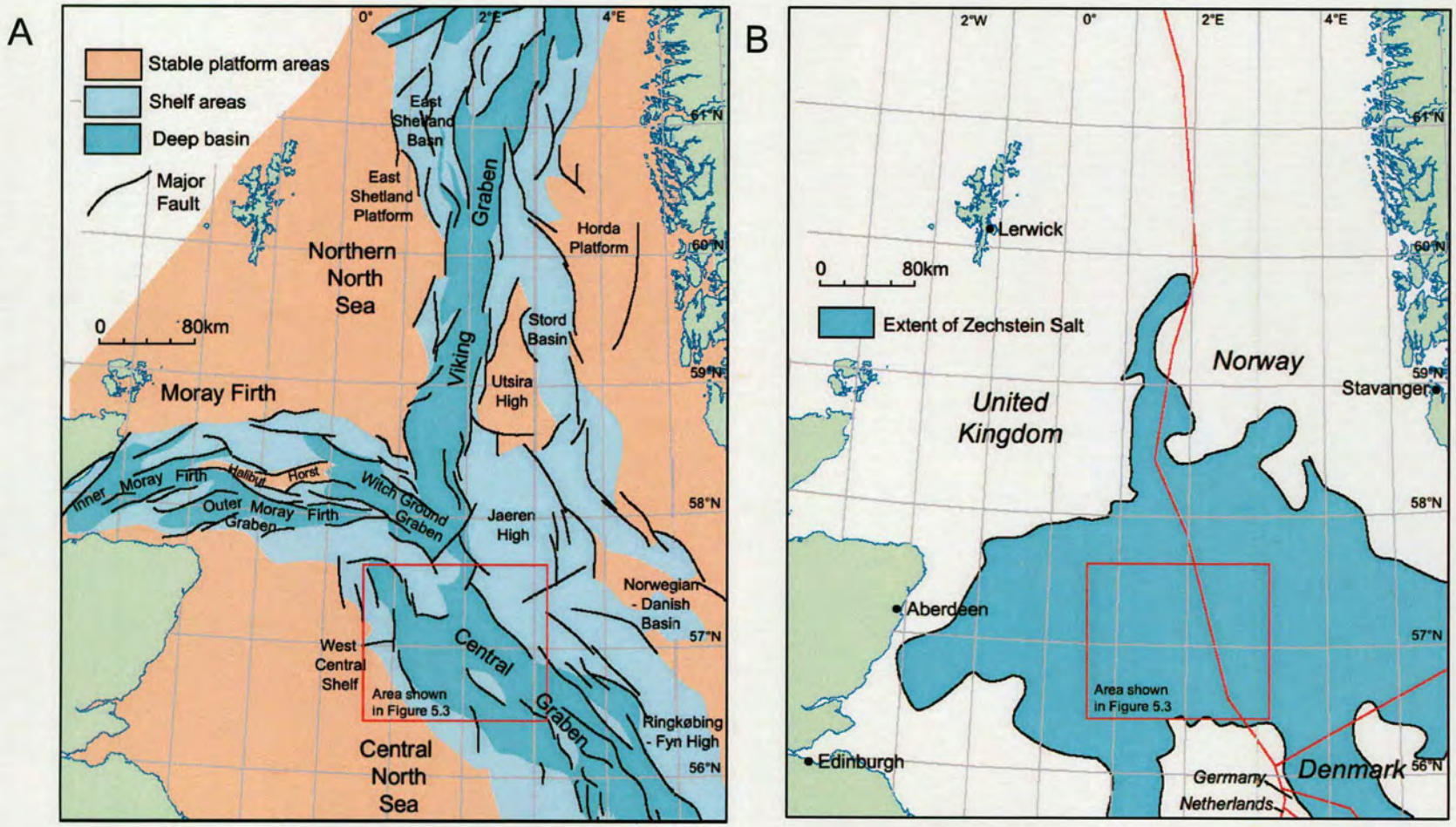

Figure 5.1. Map of the Central and Northern North Sea illustrating the morphology of the three armed Late Jurassic rift system (A) and the extent of deposition of the Upper Permian (Zechstein) salt basin.

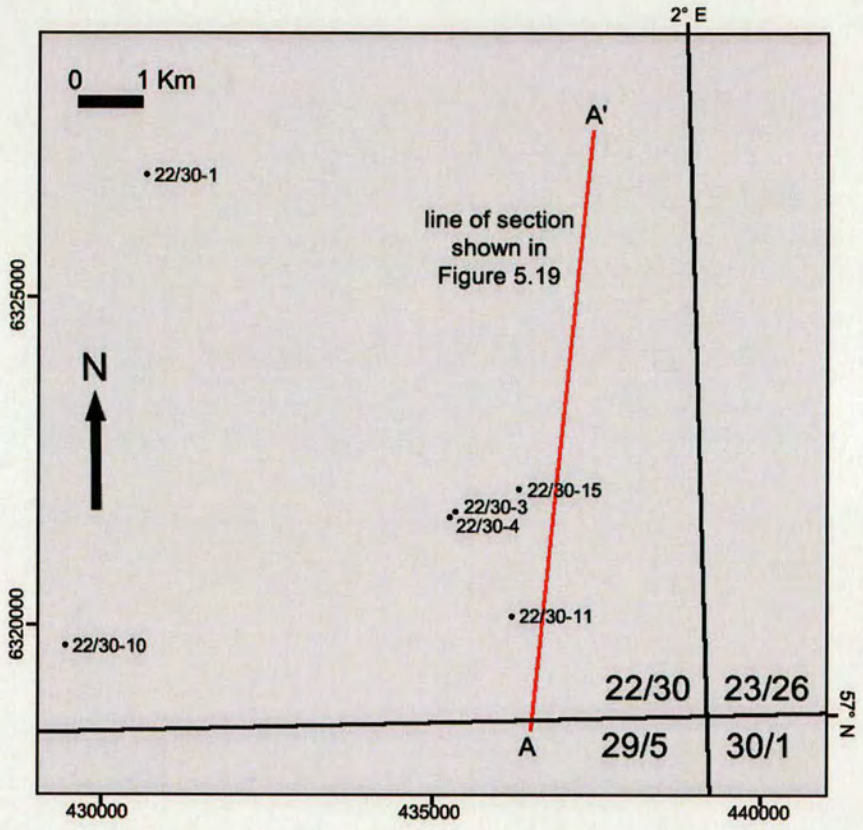

Figure 5.2. Map of the study area illustrating the well coverage in the area and the location of the seismic section shown in Figure 5.19

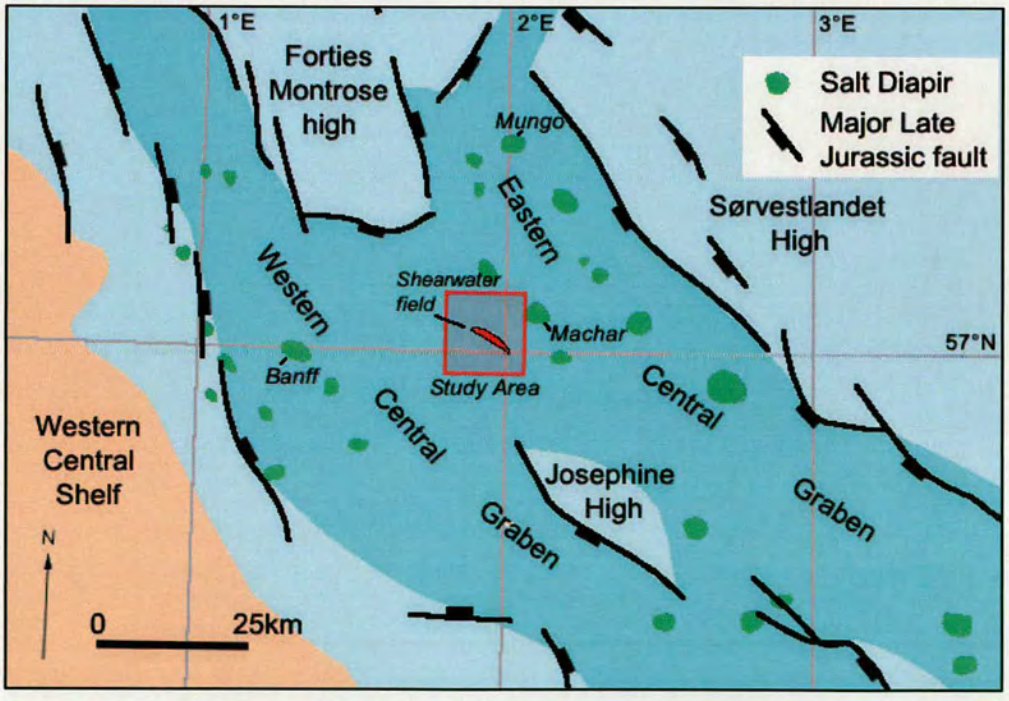

Figure 5.3. Map of the central graben area illustrating the morphology of the major Late Jurassic structures and major salt diapirs in the area as well as the location of the study area

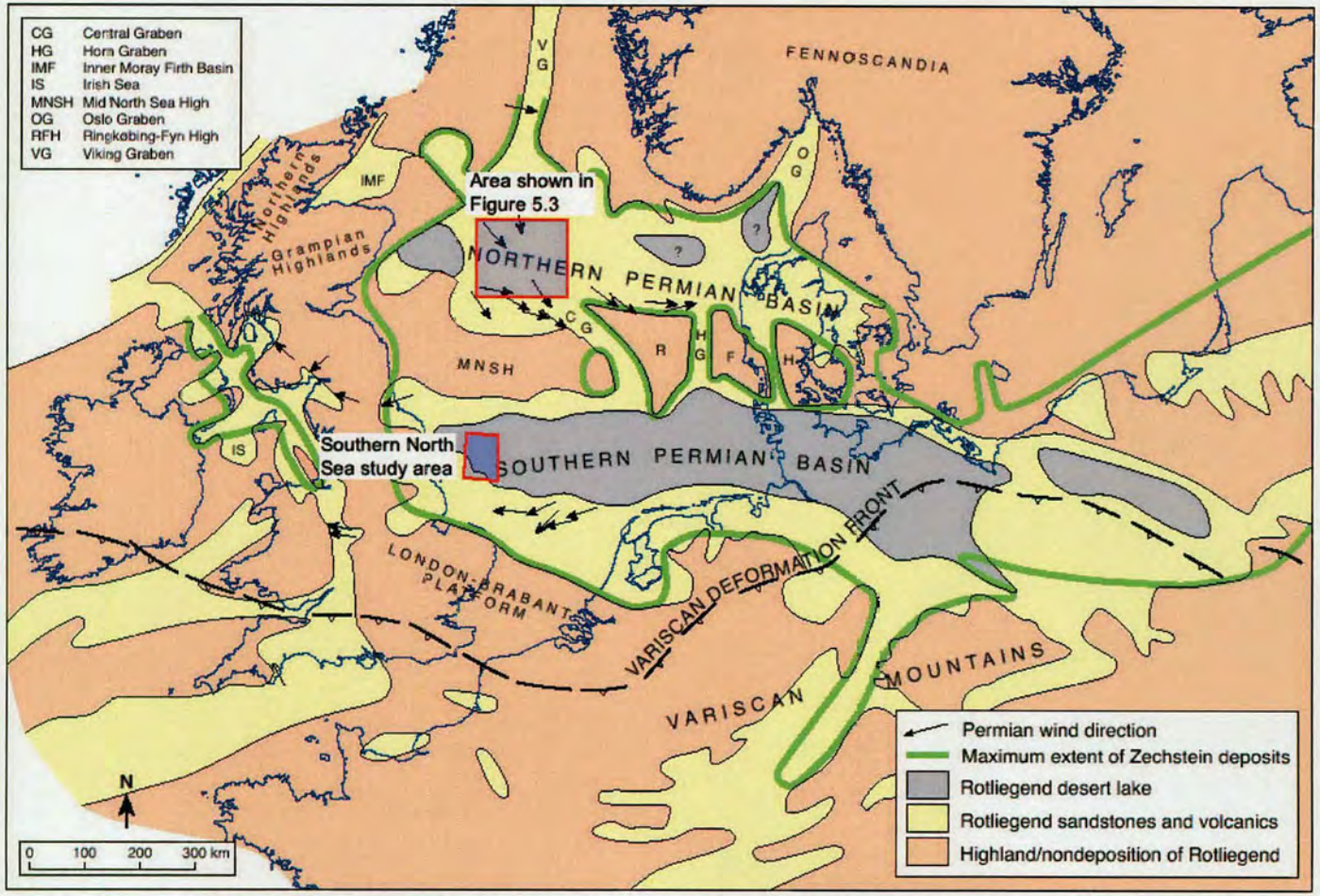

Figure 5.4. Map of NW Europe illustrating the extent of the E-W trending Northern and Southern Permian basins and the extent of deposition of Upper Permian, Zechstein Group evaporite sequences. From Glennie et al. 2003.

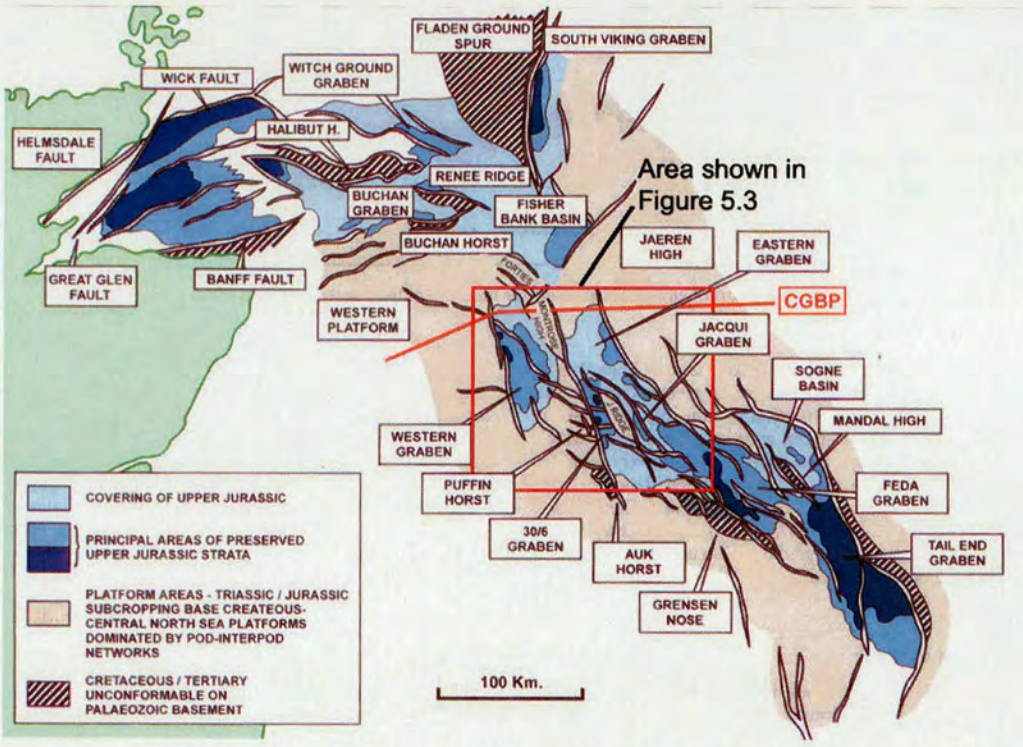

Figure 5.5. Map of the Central North Sea illustrating the main structural aspects of the Late Jurassic Rift system in the area. From Erratt et al. 1999

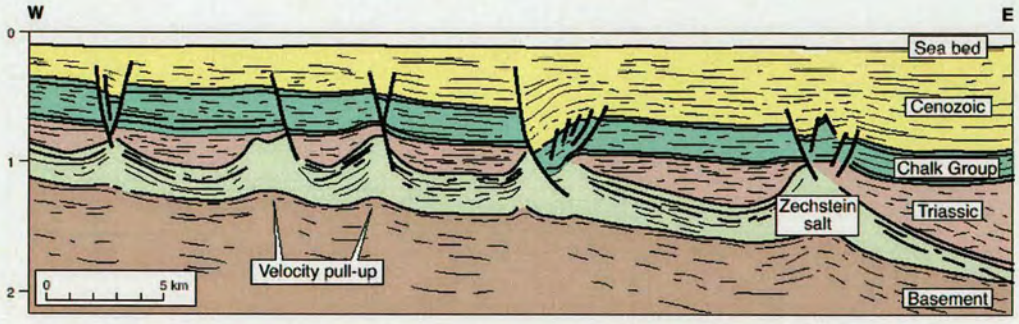

Figure 5.6. Line drawing of a seismic section illustrating the typical structural and salt tectonic style in the western platform area of the Central North Sea. From Zanella and Coward (2003).

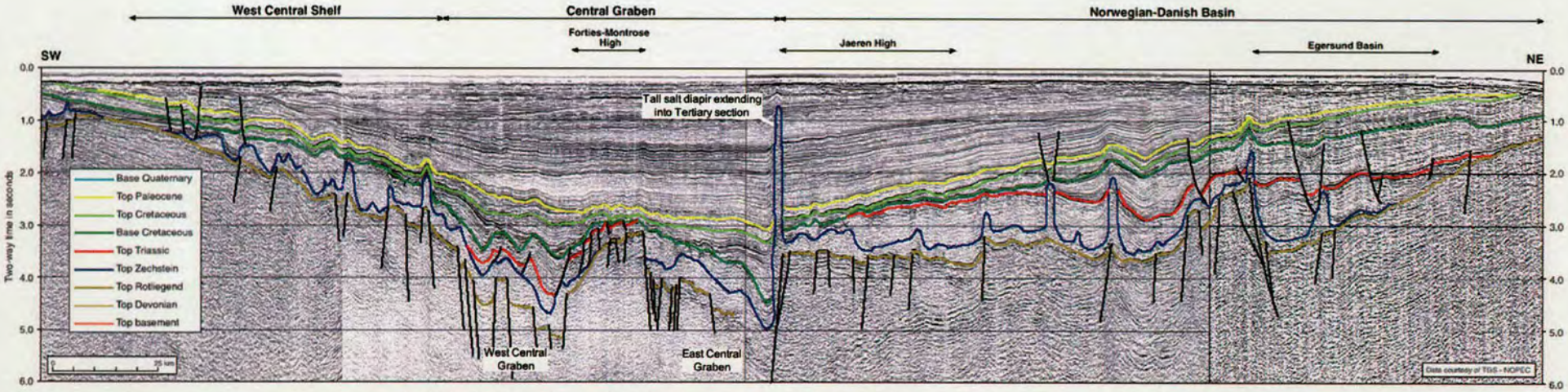

Figure 5.7. Cross section across the Central North Sea illustrating the large scale rift morphology and lack of correlation between deformation in the sub-salt and supra-salt. Modified from Zanella and Coward, 2003.

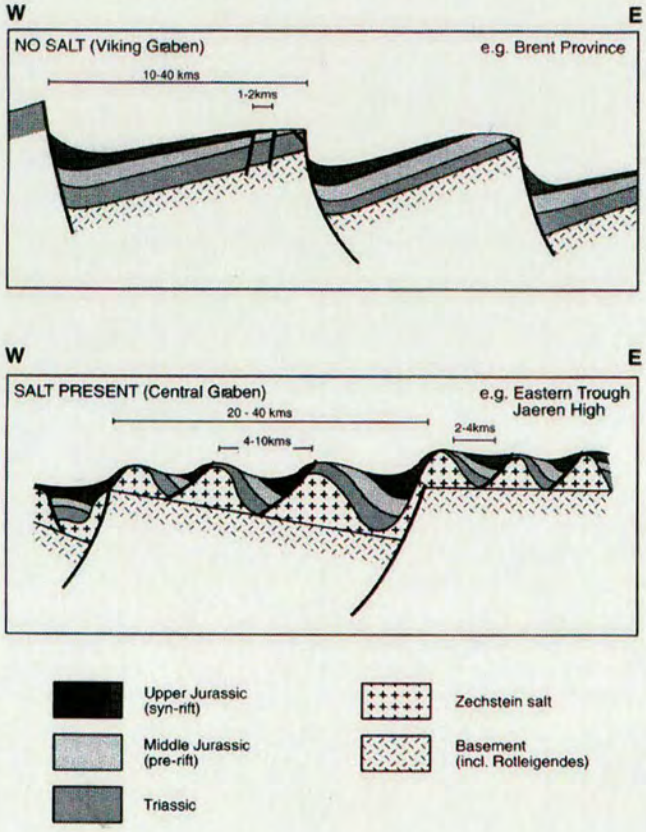

Figure 5.8. Schematic diagram illustrating the structural wavelength of sub-salt and supra-salt structures associated with Late Jurassic extension (lower) relative to the salt free Viking Graben (upper) from Hodgson et al. (1992).

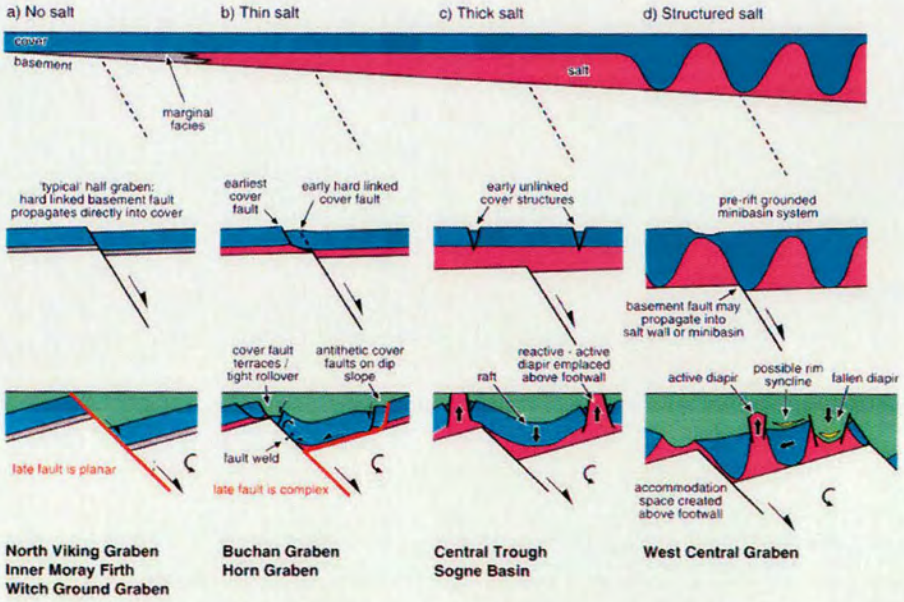

Figure 5.9. Schematic diagram illustrating how structural styles developed in the supra-salt sequence vary with changing salt thickness during Late Jurassic rift development (From Stewart and Clark, 1999)

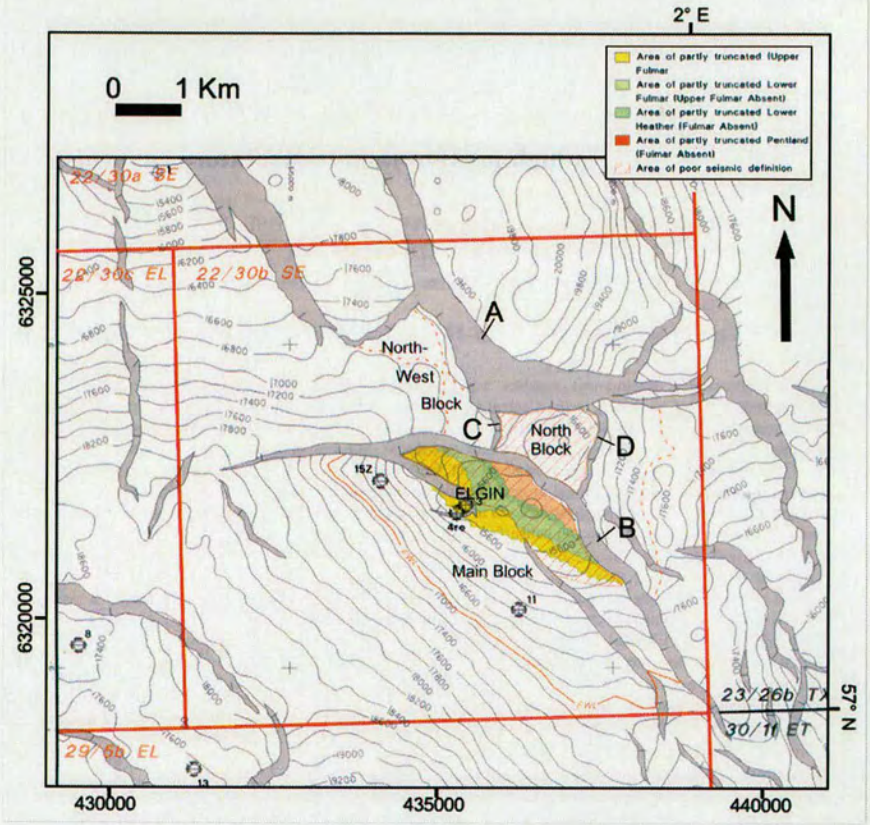

Figure 5.10. Published structural interpretation of the Shearwater prospect from Blehaut et al. (1999). Note that this figure has been modified to fit into the area shown in maps of the study area shown in this study.

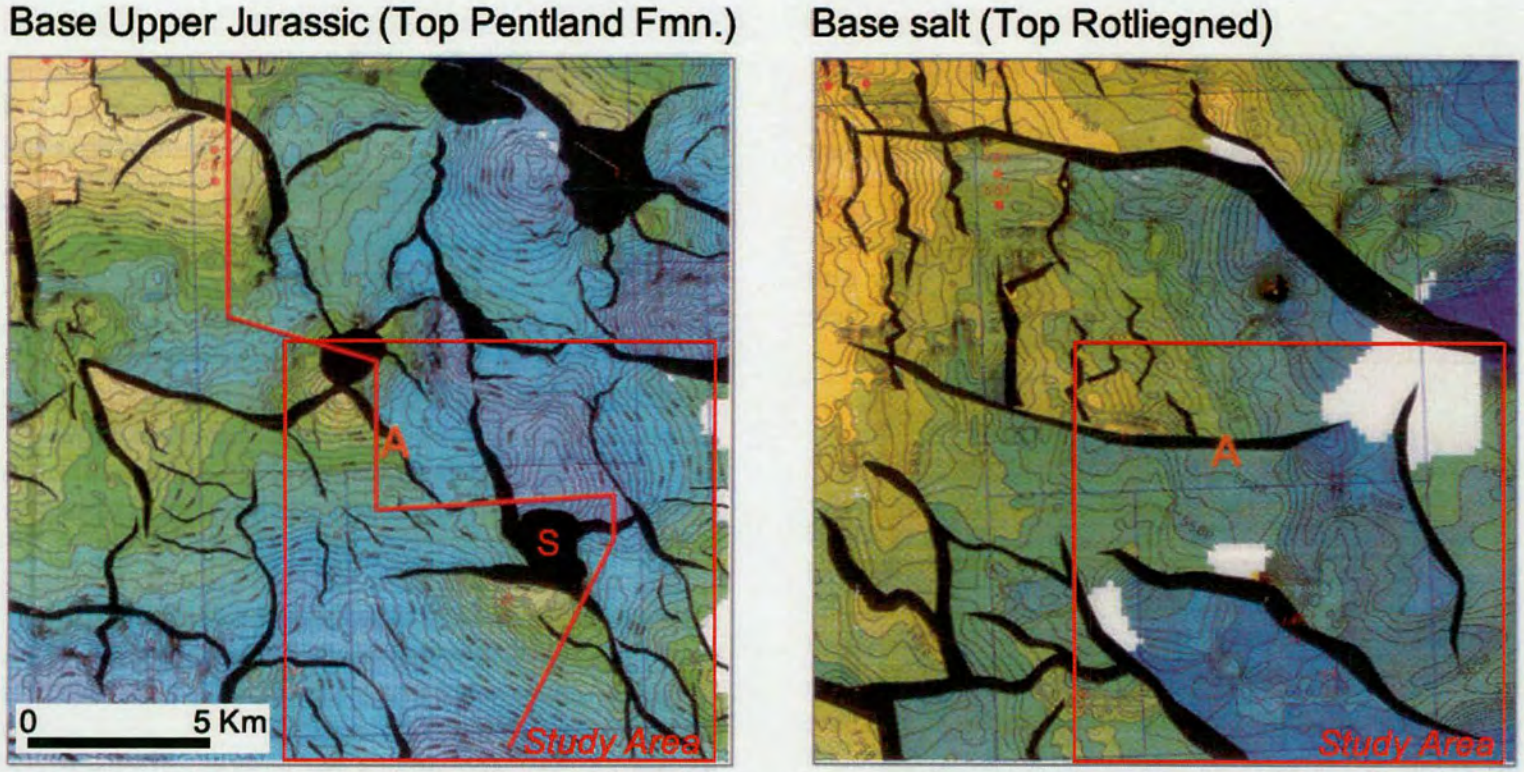

Figure 5.11. Published structure maps of the Base Upper Jurassic (pre-rift) surface (a) and base salt (b) surfaces from Helgeson (1999). Note the original maps have been modified to show the location of the study area. The location of the seismic section shown in Figure 5.12 is shown by a line marked by an A and the Shearwater Fault system is marked by an 'S'.

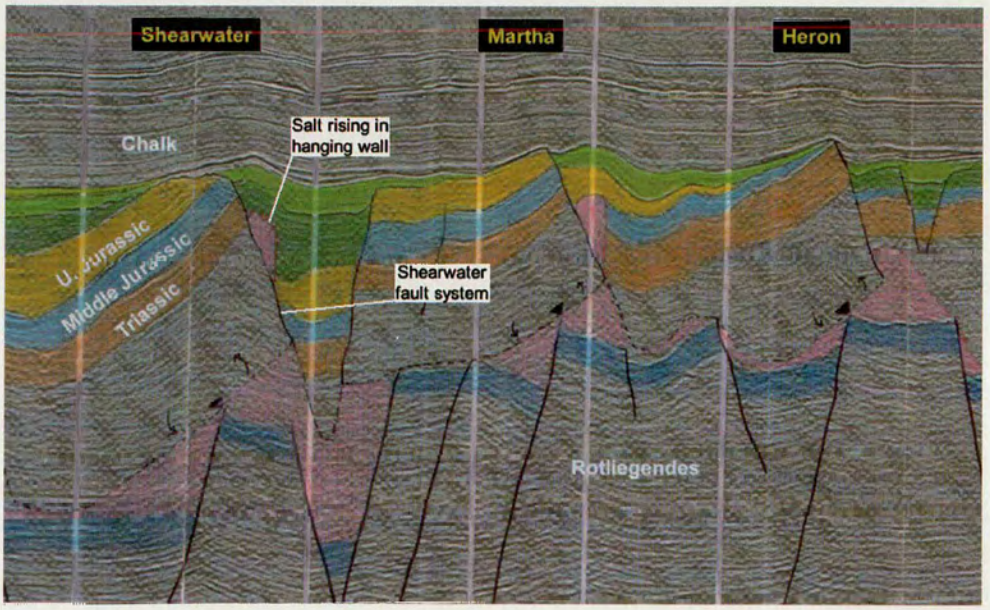

Figure 5.12. Published seismic section through part of the Central Graben including the Shearwater Fault system illustrating the structural interpretation of Helgeson (1999). Note how this section illustrates the salt associated with the Shearwater Fault system to be located in the hanging wall to the fault system. Modified from Helgeson (1999).

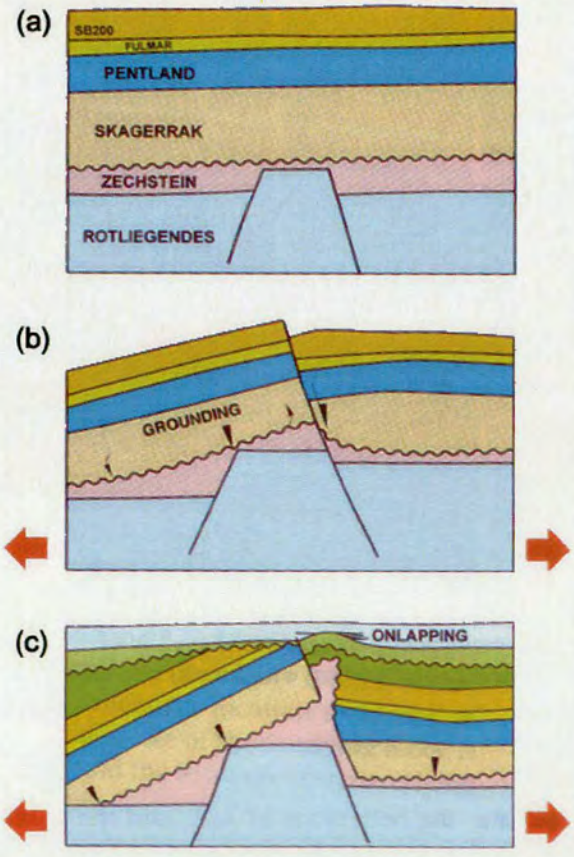

Figure 5.13. Cartoon model illustrating the development of supra-salt fault systems in the HP/HT province of the Central Graben. Modified from Helgeson (1999).

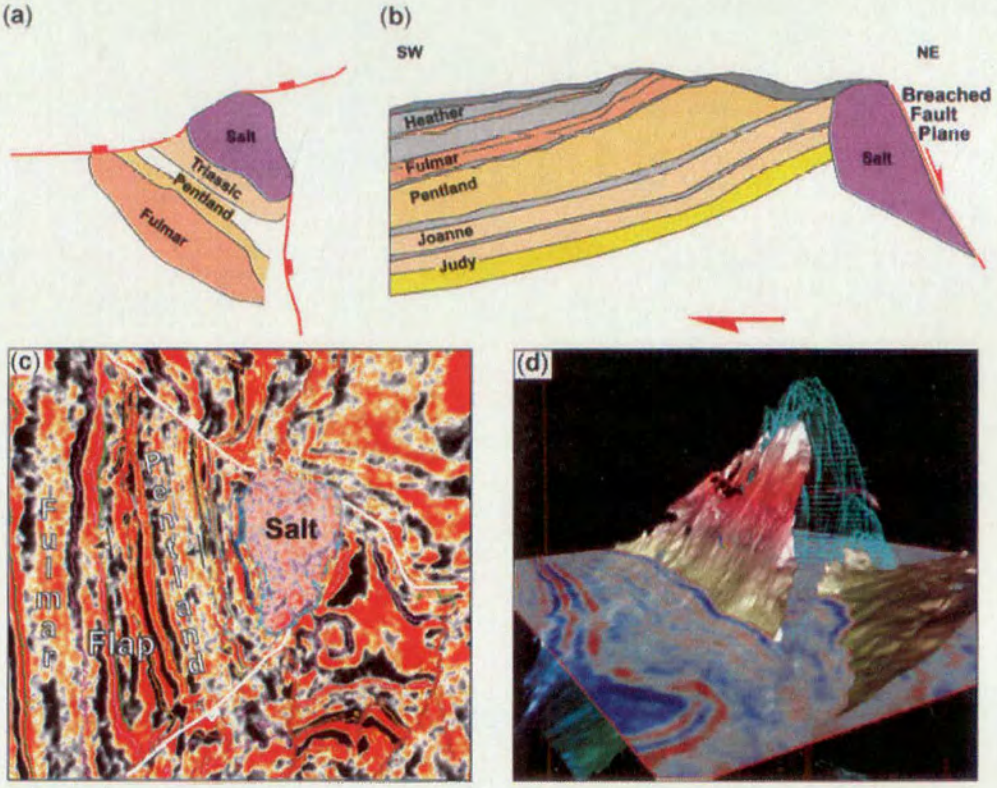

Figure 5.14. Plan view (a), cross section view (b), timeslice (c) and 3D visualisation of the Shearwater Fault System illustrating the structural interpretation of Dooley et al. (2005). The illustrated interpretation differs significantly from the interpretation detailed in this study in that it illustrates a 3 armed fault system rather than a 4 armed fault system (compare with (a) with Figure 5.21 and (c) with Figure 5.16). The illustrated interpretation also suggests the salt structure has breached the fault plane whereas in this study this is not considered to be the case. Figure from Dooley et al . (2005).

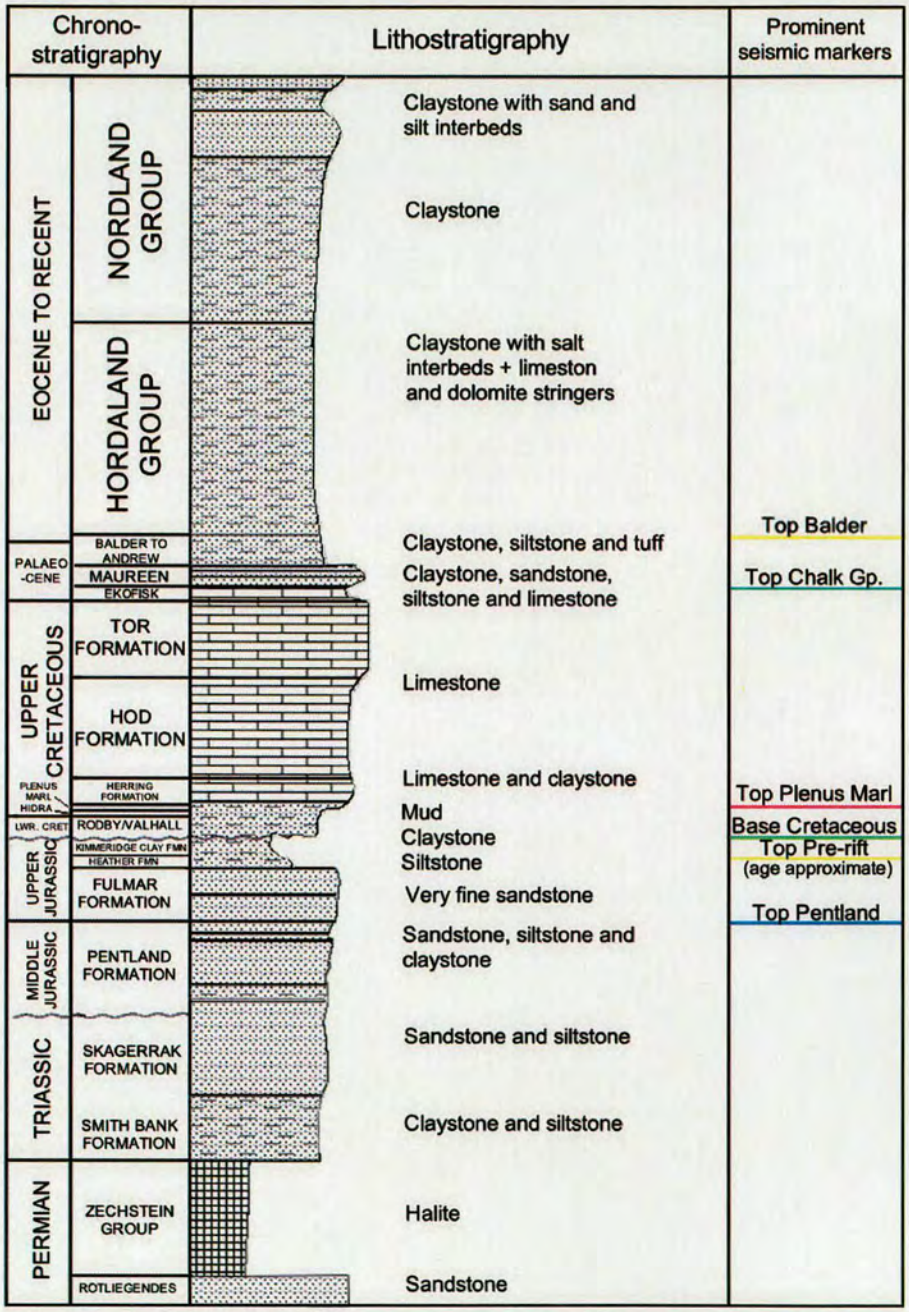

Figure 5.15. Stratigraphic column showing the main lithostratigrahic units of the study and the prominent seismic markers (after Lasocki et al., 1999).

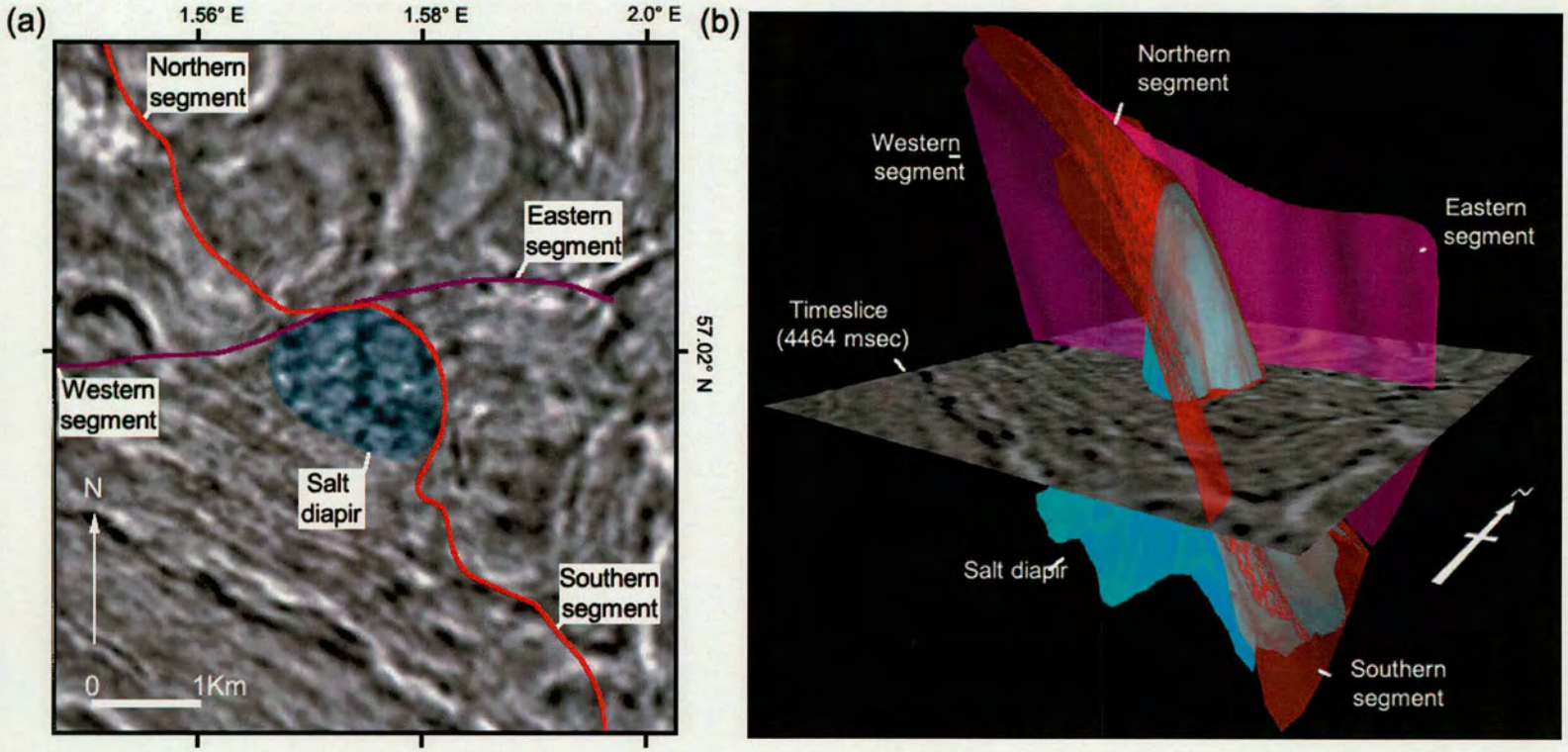

Figure 5.16. Timeslice through the central area of the Shearwater Fault system (4464 milliseconds) illustrating how fault segments intersect around the salt diapir (a) and a 3D view of the fault system illustrating the location of the timeslice (b).

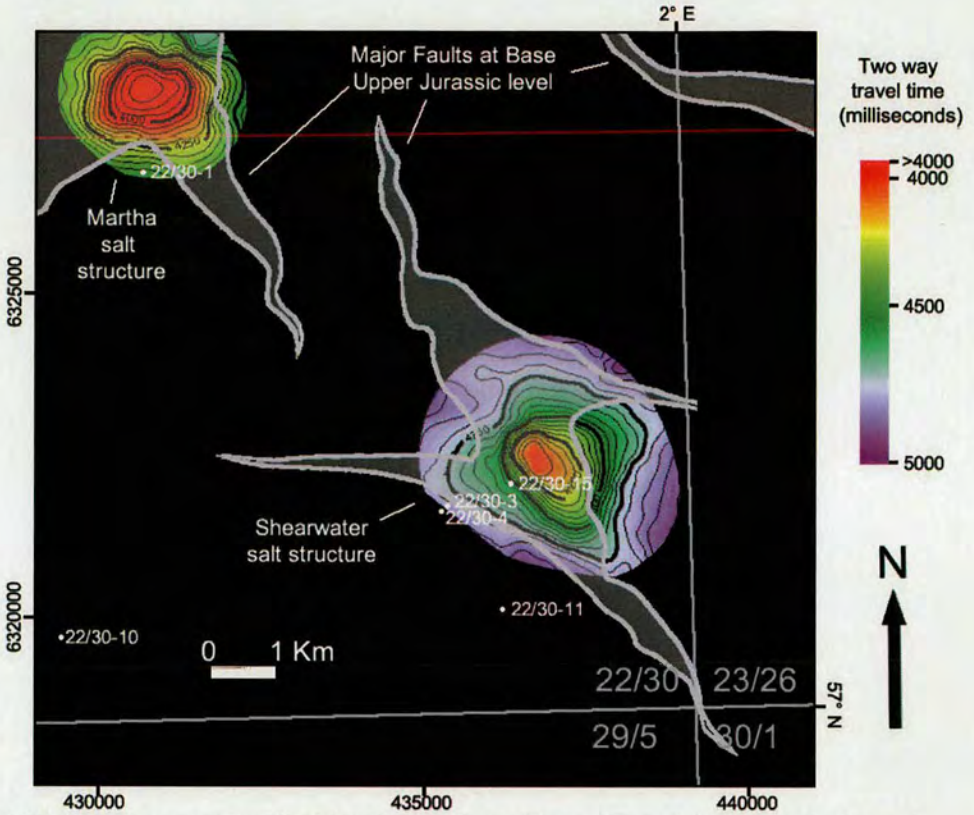

Figure 5.17. Structure map on the Top Salt horizon (Top of Permian Zechstein Group) illustrating the location of salt structures in the study area. Due to constraints of the data the Top of the salt sequence can only be resolved in the salt structures.

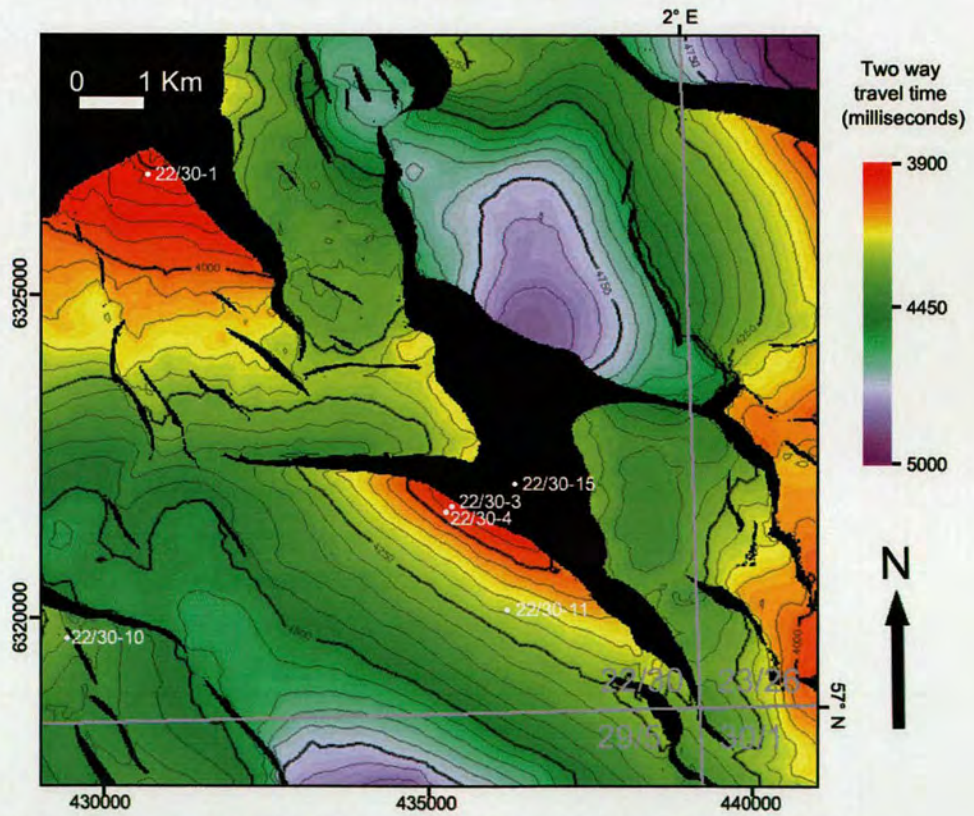

Figure 5.18. Structure map of the Pre-rift, Base Upper Jurassic (Top Pentland Formation) horizon illustrating the structural geometry developed due to the Shearwater Fault System.

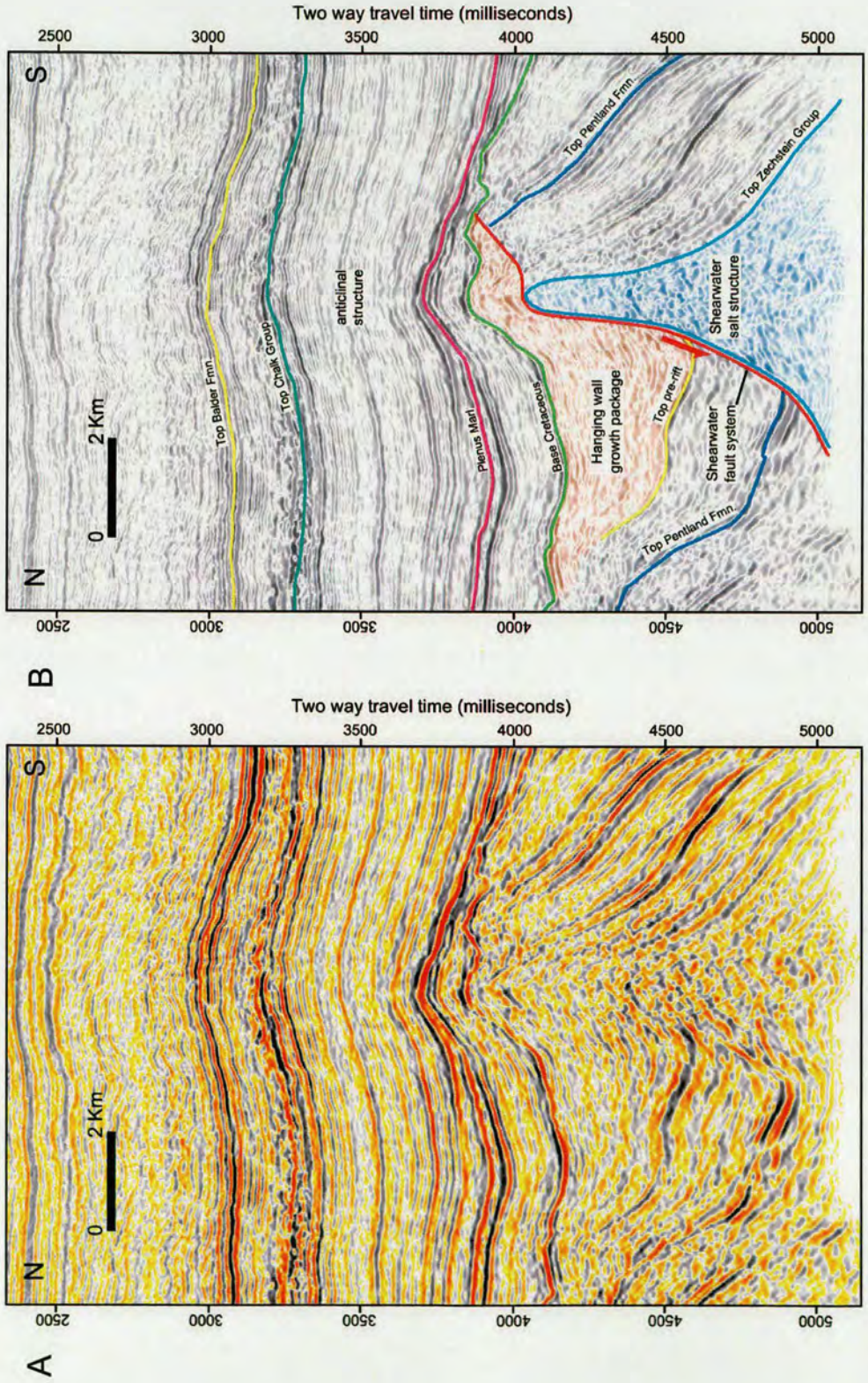

Figure 5.19. Uninterpreted (a) and interpreted (b) seismic sections through the study area illustrating the structural style of the Shearwater fault system and its relationship to the Shearwater salt structure

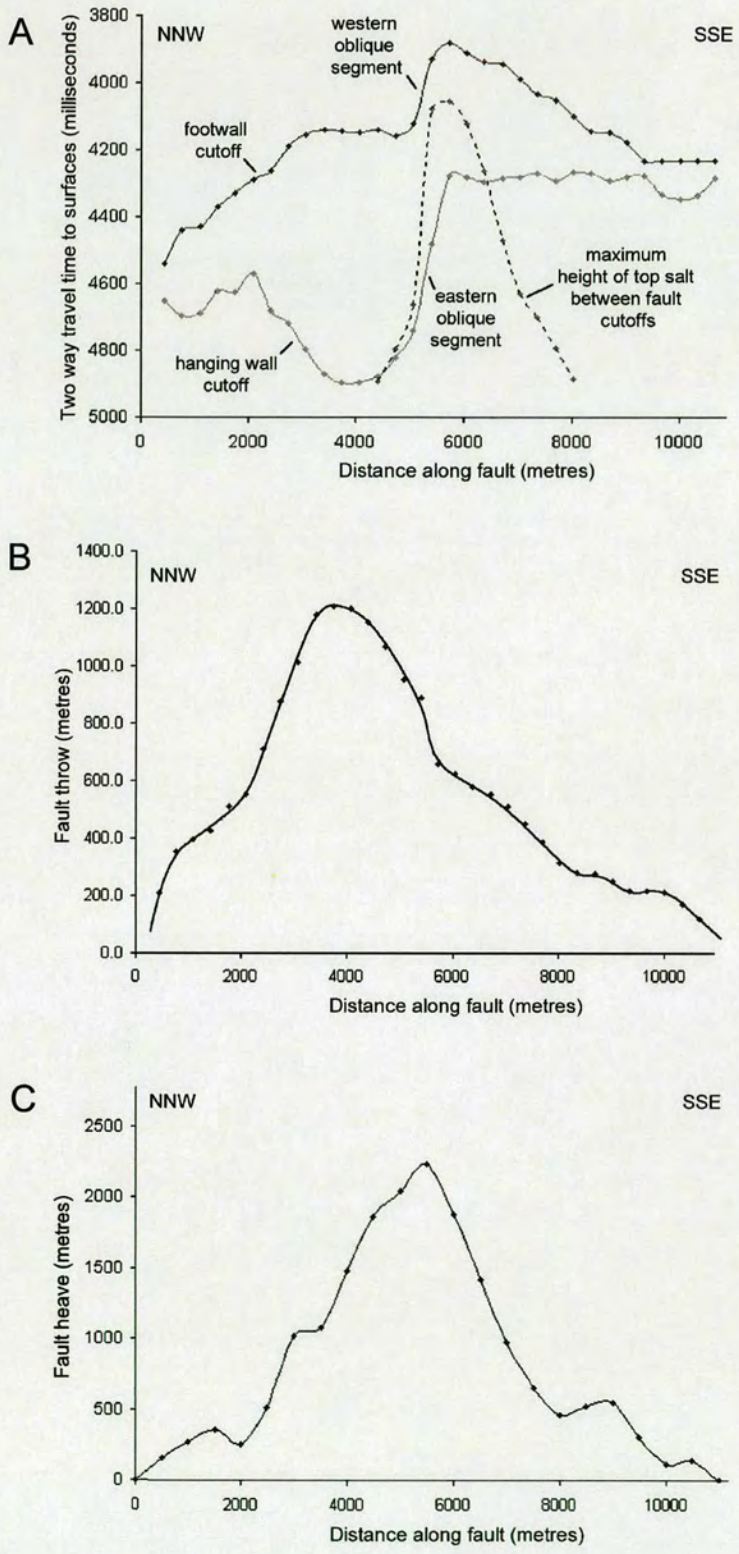

Figure 5.20. Cut-off elevation profile (A), displacement-length profile (B) and heave-length profile (C) along the NNW-SSW trending part of the Shearwater Fault System. Note B is depth converted from the original two-way travel times using the technique detailed in Appendix 1. Profiles are based on the elevations and separation of the Base Upper Jurassic (Top Pentland Formation) horizon.

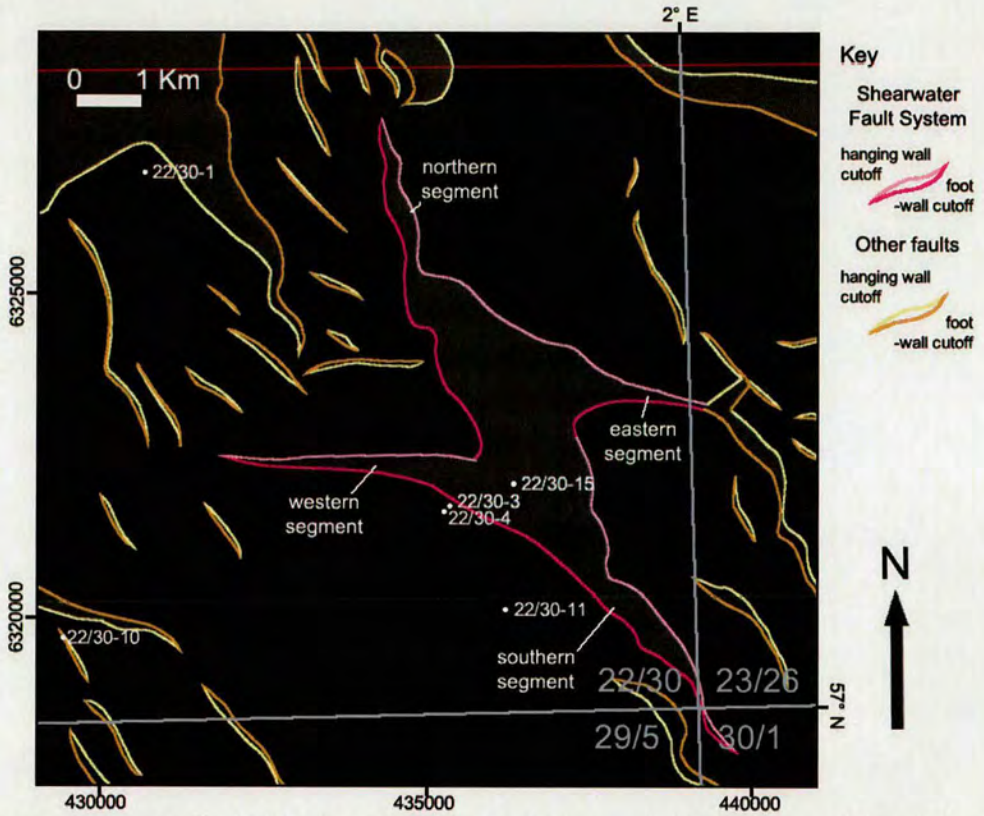

Figure 5.21. Map illustrating the location of faults mapped at Base Upper Jurassic level (Top Pentland Formation) in the study area

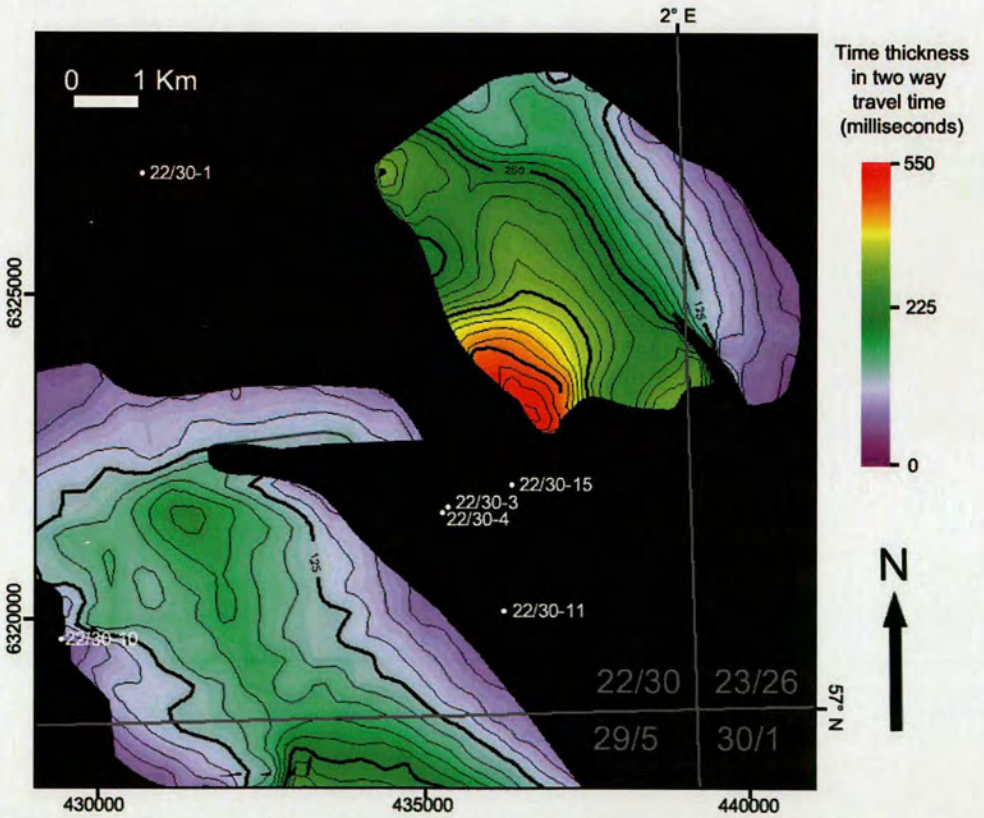

Figure 5.22. Isochron of the Upper Jurassic syn-rift sequence in the study area

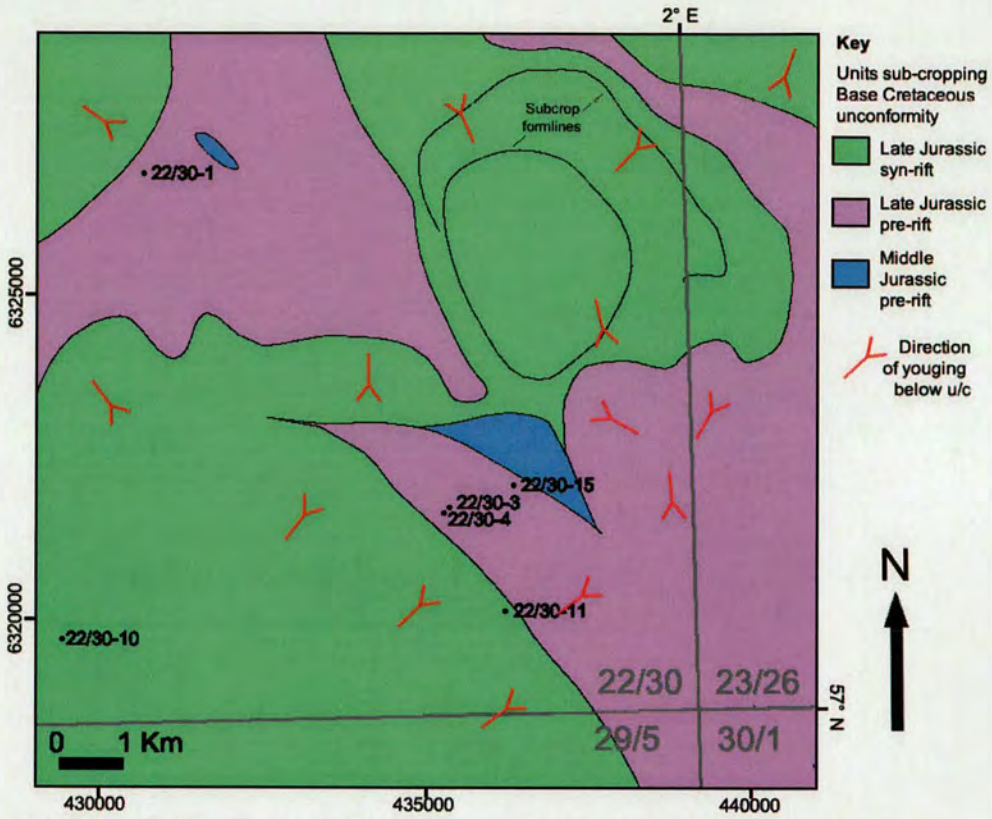

Figure 5.23. Map illustrating the units sub-cropping the Base Cretaceous Unconformity in the study area

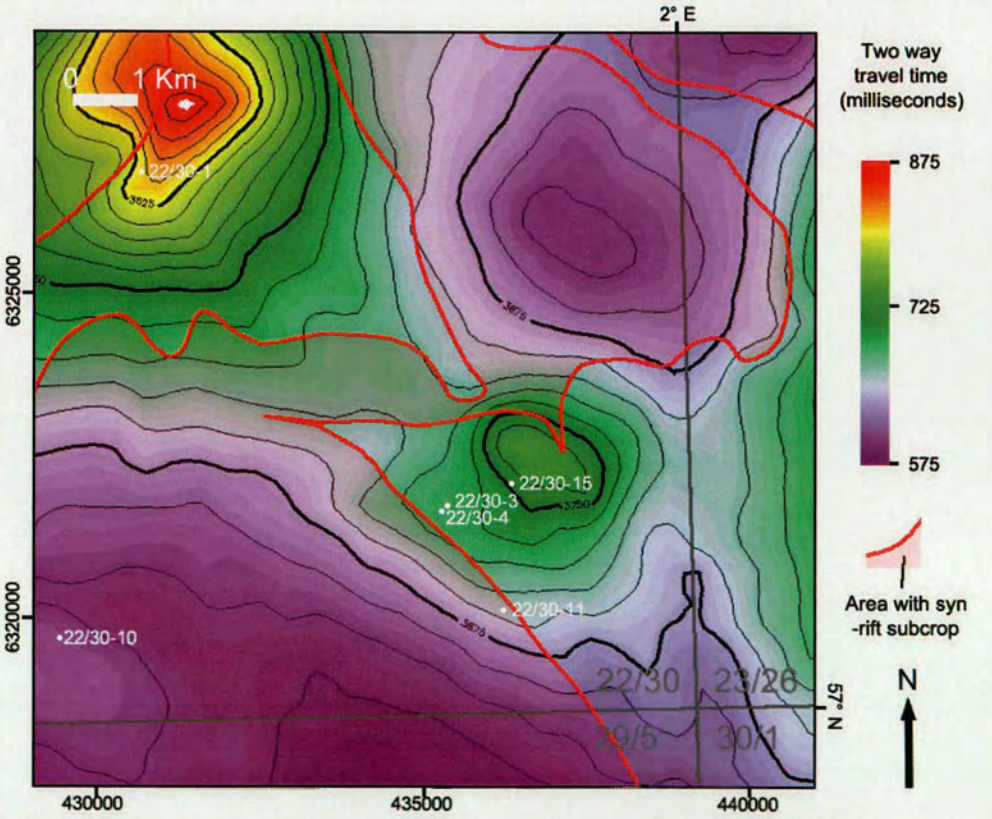

Figure 5.24. Structure map on the Upper Cretaceous Top Plenus Marl Formation horizon. Red tinted areas show where the base Cretaceous Unconformity has a syn-rift subcrop (i.e where main syn-rift depocentres are present)

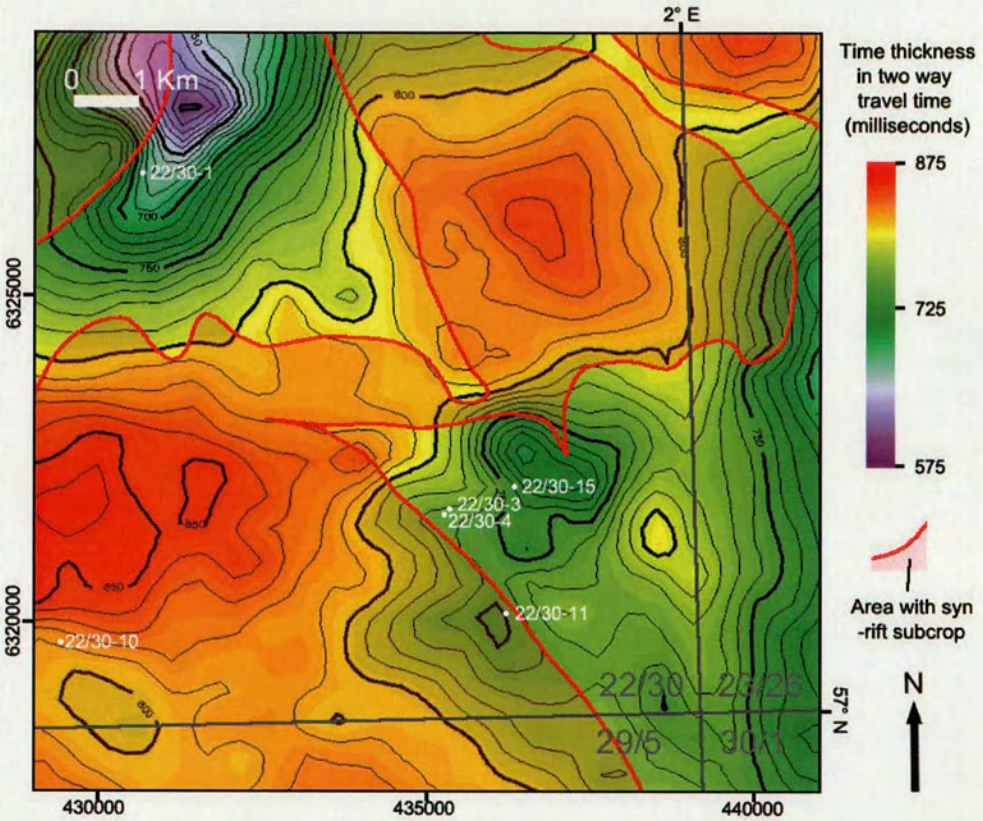

Figure 5.25. Isochron map between the Top Balder Formation and Top Plenus Marl Formation horizons consisting of most of the Upper Cretaceous and Palaeocene sequence. Red tinted areas show where the Base Cretaceous Unconformity has a syn-rift subcrop (i.e where main syn-rift depocentres are present)

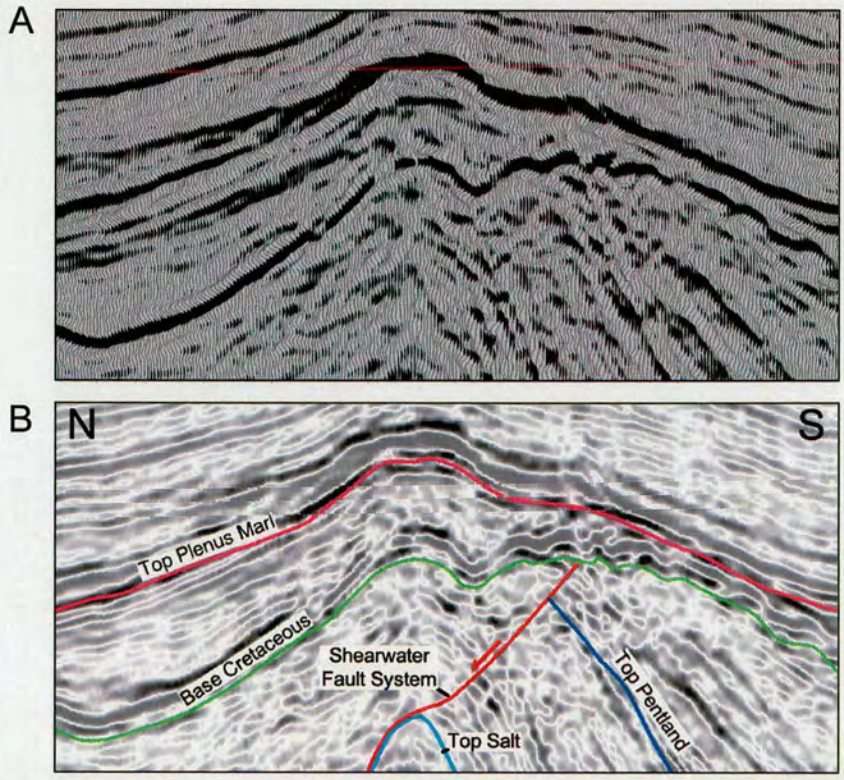

Figure 5.26. Close-up seismic section of the anticlinal structure above the Shearwater salt structure to support the interpretation that reflectors tune onto this structure rather than show evidence of onlap at Lower Cretaceous levels. The section is shown as raw uninterpreted seismic data (A) and interpreted, shaded seismic data (B).

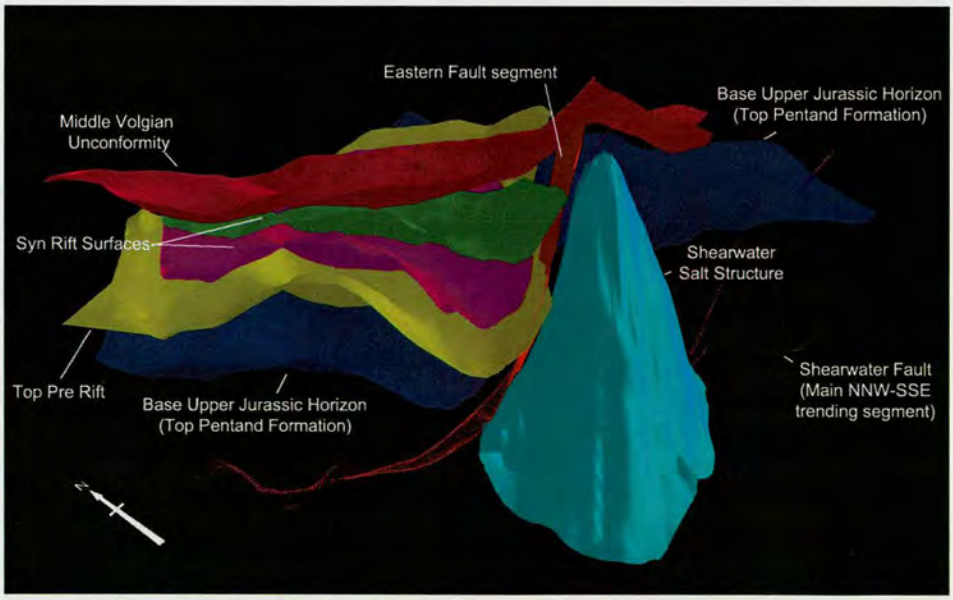

Figure 5.27. 3D visualisation illustrating the relationship between the hanging wall growth package of the Shearwater Fault System and the Shearwater salt structure. The view is looking towards the NE through the fault system. Note how the growth package thickens dramatically in the immediate vicinity of the salt structure

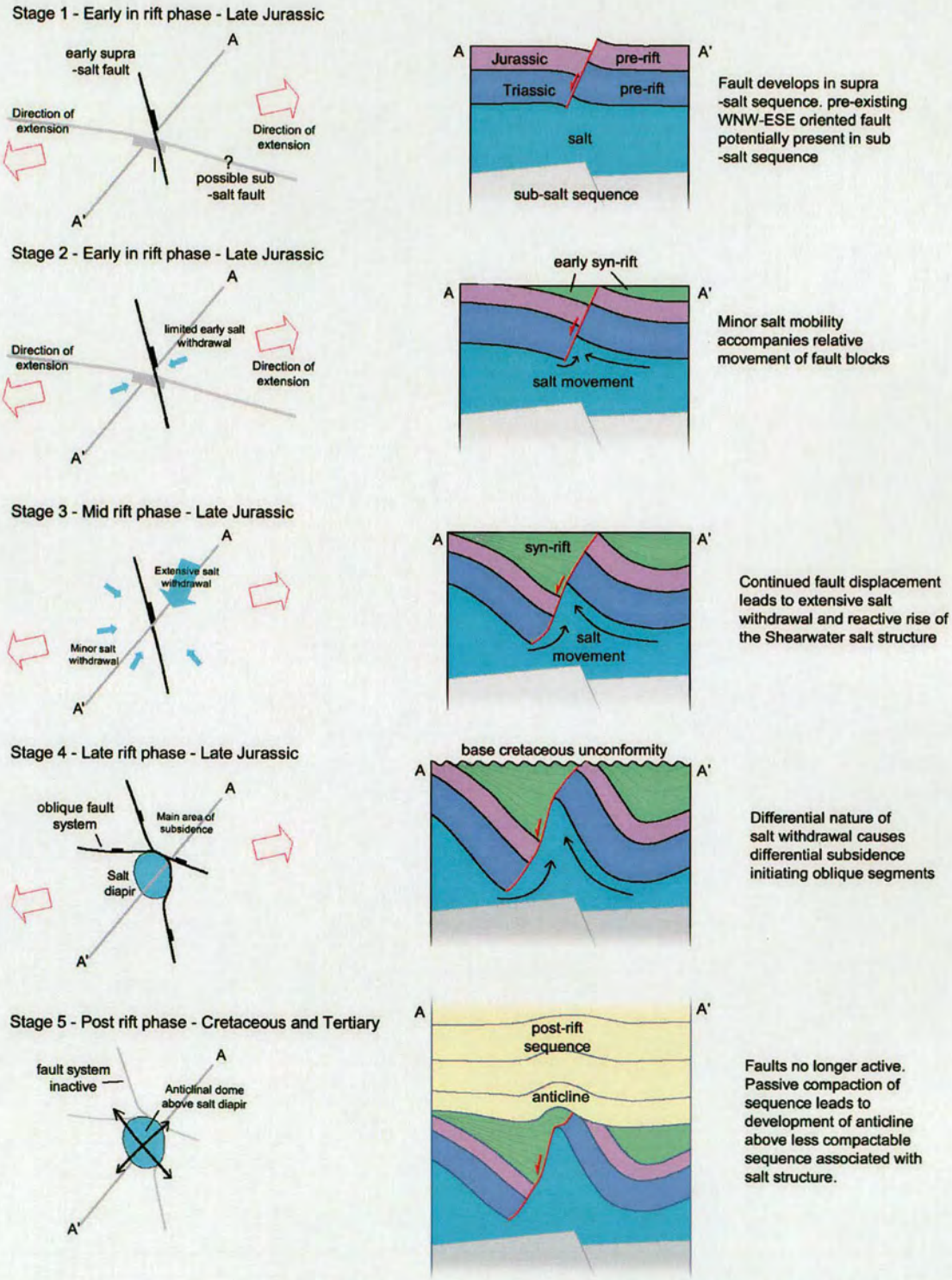

Figure 5.28. Schematic sketch model of the development of the Shearwater Fault System. Shown in plan view (left) and cross section view (right). The cross section shown is approximately along the line of section shown in Figure 5.19.

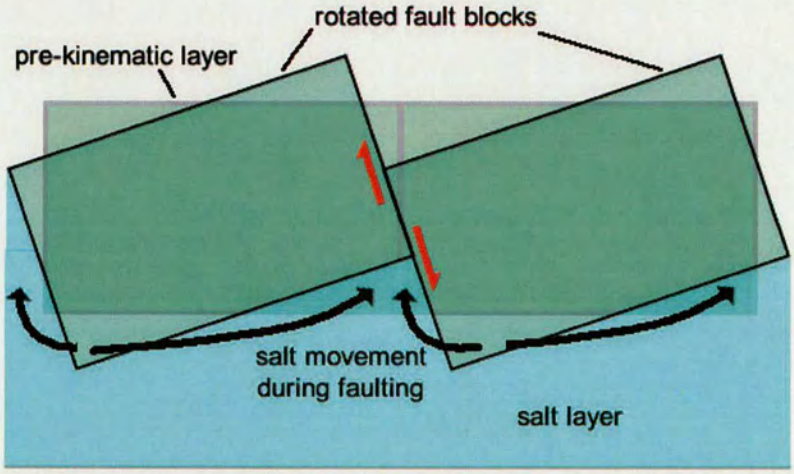

Figure 6.1. schematic section illustrating the salt movement which must accompany supra-salt faulting in order to allow the footwall and hanging wall to move relative to each other.

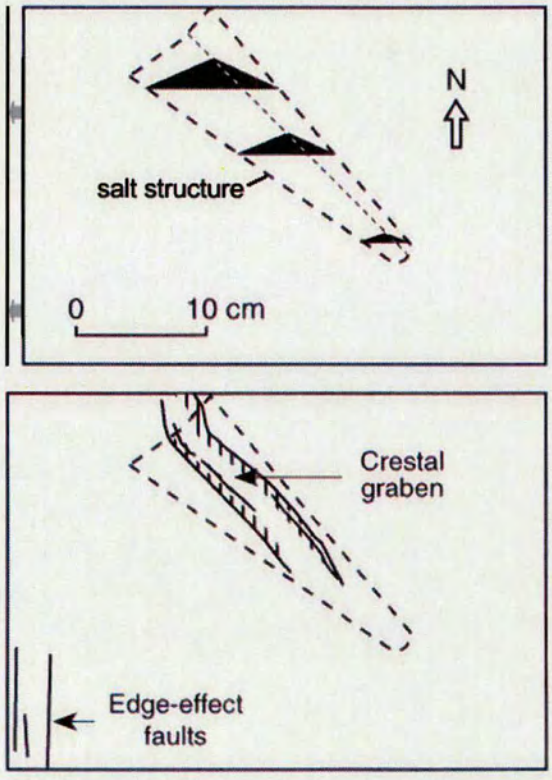

Figure 6.2. Plan view depicting two stages of a physical model where an overburden sequence developed above a pre-existing salt structure is extended slightly in an E-W direction. Note how the resultant supra-salt fault system develops above the salt structure and how it has a NW-SE orientation parallel to the pre-existing salt structure despite being oblique to the extension direction. After Ge et al., (1996).

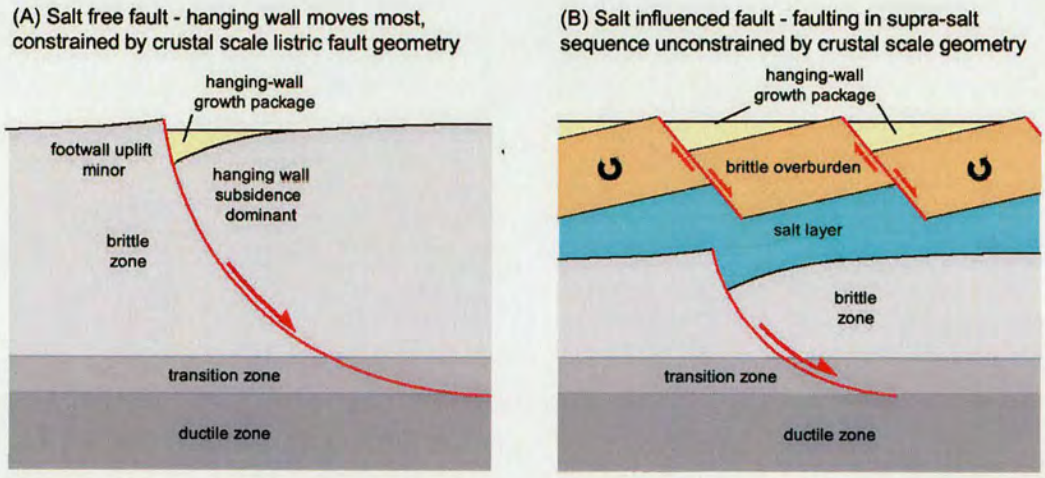

Figure 6.3. Schematic section illustrating how crustal-scale fault geometry can influence the relative constituents of fault movement. Shown is a crustal-scale listric normal fault illustrating how the fault geometry can cause a dominance of hanging wall subsidence as primary mechanism by which fault displacement is manifested (A). Also shown is the situation where a salt layer separates sub-salt and supra-salt faulting (B). In this situation the supra-salt fault geometry is not constrained by the crustal scale geometry and both footwall uplift and hanging wall subsidence are considered to be equally important in accommodating fault displacement.

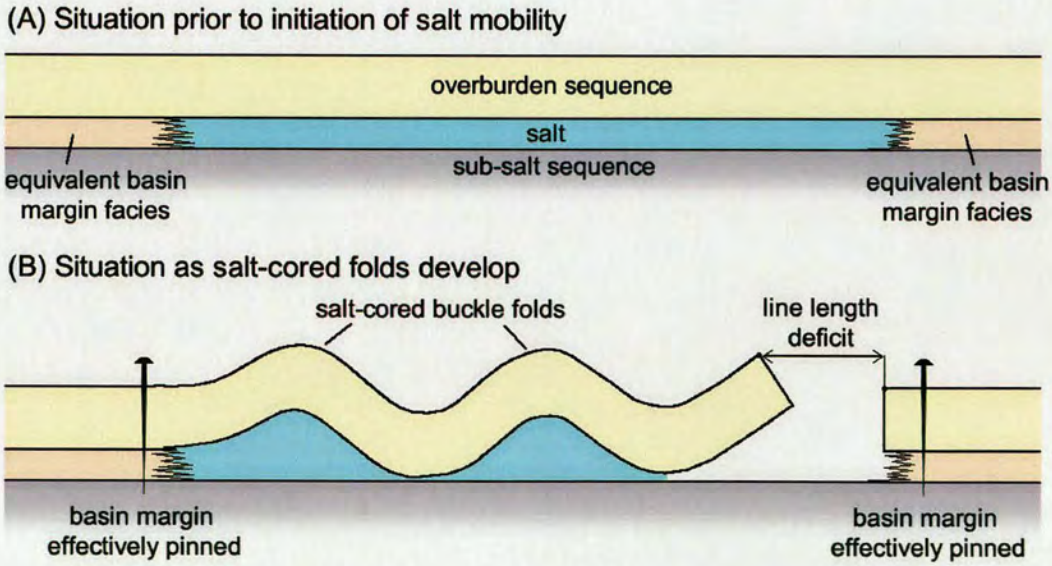

Figure 6.4. Schematic diagram illustrating a salt basin overlain by a pre-kinematic overburden sequence (A) which later became folded into a series of salt-cored buckle folds (B) without bulk crustal compression or extension. The diagram illustrates the need for compressional-style buckle folds to be balanced to extensional-style structures in the supra-salt sequence.

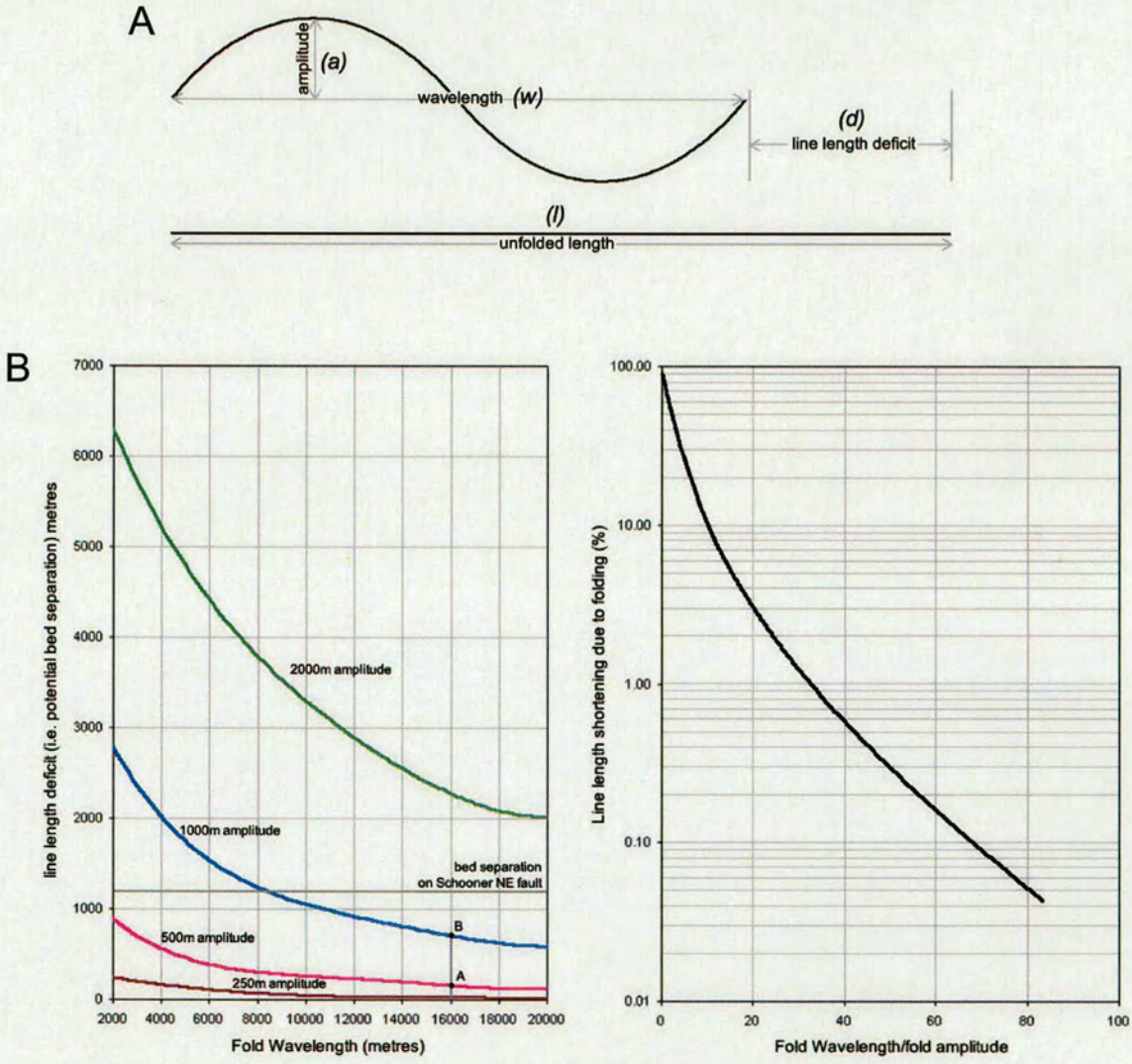

Figure 6.5. Graphs illustrating the amount of line-length shortening associated with folding and consequently the amount of apparent extension that can be associated with thin-skinned fold development. The graphs depict the amount of shortening associated with folds of various wavelengths and amplitudes (B) and a plot of the amount of shortening as a percentage of the unfolded line length (C). (A) shows illustrates the parameters used in these graphs. Points 'A' and 'B' shown in (B) are discussed in the text.

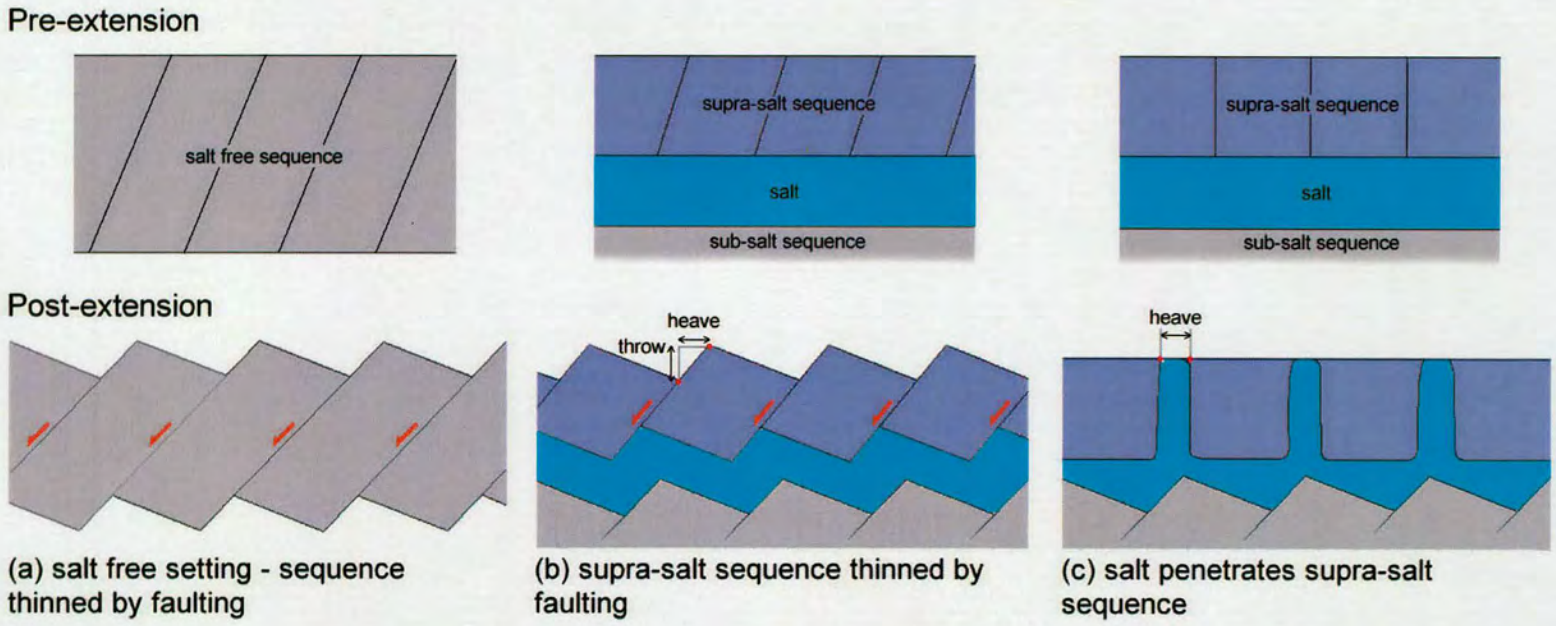

Figure 6.6. Schematic illustrations of the way the crust is thinned due to thick-skinned extension. (A) shows a situation where salt is absent and the sequence is thinned entirely through faulting. (B) shows a situation where extension is accommodated through faulting in the sub-salt and supra-salt sequence and ductile deformation in the salt sequence. (C) illustrates the supra-salt sequence being thinned, effectively through boudinage with block separation accommodated by upwelling salt. Note that in (C), only a heave component is required in the supra-salt sequence to accommodate the extension. In both (B and (C) the salt volume is balanced in the pre and post-extension cases.

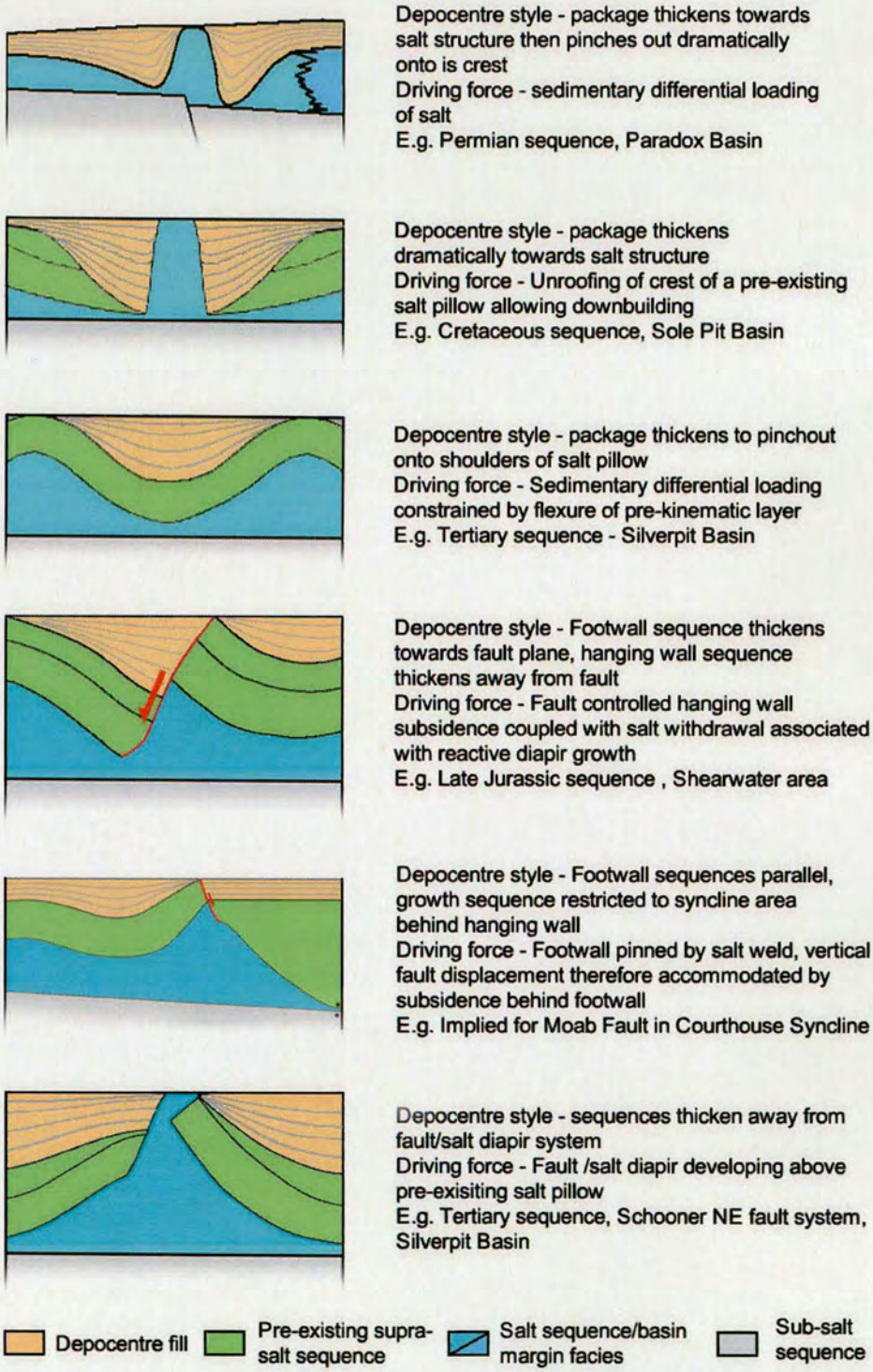

Figure 6.7. Cartoon diagrams illustrating the different salt influenced depocentres styles identified in this study

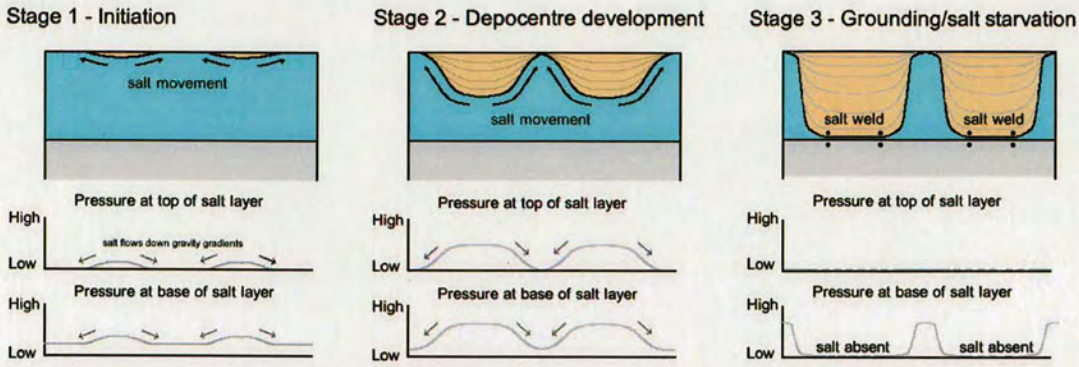

Figure 6.8. Schematic model for the development of salt withdrawal minbasins and their associated salt structures illustrated through cross sections and pressure profiles. Salt is considered to move down pressure gradients within the salt layer as a result of the pressure exerted on it by the overburden and therefore salt mobility and sedimentation are fundamentally interlinked.

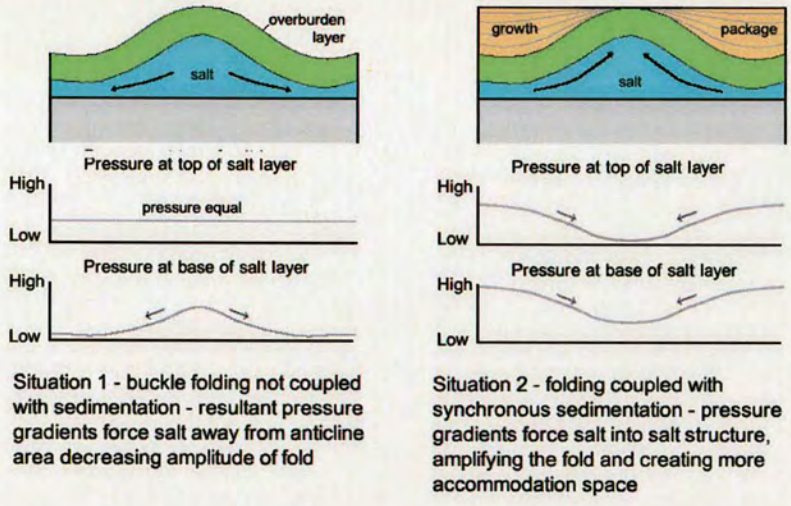

Situation 1 - buckle folding not coupled with sedimentation - resultant pressure gradients force salt away from anticline area decreasing amplitude of fold

Situation 2 - folding coupled with synchronous sedimentation - pressure gradients force salt into salt structure, amplifying the fold and creating more accommodation space

Figure 6.9. Schematic diagram illustrating pressure state in the salt layer of a buckle fold developed without synchronous sedimentation (A) and with synchronous sedimentation (B). Where no sedimentation occurs, pressure profiles indicate that salt would be forced away from the anticline, reducing the amplitude of the structure. In contrast, where synchronous sedimentation occurs, salt would be driven into the salt structure and develop a feedback mechanism between salt mobility and sedimentation similar to that in a minibasin system.

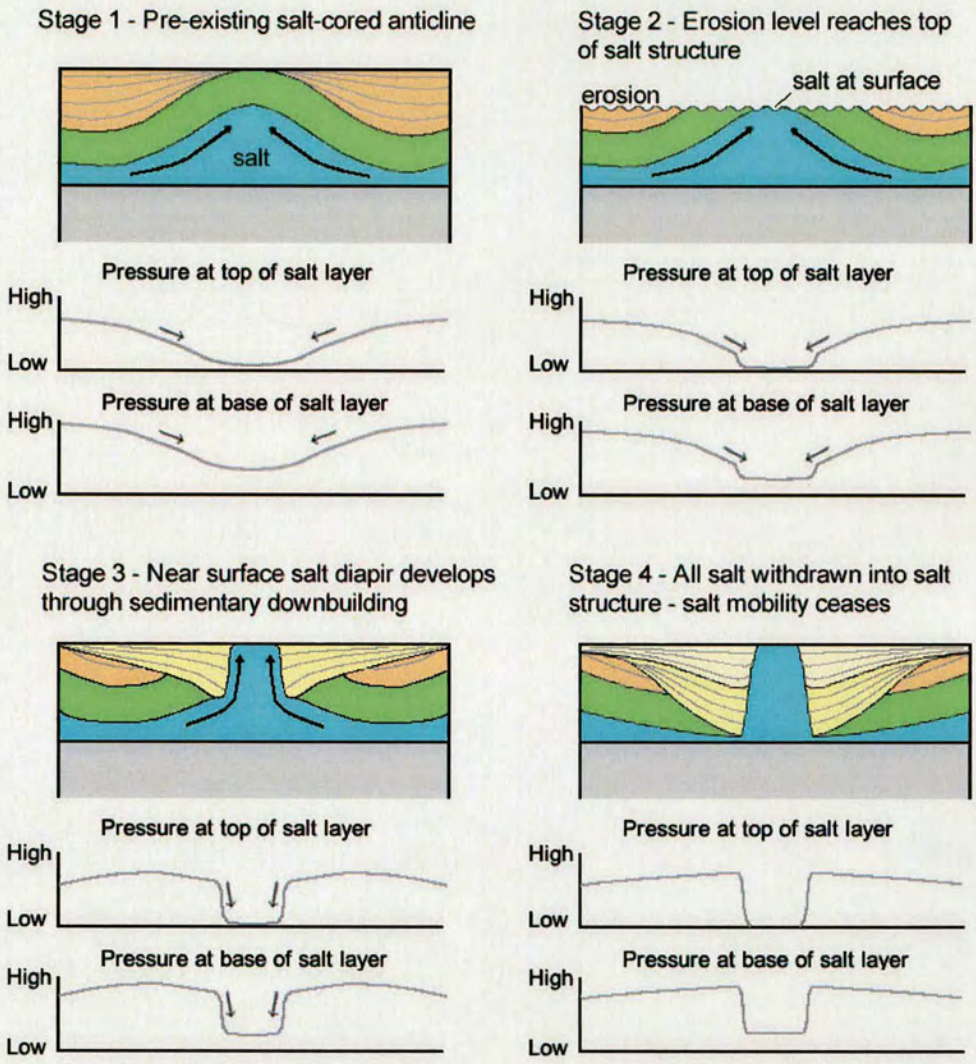

Figure 6.10. Schematic diagram illustrating the pressure state in the salt layer during the development of the illustrated depocentre style. Note how erosion changes the style of salt mobility from being constrained by flexure of the overburden layer to unconstrained downbuilding. This is analogous with the secondary peripheral sink of Trusheim (1960).

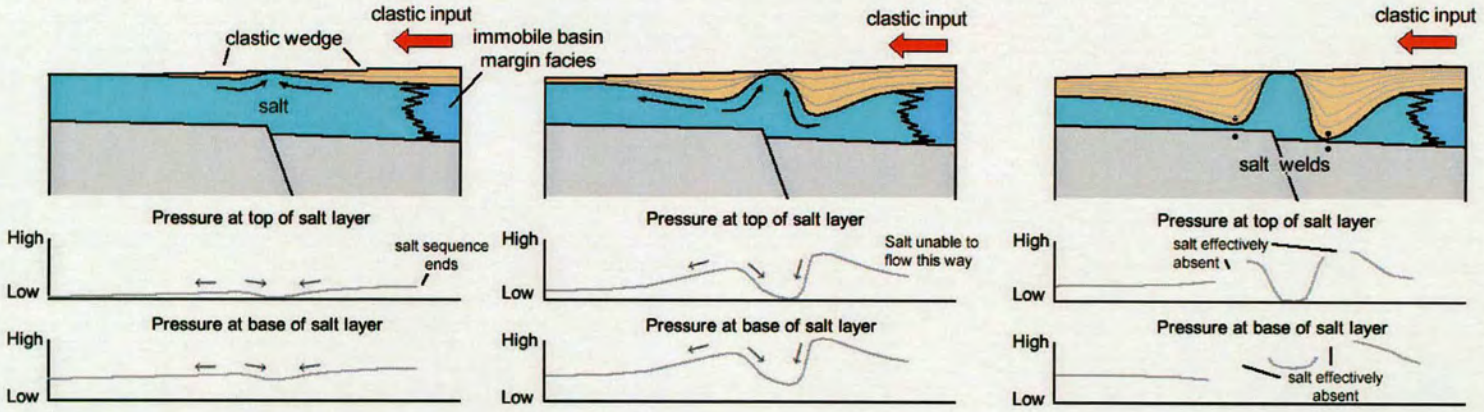

Figure 6.11. Schematic sketch illustrating the pressure state in the salt layer during the development of salt-controlled depocentres related to differential sedimentary loading with a unidirectional sediment supply.

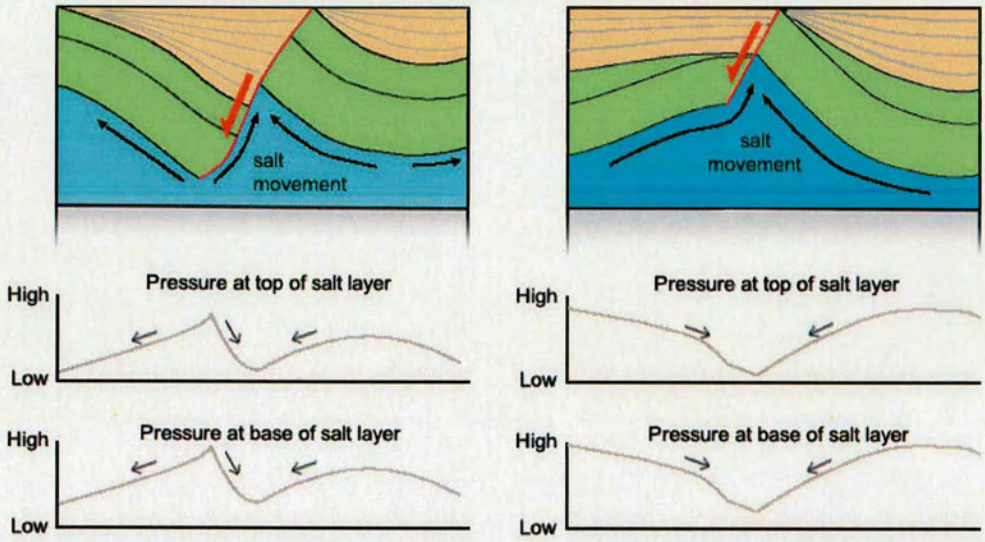

Figure 6.12. Cartoon diagrams illustrating the pressure state in the salt layer associated with the development of the depocentre style observed in the Shearwater area (A) and Schooner NE area (B). Salt is considered to flow down pressure gradients and the depocentre develops with the combined influence of fault displacement and salt mobility

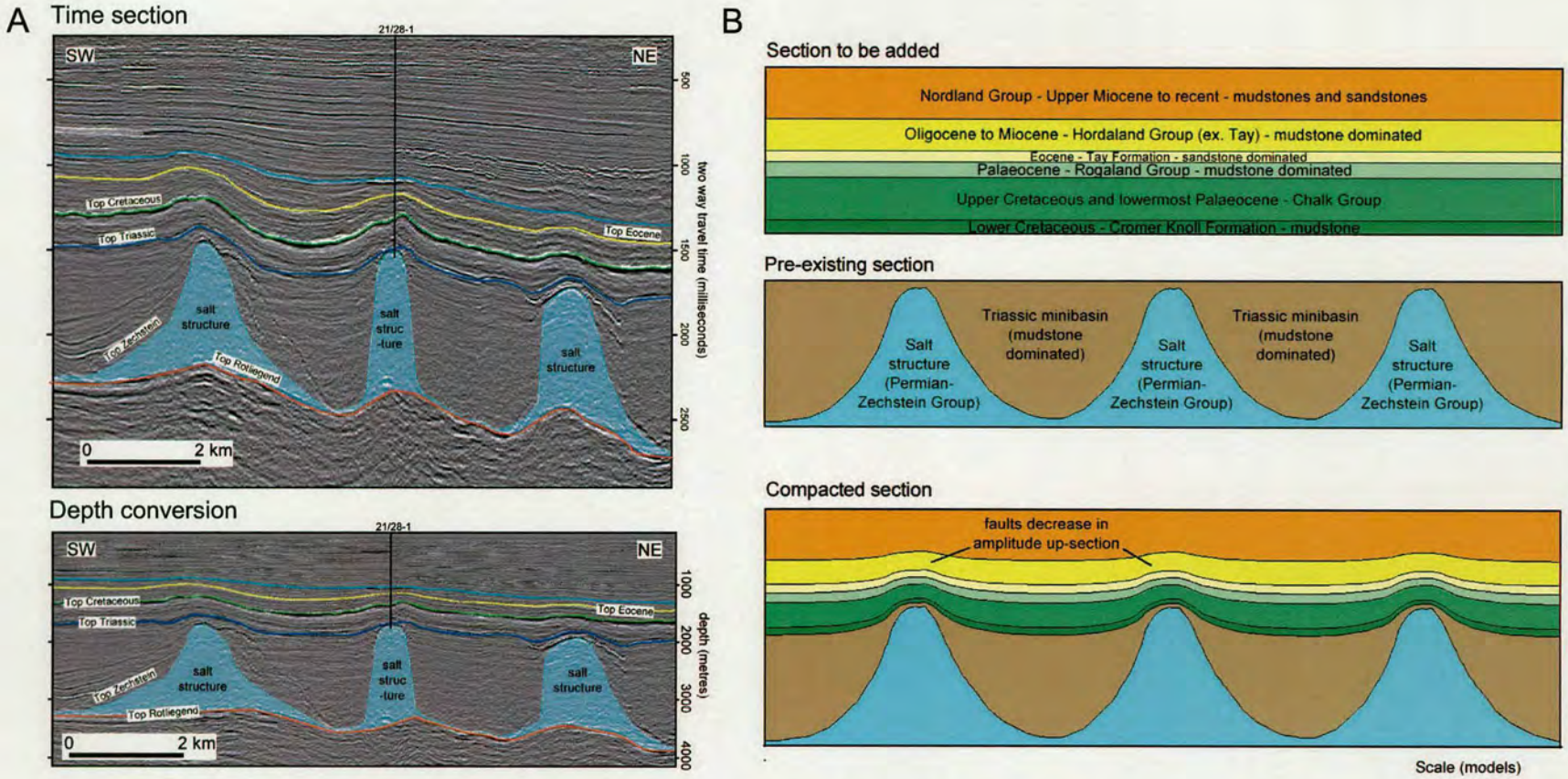

Figure 6.13. Seismic section (time) and depth converted version of the same section (A) illustrating the structural style observed in the Fyne area, Western Platform, Central North Sea. This section shows significant fold development above salt structures which decrease in amplitude up-section as is also observed in the Shearwater area. Modelling (B) shows how similar geometries were created through adding and progressively compacting an analogous section. The post Triassic sequence which was added to the model is derived from back-stripping the sequence in well 21/28-1 (shown in A).

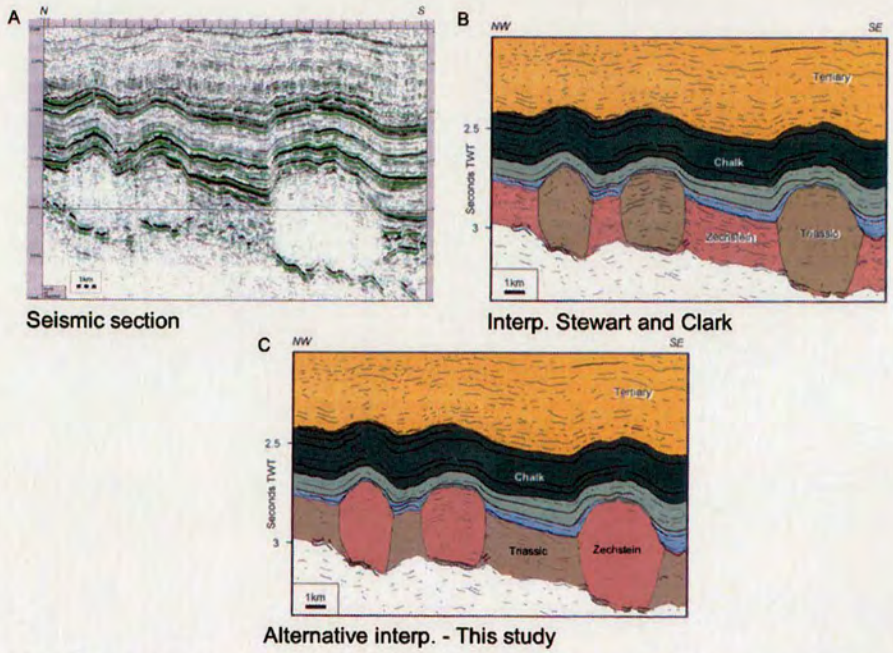

Figure 6.14. Seismic line (a) and interpretation (b) of drape folds developed in the Jæren High area, Central North Sea from Stewart and Clark (1999). An alternative interpretation is also shown (c) which suggests that the package labelled 'Zechstein' in (b) is in fact a Triassic minibasin and the package labelled 'Triassic' is a salt structure. If this interpretation were the case, drape folds would be expected to have developed due to the Triassic sequence compacting more than the Zechstein sequence.

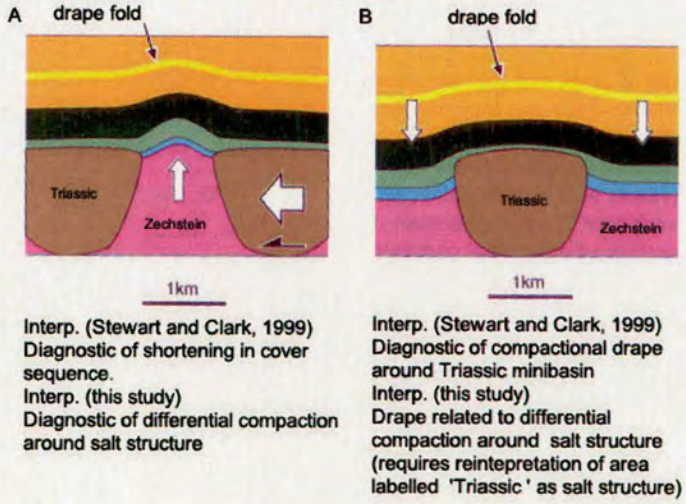

Figure 6.15. Summary diagram of some of the 'inversion' styles recognised in the Central North Sea by Stewart and Clark (1999). The situation shown in (A) is considered by them to be diagnostic of shortening in the cover sequence. In this study however, differential compaction is interpreted as the most likely mechanism to develop this structural style. Stewart and Clark (1999) do, however, interpret the situation shown in (B) to be diagnostic of compaction around a Triassic minibasin. The Triassic sequence is however considered much more compactable than the Zechstein sequence making this unlikely unless the interpreted assignment of the Zechstein and Triassic sequence is reversed as in Figure 6.14.

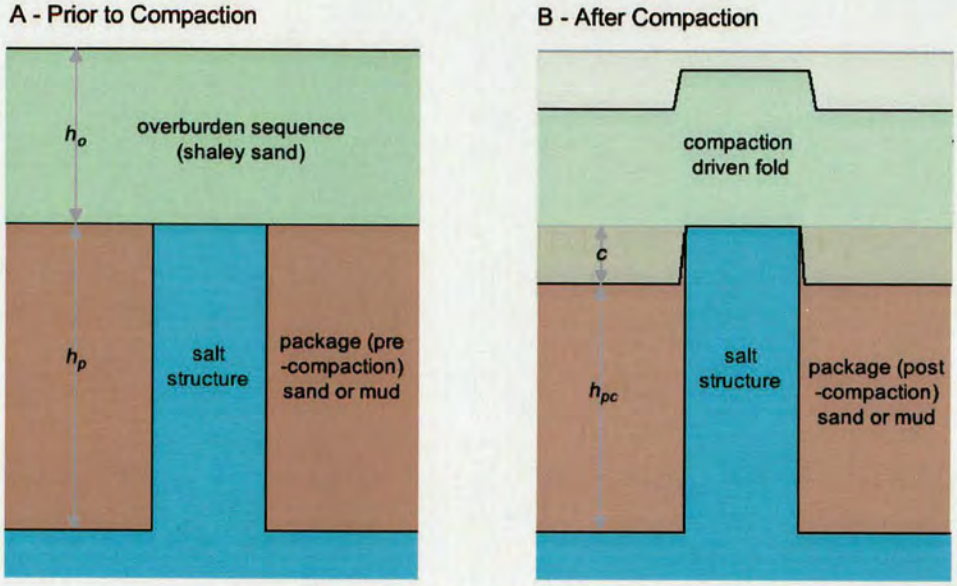

Figure 6.16. Schematic sketch illustrating the parameters used in modelling the potential height of compaction driven folds. The fold height (c) is determined by subtracting the height of the package after compaction (H_{pc}) from the height prior to compaction (H_p). Fold heights are calculated by adding varying thicknesses of overburden (H_o) to the sequence. The overburden is modelled with the properties of a shaley sand and the compacted package modelled as both sand and mud. Porosity and depth coefficient values are taken from Scalater and Christie (1980).

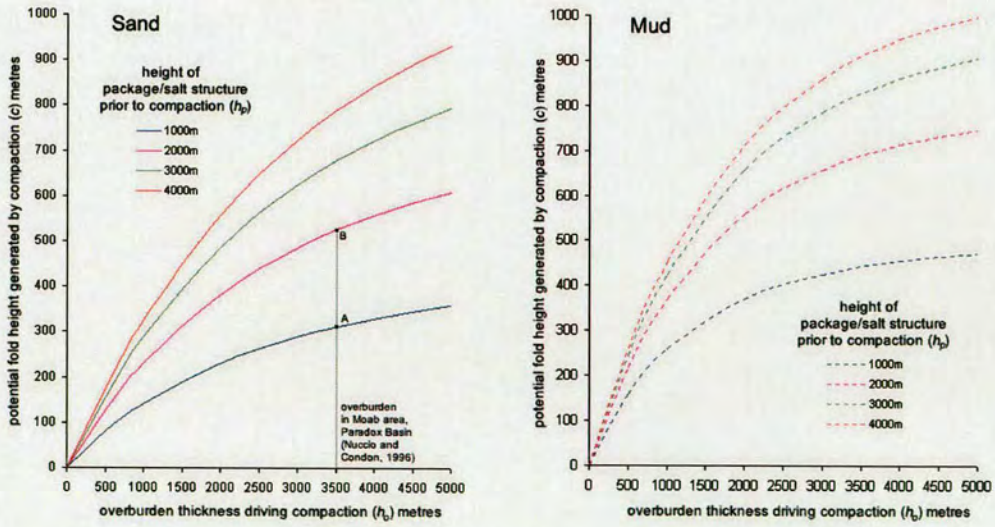

Figure 6.17. Graphs illustrating the potential fold heights generated through differential compaction of sequences adjacent to salt structures for various heights of salt structure/depocentre thicknesses and heights of overburden load. Curves are given for both a sand filled depocentre (A) and a mud filled depocentre (B). Overburden thicknesses are all given the values of a shaley sand. All initial porosity values etc. are derived from Scalater and Christie (1980).